Pathogenesis of *Streptococcus pneumoniae* - a molecular characterisation

Vikrant Minhas, B. Sc.

A thesis submitted for the fulfilment of the
Degree of Doctor of Philosophy

School of Biological Sciences
The University of Adelaide
Adelaide, South Australia, Australia

July 2020

Table of Contents

Abbreviations

µg	microgram/s
µl	microlitre/s
µM	micromolar
ABC	ATP binding cassette
Adr	Attenuator of drug resistance
ARs	Accessory regions
AI-2	Autoinducer 2
BA	Blood agar
BBB	Blood-brain barrier
BgaA	β-galactosidase
BIR	Bacteriocin immunity region
CbpA	Choline binding protein A
CbpD	Choline binding protein D
CcpA	Catabolite control protein A
CDM	Chemically defined medium
CFU	Colony forming units
ChoP	Phosphorylcholine
CPS	Capsular polysaccharide
CSP	Competence-stimulating peptide
CSF	Cerebrospinal fluid
C+Y	Casein-based, semisynthetic liquid medium
DNA	Deoxyribonucleic acid
eDNA	Extracellular DNA
DLDH	Dihydrolipoamide dehydrogenase
DMEM	Dulbecco's modified Eagle's medium
DPD	4,5-dihydroxy-2,3-pentanedione
ELISA	Enzyme-linked immunosorbent assay
ENA	European Nucleotide Archive
Eno	Enolase
FC	Fold change
FCS	Fetal calf serum
FDR	False discovery rate
Gal	Galactose
GAPDH	Glyceralde-hyde-3-phosphate dehydrogenase
GC MS	Gas chromatography mass spectrometry
gDNA	Genomic DNA
Glc	Glucose
GlpO	α-glycerophosphate oxidase
GM	Geometric mean
H_2O_2	Hydrogen peroxide
HIV	Human immunodeficiency virus
Hyl	Hyaluronate lyase
IAV	Influenza A virus
ICE	Integrative and conjugative elements
IgG	Immunoglobulin G
I.N.	Intranasal

indels	Insertions or deletions
IPD	Invasive pneumococcal disease
kDa	Kilodalton
LB	Luria-Bertani
LytA	Autolysin
AMΦ	Alveolar macrophages
iMΦ	Interstitial macrophages
MDS	Multidimensional scaling
mg	Milligram/s
ml	Millilitre/s
iMono	Inflammatory monocytes
rMono	Resident monocytes
NA	Not available
NanA	Neuraminidase
NK	Natural killer
NLR	Nucleotide-binding oligomerization domain-like receptor
NOD1	Nucleotide domain-containing protein 1
OD	Optical density
OM	Otitis media
PAF	Platelet activating factor
PAFR	Platelet activating factor receptor
PavA	Adherence and virulence protein A
PBS	Phosphate-buffered saline
PCR	Polymerase chain reaction
PCV7	Seven valent CPS conjugate vaccine
PCV13	Thirteen valent CPS conjugate vaccine
PECAM1	Platelet endothelial cell adhesion molecule 1
PgdA	Peptidoglycan-*N*-acetylglucosamine deacetylase
PIGR	Polymeric immunoglobulin receptor
PiuA	Pneumococcal iron uptake A
Ply	Pneumolysin
PPSV23	23-valent CPS vaccine
PsaA	Pneumococcal surface antigen A
PspA	Pneumococcal surface protein A
PTS	Phosphotransferase system
qRT-PCR	One-step relative quantitative real-time reverse transcription-PCR
QS	Quorum sensing
R	Rough
Raf	Raffinose
RM	Restriction/modification
RNA	Ribonucleic acid
RrgA	Ancillary pilus subunit
S	Smooth
SB	Serum broth
SD	Standard deviation
SNP	Single nucleotide polymorphism
SsbB	Single stranded DNA binding proteins
ST	Multi locus sequence typing
STD	Raffinose analytical standard

StrA	Pneumococcal sortase transpeptidase
SrtH	*N*-acetylglucosaminidase
THY	Todd-Hewitt
TLR	Toll-like receptor
URT	Upper respiratory tract
WCW	Whole cell vaccine

Declaration

I certify that this work contains no material which has been accepted for the award of any other degree or diploma in my name in any university or other tertiary institution and, to the best of my knowledge and belief, contains no material previously published or written by another person, except where due reference has been made in the text. In addition, I certify that no part of this work will, in the future, be used in a submission in my name for any other degree or diploma in any university or other tertiary institution without the prior approval of the University of Adelaide and where applicable, any partner institution responsible for the joint award of this degree.

I acknowledge that copyright of published works contained within this thesis resides with the copyright holder(s) of those works.

I give permission for the digital version of my thesis to be made available on the web, via the University's digital research repository, the Library Search and also through web search engines, unless permission has been granted by the University to restrict access for a period of time.

I acknowledge the support I have received for my research through the provision of an Australian Government Research Training Program Scholarship.

_____

Vikrant Minhas

03/07/2020

Date

Acknowledgements

First and foremost, I would like to thank my fellow Paton lab, RCID and MLS colleagues that aided me greatly throughout my PhD. I have been incredibly lucky to have gone through my PhD in such a supportive environment. Particularly I would like to thank Erin, Hui, Austen, Alex and Adrienne for their constant aid, encouragement and friendship. Thank you, Danny, Ben, Isy, Miguel, Sonia and Jill for keeping our lab company across the years, and for all the support. Kim, thank you for being the consistently uplifting person that you are, it made the tough periods that much easier. Lauren, thank you for all the incredible help throughout all this, your kindness and assistance was extremely comforting. Richard, thank you for all your help when I was starting my PhD, I look forward to seeing the great impacts that you will have throughout your political career. Patrick, who would have thought that your short placement in this lab would lead to us becoming best of friends, thank you for all your help and camaraderie. Shannon, thank you for the incredible friendship, support and kindness that you provided me throughout all this. Even if all else had failed throughout my PhD, I would still consider it an absolute success, as this is where I met you. Claudia, I cannot begin to thank you enough for all the support you gave me these past few years. Beyond the fantastic supervision you provided, there was a great friendship that I will always cherish, grazie. James, I would not be here if it were not for your support and belief in me. I have learnt so much from you, a large part of any success that comes my way throughout my career will be attributed to you.

I would like to acknowledge the contribution of the Antibiotic Resistant Sepsis Pathogens Framework Initiative consortium in the generation of *in vitro* genome and transcriptomic sequence data used in this project. The Initiative is supported by funding from Bioplatforms Australia through the Australian Government National Collaborative Research Infrastructure Strategy.

I would also like to thank my friends that put up with me throughout my PhD. When experiments weren't working, leading me to being lost and frustrated, it was incredibly comforting having the wonderful friends that I do, in which I could confide in. My greatest thanks go to my parents for all the sacrifices they made for me. Moving away from family in India to another country, so that I could have a better life, was incredibly selfless and brave. I remember how much of a struggle it was when we first moved to Australia and how much you had to give up in order to provide a privileged life for me, where I could learn and study all that I wished. I will strive to use my knowledge to help others, as you did for me. Thank you, mum and dad.

Finally, I would like to thank all the innocent mice that I inflicted pain on and killed throughout my experiments. You had no say and could do nothing about what you were put through. I am truly sorry. Those experiments were always the hardest part of this research, and they always will be. I promise that I will strive the utmost to design and create experiments that minimise animal experiments in the future, and with any luck we will eventually reach a point where these tests will no longer be necessary. I hope that your sacrifices will one day lead to some good, that one day my research will ease the pain of others. Only then will my research be of true worth.

Publications and Conference Presentations

Publications	
Thesis Chapter	**Title**
Chapter 2	V. Minhas, R.M. Harvey, L.J. McAllister, T. Seemann, A.E. Syme, S.L. Baines, J.C. Paton, C. Trappetti. (2019). Capacity to utilize raffinose dictates pneumococcal disease phenotype. *mBio.* 10: e02596-18.
Chapter 4	V. Minhas, R. Aprianto, L.J. McAllister, H. Wang, S.C. David, K.T. McLean, I. Comerford, S.R. McColl, J.C. Paton, J. Veening, C. Trappetti. (2020). In vivo dual RNAseq reveals that neutrophil recruitment underlies differential tissue tropism of *Streptococcus pneumoniae*. *Commun. Biol.* 3: 293.

Publications and accompanying authorship statements are included after the appendicies

Presentations		
Type	**Title**	**Conference**
Oral Presentation	Utilisation of a sugar may dictate disease progression in *Streptococcus pneumoniae*	Australasian Conference of Undergraduate Research (ACUR), Adelaide, SA, Sep 2017
Poster Presentation	Sugar transporter may dictate disease progression in *Streptococcus pneumoniae* serotype 14	The Molecular Biology of Bacterial Pathogens (BacPath 14), Hahndorf, SA, Sep 2017
Invited Speaker	*Streptococcus pneumoniae* - Background, experimental updates, biological questions	Bioplatforms Antibiotic Resistant Pathogen Workshop, Melbourne, Vic, Nov 2017
Poster Presentation	Utilisation of a sugar may dictate disease progression in *Streptococcus pneumoniae*	International Symposium on Pneumococci and Pneumococcal Diseases (ISPPD 11), Melbourne, Vic, April 2018
Oral Presentation	Utilisation of the sugar raffinose dictates disease progression in *Streptococcus pneumoniae*	Australian Society for Microbiology Meeting, Brisbane, Qld, July 2018
Invited Speaker	*Streptococcus pneumoniae* - Background, experimental updates, biological questions	Bioplatforms Antibiotic Resistant Pathogen Workshop, Melbourne, Vic, Nov 2018
Oral Presentation	Sickly sweet – How does a single nucleotide polymorphism affecting utilisation of the sugar raffinose dictate pneumococcal disease progression?	European Meeting on the Molecular Biology of the Pneumococcus (EuroPneumo 14), Griefswald, Germany, June 2019
Oral Presentation	*In Vivo* Dual RNAseq Analysis Reveals the Basis for Differential Tissue Tropism of Clinical Isolates of *Streptococcus pneumoniae*	Lorne Infection and Immunity 2020, Lorne, Vic, Feb 2020

Abstract

The bacterium *Streptococcus pneumoniae* is a leading cause of human morbidity and mortality. With ever increasing antibiotic resistance rates and poor coverage of current vaccines, novel therapeutics and vaccines are urgently required. However, the mechanisms underlying the differences between capacity of individual strains to cause localised vs invasive pneumococcal diseases are poorly understood. This is largely due to vast genetic diversity of strains, which can be subdivided into 100 serotypes based on the capsular polysaccharide they produce, superimposed on >12000 clonal sequence types (ST) distinguished by multi-locus sequence typing. This poor understanding of underlying disease mechanisms is impeding novel treatment design.

Previous studies have shown that even closely related strains within the same serotype and clonal type can display variations in virulence, corresponding to their isolation site in humans. In murine intranasal challenge models, serotype 14 ST15 and serotype 3 ST 180 clinical isolates from the blood tended to cause invasive disease, while corresponding ear isolates instead caused more localised disease. Focusing on the relatively few differences between these closely related strains offers an opportunity to bypass the large genetic diversity of *S. pneumoniae*.

To determine the mechanisms that dictate their progression to specific sites of the body, the blood and ear isolates pairs had their genomes and transcriptomes sequenced and compared. No significant findings came out of the transcriptomic studies, but the genomic analyses found single nucleotide polymorphisms (SNPs) in *rafR* and *rafK,* respectively, that drastically alter pneumococcal disease progression. These genes encode proteins involved in the uptake and/or metabolism of the sugar raffinose. Growth assays with raffinose as the sole carbon source showed that blood isolates grew better than ear isolates, whereas there were no differences in growth in the presence of glucose. Finally, the swapping of *rafR* alleles by allelic-exchange mutagenesis between serotype 14 ST15 blood

and ear isolates led to a concomitant swap in virulence phenotype in mice. These results suggest the ability to utilise raffinose plays a significant role in dictating pneumococcal tissue tropism and disease progression.

Using *in vivo* dual RNA sequencing on infected murine lungs in the early stages of infection, it was established that the *rafR* SNP extensively impacts both bacterial and host transcriptomes. A crucial role for IL-17 induced neutrophil recruitment was predicted, with IL-17 pathway genes upregulated in the strains cleared from the lungs. Indeed, single cell flow cytometry analysis showed the *rafR* SNP leads to increased recruitment of neutrophils in the lungs of mice infected with the strains that were subsequently cleared. Importantly, in the murine intranasal challenge models, mice depleted of neutrophils or IL-17A had significantly higher bacterial loads in the lungs 24h post-challenge. Strikingly, the strains originally cleared from the lungs were now able to persist in this niche after neutrophil depletion, at similar levels at the non-neutrophil depleted invasive strains. The findings provide novel insights into the mechanisms underlying differences in virulence phenotype among *S. pneumoniae* clinical isolates and demonstrate the wide impact of a single bacterial SNP on both bacteria metabolism and host innate immune responses.

Chapter 1

Introduction

1.1 The Pneumococcus

Streptococcus pneumoniae (the pneumococcus) is a Gram-positive, alpha haemolytic diplococcal shaped bacterial pathogen, responsible for significant human morbidity and mortality. *S. pneumoniae* is a leading cause of invasive diseases including pneumonia, bacteraemia and meningitis (Luna-Muschi et al., 2019), as well as localised diseases, such as otitis media and sinusitis (Danishyar and Ashurst, 2019). The pneumococcus is a human pathogen that transmits from human to human via secretory droplets (Weiser et al., 2018), with colonisation of the nasopharynx required for both transmission and invasion deeper into the body to cause disease (Weiser et al., 2018).The capsular polysaccharide (CPS) is the major virulence factor of *S. pneumoniae* and is used to classify the pneumococcus into at least 100 structurally distinct serotypes (Ganaie et al., 2020; Paton and Trappetti, 2019).

1.1.1 Historical background

The first recorded visualisation of the pneumococcus was in 1875 by Edwin Klebs, and in 1881 it was independently isolated by French chemist Louis Pasteur (Note de L. Pasteur, 1881) and U.S. Army physician George Sternberg (Sternberg, 1881). This bacterium was isolated by injecting saliva into rabbits; Pasteur using saliva from a child with rabies and Sternberg using his own, allowing the bacteria to be isolated from the rabbit's blood. Pasteur named the bacteria *Microbe septicemique du salive*, while Sternberg named it *Micrococcus pasteuri*. It was latter named *Diplococcus pneumoniae* in the 1920s, due to its ability to cause pneumonia and its tendency to form pairs (Austrian, 1981), then renamed

again as *Streptococcus pneumoniae* in the 1970s because of its chain-like morphology (Watson et al., 1993).

Many important contributions to science and medicine have been made due to research on *S. pneumonia*e. For instance, in 1882 the Gram stain was discovered accidentally from research aimed at elucidating the cause(s) of pneumonia. It was observed that certain bacteria were able to retain the crystal violet stain while others could not, leading to classification of organisms as either Gram positive or Gram negative (Gram, 1884). Additionally, the Quellung reaction, which allows the determination of capsular serotype of human isolates, was established after an observation that pneumococci swell when exposed to particular antisera (Neufeld, 1902). This reaction is also used for other bacteria, including *Haemophilus, Klebsiella* and *Neisseria* spp. *S. pneumoniae* has also played an important role in understanding humoral immunity and phagocytosis. It was demonstrated in the 1920s that the capsular polysaccharide (CPS) of the pneumococcus was capable of eliciting serological activity (Heidelberger and Avery, 1923) and strain specific protection in mice (Heidelberger, 1927).

Finally, the elucidation of DNA as genetic material, one of the biggest discoveries in molecular biology, was achieved using *S. pneumoniae*. Frederick Griffith observed two different types of pneumococcal colonies present on blood agar (BA) plates: smooth (S) colonies, which possessed CPS and caused lethal infections, and rough (R) colonies, which didn't possess CPS nor the ability to cause lethal infections. It was shown that R strain, incapable of naturally reverting to the S form *in vivo*, was able to acquire S morphology after injecting the R strain into mice along with a heat-killed S strain (Griffith, 1928). Subsequent isolated colonies produced CPS that was identical to the CPS produced by the S strain. This suggested that the pneumococcus was capable of taking up and incorporating genetic material from the environment, a process known as natural transformation. It was then shown that this genetic transformation could be achieved *in vitro* (Alloway, 1932). A

few years later, Oswald Avery and colleagues showed that DNA was the heredity material, by demonstrating that the capsular transformation reaction was abrogated when lysates from the smooth donor were first digested with DNAse (Avery et al., 1944).

1.1.2 Disease burden

Pneumococcal infections are most prevalent in the immunocompromised, children under five years of age and the elderly. The human nasopharynx is its main ecological niche, where it can remain asymptomatically in over 50% of children and up to 10% of adults (Bogaert, De Groot, et al., 2004; Regev-Yochay et al., 2004; Weiser et al., 2018). From the nasopharynx, certain strains of pneumococci can spread deeper into normally sterile sites of the body, such as the lungs, blood or cerebrospinal fluid, to cause invasive pneumococcal disease (IPD) (**Figure 1.1**) (Weiser et al., 2018). An estimated 1 million people die annually due to IPD, the majority of which are children less than 5 years old in developing countries (Iroh Tam et al., 2017; Kadioglu et al., 2008; WHO | Pneumococcal disease, 2014). From 2010-2011, an estimated 120 million pneumonia episodes occurred, of which 14 million progressed to severe disease (Walker et al., 2013). *S. pneumoniae* also causes highly prevalent localised diseases such as otitis media (OM) and sinusitis, with the pneumococcus being the primary causative agent of OM (Brook, 2013; Danishyar and Ashurst, 2019). Australian Aboriginal children have the highest rates of OM in the world, up to 10 times higher than the world average (Organization, 1998). IPD in Indigenous populations has also been reported at rates up to 75 times higher than non-indigenous groups (Forrest et al., 2000).

Risk factors for pneumococcal carriage in the nasopharynx include poverty, malnutrition, poor access to medical care, crowded areas such as day care centres and having younger siblings (Lynch and Zhanel, 2010). In adults, smoking cigarettes, asthma, old age, immuno-

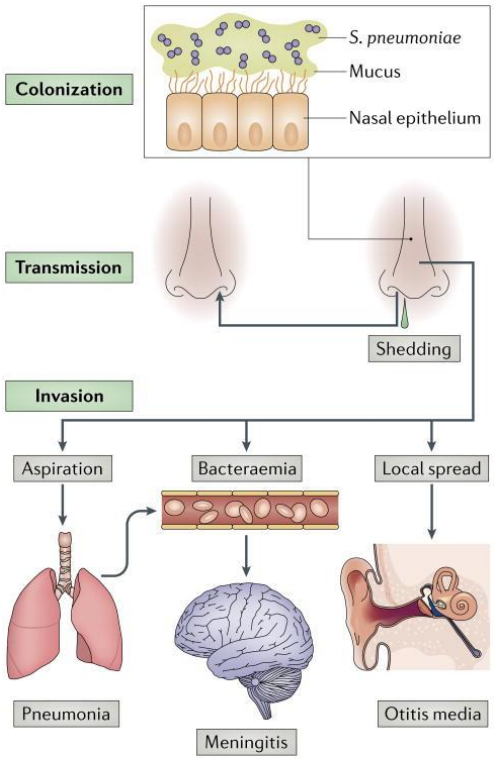

Figure 1.1. *S. pneumoniae* colonises the mucosal layer of the nasopharynx, which is a prerequisite for invasive disease and for its transmission to other hosts. From the nasopharynx, *S. pneumoniae* can be shed in nasal secretions, allowing for transmission. Dissemination from the nasopharynx along the nasal epithelium via aspiration, bacteraemia or localised spread, leads to pneumonia, meningitis or otitis media, respectively. Figure reproduced from Weiser e*t al* (2018).

compromising afflictions and prior acute respiratory infections increase the risk of nasopharyngeal carriage (Lynch and Zhanel, 2010). In Australia, the mortality rate from IPD for both children less than five years of age and for people over 65 years is less than 5% (Australian Institute of Health and Welfare, 2018). In contrast, the IPD mortality rate of children under 5 years of age in developing countries is between 10-40%, which may be in part due limited access to treatments, relatively poor healthcare systems and co-morbidities, such as malnutrition and Human immunodeficiency virus (HIV) infections (Bogaert, Hermans, et al., 2004; Harboe et al., 2009; Madeddu et al., 2010). Other respiratory pathogens, such as the influenza virus, can lead to enhanced pneumococcal infections which results in increased morbidity and mortality. An epitomised example is the 1918-19 Spanish influenza pandemic, where a significant proportion of deaths (about 50 million) were due to secondary bacterial (principally pneumococcal) infections (Morens et al., 2008). More recently, a study during the H1N1 swine flu pandemic in 2009 found

that 33% of all cases involved secondary bacterial coinfection and 62% of these were due to *S. pneumoniae* (Cillóniz et al., 2012).

1.2 Vaccine and Therapeutic Strategies

1.2.1 Antibiotics resistance

Since the introduction of penicillin in the 1940s, antibiotics have readily been used in the treatment of pneumococcal infections. However, since the detection of penicillin-resistant isolates in the 1970s, antibiotic resistance rates have increased dramatically (Cherazard et al., 2017; Lynch and Zhanel, 2009). Penicillin resistance primarily comes about through penicillin-binding protein mutations such that penicillin can no longer bind and inhibit peptidoglycan production (van der Poll and Opal, 2009). Rates of pneumococcal penicillin resistance vary greatly between regions with non-susceptibility rates surpassing 50% of isolates in East Asia and the Middle East, and 30% in Spain. Conversely, rates remain under 5% in Finland, Germany and Sweden (Bruinsma et al., 2004; Cherazard et al., 2017; El Moujaber et al., 2017; Lynch and Zhanel, 2009; Mamishi et al., 2014). It has also been shown that pneumococcal macrolide antibiotic resistance has increased in correlation with penicillin resistance, along with resistance to fluoroquinolones and tetracycline (Cherazard et al., 2017; Lynch and Zhanel, 2009). Rates of pneumococcal macrolide resistance range from 10% to over 70% around the globe (Zhanel et al., 2014), and the SENTRY Antimicrobial Surveillance Program showed that pneumococcal resistance rates in the United States against erythromycin and clindamycin have been steadily increasing since 1998 (Jones et al., 2013).

The proficient genetic transformability of *S. pneumoniae* likely mediates the rapid spread of antibiotic resistance through lateral transfer of antibiotic resistance genes and cassettes, with heavy antibiotic use also providing strong selective pressure. The escalation of antibiotic resistance globally is predominately due to the global dissemination of a handful

of serotypes, for example, serotypes 6A, 6B, 9V, 14, 14F and 23F account for the majority of macrolide resistance in *S. pneumoniae* (Lynch and Zhanel, 2009). These six serotypes, plus 15A, 19A and 19F, also accounted for the highest rates of penicillin and erythromycin resistance (Liñares et al., 2010). Increasing levels of antibiotic resistance lead to a greater reliance on preventative strategies such as vaccination programs as an alternative to reliance on antibiotics.

1.2.2 Polysaccharide vaccines and serotype replacement

A limited number of vaccines are currently utilised to prevent pneumococcal disease. As the CPS of *S. pneumoniae* is critical in pneumococcal colonisation and virulence, and is highly immunogenic in adults, it has become the major antigen target in current vaccine formulations (Bogaert, Hermans, et al., 2004). In 1977, a 14-valent purified CPS vaccine was released in the United States, providing protection against 14 of the most common invasive pneumococcal serotypes. This vaccine lessened morbidity and mortality in the healthy adult population, though unfortunately, overall pneumonia rates were unaffected (Riley et al., 1977). In 1983, a 23-valent CPS vaccine (PPSV23) was developed that provided 80-90% protection against the covered virulent serotypes. IPD rates were significantly reduced in the target population after the implementation of PPSV23, but overall rates of carriage and pneumonia have not been reduced (Fine et al., 1994; Stanek et al., 2016). Importantly, PPSV23 does not elicit immunogenicity in the groups with the greatest pneumococcal disease burden, the immunocompromised and children under 2 years old,.This is due to the inability of these populations to mount effective T-cell independent immune responses (Heilmann, 1990; Shapiro et al., 1991). To overcome this, a seven valent CPS vaccine (PCV7), covering serotypes 4, 6B, 9V, 14, 18C, 19F and 23F was developed that conjugated CPS to a protein carrier CRM197 (a non-toxic variant of diphtheria toxin). PCV7 elicits a T-cell-dependant antibody response even in infants, significantly reducing IPD and carriage in vaccinated children under 2 years old, as well

as in adult populations, due to herd immunity. However, rates of OM did not decrease (von Gottberg et al., 2014; Hammitt et al., 2006; Whitney et al., 2003). A 13-valent conjugate vaccine (PCV13), containing all 7 serotype from PCV7 plus 6 additional invasive serotypes (1, 3, 5, 6A, 7F and 19A), was later developed to increase serotype coverage (Bryant et al., 2010).

Despite the effectiveness of the CPS conjugate vaccines against the included capsular serotypes, the overall serotype coverage is limited. This facilitates the emergence of non-vaccine serotypes, which fill the unoccupied nasopharyngeal niche, and subsequently cause disease. This is termed serotype replacement and evidence for this phenomenon is clear. For example, a few years after the introduction of PCV7, pneumococcal carriage and disease due to serotypes not covered in PCV7 were shown to increase (Ghaffar et al., 2004; van Gils et al., 2009; Grivea et al., 2008; Lipsitch et al., 2007). Moreover, infection rates returned to almost pre-vaccine levels in high risk groups and antibiotic resistance in non-vaccine serotype isolates also increased (Hsu et al., 2009; Singleton et al., 2007). The continual emergence of new non-vaccine serotypes causing pneumococcal disease after introduction of PCV13 has also been observed (Corcoran et al., 2019; Kandasamy et al., 2019).

1.2.3 Protein and whole cell vaccines

Given the ongoing serotype replacement seen in pneumococcal carriage and IPD, paired with increased antibiotic resistance rates, broader preventive strategies are urgently required. Colonisation acts as a natural immunisation event by increasing anti-capsular and anti-protein antibody levels (Ferreira et al., 2013; McCool et al., 2002; Richards et al., 2010), while more recent studies have shown that anti-protein antibodies against *S. pneumoniae* are largely responsible for natural immunity (Ramos-Sevillano et al., 2019; Wilson et al., 2017). Hence, protein antigens that are highly conserved among many

pneumococcal serotypes potentially offer serotype-independent protection from IPD, thus mitigating the risk of serotype replacement (Stanek et al., 2016). In fact, recent research has shown protein antigens, such as pneumolysin (Ply), choline binding protein A (CbpA), or pneumococcal surface protein A (PspA), in multivalent combinations confer broad and strong protection (Chen et al., 2015; Olafsdottir et al., 2012). Several pneumococcal protein vaccines are undergoing or have recently undergone clinical trials. These include formulations containing Ply and pneumococcal histidine triad protein D (PhtD) (Pichichero, 2017).

Another strategy to elicit non-serotype dependant protection is the use of whole cell vaccines (WCV), e.g. immunising with killed non-encapsulated pneumococci with exposed surface protein antigens. A *lytA*-deletion mutant of *S. pneumoniae* Rx1 that expressed non-toxic Ply has been shown to elicit protection against nasopharyngeal carriage and sepsis in murine models (Babb et al., 2016, 2017; Lu et al., 2010; Malley et al., 2001). WCVs have many cost advantages over purified protein or conjugate vaccines, making them more suitable for widespread use in developing countries. Chemically killed (Moffitt and Malley, 2016) and γ-irradiated (Babb et al., 2016, 2017; David et al., 2019) pneumococcal WCVs have been developed and are in the process of undergoing pre-clinical and clinical trials to test their safety and efficacy in providing serotype independent protection.

1.3 Pneumococcal Pathogenesis

1.3.1 Colonisation and transmission

Despite the massive morbidity and mortality associated with pneumococcal disease, *S. pneumoniae* is more commonly carried asymptomatically as a commensal of the human nasopharynx, with carriage a perquisite step for pneumococcal disease. In fact, the human nasopharynx is the primary reservoir for *S. pneumoniae*. Asymptomatic carriage rates vary

markedly with age and geographic region, but are estimated to occur in 18% to >50% of healthy children and 4-10% of adults, with peak rates occurring at 2-3 years of age (Bogaert, De Groot, et al., 2004; Hosseini et al., 2015; Regev-Yochay et al., 2004; Wang et al., 2017).

Other potentially pathogenic bacterial species, including *Moraxella catarrhalis* and *Haemophilus influenzae* may co-reside in the human nasopharynx, as well as multiple serotypes/strains of pneumococci (Shiri et al., 2013; Xu and Pichichero, 2014). Intraspecies competition between pneumococcal strains has been reported to affect nasopharyngeal colonisation (Dawid et al., 2009). A study using mouse models showed that pre-existing pneumococcal colonisation prevents acquisition by a new strain (Kono et al., 2016). Passive immunisation of infant mice with anti-capsular immunoglobulin G (IgG) was also sufficient to prevent colonisation by pneumococcal strains in a serotype-specific fashion (Roche et al., 2015). Host IgA1 additionally contributes to pneumococcal clearance from mucosal surfaces of the human upper respiratory tract (URT). However, *S. pneumoniae* is believed to evade this by secretion of an IgA1 protease which cleaves the antibody hinge region, thus preventing coagulation of pneumococci (Janoff et al., 2014; Roche et al., 2015). Interactions with nasopharyngeal microflora also influence the success of pneumococcal colonisation (Shak et al., 2013). Greater microbial diversity is associated with increased acquisition of *S. pneumoniae* after intranasal (I.N.) challenge (Lysenko et al., 2007), while detection by neutrophils of Gram-negative peptidoglycan via the nucleotide-binding oligomerization domain-containing protein 1 (NOD1) triggers enhanced killing of *S. pneumoniae* (Cremers et al., 2014).

S. pneumoniae transmits from human to human mainly through contaminated secretory aerosol droplets. Crowded areas such as day care centres and hospitals help facilitate spread (Mandigers et al., 1994; Pessoa et al., 2013), as do colder months when airway secretions are more likely to occur in conjunction with viral infection of the URT (Musher, 2003;

Numminen et al., 2015). It has been shown that influenza A virus (IAV) co-infection induces higher rates of pneumococcal transmission and colonisation in mouse pups, due to increased inflammatory conditions (Nakamura et al., 2011; Richard et al., 2014). Moreover, increases in mucosal flow and secretion volume have been shown to increase pneumococcal transmission (Rodrigues et al., 2013). Pro-inflammatory affects caused by *S. pneumoniae* (induced by Ply) also lead to increases in transmission (Zafar et al., 2017). Indeed, dampening inflammation has been shown to reduce shedding and transmission in infant mice (Zafar et al., 2017).

Contact-dependant transmission of pneumococci, through secretions from infected hosts, could involve direct contact from person to person or through contact with contaminated surfaces. Transmission between littermates has been shown in the infant mouse study above, where the mouse dam was not colonised but had large numbers of pneumococci present on her teats (Zafar et al., 2017). *S. pneumoniae* can also be readily cultured from objects such as toys that colonised children recently handled (Marks et al., 2014). Bacteria can survive for days in nutrient-sufficient conditions, such as human saliva (Verhagen et al., 2014). For nutrient poor conditions such as in airway surfaces, capsule polysaccharide (CPS) and Ply expression have also been shown to promote pneumococcal survival (Hamaguchi et al., 2018; Zafar et al., 2017). Additionally, *S. pneumoniae* is able to survive desiccation for several days, while biofilm bacteria are able to retain viability more so than planktonic bacteria (Marks et al., 2014; Walsh and Camilli, 2011).

Upon entering the nasopharynx, *S. pneumoniae* is subject to entrapment by URT mucus, made up of gel like mucin glycoproteins and containing antimicrobial peptides as well as immunoglobulins (Rose and Voynow, 2006). This mucus layer acts as a barrier that prevents microorganisms from reaching the surface epithelium. These epithelial cells also provide a protective barrier for underlying tissues and organs (Brooks and Mias, 2018). Epithelial cells and mucus work in conjunction, resulting in mucociliary clearance. Here,

the negatively charged mucus traps invaders while the cilia on epithelial cells move simultaneously, directing trapped pathogens and mucus towards the mouth for expulsion (Antunes and Cohen, 2007; Nelson, Roche, et al., 2007).

For pneumococcal colonisation to successfully establish, the bacteria must adhere to the epithelial cells that line the upper respiratory tract. This adherence occurs via specific binding of pneumococcal adhesins to ligands on host receptors, e.g. choline binding proteins of pneumococci can adhere to host cell glycoconjugates (Rosenow et al., 1997). Non-specific physio-chemical interactions, such as hydrophobic interactions, between host mucosa and bacterial cells also aid adherence (Swiatlo et al., 2002). Other pneumococcal factors that aid in colonisation include phosphorylcholine (ChoP) present in the cell wall, which has affinity for the platelet activating factor receptor (PAFR) of host cells. Neuraminidase (NanA), β-galactosidase (BgaA) and *N*-acetylglucosaminidase (SrtH) may also unmask adhesin receptors through the cleavage of terminal sugars from host cell surface glycoconjugates (Kadioglu et al., 2008). Furthermore, *S. pneumoniae* can combat the lytic action of host lysozyme via two key enzymes; peptidoglycan-*N*-acetylglucosamine deacetylase (PgdA) and attenuator of drug resistance (Adr) (Davis et al., 2008).

1.3.2 Invasive pneumococcal disease

Stable colonisation of the nasopharynx is the ideal lifestyle for *S. pneumoniae*, as this allows transmission to new hosts. However, increased pneumococcal loads in the nasopharynx and loss of epithelial barrier integrity, increases the probability of invasion into deeper host tissues. IPD occurs when the pneumococcus penetrates tissues by crossing these epithelial and/or endothelial barriers, and enters the lungs, blood and/or cerebrospinal fluid (CSF) **(Figure 1.2)**.

Similar to the colonisation of the nasopharynx, invasion of the respiratory tract requires the evasion of mucus entrapment and mucociliary clearance by the CPS, and proteolytic degradation of IgA1. NanA, BgaA and StrH unmask glycan targets for adhesins, and Ply inhibits ciliary beating (Kadioglu et al., 2008). Upon contact with lung epithelial cells, apical surface adherence is mediated by ChoP, choline-binding protein A (CbpA), the ancillary pilus subunit (RrgA), adherence and virulence protein A (PavA) and large surface-exposed glycoprotein (PsrP). Adherence can occur through interaction of ChoP with PAFR and CbpA with polymeric immunoglobulin receptor (PIGR) (Zhang et al., 2000). *S. pneumoniae* is then able to induce endocytosis into the lung epithelial cells by subverting host receptor recycling pathways, facilitating release to the basolateral surface (Cundell et al., 1995). *S. pneumoniae* can also penetrate the lung epithelium via an alternative paracellular route. Here, Ply and hydrogen peroxide (H_2O_2) damage the epithelium, while hyaluronate lyase (Hy1) and plasmin, bound to the surface of pneumococci via enolase (Eno), glyceralde-hyde-3-phosphate dehydrogenase (GAPDH) or CbpE, degrade the extracellular matrix. Interactions between ChoP-PAFR and CbpA-PIGR also allow pneumococci to cross the endothelium and enter the bloodstream (Cundell et al., 1995; Zhang et al., 2000).

To cross the blood-brain barrier (BBB), *S. pneumoniae* utilise ChoP-PAFR, CbpA-PIGR and CbpA-laminin receptor binding on the brain microvascular endothelium (Brown et al., 2014; Orihuela et al., 2009). Strains that express pili use RrgA, the tip adhesin of pneumococcal pilus 1, to bind to PIGR and platelet endothelial cell adhesion molecule 1 (PECAM1) on the brain microvascular endothelium. Blockade of these two receptors lessened brain invasion rates in a mouse meningitis model (Iovino et al., 2017). Similar to respiratory tract invasion, Ply, H_2O_2 generated by α-glycerophosphate oxidase (GlpO) and activated plasmin bound to the pneumococcal surface proteins Eno, GAPDH and CbpE can lead to the compromise of the BBB (Attali, Durmort, et al., 2008; Mahdi et al., 2012;

Rayner et al., 1995). Meningitis may also occur through localised infections, or through retrograde axonal transport when pneumococci bind to gangliosides on olfactory neurons on the nasopharyngeal mucosa (van Ginkel et al., 2003). Exogenous sialic acid also stimulates this non-haematogenous spread across the BBB (Hatcher et al., 2016).

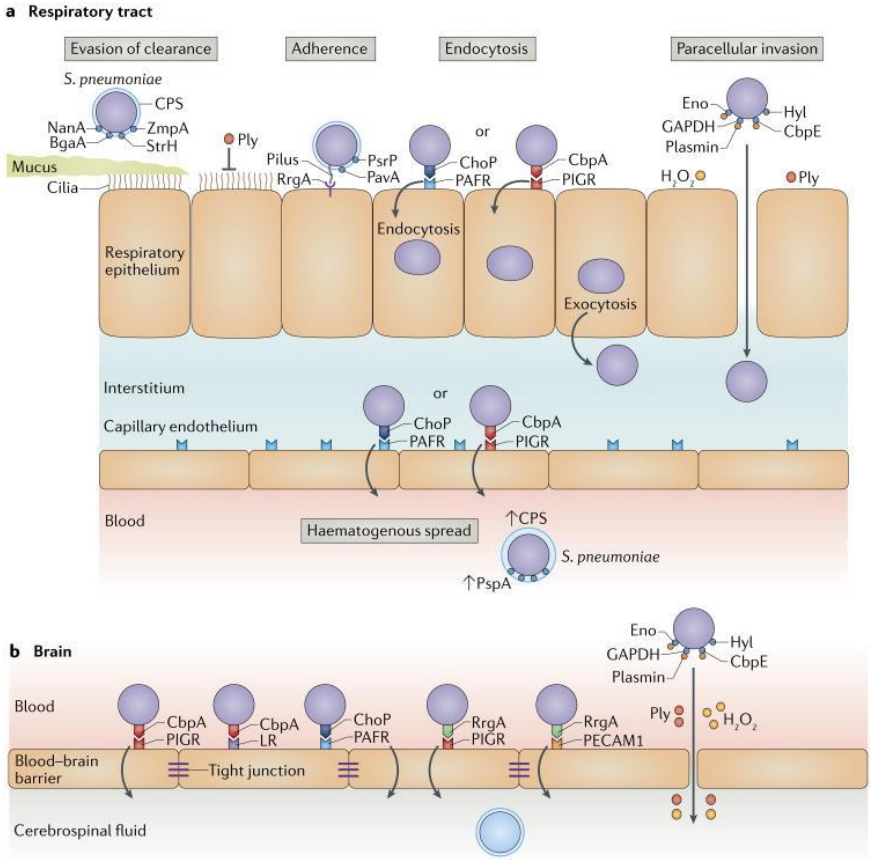

Figure 1.2. To cause Invasive Pneumococcal Disease, *S. pneumoniae* utilises a range of surface proteins and other molecules to bind to and penetrate host tissue. (a) Pneumococci cross respiratory epithelium via inducing endocytosis, providing access to the interstitium. *S. pneumoniae* can then bind to and transverse capillary endothelium, allowing access to the bloodstream, which results in haematogenous spread. From here, pneumococci can bind to and cross the blood-brain barrier (b), allowing invasion of the Cerebrospinal fluid. Figure reproduced from Weiser et al. (2018).

1.3.3 Otitis media

Many strains of *S. pneumoniae* are able to ascend the Eustachian tube to cause OM, which is a disorder resulting in inflammation of the middle ear. Infection of the middle ear is facilitated by two neuraminidases, NanA and NanB, which can cleave *N*-acetylneuraminic acid from glycoproteins and glycolipids on host cell surfaces, as well as cleaving mucins (Loughran et al., 2019). This reduces overall viscosity, improving access to the epithelial surfaces. Oligosaccharides on epithelial surfaces can then be cleaved by NanA and NanB,

exposing receptors for pneumococcal adherence (Berry et al., 1996; Stahl and O'Toole, 1972). These enzymes are evidently critical to development of OM. In a chinchilla infection model, a neuraminidase-deficient mutant was cleared twice as quickly from the middle ear compared to the wild-type *S. pneumoniae* (Tong et al., 2000). Once within the middle ear, the pneumococcus induces inflammation through cell surface proteins and Ply which contributes to hearing loss and cochlear damage (Comis et al., 1993; Tuomanen, 2000; Winter et al., 1997).

OM can be divided into 3 categories depending on the symptoms and severity of disease, acute OM, OM with effusion and chronic OM with effusion (Taylor et al., 2009). OM with effusion in the presence of signs of an infection is defined as acute OM. There are 2 subtypes of acute OM; without perforation, which usually involves the bulging of the tympanic membrane, and with perforation, which involves perforation of the tympanic membrane. When effusion discharges through a tympanic membrane perforation persistently for at least 6 weeks, it is then classified as chronic suppurative otitis media (Bergenfelz and Hakansson, 2017).

1.4 Host immune responses

1.4.1 Innate immunity

The first line of defence against *S. pneumoniae* infection is the innate immune system, which involves a non-specific and rapid response initiated against anything recognised as foreign or 'non-self'. Pathogens are recognised by innate pattern recognition receptors (PRRs) which are located on host cell surfaces or intracellularly. These will recognise pathogen-associated molecular patterns (PAMPS), such as viral dsRNA, and bacterial LPS or lipoteichoic acid, and initiate a signalling cascade leading to innate immune activation (Murphy and Weaver, 2017; Paterson and Mitchell, 2006a). Among all the PRRs identified, Toll like receptors (TLRs) are one of the largest and most well-characterised families.

TLRs are typically membrane-bound, with TLR2, TLR4 and TLR9 being the most important for recognition of *S. pneumoniae* (Richard et al., 2014; Srivastava et al., 2005; Tomlinson et al., 2014). These will recognise pneumococcal lipoproteins, the pneumococcal toxin Ply, and CpG-DNA for TLR2, 4, and 9 respectively. TLRs also play roles in the adaptive immune response as they facilitate the release of co-stimulatory molecules required for T-cell activation (Rahman et al., 2009).

Nucleotide-binding oligomerization domain-like receptors (NLRs) are another class of PRRs that recognise bacterial cell wall components. In response to ligand binding, NLRs will stimulate NF-κB, activate the inflammasome, promote cytokine production and induce inflammation (Franchi et al., 2009; Murray, 2009; Rabes et al., 2016). The protein CD14 has also been identified as a PRR through recognition of bacterial cell wall components (Anas et al., 2010). However, during *S. pneumoniae* infection, CD14 has instead been shown to facilitate pneumococcal dissemination into the respiratory tract (Dessing et al., 2007).

In response to production of inflammatory mediators, innate immune cells will be directed to the site of pathogen encounter. These cells include basophils, dendritic cells, eosinophils, Langerhans cells, mast cells, monocytes and macrophages, neutrophils and natural killer (NK) cells. Neutrophils and macrophages are critical innate immune cells for clearance of pneumococcal infection. (Craig et al., 2009; Dockrell and Brown, 2015; Murphy and Weaver, 2017; Paterson and Mitchell, 2006a; Standish and Weiser, 2009). Neutrophils are the most abundant innate cell types and are usually the first cells that travel to the site of infection (Craig et al., 2009; Kolaczkowska and Kubes, 2013). They are phagocytic cells that produce granules which break down pathogen cell walls (Falloon and Gallin, 1986; Kolaczkowska and Kubes, 2013) and can also trap *S. pneumoniae* extracellularly though fibres made from DNA (Gardiner and Andrews, 2012). Macrophages also function as phagocytic cells that engulf and kill pneumococci (Murphy and Weaver, 2017; Paterson

and Mitchell, 2006a). They target cells that have been opsonised via the complement system and Fcγ receptors (Dockrell and Brown, 2015), but they can also phagocytose non-opsonised antigens through their receptor MARCO, macrophage receptor with collagenous structure (Kraal et al., 2000).

In addition, respiratory epithelial cells are able to kill pneumococci through secretion of antimicrobial peptides such as apolactoferrin and lysozyme, that lyse cells, prevent growth, and/or sequester iron (André et al., 2015; Whitsett and Alenghat, 2015). Respiratory epithelial cells can also release cytokines and chemokines to recruit additional immune cells to the site of infection (Whitsett and Alenghat, 2015).

1.4.2 Adaptive immunity

The adaptive or acquired immune response takes longer to initiate, but is pathogen specific and highly effective. It also results in immunological memory of encountered antigens, with each subsequent response being faster and larger in magnitude. There are two types of adaptive responses, cell-mediated immunity involving T-cells and humoral immunity involving the production of antigen-specific antibodies via B-cells. Activation of B-cells and subsequent class switching results in production of functional and highly specific antibodies, mainly IgG and IgA. *S. pneumoniae* infections are controlled at mucosal sites through secretory IgA, which opsonises the bacteria to promote phagocytosis (Mook-Kanamori et al., 2011).

T-cells also play a crucial role in clearance of pneumococcal infection. These cells are split into two broad classes, helper $CD4^+$ and cytotoxic $CD8^+$ T-cells. T-cells become activated when they recognise their cognate antigen presented on the major histocompatibility complex proteins of professional antigen presenting cells (APCs). APCs include macrophages, B-cells, and dendritic cells. (Brooks and Mias, 2018). After T-cell activation, helper T cells can differentiate into either the Th1 or Th2 cell subsets. Th1 cells mainly

produce cytokines that drive inflammation and recruit additional immune cells, whilst Th2 cells interact with B-cells to promote class switching and production of antibodies (Romagnani, 1999). Research has shown that $CD4^+$ T-cells are crucial for antibody-dependent immunity to pneumococci (Malley et al., 2005).

The IL-17 producing T-helper cells (Th17) cells are an additional class of CD4+ T-cell that function in anti-pneumococcal immunity. Th17 cells release IL-17 which recruits neutrophils, monocytes and macrophages to infection sites, leading to pneumococcal clearance. Th17 responses are also linked to reduced *S. pneumoniae* carriage (Hoe et al., 2017). In contrast, $CD8^+$ T-cells directly kill infected host cells, similar to natural killer T-cells (van der Poll and Opal, 2009). Moreover, a protective role for CD8+ T-cell-mediated IFN-gamma production against *S. pneumoniae* has been suggested (Weber et al., 2011). Following resolution of infection, subsets of both T-cells and B-cells will differentiate into memory cells and remain in circulation. These memory cells are able to undergo rapid re-activation upon pathogen re-encounter, facilitating faster activation of the adaptive immune response for enhanced pathogen clearance (Sprent, 1994).

1.4.3 Other immune system factors

Cytokines are a broad category of small proteins, ~5-20 kDa, involved in cell signalling. Chemokines are a family of cytokines secreted by cells that direct immune cells to sites of infections and promote inflammation (Arango Duque and Descoteaux, 2014). Well studied examples are the cytokines TNF-α, produced by T-cells, monocytes and macrophages, and IFN-γ, produced by NK cells and T-cells in response to IL-12. These cytokines have been shown to be vital in controlling pneumococcal infections (Jeong et al., 2015; O'Brien et al., 1999; van der Poll et al., 1997; Rubins and Pomeroy, 1997; Wellmer et al., 2001; Yamamoto et al., 2004), though IFN-γ was shown in another study to instead promote pneumococcal meningitis (Mitchell et al., 2012). Moreover, *S. pneumoniae* autolysis has

been shown to prevent the production of phagocyte-activating cytokines (Martner et al., 2009).

The inflammasome is a complex of proteins, consisting of caspase 1 (a sensor protein) and an apoptosis associated Speck-like protein with a caspase recruitment domain, that indirectly identifies pathogenic molecules and subsequently regulates cytokine production (Baroja-Mazo et al., 2014; Rabes et al., 2016). The NLRP3 inflammasome has been shown to aid in the identification of *S. pneumoniae* infection, directly interacting with Ply and leading to macrophage activation and IL-1β and IL-18 release (McNeela et al., 2010; Witzenrath et al., 2011).

The complement system is a made up of small proteins that when activated enhance phagocytosis of pathogens and other invaders by coating them with opsonins (Paterson and Mitchell, 2006a). Complement can be activated through three cascade pathways: classical, alternative, and mannose-lectin pathways. The classical pathway involves complement proteins binding to antibody-antigen complexes, while the alternative and mannose-lectin pathways bind directly to PAMPs (Kadioglu and Andrew, 2004). Both the complement and mannose-lectin pathways have been shown to play important roles in host immunity to pneumococcal infection in mouse models (Ali et al., 2012; Brown, Hussell, et al., 2002). Moreover, mice lacking complement component C3 were not able to clear pneumococcal infection and had lower survival compared to wild type mice (Kerr et al., 2005).

Acute phase serum proteins are able to bind to bacterial surfaces, and they increase in the blood during acute inflammatory infection due to cytokine secretions from innate immune cells (Pepys, 1998). The three major proteins that have been linked with pneumococcal infection are C-reactive protein, serum amyloid P and mannose-binding lectin. C-reactive protein and serum amyloid P have been shown to bind to pneumococcal cell surface phosphocholine, allowing complement deposition through the classical pathway (Mukerji et al., 2012), while mannose-binding lectin has been shown to attach to pneumococcal cell

surface sugars (van Emmerik et al., 1994); low levels of this protein in serum increases the chance of death due to pneumococcal infection (Eisen et al., 2008).

1.4.4 Evasion and subversion of host defences

In order to survive in the human host, *S. pneumoniae* must be able to evade and subvert the host immune system. Acute inflammation occurs as a result of pneumococcal tissue damage, which leads to neutrophil migration to the inflamed sites. Neutrophil granules can then kill phagocytised *S. pneumoniae*, as highlighted in section 1.4.1, through the release of serine proteases (Standish and Weiser, 2009), hence immune evasion and subversion is critical. Pneumococcal CbpE aids in the prevention of neutrophil recruitment by cleaving ChoP moieties on host derived platelet-activating factor (PAF), a potent neutrophil activator (Hergott et al., 2015).

S. pneumoniae employs a range of proteins for the evasion of complement-mediated immunity, e.g. CbpA binds to factor H, a protein that inhibits activation of the alternative complement pathway (Andre et al., 2017). PspA has also been shown to obstruct complement deposition through factor B binding and preventing the formation, or increasing the dissociation rate of the alternative pathway C3 convertase (Tu et al., 1999). Released Ply also activates the classical complement pathway as it contains a domain structurally similar to the IgG Fc component, depleting serum complement components and opsonic activity (Mitchell and Dalziel, 2014; Paton et al., 1984). In fact, both Ply and PspA have been shown to be crucial for pneumococci in causing septicaemia through complement inhibition (Yuste et al., 2005). NanA, BgaA and StrH also disrupt opsonophagocytosis, likely through the deglycosylation of human proteins needed for complement deposition (Dalia et al., 2010).

S. pneumoniae can grow in both long-chains and short-chains. The long-chain forms have greater surface area and hence are more likely to induce complement activation, thus short-

chain forms are more likely to evade opsonophagocytic clearance during IPD (Dalia and Weiser, 2011). The CPS also plays critical roles in the evasion of host immunity as the negative charge of most pneumococcal CPSs also repel similarly charged sialic acid terminal glycans present in the mucosa. This aids in avoiding nasal mucus entrapment allowing pneumococci to transit and attach to epithelial cells (Nelson et al., 2007). Additionally, CPS conceals underlying bacterial surface structures,preventing the binding of immunoglobulins, C-reactive protein and complement components. For example, CPS prevents interactions of Fc and C3b bound to deeper structures in the cell wall with receptors on phagocytic cells (Hyams et al., 2010). Moreover, downregulation/shedding of CPS, together with the D-alanine present in pneumococcal cell wall decreases bacterial negative charge, which aids in evasion of positively charged antimicrobial proteins (Kietzman et al., 2016; Kovács et al., 2006; Nawrocki et al., 2014).

1.5 Pneumococcal Virulence Determinants

1.5.1 The capsular polysaccharide

The polysaccharide capsule forms the outer layer of *S. pneumoniae*, and is approximately 200-400nm thick (Skov Sørensen et al., 1988). With the exception of serotypes 3 and 37, CPS is covalently attached to the cell wall peptidoglycan (Sørensen et al., 1990). Section 1.3 outlined the roles that a few pneumococcal factors play in disease, with the CPS being the most prominent virulence factor. Indeed, within a given serotype, virulence has been shown to be directly related to capsular thickness (MacLeod and Krauss, 1950). Furthermore, although non-encapsulated pneumococci are able to colonise the upper respiratory tract and cause superficial eye infections, they rarely cause IPD (Keller et al., 2016). Nevertheless, the CPS of *S. pneumoniae* impedes adherence and thereby the invasion of host cells, as it sterically hinders interactions between cell wall surface proteins

and cognate host receptors (Talbot et al., 1996). However, pneumococci can greatly reduce CPS thickness during invasion of host cells (Hammerschmidt et al., 2005).

The 100 structurally distinct CPS serotypes differ in capacity to inhibit opsonophagocytosis and switching of the CPS of a given *S. pneumoniae* strain results in marked differences in virulence for mice (Kelly et al., 1994). Such capsule switching occurs naturally, with elevated rates of recombination and substitution occurring within the *cps* locus compared to the rest of the genome (Mostowy et al., 2017). Despite the importance of the CPS during pathogenesis, it is likely disadvantageous during colonisation. This is because colonisation involves direct interaction between pneumococcal surface adhesins and receptors on host epithelial cells. Hence, the pneumococcal adhesins need the CPS to be downregulated in order to interact with host receptors. Indeed, progression from colonisation to disease involves major changes in the expression of a range of virulence determinants in order to adapt to the different host environments (Ogunniyi et al., 2012; Orihuela, Radin, et al., 2004).

1.5.2 Virulence proteins

Virulence refers to the degree of pathology an organism is able to inflict on the host. The degree of virulence of a pathogen is often correlated with its ability to replicate in the host and may also be affected by other conditional factors. For example, pathogens encounter dynamic and varied nutritional host microenvironments that are altered during the course of disease. Hence, pathogens contain metabolic adaptations to nutrients such as carbohydrates (see section 1.5.6) that aid in virulence. *S. pneumoniae* possesses many surface and non-surface proteins that aid in virulence, and hence these are known as virulence proteins. A general overview of virulence proteins is given in **Table 1.1**. Well characterised examples include Pneumolysin, Choline-binding proteins such as PspA,

PspC/CbpA and LytA, transporters such as PsaA, PiaA and PiuA, and various LPXTG-anchored proteins (**Figure 1.3**).

Pneumolysin (Ply) is a 52 kDa soluble protein that is a potent and broad acting virulence factor belonging to the family of cholesterol-dependant cytolysins, synthesised by Gram-positive bacteria. Ply is present in essentially all pneumococcal isolates and its amino sequence is very conserved (Mitchell et al., 1990; Yun et al., 2015). However a few Ply variants have been found (Lock et al., 1996). Ply oligomorises within the membranes of target cells in groups of approximately 40 monomer subunits, forming large ring-shaped transmembrane pores roughly 260 Å in diameter. These oligomers are likely responsible for the cytolytic cell-modulatory activities of Ply, which include: inhibition of ciliary beating on respiratory epithelium and brain ependyma, inhibition of the phagocyte respiratory burst, and induction of cytokine synthesis and resultant $CD4^+$ T-cell activation and chemotaxis (Hirst et al., 2004; Kadioglu et al., 2004). Ply has also been shown, via site-directed mutagenesis, to activate the classical complement pathway independently of its cell-modulatory activities (Mitchell et al., 1991). Numerous studies have shown that both complement-activation and cell-modulatory functions of Ply impact pneumococcal virulence (Alexander et al., 1998; Berry et al., 1995; Canvin et al., 1995; Jounblat et al., 2003; Rubins et al., 1996). However, particular isolates of *S. pneumoniae* lacking haemolytic activity and complement-activating activity have been shown to be at least as virulent, if not more virulent, than isolates containing fully functional Ply, indicating additional unknown functions of this virulence factor (Alexander et al., 1998; Kirkham et al., 2006). Isolates without haemolytic activity of Ply are still able to cause TLR4 or IFN-γ responses, which suggests that there are additional unknown functions of Ply (Baba et al., 2002; Malley et al., 2003).

The Choline-binding proteins PspA, PspC/CbpA and LytA are well-characterised pneumococcal virulence factors, present on the cell wall, anchored to phosphorylcholine

(ChoP) moieties on cell wall teichoic acid and lipoteichoic acid. These proteins contain approximately 20 amino acid repeat sequences that allow for attachment to the cell surface via ChoP. PspA is highly variable between pneumococci strains; based on its N-terminal sequence it can be grouped into three families, subdivided into 6 clades (Hollingshead et al., 2000). PspA inhibits complement component C3 from binding to the pneumococcal cell surface, likely through its highly electronegative properties (Jedrzejas et al., 2001). This protein also binds lactoferrin; hence it protects *S. pneumoniae* from apolactoferrin bactericidal activity (Shaper et al., 2004). PspC/CbpA is a cell-surface multifunctional protein, with *pspC* knock out (KO) mutants showing reduced adherence to epithelial cells and sialic acid *in vitro*, as well as reduced colonisation, compared to a wild type control (Rosenow et al., 1997). PspC can also bind the polymeric immunoglobulin receptor that transports secretory IgA (Hammerschmidt et al., 2000; Zhang et al., 2000). This function may allow the first stage of translocation across respiratory epithelium by subversion of the receptor recycling pathway (Asmat et al., 2014). Additionally, PspC is able to bind factor H (Dave et al., 2004; Janulczyk et al., 2000), preventing C3b formation via the alternative pathway of the complement system, thereby inhibiting opsonisation (Quin et al., 2005). Indeed, *pspC* KO mutants have reduced virulence in mouse pneumonia and sepsis models (Iannelli et al., 2004; Jounblat et al., 2003; Quin et al., 2005). LytA is an amidase that cleaves pneumococcal peptidoglycan N-acetylmuramoyl-L-alanine bonds, leading to cell autolysis, a hallmark feature when growing pneumococci in batch culture (Lysbo Svendsen et al., 1979). However, LytA also aids in cell-wall growth and turnover. *LytA* KO mutants had reduced virulence in pneumonia and sepsis murine models (Berry et al., 1989; Berry and Paton, 2000; Canvin et al., 1995; Orihuela, Gao, et al., 2004). LytA's influence on virulence is likely due in part to the release of Ply and lipoteichoic acids and inflammatory peptidoglycan fragments from lysed pneumococci (Kadioglu et al., 2008; Mellroth et al., 2012).

Cell-surface lipoproteins that have been shown to be essential for pneumococcal virulence include the metal-binding lipoproteins pneumococcal surface antigen A (PsaA), pneumococcal iron acquisition A (PiaA) and pneumococcal iron uptake A (PiuA). PsaA is a divalent metal-ion binding component of a manganese uptake ATP-binding cassette (ABC) transport system, which accommodates both zinc and manganese ions (Dintilhac et al., 1997; Lawrence et al., 1998). *PsaA* KO mutants were unable to grow without the addition of manganese (Dintilhac et al., 1997), were deficient in adherence to mammalian cells *in vitro* (Berry and Paton, 1996; Briles et al., 2000) and were avirulent in murine pneumonia, sepsis and colonisation models (Berry and Paton, 1996; Johnson et al., 2002; Marra et al., 2002; McAllister et al., 2004). Studies with *psaA* mutants suggest that manganese uptake is essential for resistance to oxidative stress due to the production of hydrogen peroxide during pneumococcal metabolism and generation of reactive oxygen species during host innate immune responses (McAllister et al., 2004; Tseng et al., 2002). PiaA and PiuA are the lipoprotein metal-binding proteins of two ABC iron and iron-carrier uptake transporters (Cheng et al., 2013; Whalan et al., 2005). Redundancy is seen between the transporters, as both must be deleted to induce significant reduction in growth in iron-deficient medium. However, mutations in either of these transporters leads to decreases in virulence in murine pneumonia and sepsis models, while a double mutant showed the greatest decrease in virulence (Brown, Gilliland, et al., 2002).

The pneumococcal sortase transpeptidase (StrA) recognises the LPXTG amino acid motif in certain surface proteins, covalently anchoring them to the peptidoglycan. *S. pneumoniae* strains can contain either a single or multiple sortase-like genes (Bergmann and Hammerschmidt, 2006). Murine, chinchilla and *in vitro* adhesion models show SrtA plays roles in pneumococcal colonisation, pneumonia and septicaemia (Chen et al., 2005; Kharat and Tomasz, 2003; Paterson and Mitchell, 2006b). Up to 20 pneumococcal proteins, including neuraminidases and Hic, in some serotypes, are believed to be anchored by an

LPXTG motif (Bergmann and Hammerschmidt, 2006; Iannelli et al., 2002). Neuraminidases, known also as sialidases, cleave terminal sialic acid residues off glycoproteins, glycolipids, cell surface oligosaccharides and even soluble proteins such as lactoferrin and IgA2 (King et al., 2004). The pneumococcus produces at least three neuraminidases: NanA, NanB and NanC. NanA is present in all strains, NanB in most, while NanC is present in an estimated 50% of strains (Pettigrew et al., 2006). All these neuraminidases are secreted, though only NanA contains an LPXTG sequence, suggesting differing allele locations and functions, which is supported by the observation that NanB has a drastically lower optimum pH than NanA (Berry et al., 1996). Loss of function neuraminidase mutants in an acute pneumonia murine model demonstrated that both NanA and NanB play roles in pneumococcal persistence in the respiratory tract and bloodstream (Manco et al., 2006). NanC, with its primary reaction product being a nonspecific sialidase inhibitor (Owen et al., 2015), was found to be more common in isolates from cerebrospinal fluid compared to carriage isolates (Pettigrew et al., 2006).

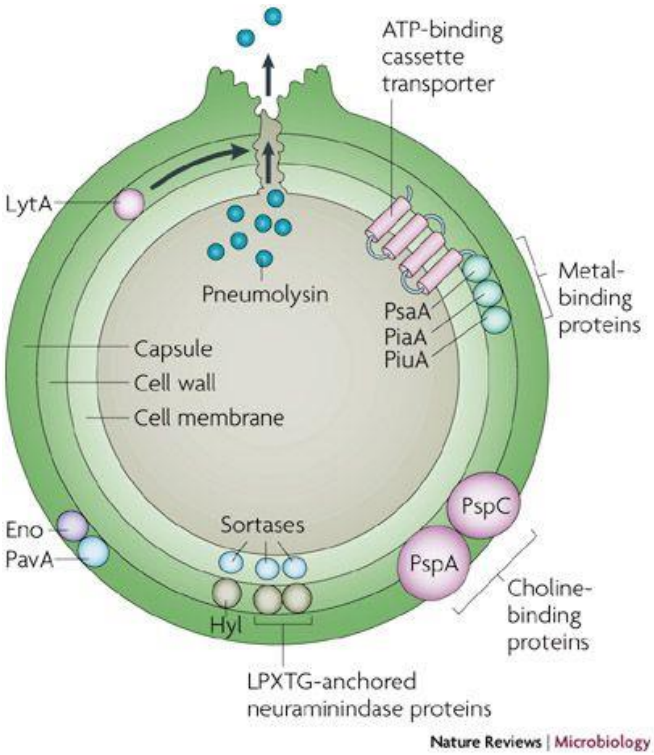

Figure 1.3. Virulence of *Streptococcus pneumoniae* is impacted by many different factors. Important and well characterised virulence factors include: the capsule; the cell wall; choline-binding proteins; pneumococcal surface proteins A and C (PspA and PspC); the LPXTG-anchored neuraminidase proteins; hyaluronate lyase (Hyl); pneumococcal adhesion and virulence A (PavA); enolase (Eno); pneumolysin; autolysin A (LytA); and the metal-binding proteins pneumococcal surface antigen A (PsaA), pneumococcal iron acquisition A (PiaA) and pneumococcal iron uptake A (PiuA). Figure reproduced from Kadioglu *et al* (2008).

Table 1.1. Major pneumococcal virulence factors. Adapted from Weiser e*t al.* (2018).

Virulence factor	Description	Function in pathogenesis	Reference
CPS	Major surface antigen	Prevents entrapment by mucus during colonization	A. L. Nelson et al, 2007
	100 structurally distinct serotypes	Inhibits opsonophagocytosis by preventing the interaction of iC3b and the Fc fragment of IgG bound to deeper bacterial surface structures with receptors on phagocytic cells	Hyams et al, 2010
ChoP on teichoic acid	PAFR ligand	Binds PAFR on surface of epithelial and endothelial cells, facilitating adherence and invasion	Cundell et al, 1996
Lipopeptides, lipoteichoic acid and peptidoglycan fragments	Pathogen-associated molecular patterns	Promote inflammation	Majcherczyk et al, 1999; Seo et al, 2008
Ply	Pore-forming toxin	Cytotoxic and pro-apoptotic for a wide variety of host cells	Rubins et al, 1996
	TLR4 ligand	Activates classical complement pathway and depletes serum opsonic activity	Andre et al, 2017
		Highly pro-inflammatory at sub-lytic levels	García-Suárez et al, 2007
		Activates TLR4, NLRP3 inflammasome and p38–MAPK pathways	McNeela et al, 2010
PspA	Choline binding protein	Limits C3 deposition on pneumococcal surface	Tu et al, 1999
		Protects against bactericidal effects of free lactoferrin	Shaper et al, 2004
CbpA (also known as PspC)	Choline binding protein	Binds C3 and factor H and limits C3b deposition on pneumococcal surface	Lu et al, 2006
		Binds PIGR and laminin receptor through separate domains	Lu et al, 2003
		Facilitates adherence and invasion of respiratory epithelium and blood–brain barrier	Prager et al, 2017
LytA	Choline binding protein	Digests cell wall	Mosser and Tomasz, 1970
	Autolysin	Releases Ply and pro-inflammatory cell wall fragments	López et al, 1997
		Mediates capsule shedding during cellular invasion	Kietzman et al, 2016
CbpD	Choline binding protein	Mediates fratricide and release of extracellular DNA	Claverys et al, 2007
	Murein hydrolase	Promotes biofilm formation	Moscoso et al, 2006
CbpE (also known as Pce)	Choline binding protein	Decreases neutrophil activity by inactivation of host PAF	Hergott et al. 2015
	Phosphorylcholine esterase	Binds plasminogen	Attali et al, 2008b
CbpG	Choline binding protein serine protease	Cell-attached form promotes adherence	Mann et al, 2006
		Extracellular form degrades fibronectin	Mann et al, 2006
		Important for mucosal and invasive disease	Mann et al, 2006
CbpL	Choline binding protein	Binds collagen, elastin and C-reactive protein	Gutiérrez-Fernández et al, 2016

		Promotes dissemination from nasopharynx to lungs and blood by inhibiting phagocytosis	Gutiérrez-Fernández et al, 2016
NanA	Neuraminidase A	Cleaves terminal sialic acid from host mucin and cell surface glycoconjugates	Manco et al, 2006
	LPXTG binding domain	Unmasks receptors for adhesins	Manco et al, 2006
		Important role in otitis media	Wren et al, 2017
		Triggers TGF-β signalling to facilitate endothelial invasion	Gratz et al, 2017
BgaA	β-Galactosidase	Sequentially cleaves sugars from host glycoconjugates	Singh et al, 2014
	LPXTG binding domain		
StrH	β-*N*-acetylglucosaminidase	Sequentially cleaves sugars from host glycoconjugates	King et al, 2006
	LPXTG binding domain		
EndoD	Endo-*N*-acetylglucosaminidase	Sequentially cleaves sugars from host glycoconjugates	Muramatsu et al, 2001
	LPXTG binding domain		
Hyl	Hyaluronate lyase	Degrades extracellular matrix, facilitating tissue penetration	Jedrzejas et al, 2002
	LPXTG binding domain		
ZmpA (also known as IgA1 protease)	Zinc metalloprotease	Cleaves human IgA1	Fasching et al, 2007
	LPXTG binding domain		
ZmpC	Zinc metalloprotease	Cleaves human matrix metalloproteinase 9	Oggioni et al, 2003
	LPXTG binding domain		
PepO	Endopeptidase	Binds fibronectin and plasminogen and Facilitates adherence and invasion	Agarwal et al, 2013
		Binds C1q to inhibit classical complement pathway	Agarwal et al. 2014
PsrP	Very large *O*-glycosylated serine-rich repeat protein	Adhesin, bind to lung cells via keratin 10	Shivshankar et al. 2009
	LPXTG binding domain	Mediates bacterial aggregation and biofilm formation in lung tissue	Blanchette-Cain et al. 2013
RrgA, RrgB and RrgC	LPXTG proteins	Adhesins, bind to a range of glycans	Gentile et al, 2011; A L Nelson et al, 2007; Shaik et al, 2014
	Structural components of pilus 1		
	Encoded by *rlrA* pathogenicity islet	Facilitate colonization and biofilm formation	LeMieux et al, 2006
	RrgA is tip adhesin	RrgA also binds PIGR and PECAM1 on endothelium of the blood–brain barrier, which promotes brain invasion	Iovino et al, 2017

PsaA	Lipoprotein	Mn uptake in host environment	Dintilhac et al, 1997
	Solute-binding component of Mn-specific transporter	Essential for pneumococcal resistance to oxidative stress in vivo	Johnston et al. 2004
AdcA and AdcAII	Lipoproteins	Zn acquisition in vivo	Bayle et al, 2011
	Solute-binding components of a single Zn-specific ABC transporter		
PiuA, PiaA and PitA	Lipoprotein	Fe acquisition in vivo	Whalan et al, 2005
	Solute-binding components of iron-specific ABC transporters		
SlrA and PpmA	Lipoproteins	Contribute to nasopharyngeal colonization	Cron et al, 2009; Hermans et al, 2006
	Peptidyl-prolyl isomerases		
PhtA, PhtB, PhtD and PhtE	Family of surface proteins with unusual His-triad motifs	Putative adhesins	Kallio et al, 2014
		Facilitate Zn acquisition together with AdcAII	Plumptre et al, 2014
PavA and PavB	Fibronectin-binding proteins	Adhere to host surfaces and important during sepsis and meningitis	Jensch et al, 2010; Pracht et al, 2005
	NCSP		
Eno	Enolase	Binds and activates plasminogen	Bergmann et al. 2001
GAPDH	Glyceraldehyde-3-phosphate dehydrogenase	Binds and activates plasminogen	Bergmann et al. 2004
SpxB	Pyruvate oxidase	Generates H_2O_2 and is important in during colonisation	Regev-Yochay et al, 2007
GlpO	α-Glycerophosphate oxidase	Generates H_2O_2 and is important during sepsis and meningitis	Mahdi et al, 2012
SodA	Mn-dependent superoxide dismutase	Resistance to oxidative stress	Yesilkaya et al, 2000
Etrx1 and Etrx2	Surface-exposed thioredoxin-family lipoproteins	Resistance to oxidative stress	Saleh et al, 2013
SpMsrAB2	Methionine sulfoxide reductase	Redox partner of Etrx1 and Etrx2	Saleh et al, 2013

1.5.3 Competence and natural transformation

Competence is the ability of bacterial cells to take up extracellular DNA (eDNA) and integrate it into their genomes via recombination, allowing the reparation of damaged DNA or the acquisition of new traits such as antibiotic resistance or virulence proteins (Alloing

et al., 1996; Johnston et al., 2014). Homologous recombination is required for successful integration of eDNA, hence the more similar eDNA is to the genome, the more likely recombination will occur (Mell and Redfield, 2014). The proteins synthesised from the *comABCDE* operon control competence in pneumococci. *ComC* encoded pre-CSP is exported via the ComAB ABC transporter/protease, where it's cleaved into the competence-stimulating peptide (CSP) upon entering the extracellular matrix (Håvarstein et al., 1995). CSP then accumulates extracellularly and subsequently binds and activates the ComD histidine kinase receptor, which is part of the ComDE two component signal transduction system. This results in ComD auto-phosphorylation, and subsequent transfer of this phosphoryl group on ComD to ComE. ComE-P binds to and activates early competence genes containing the Ceb promoter sequence. These include the *comABCDE* genes, *comM,* which provides cellular immunity against lytic enzymes, and *comX* encoding an alternative sigma factor (Håvarstein et al., 2006; Martin et al., 2013; Peterson et al., 2004). ComX controls activation of the late competence genes needed for DNA-uptake, transformation and fratricide. Fratricide is the targeted lysis of non-competent pneumococci by competent siblings, and is one method pneumococci use to access highly homologous DNA (Steinmoen et al., 2002). This process also aids in pathogenicity by regulating the release of virulence factors such as Ply (Claverys and Håvarstein, 2007). The murein hydrolase choline binding protein D (CbpD) and the early immunity protein ComM play key roles in lysing target cells (Eldholm et al., 2009; Kausmally et al., 2005). It was originally thought that fratricide only enables gene integration between pneumococci, but it has been shown that CbpD results in DNA release by closely related species, including *S. mitis* and *S. oralis*, by binding to choline containing teichoic acids (Eldholm et al., 2010; Johnsborg et al., 2008). Meanwhile, bacteriocins, the small ribosomal peptide antibiotics, facilitate antagonistic affects to differing bacterial species within the same ecological niches, providing a competitive advantage for pneumococci (Wang and Kuramitsu, 2005).

Competence in Streptococci has been shown to be tightly linked with bacteriocin production, mediated through a variety of regulatory pathways (Shanker and Federle, 2017). Indeed, lysis of non-competent *S. pneumoniae* relies on the two peptide bacteriocin CibAB, which targets cells lacking the corresponding immunity factor CibC (Guiral et al., 2005).

1.5.4 Biofilms

Biofilms are highly structured collections of cells that adhere together embedded within extracellular polymeric substances comprised of extracellular DNA, proteins and polysaccharides produced by the bacteria (Hall-Stoodley et al., 2004). *S. pneumoniae* colonise the nasopharynx as biofilms as part of microbial communities, which is recognised as a crucial step in pneumococcal pathogenesis (Hall-Stoodley et al., 2004). Biofilms are complex structures that facilitate bacterial persistence by providing protection from antimicrobial drugs and contain channels through which nutrients and signalling molecules can circulate, also enabling pneumococcal genetic exchange to take place (Cho et al., 2007; Costerton et al., 1999; Donlan and Costerton, 2002; Lewis, 2008; Marks et al., 2012). Increased antibiotic-resistance of biofilm bacteria is attributed to lower penetration of the selected drug into biofilm structures, and with corresponding phenotype shifts of biofilm bacteria (de la Fuente-Núñez et al., 2013; Nguyen et al., 2011). In fact, majority of bacterial species within the nasopharynx are not cleared from patients after antibiotic treatment (Cohen et al., 1997; Dabernat et al., 1998; Dagan et al., 1998; García-Rodríguez and Fresnadillo Martínez, 2002). Biofilms present during OM or chronic rhinosinusitis provide potential reservoirs from whence virulent bacteria can seed under the right conditions (Oggioni et al., 2006; Sanchez et al., 2011; Weimer et al., 2010).

Bacterial cells in biofilms are very close to each other, as well as to surrounding DNA. This provides an optimum environment for the exchange of genetic material, promoting survival

and adaptation to the host environment. Moreover, studies suggest that pneumococci dispersed from biofilms have distinct phenotypes. *In vivo* murine models of colonisation and dissemination have shown biofilm dispersed *S. pneumoniae* were able to colonise the nasopharynx at higher levels than broth-grown pneumococci (Trappetti et al., 2011) and disseminate to the middle ear and lungs at higher levels as well (Marks et al., 2013). Histological examination showed that mice infected with biofilm-dispersed *S. pneumoniae* had higher levels of inflammation and leukocyte infiltrates in the lungs, blood and middle ear, compared to planktonic *S. pneumoniae*-infected counterparts (Blanchette-Cain et al., 2013). These differences in virulence between biofilm, planktonic and biofilm dispersed bacteria suggest key transcriptomic differences, as another study showed virulence genes are down regulated in biofilm bacteria compared to broth-grown (Sanchez et al., 2011). Moreover, environmental changes that influence transcriptional changes, such as fever, ion concentrations, nutrient availability and pro-inflammatory cytokines (Grebe et al., 2010; Weiser, 2010), can trigger biofilm dispersal (Marks et al., 2013).

1.5.5 Quorum sensing

Quorum sensing (QS) is a communication process used by both Gram-negative and Gram-positive bacteria to coordinate population-wide responses. Three types of known QS systems in bacteria are; LuxI/LuxR-type QS in Gram-negative bacteria, oligopeptide-two component-type QS in Gram-positive bacteria and LuxS-mediated autoinducer 2 (AI-2) QS. Pneumococcal QS systems are classified into general groups based on the small peptide signals known as pheromones and their receptors; the RNPP family of regulators, double glycine peptides and Lanthinonine-containing cyclic peptides. Pheremones are released by Gram-positive bacteria and sensed in a concentration depended manner by neighbouring cells, eliciting a response such as competence regulation, biofilm development, symbiosis, sporulation and virulence factor expression (Johnston et al., 2014). As this process is based on concentrations of peptides, conditions that alter peptide

concentration (e.g. diffusion, signal degradation, sequestration, etc) impact the ability of bacteria to communicate.

The oligopeptide QS ComABCDE pathway and associated fratricide, as described in section 1.5.3, is one of the most well characterised examples of QS in *S. pneumoniae*. Another QS system in the pneumococcus is the BlpABCSRH pathway, which is similar to the Com pathway, as it regulates the production of class II bacteriocins and their corresponding immunity proteins (Knutsen et al., 2004). The Peptide BlpC activates the histidine kinase receptor BlpH, which in turn phosphorylates the response regulator BlpR (de Saizieu et al., 2000). Upon BlpC induction, *blpABC*, *blpXYZ*, and *blpSRH*, as well as several putative bacteriocins and related immunity protein genes that constitute the Bacteriocin Immunity Region (BIR), are upregulated (Dawid et al., 2007, 2009; de Saizieu et al., 2000). It has been demonstrated that the the ComABCDE and BlpABCSRH QS systems are linked, as exogenous CSP upregulated the *blp* operon, even when the *comAB* locus was deleted (Wholey et al., 2016).

The LuxS/AI-2 QS system is present in both Gram-positive and Gram-negative bacteria. Here AI-2 synthesis is catalysed by the metabolic enzyme LuxS, which generates the precursor to AI-2, 4,5-dihydroxy-2,3-pentanedione (DPD) as a by-product of the conversion of *S*-ribosylhomocysteine into homocysteine, an integral reaction of the activated methyl cycle (Winzer et al., 2003). Pneumococcal strains lacking *luxS* showed significant decreases in biofilm formation and virulence after murine intranasal challenge (Stroeher et al., 2003; Trappetti et al., 2017; Yadav et al., 2018)

1.5.6 Carbohydrate metabolism

S. pneumoniae is a fermentative bacterium, relying solely on glycolysis for energy, as it lacks an entire set of genes involved in the tricarboxylic acid cycle and an electron transport chain (Hoskins et al., 2001; Tettelin et al., 2001). This critical role for carbohydrates is

highlighted by the large number of sugar transporter genes present in the pneumococcal genome with more than 30% of all encoded transporters involved in carbohydrate uptake (Bidossi et al., 2012; Tettelin et al., 2001). At least 32 different carbohydrates are imported through 21 phosphotransferase systems (PTS) and 8 ABC transporters (Bidossi et al., 2012).

Carbohydrates imported into pneumococcal cells undergo glycolysis, where two ATP molecules and two NADH molecules are gained from the conversion of one molecule of glucose to two molecules of pyruvate. Pyruvate is then metabolised primarily to lactate via a lactate dehydrogenase, which regenerates NAD^+ (Harris and Harper, 2015). The oxidation of NADH to NAD^+ maintains redox balance, and this NADH-NAD^+ balance appears to regulate pneumococcal fermentation. An excess of easily convertible sugars, such as glucose, as well as low oxygen tension, leads to a high NADH-NAD^+ ratio, which results in homolactic fermentation, where two molecules of lactic acid are generated (Gänzle, 2015). Contrastingly, low glycolytic flux, such as during an excess of non-readily convertible sugars, and high oxygen tension, results in pneumococci undergoing mixed acid fermentation where ethanol, acetate and formate are produced (Kandler, 1983; Yesilkaya et al., 2009).

Glucose is *S. pneumoniae's* preferred source of carbon and energy (Carvalho et al., 2011) and is transported into the cell largely through PTS MalN-MalLM system. If glucose is transported via an ABC transporter, it is phosphorylated by a glucokinase Gki before entering the glycolytic pathway. However, free sugars are scarce in the human respiratory tract where the pneumococcus principally lives, with concentrations of glucose under 1 mM (Philips et al., 2003). To overcome this limitation, the pneumococcus employs a range of extracellular glycosidases, such as NanA, BgaA and StrH, that are able to cleave sugars from N-linked glycoconjugates present on epithelial surfaces (King, 2010). The sugars are then able to be taken up by the appropriate ABC or PTS transporters. Many glycosidases

that pneumococci possess target specific structures of sugars. For example, the β-galactosidase activity of BgaA only targets galactose β1-4 linked to N-acetylglucosamine, which is generally found in N-linked glycaoconjugates, while NanA cleaves α2-3- and α2-6-linked sialic acid. In fact, *S. pneumoniae* is able to grow solely on mucins, which are glycosylated macromolecules with a majority make up of carbohydrates, as a carbon source (Rose and Voynow, 2006). It has also been shown that pneumococci can alter capsule structures of certain other bacteria such as *Neisseria meningitidis* and *Haemophilus influenzae* to scavenge surface carbohydrates (Shakhnovich et al., 2002) and are able to grow on solely purified Group A Streptococcus capsule as a carbon source (Marion et al., 2012).

During pathogenesis, *S. pneumoniae* encounters several distinct environmental niches that contain various constituent nutrients, including carbohydrates, at differing levels. Hence, it is vital for pneumococci to be able to ferment a diverse range of carbohydrates. Indeed, genes encoding for 20 carbohydrate transporters are present in *S. pneumoniae's* core genome (Obert et al., 2006). In comparison, other airway commensal and pathogenic bacteria, sharing the same ecological niche, such as *N. meningitidis*, *H.influenzae* and *Morxaella catarrhalis* have much more limited carbohydrate utilisation capabilities, though *Staphylococcus aureus* is an exception (Egan and Morse, 1966; Leighton et al., 2001; Macfadyen et al., 1996; de Vries et al., 2010). These other bacterial species do not solely rely on carbohydrates for carbon and energy. Nevertheless, it is likely that the ability of *S. pneumoniae* to utilize a wider variety of carbohydrates provides a competitive advantage against other bacteria in human host niches.

Additionally, as the pneumococcus encounters a wide variety of carbon sources, it opts to preferentially use glucose or sucrose over other sugars, in order to maintain optimal growth via the catabolite control protein A (CcpA). This process is referred as carbon catabolite control, and prevents simultaneous utilisation of sugars, which would be metabolically less

efficient (Iyer et al., 2005). When there is excess glucose, the kinase HPrK phosphorylates the phosphoprotein HPr which mediates carbon catabolite repression via CcpA dependant and independent mechanisms. (Carvalho et al., 2011; Fleming et al., 2015; Iyer et al., 2005). Moreover, a mouse study found that *ccpA* deletion mutants were severely attenuated in both nasopharyngeal colonisation and lung infection, suggesting a link between carbohydrate metabolism and pneumococcal virulence (Iyer et al., 2005).

It has been shown that the metabolic capabilities of *Streptococci* are highly adapted to the environments in which they live (Price et al., 2012). Nevertheless, the pneumococcus is a human adapted bacterium, which is able to take up and metabolize a range of plant-derived sugars (Bidossi et al., 2012; Hiss, 1905; McKessar and Hakenbeck, 2007; Rosenow et al., 1999; Shafeeq et al., 2011). The metabolism of *S. pneumoniae* seems to be closer to oral streptococci than other human airway pathogens (Sitkiewicz, 2018). Hence, there is the possibility that the pneumococcus evolved from an ancestral oral streptococcal lineage, which also had wide carbohydrate metabolic capabilities. Though it is also possible that *S. pneumoniae* along with other members of the Mitis groups evolved from an ancestral lineage presumed to be pathogenic to hominoids (Kilian et al., 2008).

1.6 Genomic Diversity

S. pneumoniae's genome is incredibly diverse, as this species can be divided into over 12000 different clonal clusters, recognised through multi locus sequence typing (ST) (Enright and Spratt, 1998). Moreover, pneumococcal genes are distributed across the population (referred to as the pangenome). At least 20% of the coding sequences in any single pneumococcal isolate are not present in all strains, but rather make up part of the accessory genome, which is unevenly distributed across all isolates (Donati et al., 2010; Hiller et al., 2007). This provides the pneumococcus additional sets of accessory genes to draw from, for optimum adaptation to its environment. TIGR4, the first pneumococcal

genome to be sequenced, is approximately 2 megabases in length and contains roughly 2200 coding sequences (Tettelin et al., 2001). The pneumococcal genome has been estimated to encode 500-1100 clusters of orthologous genes, while the pangenome encodes between 5000-7000 orthologous clusters (Croucher, Finkelstein, et al., 2013; Donati et al., 2010; Gladstone et al., 2015; Tonder et al., 2017). Hence, approximately three quarters of all pneumococcal genes are distributed differentially across the species.

The accessory genome allows pneumococci to exchange DNA in settings such as biofilms in the nasopharynx, leading to strains with novel combinations of genes that may provide advantages to evade host immune responses, outcompete other colonisers or escape antibiotics (Ehrlich et al., 2005). However, the accessory genome is not solely derived from pneumococcal genes, as other colonisers of the upper respiratory tract such as *S. mitis*, *S. pseudopneumoniae, S. oralis* and *S. infantis* can contribute considerably to the pneumococcal pangenome (Donati et al., 2010; Kilian et al., 2008). Plasmids also contribute to the genetic variation seen within pneumococci, as the plasmid pDP1 was found in approximately 3% of all tested isolates (Sibold et al., 1991; Smith and Guild, 1979). However, no specific function has been described for this plasmid, or other unrelated plasmids (Santoro et al., 2019).

Many factors contribute to *S. pneumoniae's* striking ability to undergo genetic exchange, including their natural competence and biofilm lifestyle in the upper respiratory tract, as detailed above. Human intervention has also been shown to activate competence, as multiple classes of antibiotics are able to indirectly increase local CSP concentrations (Domenech et al., 2018; Prudhomme et al., 2006; Stevens et al., 2011). Additionally, pneumococci are able to protect internalised ssDNA through the production of single stranded DNA binding proteins (SsbB), which can protect the equivalent of half a genome of intracellular DNA. These resulting ssDNA-SsbB complexes can be used in subsequent recombination events, serving as DNA reservoirs (Attaiech et al., 2011). Moreover, the

recombination machinery of *S. pneumoniae* allows for highly divergent alleles or novel genes to be inserted, as it does not require extended runs of identical sequences for recombination to occur (Prudhomme et al., 2002).

S. pneumoniae is also able to perform genetic exchange through transduction, which is the horizontal gene transfer mediated by prophages that undergo lytic and lysogenic life cycles. During the lysogenic phase, these prophages are integrated into the pneumococcal genome. In the lytic phase, prophages are excised from the host genome, which then replicate and lyse the host cell in order to infect other bacterial cells. Prophages are ubiquitous and heavily present within pneumococcal genomes, present in up to 76% of tested strains (Ramirez et al., 1999). The phage integrase dictates the location where a phage integrates into the genome, with most pneumococcal prophages located within one of a few conserved locations (Brueggemann et al., 2017). Studies have highlighted the importance of prophage genes in the pneumococcal genome, with the ϕMM1-like phage increasing adherence to pharyngeal cells and inert surfaces (Loeffler and Fischetti, 2006). Additionally, the phage tail protein PblB promotes pneumococcal adherence to human epithelial cells, while also increasing nasopharyngeal colonisation and lung infection in murine pneumococcal disease models (Harvey et al., 2011; Hsieh et al., 2015). The Spn1 prophage also leads to defects in pneumococcal autolysis, increased chain length of pneumococci, decreased fitness in murine colonisation models and increased resistance to penicillin-mediated lysis (DeBardeleben et al., 2014). The genomes of *S. pneumoniae* also encode phage-related chromosomal islands (PRCIs) that are presumed to hitchhike with prophages as they are incapable of lytic cycles (Novick et al., 2010). However, the distribution of PRCIs is much less diverse than prophages, likely due to limited lateral transfer or the high specificities between PRCIs and subsets of prophages.

Conjugation, which is the process of one bacterium transferring genetic material to another through direct contact, is another method used by *S. pneumoniae* for horizontal gene

transfer of integrative and conjugative elements (ICEs). ICEs consist of conjugative transposons or integrative plasmids and undergo vertical transfer once inserted into the genome. They can alternatively undergo horizontal transfer between strains after being excised from the recipient genome (Burrus et al., 2002). ICEs can contain several kilobases of genomic material, hence allowing for significant genetic diversity to emerge from even one transfer event. Moreover, ICEs have a propensity to carry drug resistance genes and cassettes that confer resistance to antibiotics such as macrolides, tetracycline and chloramphenicol (Ayoubi et al., 1991; Chancey et al., 2015; Croucher et al., 2009).

To summarise, recombination, transformation, transduction and conjugation all play important roles that drive *S. pneumoniae's* genetic diversity and evolution. The great extent of pneumococcal genetic diversity is highlighted in its separation into 100 structurally distinct capsular serotypes, which is superimposed onto over 12000 different clonal lineages/ sequence types distinguished by multi-locus sequence typing (ST).

1.7 Research Project

1.7.1 Rationale for project

Previous studies have independently shown that strains within the same CPS serotype and clonal lineage/ST display distinct niche adaptation in mice, depending on their original site of isolation in humans (Amin et al., 2015; Croucher, Mitchell, et al., 2013; Silva et al., 2006; Trappetti et al., 2013). In the studies from the Paton lab, murine intranasal challenge models were used which mimic the natural route of infection. Serotype 3 (ST180, ST232 and ST233) blood isolates did not stably colonise the nasopharynx, but spread to the blood in 10/15 mice, while none spread to the ear. In contrast, ear isolates belonging to the same STs colonised the nasopharynx at higher levels and also spread to the ear in 7/15 mice; none caused bacteraemia (Trappetti et al., 2013). Meanwhile, serotype 14 (ST15) clinical blood isolates exhibited higher tendencies to infect the lungs compared to serotype/ST

matched ear isolates. On the other hand, the serotype 14 ST15 ear isolates infected the ear and brain at higher levels than their corresponding blood isolates, while both colonised the nasopharynx stably and neither caused bacteraemia (Amin et al., 2015). Both the serotype 3 and 14 isolates are clinically relevant as these serotypes are common causes of invasive disease. Moreover, Serotype 3 is a common cause of OM and serotype 14 is highly prevalent in children (Grabenstein and Musey, 2014; Weinberger et al., 2010).

This project was initiated to investigate the molecular differences that determine *in vivo* behaviour of blood and ear isolate pairs from each of the serotype 3 and 14 *S. pneumoniae* strains mentioned above. Although members of the same ST type have very closely related genetic backbones, they are not necessarily identical as they may have acquired distinct accessory regions, random mutations from replication errors or other genetic changes through horizontal gene transfer, which may account for differences seen in the niche adaption/virulence phenotype. The distinct phenotypes could also be due to differential expression patterns of core virulence-related or metabolic genes, post-transcriptional modifications, or a combination of scenarios. This project was designed to benefit from the involvement of our laboratory with the Antibiotic Resistant Sepsis Pathogens Framework Initiative consortium, coordinated by Bioplatforms Australia, which aimed to provide multi-omic analyses of various sepsis pathogens, including *S. pneumoniae*. It had been predetermined that omic analyses would be carried out in chemically defined media (CDM) + Glucose (Glc) or Galactose (Gal) or in human serum.

1.7.2 Hypothesis, aims and strategy

Hypothesis: Strains of *S. pneumoniae* of the same serotype and sequence type that spread to the different sites of the body (e.g. ear vs blood), although very similar, may contain distinct molecular differences that result in their varied disease progression. Genomic and transcriptomic comparisons of these serotype- and sequence type-matched strains, will

elucidate key molecular mechanisms that drive pneumococcal progression into specific sites of the body.

Aim 1: Investigate the genomic features that distinguish ear and blood isolates within a given clonal lineage and examine their impacts on *in vitro* and *in vivo* phenotypes.

Aim 2: Investigate which transcriptomic features that distinguish ear and blood isolates within a given clonal lineage and examine their impacts on *in vitro* and *in vivo* phenotypes.

Aim 3: Investigate both the pneumococcal and host transcriptomic features that determine the virulence/pathogenic phenotype of *S. pneumoniae in vivo*.

Strategy: As this project generated an immense amount of data, the following strategy was followed to prioritise the research. Genomic and transcriptomic differences found commonly within both the blood and ear isolate pairs will firstly be examined, as these findings are more likely to be widespread across *S. pneumoniae* strains. However, as the pneumococcus is a genetically diverse species there may not be many, if any common differences between the isolate pairs. If this is the case, examinations will begin on differences present within each of the pairs separately, with differences that have been shown to impact pneumococcal disease to be prioritised. The following Chapters detail the experimental techniques used to examine and analyse the findings.

Chapter 2

Genomic Comparisons of *S. pneumoniae* Clonal Clinical Isolates

2.1 Introduction

This Chapter incorporates data published in *mBio* (Minhas et al., 2019),which focuses mainly on mutations within the raffinose transport operon, and their impacts on pneumococcal disease progression. Additional data and discussion have been included in order to provide more detail on the work that was undertaken regarding the genomic comparison analyses as a whole.

As detailed in Chapter 1, *S. pneumoniae* is one of the world's foremost bacterial pathogens, yet it can asymptomatically colonise the nasopharynx. This provides a reservoir for pneumococcal transmission in the community (Kadioglu et al., 2008; Weiser et al., 2018). In a small proportion of carriers, which nevertheless translates into globally significant numbers, *S. pneumoniae* invades from its nasopharyngeal reservoir around the body to cause disease (section 1.3) (Kadioglu et al., 2008; Weiser et al., 2018). However, the molecular mechanisms whereby pneumococci transition from a commensal lifestyle to cause either localized or invasive disease are poorly understood.

The pneumococcus is a genetically plastic and diverse species, comprising at least 100 capsular serotypes, superimposed on more than 12,000 clonal lineages (sequence types [STs]) recognizable by multilocus sequence typing (Enright and Spratt, 1998). Individual *S. pneumoniae* strains can differ markedly in their virulence phenotypes, including their capacity to colonise the nasopharynx, spread from person to person, or progress to either localised or invasive infections. Capsule switching experiments have

shown that both serotype and genetic background (i.e., ST) influence virulence (Kelly et al., 1994; McAllister et al., 2011), but strain complexity has complicated attempts to examine whether there is any association between a given clonal lineage or serotype and propensity to cause localized rather than invasive infections.

To determine potential disease mechanisms of *S. pneumoniae*, the serotype 3 ST180 and serotype 14 ST15 blood and ear isolate pairs were utilised in a multi-omics study in collaboration with Bioplatforms Australia as explained in section 1.6.1. Here, these strains were subjected to comprehensive analyses, including Illumina MiSeq and PacBio SMRT genome sequencing, to obtain fully closed genomes, as well as transcriptomic (RNAseq) sequencing. To address aim 1 of this project, the genomic sequences between each serotype and ST matched pair were compared to identify any differences present. Analysis of this data allowed a thorough examination of the molecular mechanisms of serotype 3 and 14 pneumococci that determine their pathogenic profiles.

2.2 Materials and Methods

2.2.1 Bacterial strains and growth conditions

The bacterial strains used in this Chapter are listed in **Table 2.1**. *S. pneumoniae* strains were routinely grown in casein-based, semisynthetic liquid medium (C+Y) (Lacks and Hotchkiss, 1960) or serum broth (SB) (10 g/l peptone [Oxoid], 10 g/l Lab Lemco poweder [Oxoid]. 5 g/l NaCl and 10% (v/v) heat –inactivated horse serum [Gibco®, Auckland, New Zealand]) as required. Growth assays were performed using a chemically defined medium (CDM) comprising RPMI 1640 medium (Sigma-Aldrich, St. Louis, United States), supplemented with amino acids, vitamins, choline, and catalase as described previously (Kloosterman et al., 2006), supplemented with either 0.5% glucose or 0.5% raffinose. Bacteria were routinely plated on Columbia agar (39 g/l [Oxoid]) supplemented with 5% (vol/vol) defibrinated horse blood (BA) with or without gentamicin (40 µg/ml), kanamycin (500 µg/ml), or streptomycin (150 µg/ml) (as required) and incubated at 37°C in 5% CO_2 overnight. For gene expression analyses, strains were grown in CDM + glucose (Glc) medium to an Optical Density at 600 nm (OD_{600}) of 0.2, before being incubated in CDM + raffinose (Raf) for 30 min. *E. coli* strain were routinely grown in Luria-Bertani (LB) broth or agar (10 g/l trypton, 5 g/l yeast extract and 5 g/l NaCl), with or without 1.5% Bacto Agar.

2.2.2 Genome sequencing

S. pneumoniae strains were grown to mid-exponential phase in Todd-Hewitt (THY) broth supplemented with 1% yeast extract (Becton, Dickinson and Company, New Jersey, USA). Genomic DNA (gDNA) was extracted using the Qiagen genomic DNA buffer set with 100/g Genomic Tips according to the manufacturer's instructions, except mutanolysin (20 U) and sodium deoxycholate (0.1%) were included to aid cell lysis. The gDNA was sequenced at the Ramaciotti Centre for Genomics (University of New South Wales, Sydney, Australia). Illumina MiSeq (250-bp paired-end reads), as well as a PacBio RSII

instrument using one SMRT cell per strain, a 20-kb insert library, and the P6 polymerase and C4 sequencing chemistry were used for genomic sequencing before *de novo* assembly (Gladman, 2018).

Table 2.1. Bacterial strains used in this Chapter.

Strain	Description	Source	Reference
4559	*S. pneumoniae s*erotype 14 ST15	Blood	Amin et al., 2015
947	*S. pneumoniae s*erotype 14 ST15	Ear	Amin et al. 2015
4534	*S. pneumoniae s*erotype 14 ST15	Blood	Amin et al, 2015
51742	*S. pneumoniae s*erotype 14 ST15	Ear	Amin et al, 2015
$4559^{947rafR}$	4559 expressing 947 *rafR* gene		This study
$947^{4559rafR}$	947 expressing 4559 *rafR* gene		This study
180/15	*S. pneumoniae s*erotype 3 ST180	Blood	Trappetti et al, 2013
180/2	*S. pneumoniae s*erotype 3 ST180	Ear	Trappetti et al, 2013
180/15 Δ*rafK*	180/15 with *rafK* deletion		This study
180/2 Δ*rafK*	180/2 with *rafK* deletion		This study
5076	*S. pneumoniae s*erotype 23F ST81	Blood	This study
9725241	*S. pneumoniae s*erotype 23F ST81	Ear	This study
$XL10^{pAL2}$	*E. coli* XL10 containing the empty T7 vector pAL2		Chai, 2016
947^{pAL2}	947 containing the empty T7 vector pAL2		This Study
51742^{pAL2}	51742 containing the empty T7 vector pAL2		This Study
$XL10^{pAL2:4559rafR}$	*E. coli* XL10 containing pAL2 with *rafR* from 4559 inserted		This Study
$947^{pAL2:4559rafR}$	947 containing pAL2 with *rafR* from 4559 inserted		This Study
$51742^{pAL2:4559rafR}$	51742 containing pAL2 with *rafR* from 4559 inserted		This Study
$4559^{RafE\ RGD\rightarrow HAE}$	4559 with the RGD motif of RafE mutated to HAE		This Study
$947^{RafE\ RGD\rightarrow HAE}$	947 with the RGD motif of RafE mutated to HAE		This Study

2.2.3 Bioinformatic analyses

The Artemis Comparison Tool was used to compare genomes (Carver et al., 2005). MiSeq reads of 4559 and 947 and 180/15 and 180/2 were mapped to the assembled reference genome of the opposing strain with BOWTIE2 version 2.2.6 (Langmead and Salzberg, 2012). Variant calling was then performed using SAMTools version 0.1.18 (Li et al., 2009), and variants were mapped to coding sequences of the reference strain using BEDTools

version 2.25.0 (Quinlan and Hall, 2010). Single nucleotide polymorphisms (SNPs) and insertions/deletions (indels) were filtered for those with scores of 100 or greater. Artemis was used to visualize SNPs and indels (Rutherford et al., 2000). Sanger sequencing was performed to confirm the SNPs in *rafR* and *rafK* (Australian Genome Research Facility, Adelaide).

2.2.4 Phenotypic microarrays

Carbon phenotype microarray analysis was performed on the serotype 14 ST 15 strains, using the PM microplates PM1 and PM2A (Biolog, Inc.), which tested for the catabolism of 190 different carbon sources. Each well of the microarrays contained a different carbon source. Briefly, cells were suspended in the provided buffer (as per the manufacturer's instructions) to an Absorbance 590 nm (A_{590}) of 0.37. 100 µl of this suspension was added to the wells, and the A_{590} was measured after 17 h of incubation at 37°C on a SpectraMax M2 Microplate Reader (Molecular Devices, California, USA). Catabolism was measured through the reduction of a colourless tetrazolium dye by NADH, produced during catabolic activity. Absorbance values above 0.65 after subtraction from the zero carbon source blank were considered positive.

2.2.5 Growth assays

Each tested strain was grown in CDM supplemented with either 0.5% Glc (CDM+Glc), 0.5% Raf (CDM+Raf), or no sugar (CDM) from an OD_{600} of 0.05. 200 µl of inoculated culture was then incubated at 37°C for 12 h in a Costar® 96-well Flat-bottomed Cell Culture Plate (Corning Incoporated, New York, United States). The OD_{600} was measured every 15 min a SpectraMax M2 Microplate Reader (Molecular Devices). All experiments were conducted in triplicate and repeated at least two times.

2.2.6 Quantitative real-time RT-PCR

Differences in levels of gene expression were assayed by one-step relative quantitative real-time RT-PCR (qRT-PCR) in a LightCycler® 480 II cycler (Roche) essentially as described previously (Mahdi et al., 2008). The specific primers used for the various genes are listed in **Table 2.2** and were used at a final concentration of 200 nM per reaction. As an internal control, primers specific for 16S rRNA were employed. Amplification data were analysed using the comparative critical threshold cycle ($2^{-\Delta\Delta CT}$) method (Livak and Schmittgen, 2001). For analysis of raffinose operon expression *in vivo*, groups of 4 mice were challenged I.N. with 50 µl of bacterial suspension containing approximately 1×10^8 colony forming units (CFU) of 4559, 947, $4559^{947rafR}$ or $947^{4559rafR}$. 6 h post-infection, the lungs were harvested and placed in 1ml Trizol (Ambion), left at RT for 5 min then subsequently homogenised using a Precellys® 24 tissue homogeniser (Bertin Technologies, France) before storage at -80ºC. The following day, 200 µl chloroform was added to the samples and inverted to mix well, then centrifuged at 12,000 x g for 15 min at 4ºC. The resulting aqueous phase was removed and RNA extracted using the Qiagen RNeasy RNA isolation kit.

2.2.7 Polymerase chain reaction

PCR reactions were performed on a Mastercycler Flexilid thermal cycler (Eppendorf, NSW, Australia). Reactions were carried out using 2 × Phusion Flash PCR Master Mix (Thermo Fisher Scientific, Victoria, Australia), according to manufacturer's instructions. Typical reaction conditions comprised 25 cycles of denaturation at 95ºC for 30 s, annealing at 55ºC for 30 s and extension at 68ºC for 15 s per kb of expected PCR product. PCR products were then purified using a MiniElute PCR Purification Kit (Qiagen, Hilden, Germany) according to the manufacturer's instructions. To analyse PCR products or chromosomal and plasmid DNA preparations, gel electrophoresis was performed using

Table 2.2. Oligonucleotide primers used in this study. All primers used in this Chapter and subsequent Chapters were purchased from Sigma Aldrich.

Primer	Sequence (5′→3′)	Reference
rafR Flank F	GCGAACGTAGGTTACAATCGT	This study
rafR R j tail	GGAAAGGGGCCCAGGTCTCTCTAGCATGTG CTACCTCCTACC	This study
rafR F j tail	CATTATCCATTAAAAATCAAAGGGGAAATC CTACCAAGCTGTCTACC	This study
rafR Flank R	CGAACGTAGTTCAGTGGTAGAA	This study
Janus F	CCGTTTGATTTTTAATGGATAATG	Sung et al, 2001
Janus R	AGAGACCTGGGCCCCTTTCC	Sung et al., 2001
aga F	AAGGTCAGAATGGTCCACAG	This study
aga R	GCTGGAAAATCAGCCATAAA	This study
rafG F	CCTATGGCAGCCTACTCCATC	This study
rafG R	GGGTCTGTGGAATCGCATAGG	This study
rafK F	AACGACGTAGCTCCAAAAGA	This study
rafK R	GCTGGTTTACGTTCCAAGAA	This study
16s rRNA F	GGTGAGTAACGCGTAGGTAA	Trappetti et al, 2017
16s rRNA R	ACGATCCGAAAACCTTCTTC	Trappetti et al, 2017
rafR sanger	AGTAGAAGAGCTGGTGTTTG	This study
rafR sanger	TCTGTGACTAAGCCAGTTTC	This study
rafK Flank F	AGGACTTGGTTCTTGTTGAG	This study
rafK Rery tail	TTGTTCATGTAATCACTCCTTCCTACCATGA GGTGAACTCC	This study
rafK Fery tail	CGGGAGGAAATAATTCTATGAGATCAGTTA ATCTAGGGAGAG	This study
rafK Flank R	CTCAAAGGCAACTGGACAAC	This study
EcoRI-*rafR* F	GCGCGAATTCCCATTTACTTCACCTCATCAC	This study
EcoRI-*rafR* R	GCGCGAATTCGGATTTGGTAGACAGCTTGG	This study
pAL2 BamHI F	CTACTTGGAGCCACTATCGAC	This study
rafE Flank F	TGAAGTTCGGGTGGCTATTG	This study
rafE RGD R	CCAAGACCCATTTGGTGTCATGAGGACCTC CGCATGTGCGAAGGCTCCGATAACATCGGT	This study
rafE R j tail	GGAAAGGGGCCCAGGTCTCTCCATTCCATT AGAAAGCCTC	This study
rafE RGD F	ACCGATGTTATCGGAGCCTTCGCACATGCG GAGGTCCTCATGACACCAAATGGGTCTTGG	This study
rafE F j tail	CATTATCCATTAAAAATCAAAGGGTGGATT AGGAGTAGAGAGAC	This study
rafE Flank R	GGCCTGCGTAGTTGTATTGG	This study

0.8% (w/v) agarose (Agarose low EEO [AppliChem, Germany]) in TBE buffer (44.5 mM Tris, 44.5 mM boric acid, 1.25 mM EDTA, pH 8.4). Prior to loading, DNA was mixed with 1/10th volume of loading buffer (15% [w/v] Ficoll, 0.1% [w/v] bromophenol dye, 100 ng/ml RNAse A) and 0.5 μl/10ml GelRed^{TM} (Biotium, California, United States). Gels

were electrophoresed in 0.5 × TBE buffer at 180 V for at least 30 min. DNA bands were visualised by transillumination with short wavelength ultraviolet light using a Gel/Chemi Doc XR system (Bio-Rad, NSW, Australia) and analysed using Quantity One v 4.6.9 software.

2.2.8 Mutagenesis

The *rafR* gene swap between serotype 14 ST15 strains 4559 and 947, to produce $4559^{947rafR}$ and $947^{4559rafR}$, was achieved via allelic exchange mutagenesis utilising the Janus cassette, as described previously (Harvey et al., 2014; Sung et al., 2001). This involved a three-step process in which endogenous *rpsL* (which confers streptomycin sensitivity) was first replaced with the streptomycin-resistant *rpsL1* allele by direct transformation of the blood and ear isolates. The Janus cassette (comprising a kanamycin resistance marker and a dominant counterselectable $rpsL^+$ marker) was then used to replace the native *rafR* gene by direct transformation with a linear PCR product comprising the Janus cassette flanked by sequences 5′ and 3′ to *rafR* (selecting on kanamycin). In the final step, the Janus cassette in $Kan^r/Strep^s$ transformants is replaced by transformation with the alternative *rafR* allele and flanking sequences, counter selecting on streptomycin (loss of the Janus cassette reinstates the $Strep^r$ phenotype). Gene swap constructs were confirmed by Sanger DNA sequencing (AGRF, Adelaide). The *rafK* gene was also deleted from serotype 3 ST180/2 and ST180/15 by direct transformation with a linear DNA fragment comprising an erythromycin resistance cassette flanked by sequences 5′ and 3′ to *rafK* generated by overlap PCR, essentially as previously described (Trappetti et al., 2017). The *rafR* and *rafK* primers used are listed in **Table 2.2**. Mutant constructs were confirmed by Sanger sequencing (AGRF). Introduction of the RafE RGD to HAE amino acid mutation in the serotype 14 ST15 4559 and 947 strains, to produce $4559^{\text{RafE RGD}\rightarrow\text{HAE}}$ and $947^{\text{RafE RGD}\rightarrow\text{HAE}}$, utilised the Janus cassette method as well. After the Janus cassette replaced *rafE*, the *rafE* RGD primers (**Table 2.2**) incorporating the RGD→HAE mutation,

were constructed into a linear PCR product by overlap PCR and transformed into 4559 and 947.

2.2.9 Construction and integration of pAL2:4559*rafR*

The plasmid pAL2 was extracted from an *E. coli* XL10 strain by using a Qiagen Plasmid Mini Kit (Hilden, Germany). *RafR* was PCR amplified from the *S. pneumoniae* strain 4559, using the EcoRI-*rafR* primers listed in **Table 2.2**, then purified using the MiniElute PCR Purification Kit (Qiagen). The pAL2 plasmid (Addgene, Massachusetts, United States) and *rafR* PCR product were digested with EcoRI, using Shrimp Alkaline Phosphatase (rSAP) and CutSmart buffer, then ligated with T4 DNA ligase (New England Biolabs, Massachusetts, United States), creating the pAL2:4559*rafR* plasmid. Correct ligation was checked for via PCR using the pAL2 BamHI F and EcoRI-*rafR* R primers listed in **Table 2.2**. The pAL2:4559*rafR* plasmid was then transformed into the *E. coli* strain XL10 via the following method (Jechlinger et al., 1999). XL10 cells were prepared by growing cells in LB medium to roughly OD_{600} 0.60 at 37ºC, followed by incubation at 4ºC for 30 min. Cells were then centrifuged and the resulting pellet resuspended in ice cold 100 mM $MgCl_2$, followed by another centrifugation and resuspension in 100 mM $CaCl_2$, then incubation for a further 30 min at 4ºC. 30% (v/v) glycerol was added to competent cells and 100 µl aliquots were stored at -80ºC. For transformation of the plasmid DNA into competent XL10, equal volumes of KCM (100 mM KCl, 30 mM $CaCl_2$, 50mM $MgCl_2$) and competent cells were mixed together with the pAL2:4559*rafR* plasmid, then placed on ice for 30 min, followed by heat-shock at 42ºC for 90 s. The cells were then placed into 1 ml LB and incubated at 37ºC for 1 h with shaking. Successfully transformed cells were plated onto LB agar + 500 µg/ml erythromycin and incubated overnight at 37ºC. XL10 containing pAL2:4559*rafR* plasmid was grown up in LB broth to OD_{600} of 0.6 and plasmid DNA was purified using the QIAprep spin Miniprep Kit (Qiagen). Purified pAL2:4559*rafR* was then

transformed into the *S. pneumoniae* serotype 14 ST 15 ear isolates 947 and 51742, by growing the strains to an OD_{600} of 0.2 in C+Y + 0.2% glucose media, then adding 10 µl of 10 mg/ml competence stimulating peptides (CSP) 1 and 2. After 10 minutes, 200 ng of the pAL2:4559*rafR* plasmid was added then plated onto blood agar + 0.2 µg/ml erythromycin. Successful transformation was confirmed by PCR.

2.2.10 Animal studies

Animal experiments were approved by the University of Adelaide Animal Ethics Committee. Groups of outbred 6-week-old female Swiss (CD-1) mice were anesthetized by intraperitoneal injection of 10 µl/g pentobarbital sodium (Nembutal; Rhone-Merieux) and challenged intranasally (I.N.) with 50 µl of bacterial suspension containing approximately 1×10^8 CFU in SB (Amin et al., 2015). The challenge dose was confirmed retrospectively by serial dilution and plating on BA. Mice were euthanized by CO_2 asphyxiation at 24 h, and then tissue samples (lungs, nasopharynx, brain, ear, and blood) were harvested and pneumococci enumerated in tissue homogenates as described previously via serial dilution and spreading on plates containing BA plus gentamicin (Trappetti et al., 2011).

2.2.11 Adherence assays

A549 human lung alveolar carcinoma (type II pneumocyte) and Detroit 562 human nasopharyngeal cell lines were used for adherence assays. Cells were grown in CDM supplemented with 10% fetal calf serum (FCS) and 0.5% glucose, in $75cm^2$ tissue culture bottles (Becton Dickinson) at 37ºC in a 5% CO_2 atmosphere. 2×10^5 cells were seeded into each well of 24-well tissue culture trays (Becton Dickinson) for use in the adherence assays. The day prior to inoculation of pneumococcal cells to the tissue culture, CDM media was replaced with CDM + 10% FCS + 0.5% Glc or CDM + 10% FCS + 0.5% Raf in the 24-well seeded trays. *S. pneumoniae* serotype 14 ST15 strains were used for

adherence assays. 500 µl of each strain was inoculated onto washed A549 or Detroit 562 cells, to an OD_{600} of 0.2 in CDM + 0.5% Glc or Raf in triplicate. After incubation for 2 hours at 37^{o}C, the wells were washed three times with PBS and cells were detached from the plate by treatment with 100 µl of 0.25% trypsin-0.02% EDTA and 400µl of 0.1% triton x-100. Appropriate dilutions of the cultures were plated on BA to determine the number of adherent bacteria. Assays were performed in triplicate from two independent experiments.

2.2.12 ELISA for capsule quantification

Total capsular polysaccharide (CPS) produced by strains was quantified by enzyme-linked immunosorbent assay (ELISA) using a modification of the method described previously (Trappetti et al., 2011). Briefly, serial 2-fold dilutions of either purified type 14 CPS standard (American Type Culture Collection, USA) at a starting concentration of 10 µg/ml or total CPS preparations of the strains included in this study were coated on poly-L-lysine-treated Nunc MaxiSorp (Roskilde, Denmark) flat-bottom 96-well plates overnight at 4°C. After blocking with 1% fetal calf serum, the samples were reacted with a 1:10,000 dilution of *S. pneumoniae* serotype 14 typing sera (Statens Seruminstitut, Copenhagen, Denmark) for 2 h. The plates were washed five times in wash buffer (0.05% Tween 20 –phosphate-buffered saline (PBS)) and then reacted with a 1:20,000 dilution of goat anti-rabbit IgG alkaline phosphatase conjugate (Sigma-Aldrich) overnight at 4°C. After extensive washing, the plates were developed using alkaline phosphatase substrate (Sigma) in diethanolamine buffer, and the Absorbance at 405 nm was read in a Spectramax M2 spectrometer (Molecular Devices, CA, USA).

2.2.13 Gas chromatography mass spectrometry of infected murine lungs

Presence of raffinose in murine lung extracts was assayed by gas chromatography mass spectrometry (GC MS). Groups of 4 mice were I.N. challenged with 50 µl containing

1×10^8 CFU of 4559, 947 or SB. 24 h post-infection, lungs were harvested and flash frozen before being stored at -80°C, then sent to Metabolomics Australia for metabolite extraction and analysis. Here 20 mg of infected lungs were pulverised using a CryoMill cryogenic grinder and suspended in 600 µl in 3:1 MeOH:Water; 0.1 nM ^{13}C Sorbitol (ISTD). Samples then underwent GC MS analysis as previously described, in order to detect and quantify monosaccharides, disaccharides and trisaccharides (Fiehn, 2016).

2.2.14 Data availability

Genome sequences have been deposited with European Nucleotide Archive (ENA) under the accession numbers SAMEA5092021, SAMEA5092022, SAMEA5092023, and SAMEA5092024, for strains 947, 4559, 180/2, and 180/15, respectively.

2.3 Results

2.3.1 Genetic differences between serotype/ST-matched blood and ear isolates

In the first instance, draft genomes of serotype 14 ST15 strains 4559 (blood isolate) and 947 (ear isolate) were assembled from PacBio and MiSeq data and then compared (see Sections 2.2.3). The only differences in ARs were the presence of a 35-kb prophage and a 3.2-kb plasmid in 4559 and not 947, but these ARs were not present in other serotype 14 ST15 blood isolates in our collection and hence were not examined further. Seventeen SNPs and indels present within protein coding sequences of 4559 and 947 resulting in a change in the predicted amino acid sequence are listed in **Table 2.3**. The genes affected included those predicted to be involved in metabolism and energy production, transcriptional regulation, transporters, and putative virulence factors. Among the latter category, a SNP resulting in a L43P substitution was identified in *cpsE*, which encodes the glycosyl transferase that initiates assembly of the capsular polysaccharide (CPS) repeat unit. However, it has previously been shown that there is no difference in total CPS production between 4559 and 947 (Amin et al., 2015). The SNP in the putative plasmin and fibronectin-binding protein gene *pfbA* is also a conservative T318M substitution. The protein encoded by *iga* is truncated in 4559 compared to 947, but only by four amino acids. On the other hand, the *nanB* sequence in 947 has a premature stop codon that truncates the protein by 330 amino acids (47% of the 4559 protein), presumably inactivating the gene product. Mutagenesis studies have previously shown that NanB contributes to colonization of both the upper and lower respiratory tract of mice, albeit to a lesser extent than the major neuraminidase NanA (Manco et al., 2006). Nevertheless, 4559 and 947 colonize the nasopharynx equally well (Amin et al., 2015). Interestingly, SNPs were identified in two metabolic genes, coding for ATP-dependent 6-phosphofructokinase (*pfkA*) and a glycogen

synthase (*glgA*), as well as in two helix-turn-helix (HTH)-type transcriptional regulators, *scrR* and *rafR*, involved in metabolism of sucrose and raffinose, respectively. Given the importance of carbohydrate metabolism to *S. pneumoniae* (Buckwalter and King, 2012), a phenotypic microarray was employed to compare the capacity of 4559 and 947 to metabolize over 100 different carbohydrates (see Section 2.2.4). The only difference observed between the ear and blood isolates was a reduced capacity of the former (947) to induce reduction of colourless tetrazolium dye by NADH,in medium containing raffinose as the sole carbon source **(Appendices A, B, E and F)**. Moreover, the SNP in *rafR* was within a functionally important conserved signature sequence for the AraC/XylS family of transcriptional regulators (Rosenow et al., 1999), hence further examination was warranted.

Table 2.3. Genes containing indels or SNPs that led to amino acid changes, identified from the whole-genome variant calling analysis between 4559 and 947 (results for the raffinose pathway gene *rafR* are in bold face).

Locus tag in 947	**Gene**	**Product**	**Change in aa sequence in 4559 relative to 947**
0862	*pfkA*	ATP-dependent 6-phosphofructokinase	S212G
1153	*glgA*	Glycogen synthase	E174G
1345	*pncB*	Nicotinate phosphoribosyltransferase	N434D
1631	*scrR*	HTH-type transcriptional regulator	ΔL27-G28
1803	***rafR***	**HTH-type transcriptional regulator**	**D249G**
1255	*pyrP*	Uracil permease	V65A
1737	*piuA*	Fe^{3+} import ATP-binding protein	G141V
2020		ABC transporter ATP-binding protein	Y508N
0330	*cpsE*	CPS glycosyltransferase	L43P
1139	*iga*	Immunoglobulin A1 protease	Premature stop 1905 (4559) due to indel
1594	*nanB*	Sialidase B	Premature stop 362 (947) due to indel
1741	*pfbA*	Plasmin and fibronectin-binding protein A	T318M
0945	*coiA*	Competence protein	E78K
1141	*addA*	ATP-dependent helicase/nuclease subunit A	I980M
1060		Acetyl transferase	C101G
1194		Cytosolic protein containing multiple CBS domains	Premature stop 104 (947) due to SNP
1731		Hypothetical protein (no Pfam match)	H32P

Genetic differences between ear/blood isolate pairs that are common to two unrelated serotypes/ST lineages would be strong candidates for determinants of tissue tropism. Genomic comparisons were therefore also made between two serotype 3 ST180 ear and blood isolates (strains 180/2 and 180/15, respectively), which like the serotype 14 ST15 isolates, have previously been shown to exhibit distinct tissue tropism in mice in accordance with clinical isolation site (Trappetti et al., 2013). There were no differences in ARs between the two strains, while SNPs and indels impacting the deduced amino acid sequence for 27 genes were identified (**Table 2.4**). Interestingly, there were no affected genes in common with those in **Table 2.3**. However, an I227T SNP was detected in the serotype 3 *rafK* gene, encoding the ATP-binding protein component of the raffinose ABC transporter. RafK is known to be essential for activation of other *raf* operon genes, and the SNP identified in ST180 isolates is located in the conserved regulatory domain motif 1 (Tyx et al., 2011). This compares with a SNP in the raffinose pathway regulatory gene *rafR* between the serotype 14 strains. Thus, potential defects in raffinose uptake/metabolism appear to be a common feature of ear isolates from both serotypes/lineages.

2.3.2 Blood isolates utilise raffinose more efficiently than ear isolates

In view of the SNPs in genes associated with raffinose metabolism between ear and blood isolates in two unrelated serotypes/STs and the fact that the serotype 14 ear and blood isolates differed only in their ability to metabolize raffinose on phenotypic microarray analysis, *in vitro* growth phenotypes were further investigated. Strains 4559 and 947, as well as another pair of serotype 14 ST15 blood and ear isolates (4534 and 51742, respectively), were grown in a chemically defined medium (CDM) with either glucose or raffinose as the sole carbon source (designated CDM+Glc and CDM+Raf, respectively) (see section 2.2.5) (**Figure 2.1**). In CDM+Glc, there were no significant differences in

growth rates between blood and ear isolates. However, in CDM+Raf, the two blood isolates grew at a higher rate and to a higher final culture density OD_{600} than either of the serotype

Table 2.4. Genes containing indels or SNPs that led to amino acid changes, identified from the whole-genome variant calling analysis between 180/2 and 180/15 (results for the raffinose pathway gene *rafK* are in bold face).

Locus tag in 180/2	Gene	Product	Change in aa sequence of 180/15 relative to 180/2
100	*purN*	Phosphoribosyl-glycinamide	G81A
254	*rpsJ*	30S ribosomal protein S10	Y58D
285		Hypothetical protein	A81S
314	*cdsA*	Phosphatidate cytidylyltransferase	M14I
335	*adhP*	Alcohol dehydrogenase 1	M210V
403	*fabK*	Enoyl-[acyl-carrier-protein] reductase	I1029T
449		Nitronate monooxygenase	I55M
512	*glnA*	Glutamine synthetase	F22L
645	*nhaK*	Sodium, potassium, lithium and rubidium/H^+ antiporter	G190D
741		VanZ family protein	C149W
996		Hypothetical protein	H38R
1121	*clcA*	H^+/Cl^- exchange transporter	M131I
1138	*ptsH*	Phosphocarrier protein HPr	I14V
1172		Formate/nitrate transporter	A211E
1194	*glnP*	Glutamine transport system permease protein	S662A
1234		SpF43_sRNA	Y31C
1306	*alaS*	Alanine-tRNA ligase	E18A
1387	*apbE*	FAD:protein FMN transferase*	M52I
1404		LPXTG cell wall anchor domain-containing protein	ΔK112-Q119; G125K, E126T, P127E, E130V, K131N, I133D; ΔQ135-P178
1491	***rafK***	**Raffinose import ATP-binding protein**	**I227T**
1616	*dnaB*	DNA helicase	C375R
1760	*fepD_2*	Ferric enterobactin transport system permease protein	S248G
1863	*rpoC*	DNA-directed RNA polymerase subunit beta	D76E
1878	*acyP*	Acylphosphatase	V4I
1887	*rsgA*	Small ribosomal subunit biogenesis	G40S
2045	*aspS*	Aspartate tRNA ligase	E51V
2100	*dltD*	D-Alanyl-lipoteichoic acid biosynthesis protein	D151E

*FAD, flavin adenine dinucleotide; FMN, flavin mononucleotide.

14 ST15 ear isolates. Similarly, there was no significant difference in growth rates of the serotype 3 ST180 ear and blood isolates (180/15 and 180/2, respectively) in CDM+Glc,

but the blood isolate grew better than the ear isolate in CDM+Raf (**Figure 2.1**). Thus, defective growth in raffinose appears to be a common defect in ear isolates relative to serotype/ST-matched blood isolates.

The raffinose uptake/utilization operon in *S. pneumoniae* comprises genes encoding transcriptional regulators (*rafR* and *rafS*), an α-galactosidase (*aga*), the ABC transporter substrate-binding protein and two cognate permeases (*rafE*, *rafF*, and *rafG*), a sucrose phosphorylase (*gtfA*), and a protein of unknown function (*rafX*), as well as the ATP binding protein component of the transporter (*rafK*), which is separately located in the genome (Rosenow et al., 1999) (**Figure 2.2**).

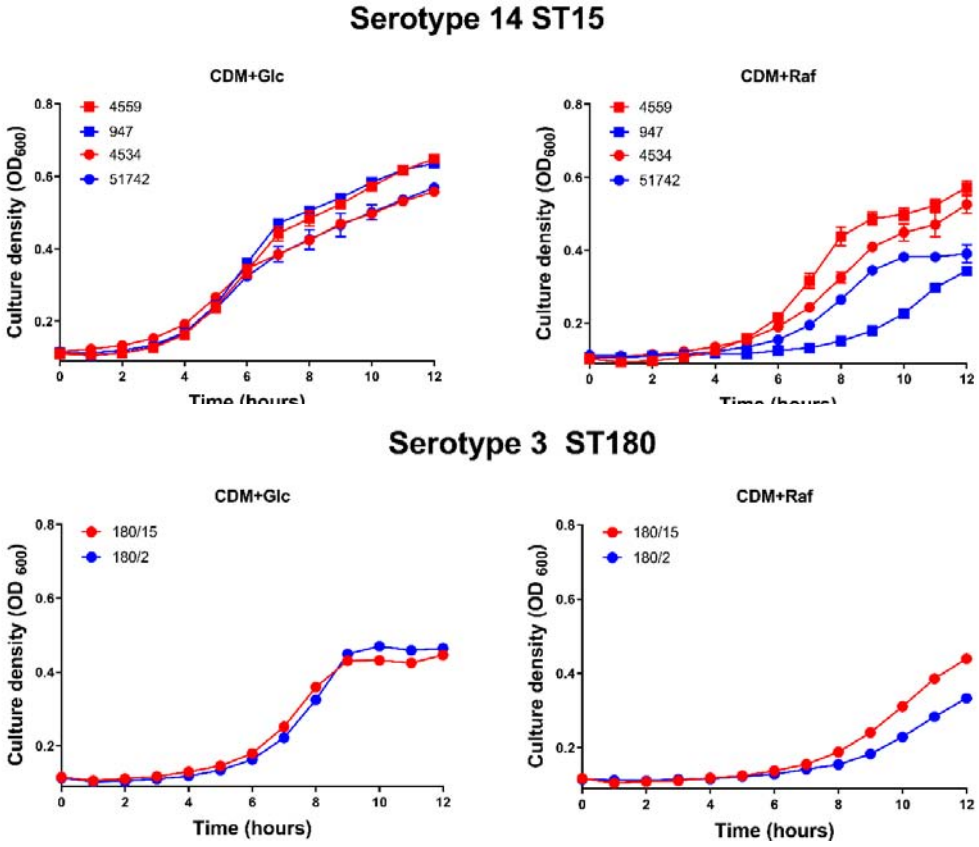

Figure 2.1. Differential growth of blood and ear isolates in raffinose. *S. pneumoniae* serotype 14 ST15 blood isolates 4559 and 4534 and ear isolates 947 and 51742 were grown in 200 µl CDM supplemented with 0.5% glucose (CDM+Glc) or 0.5% raffinose (CDM+Raf). Similar growth studies were also performed for serotype 3 ST180 strains 180/15 (blood isolate) and 180/2 (ear isolate). OD_{600} was measured every hour for 12 h. Data are mean OD_{600} ± standard deviation (SD) from a representative assay that was performed in triplicate.

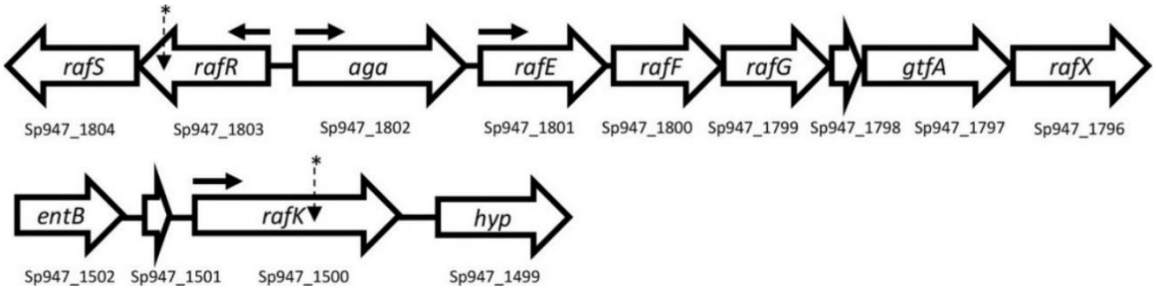

Figure 2.2. Genetic loci encoding raffinose uptake and utilization in *S. pneumoniae*. The numbers below each gene refer to the locus tags in the serotype 14 ST15 947 genome. The locations of SNPs in serotype 14 ST15 and serotype 3 ST180 isolates are indicated with asterisks; horizontal arrows show the locations of promoters.

To determine if the difference in ability to utilize raffinose between the blood and ear isolates corresponded with raffinose operon gene expression, *S. pneumoniae* serotype 14 ST15 strains 4559, 947, 4534, and 51742 and serotype 3 ST180 strains 180/2 and 180/15 were grown to the same OD_{600} (0.2) in CDM+Glc and then washed and resuspended in CDM+Raf and incubated for a further 30 min. RNA was then extracted, and levels of *aga*, *rafG* and *rafK* mRNA, representative of each of the three *rafR*-regulated transcriptional units, were then measured relative to 16S rRNA by quantitative real-time reverse transcription-PCR (qRT-PCR). In every case, expression levels for all three genes were significantly greater in the blood isolates than in the respective ear isolates (**Figure 2.3**).

As further confirmation, blood and ear isolates belonging to serotype 23F ST81 were also tested for growth in CDM+Glc and CDM+Raf, as well as for expression of *aga*, *rafG*, and *rafK* (**Figure 2.4**). Again, the blood isolate grew to a higher OD_{600} than the ear isolate in CDM+Raf, but not in CDM+Glc. Moreover, expression of all three *raf* genes were significantly higher in the blood isolate than in the ear isolate.

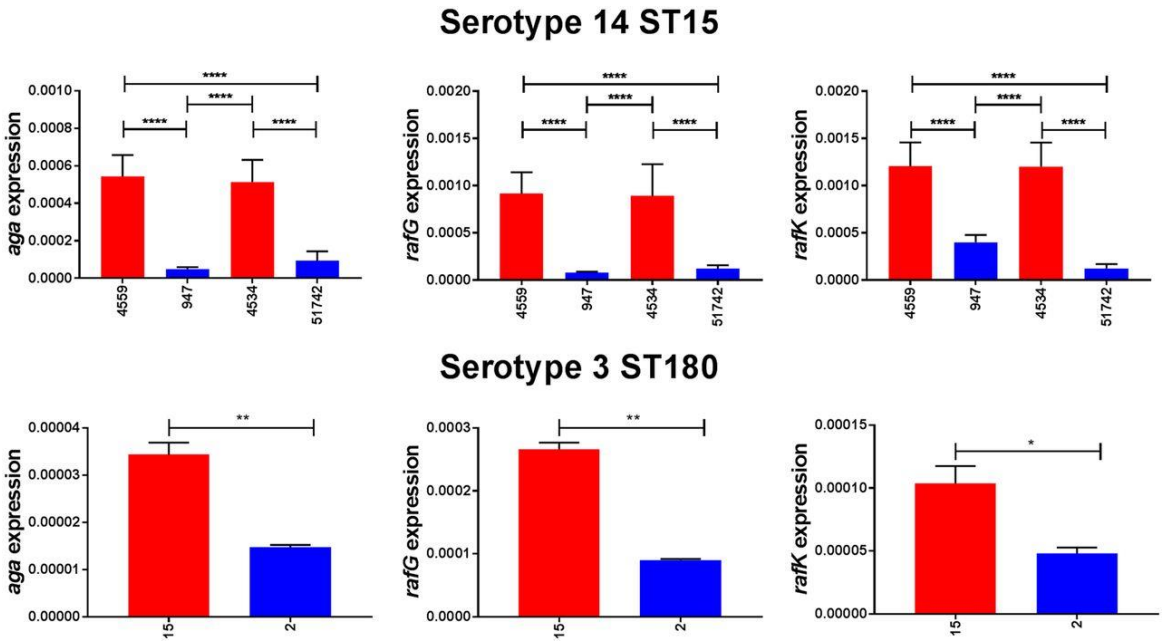

Figure 2.3. Expression of raffinose pathway genes by serotype 14 and 3 blood and ear isolates. The indicated strains were grown in CDM+Glc to an OD_{600} of 0.2, washed and resuspended in CDM+Raf, and then incubated at 37°C for a further 30 min. RNA was then extracted, and levels of *aga*, *rafG*, and *rafK* mRNA were analysed by qRT-PCR using 16S rRNA as an internal control (see Section 2.2.6). The data presented are the means ± SD from three independent experiments. *, $p < 0.05$, **, $p < 0.01$, and ****, $p < 0.0001$, by unpaired *t* test.

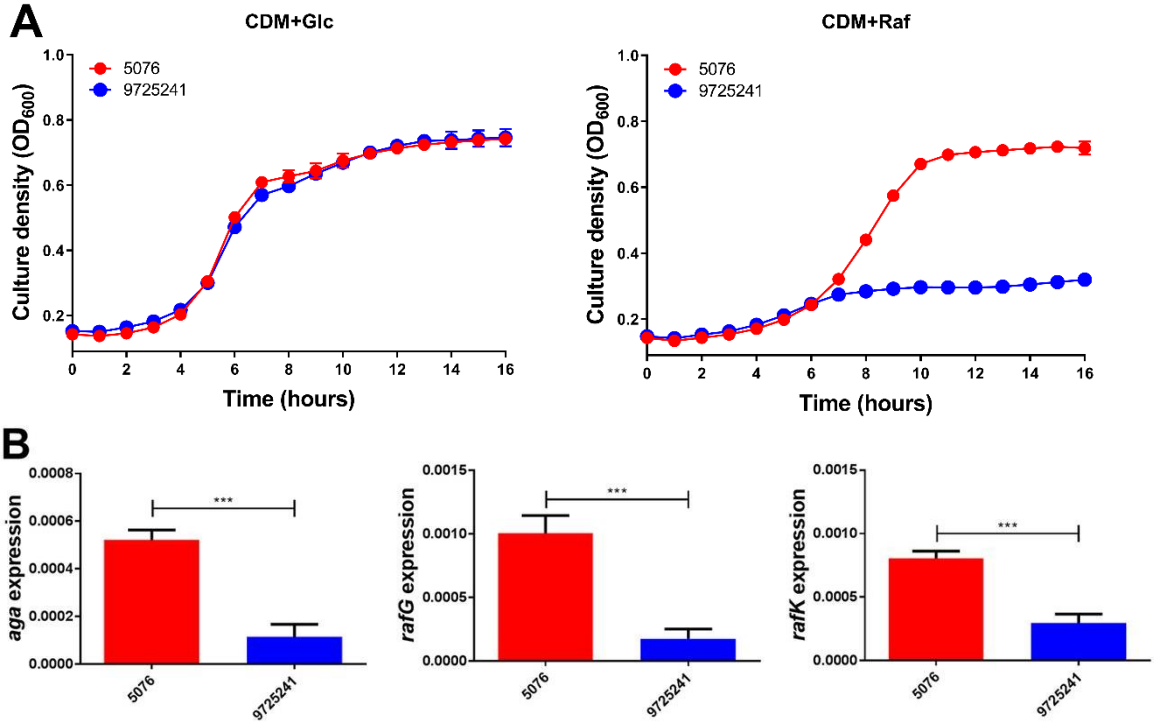

Figure 2.4. Growth phenotype and raffinose pathway gene expression in serotype 23F ST81 blood and ear isolates. (A) Growth of blood isolate 5076 and ear isolate 9725241 in CDM+Glc or CDM+Raf was monitored by OD_{600} for 12 h. Data are mean OD_{600} ± SD from a representative assay that was performed in triplicate. (B) The indicated strains were grown in CDM+Glc to an OD_{600} of 0.2, washed and resuspended in CDM+Raf, and then incubated at 37°C for a further 30 min. RNA was then extracted, and levels of *aga*, *rafG*, and *rafK* mRNA were analysed by qRT-PCR using 16S rRNA as an internal control. The data presented are the means ± SD from three independent experiments. ***, $p < 0.001$ by unpaired *t* test.

2.3.3 The SNP in 947 *rafR* is responsible for its raffinose phenotype

In order to test whether the distinct *in vitro* and *in vivo* phenotype of 947 relative to 4559 was attributable to the SNP in *rafR*, allelic-exchange mutagenesis was performed in 4559 and 947, generating a 4559 derivative with its *rafR* allele replaced by that from 947 (designated $4559^{947rafR}$) and a 947 derivative expressing the 4559 *rafR* allele ($947^{4559rafR}$) (see Section 2.2.8). Growth assays in CDM+Glc showed no significant differences in growth rates between 4559, 947, $4559^{947rafR}$, and $947^{4559rafR}$. However, in CDM+Raf, growth of $4559^{947rafR}$ was at least as poor as that of 947, while growth of $947^{4559rafR}$ was similar to that of 4559 (**Figure 2.5A**). Expression of *aga*, *rafG*, and *rafK* was then examined in 4559, 947, $4559^{947rafR}$, and $947^{4559rafR}$ by qRT-PCR after 30 min of growth in CDM+Raf. For all three genes, expression levels in $947^{4559rafR}$ were indistinguishable from those in 4559, while expression in $4559^{947rafR}$ was essentially the same as that in 947 (**Figure 2.5B**). Thus, exchange of *rafR* alleles between 4559 and 947 significantly impacts both growth phenotype and *raf* operon gene expression in CDM+Raf.

To further confirm the observed raffinose phenotype, that is 4559's *rafR* leads to greater raffinose utilisation, *rafR* from the blood isolate 4559 was inserted into the plasmid pAL2, creating the new plasmid pAL2:4559*rafR* (**Figure 2.6**), which was then introduced into the ear isolates 947 and 51742 (see Section 2.2.8). Successful insertion of *rafR* into pAL2 was confirmed by Sanger sequencing. Growth assays in CDM+Glc showed no significant differences in growth rates between 947^{pAL2}, 51742^{pAL2}, $947^{pAL2:4559rafR}$ and $51742^{pAL2:4559rafR}$. However, in CDM+Raf, $947^{pAL2:4559rafR}$ and 51742 $^{pAL2:4559rafR}$ grew to higher optical densities more efficiently than their respective wild type strains, with effect more pronounced in the 947 background (**Figure 2.7A**). Expression of *aga*, *rafG*, and *rafK* was then examined in 947^{pAL2}, 51742^{pAL2}, $947^{pAL2:4559rafR}$ and 51742 $^{pAL2:4559rafR}$ by qRT-PCR after 30 min of growth in CDM+Raf. For all three genes, expression levels in $947^{pAL2:4559rafR}$ and 51742 $^{pAL2:4559rafR}$ was significantly greater than

their respective empty vector wild types, corresponding to the results seen in the growth curves (**Figure 2.7B**). This suggests that the *rafR* allele in 4559 allows for greater raffinose utilisation compared to the *rafR* of 947.

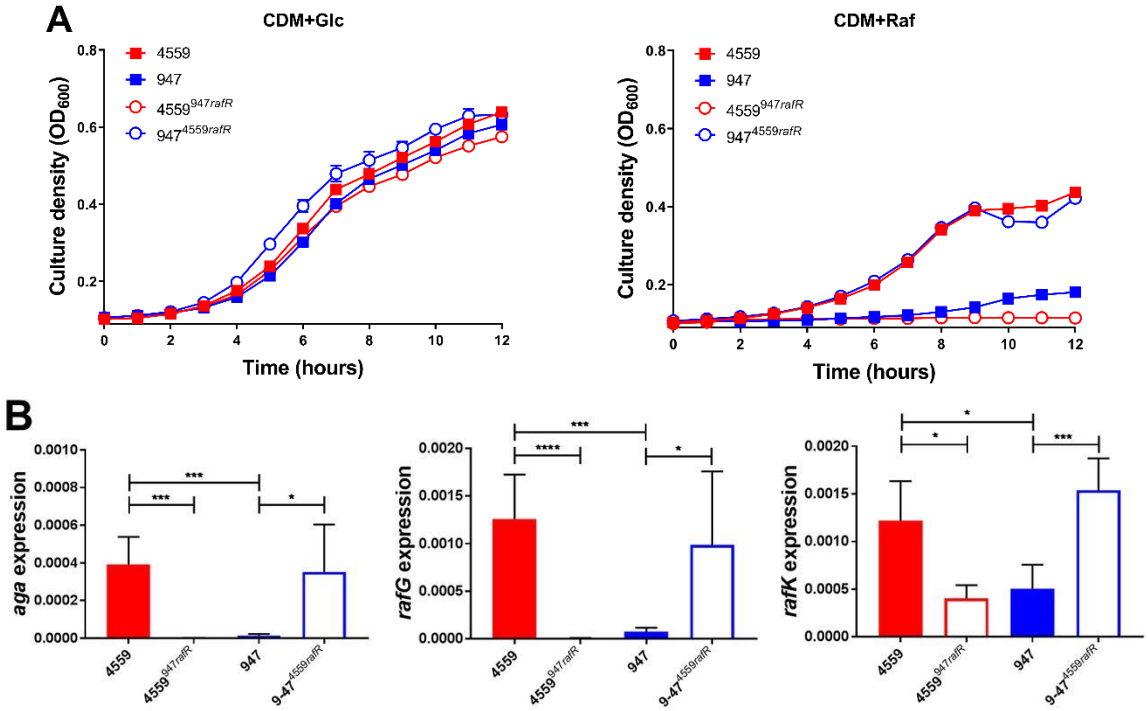

Figure 2.5. Growth phenotype and raffinose operon gene expression in *rafR* exchange mutants. (A) *S. pneumoniae* strains 4559, 947, 4559^{947rafR}, and 947^{4559rafR} were grown in CDM+Glc or CDM+Raf, and OD_{600} was monitored for 12 h. Data are mean OD_{600} ± SD from a representative assay that was performed in triplicate. (B) The indicated strains were grown in CDM+Glc to an OD_{600} of 0.2, washed and resuspended in CDM+Raf, and then incubated at 37°C for a further 30 min. RNA was then extracted, and levels of *aga*, *rafG*, and *rafK* mRNA were analysed by qRT-PCR. Data are the means ± SD from three independent experiments. *, $p < 0.05$, ***, $p < 0.001$, and ****, $p < 0.0001$, by unpaired *t* test.

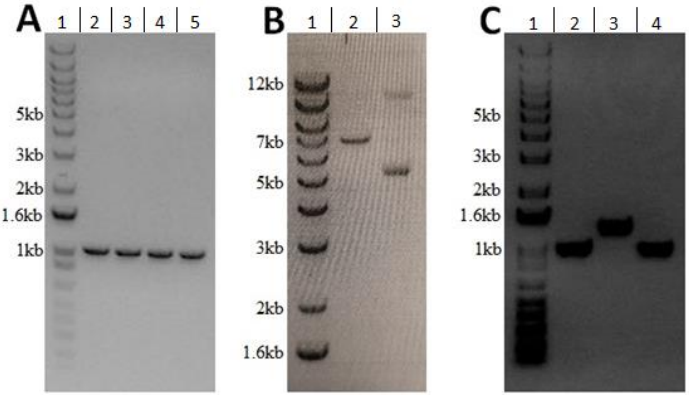

Figure 2.6. Insertion of *rafR* from 4559 into the pAL3 plasmid. Visualisation of PCRs through gel electrophoresis with 1kb plus ladder (Invitrogen) (lane 1, all images). (A) The *rafR* of 4559 was PCR amplified, then purified, with *Eco*RI sites placed at edges of the *rafR* sequence (lanes 2-5). (B) *EcoRI* digest of pAL3 (lane 2) and undigested control (lane 3). *Eco*RI digested pAL3 was then ligated with *Eco*RI digested 4559 *rafR*, and transformed into *E. coli* XL10 (see Section 2.2.9). (C) PCR amplification of DNA from a successfully transformed colony, using *rafR Eco*RI F and R primers (lane 2) and pAL2 bamHI F – *rafR Eco*RI R primers (lane 3). DNA from 4559 was used with *rafR Eco*RI F and R primers as a positive control (lane 4).

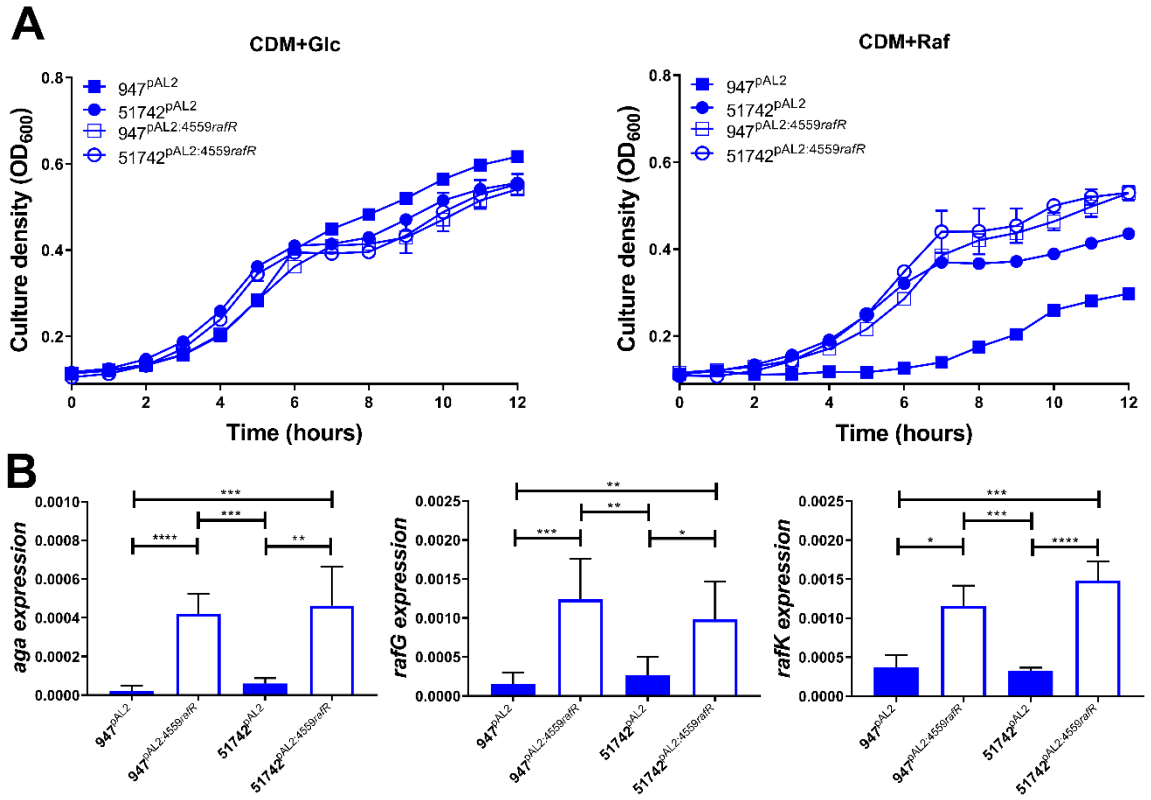

Figure 2.7. Growth phenotype and raffinose operon gene expression in serotype 14 ST 15 ear isolates mutants with 4559 *rafR* containing expression plasmid. (A) *S. pneumoniae* strains 947^{pAL2}, 51742^{pAL2}, 947$^{pAL2:4559rafR}$ and 51742 $^{pAL2:4559rafR}$ were grown in CDM+Glc or CDM+Raf, and OD_{600} was monitored for 12 h. Data are mean OD_{600} ± SD from a representative assay that was performed in triplicate. (B) The indicated strains were grown in CDM+Glc to an OD_{600} of 0.2, washed and resuspended in CDM+Raf, and then incubated at 37°C for a further 30 min. RNA was then extracted, and levels of *aga*, *rafG*, and *rafK* mRNA were analysed by qRT-PCR. Data are the means ± SD from three independent experiments. *, $p < 0.05$, **, $p < 0.001$, ***, $p < 0.001$, and ****, $p < 0.0001$, by unpaired *t* test

2.3.4 Virulence phenotypes of 4559 and 947 and their *rafR* exchange mutants

To determine whether the marked difference in virulence phenotypes of 4559 and 947 is also directly attributable to the SNP in *rafR*, 4559, 947, 4559^{947rafR} and 947^{4559rafR} were tested in a murine intranasal challenge model. Groups of Swiss mice were challenged with 10^8 CFU of each strain, and bacterial loads were quantitated in various tissues 24 h post challenge (**Figure 2.8**). No significant differences in bacterial numbers in the nasopharynx were seen between any groups (**Figure 2.8**), and no bacteria were detected in the blood of any mice (data not presented). However, 4559 was better able than 947 to persist in the lungs of infected mice, with significantly higher geometric mean (GM) bacterial load

($p < 0.0001$) and a significantly greater proportion of infected animals (14/16 versus 6/16; $p < 0.01$) (**Figure 2.8**). On the other hand, bacterial loads of 947 in the ear were significantly greater than that for mice challenged with 4559 ($p < 0.01$), and the proportion of infected mice was also significantly greater (16/16 versus 7/16; $p < 0.001$) (**Figure 2.8**). A similar trend was also seen in the brain (**Figure 2.8**).

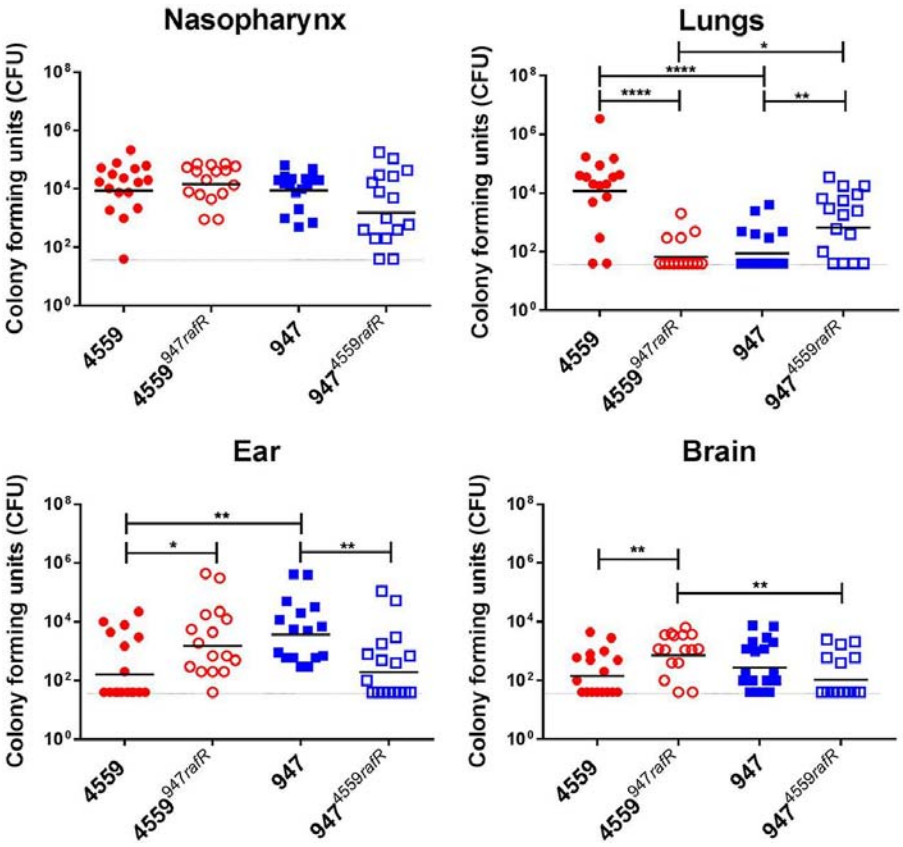

Figure 2.8. Virulence phenotype of *rafR* exchange mutants. Groups of 16 mice were infected intranasally with 10^8 CFU of the indicated strain. At 24 h, all mice from each group were euthanized and numbers of pneumococci in the indicated tissues/sites were quantitated (see Section 2.2.10). Viable counts (total CFU per tissue) are shown for each mouse at each site; horizontal bars indicate the geometric mean (GM) CFU for each group; the broken line indicates the threshold for detection. Differences in GM bacterial loads between groups are indicated by asterisks *, $p < 0.05$, **, $p < 0.01$, and ****, $p < 0.0001$, by unpaired *t* test.

Exchanging the *rafR* alleles has a striking impact on virulence phenotype. In the lungs, both the GM CFU and proportion of infected mice for the group challenged with $4559^{947rafR}$ were significantly lower than those for the 4559 group ($p < 0.0001$ and $p < 0.001$, respectively). Indeed, the virulence phenotype of $4559^{947rafR}$ was indistinguishable from that of 947. Conversely, the GM lung bacterial load and proportion of infected mice for the $947^{4559rafR}$ group were significantly greater than those for the 947

group ($P < 0.01$ and $P < 0.05$, respectively); there were no significant differences in these parameters between the $947^{4559rafR}$ and 4559 groups. In the ear, both the GM CFU and proportion of infected mice for the group challenged with $4559^{947rafR}$ were significantly greater than those for the 4559 group ($P < 0.05$ and $P < 0.01$, respectively). On the other hand, both the GM CFU and proportion of infected mice for the group challenged with $947^{4559rafR}$ were significantly lower than those for the 947 group ($P < 0.01$ in both cases). Moreover, there was no significant difference in either GM bacterial loads or proportions of infected mice between the $4559^{947rafR}$ and 947 groups or between the $947^{4559rafR}$ and 4559 groups (**Figure 2.8**). A similar pattern is seen in the brain; the GM CFU for the $4559^{947rafR}$ group was significantly greater than those for either the 4559 or $947^{4559rafR}$ groups ($P < 0.01$ in both cases). Moreover, there was no significant difference in either GM bacterial loads or proportions of infected mice between the $4559^{947rafR}$ and 947 groups or between the $947^{4559rafR}$ and 4559 group (**Figure 2.8**). Collectively, these data show that swapping the *rafR* allele between 4559 and 947 leads to a switch in their respective virulence profiles, and thus, the D49G SNP in *rafR* is entirely responsible for the observed differences in tissue tropism between the serotype 14 ST15 blood and ear isolates.

2.3.5 Mutagenesis of *rafK* in serotype 3 ST180 blood and ear isolates

Attempts to construct *rafK* exchange mutants of serotype 3 ST180 blood and ear isolates (180/15 and 180/2, respectively) analogous to the *rafR* exchange mutants constructed for the serotype 14 strains were not successful. Thus, the impact of the SNP in RafK could not be directly tested. However, the native *rafK* genes from both type 3 strains were successfully deleted (designated 180/15 Δ*rafK* and 180/2 Δ*rafK*, respectively). Both mutants were incapable of growth in CDM+Raf, and expression of *aga* and *rafG* was

virtually undetectable by qRT-PCR; *rafK* expression was also undetectable, as expected (**Figure 2.9**). Thus, the ear isolate 180/2 exhibits a phenotype that is intermediate between that of the blood isolate 180/15 and either of the two Δ*rafK* mutants, consistent with partial functionality of the ear isolate RafK. *S. pneumoniae rafK* deletion mutants have previously been shown to be outcompeted by the wild type in the murine lung and nasopharynx (Marion et al., 2011; Tyx et al., 2011). Similarly, in the present study, bacterial loads in the lungs, blood, ear, and brain were also lower for mice challenged with the 180/2 and 180/15 Δ*rafK* mutants relative to those challenged with the respective wild types at 24 h after intranasal challenge (**Figure 2.10**). This indicates that even the intermediate level of raffinose pathway gene expression exhibited by ear isolate 180/2 contributes to virulence.

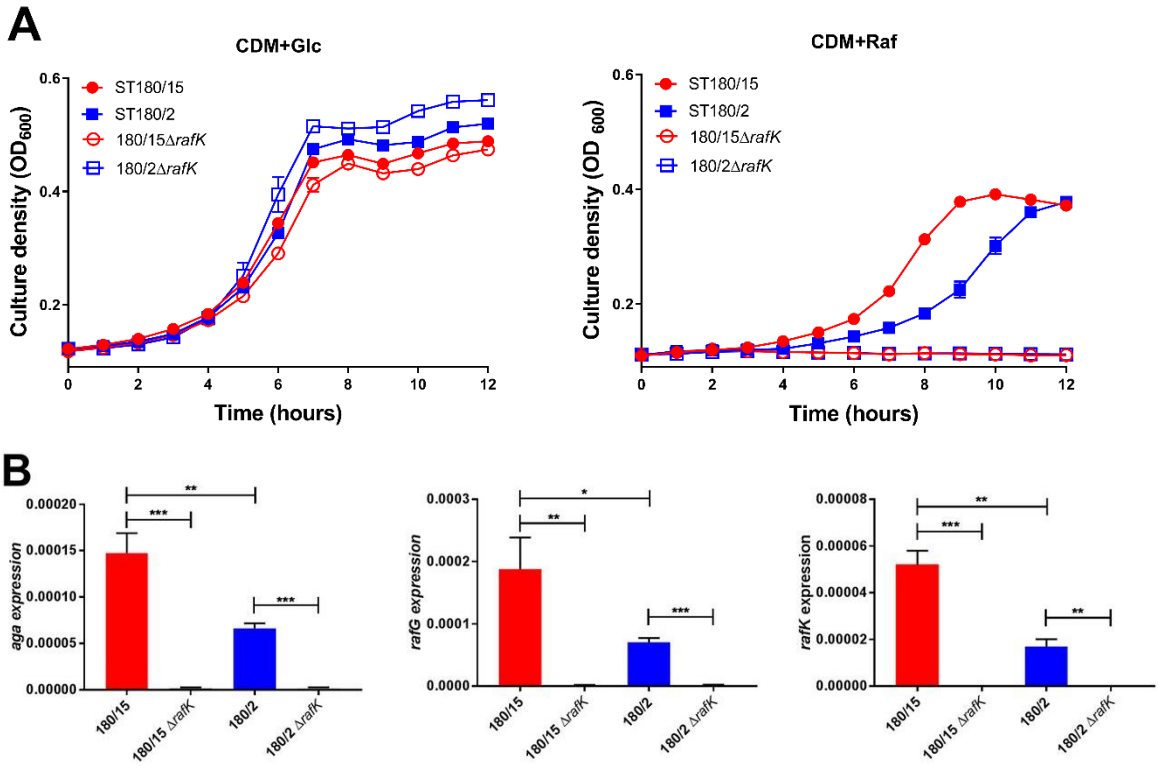

Figure 2.9. Growth phenotype and raffinose operon gene expression in Δ*rafK* mutants. (A) S. pneumoniae serotype 3 strains 180/15, 180/2, 180/15Δ*rafK*, and 180/2Δ*rafK* were grown in CDM+Glc or CDM+Raf, and OD_{600} was monitored for 12 h. Data are mean OD_{600} ± SD from a representative assay that was performed in triplicate. (B) The indicated strains were grown in CDM+Glc to an OD_{600} of 0.2, washed and resuspended in CDM+Raf, and then incubated at 37°C for a further 30 min. RNA was then extracted, and levels of *aga*, *rafG*, and *rafK* mRNA were analysed by qRT-PCR. Data are the means ± SD from three independent experiments. *, $p < 0.05$, **, $p < 0.01$, and ***, $p < 0.001$, by unpaired *t* test.

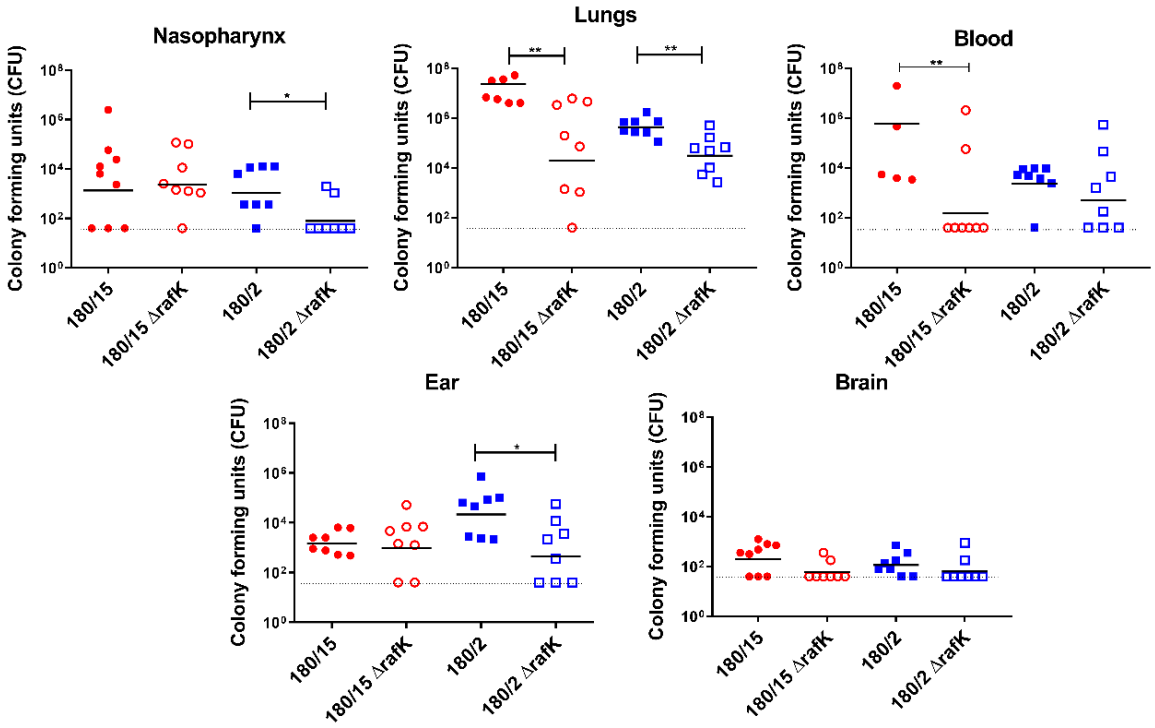

Figure 2.10. Virulence phenotype of serotype 3 ST 180 *rafK* knockout mutants. Groups of 16 mice were infected I.N. with 10^8 CFU of the indicated strain. At 24 h, all mice from each group were euthanized and numbers of pneumococci in the indicated tissues/sites were quantitated (see Section 2.2.9). Viable counts (total CFU per tissue) are shown for each mouse at each site; horizontal bars indicate the geometric mean (GM) CFU for each group; the broken line indicates the threshold for detection. Statistically significant differences in GM bacterial loads between groups are indicated by asterisks: *, $p < 0.05$ and **, $p < 0.01$, by unpaired *t* test.

2.3.6 Effects of *raf* mutations on adherence to lung epithelial cells

Given that exchanging *rafR* between 4559 and 947 had such stark impacts on murine disease progression, whether this impact was at least partly due to a direct impact of *rafR* on adherence to respiratory epithelial cell lines was investigated. Here 4559, 947, $4559^{947rafR}$, and $947^{4559rafR}$ were assessed for their adherence to A549 and Detroit 562 cell lines, in both CDM+Glc and CDM+Raf (see Section 2.2.11). The adherence of 4559 was greater than both 947 and $4559^{947rafR}$ to A549 cells, in CDM+Glc ($p < 0.01$) and CDM+Raf ($p < 0.0001$) (**Figure 2.11**). Similarly, $947^{4559rafR}$ showed significantly greater adherence to A549 cells than 947 and $4559^{947rafR}$ in CDM+Glc ($p < 0.01$ and $p < 0.001$, respectively) and CDM+Raf ($p < 0.0001$) (**Figure 2.11**). Conversely, there was no significant difference between the ability of any of the strains to adhere to Detroit 562 cells, in both CDM+Glc

and CDM+Raf (**Figure 2.11**). These results are compatible with the *in vivo* mouse virulence data, as both 4559 and 947^{4559rafR} were able to persist in the lungs significantly more so than 947 and 4559^{947rafR}, while there was no significant difference between the strains' abilities to colonise the nasopharynx (**Figure 2.8**).

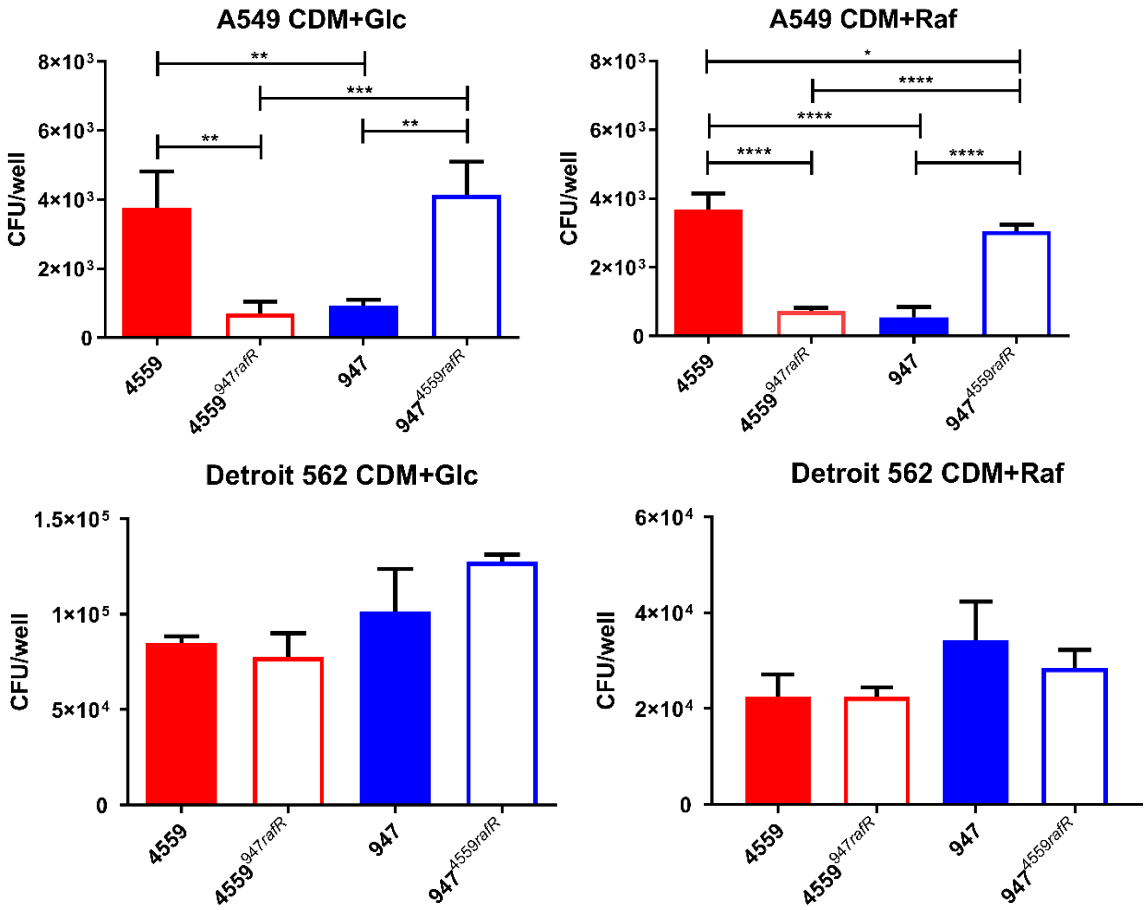

Figure 2.11. Impact of *rafR* exchange on adherence to A549 (lung epithelial) and Detroit 562 (nasopharyngeal) cells. *S. pneumoniae* strains 4559, 947, 4559^{947rafR} and 947^{4559rafR} were inoculated at OD_{600} = 0.2 onto A549 or Detroit 562 monolayers in CDM + 10% FCS + 0.5% glucose (A) or 0.5% raffinose (B), in triplicate, then tested for adherence after 2 h at 37 °C (see Section 2.2.11). Each adherence assay was performed twice, with similar results. Data presented are the means ± standard deviations from two independent experiments (*, $p < 0.05$; **, $p < 0.01$;***, $p < 0.001$;****, $p < 0.0001$; unpaired *t*-test).

To confirm that the virulence and adherence impacts of the *rafR* exchange was not due to any corresponding effects on CPS production, CPS ELISA assays were performed (see section 2.2.12). No significant difference in total CPS production was observed between 4559, 947, 4559^{947rafR}, and 947^{4559rafR} (**Figure 2.12**).

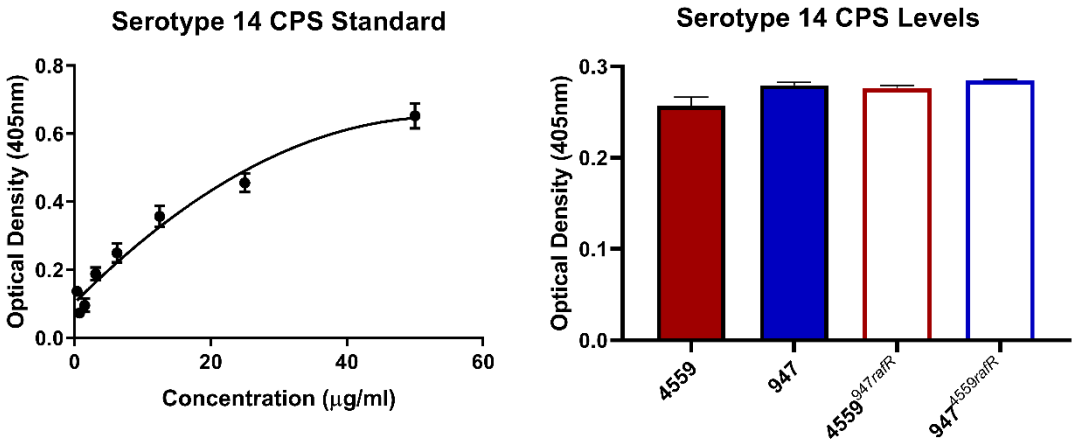

Figure 2.12. Total CPS production in serotype 14 ST 15 strains 4559, 947, $4559^{947rafR}$, and $947^{4559rafR}$ was measured by ELISA (see section 2.2.12). Serial 2-fold dilutions of a serotype 14 CPS standard and total CPS preparations of the above strains were performed, then serotype 14 typing sera (1° antibody) and goat anti-rabbit IgG (2° antibody) were used to detect CPS levels. Absorbance was read at 405nm and a resulting standard curve was generated.

RafE, the substrate binding protein of the raffinose ABC uptake system under regulation of RafR, contains a RGD motif, Arg-Gly-Asp (263-RGD-265) (Rosenow et al., 1999). The RGD motif has been reported to promote eukaryotic cell attachment (D'Souza et al., 1991) and to be crucial for interactions with the cell surface receptor integrin (Ruoslahti and Pierschbacher, 1986). To determine whether the RGD motif in RafE plays a role in pneumococcal adherence, the RGD motif was mutated to HAE (conservative amino acid changes) in 4559 and 947, generating $4559^{\text{RafE RGD→HAE}}$ and $947^{\text{RafE RGD→HAE}}$ (see Section 2.2.8). These strains were then assessed for their adherence to A549 and Detroit 562 epithelial monolayers, in both CDM+Glc and CDM+Raf. The adherence to A549 cells of both 4559 and $4559^{\text{RafE RGD→HAE}}$ were significantly greater than of 947 ($p < 0.001$ and $p < 0.01$, respectively) and $947^{\text{RafE RGD→HAE}}$ ($p < 0.05$ and $p < 0.05$, respectively) in CDM+Glc, while 4559 and $4559^{\text{RafE RGD→HAE}}$ also had significantly greater adherence than 947 ($p < 0.05$) in CDM+Raf. There was no significant sidffrence in adherence to A549 cells between 4559 and $4559^{\text{RafE RGD→HAE}}$ or between 947 and $947^{\text{RafE RGD→HAE}}$ (**Figure 2.13**). As observed in the previous experiment, there were no significant differences between any of the strains in adherence to Detroit 562 cells in either CDM+Glc and CDM+Raf (**Figure**

2.13). Thus, the RafE RGD motif is not directly affecting pneumococcal adherence to either A549 or Detroit 562 cells.

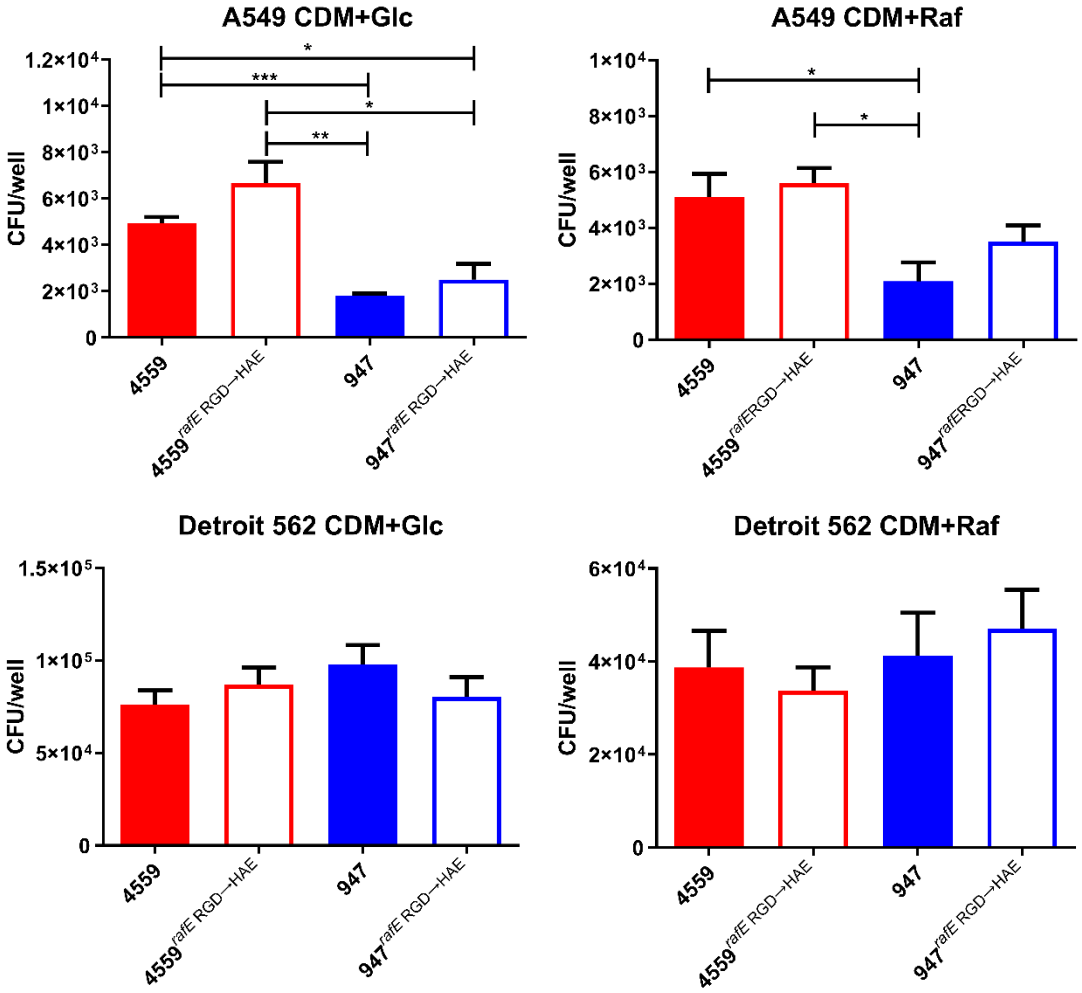

Figure 2.13. Impact of RafE RGD→HAE mutation on adherence to A549 and Detroit 562 cells. *S. pneumoniae* strains 4559, 947, 4559$^{\text{RafE RGD→HAE}}$ and 947$^{\text{RafE RGD→HAE}}$ were inoculated at OD_{600} = 0.2 onto A549 or Detroit 562 monolayers in CDM + 10% FCS + 0.5% glucose (A) or 0.5% raffinose (B), in triplicate, then tested for adherence after 2 h at 37 °C (see Section 2.2.10). Each adherence assay was performed twice, with similar results. Data presented are the means ± standard deviations from two independent experiments (*, $p < 0.05$; **, $p < 0.01$; ***, $p < 0.001$; unpaired *t*-test).

2.3.7 Detection of raffinose and *raf* operon expression in mouse lungs

Despite the apparent involvement of raffinose in pneumococcal disease progression, raffinose, a plant derived sugar, has not been directly detected in mammalian tissues. To determine raffinose's presence in murine lungs, groups of 4 mice were challenged with 10^8 CFU of either 4559, 947 or SB (mock), the lungs were then harvested 24 h post-infection.

The infected murine lungs were sent to Metabolomics Australia, where Gas chromatography-mass spectrometry (GC MS) was performed on these samples (see Section 2.2.13). This technique is capable of detecting raffinose down to a minimum of 0.01 mg/g in tissue. Sucrose was also examined in the GC MS as a positive control. Selected-ion monitoring (SIM) chromatograms of all tested samples showed detectable levels of sucrose (**Appendix I**), but levels of raffinose were under the limit of detection (**Appendix J**). Overlaid SIM chromatograms of the murine lung samples and sucrose and raffinose analytical standards, show no peak/detection of raffinose in the lungs (**Figure 2.14**).

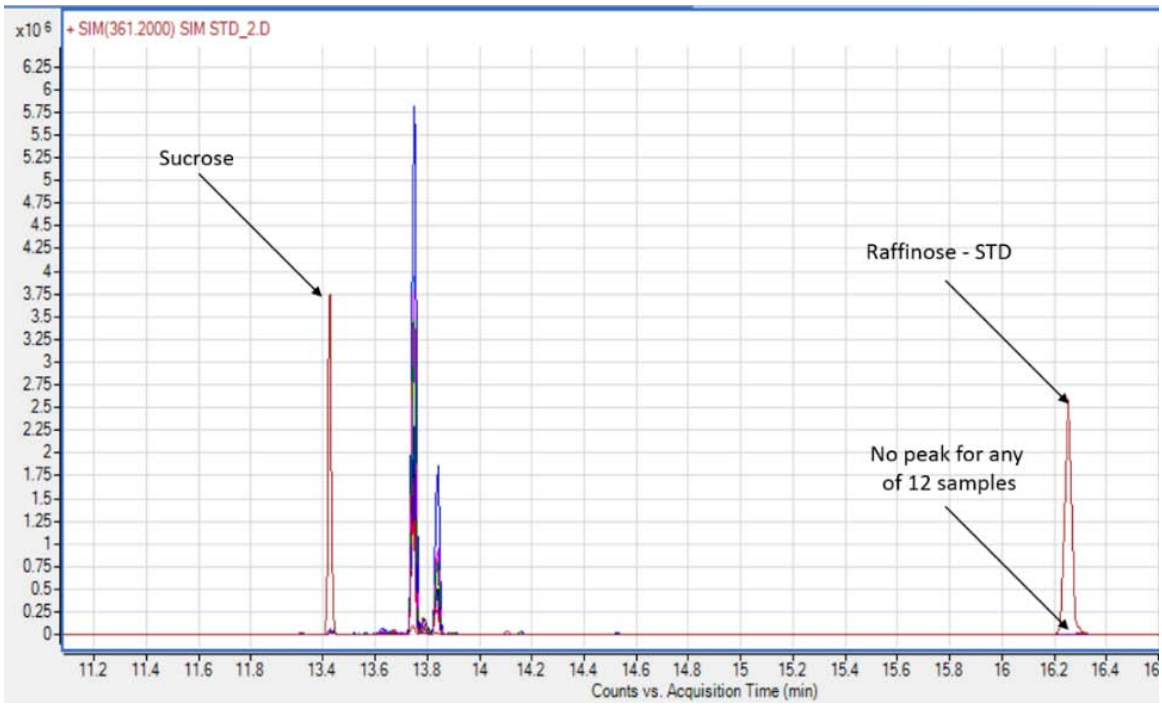

Figure 2.14. GC MS was performed at Metabolomics Australia on lungs extracted from groups of 4 mice after infectiom with 4559, 947 or SB. Lungs were harvested 24 h post-infection and underwent CryoMill extraction for polar metabolites (see section 2.2.13). Overlaid SIM chromatograms show selected-ion intensity (Y-axis) and the acquisition time (X-axis) of the 12 murine lung samples and raffinose analytical standards (STD).

As raffinose was unable to be detected in murine lungs, the activation of the raffinose operon was examined *in vivo*, in order to confirm the biological relevance of the *rafR* switch. Here murine lungs were harvested 6 h after infection with either 4559, 947, $4559^{947rafR}$, and $947^{4559rafR}$. RNA was then extracted and levels of *aga*, *rafG*, and *rafK* mRNA were then measured relative to 16S rRNA by qRT-PCR. Importantly, differential expression of these genes was observed, with *aga* expression greater in 4559 than 947 and

$4559^{947rafR}$ ($p < 0.05$, in both cases). $947^{4559rafR}$ also showed significantly greater *aga* expression than $4559^{947rafR}$ ($p < 0.05$) (**Figure 2.16**). Expression of *rafG* was also statistically significantly greater in both 4559 and $947^{4559rafR}$ than in either 947 or $4559^{947rafR}$ ($p < 0.05$, in all cases). Hence expression of the pneumococcal raffinose operon does occur *in vivo* after infection of murine lungs. These findings for *aga* and *rafG* expression are similar to that seen in cells grown *in vitro* in CDM+Raf, and implies the presence of raffinose or similar saccharides able to activate the *raf* operon within lung tissue. *RafK* expression was also detected in all infected lung extracts, but unlike the case with *in vitro* grown cells in CDM+Raf, there was no significant difference in *rafK* expression between strains.

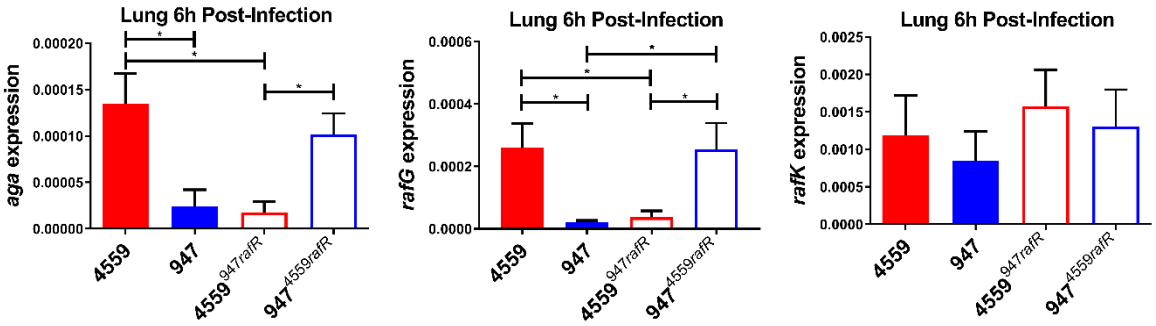

Figure 2.16. Expression of raffinose pathway genes in murine lungs. Mice were challenged I.N. with 10^8 cfu of indicated strains, then lungs were harvested 6 h post-infection. RNA was then extracted, and levels of *aga*, *rafG*, and *rafK* mRNA were analysed the means ± SD from three independent experiments. *, $p < 0.05$, by unpaired *t* test.

2.4 Discussion

Utilising both PacBio and Illumina MiSeq genomic sequencing allowed the *de novo* assembly of the serotype 14 ST15 and serotype 3 ST 180 blood and ear isolate genomes. PacBio produces long reads with high error rates while MiSeq yields much shorter reads with lower error rates (Quail et al., 2012). Thus, combining these two sequencing technologies allowed the consolidation of their advantages (long reads for PacBio and low error rate for MiSeq) whilst removing their disadvantages (high error rate for PacBio and short reads for MiSeq). Given that each sequenced blood and ear isolate pair were from the same serotype and sequence type, the low number of significant genetic differences within each pair was expected. The serotype 3 ST 180 pair had 27 indels or SNPs that lead to amino acid changes, while the serotype 14 ST 15 pair had 17 amino acid altering mutations, along with a prophage and plasmid present in 4559 but not 947 (section 2.3.1).

It was initially hoped that consistent genetic differences between blood and ear isolates might be identified for the two distinct lineages, pointing to candidate polymorphisms that are directly responsible for virulence phenotype. However, the serotype 14 ST15 and serotype 3 ST 180 blood and ear isolate pairs shared no common genetic differences. Nevertheless, SNPs in *rafR* and *rafK* within the raffinose utilisation locus were present in the ST15 and ST180 isolate pairs, respectively. As there were no other common differences between the clonal isolate pairs, the potential impact of raffinose utilisation on differential disease progression/niche adaptation was examined.

Pneumococci are strictly fermentative bacteria, relying solely on carbohydrate metabolism for energy and growth (Paixão et al., 2015). However, carbohydrate availability differs between host niches, and so the ability to respond to and utilize distinct carbohydrates is crucial for pneumococcal fitness *in vivo*. The *S. pneumoniae* genome encodes 21 phosphotransferase systems (PTSs) and up to 8 ATP binding cassette (ABC) transporters

for the import of carbohydrates (Bidossi et al., 2012; Buckwalter and King, 2012), accounting for roughly 30% of all transport systems (section 1.5.3). Previous studies have shown that several of these carbohydrate transporters, present in both the core and accessory genome, impact pneumococcal virulence. For example, a sucrose PTS and ABC transporter system of serotype 4 pneumococci have both been shown to play roles in murine colonisation and pneumonia, respectively (Iyer and Camilli, 2007), while transporters for carbohydrates such as glucose, galactose and mannose were shown to impact invasive pneumococcal disease (Hava and Camilli, 2002; Ogunniyi et al., 2012; Orihuela, Radin, et al., 2004).

Results from this Chapter further underscore the critical role played by differential carbohydrate metabolism in pneumococcal pathogenesis. It demonstrates that reduced capacity to utilise raffinose does not simply reduce pneumococcal virulence, but rather changes the nature of disease caused. In multiple serotypes/ST lineages, ear isolates had defective growth in CDM+Raf and reduced expression of raffinose pathway genes relative to their serotype/ST-matched blood isolates (section 2.3.2). Exchange of *rafR* alleles between ear and blood isolates of serotype 14 ST15 reversed these *in vitro* phenotypes (section 2.3.4). Moreover, *rafR* exchange caused blood isolates to now cause otitis media and meningitis rather than pneumonia after intranasal challenge, and conversely caused ear isolates to now target the lungs. This striking switch in *in vitro* and *in vivo* behaviours was attributable to a single, nonconservative SNP (D249G) in RafR, identifying this residue as one of critical functional importance. Significantly, the region of RafR from amino acids 226 to 268 comprises a conserved signature sequence for the AraC/XylS family of transcriptional regulators (Rosenow et al., 1999).

Interestingly, in spite of exhibiting similarly distinct *in vitro* and *in vivo* phenotypes, the serotype 3 ST180 blood and ear isolates did not share the SNP in *rafR*, but rather had a SNP in *rafK*, which encodes the ATPase required for raffinose uptake via the ABC

transport system encoded by *rafEFG*. RafK-mediated uptake of raffinose has previously been shown to be essential for induction of the *raf* operons in *S. pneumoniae* D39 (Tyx et al., 2011). Attempts to construct *rafK* exchange mutants in this lineage (analogous to the serotype 14 ST15 *rafR* exchange mutants) were not successful, likely due to the low transformability reported with serotype 3 strains (Croucher, Mitchell, et al., 2013). However, *rafK* deletion mutants of both 180/2 and 180/15 were obtained. Whereas the wild-type ear isolate 180/2 exhibited reduced growth in CDM+Raf and expression of *aga*, *rafG* and *rafK* relative to the wild-type blood isolate 180/15, both *rafK* deletion mutants were unable to grow in CDM+Raf at all, and expression of any of the *raf* operon transcripts was undetectable (section 2.3.5). Clearly, the RafK allele carried by 180/2 retains partial function. The I227T SNP that distinguishes the RafK alleles of 180/2 and 180/15 is located in the conserved regulatory domain motif 1. This domain is believed to be involved in the interaction between RafK and the enzyme dihydrolipoamide dehydrogenase (DLDH), which has been shown to modulate raffinose uptake and *raf* operon expression in *S. pneumoniae* D39 (Tyx et al., 2011). In the murine model, both *rafK* deletion mutants exhibited reduced bacterial loads in multiple host niches relative to their respective wild-type strains (section 2.3.5), consistent with previous reports (Marion et al., 2011; Tyx et al., 2011).

These findings provide an interesting example of convergent evolution, whereby pneumococci belonging to two unrelated serotypes/lineages exhibit SNPs in separate genes, each affecting raffinose uptake and utilisation, which in turn correlate with distinct pathogenic profiles in both mice and humans (the latter by inference from the clinical isolation site). In *S. pneumoniae* D39, induction of expression of the *raf* operon gene *aga* required the presence of raffinose; reduced but nevertheless significant *aga* expression also occurred in a *rafR* knockout mutant (Rosenow et al., 1999). Thus, *raf* operon expression in pneumococci can be impacted either by defects in raffinose

import (e.g., due to a defective RafK), such that insufficient exogenous raffinose (if present) is internalised to induce *raf* expression, or by functional defects in the transcriptional activator RafR, such that baseline levels of expression induced by the presence of raffinose are not further upregulated. The *raf* operons are part of the core genome of *S. pneumoniae*, and BLASTX analysis of available genomes shows that there is between 1% and 3% deduced amino acid sequence variation within any of the *raf* genes. Thus, SNPs are widespread, but it is not known which (if any) of these other SNPs impact the capacity to import or utilize raffinose or the virulence phenotype.

Notwithstanding the results presented above, the precise mechanism whereby differential raffinose uptake/utilization determines the virulence phenotype is uncertain. Raffinose is a plant-derived trisaccharide present in many staple foods, particularly beans and soy (Díaz-Batalla et al., 2006; Kumar et al., 2010). A potential complicating factor is that RafEFG is reported to be also capable of importing stachyose (Bidossi et al., 2012), while RafK has been reported to also energize uptake of sialic acid and maltotetraose via unrelated transporters (Marion et al., 2011). Thus, the SNPs observed in the present study could have pleiotropic effects. However, no differences in metabolism of these sugars between the serotype 14 ST15 blood and ear isolates were observed using phenotypic microarray analysis (**Appendices A-H**), and the serotype 3 ST180 strains were unable to grow in CDM with stachyose or sialic acid as the sole carbon source. Moreover, there was no significant difference in the growth rates of the ST180 blood and ear isolates when grown in CDM with maltotetraose.

A particularly intriguing finding of the present study was that lower raffinose uptake/utilisation by the ear isolates provided an advantage over blood isolates in the ear compartment. Interestingly, exogenous raffinose has recently been shown to promote biofilm formation by *Streptococcus mutans* by promoting aggregation of extracellular DNA into the biofilm matrix. Biofilm formation was unaffected by deletion of the α-

galactosidase gene *agaL*, indicating that the effect was unrelated to metabolism of any internalized raffinose (Nagasawa et al., 2017). Thus, it is conceivable that the reduced capacity of *S. pneumoniae* ear isolates to assimilate (and thereby deplete) raffinose from the middle ear mucosa may similarly promote pneumococcal biofilm formation in that niche, leading to otitis media.

Although humans are unable to metabolise it, dietary raffinose is known to be absorbed by the intestinal epithelium (Lobley et al., 1990), raising the possibility of at least small amounts being present on mucosal surfaces. Expression of *aga*, *rafG* and *rafK* was detected in RNA extracts of mouse lung tissue 6 h after intranasal challenge with either of the serotype 14 ST15 blood or ear isolates. Since raffinose is the only known inducer of the *raf* operon in *S. pneumoniae*, this finding is strongly indicative of the presence of bioavailable raffinose in the murine lung. However, GC MS analysis of infected lung extracts failed to detect the presence of raffinose. This may be due to the limit of detection for raffinose by GC MS. Raffinose uptake by pneumococci may be very efficient, leading to free raffinose being kept below the detection threshold of the GC MS. However, raffinose was not detected in the mock infected lung extracts. Whether this raffinose operon upregulation is due to raffinose or induced by other saccharides that are similar in structure to raffinose, capable of interacting with RafR and present in the lungs, remains to be seen.

Adherence assays showed the *rafR* mutation affect the ability of the serotype 14 ST 15 blood and ear isolates to adhere to lung epithelial cells. However, conservative mutation of a putative RGD binding motif of the raffinose ABC uptake system's substrate binding protein, RafE, did not abrogate adherence. Whether RafE could moonlight as a pneumococcal adhesin would seem unlikely given its cellular location attached to the cell membrane, beneath the cell wall and capsule, making interactions with host receptors problematic. There is also the issue of adherence occurring in CDM+Glc (**Figure 2.13**), in which raffinose gene expression, including *rafE*, would be expected to be repressed. Thus,

the raffinose operon's impact on lung epithelial adherence, and potentially on virulence as a whole, may be indirect. As *rafR* acts as the regulator for the raffinose operon, it is possible that it also acts as a regulator for other genes that in turn impact pneumococcal virulence and disease progression. Further studies looking into the impact of *rafR* on both the pneumococcal and host genome *in vivo* are needed to elucidate the precise molecular mechanisms whereby fine-tuning of levels of expression of *rafR* can have such a profound impact on pathogenic profiles of clinical isolates of *S. pneumoniae*.

Chapter 3

Transcriptomic Comparisons of *S. pneumoniae* Clonal Clinical Isolates

3.1 Introduction

In the previous Chapter, the potential effects of the genetic differences within the serotype 14 ST 15 and serotype 3 ST 180 blood and ear isolate pairs were explored, in an attempt to explain their differential disease phenotypes. Indeed, SNPs present within the genes *rafR* and *rafK* were shown in Chapter 2 to influence disease progression for the serotype 14 ST 15 and serotype 3 ST 180 blood and ear isolates, respectively (Minhas et al., 2019). Whilst there is strong evidence for the involvement of the raffinose operon in disease progression of both the examined serotype/lineages, it was unclear whether this was strictly via effects on raffinose metabolism or indirect effects on unrelated parameters. Transcriptomic analyses of the clonally-related blood and ear isolates may therefore provide insights into the underlying mechanisms.

In this Chapter, the serotype 14 ST15 and serotype 3 ST180 strains were grown in either CDM with Glc or galactose (Gal) as the sole carbon sources, or in human serum, and RNA extracts were subjected to RNA sequencing. The strains exposed to human serum mimicked the human blood environment as closely as possible without the need to infect live patients. CDM+Glc similarly mimicked this blood environment, at least in terms of carbohydrate source, as glucose is the major sugar found in the blood (McMillin, 1990). Identification of similarities between these two growth media may provide insights into how pneumococci typically behave upon invading the blood stream. Conversely, galactose is the major sugar present in the nasopharynx (Blanchette et al., 2016), thus CDM+Gal

sought to mimic the nasopharyngeal environment, which may help to elucidate the behaviour of pneumococci during colonisation.

Clearly, transcriptomic analyses of cells grown in CDM+Raf would have been highly informative in light of the findings in Chapter 2. However, the decision to use CDM+Glc and CDM+Gal was made before the genomic analyses were performed. Hence, there was no capacity in this current chapter to thoroughly expand on the raffinose related findings from the previous Chapter.

3.2 Materials and Methods

3.2.1 Preparation of *S. pneumoniae* strains

The bacterial strains used in this Chapter are listed in **Table 3.1**. Cells were routinely grown in C+Y medium (Lacks and Hotchkiss, 1960) or on BA plates with or without gentamicin (40 µg/ml), kanamycin (500 µg/ml), or spectinomycin (200 µg/ml) (as required) and incubated at 37°C in 5% CO_2 overnight (section 2.2.1). The strains 4559, 947, 180/15 and 180/2 were prepared for RNA sequencing in human serum or CDM (Kloosterman et al., 2006), with either 0.5% Glc or 0.5% galactose, in 6 biological replicates. Each strain was inoculated into CDM+Glc or CDM+Gal at an OD_{600} of 0.05, and grown to 0.25 OD_{600}. Pneumococci are unable to grow in human serum, hence strains were instead incubated in this media at 0.5 OD_{600} for 2 hours. Each sample was then pelleted and RNA extracted by the addition of 400 µl of Acid Phenol: Chloroform (5:1, pH 4.5) (Ambion), and 400 µl of 65^{o}C NAES (50mM NaAC pH 5.1 + 1% SDS) at 65^{o}C, essentially as previously described (Ogunniyi et al., 2002), except that the resulting aqueous phase was extracted using the Qiagen RNeasy RNA isolation kit. For gene expression validations, strains were similarly grown in CDM+Gal or CDM+Gal to an OD_{600} of 0.5, before RNA extraction.

3.2.2 Transcriptomic sequencing

Purified pneumococcal RNA samples were assessed by the Bioanalyzer (Agilent, Sant Clara, United States) for a RIN (RNA Integrity Number) value > 8.0, then sent to AGRF for sequencing. Then rRNA was depleted using the Ribo-Zero rRNA Removal Kit (Bacteria) and prepared for RNAseq using the TruSeq Stranded mRNA Library Prep Kit (not including the poly(A) RNA purification step) (Illumina). RNA sequencing was performed on a single Hiseq2500 lane with 100 PE chemistry and dual indexing.

Table 3.1. Bacterial strains used in this Chapter.

Strain	Description	Source	Reference
4559	*S. pneumoniae s*erotype 14 ST15	Blood	Amin et al, 2015
947	*S. pneumoniae s*erotype 14 ST15	Ear	Amin et al, 2015
4534	*S. pneumoniae s*erotype 14 ST15	Blood	Amin et al. 2015
51742	*S. pneumoniae s*erotype 14 ST15	Ear	Amin et al, 2015
180/15	*S. pneumoniae s*erotype 3 ST180	Blood	Trappetti et al, 2013
180/2	*S. pneumoniae s*erotype 3 ST180	Ear	Trappetti et al, 2013
D39 *ΔadhE*	*S. pneumoniae* serotype 2 with *adhE* deletion		This study
180/15 *ΔadhE*	*S. pneumoniae s*erotype 3 ST180 with *adhE* deletion		This study
180/2 *ΔadhE*	*S. pneumoniae s*erotype 3 ST180 with *adhE* deletion		This study
180/4	*S. pneumoniae s*erotype 3 ST180	Blood	This study
180/9	*S. pneumoniae s*erotype 3 ST180	Ear	This study
232/1	*S. pneumoniae s*erotype 3 ST232	Blood	Trappetti et al, 2013
232/11	*S. pneumoniae s*erotype 3 ST232	Ear	Trappetti et al, 2013

Demultiplexing was then performed, assigning reads to their corresponding samples, generating one FASTQ sequence file per sample. Finally, a quality check was performed on the FASTQ files using FASTQC (Andrews and Babraham Bioinformatics, 2010).

3.2.3 Bioinformatics analysis

Read counts were obtained utilising Galaxy Australia provided by the Research Computing Centre, University of Queensland, Australia. FASTQ reads of 4559 and 947 and 180/15 and 180/2 were mapped to the assembled reference genome of the other strain within each clonal lineage, using BWA-MEM version 1.1.3 (Li, 2013). Read counts for each gene were then determined using SAMTools version 0.1.18 (Li et al., 2009), and differentially expressed genes (DEG) were quantified using Degust version 4.1.1 (Powell et al., 2019). Genes were filtered for DEG Fold Change (FC) > 2 and FDR (false discovery rate) < 0.01.

3.2.4 Quantitative real time RT-PCR

Differences in levels of gene expression were validated by qRT-PCR in a Roche LC480 real-time cycler essentially as described previously (Mahdi et al., 2008). The specific

primers used for the various genes are listed in **Table 3.2** and were used at a final concentration of 200 nM per reaction. As an internal control, primers specific for 16S rRNA were employed. Amplification data were analysed using the comparative critical threshold cycle ($2^{-\Delta\Delta CT}$) method (Livak and Schmittgen, 2001).

Table 3.2. Oligonucleotide primers used in this Chapter.

Primer	Sequence (5′→3′)	Reference
TreP F	CCAGTCCTTGTTGCAGTCTG	This study
TreP R	CGCATCAGACACAACCAACA	This study
WbbI F	ATCCAGCTGATGAGGAGGAC	This study
WbbI R	CGATTGGCTTCCTCCAAACT	This study
Gtf2 F	GTCACTTTCCGTATTGCAGC	This study
Gtf2 R	GCCTGTAGCAACTCATTACTGT	This study
EpsJ_4 F	CGCTTTGATGATGAAGCAAC	This study
EpsJ_4 R	CCTGTAGGATATCCTGTACCCA	This study
ScrB F	CGACCGTACTGCCTACATGA	This study
ScrB R	GAAGGCTTGAGTTGCATAGG	This study
TreR F	CTGTCTCTCCTCCAAGAGGA	This study
TreR R	GGACCACCTTCCAAACCATC	This study
NanA_3 F	ATGTTCCCAGAAGGTCGAGC	This study
NanA_3 R	CTATAGCCAGGTTCTGTTGG	This study
GmuE F	CGTGCCAATGTACTTCACAA	This study
GmuE R	CCACACCACCGATAAACTCA	This study
BioY2 F	TCCAATTGGACCTGTTCCCT	This study
BioY2 R	CCTGCAGTAGGGCCAACTAA	This study
SpxB F	CCGTGTTGGTTGGAAACCAG	This study
SpxB R	CTTGACCAGCATCACCAAGG	This study
lytA_7 F	CTCGCTGAGTGTTGCTTATG	This study
lytA_7 R	CCTGAGCCAGAAGAAACAGC	This study
Dus F	GGATAATGAAATGCTTGCTCG	This study
Dus R	AGCACCAGTTGCTGCACCTT	This study
AcpB F	TTGATCCACGGACAAGTAGC	This study
AcpB R	GCAAGAATATTGGCTGCAGC	This study
NanE F	GCATTCGCGCAAATTCTGTG	This study
NanE R	GACTGTTGTTCCGCATTCTAC	This study
ArcC1 F	CTGTTGTAACGCAAGTTGTCG	This study
ArcC1 R	TGGTGAGGCAACGACCTTAC	This study
SorC F	CGTGTGGATGCTGCAATCGA	This study
SorC R	CAAGTGTCAAGCCATCTGCA	This study
RpiR F	CCAAGAGATGATTCGTGAGA	This study
RpiR R	CACGCTCAGCAGTTTCTATC	This study
NatA F	GAGTATTGAATGGCTGGATGG	This study
NatA R	CGTTGCTTCATGCCTAAGGA	This study
BoGH2 F	CGTTGGTATTCAGGAAGTGG	This study
BoGH2 R	CCTGTTACAGCATGACCACC	This study

PflB F	GGACGTATCATCGGTGTTTACG	This study
PflB R	CCAGGCGAACAACTTGTTGC	This study
Gtf F	GGTCATTCTCGATAGGGAGA	This study
Gtf R	AGTCAACCTTATCTGCATTGG	This study
BglH_2 F	ATCAAGGCCATGCGAGATGC	This study
BglH_2 R	CTTGCTACGTTTGAGAGTCC	This study
LacD F	TTGCCAGACTGCTTGGATGT	Trappetti et al, 2017
LacD R	ACTCAGAACCGATGCGTTCG	Trappetti et al, 2017
GalT F	GGTGTAGGAGCAATCAGTCT	Trappetti et al, 2017
GalT R	GCATCACCAATTGACATCCA	Trappetti et al, 2017
AdhR F	GCAGGAATTGGTGAGATAAA	This study
AdhR R	GTCCGATAAATTCGAGCAAT	This study
GlnP F	ACGTTCCCAACCTTCTCTGG	This study
GlnP F	CCGCCTCGAATAATCTCAGC	This study
Zwf F	GGTGTAGAAGAACGTGGTGG	This study
Zwf R	TCATCAGTTGGATGATAGAGG	This study
GlnR F	GACATGGATCGTCTGCTTGA	This study
GlnR R	GAGGAGTTCATTGTGAAGTGC	This study
AlsT F	GGAACCTTCACCCAAGTCAA	This study
AlsT R	GAGTCCACCAAAGACTGCAA	This study
LytN F	TGTAGCGCCTGTTGCAACAC	This study
LytN R	GGCTTCTGCTTCAGATCCGC	This study
ComF F	CTAACTCATTGGTCGAAGTCG	This study
ComF R	GCAACAACCCATCAGTTATTG	This study
GroL F	GCCAATAAAGAAGCTATCGC	This study
GroL R	TACTGTGAAAGGTAACCACGG	This study
PatB F	AACCCTCACAATCCTGGTGG	This study
PatB R	GGCACTGCTCAAGACGATAGC	This study
ArgG F	TGTCATTGATGTCAAGGACG	This study
ArgG R	GGTACAGCCATGAGCAATTG	This study
Ugd_2 F	CGCATAGTTGTTGGAGATGAG	This study
Ugd_2 R	GCTTAATTGCTTCTGCTTCAG	This study
SpeA F	CCTGCAAGGCAGGAGATAAG	This study
SpeA R	CCTTAGCATCTGGATGGTCC	This study
GmuA F	GTGGAGCAGCCAAATCATCC	This study
GmuA R	TGTGCGCTTCTACTAAGGAG	This study
PdhC F	CCAATGCGTAAGGTTATTGC	This study
PdhC R	CCAGTTGCTTCCATGATTGG	This study
Fhs1 F	CCATGTGACTGTTGGTCTTG	This study
Fhs1 R	GGCGTACGGTCATAGCGATA	This study
LytA_3 F	CCTGAGCAATCATCTATTCCT	This study
LytA_3 R	CGTTGCTGTTGAGGTAGTACC	This study
GuaA F	GAGACAGTAGAAGGAAGCGTG	This study
GuaA R	GGTGCTCGTCGATAGACTCA	This study
YusV F	GAGTCTTGGAAAAGATGACCTTG	This study
YusV R	CCAAGTAAGTAGTTGGCTCATC	This study
ComE F	CCTGTAGGTAGTCGAGTCAATG	This study
ComE R	GGCTAACTGCTTCTTCTCCA	This study

Eno_2 F	CTCGTGCTGCTGCTGACTAC	This study
Eno_2 R	CCAACTGGCAAGATCATGAAC	This study
PbpF_1 F	CATACCATGCAGTATGACAGC	This study
PbpF_1 R	CCAAGAACACGGTCAACCTT	This study
PurH F	CCGTGATGCAGATGCTGCTA	This study
PurH R	CTCACGGTTGAGGACGACAA	This study
ApbE F	GGTGCTGCCTCTAATCAATC	This study
ApbE R	CAGATTGATCAAGGCAGAAGT	This study
PaaI F	CGACCAAAGTAGTGAACTCG	This study
PaaI R	TGGTCAATACATCGTCGAGTT	This study
PspC F	TCGTCAAGTTCAGGCTCCTC	This study
PspC R	GGCTCTGGTTTAACCTCTGG	This study
Fba F	AGCTATCCACCTTGACCACG	This study
Fba R	CCACCGATAGTACCAACTTCA	This study
Nfr1 F	GCAGCAATCACTGGTGCTGT	This study
Nfr1 R	TGTCTGGATCTTGGTGAGCG	This study
RibF F	TGTTCCACCTGTAGAAGATGAG	This study
RibF R	GTACGACCACGAGCATTACC	This study
HemH F	CCAACACTTGGCAGAGTGAG	This study
HemH R	GTGGACGATGGTAGTTTACC	This study
DLDH F	ATGCTGCAAATCGTGGTATC	This study
DLDH R	CCGTAGCTACGAAGAAGTCC	This study
CapA F	CAGATGGGTGTTGAGTATCG	This study
CapA R	TTCAACCGTTTCAGATGGCT	This study
Pgk F	CCATTCGTGGCTATCCTTGG	This study
Pgk R	GAGTTACCGATTTCGATACC	This study
YdaF F	GTTAAGATAGACGAGGCTGA	This study
YdaF R	CCATGACACGACCTGAAGCT	This study
YbiV F	GGATGAATTAACATCTGACCTC	This study
YbiV R	GGAGGATATCAATGCAACCA	This study
CtsR F	GCTACATTCGTATAGGACGGA	This study
CtsR R	CCTGCTTGGTCATCAATTCC	This study
AdhB F	GCTGGTCTTGGTTATGTTCA	This study
AdhB R	CCAAGGCTTTGGCAACATTG	This study
PurL F	CGGTTATCGAAGCAACTGCT	This study
PurL R	ACCACCGATAGATGGCAAGC	This study
AdhE F	CCATGCCATGGTAGAGCTTG	This study
AdhE R	TGGCAGCATCCATTGGAGAC	This study
GapN F	ATTGGAGAACGTATTGGTCG	This study
GapN R	TGCAACGTTGTCCTGAGTAG	This study
PncB2 F	TACCAGACCTTGGTGGCGAC	This study
PncB2 R	CACGTTGCTGGTTCCATTGG	This study
Aadh_2 F	GCTCACTGTGAAGACGAAGG	This study
Aadh_2 R	TAGGCAGAATGTCTGACAGC	This study
PurC F	GCAGGTAAGGGAGTCTTGAA	This study
PurC R	GGAACCAGCAGTATAGTTGC	This study
Peb1A F	GGTCAAGATTCACTATGTGC	This study
Peb1A R	CCAGAAGCGTCTGTGTAGTA	This study

Rex F	CTTGGTCGTCGTGGTTTTGG	This study
Rex R	CAGGATGGTCGTCTAGGTCA	This study
CopY F	GCAGAGCGGTTTGACTGGTC	This study
CopY R	TCCCGACTTTGGTCTAGAG	This study
lmrA_1 F	CTTTGTCTCGGTTTGAATCG	This study
lmrA_1 R	CGTTCACCAACTTCAGTATCT	This study
CelA_3 F	GCAACAAAGTGCGACTGAAC	This study
CelA_3 R	CCTGCAATTTCTTTCACAGC	This study
TruC F	CCTGGAGATGTTTGCCAGTT	This study
TruC R	CGTTTGGTTGATTACCATGC	This study
MscL F	GGTGTTGTCATTGCCTCTGC	This study
MscL R	AGTTGAGCGATACGTTCGAC	This study
GlxK F	GTCTTGCCTGCTTCCGATCA	This study
GlxK R	GCAAACATAGTCGGATGTAGACC	This study
ManZ F	CAGCAACTATGGCTATCGCT	This study
ManZ R	AGCACCCATCATGAAGACAC	This study
YesO F	GCACAAGTCATGTGGGTTAG	This study
YesO R	CCTCCACCACTACGTACGTA	This study
UbiE F	CATATGCCTGATTTGGATGC	This study
UbiE R	CAGGTCTTCAGCGCTATAGAGA	This study
AgaC F	GGTGATCTGCCTACTGCTCT	This study
AgaC R	TCTGGACTGACTTTACCAGC	This study
lacE_1 F	GAATTCAGGAGCGTACGGAG	This study
lacE_1 R	CCATTCCTCTGGTAGCAACT	This study
CzcD F	GTAGCTGTTATCCTGATGGC	This study
CzcD R	CCACATTGTCCAATCGTTCC	This study
NanB F	GCACGTTATGGTGGGACTCA	This study
NanB R	CTCGTGGCCAGTAAACTAACT	This study
TabA F	CGAAGAAGCCATGGCTGTTAC	This study
TabA R	CGAACCTTGGGTTGATGTAA	This study
YxlF F	ACTGCGTCCATGGATACCTC	This study
YxlF R	CTCGCTACGCATAGCTAGAG	This study
J253	GAGGAGGATATATTTGAATACATACG	Trappetti et al, 2017
J254	TTATAATTTTTTTAATCTGTTATTTAAATA GTTTATAGTTA	Trappetti et al, 2017
adhE for	GAGATTCCTTATGACAAGAA	Trappetti et al, 2017
adhE Rev	TACTAGCTTATTATTCTAG	Trappetti et al, 2017
adhE spec for	AAATAACAGATTGAAGAAGGTATAATGTT TATCAGTCTAGAAG	Trappetti et al, 2017
adhE spec Rev	ACAAAGGATATCGTTCCTGAGGAGGATAT ATATGAATACATA	Trappetti et al, 2017

3.2.5 Mutagenesis

Transformation of the serotype 3 ST180 clinical isolates, 180/15 and 180/2, requires chromosomal DNA as the template, as previously described (Harvey et al., 2014, 2016). Hence in order to delete *rafK* in these strains, this mutation was first introduced into the

laboratory adapted D39 strain. A spectinomycin cassette PCR product flanked by *rafK* adjacent regions, was generated by overlap extension PCR as previously described (Morona et al., 2000). To achieve this, the relevant primers listed in **Table 3.2** were used to amplify *rafK* flanking products from 180/2 template DNA and to amplify the spectinomycin resistance cassette. D39 was transformed with the overlap extension PCR product, as previously described (Giammarinaro and Paton, 2002; Martin et al., 1995), and selected on spectinomycin containing BA plates. Transformants were confirmed by PCR and Sanger Sequencing. The construct used to make the 180/2 and 180/15 Δ*rafK* mutants were then generated in a two-step process, commencing with transformation with genomic DNA (gDNA) from D39 Δ*rafK*. After selection on BA plus spectinomycin, genomic DNA was extracted from one of the transformants for each of 180/2 and 180/15, and used as the donor in a second round of transformation of these strains. The transformation procedure itself was a modification of that developed previously for type 1 ST306 (Harvey et al., 2014). Strains 180/2 and 180/15 were grown overnight on BA and then inoculated into a 1:1 mixture of C+Y medium and Dulbecco's modified Eagle's medium (DMEM; Gibco, Grand Island, NY) supplemented with 10% heat-inactivated fetal calf serum (FCS). After 1 h at 37°C, the culture was diluted into fresh medium and incubated for a further 2 h at 37°C. Competence-stimulating peptide 1 (CSP-1) was added to achieve a concentration of 50 ng/ml, followed 15 min later by donor DNA (approximately 1 μg) of the appropriate 180/2 and 180/15 wild type strains. After a further 2 h of incubation at 37°C, transformation mixes were plated on BA plus spectinomycin.

3.2.6 Acetaldehyde assay

S. pneumoniae 180/15, 180/2 and respective Δ*rafK* strains were assessed for acetaldehyde production. Strains were cultured in C+Y medium until they reached an OD_{600} of 0.3, then acetaldehyde levels were measured using an aldehyde quantification kit (Abcam, England), according to the manufacturer's instructions. C+Y medium was used as a blank control.

3.2.7 Adherence and invasion assays

A549 and Detroit 562 cell lines were used for adherence assays. Cells were grown in Dulbecco's modified Eagle's medium (DMEM) supplemented with 10% fetal calf serum (FCS), in 75 cm^2 tissue culture bottles (Becton Dickinson) at 37ºC in a 5% CO_2 atmosphere. 2×10^5 cells were seeded into each well of a 24-well tissue culture trays (Becton Dickinson) for use in the adherence assays. The day prior to inoculation of pneumococcal cells to the tissue culture, the media was replaced with DMEM + 1% FCS in the 24-well seeded trays. *S. pneumoniae* strains 180/15, 180/2, 180/15 Δ*rafK* and 180/2 Δ*rafK* were used for adherence and invasion assays. 500 µl of each strain was inoculated onto washed A549 or Detroit 562 cells, at an OD_{600} of 0.2 in DMEM + 1% FCS in triplicate. After incubation for 2 hours at 37ºC, the wells were washed three times with PBS and cells were detached from the plate by treatment with 100 µl of 0.25% trypsin-0.02% EDTA and 400 µl of 0.1% triton x-100. Appropriate dilutions of the cultures were plated on BA to determine the number of adherent bacteria. Assays were performed in triplicate from two independent experiments. For quantitation of pneumococci that had invaded A549 and Detroit 562 cells, extracellular bacteria were killed through treatment with gentamicin (200 µg/ml) and penicillin G (10 µg/ml), before the addition of trypsin. Any intracellular pneumococci were then recovered after eukaryotic cell lysis, mediated by washing with 100µl of 0.25% trypsin-0.02% EDTA and 400µl of 0.1% triton x-100. 100 µl of neat samples were then plated neat on blood agar plates.

3.3 Results

3.3.1 Transcriptomic differences between serotype/ST-matched isolates

RNAseq analysis was performed on the serotype 14 ST15 blood and ear isolate (4559 and 947) and serotype 3 ST180 blood and ear isolate pairs (180/2 and 180/15). Strains were grown to mid-exponential phase in CDM+Glc and CDM+Gal, or exposed to human serum for 2 h. 6 replicates for each blood and ear isolate strain were sequenced after growth in each of three media (see Section 3.2.1 and 3.2.2). Multidimensional scaling (MDS) plots indicate the level of variation (i.e. pairwise distance between the fold change values for each gene) between each sample of the blood and ear isolates. The first dimension of each MDS plot represents a greater amount of the total variation than the second dimension, which represents more variation than the third dimension, and so on (**Figure 3.1**). Essentially, the MDS plots provide a visual representation of the similarities or distances in the FC of each gene, between samples. Each sample in the MDS plot is signified as a coloured dot, with increasing transcriptomic variation between samples represented the further apart samples are from each other. In CDM+Glc, the serotype 14 ST15 947 samples were grouped mostly together except for one replicate, and the same was the case for 4559 (**Figure 3.1A**), while over 45% of the variation was represented in the 1st MDS dimension (**Figure 3.1B**). All 947 replicates were closely grouped together in CDM+Gal while only 1 replicate for 4559 differed extensively from the rest (**Figure 3.1C**). Almost 90% of all variation seen between these samples were represented in the 1st MDS dimension (**Figure 3.1D**). In human serum, 2 replicates from 947 showed more variation compared to the rest, while for 4559 all but 1 of the replicates were grouped close together (**Figure 3.1E**). Here, over 55% of all the variation between these samples is represented in the 1st dimension (**Figure 3.1F**).

Appendices K and L list the pneumococcal genes that were significantly differentially expressed (fold change (FC) > 2, false discovery rate (FDR) < 0.01) between each of the blood and ear isolate pairs, in the 3 different media. No genes were found to be commonly differentially expressed between both the serotype 14 ST15 and serotype 3 ST180 blood and ear isolate pairs, with a FDR cut off of < 0.01. The differentially expressed gene (DEG) analysis between the serotype 14 ST15 4559 and 947 strains (**Appendix K**), found 21 genes to be significantly upregulated for 947, in CDM+Glc, including *nanA* (FC = 2.19, FDR = 0.0012) and a Sucrose-6-phosphate hydrolase (*scrB*) (FC = 2.9, FDR = 0.00025). Conversely, 7 genes were significantly upregulated for 4559 in this media, including pyruvate oxidase (*spxB*) (FC = 6.95, FDR = 4.27×10^{-8}). In CDM+Gal, 19 genes were upregulated for 947, including *scrB* (FC = 2.85, FDR = 0.00015) and a CPS synthesis positive regulator (*acpB*) (FC = 2.38, FDR < 0.0027). For 4559, 30 genes were upregulated in CDM+Gal, including *spxB* (FC = 6.01, FDR = 2.2×10^{-6}) and the Galactose-1-phosphate uridylyltransferase (*galT*) (FC = 4.15, FDR = 0.00021). Lastly, in human serum, 18 genes were upregulated in 947 which included *scrB* (FC = 6.66, FDR = 2.49×10^{-8}), while 4559 contained 5 genes that were upregulated, including *spxB* (FC = 3.44 FDR = 2.87×10^{-7}). This analysis shows that metabolic genes were heavily differentially regulated between 4559 and 947, highlighting the role of metabolism in influencing the variation seen between these two clonally matched strains.

For the serotype 3 ST180 samples grown in CDM+Glc, 180/2 replicates were grouped together within dimension 1 but were separated in dimension 2, while 180/15 had two replicates that varied from the rest on dimension 2 (**Figure 3.2A**). Almost 50% of its variation was represented in the 1st MDS dimension (**Figure 3.2B**). The replicates for both 180/2 and 180/15 were closely grouped together in the 1st dimension, respectively, but were separated along the 2nd dimension (**Figure 3.2C**). Over 40% of the variation seen between these samples were represented in the 1st MDS dimension (**Figure 3.2D**). In human serum,

both 180/2 and 180/15 samples were grouped closely together in both dimensions, except for 1 sample from both groups (**Figure 3.2E**). Over 45% of all the variation between these samples were represented in the 1st dimension (**Figure 3.2F**). Outliers within the 1st MDS dimension for each group may need to be excluded to increase chances of obtaining statistically significant DEGs.

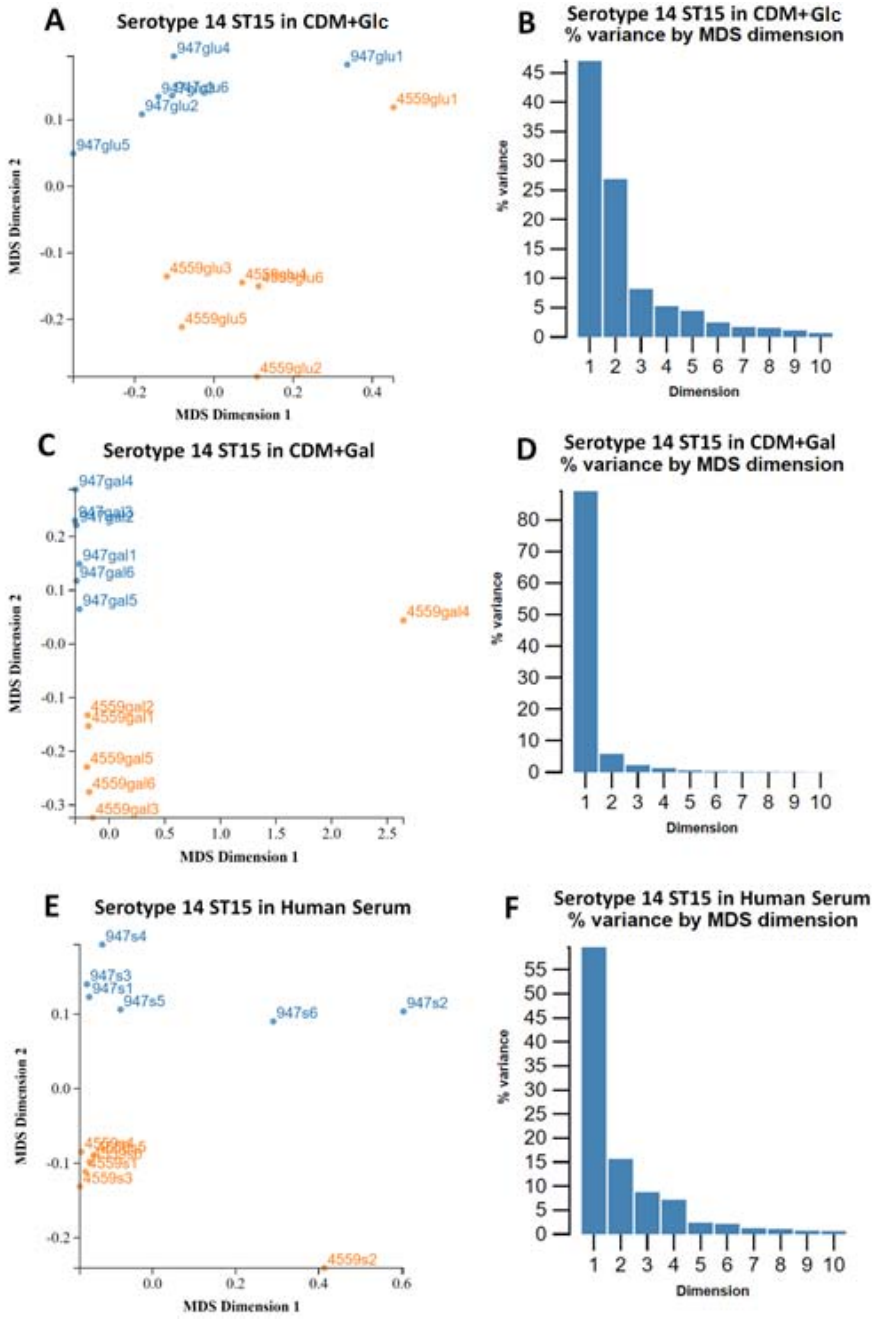

Figure 3.1. MDS plots illustrate the variation between each individual sample used in the RNA sequencing of the serotype 14 ST 15 blood and ear isolate pair, 4559 and 947. (**A**, **C**, **E**) Each dot represents a sample, with the dots closer together indicating less variation. 947 samples are represented as 947glu1-6, 947gal1-6 and 947s1-6, while 4559 samples are represented as 4559glu1-6, 4559gal1-6 and 4559s1-6. (**B**, **D**, **F**) The percentage of variance that each dimension represents is indicated in each column.

For the serotype 3 ST180 strains, the DEG analysis between the blood and ear isolate (**Appendix L**) showed that in CDM+Glc, 44 genes were upregulated in 180/2, including the Glucose-6-phosphate 1-dehydrogenase (*zwf*) (FC = 3.25, FDR = 1.32×10^{-6}). For 180/15 in CDM+Glc, 52 genes were upregulated including the dihydrolipoamide dehydrogenase *DLDH* (FC = 2.52, FDR = 1.44×10^{-7}) and the alcohol dehydrogenase (*adhE*) (FC = 3.51, FDR = 4.23×10^{-5}). In CDM+Gal 35 genes were upregulated in 180/2, which included the transcriptional repressor of the cop operon (*copY*) (FC = 2.48, FDR = 0.0070) and *zwf* (FC = 2.24, FDR = 5.80×10^{-5}). On the other hand, 180/15 in CDM+Gal contained 61 upregulated genes, including the penicillin binding protein (*pbpF_1*) (FC = 2.08, FDR = 5.48×10^{-8}), *DLDH* (FC = 2.21, FDR = 0.00052) and *adhE* (FC = 4.64, FDR = 2.09×10^{-6}). In human serum, 180/2 contained 88 genes that were upregulated which included the autolysin (*lytA*) (FC = 2.27, FDR = 0.00039). 180/15 had 55 genes upregulated in human serum, including the catabolite control protein A (*ccpA*) (FC = 2.19, FDR = 0.0052) and *DLDH* (FC = 6.61, FDR = 6.42×10^{-9}). Similar to the serotype 14 ST 15 DEG data, this analysis shows that metabolic genes were heavily differentially regulated between 180/2 and 180/15, again highlighting the role of metabolism in influencing the variation seen between these two clonally matched strains.

3.3.2 Serotype 14 ST 15 blood and ear isolate validation

To validate the data from the RNA sequencing analysis of the serotype 14 ST15 isolates, qRT-PCR (4559 and 947) was performed on fresh sample preparations, on genes that were significantly differentially expressed (FC > 2, FDR < 0.01) (**Table 3.3**). Similar to the RNAseq analysis, a FC > 2 and p value < 0.01 cut off was used to categorise genes significantly differentially expressed for the qRT-PCR validations. Hypothetical genes were omitted from the qRT-PCR validations, while only a single gene from an operon was validated if more than one gene from an operon was significantly differentially expressed

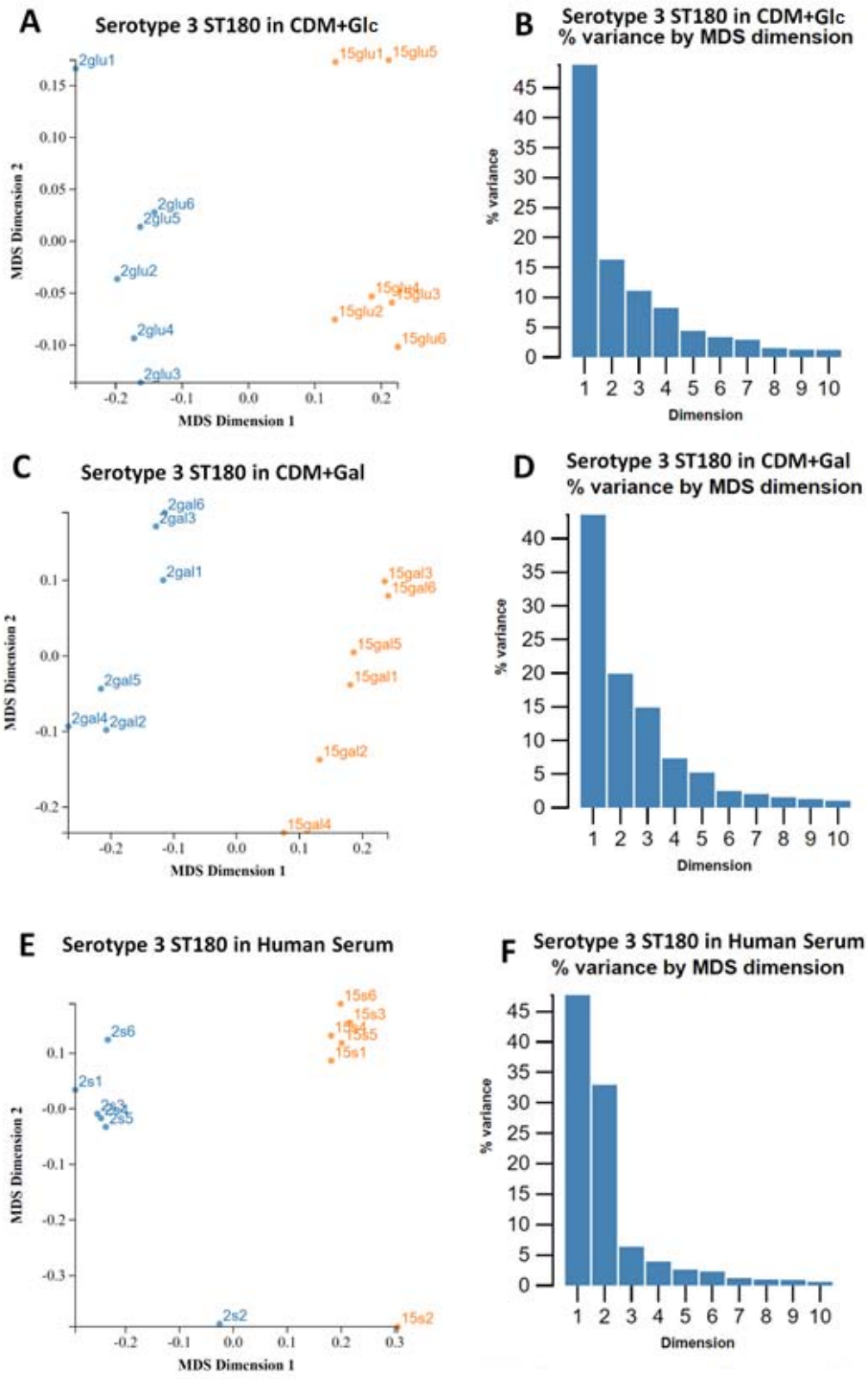

Figure 3.2. MDS plots illustrate the variation between each individual sample used in the RNA sequencing of the serotype 3 ST180 blood and ear isolate pair 180/15 and 180/2. (**A**, **C**, **E**) Each dot represents a sample, with the dots closer together indicating less variation. 180/2 samples are represented as 2glu1-6, 2gal1-6 and 2s1-6, while 180/15 samples are represented as 15glu1-6, 15gal1-6 and 15s1-6. (**B**, **D**, **F**) The percentage of variance that each dimension represents is indicated in each column.

in the RNASeq data. In CDM+Glc, 5 genes were significantly upregulated in the ear isolate 947 (*treP*, *wbbI*, *gtf2*, *scrB* and *treR*) while 3 genes were significantly upregulated in the blood isolate 4559 (*pflB*, *bglH_2*, *spxB*) which corresponded with the RNAseq data. In CDM+Gal, 5 genes were significantly upregulated in 947 (*treP*, *lytA_7*, *dus*, *acpB* and *arcC1)* while 7 genes were significantly upregulated in 4559 (*pflB*, *gtf*, *lacD*, *galT*, *exoA*, *adhR* and *spxB*).

The metabolic genes *wbbi*, *treR* and *gtf2* were significantly upregulated in 947 in CDM+Glc (**Table 3.3**) and human serum (only *wbbi* and *gtf2*) (**Appendix K**), but not in CDM+Gal. Hence, these genes are only upregulated in the blood mimicking environments. Conversely, *lytA_7*, *dus*, *acpB* and *arcC1* were significantly upregulated in 947, while *gtf1*, *lacD*, *galT*, *exoA* and *adgR* were significantly upregulated in 4559, in the nasopharynx mimicking environment CDM+Gal but not in CDM+Glc

Table 3.3. Fold change and significance (FDR or *p* value, for RNAseq and qRT-PCR, respectively) of 947 vs 4559 genes after growth in CDM+Glc or CDM+Gal for 2 h. Genes with FC greater than 2 and FDR < 0.01 in RNAseq are shown, with genes upregulated in the ear isolate 947 indicated by grayscale. For qRT-PCR, genes highlighted in blue = statistically significantly (p < 0.01) upregulated (FC > 2) in 947, while values highlighted in pink = statistically significantly (p < 0.01) upregulated (FC > 2) in 4559.

Locus tag in 947	Product	Media	RNAseq FDR	RNAseq FC	qRT-PCR *p* value	qRT-PCR FC
Sp947_chr_01629	TreP	Glu	4.99E-07	10.16	0.000643	7.65
Sp947_chr_01671	WbbI	Glu	3.30E-08	4.57	0.000931	3.25
Sp947_chr_01664	Gtf2	Glu	4.31E-09	4.56	0.008975	3.98
Sp947_chr_01674	EpsJ_4	Glu	3.84E-08	3.74	0.005638	1.76
Sp947_chr_01630	ScrB	Glu	0.000246	2.90	0.007442	2.34
Sp947_chr_01788	TreR	Glu	0.001066	2.61	0.029658	2.11
Sp947_chr_01600	NanA_3	Glu	0.001146	2.19	0.063962	1.66
Sp947_chr_01628	GmuE	Glu	0.007833	2.14	0.034275	1.83
Sp947_chr_00722	BioY2	Glu	0.005284	2.49	0.045262	2.27

Sp947_chr_00440	PflB	Glu	2.96E-05	3.16	0.003386	2.96
Sp947_chr_00679	BglH_2	Glu	0.002146	3.97	0.007221	2.68
Sp947_chr_00675	SpxB	Glu	4.72E-08	6.95	0.000848	7.49
Sp947_chr_01629	TreP	Gal	0.002858	24.5	7.63E-05	19.71
Sp947_chr_00502	lytA_7	Gal	0.002688	7.40	0.004363	8.62
Sp947_chr_00491	Dus	Gal	0.004584	7.14	0.000024	5.49
Sp947_chr_01630	ScrB	Gal	0.000152	2.85	0.076927	2.36
Sp947_chr_00065	AcpB	Gal	0.002688	2.38	0.003604	2.73
Sp947_chr_00840	NanE	Gal	9.87E-05	2.25	0.037128	1.65
Sp947_chr_02095	ArcC1	Gal	0.002442	2.21	0.009428	2.19
Sp947_chr_00066	SorC	Gal	0.004824	2.07	0.036572	1.77
Sp947_chr_00839	RpiR	Gal	0.000128	2.03	0.083943	1.32
Sp947_chr_00924	NatA	Gal	0.00857	2.00	0.053629	1.93
Sp947_chr_00594	BoGH2	Gal	0.000211	2.11	0.146262	1.28
Sp947_chr_00440	PflB	Gal	0.000229	2.21	0.001242	2.53
Sp947_chr_00023	Gtf	Gal	0.00102	2.46	0.008316	2.44
Sp947_chr_00679	BglH_2	Gal	0.001418	2.9	0.052783	2.64
Sp947_chr_01104	LacD	Gal	6.09E-06	3.74	0.003901	4.32
Sp947_chr_00119	GalT	Gal	3.93E-05	4.15	0.009235	3.67
Sp947_chr_00111	ExoA	Gal	0.000229	4.58	0.000372	3.65
Sp947_chr_00123	AdhR	Gal	8.98E-05	4.78	0.004718	4.93
Sp947_chr_00675	SpxB	Gal	2.18E-06	6.01	0.000272	5.88

To determine if other serotype 14 blood and ear isolate pairs shared the same expression differences, another serotype 14 ST15 blood (4534) and ear (51742) isolate pair, which showed similar differential virulence profiles as 4559 and 947 (Amin et al., 2015), were grown in CDM+Glc and CDM+Gal and tested via qRT-PCR for differential expression (**Table 3.4**). The scale of expression differences between this strain pair was much lower

than for 4559 vs 947. None of the tested genes showed significant differential expression at $p < 0.01$ that corresponded with the genes differentially expressed between 947 and 4559. Nevertheless, *wbbI*, *scrB*, *spxB*, *dus*, *pflB*, *lacD*, *galT* and *adhR* all showed consistent trends in common with 947 and 4559, without reaching statistical significance or FC cut off.

Table 3.4. Fold change and significance (*p* value) of 51742 vs 4534 genes after growth in CDM+Glc or CDM+Gal for 2 h. Genes with FC greater than 2 and *p* value < 0.01, as determined by qRT-PCR, are shown. FC values highlighted in blue = upregulated (not significantly) in the ear isolate 51742, while values highlighted in pink = upregulated (not significantly) in the blood isolate 4534. Genes upregulated in the ear isolate 947, compared to 4559 in the RNAseq data, indicated by grayscale.

Locus tag in 947	Product	Media	qRT-PCR *p* value	qRT-PCR FC
Sp947_chr_01629	TreP	Glu	0.185306	0.44
Sp947_chr_01671	WbbI	Glu	0.062863	1.53
Sp947_chr_01664	Gtf2	Glu	0.092957	0.79
Sp947_chr_01630	ScrB	Glu	0.038215	1.71
Sp947_chr_00440	PflB	Glu	0.375024	0.28
Sp947_chr_00679	BglH_2	Glu	0.145827	0.55
Sp947_chr_00675	SpxB	Glu	0.035284	1.42
Sp947_chr_01629	TreP	Gal	0.074102	1.01
Sp947_chr_00502	lytA_7	Gal	0.255832	0.32
Sp947_chr_00491	Dus	Gal	0.061592	1.48
Sp947_chr_00065	AcpB	Gal	0.072358	1.23
Sp947_chr_02095	ArcC1	Gal	0.345923	0.26
Sp947_chr_00440	PflB	Gal	0.084772	1.62
Sp947_chr_00023	Gtf	Gal	0.468193	0.04
Sp947_chr_01104	LacD	Gal	0.042957	1.73
Sp947_chr_00119	GalT	Gal	0.086372	0.85
Sp947_chr_00111	ExoA	Gal	0.152735	0.74
Sp947_chr_00123	AdhR	Gal	0.096313	0.49
Sp947_chr_00675	SpxB	Gal	0.077948	1.12

3.3.3 Serotype 3 ST 180 blood and ear isolate validation

To validate the data from the RNA sequencing analysis of the serotype 3 ST180 isolates, qRT-PCR (180/2 and 180/15) was performed on genes that were significantly differentially expressed (FC > 2, FDR < 0.01) (**Table 3.5**). Similar to the RNAseq analysis, a FC > 2 and *p* value < 0.01 cut off was used to categorise genes as significantly differentially expressed for the qRT-PCR validations. As with the serotype 14 ST 15 qRT-PCR validations, hypothetical genes were omitted from the qRT-PCR validations, while only a single gene from an operon was validated if more than one gene from an operon was significantly differentially expressed in the RNASeq data. In CDM+Glc, 6 genes were significantly upregulated in the ear isolate 180/2 (*glnP*, *zwf*, *lytN*, *comF*, *argG* and *speA*) while 16 genes were significantly upregulated in the blood isolate 180/15 (*guaA*, *pbpF_1*, *pspC*, *nfr1*, *hemH*, *DLDH*, *pgk*, *ydaF*, *ctsR*, *adhB*, *purL*, *adhE*, *gapN*, *pncB2*, *aadh_2* and *purC*) which corresponded with the RNAseq data. In CDM+Gal, 6 genes were significantly upregulated in 180/2 (*peb1A*, *glnR*, *groL*, *copY*, *gmuA* and *glnP*) while 14 genes were significantly upregulated in 180/15 (*pbpF_1*, *ribF*, *DLDH*, *agaC*, *adhB*, *czcD*, *nanB*, *comE*, *nadE*, *walK*, *yxlF*, *hemH*, *adhE* and *adh_2*).

For 180/2, *comF*, *speA* and *argG* were upregulated in CDM+Glc but not in CDM+Gal, while *argG* was also upregulated in human serum. For 180/15, genes that were upregulated in both CDM+Glc and human serum, but not in CDM+Gal, include; *guaA*, *aadH_2* (only in CDM+Glc), and *purL*. On the other hand, the solitary gene upregulated in only CDM+Gal for 180/2 was *copY*, while *agaC*, *nanB* and *yxlF* were upregulated in 180/15 in CDM+Gal.

Table 3.5. Fold change and significance (FDR or *p* value, for RNAseq and qRT-PCR, respectively) of 180/2 vs 180/15 genes after growth in CDM+Glc or CDM+Gal for 2 h. Genes with FC greater than 2 and FDR < 0.01 in RNAseq are shown, with genes upregulated in the ear isolate 947 indicated by grayscale. For qRT-PCR, genes highlighted in blue = statistically significantly (p < 0.01) upregulated (FC > 2) in 180/2, while values highlighted in pink = statistically significantly (p < 0.01) upregulated (FC > 2) in 180/15.

Locus tag in 180/2	Product	Media	RNAseq FDR	RNAseq FC	qRT-PCR *p* value	qRT-PCR FC
Sp180_2_chr_00600	GlnP	Glu	1.71E-07	6.28	0.000048	7.89
Sp180_2_chr_01196	Zwf	Glu	1.3E-06	3.25	0.004621	3.22
Sp180_2_chr_00511	GlnR	Glu	8.7E-05	2.93	0.008513	1.76
Sp180_2_chr_00438	AlsT	Glu	7.43E-07	2.92	0.038602	2.48
Sp180_2_chr_00152	LytN	Glu	0.00266	2.76	0.002837	2.42
Sp180_2_chr_02133	ComF	Glu	0.01515	2.55	0.007522	3.27
Sp180_2_chr_01821	GroL	Glu	0.00056	2.47	0.039636	1.36
Sp180_2_chr_01433	PatB	Glu	2.7E-05	2.31	0.017834	1.82
Sp180_2_chr_00159	ArgG	Glu	0.00826	2.3	0.005287	3.44
Sp180_2_chr_00203	Ugd_2	Glu	0.02178	2.08	0.023661	2.27
Sp180_2_chr_00888	SpeA	Glu	0.01817	2.03	0.008254	2.18
Sp180_2_chr_01941	GmuA	Glu	0.00399	2.02	0.037288	1.74
Sp180_2_chr_01125	PdhC	Glu	1.3E-06	2.01	0.019579	2.65
Sp180_2_chr_01183	Fhs1	Glu	0.00297	2.01	0.074643	1.83
Sp180_2_chr_01339	LytA_3	Glu	3.90E-08	2.02	0.052788	1.55
Sp180_2_chr_02004	GuaA	Glu	0.00279	2.03	0.006742	3.46
Sp180_2_chr_01740	PucK	Glu	0.00032	2.04	0.088329	1.42
Sp180_2_chr_01007	YusV	Glu	1.58E-07	2.05	0.029335	2.12
Sp180_2_chr_00925	ComE	Glu	0.00145	2.07	0.009186	1.89
Sp180_2_chr_01113	Eno_2	Glu	0.00309	2.07	0.061145	1.47
Sp180_2_chr_01928	PbpF_1	Glu	6.29E-07	2.08	0.007493	3.91
Sp180_2_chr_00102	PurH	Glu	0.02127	2.08	0.026429	2.12

Sp180_2_chr_01387	ApbE	Glu	2.1E-05	2.16	0.057617	1.86
Sp180_2_chr_01743	PaaI	Glu	0.00011	2.26	0.082825	1.39
Sp180_2_chr_02116	PspC	Glu	1.4E-06	2.33	0.006519	2.04
Sp180_2_chr_00598	Fba	Glu	0.0002	2.45	0.016345	2.37
Sp180_2_chr_01389	Nfr1	Glu	0.00017	2.47	0.001527	4.82
Sp180_2_chr_01095	RibF	Glu	2.37E-07	2.48	0.026611	1.93
Sp180_2_chr_00979	HemH	Glu	2.37E-07	2.48	0.008274	2.31
Sp180_2_chr_01124	DLDH	Glu	1.44E-07	2.52	0.003621	2.59
Sp180_2_chr_01372	CapA	Glu	3.66E-07	2.53	0.022548	2.04
Sp180_2_chr_00509	Pgk	Glu	0.00031	2.62	0.005369	3.36
Sp180_2_chr_01341	YdaF	Glu	3.90E-09	2.73	0.001582	2.42
Sp180_2_chr_01371	YbiV	Glu	1.51E-07	2.88	0.046273	2.25
Sp180_2_chr_02121	CtsR	Glu	1.19E-09	2.97	0.000739	3.86
Sp180_2_chr_02082	AdhB	Glu	2.6E-05	3.24	0.005783	3.02
Sp180_2_chr_00097	PurL	Glu	0.0002	3.36	0.009825	2.81
Sp180_2_chr_01942	AdhE	Glu	4.2E-05	3.51	0.006623	2.44
Sp180_2_chr_01105	GapN	Glu	9.7E-06	3.60	0.005982	3.17
Sp180_2_chr_01343	PncB2	Glu	1.13E-09	3.60	0.000417	3.52
Sp180_2_chr_01971	Adh_2	Glu	1.3E-06	4.57	0.003821	3.96
Sp180_2_chr_00096	PurC	Glu	5.12E-07	4.75	0.000832	5.11
Sp180_2_chr_01194	GlnP	Gal	2.2E-05	3.42	0.007189	2.86
Sp180_2_chr_00602	Peb1A	Gal	2.5E-05	3.42	0.000351	3.30
Sp180_2_chr_00511	GlnR	Gal	7.65E-07	3.15	0.004724	2.73
Sp180_2_chr_01077	Rex	Gal	1.3E-05	2.83	0.032782	2.15
Sp180_2_chr_01821	GroL	Gal	1.8E-05	2.69	0.001753	3.09
Sp180_2_chr_00152	LytN	Gal	0.004	2.54	0.026168	2.36
Sp180_2_chr_00706	CopY	Gal	0.007	2.48	0.008249	2.79

Sp180_2_chr_01435	lmrA_1	Gal	1.8E-05	2.37	0.026822	1.84
Sp180_2_chr_01941	GmuA	Gal	0.00192	2.27	0.009302	2.69
Sp180_2_chr_01196	Zwf	Gal	5.8E-05	2.24	0.047295	2.13
Sp180_2_chr_00600	putative GlnP	Gal	0.0009	2.24	0.009327	2.67
Sp180_2_chr_01940	CelA_3	Gal	0.00101	2.23	0.016280	2.08
Sp180_2_chr_01433	PatB	Gal	1.2E-06	2.02	0.072602	1.93
Sp180_2_chr_00980	MscL	Gal	0.0002	2.03	0.037278	1.88
Sp180_2_chr_00509	Pgk	Gal	0.01028	2.03	0.089768	1.63
Sp180_2_chr_01007	YusV	Gal	3.7E-05	2.05	0.016229	2.21
Sp180_2_chr_01111	GlxK	Gal	0.00011	2.05	0.012267	1.92
Sp180_2_chr_01928	PbpF_1	Gal	5.48E-08	2.08	0.006411	2.49
Sp180_2_chr_00924	YdaF	Gal	7.65E-07	2.08	0.052721	2.13
Sp180_2_chr_00373	ManZ	Gal	0.00069	2.1	0.029983	2.02
Sp180_2_chr_01595	YesO	Gal	0.01301	2.11	0.061589	1.77
Sp180_2_chr_01372	CapA	Gal	0.00011	2.15	0.014671	2.14
Sp180_2_chr_01095	RibF	Gal	0.00044	2.15	0.008216	2.50
Sp180_2_chr_00598	Fba	Gal	0.00321	2.15	0.026180	1.84
Sp180_2_chr_02116	PspC	Gal	3.9E-06	2.16	0.016522	2.11
Sp180_2_chr_01961	UbiE	Gal	0.00167	2.19	0.036111	1.73
Sp180_2_chr_01124	DLDH	Gal	0.00052	2.21	0.006184	2.35
Sp180_2_chr_00372	AgaC	Gal	0.00969	2.26	0.003357	3.18
Sp180_2_chr_00490	lacE_1	Gal	0.00254	2.42	0.027915	2.04
Sp180_2_chr_02082	AdhB	Gal	3.4E-06	2.45	0.002418	2.52
Sp180_2_chr_01389	Nfr1	Gal	0.00096	2.53	0.012671	2.13
Sp180_2_chr_01749	CzcD	Gal	0.02412	2.54	0.006828	3.44
Sp180_2_chr_01592	NanB	Gal	0.0018	2.64	0.009716	2.78
Sp180_2_chr_00925	ComE	Gal	2.05E-07	2.70	0.004162	2.46

Sp180_2_chr_01105	GapN	Gal	0.00037	2.73	0.024617	2.22
Sp180_2_chr_01342	NadE	Gal	1.5E-05	2.78	0.000883	3.49
Sp180_2_chr_01596	TabA	Gal	0.00399	2.81	0.016712	2.31
Sp180_2_chr_02121	CtsR	Gal	1.16E-08	2.96	0.010593	2.53
Sp180_2_chr_02118	WalK	Gal	5.48E-08	3.09	0.005344	3.05
Sp180_2_chr_01908	YxlF	Gal	1.5E-06	3.53	0.008625	3.18
Sp180_2_chr_00979	HemH	Gal	4.45E-07	4.25	0.009259	3.66
Sp180_2_chr_01942	AdhE	Gal	2.1E-06	4.64	0.000723	5.21
Sp180_2_chr_01971	Adh_2	Gal	0.00714	4.84	0.003782	4.87

To further validate the genes that were shown to be consistently significantly differentially expressed between 180/2 and 180/15 in both the RNAseq and qRT-PCR analyses, two other serotype 3 blood (180/4 and 232/1) and ear (180/9 and 232/11) isolate pairs, which showed similar differential virulence profiles as 180/2 and 180/15 (Trappetti et al., 2013), were grown in CDM+Glc or CDM+Gal and tested by qRT-PCR for differential expression (**Table 3.6**). From all tested genes, only *adhE* showed significant differential expression that corresponded for all three of the tested serotype 3 blood and ear isolate pairs.

Table 3.6. Fold change and significance (*p* value) of 180/4 vs 180/9 and 232/1 vs 232/11 genes, detected by qRT-PCR after growth in CDM+Glc or CDM+Gal for 2 h. FC values highlighted in blue = upregulated (not significantly) in the ear isolates 180/9 (A) or 232/11 (B), while values highlighted in pink = upregulated (not significantly) in the blood isolates 180/4 (A) or 232/1 (B). Genes upregulated in the ear isolate 180/2, compared to 180/15 in the RNAseq data, indicated by grayscale. Genes highlighted in yellow = statistically significantly ($p < 0.01$) upregulated (FC > 2) in 180/15 from the qRT-PCR.

Locus tag in 180/2	**Product**	**Medi a**	**(A) 180/4 vs 180/9**		**(B) 232/1 vs 232/11**	
			***p* value**	**FC**	***p* value**	**FC**
Sp180_2_chr_00600	GlnP	Glu	0.082274	0.97	0.023831	1.42
Sp180_2_chr_01196	Zwf	Glu	0.016376	1.51	0.009782	1.86
Sp180_2_chr_00152	LytN	Glu	0.096385	0.71	0.62467	0.28
Sp180_2_chr_02133	ComF	Glu	0.082755	2.26	0.271744	0.81

Sp180_2_chr_00159	ArgG	Glu	0.064521	1.32	0.002352	2.36
Sp180_2_chr_00888	SpeA	Glu	0.218174	0.63	0.582124	0.21
Sp180_2_chr_02004	GuaA	Glu	0.072628	0.93	0.008176	2.22
Sp180_2_chr_01928	PbpF_1	Glu	0.817126	0.13	0.325177	0.42
Sp180_2_chr_02116	PspC	Glu	0.042722	1.54	0.072823	1.19
Sp180_2_chr_01389	Nfr1	Glu	0.082659	1.08	0.021746	2.51
Sp180_2_chr_00979	HemH	Glu	0.271933	0.74	0.045171	1.23
Sp180_2_chr_01124	DLDH	Glu	0.046268	1.61	0.082796	0.85
Sp180_2_chr_00509	Pgk	Glu	0.019518	2.25	0.41677	1.42
Sp180_2_chr_01341	YdaF	Glu	0.152167	0.32	0.612871	0.05
Sp180_2_chr_02121	CtsR	Glu	0.093514	0.63	0.000739	1.14
Sp180_2_chr_02082	AdhB	Glu	0.036162	1.84	0.061884	1.42
Sp180_2_chr_00097	PurL	Glu	0.0002	3.36	0.009825	2.81
Sp180_2_chr_01942	AdhE	Glu	0.008192	2.47	0.0024728	3.13
Sp180_2_chr_01105	GapN	Glu	0.453829	0.11	0.062516	1.28
Sp180_2_chr_01343	PncB2	Glu	0.071599	1.78	0.129332	0.59
Sp180_2_chr_01971	Adh_2	Glu	0.246621	0.26	0.092687	0.94
Sp180_2_chr_00096	PurC	Glu	0.073928	1.16	0.076928	1.63
Sp180_2_chr_01194	GlnP	Gal	0.021559	2.06	0.056222	1.32
Sp180_2_chr_00602	Peb1A	Gal	0.092147	0.44	0.855186	0.03
Sp180_2_chr_00511	GlnR	Gal	0.023577	1.26	0.062774	0.75
Sp180_2_chr_01821	GroL	Gal	0.015825	1.84	0.249019	0.21
Sp180_2_chr_00706	CopY	Gal	0.007343	1.49	0.039582	0.93
Sp180_2_chr_01941	GmuA	Gal	0.100693	0.26	0.266912	0.31
Sp180_2_chr_00600	putative GlnP	Gal	0.098687	0.51	0.620516	0.16
Sp180_2_chr_01928	PbpF_1	Gal	0.007684	1.92	0.045814	1.76

Sp180_2_chr_01095	RibF	Gal	0.081599	0.42	0.040014	1.04
Sp180_2_chr_01124	DLDH	Gal	0.252068	0.17	0.089226	0.86
Sp180_2_chr_00372	AgaC	Gal	0.015967	2.14	0.023458	1.49
Sp180_2_chr_02082	AdhB	Gal	0.063882	1.14	0.092444	0.77
Sp180_2_chr_01749	CzcD	Gal	0.866832	0.06	0.351451	0.36
Sp180_2_chr_01592	NanB	Gal	0.039282	1.18	0.016399	1.25
Sp180_2_chr_00925	ComE	Gal	0.000816	3.17	0.032617	1.83
Sp180_2_chr_01342	NadE	Gal	0.184993	0.42	0.0012561	2.32
Sp180_2_chr_02118	WalK	Gal	0.062882	1.16	0.042771	0.98
Sp180_2_chr_01908	YxlF	Gal	0.872816	0.08	0.096838	0.55
Sp180_2_chr_00979	HemH	Gal	0.025683	1.93	0.004651	1.22
Sp180_2_chr_01942	AdhE	Gal	0.006122	3.62	0.003103	2.79

3.3.4 Effect of *adhE* deletion on serotype 3 ST180 pneumococci

As the serotype 14 ST15 qRT-PCR validation failed to show any consistently differentially regulated genes under the stringent conditions, and aldehyde-alcohol dehydrogenase E (*adhE*) was the only gene to be shown to be consistently differentially expressed between the tested serotype 3 ST 180 and ST 232 blood and ear isolate pairs, *adhE* was analysed for its effect on these strains. Subsequently, *adhE* was deleted from 180/15 and 180/2 (see Section 3.2.5). AdhE has previously been shown to catalyse the reaction between ethanol and NAD^+ to form acetaldehyde and NADH in the serotype 2 strain D39 (Luong et al., 2015). To test if AdhE levels impacted the ability of the serotype 3 ST180 strains to produce acetaldehyde, an acetaldehyde assay was performed on 180/15, 180/2 and their respective *adhE* deletion mutants, with or without ethanol supplementation. In the presence of ethanol, acetaldehyde levels were significantly higher compared to when no ethanol was added (180/15, $p < 0.05$; 180/2, $p < 0.001$; 180/15 Δ*adhE*, $p < 0.001$; 180/2 Δ*adhE*, $p <$

0.0001). However, there was no significant difference in acetaldehyde production between the wild type and *adhE* deletion strains (**Figure 3.3).**

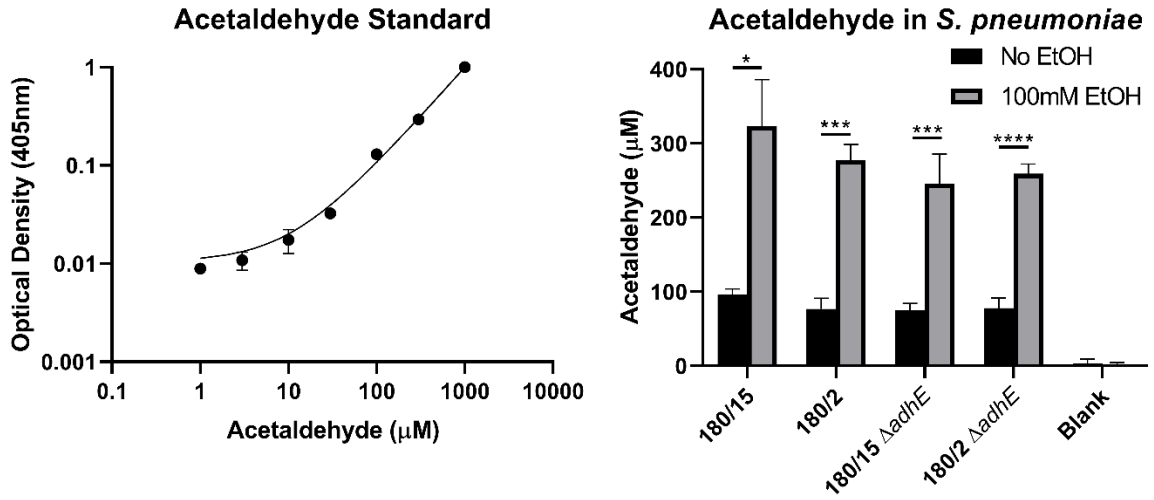

Figure 3.3. *S. pneumoniae* 180/15, 180/2 and respective Δ*adhE* strains were cultured until an OD_{600} of 0.3, and then *adhE* was induced through supplementation with 100 mM ethanol for 30 min. Bacterial cultures were analysed for acetaldehyde (sees section 3.2.6). Data are representative of two independent experiments and were analysed by one-way ANOVA (*, $p < 0.05$; ***, $p < 0.001$; ****, $p < 0.0001$).

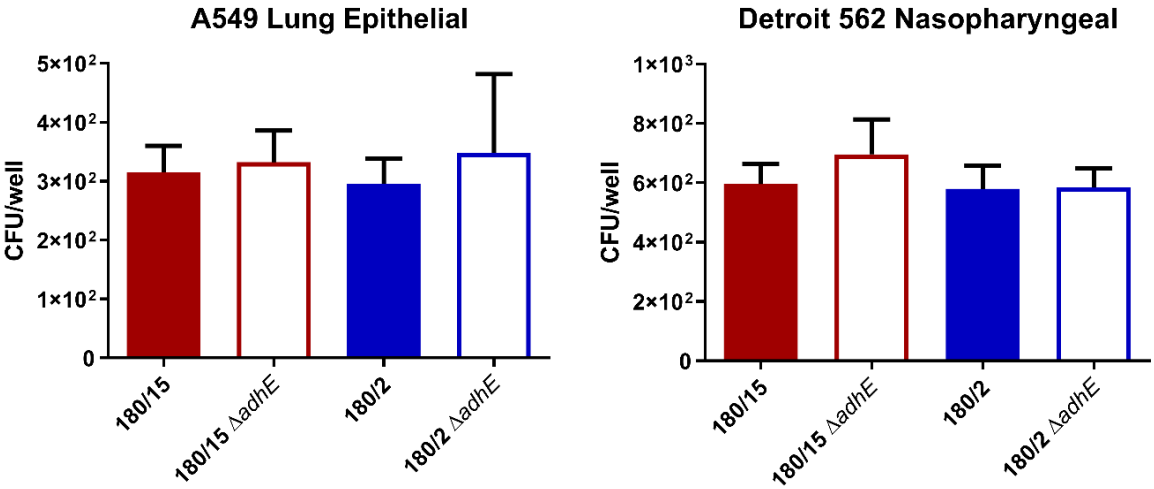

Figure 3.4. Impact of *adhE* deletion on adherence to A549 and Detroit 562 cells. *S. pneumoniae* strains 180/15, 180/2, 180/15 Δ*adhE* and 180/2 Δ*adhE* were inoculated at OD_{600} = 0.2 onto A549 or Detroit 562 monolayers in DMEM + 10% FCS, in triplicate, then tested for adherence after 2 h at 37 °C (see Section 3.2.7). Invasion assays were also performed on these cell lines and bacterial strains, although no bacteria were recovered after eukaryotic cell lysis (see section 3.2.7). Data presented are the means ± standard deviations from two independent experiments.

It has previously been shown that LAP, the alcohol acetaldehyde dehydrogenase of *Listeria monocytogenes* increases adherence by binding to the host-cell receptor HSP60 (Burkholder et al., 2009; Jagadeesan et al., 2010). Consequently, AdhE was examined for potential effects on host adherence and invasion. Adherence assays were performed on

human lung epithelial A549 and nasopharyngeal Detroit 562 cells. No significant difference was found in the adherence of 180/15 or 180/2 when compared to their respective *adhE* deletion mutants to either A549 or Detroit 562 cell lines (**Figure 3.4**), while no strains were found to invade either cell line

3.4 Discussion

The *S. pneumoniae* serotype 14 ST15 and serotype 3 ST 180 blood and ear isolate pairs were subjected to Illumina HiSeq 2500 transcriptomic sequencing after growth and/or incubation in CDM+Glc, CDM+Gal or human serum media. Each medium was selected to represent a particular biological niche, with CDM+Glc and human serum both mimicking conditions in the blood (McMillin, 1990), while CDM+Gal mimicked conditions in the nasopharynx (Blanchette et al., 2016). Hence, performing RNAseq in these media was intended to provide clues as to which pathways might be upregulated in these particular niches *in vivo*. Under each of these conditions, the transcriptomes of each of the isolate pairs were aligned to identify any DEGs, as these genes may be influencing the capacity of the bacteria to spread to distinct sites in the body. It is worth noting that the variation in levels of complement proteins and antibodies in the human sera was not provided, which could have potentially affected transcription levels.

Similar to the genomic analysis in Chapter 2, the serotype 14 ST15 and serotype 3 ST180 blood and ear isolates shared no common differentially regulated genes or pathways. This underscores the vast genetic and transcriptomic diversity between the unrelated serotype and sequence type matched pairs. However, the stringent FC (> 2) and FDR (< 0.01) conditions and sample outliers from the RNAseq analysis highlighted in the MDS plots (**Figures 3.1 and 3.2**) may have excluded many DEGs from consideration. Future analyses of these data should consider easing the FDR cut off to < 0.05 and removing data from the 1st dimension sample outliers identified in the MDS plots (see section 3.3.1).

For each blood and ear isolate pair, several genes were found to be significantly differentially regulated within one or more of the tested media. This suggests that there are large amounts of transcriptomic variation between strains, even within the same serotype and ST, which underscores the transcriptomic complexity and diversity of *S. pneumoniae*.

Many of the identified differentially expressed genes are involved in carbohydrate and amino acid metabolism, including *scrB*, *galT*, *zwf*, *ccpA*, *glnP*, *purC* and *artM*. This further highlights the importance of pneumococcal metabolic activity as a potential driver of virulence capabilities.

A handful of genes were found to be significantly differentially regulated in media that mimicked one anatomical niche only; either the blood mimicking conditions (CDM+Glc and human serum) or the nasopharyngeal mimicking condition (CDM+Gal). For example, the metabolic genes *wbbi*, *treR* and *gtf* were significantly upregulated in 947 in the blood mimicking conditions, and may play adverse roles for survival in the blood, as 947 is unable to invade the blood via the respiratory tract. Gtf genes have been identified in other *Streptococcus* species to promote and modify biofilm structures, presupposing a tendency for sessile growth not suitable in the blood (Xu et al., 2018), and hence *gtf* may be worth examining in the future. This may also be the case for *comF*, *speA, zwf* and *glnP* in the serotype 3 ST 180 background, as these genes were upregulated in blood mimicking conditions in the ear isolate 180/2. Indeed, *glnP* and *zwf* have been shown to be important for pneumococcal spread into the blood in IN murine models via *glnR* regulation, which was also shown to be upregulated in 180/2 in CDM+Glc, though this gene was under the FC > 2 cut-off (Härtel et al., 2011; Hendriksen et al., 2008).

Conversely, *guaA*, *aadH_2* and *purL* may be beneficial for the survival of 180/15 in the blood as these genes were upregulated in the blood isolate in both blood mimicking conditions. Accordingly, *purL* has been identified as a virulence gene through signature-tagged mutagenesis and invasive murine models (Polissi et al., 1998) potentially warranting further examination. CDM+Gal is a nasopharynx mimicking medium, hence any genes upregulated by the blood and ear isolate pairs may aid in colonisation of the nasopharynx. However, this is unlikely, as there is not any significant difference between

the blood and ear isolates in terms of capacity to colonise the nasopharynx (see section 2.3.4).

Genes that were found to be significantly differentially expressed in the RNAseq data were independently validated in fresh RNA extracts using qRT-PCR. However, this analysis was confined to CDM+Glc and CDM+Gal owing to limited availability of human serum. Probability value was used to determine significance here, rather than false discovery rate, as was previously used in the RNAseq analysis, as the qRT-PCR validated individual genes separately rather than in groups. Of the 31 genes that were found to be significantly differentially expressed in CDM+Glc or CDM+Gal for the serotype 14 ST15 pair in the RNAseq data, 19 of these genes were also consistently significantly differentially expressed in the independent qRT-PCR dataset. Similarly, for the serotype 3 ST180 pair, of the 85 genes that were significantly differentially expressed in the RNAseq data, 42 genes were also significantly differentially expressed in the independent qRT-PCR dataset. It is worth noting that many of the genes that were not significantly differentially expressed in the qRT-PCR dataset, still showed the same trends in relative gene expression to the RNAseq data set, just without passing the FC > 2 and/or $p < 0.01$ thresholds. Hence, the RNAseq data matches up closely with the qRT-PCR, further validating the whole transcriptome sequencing approach.

A limitation of this study is that only specific individual clinical isolates were used in the RNAseq analysis, with no certainty that any significant differences found between the blood and ear isolates would be representative of other *S. pneumoniae* blood and ear isolate pairs. Therefore, to further validate the gene regulation patterns found in the RNAseq data, qRT-PCR tested the expression of these genes in different blood and ear isolate pairs of the same serotype and sequence type. This ensured that any significant gene regulatory patterns found in the RNAseq data were widespread and present among other pneumococci that occupy the same virulence niche (i.e. blood or ear isolate). These additional strains tested

were the serotype 14 ST15 blood isolate 4534 and ear isolate 51742, serotype 3 ST180 blood isolate 180/4 and ear isolate 180/9, and the serotype 3 ST232 blood isolate 232/1 and ear isolate 232/11. Of all the genes that were tested with qRT-PCR in these other serotype- and sequence type-matched blood and ear isolate pairs, only acetaldehyde alcohol dehydrogenase (*adhE*) was found to be consistently significantly upregulated in the serotype 3 blood isolate 180/15 compared to the ear isolate 180/2, in the RNAseq and qRT-PCR analyses. This was found in both CDM+Glc and CDM+Gal.

AdhE is an alcohol dehydrogenase which plays a role in ethanol oxidation, allowing the conversion of alcohol to aldehyde through the reduction of NAD^+ to NADH (Walker, 1992). In serotype 2 *S. pneumoniae* D39, AdhE has been shown to catalyse the reaction between ethanol and NAD^+ to form acetaldehyde and NADH (Luong et al., 2015). Hence *adhE* was deleted in 180/2 and 180/15 in frame, then an acetaldehyde assay was performed to examine the role of this gene in acetaldehyde production (**Figure 3.3**). No significant difference was found between the *adhE* deletion mutants relative to their respective wild type strains. This suggests that there may be another complementary or redundant alcohol dehydrogenase present within the serotype 3 ST180 blood and ear isolate pair sequences. Indeed, there are four other annotated alcohol dehydrogenases present in the 180/2 and 180/15 genomes; Sp180_2_chr_00335, Sp180_2_chr_01747, Sp180_2_chr_01971 and Sp180_2_chr_02082. Although it would be interesting to test the impact of these other alcohol dehydrogenase genes on acetaldehyde production, this is beyond the scope of the project.

The lack of difference in acetaldehyde production between the wild-type and *adhE* deletion mutants above also suggests AdhE could serve an alternative role in these strains. For example, an alcohol acetaldehyde dehydrogenase in the Gram-positive pathogen *Listeria monocytogenes* increases adherence by binding to the host-cell receptor HSP60 (Burkholder et al., 2009; Jagadeesan et al., 2010). Thus, alcohol dehydrogenases in *S.*

pneumoniae may contribute to pneumococcal virulence by aiding adherence to respiratory epithelium. Accordingly, A549 and Detroit 562 adherence and invasion assays were performed on the 180/2 and 180/15 *adhE* deletion mutants. However, no significant differences in either parameter were found in either of the *adhE* mutants compared to their respective wild types. It is important to note however, that the thick CPS of these serotype 3 strains (Geno et al., 2015) likely impedes pneumococcal adherence to host cells *in vitro* as adherence factors may be masked. Any potential effects of *adhE* deletion *in vivo*, where the CPS could be differentially regulated, remains to be investigated. However, given the lack of evidence that AdhE effects acetaldehyde production and adherence *in vitro*, there was not sufficient justification to perform *in vivo* murine experiments as part of this study.

The raffinose pathway genes that were affected by the *rafR* and *rafK* SNPs found in Chapter 2 (see also Minhas et al. (2019), were not found to be significantly differentially expressed in the RNAseq data for both serotypes. However, this is expected due to the carbon catabolite control that silences expression of lesser utilised sugar pathways when preferred carbohydrate sources, such as glucose or galactose, are present (Iyer et al., 2005). Nevertheless DLDH, which has been found to interact with RafK to potentially regulate raffinose transport (Tyx et al., 2011), was significantly upregulated in the blood isolate 180/15 relative to the ear isolate 180/2 in both CDM+Glc and CDM+Gal. This may potentially contribute to 180/15's superior ability to utilise raffinose. Only 7 differentially expressed genes from the serotype 3 ST180 and 1 gene from serotype 14 ST15 RNAseq analyses contained SNPs that were highlighted in the genomic variant analyses in Chapter 2 (Sp180_2_chr_00100, Sp180_2_chr_00449, Sp180_2_chr_00512, Sp180_2_chr_01172, Sp180_2_chr_01194, Sp180_2_chr_01387, Sp180_2_chr_01404 and Sp947_chr_01631). Therefore, the majority of genes that were significantly differentially expressed according to the RNAseq data were not impacted by inherent differences in coding regions between the blood and ear isolates. This is not surprising, as it would not be expected for a SNP in

a given gene to impact transcription, unless present within regulatory regions or genes, although the protein product itself may be compromised.

As *adhE* was the only gene found to be commonly significantly differentially expressed between multiple serotype 3 blood and ear isolate pairs, and none were found for the serotype 14 ST 15 pairs, additional omics analyses should be used to elucidate differences between the blood and ear isolate pairs that were not picked up in the RNAseq data. Indeed, metabolomic and proteomic profiling for the serotype 14 ST15 and serotype 3 ST180 blood and ear isolates is currently being conducted by the Antibiotic Resistant Sepsis Pathogens Framework Initiative consortium. Future analysis of these data sets may uncover other mechanisms that influence how pneumococci survive in and spread around the body. Moreover, it may be worth revisiting virulence factor genes that showed differential expression without reaching statistical significance in the transcriptomic analyses, such as *nanA* for the serotype 14 ST 15 isolate pair (section 3.3.2) or *lytA* for the serotype 3 ST 180 isolate pair (section 3.3.3), if future analyses also highlight the products of these genes as potential determients of pneumococcal tissue tropism. Unfortunately, all related metabolomic and proteomic data, and associated analyses, are scheduled to be completed after the time frame of this PhD project.

Chapter 4

In vivo dual RNA analysis of *S. pneumoniae* Clonal Clinical Isolates

4.1 Introduction

This Chapter incorporates data published in *Communications Biology* (Minhas et al., 2020). This work was done in collaboration with the laboratory of Jan-Willem Veening at the University of Lausanne, Switzerland, who carried out the dual RNAseq analyses.

Chapter 2 of this thesis highlighted the impact of *rafR* regulation on disease progression in the serotype 14 ST15 blood and ear isolate pair, 4559 and 947. However, the mechanisms causing the *rafR* SNP to alter tissue tropism were not elucidated. These mechanisms presumably involve a combination of altered bacterial gene expression patterns and differences in host response elicited by such alterations. Unfortunately, the data in Chapter 3 enabled only limited conclusions to be drawn, as *in vitro* RNAseq analyses of cells grown in CDM+Raf were not performed, as the *in vitro* transcriptomic sequencing was carried out prior to identification of raffinose regulation as an important factor in pneumococcal disease progression. Due to catabolite repression of the raffinose operon in CDM+Glc or CM+Gal media (used for the *in vitro* RNAseq analyses), any impact of differential expression of the *raf* genes between isolate pairs would have been masked, and thus the data did not show any consistent results in terms of raffinose related genes. This highlights the pitfalls associated with trying to mimic conditions of distinct *in vivo* niches by growth of bacteria in different defined media or in human serum, rather than using the *in vivo* niches themselves. In order to circumvent this, Chapter 4 describes the application of a

novel RNA sequencing approach involving bacterial RNA isolation directly from *in vivo* niches.

Our laboratory has developed significant expertise in extraction of bacterial RNA from various infected mouse tissues, permitting transcriptional analysis under genuine *in vivo* conditions, initially using qRT-PCR and microarray analysis, and more recently by RNAseq (Mahdi et al., 2008; Minhas et al., 2020; Ogunniyi et al., 2012; Trappetti et al., 2011). Through initial discussion with Professor Veening, it became apparent that the yield and quality of *in vivo* RNA extracts, at least for lung tissue, should be sufficient to apply the newly developed dual RNAseq technology, which applies deep sequencing to simultaneously quantify genome-wide transcriptional responses of host and pathogen (Westermann et al., 2017; Wolf et al., 2018). This approach offers higher efficiency and more restricted technical bias compared to conventional approaches, such as assaying single species or array-based methods. Here, dual RNAseq analysis has been used to examine host-pathogen transcriptional cross-talk in the blood and ear isolates and *rafR*-swapped derivatives thereof, during the early stages of infection.

4.2 Materials and Methods

4.2.1 Bacterial strains and growth conditions

S. pneumoniae strains used in this Chapter are listed in **Table 4.1**. Cells were routinely grown in SB or plated on BA as required, then incubated at 37ºC in 5% CO_2 overnight (see section 2.2.1).

Table 4.1. Bacterial strains used in this Chapter.

Strain	Description	Source	Reference
4559	*S. pneumoniae s*erotype 14 ST15	Blood	Amin et al, 2015
947	*S. pneumoniae s*erotype 14 ST15	Ear	Amin et al, 2015
$4559^{947rafR}$	4559 expressing 947 *rafR* gene	Blood	Minhas et al, 2019
$947^{4559rafR}$	947 expressing 4559 *rafR* gene	Ear	Minhas et al, 2019

$4559^{947rafR}$ = 4559M | $947^{4559rafR}$= 947M

4.2.2 Intranasal challenge of mice and extraction of RNA

Animal experiments were approved by the University of Adelaide Animal Ethics Committee. Groups of 12 outbred 5-6-week-old female Swiss (CD-1) mice (48 in total), were anesthetized by intraperitoneal injection of pentobarbital sodium (Nembutal) and challenged intranasally (IN) with 50 µl of bacterial suspension containing approximately 1 × 10^8 CFU in SB of 4559, 947, $4559^{947rafR}$ (designated 4559M) or $947^{4559rafR}$ (designated 947M). The challenge dose was confirmed retrospectively by serial dilution and plating on BA. Mice were euthanized by CO_2 asphyxiation at 6 h and lungs placed in 1 ml TRIzol (Thermo Fisher). RNA was then extracted using acid-phenol-chloroform-isoamyl alcohol (125:21:1; pH 4.5; Ambion) and purified using the RNeasy minikit (Qiagen). For subsequent dual RNAseq analyses, there were three replicates per strain, with each replicate derived from the lungs of four mice.

4.2.3 RNA library preparation and sequencing

RNA quality was checked using chip-based capillary electrophoresis. Samples were then simultaneously depleted of murine and pneumococcal ribosomal RNAs by dual rRNA-

depletion as previously described (Aprianto et al., 2016). Stranded cDNA library preparation was performed according to the prescribed protocol (Illumina, US). Sequencing was performed for twelve samples in one lane of an Illumina NextSeq 500, High Output Flowcell in 85 single end mode. Libraries were demultiplexed and analysed further. Raw libraries are accessible at https://www.ncbi.nlm.nih.gov/geo/ with the accession number GSE123982.

4.2.4 Sequence data analysis

Quality of raw libraries was checked (FastQC v0.11.8, Babraham Bioinformatics, UK) (Andrews and Babraham Bioinformatics, 2010). In order to improve the quality of alignment, reads were trimmed using the following criteria: (i) removal of adapter sequence, if any, based on TruSeq3-SE library, (ii) removal of low quality leading and trailing nucleotides, (iii) a five-nucleotide sliding window was created for surviving reads, in which the average quality score must be above 20 and (iv) minimum remaining length must be above 50 (Trimmomatic v0.38) (Bolger et al., 2014). The quality of trimmed reads was confirmed using FastQC (Andrews and Babraham Bioinformatics, 2010).

As reference genomes, chimeric genomes were created by concatenating the in-house generated *S. pneumoniae* strain 947 or 4559 circular genomes (deposited with ENA under the accession numbers SAMEA5092021 and SAMEA5092022) into the genome of *Mus musculus* (ENSEMBL, release 94, downloaded 9 October 2018). The corresponding annotation file was downloaded at the same time. The chimeric mouse/947 genome was used as reference to align libraries from lungs infected by strain 947 (and its corresponding swap mutant 947M), while the mouse/4559 chimeric genome was used to align 4559 and 4559M libraries. Alignment was performed by RNA-STAR (v2.6.0a) (Dobin et al., 2013) with the following options: (i) alignIntronMax 1 and (ii) sjdbOverhang 84. The aligned reads were then summarized (featureCount v1.6.3) according to the chimeric annotation

file in stranded, multimapping (-M), fractionized (--fraction) and overlapping (-O) modes (Liao et al., 2014). In order to compare gene expression between strains from ear and blood isolate backgrounds, we prepared a common pneumococcal annotation file using Mauve v20150226 (Darling et al., 2004). Common genes between 947 and 4559 were defined as having common coverage at least 90% and identity at least 90%. This single-pass alignment was selected to minimise false discovery rate. However, due to this approach, the summarising process had to be adjusted, taking into account the overlapping nature of bacterial genes and their organisation into operon structures.

Pathogen and host libraries were then analysed separately in R (R v3.5.2). Since reads coming from pneumococcal genes encoding bacterial rRNA dominate the pathogen libraries (average 64.5%; range 61.4 to 67.3%), these pneumococcal ribosomal RNA reads were excluded from downstream analysis, but this was not required for murine ribosomal RNA reads due to effective eukaryotic rRNA depletion. Differential gene analysis was performed by DESeq2 v1.22.1 (Love et al., 2014) and genome-wide fold change was calculated within host and pathogen libraries for the pairwise comparisons: strains 947 to 947M, strains 947 to 4559, strains 947 to 4559M, strains 947M to 4559, strains 947M to 4559M and strains 4559 to 4559M. The value of fold change was set to zero if the corresponding adjusted p-value (*padj*) was reported to be not available (NA).

4.2.5 Quantitative real time RT-PCR

Differences in levels of gene expression observed in the dual RNAseq data were validated by one-step relative quantitative real-time RT-PCR (qRT-PCR) in a Roche LC480 real-time cycler essentially as previously described (Mahdi et al., 2008). The same RNA that was used for the dual RNAseq was used in the qRT-PCR experimental validation. 19 pneumococcal genes and 18 murine genes were chosen for the experimental validation. The murine intranasal challenge and RNA isolation was also repeated to test the

reproducibility of the dual RNAseq data. 6 pneumococcal and 6 murine genes were chosen for the reproducibility validation. The specific primers used for the various genes are listed in **Table 4.2** and were used at a final concentration of 200 nM per reaction. As an internal control, primers specific for *gyrA* for pneumococcal genes, and GAPDH for murine genes, were employed. Amplification data were analysed using the comparative critical threshold ($2^{-\Delta\Delta C_T}$) method (Livak and Schmittgen, 2001).

Table 4.2. Oligonucleotide primers used in this Chapter.

Primer	Sequence (5' → 3')	Reference
rafR F:	CCAGCCATTCGTGATACATA	Minhas et al, 2019
rafR R:	CCTCCAGTGATTCCTAACCA	Minhas et al, 2019
aga F:	AAGGTCAGAATGGTCCACAG	Minhas et al, 2019
aga R:	GCTGGAAAATCAGCCATAAA	Minhas et al, 2019
rafG F:	CCTATGGCAGCCTACTCCATC	Minhas et al, 2019
rafG R:	GGGTCTGTGGAATCGCATAGG	Minhas et al, 2019
rafK F:	GCTGGTTTACGTTCCAAGAA	Minhas et al, 2019
rafK R:	GCTGGTTTACGTTCCAAGAA	Minhas et al, 2019
Sp947_00054 F:	GCAAGACAGACTACGAAGCAG	This study
Sp947_00054 R:	TCCTCAATCCCATGAGCTC	This study
Sp947_00279 F:	GTGGCACTTGCGAATACTGT	This study
Sp947_00279 R:	GGATCAAGTCCGTCAGGAAC	This study
Sp947_00544 F:	CTGTTCGAGCCTCGTAACTC	This study
Sp947_00544 R:	CGTGGAAGGTGGATATTCTC	This study
Sp947_00675 F:	CCGTGTTGGTTGGAAACCAG	This study
Sp947_00675 R:	CTTGACCAGCATCACCAAGG	This study
Sp947_00841 F:	GGTTGCGTTGACTGGTAGTT	This study
Sp947_00841 R:	CCAATACCAGCTTCTGCTCC	This study
Sp947_01448 F:	ACAGCTCCAGCTATGAAGGG	This study
Sp947_01448 R:	AGACTGAGCCCCATAAGATG	This study
Sp947_01582 F:	GTCAACTGTGCAGGTCTTGC	This study
Sp947_01582 R:	GCTCCATCCTGCATATGCAT	This study
Sp947_01598 F:	GTTCGATTGCTATCGATGGT	This study
Sp947_01598 R:	CATCATATTCTTGGGTAACGC	This study
Sp947_01629 F:	CCAGTCCTTGTTGCAGTCTG	This study
Sp947_01629 R:	CGCATCAGACACAACCAACA	This study
Sp947_01798 F:	CGAGATATCGCTGCTGAGTA	This study
Sp947_01798 R:	CAAACGCTCTGTTCTGGAAC	This study
Sp947_01920 F:	TCCATGGATACCTCAACTCG	This study
Sp947_01920 R:	CTAGAGGCGTCGTATCTCGA	This study
Sp947_01951 F:	AATGGTCATTCCAGAAGCAG	This study
Sp947_01951 R:	CTTCTTGGATAAGCAGGTGTC	This study
Sp947_01955 F:	CCATGCCATGGTAGAGCTTG	This study
Sp947_01955 R:	TGGCAGCATCCATTGGAGAC	This study
Sp947_01982 F:	AGGCAAGCAGTACAGGCAAC	This study
Sp947_01982 R:	GTCCTGCTTGATTTCGACAG	This study
Sp947_02097 F:	CATTCTTGCTCCTCTCCAAG	This study

Sp947_02097 R:	GATTGATCATGAGACCTGCG	This study
ENSMUSG00000063021 F:	CTGCTTGCCTCTTCCTGACAT	This study
ENSMUSG00000063021 R:	ATTGGTCTAGGTGCAATGCTTC	This study
ENSMUSG00000068855 F:	AAGTGACGATCGCACAGGG	This study
ENSMUSG00000068855 R:	CGTGTTGAGTTTCACTTGCTCT	This study
ENSMUSG00000063954 F:	AACTACGCGGAGCGTGTGG	This study
ENSMUSG00000063954 R:	CGCGTCTTCTTGTTGTCGC	This study
ENSMUSG00000034855 F:	TAAACTCATGGCACCGGCAT	This study
ENSMUSG00000034855 R:	GGCATTTGGCAGCTTTACCC	This study
ENSMUSG00000048806 F:	GCACTGGGTGGAATGAGACT	This study
ENSMUSG00000048806 R:	GTGGAGAGCAGTTGAGGACA	This study
ENSMUSG00000074695 F:	AGCTGCTTGGGCTTCATAAC	This study
ENSMUSG00000074695 R:	CCCCTGCAATCACCTAATCC	This study
ENSMUSG00000000157 F:	CACCTGGCTCCTTGGAGAG	This study
ENSMUSG00000000157 R:	AGCCAAGTGGAAATCGTTGT	This study
ENSMUSG00000017300 F:	AGGAACTGGCTGAGTGCTTC	This study
ENSMUSG00000017300 R:	GCTCCATCTGCTCTCAGGTC	This study
ENSMUSG00000030730 F:	CCTCCCTACCTTGATGCCAG	This study
ENSMUSG00000030730 R:	GGAAGGGTCAAGGCTTCAGG	This study
ENSMUSG00000026407 F:	CATGAGGACCTGAGGTGCAG	This study
ENSMUSG00000026407 R:	CTGGTTTGACTCTGCTGGCT	This study
ENSMUSG00000026985 F:	GCCATGTCTTCTCAAAGCAAT	This study
ENSMUSG00000026985 R:	TGAACCCTGTAGTTTCTGGGAG	This study
ENSMUSG00000061928 F:	GGCACTGGCATAGCCTCATA	This study
ENSMUSG00000061928 R:	TTCCAGAGACTACCCCACCC	This study
ENSMUSG00000063130 F:	CCCTCCACGGGACTTTGTC	This study
ENSMUSG00000063130 R:	CAATGACCCCCAGCTCTACT	This study
ENSMUSG00000030046 F:	GCATGACCCTTTGCTGGTTG	This study
ENSMUSG00000030046 R:	CCAGATCCTGCTCATGGGTG	This study
ENSMUSG00000033765 F:	ACAAGCTCCAACTCGTCGTC	This study
ENSMUSG00000033765 R:	CTCCAGATGGCACAGCATCC	This study
ENSMUSG00000028001 F:	CTGCACCCGTTTCCTAACCT	This study
ENSMUSG00000028001 R:	CACATGGTCAAGTCCCTGCC	This study
ENSMUSG00000033860 F:	TGGAGAGACTCCAGGGATAC	This study
ENSMUSG00000033860 R:	GTTTGTCTGACAGCGCATGA	This study
ENSMUSG00000033831 F:	TGGACAGTCATACAGAACCGT	This study
ENSMUSG00000033831 R:	TTCACTCGCAGTCTTTACCTG	This study

4.2.6 Flow cytometry analysis of infected murine lungs

Groups of 8 outbred 6-week-old female Swiss (CD-1) mice (32 in total) were anesthetized and challenged with the bacterial suspension as outlined above in section 4.2.2. Mice were euthanized by CO_2 asphyxiation at 6 h, then lungs were finely macerated in 1 mL prewarmed digestion medium (DMEM + 5% FCS, 10 mM HEPES, 2.5 mM $CaCl_2$, 0.2 U/ml penicillin/gentamicin, 1 mg/ml collagenase IA, 30 U/ml DNase) and incubated at 37°C for 1 h with mixing every 20 min. The single cell suspensions were stained and fixed

using antibodies against surface markers listed in **Table 4.3**, allowing the enumeration of a number of immune cell subsets, as previously described (Yu et al., 2016). Single cells were then processed for data acquisition on a BD LSRFortessa X20 flow cytometer as previously described (David et al., 2019).

Table 4.3. List of antibodies used in this study.

Antibodies	Source	Identifier
Anti-mouse/human CD11b-PE (clone M1/70)	BioLegend	Cat# 101208, RRID: AB_312791
Anti-mouse CD11c-BV786 (clone HL3)	BD Biosciences	Cat# 563735, RRID: AB_2738394
Anti-mouse CD24-BV711 (clone M1/69)	BD Biosciences	Cat# 563450, RRID: AB_2738213
Anti-mouse CD45-FITC (clone 30-F11)	BioLegend	Cat# 103107, RRID: AB_312972
Anti-mouse CD64-BV421 (clone X54-5/7.1)	BioLegend	Cat# 139309, RRID: AB_2562694
Anti-mouse Ly6C-PerCP/Cy5.5 (clone HK1.4)	BioLegend	Cat# 128011, RRID: AB_1659242
Anti-mouse Ly6G-BUV395 (clone 1A8)	BD Biosicences	Cat# 563978, RRID: AB_2716852
Anti-mouse I-A/I-E-BV650 (clone M5/114.15.2)	BD Biosicences	Cat# 563415, RRID: AB_2738192
Anti-mouse Ly6G (clone 1A8)	Bio X Cell	Cat# BE0075-1, RRID: AB_1107721
Rat IgG2A Isotype Control (clone 54447)	R and D Systems	Cat# MAB006, RRID: AB_357349
Anti-mouse Ly-6G, Ly-6C-Biotin (clone RB6-8C5)	BD Biosicences	Cat# 553125, RRID: AB_394641
Anti-mouse IL-17A (clone 17F3)	Bio X Cell	Cat# BE0173, RRID: AB_10950102
Mouse IgG1 Isotype Control (clone MOPC-21)	Bio X Cell	Cat# BE0083, RRID: AB_1107784

4.2.7 Neutrophil depletion, IL-17A blockade and bacterial loads

Groups of 8 outbred 6-week-old female Swiss (CD-1) mice (64 in total) were intraperitoneally administered with either 350 μg of rat anti-mouse Ly6G or rat IgG2a isotype control antibodies, one and two days prior to pneumococcal challenge, or 200 μg of either monoclonal anti-mouse IL-17A or mouse IgG1 isotype control antibodies one day prior to, 2 h before and 6 h after pneumococcal challenge. Mice were also cheek bled on the day of challenge for confirmation of depletion of Ly6G-positive cells via flow

cytometry, as previously described (Faget et al., 2018). Mice were then anesthetized and challenged with the bacterial suspension for each treatment group as outlined in section 4.2.2. Mice were euthanized by CO_2 asphyxiation at 24 h, then nasopharynx and lung tissue samples were harvested, and pneumococci enumerated in tissue homogenates as described previously via serial dilution and plating on BA containing gentamicin (section 2.2.10).

4.2.8 Neutrophil and IL-17A levels after IL-17A neutralization

Groups of 3 outbred 6-week-old female Swiss (CD-1) mice were intraperitoneally administered with 200 μg of either monoclonal anti-mouse IL-17A or mouse IgG1 isotype control antibodies one day prior to and 2 h before intranasal challenge with 9-47, as described above. 6 h post-infection, lung tissue and bronchoalveolar lavage (BAL) were harvested. To quantify IL-17 levels, a mouse IL-17 DuoSet® ELISA (R&D Systems) was performed on BAL samples in duplicate, according to the manufacturer's instructions. Flow cytometry was performed on lung tissue samples, as described above, to quantify neutrophil levels after anti-mouse IL-17A treatment.

4.2.9 Statistics and reproducibility

For the RNAseq data, enrichment tests to assess enrichment were performed by the built-in function, *fisher.test()*. Corresponding *p*-values of the enrichment test were adjusted by Bonferroni correction. Resultant figures encompass data derived from three replicates per group, with each replicate derived from lungs of four mice. All other data are presented as mean ± standard error of mean (SEM) or geometric mean, and were analysed by two-tailed unpaired Student's *t*-test, one way ANOVA or Pearson correlation coefficient, using Prism v8.0d (GraphPad). Statistical significance was defined as $p < 0.05$. Data presented in figures are representative of at least two independent *in vivo* experiments, or at least 3 independent *in vitro* experiments.

4.3 Results

4.3.1 Comparative host/pathogen transcriptomics

Previous studies have shown that at 6 h after IN challenge with serotype 14 ST15 *S. pneumoniae*, numbers of blood and ear isolates (strains 4559 and 947, respectively) in murine lungs are similar (10^6 – 10^7 CFU per lung) (Amin et al., 2015). However, by 24 h, the ear isolate had been cleared from the lungs, instead spreading to the ear and brain. In contrast, the blood isolate persisted in the lungs at 24 h, but did not spread to the ear or brain (Amin et al., 2015). Thus, 6 h post infection is a critical decision point in the pathogenic process, and the similar bacterial loads in the lung at this time enables examination of host/pathogen transcriptional crosstalk without the complication of bacterial dose effects. Accordingly, groups of 12 mice were anaesthetized and challenged IN with 10^8 CFU of 4559, 947 or their respective *rafR*-swapped mutants (4559M and 947M); at 6 h, mice were euthanised, and total RNA was extracted from perfused lungs and purified. RNA from lungs of 4 mice was pooled for dual RNAseq analysis in triplicate (see section 4.2.2).

Within the sequencing libraries, an overwhelming majority of reads originate from the host genome (average 99.5%; range 99.1-99.7%), which translates into an average depth of 1.3 times (range 0.8-1.8 times). Conversely, 0.52% of the total reads originated from the pathogen genome (0.33-0.93%) (**Table 4.4**). Of these pneumococcal reads, 64.5% (61.4-67.3%) mapped onto rRNA genes and 35.5% (32.7-38.6%) mapped onto non-rRNA genes. Previous data indicate that non-depleted libraries only contain 5% non-ribosomal RNA reads; thus, this treatment enriched the non-ribosomal RNAs sevenfold. Non-ribosomal read depth was 2.7 times (1.4-4.6 times) for the pathogen genome. Further downstream analysis, including differential gene expression, excluded ribosomal reads from the pathogen library. **Appendices M-R** list pneumococcal genes that are significantly

differentially expressed (fold change (FC) > 2, $p < 0.05$) for each of the six pairwise comparisons between the four strains. Appendices S-X list murine genes that are significantly differentially expressed (FC > 1.5, $p < 0.05$) for the same pairwise comparisons. The lower FC cut-off for murine genes was chosen to strike a balance between simplicity of analysis and sensitivity. Heat maps displaying the top 50 murine and top 50 pneumococcal genes (**Fig. 4.1**) showcase the breadth of transcriptomic rewiring due to the *rafR* SNP.

Table 4.4. Host and pneumococcal read counts of RNA isolated from murine lungs 6 h post-infection, following dual RNAseq analysis.

Strain	Total Count	Murine Reads	Pneumococcal reads	% Murine	% Pneumococcal
947	46316502	46141193	175309	99.621%	0.379%
947	59564884	59248907	315977	99.470%	0.530%
947	40204707	40059925	144782	99.640%	0.360%
947M	30056978	29956541	100437	99.666%	0.334%
947M	47479606	47290932	188674	99.603%	0.397%
947M	48752703	48544160	208543	99.572%	0.428%
4559	40887116	40652817	234299	99.427%	0.573%
4559	42418850	42218273	200577	99.527%	0.473%
4559	36017301	35853955	163346	99.546%	0.454%
4559M	25210330	25045001	165329	99.344%	0.656%
4559M	52201495	51833174	368321	99.294%	0.706%
4559M	34141985	33825643	316342	99.073%	0.927%

4.3.2 RafR fine tunes carbohydrate metabolism during infection

In order to directly compare correlations in pathogen transcriptional responses in murine lungs between samples, homologous genes between the wild type ear and blood isolates were listed and used to visualise the transcriptional response in a principal component analysis (PCA) plot (**Fig. 4.2a**). Here, the pneumococcal transcriptional response of the ear isolate (strain 947, dark orange) to murine lung infection diverges considerably from the response of the blood isolate (strain 4559, dark purple). Specifically, 76 homologous genes are significantly upregulated in the ear isolate, while 40 are upregulated in the blood isolate.

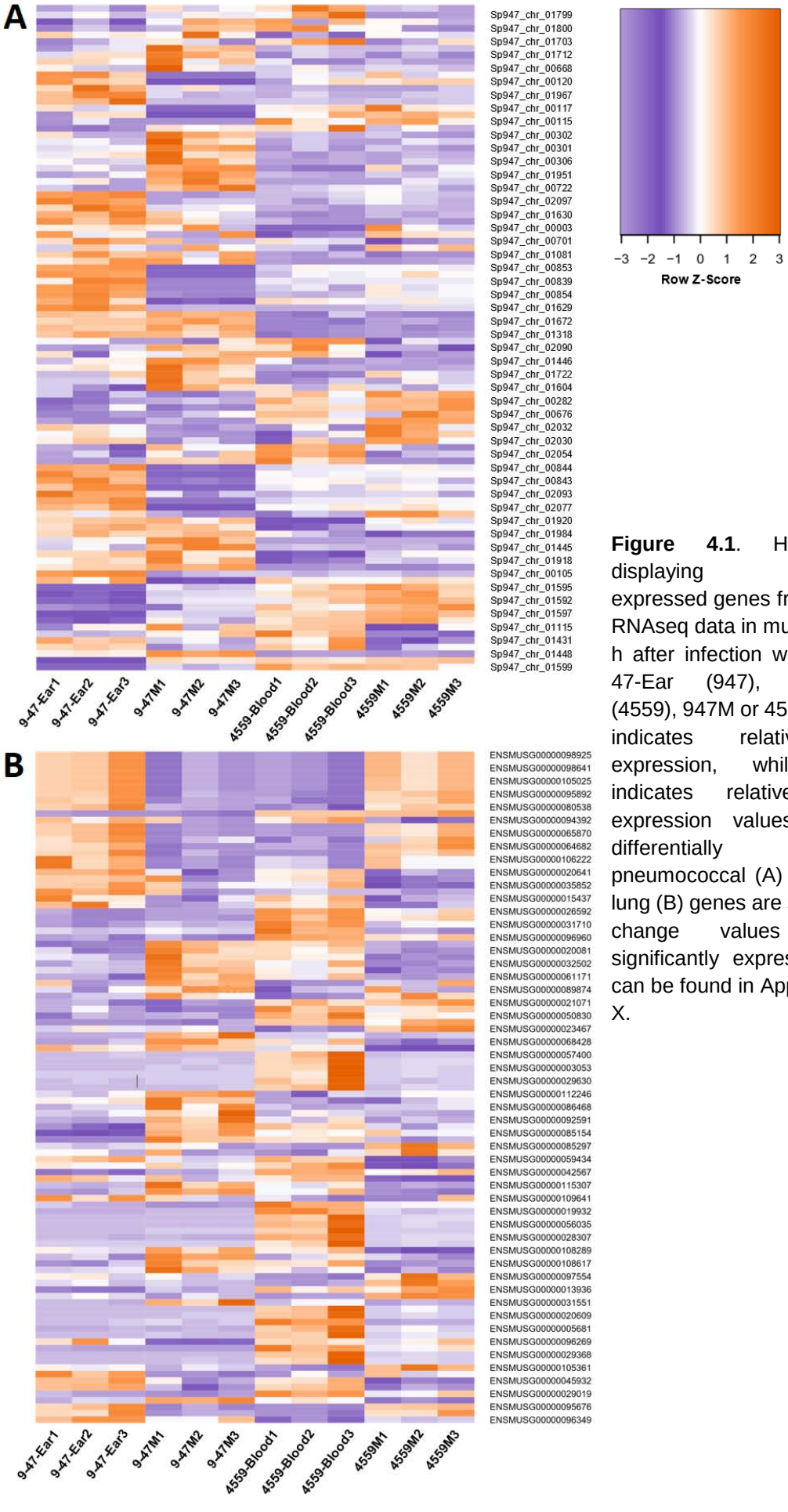

Figure 4.1. Heat maps displaying differentially expressed genes from the dual RNAseq data in murine lungs 6 h after infection with either 9-47-Ear (947), 4559-Blood (4559), 947M or 4559M. Purple indicates relatively low expression, while orange indicates relatively higher expression values. Top 50 differentially expressed pneumococcal (A) and murine lung (B) genes are shown. Fold change values of all significantly expressed genes can be found in Appendices M-X.

Upregulated genes in strain 947 include genes involved in carbohydrate metabolism, general stress response and nutrient transporters, while upregulated genes in 4559 include genes encoding small molecule permeases and nisin biosynthesis orthologous proteins.

Furthermore, replacing *rafR* of 947 with the allele from the 4559 (designated strain 947M) dissociates its transcriptional response considerably from its parental strain (**Fig. 4.2a**; 947, dark orange to 947M, light orange). These large-scale transcriptomic differences between 947 and 947M may explain the impact of the *rafR* SNP on *in vivo* tissue tropism. Specifically, 87 genes were upregulated in the wild type strain (947) while 36 genes were upregulated in the otherwise isogenic *rafR* swap strain (947M, **Fig. 4.2b**), with differentially expressed genes spread across the pneumococcal genome. Presence of the blood isolate *rafR* allele in 947 activates the expression of major genes pertaining to carbohydrate metabolism, including *adhA* (alcohol dehydrogenase) and *spxB* (pyruvate oxidase), as well as genes encoding permeases, including *glnH6P6* (transporting arginine, cysteine) and *ycjOP-yesO* (transporting multiple sugars). Also, a subset of genes with function in carbohydrate metabolism are repressed in the *rafR*-swap strain, such as glycogen synthesis (*glgACD*), sucrose metabolism (*scrB*) and ribulose metabolism (*ulaDEF*). Expression of seven genes encoding ATPase subunits (*ntpABCDEGK*) and genes for iron (*piuB*) and sugar (*scrA, satABC*, *gadEW*) permeases are also repressed.

On the other hand, replacing the blood isolate *rafR* with the ear allele (strain 4559M) does not noticeably interrupt pneumococcal transcriptional response to murine lung (**Fig. 4.2a**; 4559, dark purple to 4559M, light purple), despite the different *in vivo* behaviours of 4559 and 4559M. Essentially, the *rafR* swap activated only two genes: *yxlF,* encoding a putative subunit of an ABC transporter and *phoU1* encoding a phosphate transporter; and repressed 35 genes, mostly contained in a single genomic island (**Fig. 4.2c**, upregulated in 4559). The genomic island consists of 28 consecutive genes encoding subunits of bacteriophage(s), interspaced by *dnaC,* encoding a DNA replication protein and *lytA*, encoding autolysin.

The activation of bacteriophage-associated genes indicates that the original isolate (strain 4559) endures host-derived stress, unlike the *rafR* swap mutant (strain 4559M). Other genes repressed in 4559M include *adhAE* (alcohol dehydrogenases), *gtfA* (sucrose phosphorylase) and *rafEG* (raffinose transporter). Conversely, 947M and 4559 showcased similar *in vivo* behaviours yet displayed varied transcriptomes in murine lungs post-infection (**Fig. 4.2a**). Hence, transcriptional profiling was unable to predict tissue tropism in this case. Taken together, the single D249G SNP in *rafR* interferes with global gene expression within the already transcriptionally-distinct parental clinical isolates. This effect was more pronounced in 947 than 4559.

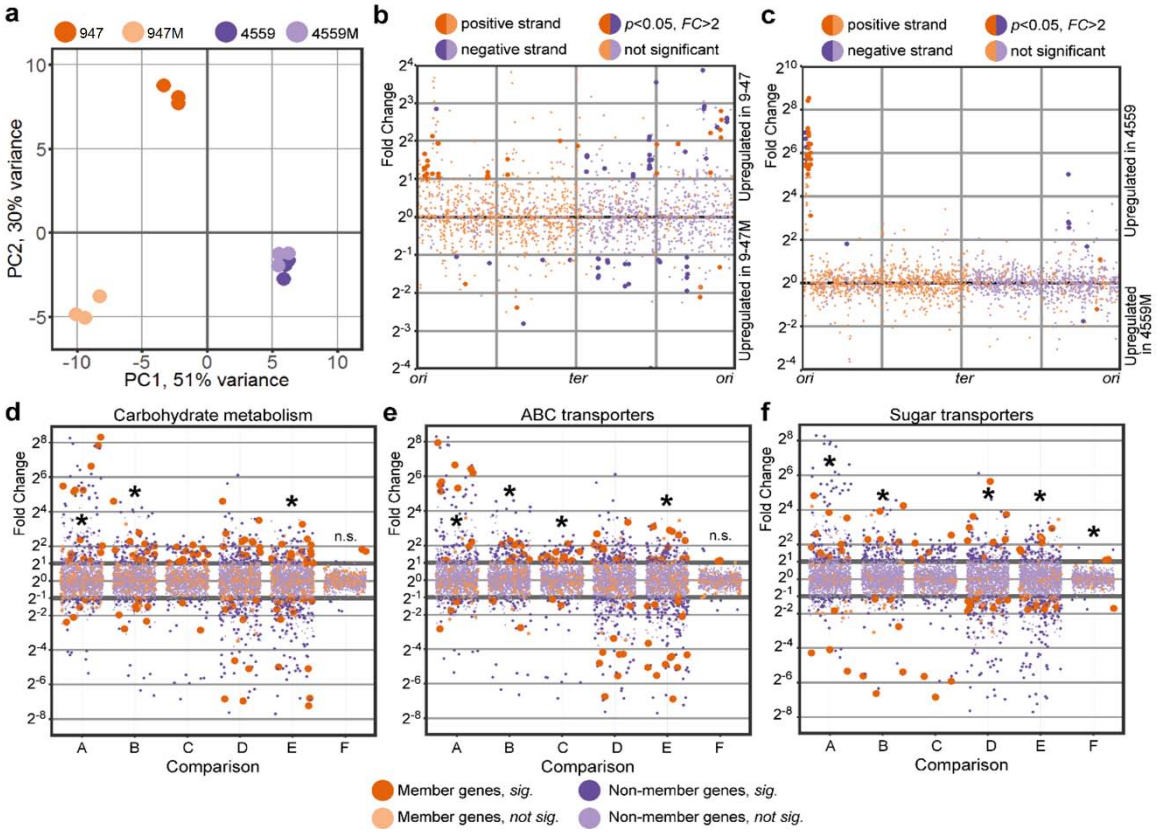

Figure 4.2. Pathogen transcriptional responses in murine lung. **(a)**. PCA plot showing divergence of transcriptional response to lung infection within the ear (947) and blood isolates (4559). *rafR* swap (947M) rewires pneumococcal transcriptional response only in the ear isolate background but not in the blood isolate. (**b)**. Differential expression due to the *rafR* swap in the ear isolate background is spread throughout the pneumococcal genome, (**c**) while in the blood isolate background, differential expression due to the *rafR* swap is limited to a genomic island. Functional enrichment showed specific function being differentially expressed, including carbohydrate metabolism (**d**), ABC transporters (**e**) and sugar transporters (**f**). A: comparison of 947 to 947M; B: 947 to 4559; C: 947 to 4559M; D: 947M to 4559; E: 947M to 4559M and F: 4559 to 4559M. * denotes statistically significant functional enrichment for the indicated strain-strain comparison.

Next, quantified enrichment analyses were performed on specific gene functions. Carbohydrate metabolism is enriched in the differentially expressed genes between the strains, particularly when comparing the ear isolate to its cognate *rafR* swap (**Fig. 4.2d**; *comparison A*, 947 vs 947M, $p = 0.03$), comparing the two clinical isolates (*comparison B,* 947 vs 4559, $p = 0.017$) and comparing the swap cognates (*comparison E,* 947M vs. 4559M, $p = 0.041$). Another function, ABC transporters, is also enriched in the comparison within the ear isolates (**Fig. 4.2e**; *comparison A*, 947 vs. 947M, $p = 0.049$), between the original isolates (*comparison B,* 947 vs 4559, $p = 0.014$), between the ear isolate and the blood isolate with the *rafR* 746G (*comparison C*, 947 vs. 4559M, $p = 0.01$) and between the *rafR* cognates (*comparison E*, 947M vs. 4559M, $p = 1.8 \times 10^{-4}$).

Additionally, since the pneumococcal genome has an exceptionally high number of sugar transporters (Bidossi et al., 2012), we quantified enrichment for this function (**Fig. 4.2f)**. Sugar transporters are enriched in almost all comparisons (except between 4559 and 4559M), highlighting the role of *rafR* in the widespread regulation of pneumococcal sugar importers. Specifically, ear and blood isolates behave differently in regard to sugar transporter expression (947 vs. 4559; **Fig. 4.2f**, *comparison B*). The ear isolate upregulated *scrA* (encoding a mannose and trehalose transporter) and *ulaA* (ascorbate transporter), while the blood isolate upregulated *ycjOP-yesO* (alternative sugar transporters)*, rafE* (raffinose transporter) and *malFG* (maltose transporter). Furthermore, *rafR* swap in the ear isolate background (947 vs. 947M; **Fig. 4.2f**, *comparison A*) reduced the expression of *gadEW* (encoding sorbose and mannose transporter), *satABC* (arabinose and lactose transporter), *ulaAC* and *glpF* (glycerol transporter), while the swap activated the expression of *ycjOP-yesO* and *bguD* (encoding complex polysaccharide transporters). In contrast, *rafR* swap in the blood isolate background (4559 vs. 4559M; **Fig. 4.2f**, *comparison F*) downregulated the expression of *rafEG* and *malD* (maltose transporter). The enrichment analysis reveals that the D249G SNP in *rafR* directly and indirectly affects the expression

of genes encoding sugar transporters, other (ABC) transporters and carbohydrate metabolism.

Genes that were commonly up or down regulated between the strains with a given virulence phenotype were also identified (**Table 4.5**). *adhP* (Sp947_00279) was significantly upregulated in both strains that persisted in lungs (947M and 4559), while 8 genes from the genomic region Sp947_0842 to Sp947_0855, as well as Sp947_00631 and Sp947_02096, were significantly upregulated in strains that were cleared from lungs by 24 h (947 and 4559M). These genes include neuraminidase *nanB*, and alpha-glycerophosphate oxidase *glpO* (**Table 4.5**). All other differentially expressed pneumococcal genes are listed in **Appendices M-R**.

Table 4.5. Pneumococcal genes that were consistently up or down regulated between strains that persisted in murine lungs (4559 and 947M) or between the strains that were cleared from the lungs (947 and 4559M).

Gene (locus tag)	Comparison	Fold Change	padj
adhP (Sp947_00279)	947 vs 947M	0.48	0.004
adhP (Sp947_00279)	947 vs 4559	0.32	5.38×10^{-7}
adhP (Sp947_00279)	947M vs 4559M	2.39	0.00018
adhP (Sp947_00279)	4559 vs 4559M	3.53	2.23×10^{-8}
nanB (Sp947_00844)	947 vs 947M	313	3.08×10^{-1}
nanB (Sp947_00844)	947 vs 4559	2.53	1.14×10^{-8}
nanB (Sp947_00844)	947M vs 4559M	0.01	4.59×10^{-8}
glpO (Sp947_02129)	947 vs 947M	5.86	1.19×10^{-37}
glpO (Sp947_02129)	947 vs 4559	1.89	2.26×10^{-7}
glpO (Sp947_02129)	947M vs 4559M	0.25	3.55×10^{-23}

4.3.3 RafR-specific rewiring of host transcriptional responses

The measured murine transcriptional response represents aggregate gene expression of all (host) cells present during pneumococcal lung infection. These include epithelial cells, endothelial cells of lung vasculature, smooth muscle cells, fibroblasts, activated and non-activated immune cells. The host transcriptional response was specific to the infecting pneumococcal strain (**Fig. 4.3a**). Specifically, there was a diverging host response to the ear isolate (947, dark orange) and blood isolate (4559, dark purple). Interestingly, *rafR* swap in blood isolate background (4559M, light purple) mimicked the lung response to the

wild type ear isolate (947, dark orange); these two strains harbour the D249 *rafR* allele. Surprisingly, the *rafR* swap in the 947 background (947M, light orange) which harbours the G249 allele, did not drive the host response to mimic those of the wild type 4559 strain (dark purple) that also has the G249 allele, but rather towards a new, third position of genome-wide expression.

Genome-wide plotting of murine transcriptional responses to *S. pneumoniae* strains 947 and 4559 showed extensive rewiring of gene expression across the murine chromosomes, consistent with their different tissue tropisms *in vivo* (**Fig. 4.3b**). Specifically, 433 murine genes are activated upon infection by 947 (FC > 1.5, $p < 0.05$), while 787 genes are activated by infection with 4559 (FC > 1.5, $p < 0.05$). Of the 947-upregulated murine genes, only 37% were protein-coding, with the majority encoding pseudogenes and small RNAs. Conversely, of the 787 4559-upregulated murine genes, 80% were protein-coding, while the rest encoded small RNAs. The 4559-upregulated genes encode proteins involved in multiple pathways such as general metabolism, peroxisome proliferator-activated receptor (PPAR) signalling, steroid hormone biosynthesis and cAMP signalling. Although both strains belong to the same capsular serotype and ST (Amin et al., 2015) the data strongly suggests wildly diverging isolate-specific host responses during early infection, with the *rafR* SNP varying the host response considerably. Interestingly, the host transcriptional response to 4559M closely resembles that of 947 (**Fig. 4.3a**), suggesting that the *rafR* SNP plays a crucial role in the distinct response to 947 vs 4559. However, the host transcriptional response to 4559 does not closely resemble the response to 947M, despite the similar *in vivo* tissue tropism these strains display. This suggests, unsurprisingly, that the host transcriptional response to pneumococcal infection does not perfectly correlate with *in vivo* outcomes.

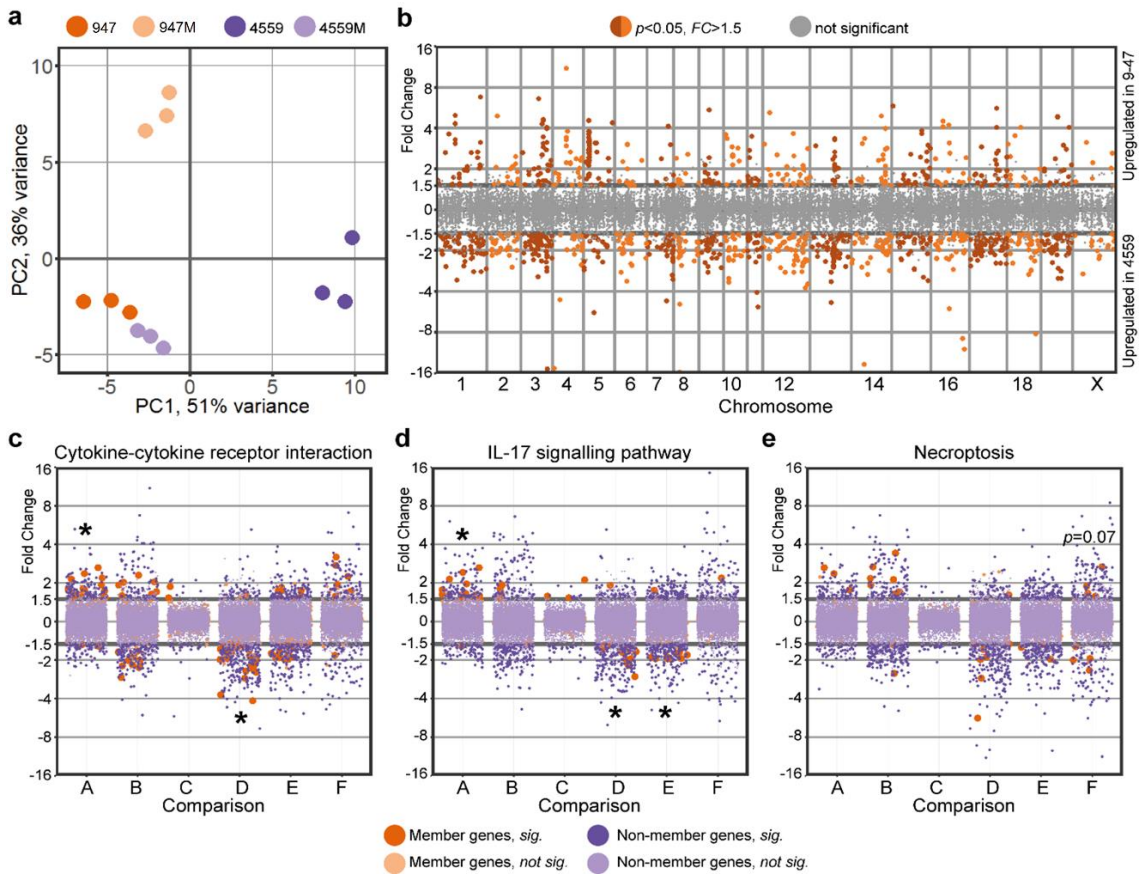

Figure 4.3. Single nucleotide polymorphism in pneumococcal *rafR* drives diverging host response. (**a**). PCA plot illustrates murine lung response to the pneumococcal strains. Interestingly, host transcriptional response to *rafR* swap in blood isolate (4559M, light purple) is similar to the murine response to the original ear strain (947, dark orange). (**b**). Differential gene expression of transcriptional response to pneumococcal ear and blood isolates shows a widespread transcriptional rewiring. Specifically, 433 genes are activated in response to infection by ear isolate (947) while 787 genes are activated (*FC* > 1.5, $p < 0.05$) by blood isolate (4559). Specific gene ontology terms are enriched in differentially expressed host genes in response to pneumococcal infection: cytokine-cytokine receptor interaction (**c**), interleukin-17 signalling pathway (**d**) and necroptosis (**e**). A: comparison between 947 to 947M; B: 947 to 4559; C: 947 to 4559M; D: 947M to 4559; E: 947M to 4559M and F: 4559 to 4559M. * denotes statistically significant functional enrichment for the indicated strain-strain comparison.

In addition, *rafR* swap in the ear isolate background (947M) expressing the G249 *rafR* allele activated 271 murine genes (FC > 1.5, $p < 0.05$), while it repressed 479 genes. The G249 *rafR*-activated genes include those involved in the Wnt signalling pathway (*Fzd2, Lgr6, Rspo1, Sost, Sox17, Wnt3a, Wnt7a*) and general calcium signalling pathway (*Adra1a, Adra1b, Adrb3, Cckar, Grin2c, P2rx6, Tacr1, Tacr2*). Conversely, 52% of the G249 *rafR*-repressed genes in lungs infected with 947M encode RNA features and 18 chemokines, chemokine ligands, interferons and interleukins. On the other hand, *rafR* swap in the blood isolate background (4559M) expressing the D249 *rafR* allele activated 328 murine genes

(FC > 1.5, $p < 0.05$), and repressed 472 genes. 73% of the D249 *rafR*-activated murine genes encode RNA features and 33 encode histone proteins. The activation of these histone proteins suggests a massive reorganisation of gene regulation with numerous potential downstream impacts. In contrast, D249 *rafR*-repressed genes include genes encoding calmodulins (*Calm4, Calm13* and *Camk2a*) and phospholipases A2 (*Pla2g4b, Pla2g4d* and *Pla2g4f*).

Moreover, there are only 132 differentially expressed host genes in response to wild type 947 compared to the response to strain 4559M (both having the D249 *rafR* allele), with 38 genes upregulated in strain 947 and 94 in strain 4559M. Fascinatingly, the D249 *rafR* allele (strains 947 and 4559M) is associated with a significant upregulation of RNA features, including antisense, intronic, long intergenic non-coding RNAs (lincRNAs) and micro RNAs (miRNAs). The resulting abundance of RNA species in murine cells upon pneumococcal infection has the potential for even more widespread transcriptional rewiring and fine-tuning of gene products later in the infection.

A quantified functional enrichment showed that certain gene functions are enriched in the murine response to pneumococcal strains. In particular, cytokine-cytokine receptor interaction is enriched in differentially expressed host genes because of *rafR* swap in the ear isolate background (**Fig. 4.3c**, *comparison A*, 947 vs. 947M, $p = 9.5\times10^{-4}$). Concurrently, this function is enriched in differentially expressed genes between mice infected with 947M and those infected with 4559 (*comparison D,* $p = 1.8\times10^{-4}$). Since both strains harbour the G249 *rafR* allele, the differentially expressed genes encoding cytokines and cytokine receptors are most likely attributable to unrelated genetic differences between the clinical isolates. Interestingly, this function is not enriched in differentially expressed genes between the *rafR* swap in the blood isolate background (4559M) and the wild type 947 (*comparison C*), both of which have the D249 *rafR* allele. Genes encoding chemokine ligands (*Cxcl2, Cxcl3, Cxcl10* and *Ccl20*), interleukin 17F

(*Il17f*), interferon beta (*Ifnb1*) and a receptor of TNF (*Tnfrsf18*) are the common differentially expressed genes in lungs of mice infected with 947, 947M and 4559, with ascending expression from responses to 947M, 947 and 4559. Other genes encoding chemokine ligands (*Ccl3, Ccl4, Ccl17, Ccl24, Cxcl5, Cxcl11* and *Xcl1*), interleukins (*Il1rn* and *Il13ra2*) and interferon gamma (*Ifng*) are more highly expressed in the ear isolate-infected lung (947) than in lungs infected by the *rafR* swap ear isolate (947M). Finally, genes encoding chemokine receptors (*Ccr1* and *Ccr6*), interleukin receptors (*Il1r2, Il10ra, Il17a, Il18rap, Il20ra, Il20rb, Il22* and *Il23r*), and interleukins (*Il1f5, Il1f6, Il1f8* and *Il6*) are more highly expressed in lungs infected by 4559 compared to the *rafR* swap in in the ear isolate background (947M).

Interleukin 17, as part of the cytokine response, activates multitudes of downstream targets in defence against infectious agents (Onishi and Gaffen, 2010), and thus plays a central role in host response to pneumococcal infection. Here, we observe the same pattern of diverging activation among murine responses to the pneumococcal strains (**Fig. 4.3d**), with IL-17-associated genes being enriched in differentially expressed genes among the host transcriptional response to the *rafR* swap in the ear isolate background (*comparison A*, 947 vs. 947M, $p = 9.5\times10^{-4}$). These genes are also enriched amongst the host response to pneumococcal strains with the G249 *rafR* allele (*comparison D*, 947M vs. 4559, $p = 7.5\times10^{-4}$) and to the *rafR* swap cognates (*comparison E*, 947M vs. 4559M, $p = 0.022$). However, there was no enrichment of IL-17 associated genes amongst the host response to pneumococcal strains with the D249 *rafR* allele (*comparison C*, 947 vs. 4559M). Common differentially expressed genes of this function include genes encoding interleukin 17F (*Il17f*) and chemokine ligands (*Cxcl2, Cxcl3* and *Ccl20*), with ascending expression level of response to 947M, 947 and 4559. Specifically, the products of these genes regulate the recruitment of neutrophils and activate immune responses to extracellular pathogens.

In addition to the above, necroptosis, a programmed cell death, is almost significantly enriched ($p = 0.07$) in differentially expressed murine genes because of the *rafR* swap in the blood isolate background (**Fig. 4.3e**, *comparison F,* 4559 vs. 4559M). Genes encoding histone cluster 2 (*Hist2h2ac, Hisr2h2aa1, Hist2h2aa2* and *H2afx*) are more highly expressed in murine lungs infected with 4559, while those encoding phospholipases A2 (*Pla2g4b, Pla2g4f* and *Pla2g4d*) and a subunit of calcium/calmodulin-dependent protein kinase II (*Camk2a*) are more highly expressed in the transcriptional response to the *rafR* swap in the blood isolate background (4559M).

4.3.4 Validation of host/pathogen transcriptomics

To validate the findings from the dual RNAseq, qRT-PCR was performed on the same RNA samples from the lungs 6 h post-infection. 19 pneumococcal and 18 murine genes were chosen for this validation, with the primers used listed in **Table 4.2**. A total of 76 pneumococcal and 72 murine gene Log_2 FC comparisons were performed, with a high degree of correlation observed for both pneumococcal ($R^2 > 0.73$, Pearson) and murine genes ($R^2 > 0.81$, Pearson) (**Fig. 4.4A**). To validate the reproducibility of the dual RNAseq data, lung RNA samples 6 h post-infection from a different experiment were analysed with qRT-PCR. Here, 6 pneumococcal and 6 murine genes were chosen, and 24 pneumococcal and 24 murine gene log_2 FC comparisons were performed. A high degree of correlation was also observed here, for both pneumococcal ($R^2 > 0.77$, Pearson) and murine genes ($R^2 > 0.73$, Pearson) (**Fig. 4.4B**).

4.3.5 Immune cell subsets present in infected lung tissue

The host RNAseq data represent the pooled transcriptional responses of all cell types present in the lungs at the time of RNA extraction. Thus, some of the transcriptomic differences may be attributable to alterations in the relative abundance of given cell types,

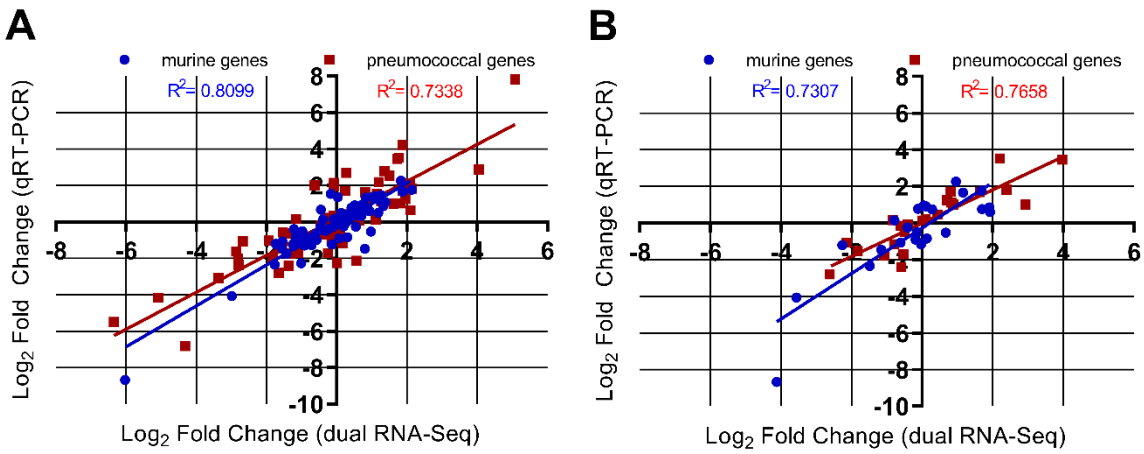

Figure 4.4. Gene expression values from the dual RNAseq were confirmed by qRT-PCR, using (**A)** the same isolated RNA used for the dual RNAseq or (**B)** isolated RNA from a repeated experiment. (**A**) 18 murine and 19 pneumococcal genes were chosen as experimental validation targets. Log_2 fold changes were plotted from qRT-PCR against dual RNAseq log fold changes for 947 vs 4559, 947 vs 947M, 947M vs 4559M and 4559 vs 4559M comparisons. A total of 72 murine and 76 pneumococcal comparisons were plotted, with a high degree of correlation observed for both species ($R^2 > 0.73$, Pearson). (**B**) 6 murine and 6 pneumococcal genes were chosen as targets to test the reproducibility of the dual RNAseq data. Log_2 fold changes were plotted from qRT-PCR against dual RNAseq log fold changes for 947 vs 4559, 947 vs 947M, 947M vs 4559M and 4559 vs 4559M comparisons. A total of 24 murine and 24 pneumococcal comparisons were plotted, with a high degree of correlation observed for both species ($R^2 > 0.73$, Pearson).

for example, by differential recruitment of immune cell subsets to the site of infection. Accordingly, flow cytometry was used to quantify immune cell subsets present in lung tissue 6 h after infection with either 947, 4559, 947M or 4559M. The surface marker staining panel used (**Table 4.3**) and appropriate gating strategy (**Appendix Y**) allowed the identification and enumeration of natural killer (NK) cells, neutrophils, eosinophils, inflammatory monocytes (iMono), resident monocytes (rMono), alveolar macrophages (AMΦ), interstitial macrophages (iMΦ), CD11b-negative dendritic cells (CD11b-DC), CD11b-positive dendritic cells (CD11b+ DC), T cells and B cells (Yu et al., 2016). Of these, neutrophils, by far the most abundant cell type, were present in significantly higher numbers in murine lungs infected with 947 (vs 4559, $p < 0.01$; vs 947M, $p < 0.05$) and 4559M (vs 4559, $p < 0.05$) (**Fig. 4.5**), both of which have the D249 *rafR* allele and were cleared from the lungs 24 h post-infection. NK cells were also found to be significantly higher in lungs infected with 947 (vs 4559, $p < 0.01$; vs 947M, $p < 0.05$), while eosinophils were raised in 4559M infected lungs (vs 4559, $p < 0.05$) (**Fig. 4.5**). However, since the

numbers of NK cells and eosinophils were much lower than neutrophils, their contribution to total lung mRNA and their impact on tissue tropism may be less pronounced. Moreover, the large difference in neutrophil recruitment to the lungs 6 post-infection aligns with the differential IL-17 response highlighted in the dual RNAseq data. The higher number of neutrophils in murine lungs infected with 947 and 4559M is likely to facilitate their clearance from this niche.

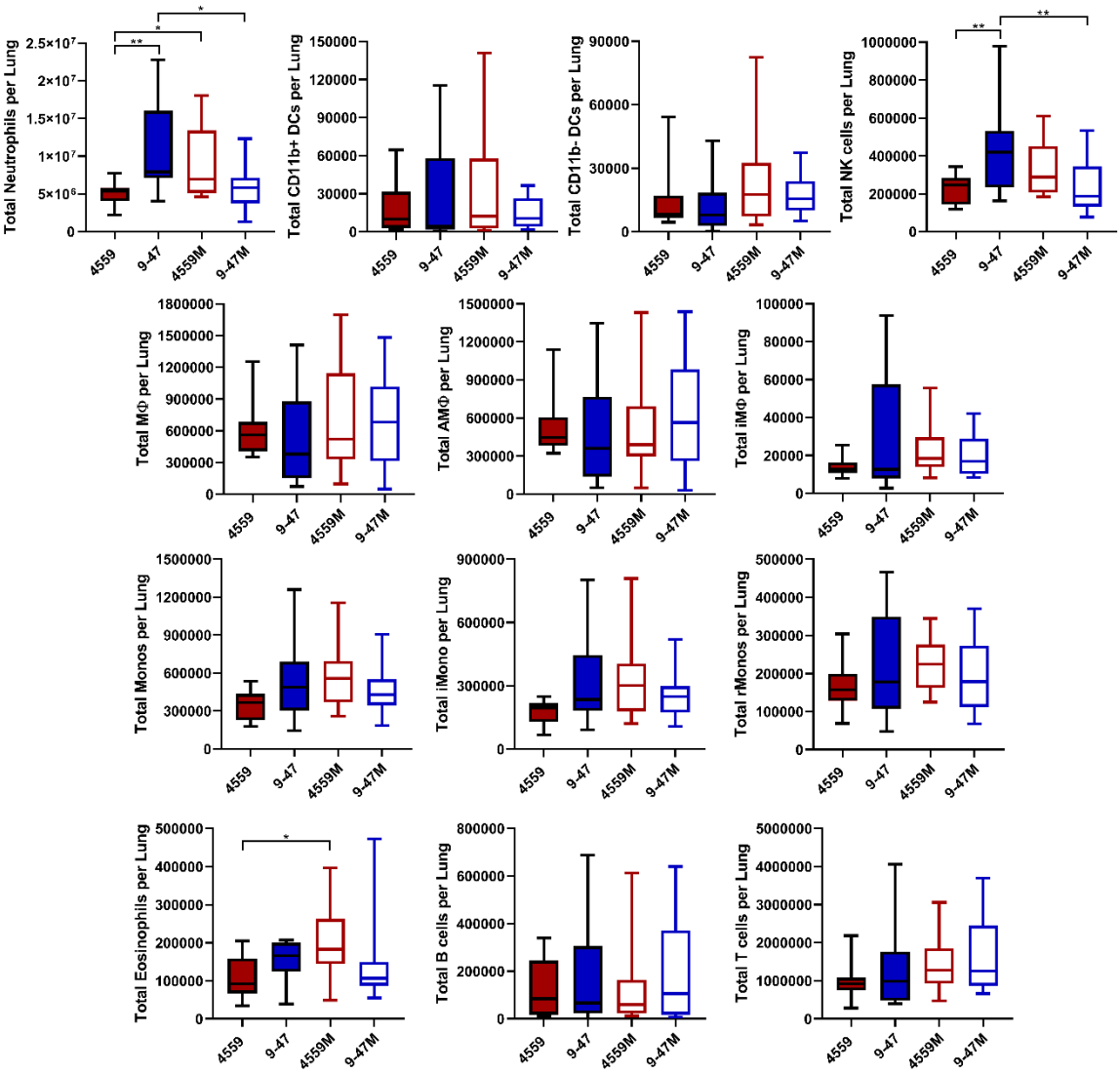

Fig. 4.5. Quantification of immune cell subsets in murine lungs 6 h post infection. Groups of 8 mice per strain were challenged with either 947, 4559, 947M or 4559M. Single cell lung suspensions were prepared and stained with antibodies against various surface markers (**Table 4.3**) then analysed by flow cytometry. Populations enumerated include: natural killer (NK) cells, neutrophils, eosinophils, inflammatory monocytes (iMono), resident monocytes (rMono), alveolar macrophages (AMΦ), interstitial macrophages (iMΦ), CD11b-negative dendritic cells (CD11b- DC), CD11b-positive dendritic cells (CD11b+ DC), T cells and B cells. Graphs shown represent pooled data from two independent experiments. All quantitative data are presented as mean ± S.E.M (n = 16 for each group), analysed by one-way ANOVA (*$p < 0.05$; **$p < 0.01$).

4.3.6 Impact of neutrophil depletion and IL-17A neutralization

The greater abundance of neutrophils in lungs infected with strains containing the D249 *rafR* allele that are cleared from the lungs by 24 h suggests that the recruitment and presence of neutrophils is crucial for bacterial clearance from the lung. Thus, differential neutrophil recruitment might be the underlying mechanism for the observed RafR-dependent tropism. To test this, we investigated the importance of neutrophils for persistence of pneumococci in the lungs in the IN challenge model. Injection of anti-mouse Ly6G was used to deplete neutrophils in 32 mice, alongside an isotype control group treated with rat IgG2a. Neutrophil depletion was confirmed in the blood prior to challenge using flow cytometry (Appendix Z), with a 76.35% decrease in neutrophils in the anti-mouse Ly6G treated mice, relative to the isotype control-treated group ($p < 0.0001$) (**Fig. 4.6A**). Mice were then challenged with 10^8 CFU of each strain, for both treatment groups. Bacterial loads were quantified in the nasopharynx and lungs 24 h post-challenge. No significant differences in bacterial numbers in the nasopharynx were seen between strains within each treatment group (**Fig. 4.7A**). Also, for both treatments, the numbers of bacteria in the lungs infected with 4559 and 947M were significantly higher than 947 and 4559M (**Fig. 4.7B**), which is consistent with our previous findings (Minhas et al., 2019). However, the anti-Ly6G-treated groups showed significantly higher lung bacterial loads compared to their respective isotype controls: 4559 anti-Ly6G vs 4559 control ($p < 0.001$), 947-Blood anti-Ly6G vs 947-Blood control ($p < 0.01$), 4559M anti-Ly6G vs 4559M control ($p < 0.01$) and 947M anti-Ly6G vs 947M control ($p < 0.05$) (**Fig. 4.7B**). Importantly, the lung bacterial loads of anti-Ly6G-treated 947 and 4559M groups were not significantly different to the isotype control-treated 4559 group (**Fig. 4.7B**). Thus, restriction of neutrophil infiltration into the lungs by depleting circulating neutrophils in mice challenged with the strains expressing the D249 *rafR* allele resulted in enhanced lung bacterial loads at 24 h

similar to that seen in untreated mice challenged with the strains expressing the G249 *rafR* allele.

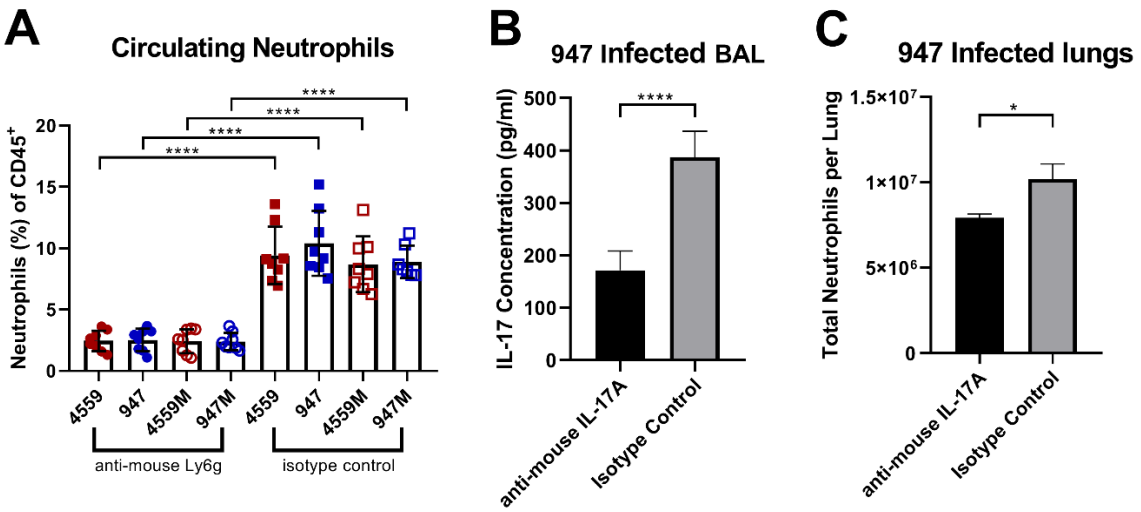

Figure 4.6. Effect of anti-mouse Ly6G and anti-mouse IL-17A treatment on neutrophil and IL-17A levels. **A** Groups of 8 mice per strain were treated with either 350 µg of rat anti-mouse Ly6G or rat IgG2a isotype control antibodies (see section 4.2.7) Percentage of circulating neutrophils relative to live ($CD45^+$) cells were calculated. Differences in circulating neutrophils between groups are indicated by asterisks: ****, $p < 0.0001$, by one-way ANOVA. **B & C** Groups of 3 outbred 6-week-old female Swiss (CD-1) mice were treated with either monoclonal anti-mouse IL-17A or mouse IgG1 isotype control antibodies (see section 4.2.8). **B** BAL was harvested 6 h post-infection and an IL-17 ELISA was performed to calculate IL-17 levels after anti-mouse IL-17A treatment. Differences in BAL IL-17 levels between groups are indicated by asterisks: ****, $p < 0.0001$, by two-tailed unpaired Student's *t*-test. **C** Lung tissue was also harvested 6 h post-infection and stained with antibodies against neutrophil surface markers (**Table 3**), then analysed by flow cytometry. Differences in lung neutrophil levels between groups are indicated by asterisks: *, $p < 0.05$, by two-tailed unpaired Student's *t*-test.

Given the known involvement of IL-17 in neutrophil recruitment into the lungs after infection (Lindén et al., 2005; McCarthy et al., 2014; Ritchie et al., 2018; Stoppelenburg et al., 2013), we also investigated the *in vivo* significance of the *rafR*-mediated differential expression of IL-17-associated genes between the various *S. pneumoniae* strains. Groups of mice were injected with anti-mouse IL-17A, or a control murine IgG1 antibody, before and after pneumococcal challenge. IL-17A depletion was confirmed by ELISA on separate 9-47-infected bronchoalveolar lavage (BAL) samples, with a 55.63% reduction in IL-17A levels seen in anti-mouse IL-17A treated mice relative to the isotype control group ($p < 0.0001$) (**Fig. 4.6B**). The effect of this IL-17A depletion on neutrophil levels was also tested using flow cytometry on infected 9-47 lung tissue, with a 22.23% decrease in neutrophils

seen in the anti-mouse IL-17A-treated mice, relative to the isotype control-treated group ($p < 0.05$) (**Fig. 4.6C**).

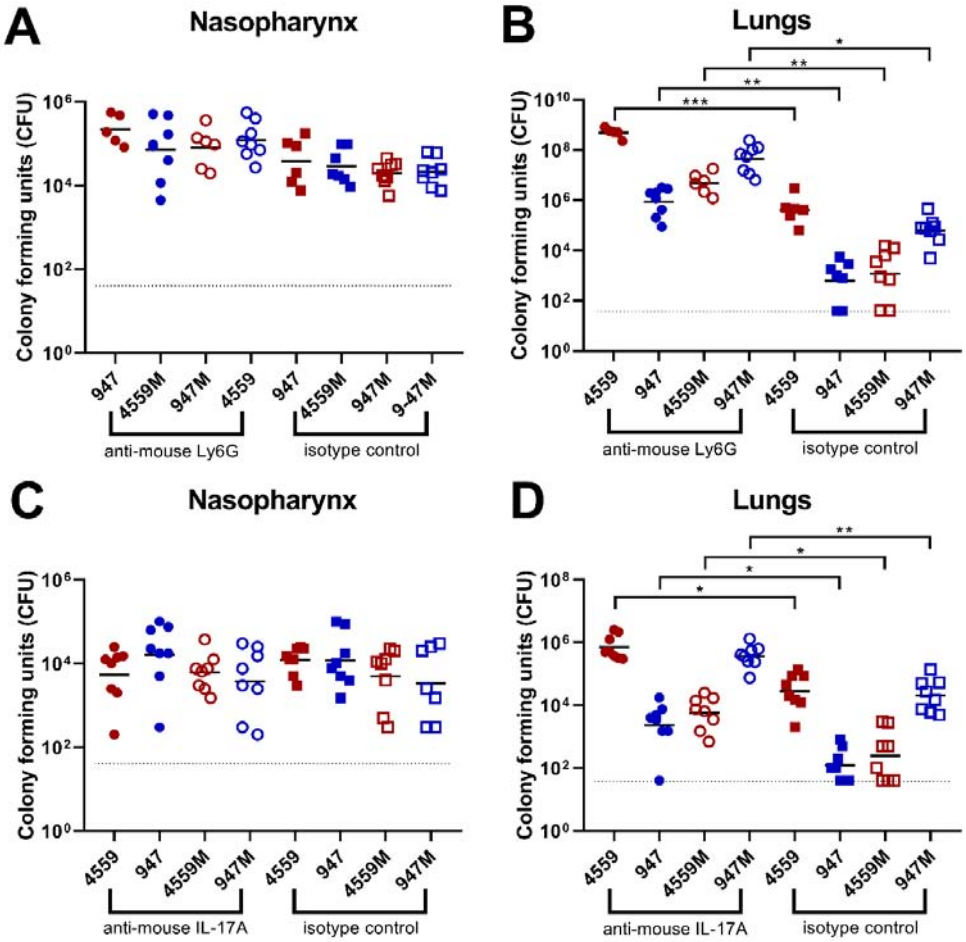

Figure 4.7. Impact of neutrophil depletion or anti-IL-17A on pneumococcal virulence. Groups of 8 mice were treated with either 350 µg of rat anti-mouse Ly6G or rat IgG2a isotype control, one and two days prior to pneumococcal challenge (A & B), or with IL-17A or mouse IgG1 isotype control (C & D), one day before, 2 h before and 6 h after intranasal challenge (A, B, C & D). 24 h post-infection, numbers of pneumococci in the nasopharynx and lungs were quantitated (see section 4.2.8). NB: n is <8 for some groups because didn't survive the challenge procedure, or until the time of harvest. Viable counts (total CFU per tissue) are shown for each mouse at each site; horizontal bars indicate the geometric mean (GM) CFU for each group; the broken line indicates the threshold for detection. Differences in GM bacterial loads between groups are indicated by asterisks: *, $p < 0.05$, **, $p < 0.01$, ***, $p < 0.001$, by unpaired *t*-test.

Bacterial loads were quantified in the nasopharynx and lungs 24 h post-challenge. Again, no significant differences between strains in bacterial numbers in the nasopharynx were seen within each treatment group (**Fig. 4.7C**). However, similar to the results obtained using anti-Ly6G, groups treated with anti-IL-17A showed significantly higher bacterial numbers in the lungs compared to their respective isotype controls; 4559 anti-IL-17A vs 4559 control ($p < 0.05$); 947-Blood anti-IL-17A vs 947-Blood control ($p < 0.05$); 4559M

anti-IL-17A vs 4559M control ($p < 0.05$); and 947M anti-IL-17A vs 947M control ($p < 0.01$) (**Fig. 4.7D**). Nevertheless, the impact of anti-IL-17 treatment on lung bacterial loads was not quite as dramatic as that of anti-Ly6G, as the number of bacteria in the lungs of anti-IL-17A-treated 947 and 4559M groups remained significantly lower relative to the isotype control treated 4559 group (both $p < 0.05$) (**Fig. 4.7D**). Together, these results show that pneumococcal strains carrying the D249 *rafR* allele caused a rapid influx of neutrophils, partly controlled by IL-17 expression in the host, leading to clearance from the lung, while the G249 *rafR* strains managed to remain 'stealthy' and hence were able to persist.

4.4 Discussion

In this Chapter, a dual RNAseq approach was used, validated by qRT-PCR, to elucidate the complex interspecies interactions between murine lung cells and infecting *S. pneumoniae* blood and ear isolates that are closely related (same capsular serotype and ST type), but exhibit distinct virulence phenotypes in accordance with their original clinical isolation site. These differences are largely, but not completely, driven by a D249G SNP in the raffinose pathway transcriptional regulator gene *rafR*, which extensively impacts the bacterial transcriptome in the lung environment. The SNP affects expression of genes encoding multiple transmembrane transporters, including those for various sugars, and fine-tunes pneumococcal carbohydrate metabolism (section 4.3.2). This indicates that the differential expression of sugar catabolism pathways provides specific advantages in distinct host niches, implying differential niche-specific availability of one carbohydrate source versus another.

Free sugars are in low abundance in the upper respiratory tract, but *S. pneumoniae* expresses a range of surface-associated exoglycosidases that enable it to scavenge constituent sugars (including galactose, *N*-acetylglucosamine, sialic acid and mannose) from complex host glycans present in respiratory secretions and on the epithelial surface (Andreassen et al., 2020; Buckwalter and King, 2012; King et al., 2006; Paixão et al., 2015; Robb et al., 2017; Shelburne et al., 2008). Conversely, glucose is readily available in the blood and also in inflamed tissues, implying a marked alteration in the availability of this preferred carbohydrate source as invasive disease progresses (Philips et al., 2003). All these variations, and the downstream consequences thereof, are ultimately sensed by host cells, including epithelial and immune cells, resulting in the observed divergence of host responses to the various strains, particularly with respect to expression of genes encoding cytokine and chemokine ligands and receptors, as well as those associated with

programmed cell death (section 4.3.3).Examination of the nature of the host response provided important clues regarding the mechanism whereby the *rafR* SNP impacts virulence phenotype. By way of example, the dual RNAseq data showed that expression of IL-17 related genes were enriched in mice infected with 947 and 4559M. These strains express the D249 *rafR* allele and are cleared from the lungs by 24 h post-challenge. It is well known that IL-17 drives neutrophil recruitment into the lungs after infection (Lindén et al., 2005; McCarthy et al., 2014; Ritchie et al., 2018; Stoppelenburg et al., 2013). Indeed, the results in this Chapter showed that neutrophils were present in the lungs 6 h post challenge at significantly higher numbers in mice infected with 947 and 4559M compared with the strains expressing the G249 *rafR* allele (**Fig. 4.5**), as predicted by the dual RNAseq data. Moreover, it was shown that neutrophil depletion by treatment with anti-Ly6G increased bacterial numbers in the lungs of mice, relative to the isotype controls. Strikingly, pneumococcal numbers in the lungs of anti-Ly6G treated mice infected with 947 and 4559M were not significantly different to that of isotype control-treated 4559 infected mice (**Fig. 4.7B**), underscoring the impact of RafR-mediated neutrophil recruitment on murine lung clearance. *In vivo* neutralization of IL-17A also resulted in an increase in bacterial loads in the lungs of mice, relative to the isotype controls, for all challenge strains (**Fig. 4.7D**), although not to the same extent as seen for neutrophil-depleted mice (**Fig. 4.7B**). The difference between the impact of IL-17A neutralization vs neutrophil depletion is likely due to the action of alternative neutrophil recruitment pathways (Craig et al., 2009; Peñaloza et al., 2015).

These findings demonstrate that the *rafR* SNP examined in this study has a wide-spread effect on both the bacterial and host transcriptomes, with the strains expressing the G249 allele triggering a strong pro-inflammatory IL-17 response in the lungs post-infection. This response leads to an influx of neutrophils to the lungs, resulting in the clearance of bacteria. Conversely, expression of the G249 *rafR* allele results in a more subdued IL-17 host

response, allowing for bacterial persistence in the lungs. Thus, the findings clearly indicate that modulation of neutrophil recruitment during the early stage of infection plays a key role in the capacity of a given *S. pneumoniae* strain to persist in the lungs, and the nature of disease ultimately caused by it.

The downstream experimental analyses of the dual RNAseq data in this chapter were confined predominately to examining the impact of neutrophil recruitment and IL-17 on ability to persist in murine lungs, largely due to compatability with the results of the flow cytometry analyses of cells from infected lung tissue. As the data sets that arise from dual RNAseq experiments are so large, the functional enrichment analyses provided a strategy to focus on classes of genes that are over-represented within the data. This allows focus to be placed on genes that are more likely to be playing roles in the behaviour of the strains, but also results in the focus of analysis being narrow. Beyond IL-17 signalling, the host functional enrichment analyses also identified cytokine-cytokine receptor interactions and necroptosis pathways as being differentially regulated between the serotype 14 ST 15 strains. Further analysis of these additional host-specific areas was outside the scope of the current project, but could be explored in future studies.

In fact, recent studies have shown that necroptosis influences the outcome of pneumococcal infection, through the loss of immune cells or by controlling excessive proinflammatory signalling (Ahn and Prince, 2017; Hakansson and Bergenfelz, 2017; Riegler et al., 2019). Moreover, pore forming toxins such Ply are known to induce necroptosis during pneumonia (Gonzalez-Juarbe et al., 2018, p.; González-Juarbe et al., 2015), though *ply* was not highlighted as significantly differentially expressed in the dual RNAseq data shown in this Chapter. Validation of an impact of RafR on necroptosis could follow a similar route to the flow cytometry experiments of murine lungs 6 h post-infection detailed in this Chapter (section 4.2.6). Necroptotic cells can be identified by staining with Annexin V or propidium iodide (Battaglia, 2017). Moreover, cell death kinetic and morphology assays

and live imaging can be used to distinguish necroptotic and apoptotic cells (Shlomovitz et al., 2018).

The bacterial genes that were commonly up or down regulated between the strains that persisted in murine lungs (4559 and 947M) or between the strains that were cleared from the lungs (947 and 4559M), may be determinants of the distinct virulence phenotypes of the blood and ear isolates (section 4.3.2). Hence their examination through KO or overexpression experiments in murine models is warranted in the future. Both *adhP* and *glpO* were upregulated in the strains that persisted in the lungs, and hence may play roles in preventing neutrophil recruitment to this niche. Other studies have shown that these genes play roles in pneumococcal virulence; GlpO aids in nasopharyngeal colonisation and meningitis (Mahdi et al., 2012, 2017), while AdhP potentiated Ply and infection in a murine infection model (Luong et al., 2015). In contrast, the data showed *nanB* was upregulated in the strains that were cleared from the lungs compared to the strains that persisted, thus this gene may play a role in neutrophil recruitment. Additionally, NanB functions in sialic acid acquisition, and this sugar has been shown to contribute towards biofilm formation (Parker et al., 2009; Trappetti et al., 2009). Therefore, it is possible that the upregulation of *nanB* in 947 and 4559M may result in their increased propensity to infect and persist the middle ear.

NK cells were shown to be present at significantly higher numbers in murine lungs infected with 947 (which were cleared from the lungs) compared to 4559 and 947M (that persisted in the lungs), whereas a similar significant result was seen for eosinophils in 4559M compared to 4559 (section 4.3.5). Hence, heightened NK cell and eosinophil responses may also contribute towards the clearance of these pneumococcal strains from the lungs. To examine if this is the case, future experiments could take a similar approach as the murine neutrophil depletion experiments detailed in this Chapter (section 4.2.7), using the

Siglec-F antibody to deplete eosinophils (Zimmermann et al., 2008) and NK1.1 to deplete NK cells (Waggoner et al., 2014).

Chapter 2 of this thesis showed that in spite of early clearance from the lung, ear isolate 947 and *rafR*-swapped 4559M, both expressing the D249 *rafR* allele, have an enhanced capacity to spread to and/or proliferate in the ear and brain compartments (Minhas et al., 2019). It is not known whether differential carbohydrate metabolism better adapts these strains to utilise alternative carbohydrate sources in these niches, or whether altered host pro-inflammatory responses contribute to ascension of the Eustachian tube and/or penetration of the blood-brain barrier. Unfortunately, the total numbers of pneumococci present in these niches are too low for pathogen-host transcriptomic analyses to be conducted using available technologies.

Intra-species variation in virulence phenotype is a common feature of pathogenic microorganisms, which by nature are genetically diverse. *S. pneumoniae* is an exemplar of such diversity comprising at least 100 capsular serotypes superimposed on over 12,000 MLST types, and with a core genome that accounts for only 70% of genes (Weiser et al., 2018). Nevertheless, stark differences in pathogenic profile can result from the smallest of genetic differences between strains, as exemplified by the profound impact of a single SNP on both bacterial and host transcriptomes reported in this Chapter.

Chapter 5

Final Discussion

The work described in this thesis circumvented issues regarding pneumococcal genomic diversity that have complicated previous attempts to pinpoint factors responsible for the spread of pneumococci into specific sites of the body. This was done by examining closely related strains of the same serotype and ST that have been shown to display distinct tissue tropism in mice that appear to correlate with their initial isolation site in the human body (Amin et al., 2015; Trappetti et al., 2013). It was hypothesised that by examining the relatively few differences within the closely related blood and ear isolate pairs from the serotype 3 ST180 and serotype 14 ST15 clonal lineages, mechanisms dictating their spread to specific sites in the body could be elucidated.

Chapter 2 of this thesis examined genomic differences between the blood and ear isolate pairs. Among other genetic differences, SNPs leading to non-conserved amino acid substitutions were found in the *raf* genes *rafR* (for serotype 14) and *rafK* (for serotype 3), which were subsequently highlighted as potential determinants of tissue tropism. It was not possible to directly attribute the distinct virulence phenotypes of the serotype 3 ST180 blood and ear isolates to the SNP in *rafK*, due to the inability to swap their *rafK* alleles. However, through IN murine challenges with *rafK* KO mutants (section 2.3.5), it is clear that the ability to utilise raffinose and/or downstream consequences thereof, strongly impact the capacity of these strains to cause disease. For the serotype 14 ST 15 isolate pair, swapping the *rafR* alleles between the blood and ear isolate led to concurrent switches in their disease progression following IN murine challenge (section 2.3.4). This was a significant finding for the research field of *S. pneumoniae* disease, as it showed how a

single SNP could alter the tissue tropism of pneumococcal strains while also highlighting the major impact of raffinose regulation on disease progression.

An interesting observation from Chapter 2 was that adherence assays with the serotype 14 ST 15 isolates, and their respective *rafR* swapped mutants, showed the strains able survive in the lung exhibited significantly greater adherence to A549 cells than the strains that were cleared (section 2.3.6), suggesting a role for RafR in adherence. However, this phenotype was seen in CDM media with either Raf or Glc as sole carbon source. In CDM+Glc, the raffinose operon would have been repressed to due to catabolite repression (Carvalho et al., 2011; Fleming et al., 2015; Iyer et al., 2005), suggesting there are additional unknown factors at play. Indeed, analysis of the dual RNAseq data from chapter 4 revealed that exchanging *rafR* alleles led to major alteration in transcriptional patterns in both host and pathogen (sections 4.3.2 and 4.3.3), including bacterial genes that are not related to carbohydrate metabolism.

Notably, the disease progression phenotypes of the serotype 14 ST15 blood and ear isolates were not completely switched after *rafR* allelic exchange. At 24 h post-challenge, the numbers of the *rafR*-swapped 947 strain present in the lungs were roughly one log lower than that for the wild type blood isolate 4559, while the *rafR*-swapped 4559 strain displayed slightly lower spread to the ear than the wild type ear isolate 947 (section 2.3.4). This suggests that there are additional unknown factors outside the *raf* operon that are contributing to the differential virulence phenotype of these otherwise closely related pneumococcal isolates.

Despite the apparent importance of raffinose utilisation in the disease progression of *S. pneumoniae*, GC MS was unable to detect the presence of free raffinose in murine lungs post-infection. However, qRT-PCR analysis of infected lung tissue found that the raffinose operon was activated, indicative of the presence of the sugar (section 2.3.7). Activation of

the raffinose operon early in the course of infection may have led to consumption of much of the free raffinose present in the lungs, resulting in levels below the detectable threshold. Additional GC MS analyses of uninfected lung tissue and at earlier timepoints may therefore be informative. Another possibility is that there may be other carbohydrates present in lung mucus that mimic raffinose sufficiently to induce raffinose operon expression. Nevertheless, the precise mechanisms underlying the effect of the raffinose operon on disease progression remain to be elucidated.

As explored in the section 2.4, the findings of Chapter 2 suggest an example of convergent evolution, where unrelated serotypes/lineages exhibit SNPs in separate genes affecting raffinose utilisation, which impacts their virulence phenotype. BLASTX analysis of available *S. pneumoniae* genomes highlighted that SNPs are widespread in the *raf* genes. Whether these other SNPs impact raffinose utilisation or virulence phenotype is unknown, but is clearly worthy of investigation.

Finally, in addition to the aforementioned SNPs, the serotype 3 ST180 isolate pair had 26 other SNPs or indels, while the serotype 14 ST15 pair had 16 other SNPs or indels, as well as a 35-kb prophage and a 3.2-kb plasmid in 4559 but not in 947 (section 2.3.1). Many of these genomic differences were not within recognised virulence factor genes. Future work should include examination of these other genomic differences, using a similar approach to that used in Chapter 2, namely construction of gene-swap mutants in both blood and ear isolate backgrounds. To further determine the effect of raffinose utilization on pneumococcal virulence in different tissues, future experiments could be performed with the addition of external raffinose in *in vivo* and *ex vivo* assays or using inoculum prepared in the presence of raffinose. Additionally, given the potential impact of carbohydrate metabolism on pneumococcal virulence phenotype, it would make sense to target other metabolic related genes in the first instance, such as *pfkA* and *nanB* for the serotype 14 isolate pair and *adhP* and *glnP* for the serotype 3 isolate pair. However, as there are no

other common SNPs between the serotype 3 and 14 blood and ear isolate pairs, the general applicability of any findings to other pneumococcal strains may be more limited.

The transcriptomic comparisons detailed in Chapter 3 followed a similar line of analysis as the genomic comparisons in Chapter 2. The transcriptomes of each isolate pair were analysed for differentially expressed genes in the three media types, followed by qRT-PCR validations in the sequenced isolate pairs and other corresponding isolate pairs of the same serotype and/or ST. Of all the qRT-PCR validations conducted, only the aldehyde-alcohol dehydrogenase E (*adhE*) was found to be commonly significantly differentially expressed within the tested serotype 3 ST 180 strains (section 3.3.3). Unfortunately, *adhE* KO mutants were unable to show any significant impact of acetaldehyde production or adherence to lung epithelial or nasopharyngeal cells (section 3.3.4), hence *in vivo* experiments were not performed.

The stringent cut off conditions utilised in the differential gene expression analyses may have excluded important gene regulation patterns that influence tissue tropism of the pneumococcal isolate pairs. Therefore, changing the p value cut off to < 0.05, then performing function enrichment analyses (Hawkins et al., 2010) may uncover determinants of pneumococcal disease progression that were overlooked in Chapter 3. Moreover, as the ST180 and ST232 clonal lineages are not from the same lineage, it may be worth examining differences common to only the ST180 blood and ear isolate pairs in the future.

The sequence of genes and their expression patterns do not represent the only potential factors that could differentiate blood and ear isolate pairs. Hence, it is likely that the other omics platforms may uncover other candidate virulence-related factors that the genomic and transcriptomic analyses missed. The PacBio genomic sequencing contains the methylome data of the sequenced pneumococcal strains, but this was not analysed due to time constraints. Importantly, epigenetic changes have been shown to influence

pneumococcal virulence phenotype, resulting from recombinational exchanges at the locus encoding a Type I restriction/modification (RM) system. In strain D39, switching between six possible restriction site target specificities for the enzyme SpnD39III, generated six alternative genome-wide methylation patterns, which was shown to influence both gene expression profiles and *in vivo* virulence phenotype (Manso et al., 2014). Hence, future experiments should compare the methylome data within the blood and ear isolates. Nevertheless, it would be predicted that if epigenetic phase variation was the basis for the distinct phenotypes of blood and ear isolates, this would be reflected in transcriptomic patterns. Thus, it seems improbable that such a mechanism is a predominant underlying cause of the observed phenotypic variation of these blood and ear isolate pairs.

The comprehensive multi-omics program conducted under the auspices of Bioplatforms Australia that generated the data analysed in Chapers 2 and 3 also includes metabolomic and proteomic analyses of the blood and ear isolates under the same three media conditions as the transcriptomic analyses. It is plausible that potentially significant differences in the cellular levels of proteins and/or metabolic pathway products/intermediates may not be evident from the genome or transcriptome. Thus, it will be important to compare the metabolome and proteome between the blood and ear isolate pairs when these data become available. Investigations could include mutational studies of candidate proteins in which their respective genes are either deleted, modified or over expressed, thereby testing the impact of highlighted factors on the ability of the pneumococcal strains to spread to specific sites in the body. The metabolomics data may also yield clues regarding pathways that are up- or down-regulated between the blood and ear isolate pairs. Important genes within these pathways could then be mutated in a similar fashion to the proposed proteomic investigations. That said, there is a possibility that some of the metabolic genes will be essential for pneumococcal viability, thereby limiting suitable mutations to those that do not involve deletion.

Although the results from the *rafR* swap experiments in Chapter 2 suggested that the efficient utilisation of raffinose and/or downstream effects thereof, play significant roles in dictating where pneumococcal strains spread to around the body, the mechanisms behind this were not elucidated. Furthermore, these differences in raffinose operon expression were not picked in the *in vitro* transcriptomics in any of the three media, most probably due to catabolite repression (Iyer et al., 2005). In fact, the most ideal conditions to perform transcriptomic analyses are *in vivo*. Thus technology and experimental techniques were refined during this project that allowed *in vivo* dual RNAseq to become viable, as detailed in chapter 4 and Minhas et al. (2020).

To understand how the *rafR* SNP caused such a drastic switch in disease progression when alleles were swapped between 4559 and 947, *in vivo* dual RNAseq was used to examine pathogen and host transcriptomes in murine lung tissue 6 h post-infection. This allowed a thorough investigation of how the *rafR* SNP affects the transcriptional cross-talk between host and pathogen. The dual-RNAseq data predicted that IL-17 signalling and neutrophil recruitment were impacted due to the *rafR* SNP (section 4.3.3), potentially influenced by corresponding changes in regulation of carbohydrate uptake and metabolism (section 4.3.2). Flow cytometry (section 4.3.5) paired with neutrophil depletion and IL-17 neutralisation in mice prior to I.N. challenge (section 4.3.6), confirmed the crucial influence of the RafR allele on the ability of the blood and ear isolates to persist in the lungs. Though the dual RNAseq data provided great insights into how the *rafR* SNP affects persistence in the lungs post-infection, much still needs to be elucidated. For example, studies on exactly how the changes in bacterial transcriptome lead to differential neutrophil recruitment in the host will need to be done in the future. A reasonable place to start for future experiments would be analysing the bacterial genes that were commonly up or down regulated between the strains that persisted in murine lungs (4559 and $947^{4559rafR}$) or between the strains that were cleared from the lungs (947 and $4559^{947rafR}$), as these may be

determinants of the distinct virulence phenotypes of the blood and ear isolates (section 4.3.2), as detailed in the Chapter 4 discussion.

As the importance of IL-17 and neutrophil recruitment on pathogen clearance was already described in the literature (Lindén et al., 2005; McCarthy et al., 2014; Ritchie et al., 2018; Stoppelenburg et al., 2013), these related findings were not significant breakthroughs in this Chapter. However, elucidation of the influence of RafR on global pneumococcal gene regulation and the impact of carbohydrate metabolism on pneumococcal virulence in general, were significant advances for the field. The *in vivo* dual RNAseq and accompanying analyses were additionally significant breakthroughs in pneumococcal research, showcasing how dual RNAseq can provide mechanistic insights into host-pathogen interactions that have real phenotypic effects *in vivo*. However, the precise mechanisms that cause the *rafR* SNP to alter inflammation and neutrophil infiltration into the lungs 6 h post-infection is not clear. Hence, future studies should focus on elucidating these mechanisms by analysing pneumococcal factors that were commonly upregulated in the strain that persisted in the lungs or commonly upregulated in the cleared strains. Additionally, performing *in vivo* dual RNAseq in murine lungs after I.N. challenge with the serotype 3 ST180 blood and ear isolate pair, given that they also exhibit distinct *in vivo* phenotypes. Additionally, performing dual RNAseq on RNA extracts of infected ear tissue using a mouse OM model would be extremely informative, if enough bacterial RNA can be extracted from this niche. This would provide important information on the pathogen-host interactions that impact the translocation and subsequent persistence of pneumococci in the middle ear compartment.

Results from the genomic and transcriptomic analyses in Chapters 2, 3 and 4 highlighted carbohydrate uptake and metabolic genes as major differentiating factors between the blood and ear isolate pairs. These data support the notion that carbohydrate utilisation plays

key roles in pneumococcal disease progression and tissue tropism, which has been showcased throughout the literature (Buckwalter and King, 2012; Echlin et al., 2020; Engholm et al., 2017; Hatcher et al., 2016; Hobbs et al., 2018; Hu et al., 2019; Kahya et al., 2017; Motib et al., 2019; Robb et al., 2017; Trappetti et al., 2017; Yadav et al., 2018). A critical role of carbohydrate utilisation on pneumococcal virulence is not surprising given the varied constituent nutrients in distinct host niches and the ability of pneumococci to utilise a vast array of carbohydrates (Bidossi et al., 2012).

This PhD project aimed to decipher the mechanisms that allow pneumococcal strains to spread to specific sites in the body. Instead of looking at what invasive isolates had in common, and risking being overwhelmed by the genomic diversity of the species, closely related clonal strains that nevertheless spread to different sites in the body were analysed. This bypassed most of the pneumococcal genetic diversity (i.e. white noise) that has hindered past attempts to analyse pneumococcal virulence mechanisms. Analyses of the omics data detailed in this thesis highlights that strains belonging to the same serotype and ST can exhibit significant variability, which likely influences differential tissue tropism. This project highlighted the importance of raffinose regulation, and carbohydrate metabolism in general, for pneumococcal tissue tropism. Although not all the mechanisms relating to the tissue tropism of the blood and ear isolate pairs were elucidated, significant steps were taken in uncovering how these strains spread around the body to cause disease, which may one day be used to inform the design of novel drug and vaccine candidates.

References

Agarwal, V., Kuchipudi, A., Fulde, M., Riesbeck, K., Bergmann, S. and Blom, A.M. (2013). *Streptococcus pneumoniae* endopeptidase O (PepO) is a multifunctional plasminogen- and fibronectin-binding protein, facilitating evasion of innate immunity and invasion of host cells. *J. Biol. Chem.* 288: 6849–6863.

Agarwal, V., Sroka, M., Fulde, M., Bergmann, S., Riesbeck, K. and Blom, A.M. (2014). Binding of *Streptococcus pneumoniae* endopeptidase O (PepO) to complement component C1q modulates the complement attack and promotes host cell adherence. *J. Biol. Chem.* 289: 15833–15844.

Ahn, D. and Prince, A. (2017). Participation of necroptosis in the host response to acute bacterial pneumonia. *J. Innate. Immun*. 9: 262–270.

Alexander, J.E., Berry, A.M., Paton, J.C., Rubins, J.B., Andrew, P.W. and Mitchell, T.J. (1998). Amino acid changes affecting the activity of pneumolysin alter the behaviour of pneumococci in pneumonia. *Microb. Pathog.* 24: 167–174.

Ali, Y.M., Lynch, N.J., Haleem, K.S., Fujita, T., Endo, Y., Hansen, S. and Holmskov, U. (2012). The lectin pathway of complement activation is a critical component of the innate immune response to pneumococcal infection. *PLoS Pathog.* 8: e1002793.

Alloing, G., Granadel, C., Morrison, D.A. and Claverys, J.P. (1996). Competence pheromone, oligopeptide permease, and induction of competence in *Streptococcus pneumoniae*. *Mol. Microbiol.* 21: 471–478.

Alloway, J.L. (1932). The transformation in vitro of R pneumococci into S forms of different specific types by the use of filtered pneumococcues extracts. *J. Exp. Med.* 55: 91–99.

Amin, Z., Harvey, R.M., Wang, H., Hughes, C.E., Paton, A.W., Paton, J.C. and Trappetti, C. (2015). Isolation site influences virulence phenotype of serotype 14 *Streptococcus pneumoniae* strains belonging to multilocus sequence type 15. *Infect. Immun.* 83: 4781–90.

Anas, A., van der Poll, T. and de Vos, A.F. (2010). Role of CD14 in lung inflammation and infection. *Crit. Care.* 14: 209.

Andre, G.O., Converso, T.R., Politano, W.R., Ferraz, L.F.C., Ribeiro, M.L., Leite, L.C.C. and Darrieux, M. (2017). Role of *Streptococcus pneumoniae* proteins in evasion of complement-mediated immunity. *Front. Microbiol.* 8: 224.

André, G.O., Politano, W.R., Mirza, S., Converso, T.R., Ferraz, L.F.C., Leite, L.C.C. and Darrieux, M. (2015). Combined effects of lactoferrin and lysozyme on *Streptococcus pneumoniae* killing. *Microb. Pathog.* 89: 7–17.

Andreassen, P.R., Trappetti, C., Minhas, V., Nielsen, F.D., Pakula, K., Paton, J.C. and Jørgensen, M.G. (2020). Host-glycan metabolism is regulated by a species-conserved two-component system in *Streptococcus pneumoniae. PLoS Pathog.* 16: e1008332.

Andrews, S. (2010). FastQC: A quality control tool for high throughput sequence data. *Babraham Bioinformatics*. https://doi.org/citeulike-article-id:11583827.

Antunes, M.B. and Cohen, N.A. (2007). Mucociliary clearance--A critical upper airway host defense mechanism and methods of assessment. *Curr. Opin. Allergy CL.* 7: 5–10.

Aprianto, R., Slager, J., Holsappel, S. and Veening, J.W. (2016). Time-resolved dual RNA-seq reveals extensive rewiring of lung epithelial and pneumococcal transcriptomes during early infection. *Genome Biol.* 17: 198.

Arango Duque, G. and Descoteaux, A. (2014). Macrophage cytokines: Involvement in immunity and infectious diseases. *Front Immunol.* 5: 491.

Asmat, T.M., Agarwal, V., Saleh, M. and Hammerschmidt, S. (2014). Endocytosis of *Streptococcus pneumoniae* via the polymeric immunoglobulin receptor of epithelial cells relies on clathrin and caveolin dependent mechanisms. *Int. J. Med. Microbiol.* 304: 1233–1246.

Attaiech, L., Olivier, A., Mortier-Barrière, I., Soulet, A.-L., Granadel, C., Martin, B. and Polard, P. (2011). Role of the single-stranded DNA–binding protein SsbB in pneumococcal transformation: Maintenance of a reservoir for genetic plasticity. *PLoS Genet.* 7: e1002156.

Attali, C., Durmort, C., Vernet, T. and Di Guilmi, A.M. (2008). The interaction of *Streptococcus pneumoniae* with plasmin mediates transmigration across endothelial and epithelial monolayers by intercellular junction cleavage. *Infect. Immun.* 76: 5350–5356.

Attali, C., Frolet, C., Durmort, C., Offant, J., Vernet, T. and Di Guilmi, A.M. (2008). *Streptococcus pneumoniae* choline-binding protein E interaction with plasminogen/plasmin stimulates migration across the extracellular matrix. *Infect. Immun.* 76: 466–476.

Australian Institute of Health and Welfare. (2018). Pneumococcal disease in Australia, *Australian Institute of Health and Welfare*, available at: https://www.aihw.gov.au/reports/immunisation/vaccine-preventable-diseases/contents.

Austrian, R. (1981). Pneumococcus: The first one hundred years. *Rev. Infect. Dis.*3: 183–189.

Avery, O.T., Macleod, C.M. and McCarty, M. (1944). Studies on the chemical natures of the substance inducing transformation of pneumococcal types: Induction of transformation by a desoxyribonucleic acid fraction isolated from pneumococcus type III. *J. Exp. Med.* 79: 137–58.

Ayoubi, P., Kilic, A.O. and Vijayakumar, M.N. (1991). Tn5253, the pneumococcal omega (cat tet) BM6001 element, is a composite structure of two conjugative transposons, Tn5251 and Tn5252. J. Bacteriol. 173: 1617–1622.

Baba, H., Kawamura, I., Kohda, C., Nomura, T., Ito, Y., Kimoto, T. and Watanabe, I. (2002). Induction of gamma interferon and nitric oxide by truncated pneumolysin that lacks pore-forming activity. *Infect. Immun.* 70: 107–113.

Babb, R., Chen, A., Hirst, T.R., Kara, E.E., McColl, S.R., Ogunniyi, A.D., Paton, J.C. and Alsharifi, M. (2016). Intranasal vaccination with γ-irradiated *Streptococcus pneumoniae* whole-cell vaccine provides serotype-independent protection mediated by B-cells and innate IL-17 responses. *Clin. Sci.* 130: 697–710.

Babb, R., Chen, A., Ogunniyi, A.D., Hirst, T.R., Kara, E.E., McColl, S.R., Alsharifi, M., Paton, J.C. (2017). Enhanced protective responses to a serotype-independent pneumococcal vaccine when combined with an inactivated influenza vaccine. *Clin. Sci.* 131: 169–180.

Baroja-Mazo, A., Martín-Sánchez, F., Gomez, A.I., Martínez, C.M., Amores-Iniesta, J., Compan, V., Barberà-Cremades, M., et al. (2014). The NLRP3 inflammasome is released as a particulate danger signal that amplifies the inflammatory response. *Nat. Immunol.* 15: 738–748.

Battaglia, G. (2017). Assessing cell health: Necroptosis, *Bioradiations*. Available at: https://www.bioradiations.com/assessing-cell-health-necroptosis.

Bayle, L., Chimalapati, S., Schoehn, G., Brown, J., Vernet, T. and Durmort, C. (2011). Zinc uptake by *Streptococcus pneumoniae* depends on both AdcA and AdcAII and is essential for normal bacterial morphology and virulence. *Mol. Microbiol.* 82: 904–916.

Bergenfelz, C. and Hakansson, A.P. (2017). *Streptococcus pneumoniae* otitis media pathogenesis and how it informs our understanding of vaccine strategies. *Curr. Otorhinolayrngol. Rep.* 5: 115–124.

Bergmann, S. and Hammerschmidt, S. (2006). Versatility of pneumococcal surface proteins. *Microbiol.* 152: 295–303.

Bergmann, S., Rohde, M., Chhatwal, G.S. and Hammerschmidt, S. (2001). Alpha-Enolase of *Streptococcus pneumoniae* is a plasmin(ogen)-binding protein displayed on the bacterial cell surface. *Mol. Microbiol.* 40: 1273–1287.

Bergmann, S., Rohde, M. and Hammerschmidt, S. (2004). Glyceraldehyde-3-phosphate dehydrogenase of *Streptococcus pneumoniae* is a surface-displayed plasminogen-binding protein. *Infect. Immun.* 72: 2416–2419.

Berry, A.M., Alexander, J.E., Mitchell, T.J., Andrew, P.W., Hansman, D. and Paton, J.C. (1995). Effect of defined point mutations in the pneumolysin gene on the virulence of *Streptococcus pneumoniae*. *Infect. Immun.* 63: 1969–1974.

Berry, A.M., Lock, R.A., Hansman, D. and Paton, J.C. (1989). Contribution of autolysin to virulence of *Streptococcus pneumoniae. Infect. Immun.* 57: 2324–2330.

Berry, A.M., Lock, R.A. and Paton, J.C. (1996). Cloning and characterization of nanB, a second *Streptococcus pneumoniae* neuraminidase gene, and purification of the NanB enzyme from recombinant Escherichia coli. *J. Bacteriol.* 178: 4854–4860.

Berry, A.M. and Paton, J.C. (1996). Sequence heterogeneity of PsaA, a 37-kilodalton putative adhesin essential for virulence of *Streptococcus pneumoniae*. *Infect. Immun.* 64: 5255–5262.

Berry, A.M. and Paton, J.C. (2000). Additive attenuation of virulence of *Streptococcus pneumoniae* by mutation of the genes encoding pneumolysin and other putative pneumococcal virulence proteins. *Infect. Immun.* 68: 133–140.

Bidossi, A., Mulas, L., Decorosi, F., Colomba, L., Ricci, S., Pozzi, G., Deutscher, J., et al. (2012). A functional genomics approach to establish the complement of carbohydrate transporters in *Streptococcus pneumoniae. PLoS One.* 7: e33320.

Blanchette, K.A., Shenoy, A.T., Milner, J., Gilley, R.P., McClure, E., Hinojosa, C.A., Kumar, N., et al. (2016). Neuraminidase A-exposed galactose promotes *Streptococcus pneumoniae* biofilm formation during colonization. *Infect. Immun.* 84: 2922–2932.

Blanchette-Cain, K., Hinojosa, C.A., Babu, R.A.S., Lizcano, A., Gonzalez-Juarbe, N., Munoz-Almagro, C., Sanchez, C.J., et al. (2013). *Streptococcus pneumoniae* biofilm formation is strain dependent, multifactorial, and associated with reduced invasiveness and immunoreactivity during colonization. m*Bio.* 4: e00745-13.

Bogaert, D., De Groot, R. and Hermans, P.W.M. (2004). *Streptococcus pneumoniae* colonisation: The key to pneumococcal disease. *Lancet. Infect. Dis.* 4: 144–154.

Bogaert, D., Hermans, P.W.M., Adrian, P.V., Rümke, H.C. and de Groot, R. (2004). Pneumococcal vaccines: an update on current strategies. *Vaccine*. 22: 2209–2220.

Bolger, A.M., Lohse, M. and Usadel, B. (2014). Trimmomatic: a flexible trimmer for Illumina sequence data. *Bioinformatics.* 30: 2114–2120.

Briles, D.E., Ades, E., Paton, J.C., Sampson, J.S., Carlone, G.M., Huebner, R.C., Virolainen, A., et al. (2000). Intranasal immunization of mice with a mixture of the pneumococcal proteins PsaA and PspA is highly protective against nasopharyngeal carriage of *Streptococcus pneumoniae*. *Infect. Immun.* 68: 796–800.

Brook, I. (2013). Acute Sinusitis in Children, *Pediatr. Clin. North Am.* 60: 409–424.

Brooks, L.R.K. and Mias, G.I. (2018). *Streptococcus pneumoniae*'s virulence and host immunity: aging, diagnostics, and prevention. *Front. Immunol.* 9: 1366.

Brown, A.O., Mann, B., Gao, G., Hankins, J.S., Humann, J., Giardina, J., Faverio, P., et al. (2014). *Streptococcus pneumoniae* translocates into the myocardium and forms unique microlesions that disrupt cardiac function. *PLoS Pathog.* 10: e1004383.

Brown, J.S., Gilliland, S.M., Ruiz-Albert, J. and Holden, D.W. (2002). Characterization of pit, a *Streptococcus pneumoniae* iron uptake ABC transporter. *Infect. Immun.* 70: 4389–4398.

Brown, J.S., Hussell, T., Gilliland, S.M., Holden, D.W., Paton, J.C., Ehrenstein, M.R., Walport, M.J., et al. (2002). The classical pathway is the dominant complement pathway required for innate immunity to *Streptococcus pneumoniae* infection in mice. *PNAS.* 99: 16969–16974.

Brueggemann, A.B., Harrold, C.L., Rezaei Javan, R., van Tonder, A.J., McDonnell, A.J. and Edwards, B.A. (2017). Pneumococcal prophages are diverse, but not without structure or history. *Sci. Rep.* 7: 42976.

Bruinsma, N., Kristinsson, K.G., Bronzwaer, S., Schrijnemakers, P., Degener, J., Tiemersma, E., Hryniewicz, W., et al. (2004). Trends of penicillin and erythromycin resistance among invasive *Streptococcus pneumoniae* in Europe. *J. Antimicrob. Chemother.* 54: 1045–1050.

Bryant, K.A., Block, S.L., Baker, S.A., Gruber, W.C., Scott, D.A. and PCV13 Infant Study Group. (2010). Safety and immunogenicity of a 13-valent pneumococcal conjugate vaccine. *Pediatrics*. 125: 866–875.

Buckwalter, C.M. and King, S.J. (2012). Pneumococcal carbohydrate transport: Food for thought. *Trends in Microbiol.* 20: 517–522.

Burkholder, K.M., Kim, K.-P., Mishra, K.K., Medina, S., Hahm, B.-K., Kim, H. and Bhunia, A.K. (2009). Expression of LAP, a SecA2-dependent secretory protein, is induced under anaerobic environment. *Microbes Infect.* 11: 859–867.

Burrus, V., Pavlovic, G., Decaris, B. and Guédon, G. (2002). Conjugative transposons: The tip of the iceberg. *Mol. Microbiol.* 46: 601–610.

Canvin, J.R., Marvin, A.P., Sivakumaran, M., Paton, J.C., Boulnois, G.J., Andrew, P.W. and Mitchell, T.J. (1995). The role of pneumolysin and autolysin in the pathology of pneumonia and septicemia in mice infected with a type 2 pneumococcus. *J. Inect. Dis.* 172: 119–123.

Carvalho, S.M., Kloosterman, T.G., Kuipers, O.P. and Neves, A.R. (2011). CcpA ensures optimal metabolic fitness of *Streptococcus pneumoniae*. *PLoS One.* 6: e26707.

Carver, T.J., Rutherford, K.M., Berriman, M., Rajandream, M.-A., Barrell, B.G. and Parkhill, J. (2005). ACT: the Artemis comparison tool. *Bioinformatics*. 21: 3422–3423.

Chai, M.H.C. (2016). Characterisation of *Streptococcus pneumoniae* opacity phase variation. Available at: https://doi.org/10.4225/55/58dc7eaca367a.

Chancey, S.T., Agrawal, S., Schroeder, M.R., Farley, M.M., Tettelin, H. and Stephens, D.S. (2015). Composite mobile genetic elements disseminating macrolide resistance in *Streptococcus pneumoniae*. *Front. Microbiol.* 9;6: 26.

Chen, A., Mann, B., Gao, G., Heath, R., King, J., Maissoneuve, J., Alderson, M., et al. (2015). Multivalent pneumococcal protein vaccines comprising pneumolysoid with epitopes/fragments of CbpA and/or PspA elicit strong and broad protection. *Clin. Vaccine Immunol.* 22: 1079–1089.

Chen, S., Paterson, G.K., Tong, H.H., Mitchell, T.J. and DeMaria, T.F. (2005). Sortase A contributes to pneumococcal nasopharyngeal colonization in the chinchilla model. *FEMS Microbiol. Lett.* 253: 151–154.

Cheng, W., Li, Q., Jiang, Y.-L., Zhou, C.-Z. and Chen, Y. (2013). Structures of *Streptococcus pneumoniae* piaa and its complex with ferrichrome reveal insights into the substrate binding and release of high affinity iron transporters. *PLoS One.* 12: e71451.

Cherazard, R., Epstein, M., Doan, T.-L., Salim, T., Bharti, S. and Smith, M.A. (2017). Antimicrobial resistant *Streptococcus pneumoniae*: prevalence, mechanisms, and clinical implications. *Am. J. Ther.* 24: e361–e369.

Cho, H., Jönsson, H., Campbell, K., Melke, P., Williams, J.W., Jedynak, B., Stevens, A.M., et al. (2007). Self-organization in high-density bacterial colonies: efficient crowd control. *PLoS Biol.* 5: e302.

Cillóniz, C., Ewig, S., Menéndez, R., Ferrer, M., Polverino, E., Reyes, S., Gabarrús, A., et al. (2012). Bacterial co-infection with H1N1 infection in patients admitted with community acquired pneumonia. *J. Infect.* 65: 223–230.

Claverys, J.-P. and Håvarstein, L.S. (2007). Cannibalism and fratricide: Mechanisms and raisons d'être. *Nat. Rev. Microbiol.* 5: 219–229.

Claverys, J.-P., Martin, B. and Håvarstein, L.S. (2007). Competence-induced fratricide in streptococci. *Mol. Microbiol.* 64: 1423–1433.

Cohen, R., Bingen, E., Varon, E., Rocque, F.D.L., Brahimi, N., Levy, C., Boucherat, M., et al. (1997). Change in nasopharyngeal carriage of *Streptococcus pneumoniae* resulting from antibiotic therapy for acute otitis media in children. *Pediatr. Infect. Dis. Journal.* 16: 555–560.

Comis, S.D., Osborne, M.P., Stephen, J., Tarlow, M.J., Hayward, T.L., Mitchell, T.J., Andrew, P.W., et al. (1993). Cytotoxic effects on hair cells of guinea pig cochlea produced by pneumolysin, the thiol activated toxin of *Streptococcus pneumoniae*. *Acta Oto-Laryngol.* 113: 152–159.

Corcoran, M., Mereckiene, J., Murchan, S., McElligott, M., 'Flanagan, D., Cotter, S., Cunney, R., et al. (2019). Is it time to review the vaccination strategy to protect adults against invasive pneumococcal disease? *Ir. Med. J.* 112: 894.

Costerton, J.W., Stewart, P.S. and Greenberg, E.P. (1999). Bacterial biofilms: A common cause of persistent infections. *Science.* 284: 1318–1322.

Craig, A., Mai, J., Cai, S. and Jeyaseelan, S. (2009). Neutrophil recruitment to the lungs during bacterial pneumonia. *Infect. Immun.* 77: 568–575.

Cremers, A.J., Zomer, A.L., Gritzfeld, J.F., Ferwerda, G., van Hijum, S.A., Ferreira, D.M., Shak, J.R., et al. (2014). The adult nasopharyngeal microbiome as a determinant of pneumococcal acquisition. *Microbiome*. 2: 44.

Cron, L.E., Bootsma, H.J., Noske, N., Burghout, P., Hammerschmidt, S. and Hermans, P.W.M. (2009). Surface-associated lipoprotein PpmA of *Streptococcus pneumoniae* is involved in colonization in a strain-specific manner. *Microbiol.* 155: 2401–2410.

Croucher, N.J., Finkelstein, J.A., Pelton, S.I., Mitchell, P.K., Lee, G.M., Parkhill, J., Bentley, S.D., et al. (2013). Population genomics of post-vaccine changes in pneumococcal epidemiology. *Nature Genet.* 45: 656–663.

Croucher, N.J., Mitchell, A.M., Gould, K.A., Inverarity, D., Barquist, L., Feltwell, T., Fookes, M.C., et al. (2013). Dominant role of nucleotide substitution in the diversification of serotype 3 pneumococci over decades and during a single infection. *PLoS Genet.* 9: e1003868.

Croucher, N.J., Walker, D., Romero, P., Lennard, N., Paterson, G.K., Bason, N.C., Mitchell, A.M., et al. (2009). Role of conjugative elements in the evolution of the multidrug-resistant pandemic clone *Streptococcus pneumoniae S*pain23F st81. *J. Bacteriol.* 191: 1480–1489.

Cundell, D.R., Gerard, C., Idanpaan-Heikkila, I., Tuomanen, E.I. and Gerard, N.P. (1996). PAf receptor anchors *Streptococcus pneumoniae* to activated human endothelial cells. *Adv. Exp. Med. Biol.* 416: 89–94.

Cundell, D.R., Gerard, N.P., Gerard, C., Idanpaan-Heikkila, I. and Tuomanen, E.I. (1995). *Streptococcus pneumoniae* anchor to activated human cells by the receptor for platelet-activating factor. *Nature.* 377: 435–438.

Dabernat, H., Geslin, P., Megraud, F., Bégué, P., Boulesteix, J., Dubreuil, C., de La Roque, F., et al. (1998). Effects of cefixime or co-amoxiclav treatment on nasopharyngeal carriage of *Streptococcus pneumoniae* and Haemophilus influenzae in children with acute otitis media. *J. Antimicrob. Chemother.* 41: 253–258.

Dagan, R., Leibovitz, E., Greenberg, D., Yagupsky, P., Fliss, D. and Leiberman, A. (1998). Dynamics of pneumococcal nasopharyngeal colonization during the first days of antibiotic treatment in pediatric patients. *Pediatr. Infect. Dis. J.* 17: 880–885.

Dalia, A.B., Standish, A.J. and Weiser, J.N. (2010). Three surface exoglycosidases from *Streptococcus pneumoniae*, NanA, BgaA, and StrH, promote resistance to opsonophagocytic killing by human neutrophils. *Infect. Immun.* 78: 2108–2116.

Dalia, A.B. and Weiser, J.N. (2011). Minimization of bacterial size allows for complement evasion and is overcome by the agglutinating effect of antibody. *Cell Host Microbe.* 10: 486–496.

Danishyar, A. and Ashurst, J. V. (2019). *Otitis, Media, Acute*. *StatPearls*. Available from: https://www.ncbi.nlm.nih.gov/books/NBK470332/

Darling, A.C.E., Mau, B., Blattner, F.R. and Perna, N.T. (2004). Mauve: Multiple alignment of conserved genomic sequence with rearrangements. *Genome Res.* 14: 1394–1403.

Dave, S., Carmicle, S., Hammerschmidt, S., Pangburn, M.K. and McDaniel, L.S. (2004). Dual roles of PspC, a surface protein of *Streptococcus pneumoniae*, in binding human secretory IgA and factor H. *J. Immunol.* 173: 471–477.

David Powell, Michael Milton, Andrew Perry and Kim Santos. (2019). *Drpowell/Degust 4.1.1*, Zenod. Available at: https://doi.org/10.5281/zenodo.3501067.

David, S.C., Laan, Z., Minhas, V., Chen, A.Y., Davies, J., Hirst, T.R., McColl, S.R., et al. (2019). Enhanced safety and immunogenicity of a pneumococcal surface antigen A mutant whole-cell inactivated pneumococcal vaccine. *Immunol. Cell Biol.* 97: 726–739.

Davis, K.M., Akinbi, H.T., Standish, A.J. and Weiser, J.N. (2008). Resistance to mucosal lysozyme compensates for the fitness deficit of peptidoglycan modifications by *Streptococcus pneumoniae*. *PLoS Pathog.* 4: e1000241.

Dawid, S., Roche, A.M. and Weiser, J.N. (2007). The blp bacteriocins of *Streptococcus pneumoniae* mediate intraspecies competition both in vitro and in vivo. *Infect. Immun.* 75: 443–451.

Dawid, S., Sebert, M.E. and Weiser, J.N. (2009). Bacteriocin activity of *Streptococcus pneumoniae* is controlled by the serine protease HtrA via posttranscriptional regulation. *J. Bacteriol.* 191: 1509–1518.

DeBardeleben, H.K., Lysenko, E.S., Dalia, A.B. and Weiser, J.N. (2014). Tolerance of a Phage Element by *Streptococcus pneumoniae* Leads to a Fitness Defect during Colonization. *J. Bacteriol.* 196: 2670–2680.

Dessing, M.C., Knapp, S., Florquin, S., de Vos, A.F. and van der Poll, T. (2007). CD14 facilitates invasive respiratory tract infection by *Streptococcus pneumoniae*. *Am. J. Respir. Crit. Care Med.* 175: 604–611.

Díaz-Batalla, L., Widholm, J.M., Fahey, George C., Castaño-Tostado, E. and Paredes-López, O. (2006). Chemical components with health implications in wild and cultivated mexican common bean seeds (*Phaseolus vulgaris* L.). *J. Agric. Food Chem.* 54: 2045–2052.

Dintilhac, A., Alloing, G., Granadel, C. and Claverys, J.-P. (1997). Competence and virulence of *Streptococcus pneumoniae*: Adc and PsaA mutants exhibit a requirement for Zn and Mn resulting from inactivation of putative ABC metal permeases. *Mol. Microbiol.* 25: 727–739.

Dobin, A., Davis, C.A., Schlesinger, F., Drenkow, J., Zaleski, C., Jha, S., Batut, P., et al. (2013). STAR: ultrafast universal RNA-seq aligner. *Bioinformatics.* 29: 15–21.

Dockrell, D.H. and Brown, J.S. (2015). Chapter 21 - *Streptococcus pneumoniae* interactions with macrophages and mechanisms of immune evasion. *Academic Press*, Amsterdam. pp. 401–422.

Domenech, A., Slager, J. and Veening, J.-W. (2018). Antibiotic-induced cell chaining triggers pneumococcal competence by reshaping quorum sensing to autocrine-like signaling. *Cell Rep.* 9: 2390-2400.

Donati, C., Hiller, N.L., Tettelin, H., Muzzi, A., Croucher, N.J., Angiuoli, S.V., Oggioni, M., et al. (2010). Structure and dynamics of the pan-genome of *Streptococcus pneumoniae* and closely related species. *Genome Biol.* 11: R107.

Donlan, R.M. and Costerton, J.W. (2002). Biofilms: Survival mechanisms of clinically relevant microorganisms. *Clin. Microbiol. Rev.* 15: 167–193.

D'Souza, S.E., Ginsberg, M.H. and Plow, E.F. (1991). Arginyl-glycyl-aspartic acid (RGD): A cell adhesion motif. *Trends Biochem. Sci.* 16: 246–250.

Echlin, H., Frank, M., Rock, C. and Rosch, J.W. (2020). Role of the pyruvate metabolic network on carbohydrate metabolism and virulence in *Streptococcus pneumoniae*. *Mol. Microbiol.* Available at: https://doi.org/10.1111/mmi.14557.

Egan, J.B. and Morse, M.L. (1966). Carbohydrate transport in *Staphylococcus aureus*: III. Studies of the transport process. *Biochim. Biophys. Acta*. 112: 63–73.

Ehrlich, G.D., Hu, F.Z., Shen, K., Stoodley, P. and Post, J.C. (2005). Bacterial plurality as a general mechanism driving persistence in chronic infections. *Clin. Orthop. Relat. Res.* 437: 20–24.

Eisen, D.P., Dean, M.M., Boermeester, M.A., Fidler, K.J., Gordon, A.C., Kronborg, G., Kun, J.F.J., et al. (2008). Low serum mannose-binding lectin level increases the risk of death due to pneumococcal infection. *Clin. Infect. Dis*. 47: 510–516.

El Moujaber, G., Osman, M., Rafei, R., Dabboussi, F. and Hamze, M. (2017). Molecular mechanisms and epidemiology of resistance in *Streptococcus pneumoniae* in the Middle East region. *J. Med. Microbiol.* 66: 847–858.

Eldholm, V., Johnsborg, O., Haugen, K., Ohnstad, H.S. and Håvarstein, L.S. (2009). Fratricide in *Streptococcus pneumoniae*: Contributions and role of the cell wall hydrolases CbpD, LytA and LytC. *Microbiol.* 155: 2223–2234.

Eldholm, V., Johnsborg, O., Straume, D., Ohnstad, H.S., Berg, K.H., Hermoso, J.A. and Håvarstein, L.S. (2010). Pneumococcal CbpD is a murein hydrolase that requires a dual cell envelope binding specificity to kill target cells during fratricide. *Mol. Microbiol.* 4: 905–917.

van Emmerik, L.C., Kuijper, E.J., Fijen, C.A., Dankert, J. and Thiel, S. (1994). Binding of mannan-binding protein to various bacterial pathogens of meningitis. *Clin. Exp. Immunol.* 97: 411–416.

Engholm, D.H., Kilian, M., Goodsell, D.S., Andersen, E.S. and Kjærgaard, R.S. (2017). A visual review of the human pathogen *Streptococcus pneumoniae*. *FEMS Microbiol. Rev.* 41: 854–879.

Enright, M.C. and Spratt, B.G. (1998). A multilocus sequence typing scheme for *Streptococcus pneumoniae*: identification of clones associated with serious invasive disease. *Microbiol.* 144: 3049–3060.

Faget, J., Boivin, G., Ancey, P.-B., Gkasti, A., Mussard, J., Engblom, C., Pfirschke, C., et al. (2018). Efficient and specific Ly6G$^+$ cell depletion: A change in the current practices toward more relevant functional analyses of neutrophils. *BioRxiv.* Available at: https://doi.org/10.1101/498881.

Falloon, J. and Gallin, J.I. (1986). Neutrophil granules in health and disease. *J. Allergy Clin. Immunol.* 77: 653–662.

Fasching, C.E., Grossman, T., Corthésy, B., Plaut, A.G., Weiser, J.N. and Janoff, E.N. (2007). Impact of the molecular form of immunoglobulin A on functional activity in defense against *Streptococcus pneumoniae. Infect. Immun.* 75: 1801–1810.

Ferreira, D.M., Neill, D.R., Bangert, M., Gritzfeld, J.F., Green, N., Wright, A.K.A., Pennington, S.H., et al. (2013). Controlled human infection and rechallenge with *Streptococcus pneumoniae* reveals the protective efficacy of carriage in healthy adults. *Am. J. Respir. Crit. Care Med.* 187: 855–864.

Fiehn, O. (2016). Metabolomics by gas chromatography-mass spectrometry: combined targeted and untargeted profiling. *Curr. Protoc. Mol. Biol.* 114: 30.4.1–30.4.32

Fine, M.J., Smith, M.A., Carson, C.A., Meffe, F., Sankey, S.S., Weissfeld, L.A., Detsky, A.S., et al. (1994). Efficacy of pneumococcal vaccination in adults. A meta-analysis of randomized controlled trials. *Ann. Intern. Med.* 154: 2666–2677.

Fleming, E., Lazinski, D.W. and Camilli, A. (2015). Carbon catabolite repression by seryl phosphorylated HPr is essential to *Streptococcus pneumoniae* in carbohydrate-rich environments. *Mol. Microbiol.* 97: 360–380.

Forrest, J., PB, M. and MA, B. (2000). Pneumococcal disease in Australia. *Commun. Dis. Intell.* 24: 89–92.

Franchi, L., Warner, N., Viani, K. and Nuñez, G. (2009). Function of Nod-like receptors in microbial recognition and host defense. *Immunol. Rev.* 227: 106–128.

de la Fuente-Núñez, C., Reffuveille, F., Fernández, L. and Hancock, R.E. (2013). Bacterial biofilm development as a multicellular adaptation: Antibiotic resistance and new therapeutic strategies. *Curr. Opin. Microbiol.* Vol. 16 No. 5, pp. 580–589.

Ganaie, F., Saad, J.S., McGee, L., Tonder, A.J. van, Bentley, S.D., Lo, S.W., Gladstone, R.A., et al. (2020). A new pneumococcal capsule type, 10D, is the 100th serotype and has a large CPS fragment from an oral Streptococcus. *mBio.* 11: e00937-20.

Gänzle, M.G. (2015). Lactic metabolism revisited: Metabolism of lactic acid bacteria in food fermentations and food spoilage. *Curr. Opin. Food Sci.* 2: 106–117.

García-Rodríguez, J.A. and Fresnadillo Martínez, M.J. (2002). Dynamics of nasopharyngeal colonization by potential respiratory pathogens. *J. Antimicrob. Chemother.* 50: 59–73.

García-Suárez, M. del M., Flórez, N., Astudillo, A., Vázquez, F., Villaverde, R., Fabrizio, K., Pirofski, L.-A., et al. (2007). The role of pneumolysin in mediating lung damage in a lethal pneumococcal pneumonia murine model. *Respir. Res.* 8: 3.

Gardiner, E.E. and Andrews, R.K. (2012). Neutrophil extracellular traps (NETs) and infection-related vascular dysfunction. *Blood Rev.* 26: 255–259.

Geno, K.A., Gilbert, G.L., Song, J.Y., Skovsted, I.C., Klugman, K.P., Jones, C., Konradsen, H.B., et al. (2015). Pneumococcal capsules and their types: Past, present, and future. *Clin. Microbiol. Rev.* 28: 871–899.

Gentile, M.A., Melchiorre, S., Emolo, C., Moschioni, M., Gianfaldoni, C., Pancotto, L., Ferlenghi, I., et al. (2011). Structural and functional characterization of the *Streptococcus pneumoniae* RrgB pilus backbone D1 domain. *The J. Biol. Chem.* 286: 14588–14597.

Ghaffar, F., Barton, T., Lozano, J., Muniz, L.S., Hicks, P., Gan, V., Ahmad, N., et al. (2004). Effect of the 7-valent pneumococcal conjugate vaccine on nasopharyngeal colonization by *Streptococcus pneumoniae* in the first 2 years of life. *Clin. Infect. Dis.*39: 930–938.

Giammarinaro, P. and Paton, J.C. (2002). Role of RegM, a homologue of the catabolite repressor protein CcpA, in the virulence of *Streptococcus pneumoniae*. *Infect. Immun.* 70: 5454–5461.

van Gils, E.J.M., Veenhoven, R.H., Hak, E., Rodenburg, G.D., Bogaert, D., Ijzerman, E.P.F., Bruin, J.P., et al. (2009). Effect of reduced-dose schedules with 7-valent pneumococcal conjugate vaccine on nasopharyngeal pneumococcal carriage in children: A randomized controlled trial. *JAMA*. 302: 159–167.

van Ginkel, F.W., McGhee, J.R., Watt, J.M., Campos-Torres, A., Parish, L.A. and Briles, D.E. (2003). Pneumococcal carriage results in ganglioside-mediated olfactory tissue infection, *PNAS.* 100: 14363–14367.

Gladman, S. (2018). De novo genome assembly for illumina data - bioinformatics documentation. Available at: https://www.melbournebioinformatics.org.au/tutorials/tutorials/assembly/assembly-protocol/.

Gladstone, R.A., Jefferies, J.M., Tocheva, A.S., Beard, K.R., Garley, D., Chong, W.W., Bentley, S.D., et al. (2015). Five winters of pneumococcal serotype replacement in UK carriage following PCV introduction. *Vaccine.* 33: 2015–2021.

Gonzalez-Juarbe, N., Bradley, K.M., Riegler, A.N., Reyes, L.F., Brissac, T., Park, S.-S., Restrepo, M.I., et al. (2018). Bacterial pore-forming toxins promote the activation of caspases in parallel to necroptosis to enhance alarmin release and inflammation during pneumonia. *Sci. Rep.* 8: 5846.

González-Juarbe, N., Gilley, R.P., Hinojosa, C.A., Bradley, K.M., Kamei, A., Gao, G., Dube, P.H., et al. (2015). Pore-forming toxins induce macrophage necroptosis during acute bacterial pneumonia. *PLoS Pathog.* 11: e1005337.

von Gottberg, A., de Gouveia, L., Tempia, S., Quan, V., Meiring, S., von Mollendorf, C., Madhi, S.A., et al. (2014). Effects of vaccination on invasive pneumococcal disease in South Africa. *N. Engl. J. Med.* 371: 1889–1899.

Grabenstein, J.D. and Musey, L.K. (2014). Differences in serious clinical outcomes of infection caused by specific pneumococcal serotypes among adults. *Vaccine.* 32: 2399–2405.

Gram, C. (1884). Ueber die isolirte Farbung der Schizomyceten, *Schnitt Aund Trockenpraparaten. Fortschr. Med.* 2: 185-189.

Gratz, N., Loh, L.N., Mann, B., Gao, G., Carter, R., Rosch, J. and Tuomanen, E.I. (2017). Pneumococcal neuraminidase activates TGF-β signalling. *Microbiol.* 163: 1198–1207.

Grebe, K.M., Takeda, K., Hickman, H.D., Bailey, A.L., Bailey, A.M., Embry, A.C., Bennink, J.R., et al. (2010). Cutting edge: Sympathetic nervous system increases proinflammatory cytokines and exacerbates influenza A virus pathogenesis. *J. Immunol.* 184: 540–544.

Griffith, F. (1928). The significance of pneumococcal types. *J. Hyg.* 27: 113–59.

Grivea, I.N., Panagiotou, M., Tsantouli, A.G. and Syrogiannopoulos, G.A. (2008). Impact of heptavalent pneumococcal conjugate vaccine on nasopharyngeal carriage of penicillin-resistant *Streptococcus pneumoniae* among day-care center attendees in central Greece. *Pediatr. Infect. Dis. Journal.* 27: 519–525.

Guiral, S., Mitchell, T.J., Martin, B. and Claverys, J.-P. (2005). Competence-programmed predation of noncompetent cells in the human pathogen *Streptococcus pneumoniae*: Genetic requirements. *PNAS.* 102: 8710–8715.

Gutiérrez-Fernández, J., Saleh, M., Alcorlo, M., Gómez-Mejía, A., Pantoja-Uceda, D., Treviño, M.A., Voß, F., et al. (2016). Modular architecture and unique teichoic acid recognition features of choline-binding protein l (CbpL) contributing to pneumococcal pathogenesis. *Sci. Rep.* 6: 1–19.

Hakansson, A.P. and Bergenfelz, C. (2017). Low NF-κB activation and necroptosis in alveolar macrophages: A new virulence property of *Streptococcus pneumoniae*. *J. Inect. Dis.* 216: 402–404.

Hall-Stoodley, L., Costerton, J.W. and Stoodley, P. (2004). Bacterial biofilms: From the natural environment to infectious diseases. *Nat. Rev. Microbiology.* 2: 95–108.

Hamaguchi, S., Zafar, M.A., Cammer, M. and Weiser, J.N. (2018). Capsule prolongs survival of *Streptococcus pneumoniae* during starvation. *Infect. Immun.* 86: e00802-17.

Hammerschmidt, S., Tillig, M.P., Wolff, S., Vaerman, J.-P. and Chhatwal, G.S. (2000). Species-specific binding of human secretory component to SpsA protein of *Streptococcus pneumoniae* via a hexapeptide motif. *Mol. Microbiol.* 36: 726–736.

Hammerschmidt, S., Wolff, S., Hocke, A., Rosseau, S., Müller, E. and Rohde, M. (2005). Illustration of pneumococcal polysaccharide capsule during adherence and invasion of epithelial cells. *Infect. Immun.* 73: 4653–4667.

Hammitt, L.L., Bruden, D.L., Butler, J.C., Baggett, H.C., Hurlburt, D.A., Reasonover, A. and Hennessy, T.W. (2006). Indirect effect of conjugate vaccine on adult carriage of *Streptococcus pneumoniae*: An explanation of trends in invasive pneumococcal disease. *J. Inect. Dis.* 193: 1487–1494.

Harboe, Z.B., Thomsen, R.W., Riis, A., Valentiner-Branth, P., Christensen, J.J., Lambertsen, L., Krogfelt, K.A., et al. (2009). Pneumococcal serotypes and mortality following invasive pneumococcal disease: A population-based cohort study. *PLoS Med.* 6: 1000081.

Harris, R.A. and Harper, E.T. (2015). Glycolytic pathway. *ELS*. 1–8: e0000619.

Härtel, T., Klein, M., Koedel, U., Rohde, M., Petruschka, L. and Hammerschmidt, S. (2011). Impact of glutamine transporters on pneumococcal fitness under infection-related conditions. *Infect. Immun.* 79: 44–58.

Harvey, R.M., Hughes, C.E., Paton, A.W., Trappetti, C., Tweten, R.K. and Paton, J.C. (2014). The impact of pneumolysin on the macrophage response to *Streptococcus pneumoniae* is strain-dependent. *PLoS One.* 9: e103625.

Harvey, R.M., Stroeher, U.H., Ogunniyi, A.D., Smith-Vaughan, H.C., Leach, A.J. and Paton, J.C. (2011). A variable region within the genome of *Streptococcus pneumoniae* contributes to strain-strain variation in virulence. *PLoS One.* 6: e0019650.

Harvey, R.M., Trappetti, C., Mahdi, L.K., Wang, H., McAllister, L.J., Scalvini, A., Paton, A.W., et al. (2016). The variable region of pneumococcal pathogenicity island 1 is responsible for unusually high virulence of a serotype 1 isolate. *Infect. Immun.* 84: 822–832.

Hatcher, B.L., Hale, J.Y. and Briles, D.E. (2016). Free sialic acid acts as a signal that promotes *Streptococcus pneumoniae* invasion of nasal tissue and nonhematogenous invasion of the central nervous system. *Infect. Immun.* 84: 2607–2615.

Hava, D.L. and Camilli, A. (2002). Large-scale identification of serotype 4 *Streptococcus pneumoniae* virulence factors. *Mol. Microbiol.* 45: 1389–1406.

Håvarstein, L.S., Coomaraswamy, G. and Morrison, D.A. (1995). An unmodified heptadecapeptide pheromone induces competence for genetic transformation in *Streptococcus pneumoniae*. *PNAS.* 92: 11140–11144.

Håvarstein, L.S., Martin, B., Johnsborg, O., Granadel, C. and Claverys, J.-P. (2006). New insights into the pneumococcal fratricide: Rto clumping and identification of a novel immunity factor. *Mol. Microbiol.* 59: 1297–1307.

Hawkins, T., Chitale, M. and Kihara, D. (2010). Functional enrichment analyses and construction of functional similarity networks with high confidence function prediction by PFP. *BMC Bioinform.* 11: 265.

Heidelberger, M. and Avery, O.T. (1923). The soluble specific substance of pneumococcus. *J. Exp. Med.* 38: 73–9.

Heidelberger, Michael. (1927). Immunologically Specific Polysaccharides. *Chem. Rev.* 3: 403–423.

Heilmann, C. (1990). Human B and T lymphocyte responses to vaccination with pneumococcal polysaccharides. *APMIS.* 15: 1–23.

Hendriksen, W.T., Kloosterman, T.G., Bootsma, H.J., Estevão, S., de Groot, R., Kuipers, O.P. and Hermans, P.W.M. (2008). Site-specific contributions of glutamine-dependent regulator GlnR and GlnR-regulated genes to virulence of *Streptococcus pneumoniae. Infect. Immun.* 76: 1230–1238.

Hergott, C.B., Roche, A.M., Naidu, N.A., Mesaros, C., Blair, I.A. and Weiser, J.N. (2015). Bacterial exploitation of phosphorylcholine mimicry suppresses inflammation to promote airway infection. *J. Clin. Invest.* 125: 3878–3890.

Hermans, P.W.M., Adrian, P.V., Albert, C., Estevão, S., Hoogenboezem, T., Luijendijk, I.H.T., Kamphausen, T., et al. (2006). The streptococcal lipoprotein rotamase A (SlrA) is a functional peptidyl-prolyl isomerase involved in pneumococcal colonization. *The J. Biol. Chem.* 281: 968–976.

Hiller, N.L., Janto, B., Hogg, J.S., Boissy, R., Yu, S., Powell, E., Keefe, R., et al. (2007). Comparative genomic analyses of seventeen *Streptococcus pneumoniae* strains: Insights into the pneumococcal supragenome. *J. Bacteriol.* 189: 8186–8195.

Hirst, R.A., Kadioglu, A., O'Callaghan, C. and Andrew, P.W. (2004). The role of pneumolysin in pneumococcal pneumonia and meningitis. *Clin. Exp. Immunol.* 138: 195–201.

Hiss, P.H. (1905). A contribution to the physiological differentiation of pneumococcus and streptococcus, and to methods of staining capsules. *J. Exp. Med.* 6: 317–345.

Hobbs, J.K., Pluvinage, B. and Boraston, A.B. (2018). Glycan-metabolizing enzymes in microbe-host interactions: The *Streptococcus pneumoniae* paradigm. *FEBS Lett.* 592: 3865–3897.

Hoe, E., Anderson, J., Nathanielsz, J., Toh, Z.Q., Marimla, R., Balloch, A. and Licciardi, P.V. (2017). The contrasting roles of Th17 immunity in human health and disease. *Microbiol. Immunol.* 61: 49–56.

Hollingshead, S.K., Becker, R. and Briles, D.E. (2000). Diversity of PspA: Mosaic genes and evidence for past recombination in *Streptococcus pneumoniae*. *Infect. Immun.* 68: 5889–5900.

Hoskins, J., Alborn, W.E., Arnold, J., Blaszczak, L.C., Burgett, S., DeHoff, B.S., Estrem, S.T., et al. (2001). Genome of the bacterium *Streptococcus pneumoniae* Strain R6. *J. Bacteriol.* 183: 5709–5717.

Hosseini, S.M., Poorolajal, J., Karami, M. and Ameri, P. (2015). Prevalence of nasopharyngeal carriage of *Streptococcus pneumoniae* in Iran: A meta-analysis. *J. Res. Health Sci.* 15: 41–146.

Hsieh, Y.-C., Lin, T.-L., Lin, C.-M. and Wang, J.-T. (2015). Identification of PbIB mediating galactose-specific adhesion in a successful *Streptococcus pneumoniae* clone. *Sci. Rep.* 5: 12265.

Hsu, H.E., Shutt, K.A., Moore, M.R., Beall, B.W., Bennett, N.M., Craig, A.S., Farley, M.M., et al. (2009). Effect of pneumococcal conjugate vaccine on pneumococcal meningitis. *N. Engl. J. Med.* 360: 244–256.

Hu, F.Z., Król, J.E., Tsai, C.H.S., Eutsey, R.A., Hiller, L.N., Sen, B., Ahmed, A., et al. (2019). Deletion of genes involved in the ketogluconate metabolism, Entner-Doudoroff pathway, and glucose dehydrogenase increase local and invasive virulence phenotypes in *Streptococcus pneumoniae*. *PLoS One.* 14: e0209688.

Hyams, C., Camberlein, E., Cohen, J.M., Bax, K. and Brown, J.S. (2010). The *Streptococcus pneumoniae* capsule inhibits complement activity and neutrophil phagocytosis by multiple mechanisms. *Infect. Immun.* 78: 704–715.

Iannelli, F., Chiavolini, D., Ricci, S., Oggioni, M.R. and Pozzi, G. (2004). Pneumococcal surface protein c contributes to sepsis caused by *Streptococcus pneumoniae* in mice. *Infect. Immun.* 72: 3077–3080.

Iannelli, F., Oggioni, M.R. and Pozzi, G. (2002). Allelic variation in the highly polymorphic locus PspC of *Streptococcus pneumoniae. Gene.* 284: 63–71.

Iovino, F., Engelen-Lee, J.-Y., Brouwer, M., van de Beek, D., van der Ende, A., Valls Seron, M., Mellroth, P., et al. (2017). PIgR and PECAM-1 bind to pneumococcal adhesins RrgA and PspC mediating bacterial brain invasion. *J. Exp. Med.* 214: 1619–1630.

Iroh Tam, P.-Y., Thielen, B.K., Obaro, S.K., Brearley, A.M., Kaizer, A.M., Chu, H. and Janoff, E.N. (2017). Childhood pneumococcal disease in Africa – A systematic review and meta-analysis of incidence, serotype distribution, and antimicrobial susceptibility. *Vaccine.* 35: 1817–1827.

Iyer, R., Baliga, N.S. and Camilli, A. (2005). Catabolite control protein a (CcpA) contributes to virulence and regulation of sugar metabolism in *Streptococcus pneumoniae. J. Bacteriol.* 187: 8340–8349.

Iyer, R. and Camilli, A. (2007). Sucrose metabolism contributes to in vivo fitness of *Streptococcus pneumoniae. Mol. Microbiol.* 66: 1–13.

Jagadeesan, B., Koo, O.K., Kim, K.-P., Burkholder, K.M., Mishra, K.K., Aroonnual, A. and Bhunia, A.K. (2010). LAP, an alcohol acetaldehyde dehydrogenase enzyme in Listeria, promotes bacterial adhesion to enterocyte-like Caco-2 cells only in pathogenic species. *Microbiol.* 156: 2782–2795.

Janoff, E.N., Rubins, J.B., Fasching, C., Charboneau, D., Rahkola, J.T., Plaut, A.G. and Weiser, J.N. (2014). Pneumococcal IgA1 protease subverts specific protection by human IgA1. *Mucosal Immunology*. 7: 249–256.

Janulczyk, R., Iannelli, F., Sjöholm, A.G., Pozzi, G. and Björck, L. (2000). Hic, a novel surface protein of *Streptococcus pneumoniae* that interferes with complement function. *J. Biol. Chem.* 275: 37257–37263.

Jechlinger, W., Szostak, M.P., Witte, A. and Lubitz, W. (1999). Altered temperature induction sensitivity of the lambda pR/cI857 system for controlled gene E expression in *Escherichia coli. FEMS Microbiol. Lett.* 173: 347–352.

Jedrzejas, M.J., Lamani, E. and Becker, R.S. (2001). Characterization of selected strains of pneumococcal surface protein A. *J. Biol. Chem.* 276: 33121–33128.

Jedrzejas, M.J., Mello, L.V., de Groot, B.L. and Li, S. (2002). Mechanism of hyaluronan degradation by *Streptococcus pneumoniae* hyaluronate lyase. Structures of complexes with the substrate. *J. Biol. Chem.* 277: 28287–28297.

Jensch, I., Gámez, G., Rothe, M., Ebert, S., Fulde, M., Somplatzki, D., Bergmann, S., et al. (2010). PavB is a surface-exposed adhesin of *Streptococcus pneumoniae* contributing to nasopharyngeal colonization and airways infections. *Mol. Microbiol.* 77: 22–43.

Jeong, D.-G., Seo, J.-H., Heo, S.-H., Choi, Y.-K. and Jeong, E.-S. (2015). Tumor necrosis factor-alpha deficiency impairs host defense against *Streptococcus pneumoniae*. *Lab. Anim. Res.* 31: 78–85.

Johnsborg, O., Eldholm, V., Bjørnstad, M.L. and Håvarstein, L.S. (2008). A predatory mechanism dramatically increases the efficiency of lateral gene transfer in *Streptococcus pneumoniae* and related commensal species. *Mol. Microbiol.* 69: 245–253.

Johnson, S.E., Dykes, J.K., Jue, D.L., Sampson, J.S., Carlone, G.M. and Ades, E.W. (2002). Inhibition of pneumococcal carriage in mice by subcutaneous immunization with peptides from the common surface protein pneumococcal surface adhesin A. *J. Inect. Dis. 1*85: 489–496.

Johnston, C., Martin, B., Fichant, G., Polard, P. and Claverys, J.-P. (2014). Bacterial transformation: Distribution, shared mechanisms and divergent control. *Nat. Rev. Microbiology*. 12: 181–196.

Johnston, J.W., Myers, L.E., Ochs, M.M., Benjamin, W.H., Briles, D.E. and Hollingshead, S.K. (2004). Lipoprotein PsaA in virulence of *Streptococcus pneumoniae*: Surface accessibility and role in protection from superoxide. *Infect. Immun.* 72: 5858–5867.

Jones, R.N., Sader, H.S., Mendes, R.E. and Flamm, R.K. (2013). Update on antimicrobial susceptibility trends among *Streptococcus pneumoniae* in the United States: Report of ceftaroline activity from the SENTRY Antimicrobial Surveillance Program (1998-2011). *Diag. Microbiol. Infect. Dis.* 75: 107–109.

Jounblat, R., Kadioglu, A., Mitchell, T.J. and Andrew, P.W. (2003). Pneumococcal behavior and host responses during bronchopneumonia are affected differently by the cytolytic and complement-activating activities of pneumolysin. *Infect. Immun.* 71: 1813–1819.

Kadioglu, A. and Andrew, P.W. (2004). The innate immune response to pneumococcal lung infection: The untold story. *Trends Immunol.* 25: 143–149.

Kadioglu, A., Coward, W., Colston, M.J., Hewitt, C.R.A. and Andrew, P.W. (2004). CD4-T-lymphocyte interactions with pneumolysin and pneumococci suggest a crucial

protective role in the host response to pneumococcal infection. *Infect. Immun.* 72: 2689–2697.

Kadioglu, A., Weiser, J.N., Paton, J.C. and Andrew, P.W. (2008). The role of *Streptococcus pneumoniae* virulence factors in host respiratory colonization and disease. *Nature Rev. Microbiol.* 6: 288–301.

Kahya, H.F., Andrew, P.W. and Yesilkaya, H. (2017). Deacetylation of sialic acid by esterases potentiates pneumococcal neuraminidase activity for mucin utilization, colonization and virulence. *PLoS Pathog.* 13: e1006263.

Kallio, A., Sepponen, K., Hermand, P., Denoël, P., Godfroid, F. and Melin, M. (2014). Role of Pht proteins in attachment of *Streptococcus pneumoniae* to respiratory epithelial cells. *Infect. Immun.* 82: 1683–1691.

Kandasamy, R., Voysey, M., Collins, S., Berbers, G., Robinson, H., Noel, I., Hughes, H., et al. (2019). Persistent circulation of vaccine serotypes and serotype replacement after five years of UK infant immunisation with PCV13. *J. Inect. Dis.* 221: 1361-1370.

Kandler, O. (1983). Carbohydrate metabolism in lactic acid bacteria. *Anton. Leeuw. Int. J*. 49: 209–224.

Kausmally, L., Johnsborg, O., Lunde, M., Knutsen, E. and Håvarstein, L.S. (2005). Choline-binding protein D (CbpD) in *Streptococcus pneumoniae* is essential for competence-induced cell lysis. *J. Bacteriol.* 187: 4338–4345.

Keller, L.E., Robinson, D.A. and McDaniel, L.S. (2016). Nonencapsulated *Streptococcus pneumoniae*: Emergence and pathogenesis. *mBio.* 7: e01792-15.

Kelly, T., Dillard, J.P. and Yother, J. (1994). Effect of genetic switching of capsular type on virulence of *Streptococcus pneumoniae*. *Infect. Immun.* 62: 1813–1819.

Kerr, A.R., Paterson, G.K., Riboldi-Tunnicliffe, A. and Mitchell, T.J. (2005). Innate immune defense against pneumococcal pneumonia requires pulmonary complement component C3. *Infect. Immun.* 73: 4245–4252.

Kharat, A.S. and Tomasz, A. (2003). Inactivation of the SrtA gene affects localization of surface proteins and decreases adhesion of *Streptococcus pneumoniae* to human pharyngeal cells in vitro. *Infect. Immun.* 71: 2758–2765.

Kietzman, C.C., Gao, G., Mann, B., Myers, L. and Tuomanen, E.I. (2016). Dynamic capsule restructuring by the main pneumococcal autolysin LytA in response to the epithelium. *Nature Commun.* 7: e10859.

Kilian, M., Poulsen, K., Blomqvist, T., Håvarstein, L.S., Bek-Thomsen, M., Tettelin, H. and Sørensen, U.B.S. (2008). Evolution of *Streptococcus pneumoniae* and its close commensal relatives. *PLoS One.* 3: e2683.

King, S.J. (2010). Pneumococcal modification of host sugars: A major contributor to colonization of the human airway? *Mol. Oral Microbiol.* 25: 15–24.

King, S.J., Hippe, K.R., Gould, J.M., Bae, D., Peterson, S., Cline, R.T., Fasching, C., et al. (2004). Phase variable desialylation of host proteins that bind to *Streptococcus pneumoniae* in vivo and protect the airway. *Mol. Microbiol.* 54: 159–171.

King, S.J., Hippe, K.R. and Weiser, J.N. (2006). Deglycosylation of human glycoconjugates by the sequential activities of exoglycosidases expressed by *Streptococcus pneumoniae*. *Mol. Microbiol.* 59: 961–974.

Kirkham, L.-A.S., Jefferies, J.M.C., Kerr, A.R., Jing, Y., Clarke, S.C., Smith, A. and Mitchell, T.J. (2006). Identification of invasive serotype 1 pneumococcal isolates that express nonhemolytic pneumolysin. *J. Clin. Microbiol.* 44: 151–159.

Kloosterman, T.G., Bijlsma, J.J.E., Kok, J. and Kuipers, O.P. (2006). To have neighbour's fare: extending the molecular toolbox for *Streptococcus pneumoniae*. *Microbiology.* 152: 351–359.

Knutsen, E., Ween, O. and Håvarstein, L.S. (2004). Two separate quorum-sensing systems upregulate transcription of the same ABC transporter in *Streptococcus pneumoniae. J. Bacteriol.* 186: 3078–3085.

Kolaczkowska, E. and Kubes, P. (2013). Neutrophil recruitment and function in health and inflammation. *Nature Rev. Immunol.* 13: 159–175.

Kono, M., Zafar, M.A., Zuniga, M., Roche, A.M., Hamaguchi, S. and Weiser, J.N. (2016). Single cell bottlenecks in the pathogenesis of *Streptococcus pneumoniae*. *PLoS Pathog.* 12: e1005887.

Kovács, M., Halfmann, A., Fedtke, I., Heintz, M., Peschel, A., Vollmer, W., Hakenbeck, R., et al. (2006). A functional *dlt* operon, encoding proteins required for incorporation of D-alanine in teichoic acids in Gram-positive bacteria, confers resistance to cationic antimicrobial peptides in *Streptococcus pneumoniae*. *J. Bacteriol.* 188: 5797–5805.

Kraal, G., van der Laan, L.J., Elomaa, O. and Tryggvason, K. (2000). The macrophage receptor MARCO. *Microbes Infect.* 2: 313–316.

Kumar, V., Rani, A., Goyal, L., Dixit, A.K., Manjaya, J.G., Dev, J. and Swamy, M. (2010). Sucrose and raffinose family oligosaccharides (RFOS) in soybean seeds as influenced by genotype and growing location. *J. Agric. Food Chem.* 58: 5081–5085.

Lacks, S. and Hotchkiss, R.D. (1960). A study of the genetic material determining an enzyme activity in Pneumococcus. *Biochimica et Biophysica Acta.* 39: 508–518.

Langmead, B. and Salzberg, S.L. (2012). Fast gapped-read alignment with Bowtie 2. *Nature Methods.* 9: 357–359.

Lawrence, M.C., Pilling, P.A., Epa, V.C., Berry, A.M., Ogunniyi, A.D. and Paton, J.C. (1998). The crystal structure of pneumococcal surface antigen PsaA reveals a metal-binding site and a novel structure for a putative ABC-type binding protein. *Structure*. 6: 1553–1561.

Leighton, M.P., Kelly, D.J., Williamson, M.P. and Shaw, J.G. (2001). An NMR and enzyme study of the carbon metabolism of *Neisseria meningitidis. Microbiol.* 147: 1473–1482.

LeMieux, J., Hava, D.L., Basset, A. and Camilli, A. (2006). RrgA and RrgB are components of a multisubunit pilus encoded by the *Streptococcus pneumoniae rlrA* pathogenicity islet. *Infect. Immun.* 74: 2453–2456.

Lewis, K. (2008). Multidrug tolerance of biofilms and persister cells. *Curr. Topics Microbiol. Immunol.* 322: 107–131.

Li, H. (2013). Aligning sequence reads, clone sequences and assembly contigs with BWA-MEM, *ArXiv:1303.3997 [Q-Bio]*, available at: http://arxiv.org/abs/1303.3997.

Li, H., Handsaker, B., Wysoker, A., Fennell, T., Ruan, J., Homer, N., Marth, G., et al. (2009). The sequence alignment/map format and samtools. *Bioinformatics*. 25: 2078–2079.

Liao, Y., Smyth, G.K. and Shi, W. (2014). FeatureCounts: An efficient general purpose program for assigning sequence reads to genomic features. *Bioinformatics.* 30: 923–930.

Liñares, J., Ardanuy, C., Pallares, R. and Fenoll, A. (2010). Changes in antimicrobial resistance, serotypes and genotypes in *Streptococcus pneumoniae* over a 30-year period. *Clin. Microbiol. Infect.* 16: 402–410.

Lindén, A., Laan, M. and Anderson, G.P. (2005). Neutrophils, interleukin-17A and lung disease. *Europ. Resp. J.* 25: 159–172.

Lipsitch, M., O'Neill, K., Cordy, D., Bugalter, B., Trzcinski, K., Thompson, C.M., Goldstein, R., et al. (2007). Strain characteristics of *Streptococcus pneumoniae* carriage and invasive disease isolates during a cluster-randomized clinical trial of the 7-valent pneumococcal conjugate vaccine. *J. Inect. Dis.* 196: 1221–1227.

Livak, K.J. and Schmittgen, T.D. (2001). Analysis of relative gene expression data using real-time quantitative PCR and the 2(-Delta Delta C(T)) Method. *Methods.* 25: 402–408.

Lobley, R.W., Burrows, P.C., Warwick, R., Dawson, D.J. and Holmes, R. (1990). Simultaneous assessment of intestinal permeability and lactose tolerance with orally administered raffinose, lactose and L-arabinose. *Clin. Sci.* 79: 175–83.

Lock, R.A., Zhang, Q.Y., Berry, A.M. and Paton, J.C. (1996). Sequence variation in the *Streptococcus pneumoniae* pneumolysin gene affecting haemolytic activity and electrophoretic mobility of the toxin. *Microb. Pathog.* 21: 71–83.

Loeffler, J.M. and Fischetti, V.A. (2006). Lysogeny of *Streptococcus pneumoniae* with Mm1 phage: Improved adherence and other phenotypic changes. *Infect. Immun.* 74: 4486–4495.

López, R., García, E., García, P. and García, J.L. (1997). The pneumococcal cell wall degrading enzymes: A modular design to create new lysins? *Microbial Drug Resis.* 3: 199–211.

Loughran, A.J., Orihuela, C.J. and Tuomanen, E.I. (2019). *Streptococcus pneumoniae*: Invasion and inflammation. *Microbiol. Spect.* 7: e30004.

Love, M.I., Huber, W. and Anders, S. (2014). Moderated estimation of fold change and dispersion for RNA-seq data with DESeq2. *Genome Biol.* 15: 550.

Lu, L., Lamm, M.E., Li, H., Corthesy, B. and Zhang, J.-R. (2003). The human polymeric immunoglobulin receptor binds to *Streptococcus pneumoniae* via domains 3 and 4. *J. Biol. Chem.* 278: 48178–48187.

Lu, L., Ma, Y. and Zhang, J.-R. (2006). *Streptococcus pneumoniae* Recruits Complement Factor H through the Amino Terminus of CbpA. *J. Biol. Chem.* 281: 15464–15474.

Lu, Y.-J., Leite, L., Gonçalves, V.M., Dias, W. de O., Liberman, C., Fratelli, F., Alderson, M., et al. (2010). GMP-grade pneumococcal whole-cell vaccine injected subcutaneously protects mice from nasopharyngeal colonization and fatal aspiration-sepsis. *Vaccine.* 28: 7468–7475.

Luna-Muschi, A., Castillo-Tokumori, F., Deza, M.P., Mercado, E.H., Egoavil, M., Sedano, K., Castillo, M.E., et al. (2019). Invasive pneumococcal disease in hospitalised children from Lima, Peru before and after introduction of the 7-valent conjugated vaccine. *Epidemiol. Infect.* 147: e91.

Luong, T.T., Kim, E.-H., Bak, J.P., Nguyen, C.T., Choi, S., Briles, D.E., Pyo, S., et al. (2015). Ethanol-induced alcohol dehydrogenase A (AdhE) potentiates pneumolysin in *Streptococcus pneumoniae. Infect. Immun.* 83: 108–119.

Lynch, J.P. and Zhanel, G.G. (2009). *Streptococcus pneumoniae*: Does antimicrobial resistance matter? *Semin. Res. Crit. Care Med.* 30: 210–238.

Lynch, J.P. and Zhanel, G.G. (2010). *Streptococcus pneumoniae*: Epidemiology and risk factors, evolution of antimicrobial resistance, and impact of vaccines. *Curr. Opin. Pulmon. Med.* 16: 1.

Lysbo Svendsen, T., Rasmussen, S., Nielsen, P.E., Hartling, O. and Trap-Jensen, J. (1979). Hemodynamic effects of acute and long-term treatment with labetalol. *Acta Medica Scandin.* 625: 49–53.

Lysenko, E.S., Clarke, T.B., Shchepetov, M., Ratner, A.J., Roper, D.I., Dowson, C.G. and Weiser, J.N. (2007). Nod1 signaling overcomes resistance of *S. pneumoniae* to opsonophagocytic killing. *PLoS Pathog.* 3: e118.

Macfadyen, L.P., Dorocicz, I.R., Reizer, J., Saier, M.H. and Redfield, R.J. (1996). Regulation of competence development and sugar utilization in *Haemophilus influenzae* Rd by a phosphoenolpyruvate:fructose phosphotransferase system. *Mol. Microbiol.* 21: 941–952.

MacLeod, C.M. and Krauss, M.R. (1950). Relation of virulence of penumococcal strains for mice to the quantity of capsular polysachharide formed in vitro. *J. Exp. Med.* 92: 1–9.

Madeddu, G., Laura Fiori, M. and Stella Mura, M. (2010). Bacterial community-acquired pneumonia in HIV-infected patients. *Curr. Opin. Pulmon. Med.* 16: 201–7.

Mahdi, L.K., Higgins, M.A., Day, C.J., Tiralongo, J., Hartley-Tassell, L.E., Jennings, M.P., Gordon, D.L., et al. (2017). The pneumococcal alpha-glycerophosphate oxidase enhances nasopharyngeal colonization through binding to host glycoconjugates, *EBioMedicine*. 18: 236–243.

Mahdi, L.K., Ogunniyi, A.D., LeMessurier, K.S. and Paton, J.C. (2008). Pneumococcal virulence gene expression and host cytokine profiles during pathogenesis of invasive disease. *Infect. Immun.* 76: 646–657.

Mahdi, L.K., Wang, H., Van der Hoek, M.B., Paton, J.C. and Ogunniyi, A.D. (2012). Identification of a novel pneumococcal vaccine antigen preferentially expressed during meningitis in mice. *J. Clin. Invest.* 122: 2208–2220.

Majcherczyk, P.A., Langen, H., Heumann, D., Fountoulakis, M., Glauser, M.P. and Moreillon, P. (1999). Digestion of *Streptococcus pneumoniae* cell walls with its major peptidoglycan hydrolase releases branched stem peptides carrying proinflammatory activity. *J. Biol. Chem. 2*74: 12537–12543.

Malley, R., Henneke, P., Morse, S.C., Cieslewicz, M.J., Lipsitch, M., Thompson, C.M., Kurt-Jones, E., et al. (2003). Recognition of pneumolysin by Toll-like receptor 4 confers resistance to pneumococcal infection. *PNAS.* 100: 1966–1971.

Malley, R., Lipsitch, M., Stack, A., Saladino, R., Fleisher, G., Pelton, S., Thompson, C., et al. (2001). Intranasal immunization with killed unencapsulated whole cells prevents colonization and invasive disease by capsulated pneumococci. *Infect. Immun.* 69: 4870–4873.

Malley, R., Trzcinski, K., Srivastava, A., Thompson, C.M., Anderson, P.W. and Lipsitch, M. (2005). CD4+ T cells mediate antibody-independent acquired immunity to pneumococcal colonization. *PNAS.* 102: 4848–4853.

Mamishi, S., Moradkhani, S., Mahmoudi, S., Hosseinpour - Sadeghi, R. and Pourakbari, B. (2014). Penicillin-Resistant trend of *Streptococcus pneumoniae* in Asia: A systematic review. *Iran. J. Microbiol.* 6: 198–210.

Manco, S., Hernon, F., Yesilkaya, H., Paton, J.C., Andrew, P.W. and Kadioglu, A. (2006). Pneumococcal neuraminidases A and B both have essential roles during infection of the respiratory tract and sepsis. *Infect. Immun.* 74: 4014–4020.

Mandigers, C.M., Diepersloot, R.J., Dessens, M., Mol, S.J. and Klingeren, B. van. (1994). A hospital outbreak of penicillin-resistant pneumococci in The Netherlands. *Europ. Resp. J.* 7: 1635–1639.

Mann, B., Orihuela, C., Antikainen, J., Gao, G., Sublett, J., Korhonen, T.K. and Tuomanen, E. (2006). Multifunctional role of choline binding protein G in pneumococcal pathogenesis. *Infect. Immun.* 74: 821–829.

Manso, A.S., Chai, M.H., Atack, J.M., Furi, L., De Ste Croix, M., Haigh, R., Trappetti, C., et al. (2014). A random six-phase switch regulates pneumococcal virulence via global epigenetic changes. *Nature Commun.* 5: 1–9.

Marion, C., Aten, A.E., Woodiga, S.A. and King, S.J. (2011). Identification of an ATPase, MsmK, which energizes multiple carbohydrate ABC transporters in *Streptococcus pneumoniae. Infect. Immun.* 79: 4193–4200.

Marion, C., Stewart, J.M., Tazi, M.F., Burnaugh, A.M., Linke, C.M., Woodiga, S.A. and King, S.J. (2012). *Streptococcus pneumoniae* can utilize multiple sources of hyaluronic acid for growth. *Infect. Immun.* 80: 1390–1398.

Marks, L.R., Davidson, B.A., Knight, P.R. and Hakansson, A.P. (2013). Interkingdom signaling induces *Streptococcus pneumoniae* biofilm dispersion and transition from asymptomatic colonization to disease. *mBio.* 4: e00438-13.

Marks, L.R., Reddinger, R.M. and Hakansson, A.P. (2012). High levels of genetic recombination during nasopharyngeal carriage and biofilm formation in *Streptococcus pneumoniae. mBio.* 3: e00200-12.

Marks, L.R., Reddinger, R.M. and Hakansson, A.P. (2014). Biofilm formation enhances fomite survival of *Streptococcus pneumoniae* and *Streptococcus pyogenes. Infect. Immun.* 82: 1141–1146.

Marra, A., Lawson, S., Asundi, J.S., Brigham, D. and Hromockyj, A.E. (2002). In vivo characterization of the *psa* genes from *Streptococcus pneumoniae* in multiple models of infection. *Microbiology.* 148: 1483–1491.

Martin, B., Garcia, P., Castanié, M.P., Glise, B. and Claverys, J.P. (1995). The *recA* gene of *Streptococcus pneumoniae* is part of a competence-induced operon and controls an SOS regulon. *Develop. Biol. Standard.* 85: 293–300.

Martin, B., Soulet, A.-L., Mirouze, N., Prudhomme, M., Mortier-Barrière, I., Granadel, C., Noirot-Gros, M.-F., et al. (2013). ComE/ComE~P interplay dictates activation or extinction status of pneumococcal X-state (competence). *Mol. Microbiol.* 87: 394–411.

Martner, A., Skovbjerg, S., Paton, J.C. and Wold, A.E. (2009). *Streptococcus pneumoniae* autolysis prevents phagocytosis and production of phagocyte-activating cytokines. *Infect. Immun.* 77: 3826–3837.

McAllister, L.J., Ogunniyi, A.D., Stroeher, U.H., Leach, A.J. and Paton, J.C. (2011). Contribution of serotype and genetic background to virulence of serotype 3 and serogroup 11 pneumococcal isolates, *Infect. Immun.* Vol. 79 No. 12, pp. 4839–4849.

McAllister, L.J., Tseng, H.-J., Ogunniyi, A.D., Jennings, M.P., McEwan, A.G. and Paton, J.C. (2004). Molecular analysis of the Psa permease complex of *Streptococcus pneumoniae*. *Mol. Microbiol.* 53: 889–901.

McCarthy, M.K., Zhu, L., Procario, M.C. and Weinberg, J.B. (2014). IL-17 contributes to neutrophil recruitment but not to control of viral replication during acute mouse adenovirus type 1 respiratory infection. *Virology.* 456–457: 259–267.

McCool, T.L., Cate, T.R., Moy, G. and Weiser, J.N. (2002). The immune response to pneumococcal proteins during experimental human carriage. *J. Exp. Med.* 195: 359–365.

McKessar, S.J. and Hakenbeck, R. (2007). The two-component regulatory system TCS08 is involved in cellobiose metabolism of *Streptococcus pneumoniae* R6. *J. Bacteriol.* 189: 1342–1350.

McMillin, J.M. (1990). Blood glucose, in Walker, H.K., Hall, W.D. and Hurst, J.W. (Eds.). Clinical Methods: The History, Physical, and Laboratory Examinations, 3rd ed. *Butterworths, Boston.* Available at: http://www.ncbi.nlm.nih.gov/books/NBK248/.

McNeela, E.A., Burke, A., Neill, D.R., Baxter, C., Fernandes, V.E., Ferreira, D., Smeaton, S., et al. (2010). Pneumolysin activates the NLRP3 inflammasome and promotes proinflammatory cytokines independently of TLR4. *PLoS Pathog.* 6: e1001191.

Mell, J.C. and Redfield, R.J. (2014). Natural competence and the evolution of DNA uptake specificity. *J. Bacteriol.* 196: 1471–1483.

Mellroth, P., Daniels, R., Eberhardt, A., Rönnlund, D., Blom, H., Widengren, J., Normark, S., et al. (2012). LytA, major autolysin of *Streptococcus pneumoniae*, requires access to nascent peptidoglycan. *The J. Biol. Chem.* 287: 11018–11029.

Minhas, V., Aprianto, R., McAllister, L.J., Wang, H., David, S.C., McLean, K.T., Comerford, I., et al. (2020). In vivo dual RNA-seq reveals that neutrophil recruitment underlies differential tissue tropism of *Streptococcus pneumoniae*. *Commun. Biol.* 3: 1–12.

Minhas, V., Harvey, R.M., McAllister, L.J., Seemann, T., Syme, A.E., Baines, S.L., Paton, J.C., et al. (2019). Capacity to utilize raffinose dictates pneumococcal disease phenotype. *mBio.* 10: e02596-18.

Mitchell, A.J., Yau, B., McQuillan, J.A., Ball, H.J., Too, L.K., Abtin, A., Hertzog, P., et al. (2012). Inflammasome-dependent IFN-γ drives pathogenesis in *Streptococcus pneumoniae* meningitis. *J. Immunol.* 189: 4970–4980.

Mitchell, T.J., Andrew, P.W., Saunders, F.K., Smith, A.N. and Boulnois, G.J. (1991). Complement activation and antibody binding by pneumolysin via a region of the toxin homologous to a human acute-phase protein. *Mol. Microbiol.* 5: 1883–1888.

Mitchell, T.J. and Dalziel, C.E. (2014). The biology of pneumolysin. *Subcell. Biochem.* 80: 145–160.

Mitchell, T.J., Mendez, F., Paton, J.C., Andrew, P.W. and Boulnois, G.J. (1990). Comparison of pneumolysin genes and proteins from *Streptococcus pneumoniae* types 1 and 2. *Nucleic Acids Res.* 18: 4010.

Moffitt, K. and Malley, R. (2016). Rationale and prospects for novel pneumococcal vaccines. *Hum. Vaccin. Immunother.* 12: 383–392.

Mook-Kanamori, B.B., Geldhoff, M., van der Poll, T. and van de Beek, D. (2011). Pathogenesis and pathophysiology of pneumococcal meningitis. *Clin. Microbiol. Rev.* 24: 557–591.

Morens, D.M., Taubenberger, J.K. and Fauci, A.S. (2008). Predominant role of bacterial pneumonia as a cause of death in pandemic influenza: Implications for pandemic influenza preparedness. *J. Inect. Dis.* 198: 962–970.

Morona, J.K., Paton, J.C., Miller, D.C. and Morona, R. (2000). Tyrosine phosphorylation of CpsD negatively regulates capsular polysaccharide biosynthesis in *Streptococcus pneumoniae. Mol. Microbiol.* 35: 1431–1442.

Moscoso, M., García, E. and López, R. (2006). Biofilm formation by *Streptococcus pneumoniae*: Role of choline, extracellular DNA, and capsular polysaccharide in microbial accretion. *J. Bacteriol.* 188: 7785–7795.

Mosser, J.L. and Tomasz, A. (1970). Choline-containing teichoic acid as a structural component of pneumococcal cell wall and its role in sensitivity to lysis by an autolytic enzyme. *J. Biol. Chem.* 245: 287–298.

Mostowy, R.J., Croucher, N.J., De Maio, N., Chewapreecha, C., Salter, S.J., Turner, P., Aanensen, D.M., et al. (2017). Pneumococcal capsule synthesis locus CPS as evolutionary hotspot with potential to generate novel serotypes by recombination. *Mol. Biol. Evol.* 34: 2537–2554.

Motib, A.S., Al-Bayati, F.A.Y., Manzoor, I., Shafeeq, S., Kadam, A., Kuipers, O.P., Hiller, N.L., et al. (2019). TprA/PhrA quorum sensing system has a major effect on pneumococcal survival in respiratory tract and blood, and its activity is controlled by CcpA and GlnR. *Front. Cell. Infect. Microbiol.* 9: 326.

Mukerji, R., Mirza, S., Roche, A.M., Widener, R.W., Croney, C.M., Rhee, D.-K., Weiser, J.N., et al. (2012). Pneumococcal surface protein A inhibits complement deposition on the pneumococcal surface by competing with the binding of C-reactive protein to cell-surface phosphocholine. *J. Immunol.* 189: 5327–5335.

Muramatsu, H., Tachikui, H., Ushida, H., Song, X., Qiu, Y., Yamamoto, S. and Muramatsu, T. (2001). Molecular cloning and expression of endo-beta-N-acetylglucosaminidase D, which acts on the core structure of complex type asparagine-linked oligosaccharides. *J. Biochem.* 129: 923–928.

Murphy, K. and Weaver, C. (2017). Chapter 02- innate immunity: The first lines of defense. *Janeway's Immunobiology*. Available at: https://www.vitalsource.com/products/chapter-02-innate-immunity-the-first-lines-of-kenneth-murphy-casey-weaver-v9781315533247ch02.

Murray, P.J. (2009). Beyond peptidoglycan for Nod2. *Nat. Immunol.* 10: 1053–1054.

Musher, D.M. (2003). How contagious are common respiratory tract infections? *The N. Engl. J. Med.* 348: 1256–1266.

Nagasawa, R., Sato, T. and Senpuku, H. (2017). Raffinose induces biofilm formation by *Streptococcus mutans* in low concentrations of sucrose by increasing production of extracellular DNA and fructan. *Appl. Environ. Microbiol.* 83: e00869-17.

Nakamura, S., Davis, K.M. and Weiser, J.N. (2011). Synergistic stimulation of type I interferons during influenza virus coinfection promotes *Streptococcus pneumoniae* colonization in mice. *J. Clin. Invest.* 121: 3657–3665.

Nawrocki, K.L., Crispell, E.K. and McBride, S.M. (2014). Antimicrobial peptide resistance mechanisms of Gram-positive bacteria. *Antibiotics.* 3: 461–492.

Nelson, A.L., Ries, J., Bagnoli, F., Dahlberg, S., Fälker, S., Rounioja, S., Tschöp, J., et al. (2007). RrgA is a pilus-associated adhesin in *Streptococcus pneumoniae. Mol. Microbiol.* 66: 329–340.

Nelson, A.L., Roche, A.M., Gould, J.M., Chim, K., Ratner, A.J. and Weiser, J.N. (2007). Capsule enhances pneumococcal colonization by limiting mucus-mediated clearance. *Infect. Immun.* 75: 83–90.

Neufeld, F. (1902). Ueber die Agglutination der Pneumokokken und über die Theorieen der Agglutination. *Zeitschrift Für Hygiene Und Infektionskrankheiten*. 40: 54–72.

Nguyen, D., Joshi-Datar, A., Lepine, F., Bauerle, E., Olakanmi, O., Beer, K., McKay, G., et al. (2011). Active starvation responses mediate antibiotic tolerance in biofilms and nutrient-limited bacteria. *Science.* 334: 982–986.

Note de L. Pasteur. (1881). Maison de Louis Pasteur à Arbois - Publications de Louis Pasteur dans les Comptes rendus. *Comptes Rendus de l'Académie Des Sciences de Paris.* 92: 159.

Novick, R.P., Christie, G.E. and Penadés, J.R. (2010). The phage-related chromosomal islands of Gram-positive bacteria. *Nature Rev. Microbiol.* 8: 541–551.

Numminen, E., Chewapreecha, C., Turner, C., Goldblatt, D., Nosten, F., Bentley, S.D., Turner, P., et al. (2015). Climate induces seasonality in pneumococcal transmission. *Sci. Rep.* 5: 11344.

Obert, C., Sublett, J., Kaushal, D., Hinojosa, E., Barton, T., Tuomanen, E.I. and Orihuela, C.J. (2006). Identification of a candidate *Streptococcus pneumoniae* core genome and

regions of diversity correlated with invasive pneumococcal disease. *Infect. Immun.* 74: 4766–4777.

O'Brien, D.P., Briles, D.E., Szalai, A.J., Tu, A.-H., Sanz, I. and Nahm, M.H. (1999). Tumor necrosis factor alpha receptor I is important for survival from *Streptococcus pneumoniae* infections. *Infect. Immun.* 67: 595–601.

Oggioni, M.R., Memmi, G., Maggi, T., Chiavolini, D., Iannelli, F. and Pozzi, G. (2003). Pneumococcal zinc metalloproteinase ZmpC cleaves human matrix metalloproteinase 9 and is a virulence factor in experimental pneumonia. *Mol. Microbiol.* 49: 795–805.

Oggioni, M.R., Trappetti, C., Kadioglu, A., Cassone, M., Iannelli, F., Ricci, S., Andrew, P.W., et al. (2006). Switch from planktonic to sessile life: A major event in pneumococcal pathogenesis. *Mol. Microbiol.* 61: 1196–1210.

Ogunniyi, A.D., Giammarinaro, P. and Paton, J.C. (2002). The genes encoding virulence-associated proteins and the capsule of *Streptococcus pneumoniae* are upregulated and differentially expressed in vivo. *Microbiology.* 148: 2045–2053.

Ogunniyi, A.D., Mahdi, L.K., Trappetti, C., Verhoeven, N., Mermans, D., Van der Hoek, M.B., Plumptre, C.D., et al. (2012). Identification of genes that contribute to the pathogenesis of invasive pneumococcal disease by in vivo transcriptomic analysis. *Infect. Immun.* 80: 3268–3278.

Olafsdottir, T.A., Lingnau, K., Nagy, E. and Jonsdottir, I. (2012). Novel protein-based pneumococcal vaccines administered with the Th1-promoting adjuvant IC31 induce protective immunity against pneumococcal disease in neonatal mice. *Infect. Immun.* 80: 461–468.

Onishi, R.M. and Gaffen, S.L. (2010). Interleukin-17 and its target genes: Mechanisms of interleukin-17 function in disease. *Immunology. 1*29: 311–321.

Organization, W.H. (1998). Prevention of hearing impairment from chronic otitis media. Report of a WHO/CIBA foundation workshop, London, November 12–21, 1996, available at: https://apps.who.int/iris/handle/10665/63870.

Orihuela, C.J., Gao, G., Francis, K.P., Yu, J. and Tuomanen, E.I. (2004). Tissue-specific contributions of pneumococcal virulence factors to pathogenesis. *J. Inect. Dis.* 190: 1661–1669.

Orihuela, C.J., Mahdavi, J., Thornton, J., Mann, B., Wooldridge, K.G., Abouseada, N., Oldfield, N.J., et al. (2009). Laminin receptor initiates bacterial contact with the blood brain barrier in experimental meningitis models. *J. Clin. Invest.* 119: 1638–1646.

Orihuela, C.J., Radin, J.N., Sublett, J.E., Gao, G., Kaushal, D. and Tuomanen, E.I. (2004). Microarray analysis of pneumococcal gene expression during invasive disease. *Infect. Immun.* 72: 5582–5596.

Owen, C.D., Lukacik, P., Potter, J.A., Sleator, O., Taylor, G.L. and Walsh, M.A. (2015). *Streptococcus pneumoniae* NanC structural infishts into the specificity and mechanism of a sialidase that produces a sialidase inhibitor. *J. Biol. Chem.* 290: 27736–27748.

Paixão, L., Caldas, J., Kloosterman, T.G., Kuipers, O.P., Vinga, S. and Neves, A.R. (2015). Transcriptional and metabolic effects of glucose on *Streptococcus pneumoniae* sugar metabolism. *Front. Microbiol.* 6: 1041.

Parker, D., Soong, G., Planet, P., Brower, J., Ratner, A.J. and Prince, A. (2009). The NanA neuraminidase of *Streptococcus pneumoniae* is involved in biofilm formation. *Infect. Immun.* 77: 3722–3730.

Paterson, G.K. and Mitchell, T.J. (2006a). Innate immunity and the pneumococcus. *Microbiol.* 152: 285–293.

Paterson, G.K. and Mitchell, T.J. (2006b). The role of *Streptococcus pneumoniae* sortase A in colonisation and pathogenesis. *Microbes Infect.* 8: 145–153.

Paton, J.C., Rowan-Kelly, B. and Ferrante, A. (1984). Activation of human complement by the pneumococcal toxin pneumolysin. *Infect. Immun.* 43: 1085–1087.

Paton, J.C. and Trappetti, C. (2019). *Streptococcus pneumoniae* capsular polysaccharide. *Microbiol. Spect.* 7: 2.

Peñaloza, H.F., Nieto, P.A., Muñoz-Durango, N., Salazar-Echegarai, F.J., Torres, J., Parga, M.J., Alvarez-Lobos, M., et al. (2015). Interleukin-10 plays a key role in the modulation of neutrophils recruitment and lung inflammation during infection by *Streptococcus pneumoniae*. *Immunology.* 146: 100–112.

Pepys, M.B. (1998). Acute phase proteins, in Delves, P.J. (Ed.). *Encyclopedia of Immunology (Second Edition).* Elsevier, Oxford, pp. 18–20.

Pessoa, D., Hoti, F., Syrjänen, R.K., Sá-Leão, R., Kaijalainen, T.H., Gomes, M.G.M. and Auranen, K. (2013). Comparative analysis of *Streptococcus pneumoniae* transmission in Portuguese and Finnish day-care centres. *BMC Infect. Dis.* 13: 180.

Peterson, S.N., Sung, C.K., Cline, R., Desai, B.V., Snesrud, E.C., Luo, P., Walling, J., et al. (2004). Identification of competence pheromone responsive genes in *Streptococcus pneumoniae* by use of DNA microarrays. *Mol. Microbiol.* 51: 1051–1070.

Pettigrew, M.M., Fennie, K.P., York, M.P., Daniels, J. and Ghaffar, F. (2006). Variation in the presence of neuraminidase genes among *Streptococcus pneumoniae* isolates with identical sequence types. *Infect. Immun.* 74: 3360–3365.

Philips, B.J., Meguer, J.-X., Redman, J. and Baker, E.H. (2003). Factors determining the appearance of glucose in upper and lower respiratory tract secretions. *Intensive Care Med.* 29: 2204–2210.

Pichichero, M.E. (2017). Pneumococcal whole-cell and protein-based vaccines: Changing the paradigm. *Expert Rev. Vaccines.* 16: 1181–1190.

Plumptre, C.D., Hughes, C.E., Harvey, R.M., Eijkelkamp, B.A., McDevitt, C.A. and Paton, J.C. (2014). Overlapping functionality of the Pht proteins in zinc homeostasis of *Streptococcus pneumoniae. Infect. Immun.* 82: 4315–4324.

Polissi, A., Pontiggia, A., Feger, G., Altieri, M., Mottl, H., Ferrari, L. and Simon, D. (1998). Large-scale identification of virulence genes from *Streptococcus pneumoniae*. *Infect. Immun.* 66: 5620–5629.

van der Poll, T., Keogh, C.V., Buurman, W.A. and Lowry, S.F. (1997). Passive immunization against tumor necrosis factor-alpha impairs host defense during pneumococcal pneumonia in mice. *Am. J. Respir. Crit. Care Med.* 155: 603–608.

van der Poll, T. and Opal, S.M. (2009). Pathogenesis, treatment, and prevention of pneumococcal pneumonia. *Lancet.* 374: 1543–1556.

Pracht, D., Elm, C., Gerber, J., Bergmann, S., Rohde, M., Seiler, M., Kim, K.S., et al. (2005). PavA of *Streptococcus pneumoniae* modulates adherence, invasion, and meningeal inflammation. *Infect. Immun.* 73: 2680–2689.

Prager, O., Friedman, A. and Nebenzahl, Y.M. (2017). Role of neural barriers in the pathogenesis and outcome of *Streptococcus pneumoniae* meningitis (Review). *Exp. Ther. Med.* 13: 799–809.

Price, C.E., Zeyniyev, A., Kuipers, O.P. and Kok, J. (2012). From meadows to milk to mucosa - Adaptation of Streptococcus and Lactococcus species to their nutritional environments. *FEMS Microbiol. Rev.* 36: 949–971.

Prudhomme, M., Attaiech, L., Sanchez, G., Martin, B. and Claverys, J.-P. (2006). Antibiotic stress induces genetic transformability in the human pathogen *Streptococcus pneumoniae. Science.* 313: 89–92.

Prudhomme, M., Libante, V. and Claverys, J.-P. (2002). Homologous recombination at the border: Insertion-deletions and the trapping of foreign DNA in *Streptococcus pneumoniae*. *PNAS.* 99: 2100–2105.

Quail, M.A., Smith, M., Coupland, P., Otto, T.D., Harris, S.R., Connor, T.R., Bertoni, A., et al. (2012). A tale of three next generation sequencing platforms: Comparison of Ion Torrent, Pacific Biosciences and Illumina MiSeq sequencers. *BMC Genomics*. 13: 341.

Quin, L.R., Carmicle, S., Dave, S., Pangburn, M.K., Evenhuis, J.P. and McDaniel, L.S. (2005). In vivo binding of complement regulator factor H by *Streptococcus pneumoniae. J. Inect. Dis.* 192: 1996–2003.

Quinlan, A.R. and Hall, I.M. (2010). BEDTools: A flexible suite of utilities for comparing genomic features. *Bioinformatics.* 26: 841–842.

Rabes, A., Suttorp, N. and Opitz, B. (2016). Inflammasomes in pneumococcal infection: Innate immune sensing and bacterial evasion strategies. *Current Topics Microbiol. Immunol.* 397: 215–227.

Rahman, A.H., Taylor, D.K. and Turka, L.A. (2009). The contribution of direct TLR signaling to T cell responses. *Immunologic Res.* 45: 25–36.

Ramirez, M., Severina, E. and Tomasz, A. (1999). A high incidence of prophage carriage among natural isolates of *Streptococcus pneumoniae*. *J. Bacteriol.* 181: 3618–3625.

Ramos-Sevillano, E., Ercoli, G. and Brown, J.S. (2019). Mechanisms of naturally acquired immunity to *Streptococcus pneumoniae*. *Front. Immunol.* 10: 358.

Rayner, C.F., Jackson, A.D., Rutman, A., Dewar, A., Mitchell, T.J., Andrew, P.W., Cole, P.J., et al. (1995). Interaction of pneumolysin-sufficient and -deficient isogenic variants of *Streptococcus pneumoniae* with human respiratory mucosa. *Infect. Immun.* 63: 442–447.

Regev-Yochay, G., Raz, M., Dagan, R., Porat, N., Shainberg, B., Pinco, E., Keller, N., et al. (2004). Nasopharyngeal carriage of *Streptococcus pneumoniae* by adults and children in community and family settings. *Clin. Infect. Dis.* 38: 632–639.

Regev-Yochay, G., Trzcinski, K., Thompson, C.M., Lipsitch, M. and Malley, R. (2007). SpxB is a suicide gene of *Streptococcus pneumoniae* and confers a selective advantage in an in vivo competitive colonization model. *J. Bacteriol. 1*89: 6532–6539.

Richard, A.L., Siegel, S.J., Erikson, J. and Weiser, J.N. (2014). TLR2 signaling decreases transmission of *Streptococcus pneumoniae* by limiting bacterial shedding in an infant mouse Influenza A co-infection model. *PLoS Pathog.* 10: e1004339.

Richards, L., Ferreira, D.M., Miyaji, E.N., Andrew, P.W. and Kadioglu, A. (2010). The immunising effect of pneumococcal nasopharyngeal colonisation; protection against future colonisation and fatal invasive disease. *Immunobiology*. 215: 251–263.

Riegler, A.N., Brissac, T., Gonzalez-Juarbe, N. and Orihuela, C.J. (2019). Necroptotic cell death promotes adaptive immunity against colonizing pneumococci. *Front. Immunol.* 10: 00615.

Riley, I.D., Tarr, P.I., Andrews, M., Pfeiffer, M., Howard, R., Challands, P. and Jennison, G. (1977). Immunisation with a polyvalent pneumococcal vaccine. Reduction of adult respiratory mortality in a new Guinea highlands community. *Lancet.* 1: 1338–1341.

Ritchie, N.D., Ritchie, R., Bayes, H.K., Mitchell, T.J. and Evans, T.J. (2018). IL-17 can be protective or deleterious in murine pneumococcal pneumonia. *PLoS Pathog.* 14: e1007099.

Robb, M., Hobbs, J.K., Woodiga, S.A., Shapiro-Ward, S., Suits, M.D.L., McGregor, N., Brumer, H., et al. (2017). Molecular characterization of N-glycan degradation and transport in *Streptococcus pneumoniae* and its contribution to virulence. *PLoS Pathog.* 13: e1006090.

Roche, A.M., Richard, A.L., Rahkola, J.T., Janoff, E.N. and Weiser, J.N. (2015). Antibody blocks acquisition of bacterial colonization through agglutination. *Mucosal Immunol.* 8: 176–185.

Rodrigues, F., Foster, D., Nicoli, E., Trotter, C., Vipond, B., Muir, P., Gonçalves, G., et al. (2013). Relationships between rhinitis symptoms, respiratory viral infections and nasopharyngeal colonization with *Streptococcus pneumoniae*, *Haemophilus influenzae* and *Staphylococcus aureus* in children attending daycare. *Pediatr. Infect. Dis. Journal.* 32: 227–232.

Romagnani, S. (1999). Th1/Th2 cells. *Inflamm. Bowel Dis.* 5: 285–294.

Rose, M.C. and Voynow, J.A. (2006). Respiratory tract mucin genes and mucin glycoproteins in health and disease. *Physiol. Rev.* 86: 245–278.

Rosenow, C., Maniar, M. and Trias, J. (1999). Regulation of the alpha-galactosidase activity in *Streptococcus pneumoniae*: Characterization of the raffinose utilization system. *Genome Res.* 9: 1189–1197.

Rosenow, C., Ryan, P., Weiser, J.N., Johnson, S., Fontan, P., Ortqvist, A. and Masure, H.R. (1997). Contribution of novel choline-binding proteins to adherence, colonization and immunogenicity of *Streptococcus pneumoniae. Mol. Microbiol.* 25: 819–829.

Rubins, J.B., Charboneau, D., Fasching, C., Berry, A.M., Paton, J.C., Alexander, J.E., Andrew, P.W., et al. (1996). Distinct roles for pneumolysin's cytotoxic and complement activities in the

pathogenesis of pneumococcal pneumonia. *Am. J. Respir. Crit. Care Med.* 153: 1339–1346.
Rubins, J.B. and Pomeroy, C. (1997). Role of gamma interferon in the pathogenesis of bacteremic pneumococcal pneumonia. *Infect. Immun.* 65: 2975–2977.
Ruoslahti, E. and Pierschbacher, M.D. (1986). Arg-Gly-Asp: A versatile cell recognition signal. *Cell.* 44: 517–518.
Rutherford, K., Parkhill, J., Crook, J., Horsnell, T., Rice, P., Rajandream, M.-A. and Barrell, B. (2000). Artemis: Sequence visualization and annotation. *Bioinformatics.*16: 944–945.
de Saizieu, A., Gardès, C., Flint, N., Wagner, C., Kamber, M., Mitchell, T.J., Keck, W., et al. (2000). Microarray-based identification of a novel *Streptococcus pneumoniae* regulon controlled by an autoinduced peptide. *J. Bacteriol.* 182: 4696–4703.
Saleh, M., Bartual, S.G., Abdullah, M.R., Jensch, I., Asmat, T.M., Petruschka, L., Pribyl, T., et al. (2013). Molecular architecture of *Streptococcus pneumoniae* surface thioredoxin-fold lipoproteins crucial for extracellular oxidative stress resistance and maintenance of virulence. *EMBO Mol. Med.* 5: 1852–1870.
Sanchez, C.J., Kumar, N., Lizcano, A., Shivshankar, P., Hotopp, J.C.D., Jorgensen, J.H., Tettelin, H., et al. (2011). *Streptococcus pneumoniae* in biofilms are unable to cause invasive disease due to altered virulence determinant production. *PLoS One.* 6: e28738.
Santoro, F., Iannelli, F. and Pozzi, G. (2019). Genomics and genetics of *Streptococcus pneumoniae*. *Microbiol. Spect.* 7: 0025.
Seo, H.S., Michalek, S.M. and Nahm, M.H. (2008). Lipoteichoic acid is important in innate immune responses to gram-positive bacteria. *Infect. Immun.* 76: 206–213.
Shafeeq, S., Kloosterman, T.G. and Kuipers, O.P. (2011). CelR-mediated activation of the cellobiose-utilization gene cluster in *Streptococcus pneumoniae*. *Microbiol.* 157: 2854–2861.
Shaik, M.M., Maccagni, A., Tourcier, G., Di Guilmi, A.M. and Dessen, A. (2014). Structural basis of pilus anchoring by the ancillary pilin RrgC of *Streptococcus pneumoniae. The J. Biol. Chem.* 289: 16988–16997.
Shak, J.R., Vidal, J.E. and Klugman, K.P. (2013). Influence of bacterial interactions on pneumococcal colonization of the nasopharynx. *Trends in Microbiol.* 21: 129–135.
Shakhnovich, E.A., King, S.J. and Weiser, J.N. (2002). Neuraminidase expressed by *Streptococcus pneumoniae* desialylates the lipopolysaccharide of *Neisseria meningitidis* and *Haemophilus influenzae*: A paradigm for interbacterial competition among pathogens of the human respiratory tract. *Infect. Immun.* 70: 7161–7164.
Shanker, E. and Federle, M.J. (2017). Quorum sensing regulation of competence and bacteriocins in *Streptococcus pneumoniae* and *mutans. Genes.* 8: 10015.
Shaper, M., Hollingshead, S.K., Benjamin, W.H. and Briles, D.E. (2004). PspA protects *Streptococcus pneumoniae* from killing by apolactoferrin, and antibody to PspA enhances killing of pneumococci by apolactoferrin. *Infect. Immun.* 72: 5031–5040.
Shapiro, E.D., Berg, A.T., Austrian, R., Schroeder, D., Parcells, V., Margolis, A., Adair, R.K., et al. (1991). The protective efficacy of polyvalent pneumococcal polysaccharide vaccine. *N. Engl. J. Med.* 325: 1453–1460.
Shelburne, S.A., Davenport, M.T., Keith, D.B. and Musser, J.M. (2008). The role of complex carbohydrate catabolism in the pathogenesis of invasive streptococci. *Trends Microbiol.* 16: 318–325.
Shiri, T., Nunes, M.C., Adrian, P.V., Van Niekerk, N., Klugman, K.P. and Madhi, S.A. (2013). Interrelationship of *Streptococcus pneumoniae*, *Haemophilus influenzae* and *Staphylococcus aureus* colonization within and between pneumococcal-vaccine naïve mother-child dyads. *BMC Infect. Dis.* 13: 483.
Shivshankar, P., Sanchez, C., Rose, L.F. and Orihuela, C.J. (2009). The *Streptococcus pneumoniae* adhesin PsrP binds to Keratin 10 on lung cells. *Mol. Microbiol.* 73: 663–679.
Shlomovitz, I., Zargarian, S., Erlich, Z., Edry-Botzer, L. and Gerlic, M. (2018). Distinguishing necroptosis from apoptosis. *Methods Mol. Biol.* 1857: 35–51.

Sibold, C., Markiewicz, Z., Latorre, C. and Hakenbeck, R. (1991). Novel plasmids in clinical strains of *Streptococcus pneumoniae*. *FEMS Microbiol. Lett.* 77: 91–95.
Silva, N.A., McCluskey, J., Jefferies, J.M.C., Hinds, J., Smith, A., Clarke, S.C., Mitchell, T.J., et al. (2006). Genomic diversity between strains of the same serotype and multilocus sequence type among pneumococcal clinical isolates. *Infect. Immun.* 74: 3513–3518.
Singh, A.K., Pluvinage, B., Higgins, M.A., Dalia, A.B., Woodiga, S.A., Flynn, M., Lloyd, A.R., et al. (2014). Unravelling the multiple functions of the architecturally intricate *Streptococcus pneumoniae* β-galactosidase, BgaA. *PLoS Pathog.* 10: e1004364.
Singleton, R.J., Hennessy, T.W., Bulkow, L.R., Hammitt, L.L., Zulz, T., Hurlburt, D.A., Butler, J.C., et al. (2007). Invasive pneumococcal disease caused by nonvaccine serotypes among Alaska native children with high levels of 7-valent pneumococcal conjugate vaccine coverage. *JAMA.* 297: 1784–1792.
Sitkiewicz, I. (2018). How to become a killer, or is it all accidental? Virulence strategies in oral streptococci. *Mol. Oral Microbiol.* 33: 1–12.
Skov Sørensen, U.B., Blom, J., Birch-Andersen, A. and Henrichsen, J. (1988). Ultrastructural localization of capsules, cell wall polysaccharide, cell wall proteins, and F antigen in pneumococci. *Infect. Immun.* 56: 1890–1896.
Smith, M.D. and Guild, W.R. (1979). A plasmid in *Streptococcus pneumoniae*. *J. Bacteriol.* 137: 735–739.
Sørensen, U.B.S., Henrichsen, J., Chen, H.-C. and Szu, S.C. (1990). Covalent linkage between the capsular polysaccharide and the cell wall peptidoglycan of *Streptococcus pneumoniae* revealed by immunochemical methods. *Microb. Pathog.* 8: 325–334.
Sprent, J. (1994). T and B memory cells. *Cell.* 76: 315–322.
Srivastava, A., Henneke, P., Visintin, A., Morse, S.C., Martin, V., Watkins, C., Paton, J.C., et al. (2005). The apoptotic response to pneumolysin is Toll-like receptor 4 dependent and protects against pneumococcal disease. *Infect. Immun.* 73: 6479–6487.
Stahl, W.L. and O'Toole, R.D. (1972). Pneumococcal neuraminidase: Purification and properties. *Biochimica Et Biophysica Acta.* 268: 480–487.
Standish, A.J. and Weiser, J.N. (2009). Human neutrophils kill *Streptococcus pneumoniae* via serine proteases. *J. Immunol.* 183: 2602–2609.
Stanek, R.J., Norton, N.B. and Mufson, M.A. (2016). A 32-year study of the effect of pneumococcal vaccines on invasive *Streptococcus pneumoniae* disease. *Am. J.Med. Sci.* 352: 563–573.
Steinmoen, H., Knutsen, E. and Håvarstein, L.S. (2002). Induction of natural competence in *Streptococcus pneumoniae* triggers lysis and DNA release from a subfraction of the cell population. *PNAS.* 99: 7681–7686.
Sternberg, G. (1881). A Fatal Form of Septicaemia in the Rabbit Produced by the Subcutaneous Injection of Human Saliva: An Experimental Research. *Printed by John Murphy & Co., Baltimore*.
Stevens, K.E., Chang, D., Zwack, E.E. and Sebert, M.E. (2011). Competence in *Streptococcus pneumoniae* is regulated by the rate of ribosomal decoding errors. *mBio.* 2: e00071-11.
Stoppelenburg, A.J., Salimi, V., Hennus, M., Plantinga, M., Veld, R.H. in 't, Walk, J., Meerding, J., et al. (2013). Local IL-17A potentiates early neutrophil recruitment to the respiratory tract during severe RSV infection. *PLoS One.* 8: e78461.
Stroeher, U.H., Paton, A.W., Ogunniyi, A.D. and Paton, J.C. (2003). Mutation of *luxS* of *Streptococcus pneumoniae* affects virulence in a mouse model. *Infect. Immun.* 71: 3206–3212.
Sung, C.K., Li, H., Claverys, J.P. and Morrison, D.A. (2001). An rpsl cassette, janus, for gene replacement through negative selection in *Streptococcus pneumoniae. Appl. Environ. Microbiol.* 67: 5190–5196.
Swiatlo, E., Champlin, F.R., Holman, S.C., Wilson, W.W. and Watt, J.M. (2002). Contribution of choline-binding proteins to cell surface properties of *Streptococcus pneumoniae*. *Infect. Immun.* 70: 412–415.

Talbot, U.M., Paton, A.W. and Paton, J.C. (1996). Uptake of *Streptococcus pneumoniae* by respiratory epithelial cells. *Infect. Immun.* 64: 3772–3777.

Taylor, P.S., Faeth, I., Marks, M.K., Del Mar, C.B., Skull, S.A., Pezzullo, M.L., Havyatt, S.M., et al. (2009). Cost of treating otitis media in Australia. *Exp. Rev. Pharmacoeconomics Outcomes Res.* 9: 133–141.

Tettelin, H., Nelson, K.E., Paulsen, I.T., Eisen, J.A., Read, T.D., Peterson, S., Heidelberg, J., et al. (2001). Complete genome sequence of a virulent isolate of *Streptococcus pneumoniae*. *Science.* 293: 498–506.

Tomlinson, G., Chimalapati, S., Pollard, T., Lapp, T., Cohen, J., Camberlein, E., Stafford, S., et al. (2014). TLR-mediated inflammatory responses to *Streptococcus pneumoniae* are highly dependent on surface expression of bacterial lipoproteins. *J. Immunol.* 193: 3736–3745.

Tonder, A.J. van, Bray, J.E., Jolley, K.A., Quirk, S.J., Haraldsson, G., Maiden, M.C., Bentley, S.D., et al. (2017). Heterogeneity among estimates of the core genome and pan-genome in different pneumococcal populations. *BioRxiv.* Available at: https://www.biorxiv.org/content/10.1101/133991v1.

Tong, H.H., Blue, L.E., James, M.A. and DeMaria, T.F. (2000). Evaluation of the virulence of a *Streptococcus pneumoniae* neuraminidase-deficient mutant in nasopharyngeal colonization and development of otitis media in the chinchilla model. *Infect. Immun.* 68: 921–924.

Trappetti, C., Kadioglu, A., Carter, M., Hayre, J., Iannelli, F., Pozzi, G., Andrew, P.W., et al. (2009). Sialic acid: A preventable signal for pneumococcal biofilm formation, colonization, and invasion of the host. *J. Inect. Dis.* 199: 1497–1505.

Trappetti, C., Maten, E. van der, Amin, Z., Potter, A.J., Chen, A.Y., Mourik, P.M. van, Lawrence, A.J., et al. (2013). Site of isolation determines biofilm formation and virulence phenotypes of *Streptococcus pneumoniae* serotype 3 clinical isolates. *Infect. Immun.* 81: 505–513.

Trappetti, C., McAllister, L.J., Chen, A., Wang, H., Paton, A.W., Oggioni, M.R., McDevitt, C.A., et al. (2017). Autoinducer 2 signaling via the phosphotransferase frua drives galactose utilization by *Streptococcus pneumoniae*, resulting in hypervirulence. *mBio.* 8: e02269.

Trappetti, C., Ogunniyi, A.D., Oggioni, M.R. and Paton, J.C. (2011). Extracellular matrix formation enhances the ability of *Streptococcus pneumoniae* to cause invasive disease. *PLoS One.* 6: e19844.

Tseng, H.-J., McEwan, A.G., Paton, J.C. and Jennings, M.P. (2002). Virulence of *Streptococcus pneumoniae*: PsaA mutants are hypersensitive to oxidative stress. *Infect. Immun.* 70: 1635–1639.

Tu, A.H., Fulgham, R.L., McCrory, M.A., Briles, D.E. and Szalai, A.J. (1999). Pneumococcal surface protein A inhibits complement activation by *Streptococcus pneumoniae. Infect. Immun.* 67: 4720–4724.

Tuomanen, E.I. (2000). Pathogenesis of pneumococcal inflammation: Otitis media. *Vaccine.* 19: S38-40.

Tyx, R.E., Roche-Hakansson, H. and Hakansson, A.P. (2011). Role of dihydrolipoamide dehydrogenase in regulation of raffinose transport in *Streptococcus pneumoniae. J. Bacteriol.* 193: 3512–3524.

Verhagen, L.M., de Jonge, M.I., Burghout, P., Schraa, K., Spagnuolo, L., Mennens, S., Eleveld, M.J., et al. (2014). Genome-wide identification of genes essential for the survival of *Streptococcus pneumoniae* in human saliva. *PLoS One.* 9: e89541.

de Vries, S.P.W., van Hijum, S.A.F.T., Schueler, W., Riesbeck, K., Hays, J.P., Hermans, P.W.M. and Bootsma, H.J. (2010). Genome analysis of *Moraxella catarrhalis* strain BBH18, [corrected] a human respiratory tract pathogen. *J. Bacteriol.* 192: 3574–3583.

Waggoner, S.N., Daniels, K.A. and Welsh, R.M. (2014). Therapeutic depletion of natural killer cells controls persistent infection. *J. Virology.* 88: 1953–1960.

Walker, C.L.F., Rudan, I., Liu, L., Nair, H., Theodoratou, E., Bhutta, Z.A., O'Brien, K.L., et al. (2013). Global burden of childhood pneumonia and diarrhoea. *Lancet.* 381: 1405–1416.

Walker, J.R.L. (1992). Spectrophotometric determination of enzyme activity: Alcohol dehydrogenase (ADH). *Biochemical Edu.* 20: 42–43.
Walsh, R.L. and Camilli, A. (2011). *Streptococcus pneumoniae* is desiccation tolerant and infectious upon rehydration. *mBio.* 2: e00092-00011.
Wang, B.-Y. and Kuramitsu, H.K. (2005). Interactions between oral bacteria: Inhibition of *Streptococcus mutans* bacteriocin production by *Streptococcus gordonii. Appl. Environ. Microbiol.* 71: 354–362.
Wang, L., Fu, J., Liang, Z. and Chen, J. (2017). Prevalence and serotype distribution of nasopharyngeal carriage of *Streptococcus pneumoniae* in China: A meta-analysis. *BMC Infect. Dis.* 17: 765.
Watson, D.A., Musher, D.M., Jacobson, J.W. and Verhoef, J. (1993). A brief history of the pneumococcus in biomedical research: A panoply of scientific discovery. *Clin. Infect. Dis.* 17: 913–24.
Weber, S.E., Tian, H. and Pirofski, L. (2011). CD8+ cells enhance resistance to pulmonary serotype 3 *Streptococcus pneumoniae* infection in mice. *J. Immunol.* 186: 432–442.
Weimer, K.E.D., Armbruster, C.E., Juneau, R.A., Hong, W., Pang, B. and Swords, W.E. (2010). Coinfection with *Haemophilus influenzae* promotes pneumococcal biofilm formation during experimental otitis media and impedes the progression of pneumococcal disease. *J. Inect. Dis.* 202: 1068–1075.
Weinberger, D.M., Harboe, Z.B., Sanders, E.A.M., Ndiritu, M., Klugman, K.P., Rückinger, S., Dagan, R., et al. (2010). Association of serotype with risk of death due to pneumococcal pneumonia: A meta-analysis. *Clin. Infect. Dis.*51: 692–699.
Weiser, J.N. (2010). The pneumococcus: Why a commensal misbehaves. *J. Mol. Med.* 88: 97–102.
Weiser, J.N., Ferreira, D.M. and Paton, J.C. (2018). *Streptococcus pneumoniae*: Transmission, colonization and invasion. *Nature Rev. Microbiol. 1*6: 355–367.
Wellmer, A., Gerber, J., Ragheb, J., Zysk, G., Kunst, T., Smirnov, A., Brück, W., et al. (2001). Effect of deficiency of tumor necrosis factor alpha or both of its receptors on *Streptococcus pneumoniae* central nervous system infection and peritonitis. *Infect. Immun.* 69: 6881–6886.
Westermann, A.J., Barquist, L. and Vogel, J. (2017). Resolving host-pathogen interactions by dual RNA-seq. *PLoS Pathog.* 13: e1006033.
Whalan, R.H., Funnell, S.G.P., Bowler, L.D., Hudson, M.J., Robinson, A. and Dowson, C.G. (2005). PiuA and PiaA, iron uptake lipoproteins of *Streptococcus pneumoniae*, elicit serotype independent antibody responses following human pneumococcal septicaemia. *FEMS Immunol.Med. Microbiol.* 43: 73–80.
Whitney, C.G., Farley, M.M., Hadler, J., Harrison, L.H., Bennett, N.M., Lynfield, R., Reingold, A., et al. (2003). Decline in invasive pneumococcal disease after the introduction of protein-polysaccharide conjugate vaccine. *N. Engl. J. Med.* 348: 1737–1746.
Whitsett, J.A. and Alenghat, T. (2015). Respiratory epithelial cells orchestrate pulmonary innate immunity. *Nat. Immunol.* 16: 27–35.
WHO | Pneumococcal disease. (2014). *WHO*, World Health Organization.
Wholey, W.-Y., Kochan, T.J., Storck, D.N. and Dawid, S. (2016). Coordinated bacteriocin expression and competence in *Streptococcus pneumoniae* contributes to genetic adaptation through neighbor predation. *PLoS Pathog.* 12: e1005413.
Wilson, R., Cohen, J.M., Reglinski, M., Jose, R.J., Chan, W.Y., Marshall, H., Vogel, C. de, et al. (2017). Naturally acquired human immunity to pneumococcus is dependent on antibody to protein antigens. *PLoS Pathog.* 13: e1006137.
Winter, A.J., Comis, S.D., Osborne, M.P., Tarlow, M.J., Stephen, J., Andrew, P.W., Hill, J., et al. (1997). A role for pneumolysin but not neuraminidase in the hearing loss and cochlear damage induced by experimental pneumococcal meningitis in guinea pigs. *Infect. Immun.* 65: 4411–4418.
Winzer, K., Hardie, K.R. and Williams, P. (2003). LuxS and autoinducer-2: their contribution to quorum sensing and metabolism in bacteria. *Adv. Appl. Microbiol.* 53: 291–396.

Witzenrath, M., Pache, F., Lorenz, D., Koppe, U., Gutbier, B., Tabeling, C., Reppe, K., et al. (2011). The NLRP3 inflammasome is differentially activated by pneumolysin variants and contributes to host defense in pneumococcal pneumonia. *J. Immunol.* 187: 434–440.

Wolf, T., Kämmer, P., Brunke, S. and Linde, J. (2018). Two's company: Studying interspecies relationships with dual RNA-seq., *Curr. Opin. Microbiol.* 42: 7–12.

Wren, J.T., Blevins, L.K., Pang, B., Roy, A.B., Oliver, M.B., Reimche, J.L., Wozniak, J.E., et al. (2017). Pneumococcal neuraminidase A (nanA) promotes biofilm formation and synergizes with influenza A virus in nasal colonization and middle ear infection. *Infect. Immun.* 85: e01044-16.

Xu, Q. and Pichichero, M.E. (2014). Co-colonization by *Haemophilus influenzae* with *Streptococcus pneumoniae* enhances pneumococcal-specific antibody response in young children. *Vaccine.* 32: 706–711.

Xu, R.-R., Yang, W.-D., Niu, K.-X., Wang, B. and Wang, W.-M. (2018). An update on the evolution of glucosyltransferase (*gtf*) genes in Streptococcus. *Front. Microbiol.* 9: e02979.

Yadav, M.K., Vidal, J.E., Go, Y.Y., Kim, S.H., Chae, S.-W. and Song, J.-J. (2018). The LuxS/AI-2 quorum-sensing system of *Streptococcus pneumoniae* is required to cause disease, and to regulate virulence- and metabolism-related genes in a rat model of middle ear infection. *Front. Cell. Infect. Microbiol.* 8: e00138.

Yamamoto, N., Kawakami, K., Kinjo, Y., Miyagi, K., Kinjo, T., Uezu, K., Nakasone, C., et al. (2004). Essential role for the p40 subunit of interleukin-12 in neutrophil-mediated early host defense against pulmonary infection with *Streptococcus pneumoniae*: involvement of interferon-gamma. *Microbes Infect.* 6: 1241–1249.

Yesilkaya, H., Kadioglu, A., Gingles, N., Alexander, J.E., Mitchell, T.J. and Andrew, P.W. (2000). Role of manganese-containing superoxide dismutase in oxidative stress and virulence of *Streptococcus pneumoniae*. *Infect. Immun.* 68: 2819–2826.

Yesilkaya, H., Spissu, F., Carvalho, S.M., Terra, V.S., Homer, K.A., Benisty, R., Porat, N., et al. (2009). Pyruvate formate lyase is required for pneumococcal fermentative metabolism and virulence. *Infect. Immun.* 77: 5418–5427.

Yu, Y.-R.A., O'Koren, E.G., Hotten, D.F., Kan, M.J., Kopin, D., Nelson, E.R., Que, L., et al. (2016). A protocol for the comprehensive flow cytometric analysis of immune cells in normal and inflamed murine non-lymphoid tissues. *PLoS One.* 11: e0150606.

Yun, K.W., Lee, H., Choi, E.H. and Lee, H.J. (2015). Diversity of pneumolysin and pneumococcal histidine triad protein D of *Streptococcus pneumoniae* isolated from invasive diseases in korean children. *PLoS One.* 10: e0134055.

Yuste, J., Botto, M., Paton, J.C., Holden, D.W. and Brown, J.S. (2005). Additive inhibition of complement deposition by pneumolysin and PspA facilitates *Streptococcus pneumoniae* septicemia. *J. Immunol.* 175: 1813–1819.

Zafar, M.A., Wang, Y., Hamaguchi, S. and Weiser, J.N. (2017). Host-to-host transmission of *Streptococcus pneumoniae* is driven by its inflammatory toxin, pneumolysin. *Cell Host Microbe.* 21: 73–83.

Zhanel, G.G., Wolter, K.D., Calciu, C., Hogan, P., Low, D.E., Weiss, K. and Karlowsky, J.A. (2014). Clinical cure rates in subjects treated with azithromycin for community-acquired respiratory tract infections caused by azithromycin-susceptible or azithromycin-resistant *Streptococcus pneumoniae*: Analysis of Phase 3 clinical trial data. *J. Antimicrob. Chemother.* 69: 2835–2840.

Zhang, J.R., Mostov, K.E., Lamm, M.E., Nanno, M., Shimida, S., Ohwaki, M. and Tuomanen, E. (2000). The polymeric immunoglobulin receptor translocates pneumococci across human nasopharyngeal epithelial cells. *Cell.* 102: 827–837.

Zimmermann, N., McBride, M.L., Yamada, Y., Hudson, S.A., Jones, C., Cromie, K.D., Crocker, P.R., et al. (2008). Siglec-F antibody administration to mice selectively reduces blood and tissue eosinophils. *Allergy.* 63: 1156–1163.

Appendicies

Appendix A. Phenotype Microarray of 4559, Biolog PM1 plate. Catabolism was measured through the reduction of a colourless tetrazolium dye by NADH, produced during catabolic activity. A_{590} values above 0.65 were considered positive (see section 2.2.4).

Negative control	**L-Arabinose**	**N-Acetyl-D-Glucosamine**	**D-Saccharic Acid**	**Succinic Acid**	**D-Galactose**
0.424	0.764	1.233	0.395	0.403	1.389
D-Serine	**D-Sorbitol**	**Glycerol**	**L-Fucose**	**D-Glucuronic Acid**	**D-Gluconic Acid**
0.403	0.618	1.006	0.595	0.425	0.489
D-Glucose-6-Phosphate	**D-Galactonic Acid-γ-Lactone**	**D, L-Malic Acid**	**D-Ribose**	**Tween 20**	**L-Rhamnose**
0.461	0.187	0.39	0.909	0.636	0.641
L-Asparagine	**D-Aspartic Acid**	**D-Glucosaminic Acid**	**1,2-Propanediol**	**Tween 40**	**α-Keto-Glutaric Acid**
0.409	0.436	0.422	0.636	0.697	0.406
L-Glutamine	**M-Tartaric Acid**	**D-Glucose-1-Phosphate**	**D-Fructose-6-Phosphate**	**Tween 80**	**α-Hydroxy Glutaric Acid-γ-Lactone**
0.393	0.426	0.421	0.412	0.373	0.312
Glycyl-L-Aspartic Acid	**Citric Acid**	**M-Inositol**	**D-Threonine**	**Fumaric Acid**	**Bromo Succinic Acid**
0.453	0.451	0.447	0.439	0.42	0.354
Glycyl-L-Glutamic Acid	**Tricarballylic Acid**	**L-Serine**	**L-Threonine**	**L-Alanine**	**L-Alanyl-Glycine**
0.456	0.339	0.373	0.387	0.344	0.347
Glycyl-L-Proline	**p-Hydroxy Phenyl Acetic Acid**	**m-Hydroxy Phenyl Acetic Acid**	**Tyramine**	**D-Psicose**	**L-Lyxose**
0.33	0.184	0.211	0.239	0.584	0.924
L-Aspartic Acid	**L-Proline**	**D-Alanine**	**D-Trehalose**	**D-Mannose**	**Dulcitol**
0.381	0.388	0.386	1.266	1.292	0.451
D,L-α-Glycerol-Phosphate	**D-Xylose**	**L-Lactic Acid**	**Formic Acid**	**D-Mannitol**	**L-Glutamic Acid**
0.467	0.839	0.916	0.423	0.586	0.378
D-Fructose	**Acetic Acid**	**α-D-Glucose**	**Maltose**	**D-Melibiose**	**Thymidine**
1.269	0.664	1.266	1.351	1.277	0.496
α-Keto-Butyric Acid	**α-Methyl-D-Galactoside**	**α-D-Lactose**	**Lactulose**	**Sucrose**	**Uridine**
0.429	0.913	1.339	1.347	1.237	0.785
α-Hydroxy Butyric Acid	**β-Methyl-D-Glucoside**	**Adonitol**	**Maltotriose**	**2-Deoxy Adenosine**	**Adenosine**
0.464	0.403	0.309	0.379	1.047	0.538
Propionic Acid	**Mucic Acid**	**Glycolic Acid**	**Glyoxylic Acid**	**D-Cellobiose**	**Inosine**
0.584	0.46	0.342	0.408	0.784	0.437

Acetoacetic Acid	N-Acetyle-β-D-Mannosamine	Mono Methyl Succinate	Methyl Pyruvate	D-Malic Acid	L-Malic Acid
0.782	1.198	0.369	0.401	0.373	0.376
Glucuronamide	**Pyruvic Acid**	**L-GalactonicAcid-γ-Lactone**	**D-Galacturonic acid**	**Phenylethyl-amine**	**2-Aminoethano**
0.431	0.633	0.392	0.392	0.358	0.311

Appendix B. Phenotype Microarray of 947, Biolog PM1 plate. Catabolism was measured through the reduction of a colourless tetrazolium dye by NADH, produced during catabolic activity. A_{590} values above 0.65 were considered positive (see section 2.2.4).

Negative control	**L-Arabinose**	**N-Acetyl-D-Glucosamine**	**D-Saccharic Acid**	**Succinic Acid**	**D-Galactose**
0.483	0.859	0.933	0.439	0.451	0.947
D-Serine	**D-Sorbitol**	**Glycerol**	**L-Fucose**	**D-Glucuronic Acid**	**D-Gluconic Acid**
0.421	0.582	0.756	0.658	0.497	0.485
D-Glucose-6-Phosphate	**D-Galactonic Acid-γ-Lactone**	**D, L-Malic Acid**	**D-Ribose**	**Tween 20**	**L-Rhamnose**
0.543	0.23	0.451	0.947	0.732	0.71
L-Asparagine	**D-Aspartic Acid**	**D-Glucosaminic Acid**	**1,2-Propanediol**	**Tween 40**	**α-Keto-Glutaric Acid**
0.468	0.483	0.462	0.593	0.645	0.45
L-Glutamine	**M-Tartaric Acid**	**D-Glucose-1-Phosphate**	**D-Fructose-6-Phosphate**	**Tween 80**	**α-Hydroxy Glutaric Acid-γ-Lactone**
0.366	0.389	0.485	0.51	0.691	0.384
Glycyl-L-Aspartic Acid	**Citric Acid**	**M-Inositol**	**D-Threonine**	**Fumaric Acid**	**Bromo Succinic Acid**
0.453	0.451	0.447	0.439	0.42	0.354
Glycyl-L-Glutamic Acid	**Tricarballylic Acid**	**L-Serine**	**L-Threonine**	**L-Alanine**	**L-Alanyl-Glycine**
0.434	0.377	0.382	0.411	0.378	0.396
Glycyl-L-Proline	**p-Hydroxy Phenyl Acetic Acid**	**m-Hydroxy Phenyl Acetic Acid**	**Tyramine**	**D-Psicose**	**L-Lyxose**
0.406	0.213	0.21	0.263	0.671	0.985
L-Aspartic Acid	**L-Proline**	**D-Alanine**	**D-Trehalose**	**DMannose**	**Dulcitol**
0.481	0.407	0.418	1.003	0.97	0.513
D,L-α-Glycerol-Phosphate	**D-Xylose**	**L-Lactic Acid**	**Formic Acid**	**D-Mannitol**	**L-Glutamic Acid**
0.519	0.901	0.639	0.667	0.539	0.408
D-Fructose	**Acetic Acid**	**α-D-Glucose**	**Maltose**	**D-Melibiose**	**Thymidine**
1	0.703	0.993	1.087	0.712	0.408
α-Keto-Butyric Acid	**α-Methyl-D-Galactoside**	**α-D-Lactose**	**Lactulose**	**Sucrose**	**Uridine**
0.406	0.721	0.991	0.964	1.072	0.624
α-Hydroxy Butyric Acid	**β-Methyl-D-Glucoside**	**Adonitol**	**Maltotriose**	**2-Deoxy Adenosine**	**Adenosine**
0.415	0.765	0.486	1.05	0.35	0.495
Propionic Acid	**Mucic Acid**	**Glycolic Acid**	**Glyoxylic Acid**	**D-Cellobiose**	**Inosine**
0.584	0.46	0.342	0.408	0.784	0.437
Acetoacetic Acid	**N-Acetyle-β-D-Mannosamine**	**Mono Methyl Succinate**	**Methyl Pyruvate**	**D-Malic Acid**	**L-Malic Acid**
0.797	0.937	0.414	0.347	0.382	0.437

Glucuronamide	Pyruvic Acid	L-GalactonicAcid-γ-Lactone	D-Galacturonic acid	Phenylethyl-amine	2-Aminoethano
0.504	0.523	0.446	0.445	0.413	0.337

Appendix C. Phenotype Microarray of 4559^{947rafR}, Biolog PM1 plate. Catabolism was measured through the reduction of a colourless tetrazolium dye by NADH, produced during catabolic activity. A_{590} values above 0.65 were considered positive (see section 2.2.4).

Negative control	**L-Arabinose**	**N-Acetyl-D-Glucosamine**	**D-Saccharic Acid**	**Succinic Acid**	**D-Galactose**
0.472	0.856	1.504	0.47	0.545	1.719
D-Serine	**D-Sorbitol**	**Glycerol**	**L-Fucose**	**D-Glucuronic Acid**	**D-Gluconic Acid**
0.49	0.674	1.529	0.662	0.563	0.543
D-Glucose-6-Phosphate	**D-Galactonic Acid-γ-Lactone**	**D, L-Malic Acid**	**D-Ribose**	**Tween 20**	**L-Rhamnose**
0.538	0.37	0.5	1.077	0.695	0.697
L-Asparagine	**D-Aspartic Acid**	**D-Glucosaminic Acid**	**1,2-Propanediol**	**Tween 40**	**α-Keto-Glutaric Acid**
0.464	0.522	0.543	0.658	0.627	0.446
L-Glutamine	**M-Tartaric Acid**	**D-Glucose-1-Phosphate**	**D-Fructose-6-Phosphate**	**Tween 80**	**α-Hydroxy Glutaric Acid-γ-Lactone**
0.444	0.442	0.523	0.576	0.647	0.51
Glycyl-L-Aspartic Acid	**Citric Acid**	**M-Inositol**	**D-Threonine**	**Fumaric Acid**	**Bromo Succinic Acid**
0.539	0.538	0.54	0.508	0.507	0.463
Glycyl-L-Glutamic Acid	**Tricarballylic Acid**	**L-Serine**	**L-Threonine**	**L-Alanine**	**L-Alanyl-Glycine**
0.474	0.45	0.494	0.523	0.489	0.535
Glycyl-L-Proline	**p-Hydroxy Phenyl Acetic Acid**	**m-Hydroxy Phenyl Acetic Acid**	**Tyramine**	**D-Psicose**	**L-Lyxose**
0.454	0.381	0.39	0.416	1.356	1.092
L-Aspartic Acid	**L-Proline**	**D-Alanine**	**D-Trehalose**	**DMannose**	**Dulcitol**
0.499	0.492	0.51	1.634	1.612	0.611
D,L-α-Glycerol-Phosphate	**D-Xylose**	**L-Lactic Acid**	**Formic Acid**	**D-Mannitol**	**L-Glutamic Acid**
0.573	0.978	0.946	0.557	0.784	0.493
D-Fructose	**Acetic Acid**	**α-D-Glucose**	**Maltose**	**D-Melibiose**	**Thymidine**
1.631	0.699	1.648	1.619	0.715	0.65
α-Keto-Butyric Acid	**α-Methyl-D-Galactoside**	**α-D-Lactose**	**Lactulose**	**Sucrose**	**Uridine**
0.489	0.551	1.702	1.758	1.577	0.876
α-Hydroxy Butyric Acid	**β-Methyl-D-Glucoside**	**Adonitol**	**Maltotriose**	**2-Deoxy Adenosine**	**Adenosine**
0.494	1.339	0.54	1.577	0.546	0.778
Propionic Acid	**Mucic Acid**	**Glycolic Acid**	**Glyoxylic Acid**	**D-Cellobiose**	**Inosine**
0.643	0.491	0.487	0.462	1.395	0.71
Acetoacetic Acid	**N-Acetyle-β-D-Mannosamine**	**Mono Methyl Succinate**	**Methyl Pyruvate**	**D-Malic Acid**	**L-Malic Acid**
0.905	1.731	0.543	0.543	0.494	0.538

Glucuronamide	Pyruvic Acid	L-GalactonicAcid-γ-Lactone	D-Galacturonic acid	Phenylethyl-amine	2-Aminoethano
0.552	0.673	0.545	0.586	0.533	0.461

Appendix D. Phenotype Microarray of 947^{4559rafR}, Biolog PM1 plate. Catabolism was measured through the reduction of a colourless tetrazolium dye by NADH, produced during catabolic activity. A_{590} values above 0.65 were considered positive (see section 2.2.4).

Negative control	**L-Arabinose**	**N-Acetyl-D-Glucosamine**	**D-Saccharic Acid**	**Succinic Acid**	**D-Galactose**
0.488	0.748	1.094	0.443	0.457	1.262
D-Serine	**D-Sorbitol**	**Glycerol**	**L-Fucose**	**D-Glucuronic Acid**	**D-Gluconic Acid**
0.463	0.658	0.774	0.8	0.511	0.504
D-Glucose-6-Phosphate	**D-Galactonic Acid-γ-Lactone**	**D, L-Malic Acid**	**D-Ribose**	**Tween 20**	**L-Rhamnose**
0.565	0.214	0.505	0.999	0.659	0.761
L-Asparagine	**D-Aspartic Acid**	**D-Glucosaminic Acid**	**1,2-Propanediol**	**Tween 40**	**α-Keto-Glutaric Acid**
0.442	0.479	0.525	1.033	0.613	0.407
L-Glutamine	**M-Tartaric Acid**	**D-Glucose-1-Phosphate**	**D-Fructose-6-Phosphate**	**Tween 80**	**α-Hydroxy Glutaric Acid-γ-Lactone**
0.386	0.341	0.529	0.568	0.751	0.392
Glycyl-L-Aspartic Acid	**Citric Acid**	**M-Inositol**	**D-Threonine**	**Fumaric Acid**	**Bromo Succinic Acid**
0.479	0.466	0.453	0.442	0.452	0.387
Glycyl-L-Glutamic Acid	**Tricarballylic Acid**	**L-Serine**	**L-Threonine**	**L-Alanine**	**L-Alanyl-Glycine**
0.492	0.38	0.399	0.067	0.391	0.397
Glycyl-L-Proline	**p-Hydroxy Phenyl Acetic Acid**	**m-Hydroxy Phenyl Acetic Acid**	**Tyramine**	**D-Psicose**	**L-Lyxose**
0.428	0.195	0.217	0.258	0.733	1.067
L-Aspartic Acid	**L-Proline**	**D-Alanine**	**D-Trehalose**	**DMannose**	**Dulcitol**
0.426	0.434	0.462	1.218	1.247	0.519
D,L-α-Glycerol-Phosphate	**D-Xylose**	**L-Lactic Acid**	**Formic Acid**	**D-Mannitol**	**L-Glutamic Acid**
0.478	0.984	0.814	0.484	0.6	0.565
D-Fructose	**Acetic Acid**	**α-D-Glucose**	**Maltose**	**D-Melibiose**	**Thymidine**
1.146	0.647	1.211	1.35	0.976	0.491
α-Keto-Butyric Acid	**α-Methyl-D-Galactoside**	**α-D-Lactose**	**Lactulose**	**Sucrose**	**Uridine**
0.474	0.891	1.259	1.24	1.27	0.807
α-Hydroxy Butyric Acid	**β-Methyl-D-Glucoside**	**Adonitol**	**Maltotriose**	**2-Deoxy Adenosine**	**Adenosine**
0.45	0.975	0.526	1.353	0.45	0.682
Propionic Acid	**Mucic Acid**	**Glycolic Acid**	**Glyoxylic Acid**	**D-Cellobiose**	**Inosine**
0.638	0.462	0.388	0.389	1.175	0.624
Acetoacetic Acid	**N-Acetyle-β-D-Mannosamine**	**Mono Methyl Succinate**	**Methyl Pyruvate**	**D-Malic Acid**	**L-Malic Acid**
0.821	1.233	0.442	0.551	0.418	0.412

Glucuronamide	Pyruvic Acid	L-GalactonicAcid-γ-Lactone	D-Galacturonic acid	Phenylethyl-amine	2-Aminoethano
0.527	0.68	0.619	0.492	0.492	0.371

Appendix E. Phenotype Microarray of 4559, Biolog PM2 plate. Catabolism was measured through the reduction of a colourless tetrazolium dye by NADH, produced during catabolic activity. A_{590} values above 0.65 were considered positive (see section 2.2.4). Values for raffinose are highlighted in yellow.

Negative Control	Chondroitin Sulfate c	α-Cyclodextrin	β-Cyclodextrin	γ-Cyclodextrin	Dextrin
0.569	0.73	0.615	0.424	0.405	1.197
N-Acetyl-D-Galactosamine	N-Acetyl-Neuraminic Acid	β-D-Allose	Amygdalin	D-Arabinose	D-Arabitol
1.134	0.669	0.664	0.669	0.841	0.515
Gentiobiose	L-Glucose	Lactitol	D-Melezitose	Maltitol	α-Methyl-D-Glucoside
0.679	0.595	0.825	0.658	0.613	0.741
D-Raffinose	Salicin	Sedoheptulosan	L-Sorbose	Stachyose	D-Tagatose
1.618	0.919	0.553	0.684	1.627	0.978
Capric Acid	Caproic Acid	Citraconic Acid	Citramalic Acid	D-Glucosamine	2-Hydroxy Benzoic Acid
0.404	0.681	0.429	0.547	1.458	0.368
D-Lactic Acid Methyl Ester	Malonic Acid	Melibionic Acid	Oxalic Acid	Oxalomalic Acid	Quinic Acid
0.556	0.546	0.769	0.592	0.591	0.512
Acetamide	L-Alaninamide	N-Acetyl-L-Glutamic Acid	L-Arginine	Glycine	L-Histidine
0.571	0.566	0.603	0.617	0.496	0.481
L-Ornithine	L-Phenylalanine	L-Pyroglutamic Acid	L-Valine	D,L-Carnitine	Sec-Butylamine
0.547	0.622	0.591	0.555	0.541	0.682
Gelatin	Glycogen	Inulin	Laminarin	Mannan	Pectin
0.587	0.582	1.31	0.527	0.367	0.47
L-Arabitol	Arbutin	2-Deoxy-D-Ribose	I-Erythritol	D-Fucose	3-0-β-D-Galactopyranosyl-D-Arabinose
0.53	0.379	0.834	0.481	0.804	1.331
β-Methyl-D-Galactoside	3-Methyl Glucose	β-Methyl-D-Glucuronic Acid	α-Methyl-D-Mannoside	β-Methyl-D-Xyloside	Palatinose
0.815	0.769	0.509	0.535	0.493	1.091
Turanose	Xylitol	N-Acetyl-D-Glucosaminitol	γ-Amino Butyric Acid	δ-Amino Valeric Acid	Butyric Acid
0.775	0.507	0.659	0.448	0.461	0.561
4-Hydroxy Benzoic Acid	β-Hydroxy Butyric Acid	γ-Hydroxy Butyric Acid	α-Keto-Valeric Acid	Itaconic Acid	5-Keto-D-Gluconic Acid
0.42	0.54	0.518	0.39	0.526	0.841
D-Ribono-1,4-Lactone	Sebacic Acid	Sorbic Acid	Succinamic Acid	D-Tartaric Acid	L-Tartaric Acid
0.381	0.468	0.8	0.448	0.461	0.529
L-Homoserine	Hydroxy-L-Proline	L-Isoleucine	L-Leucine	L-Lysine	L-Methionine
0.491	0.506	0.527	0.49	0.423	0.402

D.L-Octopamine	Putrescine	Dihydroxy Acetone	2,3-Butanediol	2,3-Butanone	3-Hydroxy 2-Butanone
0.438	0.496	1.022	0.514	0.369	0.547

Appendix F. Phenotype Microarray of 947, Biolog PM2 plate. Catabolism was measured through the reduction of a colourless tetrazolium dye by NADH, produced during catabolic activity. A_{590} values above 0.65 were considered positive (see section 2.2.4). Values for raffinose are highlighted in yellow.

Negative Control	Chondroitin Sulfate c	α-Cyclodextrin	β-Cyclodextrin	γ-Cyclodextrin	Dextrin
0.632	0.801	0.621	0.384	0.383	1.131
N-Acetyl-D-Galactosamine	N-Acetyl-Neuraminic Acid	β-D-Allose	Amygdalin	D-Arabinose	D-Arabitol
1.121	0.981	0.796	0.736	0.969	0.624
Gentiobiose	L-Glucose	Lactitol	D-Melezitose	Maltitol	α-Methyl-D-Glucoside
0.801	0.67	0.881	0.679	0.735	0.897
D-Raffinose	Salicin	Sedoheptulosan	L-Sorbose	Stachyose	D-Tagatose
0.427	1.001	0.649	0.69	1.444	1.01
Capric Acid	Caproic Acid	Citraconic Acid	Citramalic Acid	D-Glucosamine	2-Hydroxy Benzoic Acid
0.381	0.677	0.495	0.651	1.358	0.424
D-Lactic Acid Methyl Ester	Malonic Acid	Melibionic Acid	Oxalic Acid	Oxalomalic Acid	Quinic Acid
0.647	0.629	0.723	0.679	0.585	0.542
Acetamide	L-Alaninamide	N-Acetyl-L-Glutamic Acid	L-Arginine	Glycine	L-Histidine
0.83	0.611	0.59	0.613	0.566	0.558
L-Ornithine	L-Phenylalanine	L-Pyroglutamic Acid	L-Valine	D,L-Carnitine	Sec-Butylamine
0.565	0.609	0.718	0.599	0.636	0.764
Gelatin	Glycogen	Inulin	Laminarin	Mannan	Pectin
0.697	0.669	1.152	0.597	0.386	0.528
L-Arabitol	Arbutin	2-Deoxy-D-Ribose	I-Erythritol	D-Fucose	3-0-β-D-Galactopyranosyl-D-Arabinose
0.675	0.466	0.88	0.52	0.876	1.178
β-Methyl-D-Galactoside	3-Methyl Glucose	β-Methyl-D-Glucuronic Acid	α-Methyl-D-Mannoside	β-Methyl-D-Xyloside	Palatinose
0.921	1.006	0.606	0.585	0.59	1.196
Turanose	Xylitol	N-Acetyl-D-Glucosaminitol	γ-Amino Butyric Acid	δ-Amino Valeric Acid	Butyric Acid
0.936	0.631	0.696	0.5	0.483	0.643
4-Hydroxy Benzoic Acid	β-Hydroxy Butyric Acid	γ-Hydroxy Butyric Acid	α-Keto-Valeric Acid	Itaconic Acid	5-Keto-D-Gluconic Acid
0.463	0.605	0.573	0.433	0.59	0.957
D-Ribono-1,4-Lactone	Sebacic Acid	Sorbic Acid	Succinamic Acid	D-Tartaric Acid	L-Tartaric Acid
0.471	0.523	0.892	0.521	0.56	0.564
L-Homoserine	Hydroxy-L-Proline	L-Isoleucine	L-Leucine	L-Lysine	L-Methionine
0.597	0.611	0.585	0.587	0.536	0.487

D.L-Octopamine	Putrescine	Dihydroxy Acetone	2,3-Butanediol	2,3-Butanone	3-Hydroxy 2-Butanone
0.539	0.571	1.118	0.594	0.401	0.577

Appendix G. Phenotype Microarray of 4559^{947rafR}, Biolog PM2 plate. Catabolism was measured through the reduction of a colourless tetrazolium dye by NADH, produced during catabolic activity. A_{590} values above 0.65 were considered positive (see section 2.2.4). Values for raffinose are highlighted in yellow.

Negative Control	Chondroitin Sulfate c	α-Cyclodextrin	β-Cyclodextrin	γ-Cyclodextrin	Dextrin
0.276	0.482	0.28	0.147	0.14	0.745
N-Acetyl-D-Galactosamine	N-Acetyl-Neuraminic Acid	β-D-Allose	Amygdalin	D-Arabinose	D-Arabitol
0.887	1.177	0.323	0.395	0.572	0.296
Gentiobiose	L-Glucose	Lactitol	D-Melezitose	Maltitol	α-Methyl-D-Glucoside
0.395	0.314	0.612	0.31	0.37	0.477
D-Raffinose	Salicin	Sedoheptulosan	L-Sorbose	Stachyose	D-Tagatose
0.469	0.683	0.316	0.33	0.383	0.7
Capric Acid	Caproic Acid	Citraconic Acid	Citramalic Acid	D-Glucosamine	2-Hydroxy Benzoic Acid
0.106	0.349	0.198	0.24	1.038	0.6
D-Lactic Acid Methyl Ester	Malonic Acid	Melibionic Acid	Oxalic Acid	Oxalomalic Acid	Quinic Acid
0.271	0.273	0.301	0.425	0.289	0.233
Acetamide	L-Alaninamide	N-Acetyl-L-Glutamic Acid	L-Arginine	Glycine	L-Histidine
0.292	0.27	0.269	0.281	0.225	0.242
L-Ornithine	L-Phenylalanine	L-Pyroglutamic Acid	L-Valine	D,L-Carnitine	Sec-Butylamine
0.237	0.281	0.304	0.277	0.266	0.427
Gelatin	Glycogen	Inulin	Laminarin	Mannan	Pectin
0.329	0.343	0.871	0.304	0.173	0.262
L-Arabitol	Arbutin	2-Deoxy-D-Ribose	I-Erythritol	D-Fucose	3-0-β-D-Galactopyranosyl-D-Arabinose
0.3	0.165	0.61	0.26	0.743	0.988
β-Methyl-D-Galactoside	3-Methyl Glucose	β-Methyl-D-Glucuronic Acid	α-Methyl-D-Mannoside	β-Methyl-D-Xyloside	Palatinose
0.636	0.528	0.292	0.298	0.293	0.853
Turanose	Xylitol	N-Acetyl-D-Glucosaminitol	γ-Amino Butyric Acid	δ-Amino Valeric Acid	Butyric Acid
0.593	0.282	0.399	0.247	0.236	0.368
4-Hydroxy Benzoic Acid	β-Hydroxy Butyric Acid	γ-Hydroxy Butyric Acid	α-Keto-Valeric Acid	Itaconic Acid	5-Keto-D-Gluconic Acid
0.166	0.282	0.293	0.171	0.318	0.585
D-Ribono-1,4-Lactone	Sebacic Acid	Sorbic Acid	Succinamic Acid	D-Tartaric Acid	L-Tartaric Acid
0.149	0.215	0.523	0.246	0.26	0.266
L-Homoserine	Hydroxy-L-Proline	L-Isoleucine	L-Leucine	L-Lysine	L-Methionine
0.237	0.249	0.259	0.279	0.239	0.207

D.L-Octopamine	Putrescine	Dihydroxy Acetone	2,3-Butanediol	2,3-Butanone	3-Hydroxy 2-Butanone
0.183	0.257	0.765	0.305	0.157	0.284

Appendix H. Phenotype Microarray of 947^{4559rafR}, Biolog PM2 plate. Catabolism was measured through the reduction of a colourless tetrazolium dye by NADH, produced during catabolic activity. A_{590} values above 0.65 were considered positive (see section 2.2.4). Values for raffinose are highlighted in yellow.

Negative Control	Chondroitin Sulfate c	α-Cyclodextrin	β-Cyclodextrin	γ-Cyclodextrin	Dextrin
0.612	0.944	0.55	0.43	0.427	1.24
N-Acetyl-D-Galactosamine	N-Acetyl-Neuraminic Acid	β-D-Allose	Amygdalin	D-Arabinose	D-Arabitol
1.351	0.89	0.593	0.72	0.868	0.56
Gentiobiose	L-Glucose	Lactitol	D-Melezitose	Maltitol	α-Methyl-D-Glucoside
0.776	0.602	0.933	0.596	0.695	0.84
D-Raffinose	Salicin	Sedoheptulosan	L-Sorbose	Stachyose	D-Tagatose
1.454	1.113	0.615	0.593	1.489	0.966
Capric Acid	Caproic Acid	Citraconic Acid	Citramalic Acid	D-Glucosamine	2-Hydroxy Benzoic Acid
0.417	0.653	0.493	0.575	1.451	0.442
D-Lactic Acid Methyl Ester	Malonic Acid	Melibionic Acid	Oxalic Acid	Oxalomalic Acid	Quinic Acid
0.64	0.645	0.727	0.696	0.547	0.504
Acetamide	L-Alaninamide	N-Acetyl-L-Glutamic Acid	L-Arginine	Glycine	L-Histidine
0.585	1.075	1.138	0.542	0.529	0.511
L-Ornithine	L-Phenylalanine	L-Pyroglutamic Acid	L-Valine	D,L-Carnitine	Sec-Butylamine
0.547	0.557	0.631	0.553	0.579	0.695
Gelatin	Glycogen	Inulin	Laminarin	Mannan	Pectin
0.638	0.587	1.12	0.588	0.397	0.533
L-Arabitol	Arbutin	2-Deoxy-D-Ribose	I-Erythritol	D-Fucose	3-0-β-D-Galactopyranosyl-D-Arabinose
0.591	0.42	0.831	0.495	0.952	1.305
β-Methyl-D-Galactoside	3-Methyl Glucose	β-Methyl-D-Glucuronic Acid	α-Methyl-D-Mannoside	β-Methyl-D-Xyloside	Palatinose
1.009	0.876	0.533	0.577	0.54	1.169
Turanose	Xylitol	N-Acetyl-D-Glucosaminitol	γ-Amino Butyric Acid	δ-Amino Valeric Acid	Butyric Acid
0.964	0.591	0.661	0.511	0.476	0.624
4-Hydroxy Benzoic Acid	β-Hydroxy Butyric Acid	γ-Hydroxy Butyric Acid	α-Keto-Valeric Acid	Itaconic Acid	5-Keto-D-Gluconic Acid
0.431	0.522	0.283	0.431	0.584	0.796
D-Ribono-1,4-Lactone	Sebacic Acid	Sorbic Acid	Succinamic Acid	D-Tartaric Acid	L-Tartaric Acid
0.443	0.474	0.835	0.495	0.506	0.497
L-Homoserine	Hydroxy-L-Proline	L-Isoleucine	L-Leucine	L-Lysine	L-Methionine
0.533	0.523	0.556	0.529	0.464	0.476

D.L-Octopamine	Putrescine	Dihydroxy Acetone	2,3-Butanediol	2,3-Butanone	3-Hydroxy 2-Butanone
0.468	0.548	0.995	0.556	0.389	0.633

Appendix I: Sucrose intensity of gas chromatography mass spectrometry, selected-ion monitoring analysis on pneumococcal infected murine lungs

Name	Retention Time	SIM Intensity	Qualifier (437.2) Ion Ratio
Analytical standard A	13.432	4299424	15.4
Analytical standard B	13.428	3241463	15.6
947 A	13.428	46874	11.2
947 B	13.428	63609	9.1
947 C	13.428	62015	12.9
947 D	13.428	58606	10.8
4559 A	13.428	67667	10.8
4559 B	13.428	32775	12.6
4559 C	13.428	49602	11.9
4559 D	13.428	32432	11.5
Serum broth A	13.428	37540	11
Serum broth B	13.428	74120	8.5
Serum broth C	13.428	57343	8.9
Serum broth D	13.428	41296	10

Appendix J: Raffinose intensity of gas chromatography mass spectrometry, selected-ion monitoring analysis on pneumococcal infected murine lungs.

Name	Retention Time	SIM Intensity	Qualifier (437.2) Ion Ratio
Analytical standard	16.263	7096929	9.9
Analytical standard	16.255	4764259	9.6
Ear isolate	16.255	2478	26.7
Ear isolate	16.255	1840	18.4
Ear isolate	16.298	3100	32.7
Ear isolate	16.255	1627	28.7
Blood isolate	16.255	2930	N/A
Blood isolate	16.255	802	39.9
Blood isolate	16.298	35965	7.8
Blood isolate	16.298	16507	13.2
Serum broth	16.298	7043	10.9
Serum broth	16.298	15588	8
Serum broth	16.298	9152	7.8
Serum broth	16.298	7103	7.1

Appendix K: Differential gene expression of *S. pneumoniae* 4559 vs 947 in CDM+Glc (Glu), CDM+Gal and human serum mediums. Genes wfith fold change (FC) greater than 2 and FDR < 0.01 are shown. FC values highlighted in blue = upregulated in 947, while values highlighted in red = upregulated in 4559.

Locus tag in 947	Product	Media	FDR	FC
Sp947_chr_01629	treP PTS system trehalose-specific EIIBC component	Glu	4.99E-07	10.16
Sp947_chr_01671	wbbI Beta-1,6-galactofuranosyltransferase	Glu	3.30E-08	4.57
Sp947_chr_01664	gtf2 Glycosyltransferase-stabilizing protein	Glu	4.31E-09	4.56
Sp947_chr_01665	gtf1 Glycosyltransferase	Glu	3.36E-09	4.5
Sp947_chr_01663	Hypothetical protein	Glu	7.47E-08	4.42
Sp947_chr_01670	secY2 Accessory Sec system protein translocase subunit	Glu	2.70E-08	4.34
Sp947_chr_01666	secA_2 Protein translocase subunit	Glu	4.72E-08	4.33
Sp947_chr_01669	Hypothetical protein	Glu	4.72E-08	4.22
Sp947_chr_01672	gspA_1 General stress protein A	Glu	3.30E-08	4.2
Sp947_chr_01668	asp2 Accessory Sec system protein	Glu	7.59E-07	4.09
Sp947_chr_01667	Accessory Sec system protein Asp3	Glu	1.87E-05	4.05
Sp947_chr_01662	Hypothetical protein	Glu	4.72E-08	3.92
Sp947_chr_01673	gspA_1 General stress protein A	Glu	1.07E-08	3.9
Sp947_chr_01675	Hypothetical protein	Glu	3.78E-08	3.84
Sp947_chr_01674	epsJ_4 putative glycosyltransferase	Glu	3.84E-08	3.74
Sp947_chr_01868	Hypothetical protein	Glu	0.00933	3.16
Sp947_chr_01631	HTH-type transcriptional regulator DegA	Glu	6.21E-05	2.94
Sp947_chr_01630	scrB Sucrose-6-phosphate hydrolase	Glu	0.000246	2.9
Sp947_chr_01788	HTH-type transcriptional regulator TreR	Glu	0.001066	2.61
Sp947_chr_01600	nanA_3 Sialidase A	Glu	0.001146	2.19
Sp947_chr_01628	gmuE Putative fructokinase	Glu	0.007833	2.14
Sp947_chr_00722	Biotin transporter BioY2	Glu	0.005284	2.49
Sp947_chr_00440	pflB Formate acetyltransferase	Glu	2.96E-05	3.16
Sp947_chr_00679	bglH_2 Aryl-phospho-beta-D-glucosidase	Glu	0.002146	3.97
Sp947_chr_00678	Hypothetical protein	Glu	3.06E-06	5.56
Sp947_chr_00677	Hypothetical protein	Glu	9.00E-07	5.57
Sp947_chr_00676	Hypothetical protein	Glu	3.84E-08	5.88
Sp947_chr_00675	spxB Pyruvate oxidase	Glu	4.72E-08	6.95
Sp947_chr_01629	treP PTS system trehalose-specific EIIBC component	Gal	0.002858	24.5
Sp947_chr_00499	hypothetical protein	Gal	0.002594	9.25
Sp947_chr_00498	hypothetical protein	Gal	0.006684	9.2
Sp947_chr_00500	hypothetical protein	Gal	0.002442	8.36
Sp947_chr_00502	lytA_7 Autolysin	Gal	0.002688	7.4
Sp947_chr_00501	Hypothetical protein	Gal	0.005244	7.34
Sp947_chr_00491	dus putative tRNA-dihydrouridine synthase	Gal	0.004584	7.14
Sp947_chr_00493	Hypothetical protein	Gal	0.007566	6.29
Sp947_chr_01675	Hypothetical protein	Gal	0.000316	4.63
Sp947_chr_01630	scrB Sucrose-6-phosphate hydrolase	Gal	0.000152	2.85
Sp947_chr_01631	HTH-type transcriptional regulator DegA	Gal	0.000229	2.68
Sp947_chr_00065	acpB Capsule synthesis positive regulator AcpB	Gal	0.002688	2.38
Sp947_chr_00840	nanE Putative N-acetylmannosamine-6-phosphate 2-epimerase	Gal	9.87E-05	2.25
Sp947_chr_02095	arcC1 Carbamate kinase 1	Gal	0.002442	2.21
Sp947_chr_00646	Hypothetical protein	Gal	0.00102	2.19
Sp947_chr_00066	sorC PTS system sorbose-specific EIIC component	Gal	0.004824	2.07
Sp947_chr_00839	HTH-type transcriptional regulator RpiR	Gal	0.000128	2.03
Sp947_chr_00841	nanA N-acetylneuraminate lyase	Gal	9.64E-05	2.01
Sp947_chr_00924	natA ABC transporter ATP-binding protein	Gal	0.00857	2

Sp947_chr_00592	gatC_2 PTS system galactitol-specific EIIC component	Gal	0.004291	2
Sp947_chr_00594	Beta-galactosidase BoGH2	Gal	0.000211	2.11
Sp947_chr_00440	pflB Formate acetyltransferase	Gal	0.000229	2.21
Sp947_chr_01097	Hypothetical protein	Gal	0.001418	2.32
Sp947_chr_01096	Hypothetical protein	Gal	0.002195	2.43
Sp947_chr_01098	Hypothetical protein	Gal	0.003998	2.43
Sp947_chr_00023	Glycosyltransferase	Gal	0.00102	2.46
Sp947_chr_01099	Hypothetical protein	Gal	0.000172	2.5
Sp947_chr_00679	bglH_2 Aryl-phospho-beta-D-glucosidase	Gal	0.001418	2.9
Sp947_chr_01104	lacD Tagatose 1,6-diphosphate aldolase	Gal	6.09E-06	3.74
Sp947_chr_01103	lacC Tagatose-6-phosphate kinase	Gal	1.63E-05	3.93
Sp947_chr_00116	Hypothetical protein	Gal	0.000849	3.96
Sp947_chr_00112	Hypothetical protein	Gal	0.001314	4.04
Sp947_chr_01102	lacB Galactose-6-phosphate isomerase subunit	Gal	2.28E-05	4.05
Sp947_chr_00117	dpnC Type-2 restriction enzyme DpnI	Gal	0.000381	4.05
Sp947_chr_00118	paaI Acyl-coenzyme A thioesterase	Gal	0.000365	4.06
Sp947_chr_00119	galT Galactose-1-phosphate uridylyltransferase	Gal	3.93E-05	4.15
Sp947_chr_00122	adh_1 Alcohol dehydrogenase	Gal	0.000805	4.16
Sp947_chr_00114	hypothetical protein	Gal	0.00102	4.16
Sp947_chr_00115	hypothetical protein	Gal	0.001218	4.24
Sp947_chr_01101	lacA Galactose-6-phosphate isomerase subunit	Gal	1.63E-05	4.24
Sp947_chr_00120	galK_2 Galactokinase	Gal	0.000211	4.28
Sp947_chr_00121	lacR_3 HTH-type transcriptional regulator LacR	Gal	9.64E-05	4.42
Sp947_chr_00111	exoA Exodeoxyribonuclease	Gal	0.000229	4.58
Sp947_chr_00113	Hypothetical protein	Gal	0.005561	4.61
Sp947_chr_00123	adhR HTH-type transcriptional regulator AdhR	Gal	8.98E-05	4.78
Sp947_chr_00676	Hypothetical protein	Gal	2.18E-06	5.9
Sp947_chr_00675	spxB Pyruvate oxidase	Gal	2.18E-06	6.01
Sp947_chr_00678	Hypothetical protein	Gal	2.18E-06	6.13
Sp947_chr_00677	Hypothetical protein	Gal	0.000104	6.21
Sp947_chr_01629	treP PTS system trehalose-specific EIIBC component	Serum	1.22E-05	27.8
Sp947_chr_01630	scrB Sucrose-6-phosphate hydrolase	Serum	2.49E-08	6.66
Sp947_chr_01631	HTH-type transcriptional regulator DegA	Serum	1.26E-07	6.11
Sp947_chr_01675	Hypothetical protein	Serum	2.49E-08	5.41
Sp947_chr_01674	epsJ_4 putative glycosyltransferase	Serum	1.26E-08	4.69
Sp947_chr_01673	gspA_1 General stress protein A	Serum	6.83E-09	4.47
Sp947_chr_01670	secY2 Accessory Sec system protein translocase subunit	Serum	2.33E-07	4.25
Sp947_chr_01672	gspA_1 General stress protein A	Serum	2.49E-08	4.18
Sp947_chr_01628	gmuE Putative fructokinase	Serum	5.13E-05	4.09
Sp947_chr_01671	wbbI Beta-1,6-galactofuranosyltransferase	Serum	8.80E-08	3.98
Sp947_chr_01663	Hypothetical protein	Serum	5.88E-07	3.96
Sp947_chr_01664	gtf2 Glycosyltransferase-stabilizing protein	Serum	6.92E-08	3.9
Sp947_chr_01665	gtf1 Glycosyltransferase	Serum	2.33E-07	3.89
Sp947_chr_01668	asp2 Accessory Sec system protein	Serum	1.22E-05	3.88
Sp947_chr_01666	secA_2 Protein translocase subunit	Serum	6.77E-06	3.8
Sp947_chr_01669	Hypothetical protein	Serum	2.46E-06	3.74
Sp947_chr_01667	Accessory Sec system protein Asp3	Serum	8.85E-05	3.7
Sp947_chr_01662	Hypothetical protein	Serum	5.78E-05	3.28
Sp947_chr_00678	Hypothetical protein	Serum	0.005505	3.49
Sp947_chr_00722	Biotin transporter BioY2	Serum	1.02E-05	3.79
Sp947_chr_00675	spxB Pyruvate oxidase	Serum	2.87E-07	4.33
Sp947_chr_00677	Hypothetical protein	Serum	2.96E-05	4.72
Sp947_chr_00676	Hypothetical protein	Serum	1.26E-08	4.88

Appendix L: Differential gene expression of *S. pneumoniae* 180/15 vs 180/2 in CDM+Glc (Glu), CDM+Gal and human serum mediums. Genes with fold change (FC) greater than 2 and FDR < 0.01 are shown. FC values highlighted in blue = upregulated in 180/2, while values highlighted in red = upregulated in 180/15.

Locus tag in 180_2	Product	Media	FDR	FC
Sp180_2_chr_00600	putative glutamine ABC transporter permease protein GlnP	Glu	1.71E-07	6.28
Sp180_2_chr_00603	Glutamine transport ATP-binding protein GlnQ	Glu	8.78E-07	5.94
Sp180_2_chr_00601	putative glutamine ABC transporter permease protein GlnM	Glu	4.73E-08	5.66
Sp180_2_chr_00602	Major cell-binding factor peb1A	Glu	2.37E-07	5.58
Sp180_2_chr_00162	Hypothetical protein	Glu	0.00038	4.47
Sp180_2_chr_00161	Hypothetical protein	Glu	0.00023	4.06
Sp180_2_chr_00513	Hypothetical protein	Glu	5.1E-06	4.05
Sp180_2_chr_01195	Arginine transport ATP-binding protein ArtM	Glu	2.2E-05	3.93
Sp180_2_chr_00813	Hypothetical protein	Glu	3.1E-05	3.52
Sp180_2_chr_01194	Glutamine transport system permease protein GlnP	Glu	1.6E-05	3.41
Sp180_2_chr_00160	Hypothetical protein	Glu	0.00078	3.37
Sp180_2_chr_01196	Glucose-6-phosphate 1-dehydrogenase zwf	Glu	1.3E-06	3.25
Sp180_2_chr_00555	Hypothetical protein	Glu	0.00429	3.09
Sp180_2_chr_01980	Hypothetical protein	Glu	9.1E-05	3.07
Sp180_2_chr_00511	HTH-type transcriptional regulator GlnR	Glu	8.7E-05	2.93
Sp180_2_chr_00438	Amino-acgene_id carrier protein AlsT	Glu	7.43E-07	2.92
Sp180_2_chr_00512	Glutamine synthetase glnA	Glu	0.00014	2.83
Sp180_2_chr_00152	putative cell wall hydrolase LytN	Glu	0.00266	2.76
Sp180_2_chr_01077	Redox-sensing transcriptional repressor Rex	Glu	1.7E-06	2.72
Sp180_2_chr_01076	Putative glutamine amgene_idotransferase	Glu	1.3E-06	2.65
Sp180_2_chr_00515	Hypothetical protein	Glu	9.95E-08	2.56
Sp180_2_chr_02133	ComF operon protein 1	Glu	0.01515	2.55
Sp180_2_chr_01822	groS 10 kDa chaperonin	Glu	0.00035	2.55
Sp180_2_chr_01821	groL 60 kDa chaperonin	Glu	0.00056	2.47
Sp180_2_chr_01434	Cystathionine gamma-synthase/O-acetylhomoserine (thiol)-lyase metI	Glu	8E-05	2.42
Sp180_2_chr_01404	Hypothetical protein	Glu	2.1E-06	2.39
Sp180_2_chr_01435	Multgene_idrug resistance ABC transporter ATP-binding and permease protein lmrA_1	Glu	0.00083	2.35
Sp180_2_chr_01436	Multgene_idrug resistance ABC transporter ATP-binding and permease protein lmrA_2	Glu	0.00076	2.32
Sp180_2_chr_01433	Cystathionine beta-lyase PatB	Glu	2.7E-05	2.31
Sp180_2_chr_00159	Argininosuccinate synthase argG	Glu	0.00826	2.3
Sp180_2_chr_01075	Hypothetical protein	Glu	1.3E-06	2.28
Sp180_2_chr_01776	Hypothetical protein	Glu	3.2E-05	2.28
Sp180_2_chr_01437	Hypothetical protein	Glu	0.0013	2.26
Sp180_2_chr_00516	Hypothetical protein	Glu	1.6E-06	2.25
Sp180_2_chr_01347	Hypothetical protein	Glu	0.0032	2.21
Sp180_2_chr_01777	Hypothetical protein	Glu	0.00015	2.18
Sp180_2_chr_01778	Hypothetical protein	Glu	6.1E-05	2.17
Sp180_2_chr_00203	UDP-glucose 6-dehydrogenase ugd_2	Glu	0.02178	2.08
Sp180_2_chr_00609	Hypothetical protein	Glu	9.9E-06	2.06
Sp180_2_chr_00158	Arginine-binding extracellular protein ArtP	Glu	0.0087	2.05
Sp180_2_chr_00888	Arginine decarboxylase speA	Glu	0.01817	2.03
Sp180_2_chr_01941	PTS system oligo-beta-mannosgene_ide-specific EIIA component gmuA	Glu	0.00399	2.02
Sp180_2_chr_01940	PTS system cellobiose-specific EIIB component celA_3	Glu	0.00391	2.02

Sp180_2_chr_01346	Hypothetical protein	Glu	0.00625	2.01
Sp180_2_chr_01125	Dihydrolipoyllysine-resgene_idue acetyltransferase component of pyruvate dehydrogenase complex pdhC	Glu	1.3E-06	2.01
Sp180_2_chr_01183	Formate--tetrahydrofolate ligase 1 fhs1	Glu	0.00297	2.01
Sp180_2_chr_01339	Autolysin lytA_3	Glu	3.90E-08	2.02
Sp180_2_chr_01126	2-oxoisovalerate dehydrogenase subunit beta bfmBAB	Glu	1.9E-06	2.02
Sp180_2_chr_02004	Putative glutamine amgene_idotransferase	Glu	0.00279	2.03
Sp180_2_chr_01740	Uric acgene_id permease PucK	Glu	0.00032	2.04
Sp180_2_chr_01007	putative sgene_iderophore transport system ATP-binding protein YusV	Glu	1.58E-07	2.05
Sp180_2_chr_00925	ComE operon protein 1	Glu	0.00145	2.07
Sp180_2_chr_01113	Enolase eno_2	Glu	0.00309	2.07
Sp180_2_chr_01006	putative sgene_iderophore transport system permease protein YfhA	Glu	1.79E-07	2.08
Sp180_2_chr_01928	Penicillin-binding protein 1F pbpF_1	Glu	6.29E-07	2.08
Sp180_2_chr_00102	Bifunctional purine biosynthesis protein PurH	Glu	0.02127	2.08
Sp180_2_chr_00101	Hypothetical protein	Glu	0.01241	2.14
Sp180_2_chr_01387	FAD:protein FMN transferase apbE	Glu	2.1E-05	2.16
Sp180_2_chr_01111	Glycerate kinase glxK	Glu	8.06E-07	2.19
Sp180_2_chr_00981	Hypothetical protein	Glu	9.8E-06	2.25
Sp180_2_chr_01743	Acyl-coenzyme A thioesterase PaaI	Glu	0.00011	2.26
Sp180_2_chr_01112	Hypothetical protein	Glu	1.1E-06	2.27
Sp180_2_chr_02117	Hypothetical protein	Glu	3.35E-07	2.27
Sp180_2_chr_00100	Phosphoribosylglycinamgene_ide formyltransferase purN	Glu	0.0114	2.32
Sp180_2_chr_02116	IgA FC receptor bag	Glu	1.4E-06	2.33
Sp180_2_chr_00099	Phosphoribosylformylglycinamgene_idine cyclo-ligase purM	Glu	0.00788	2.39
Sp180_2_chr_02136	Hypothetical protein	Glu	0.00041	2.39
Sp180_2_chr_00598	Fructose-bisphosphate aldolase fba	Glu	0.0002	2.45
Sp180_2_chr_01340	Hypothetical protein	Glu	1.44E-07	2.46
Sp180_2_chr_01389	NADH-dependent flavin reductase subunit 1 nfr1	Glu	0.00017	2.47
Sp180_2_chr_01095	Riboflavin biosynthesis protein RibF	Glu	2.37E-07	2.48
Sp180_2_chr_00979	Ferrochelatase hemH	Glu	2.37E-07	2.48
Sp180_2_chr_01124	Dihydrolipoamide dehydrogenase	Glu	1.44E-07	2.52
Sp180_2_chr_01372	Capsule biosynthesis protein CapA	Glu	3.66E-07	2.53
Sp180_2_chr_00509	Phosphoglycerate kinase pgk	Glu	0.00031	2.62
Sp180_2_chr_00098	Amgene_idophosphoribosyltransferase purF	Glu	0.00339	2.67
Sp180_2_chr_01341	Putative ribosomal N-acetyltransferase YdaF	Glu	3.90E-09	2.73
Sp180_2_chr_01388	NADH-dependent flavin reductase subunit 2 nfr2	Glu	2E-05	2.83
Sp180_2_chr_01371	Sugar phosphatase YbiV	Glu	1.51E-07	2.88
Sp180_2_chr_01123	Lipoate-protein ligase LplJ	Glu	1.45E-08	2.96
Sp180_2_chr_02121	Transcriptional regulator CtsR	Glu	1.19E-09	2.97
Sp180_2_chr_01370	Hypothetical protein	Glu	6.38E-08	3.06
Sp180_2_chr_02082	Alcohol dehydrogenase 2 adhB	Glu	2.6E-05	3.24
Sp180_2_chr_02118	Sensor histgene_idine kinase WalK	Glu	2.02E-09	3.25
Sp180_2_chr_00097	Phosphoribosylformylglycinamgene_idine synthase purL	Glu	0.0002	3.36
Sp180_2_chr_02119	Phosphate regulon transcriptional regulatory protein PhoB	Glu	1.13E-09	3.4
Sp180_2_chr_01942	Aldehyde-alcohol dehydrogenase adhE	Glu	4.2E-05	3.51
Sp180_2_chr_01105	NADP-dependent glyceraldehyde-3-phosphate dehydrogenase	Glu	9.7E-06	3.6
Sp180_2_chr_01343	Nicotinate phosphoribosyltransferase pncB2	Glu	1.13E-09	3.6
Sp180_2_chr_02120	ATP-dependent Clp protease ATP-binding subunit ClpC	Glu	5.31E-10	3.75
Sp180_2_chr_01342	NH(3)-dependent NAD(+) synthetase nadE	Glu	1.13E-09	3.83

Sp180_2_chr_00571	Hypothetical protein	Glu	9.7E-06	4.29
Sp180_2_chr_01971	Alcohol dehydrogenase adh_2	Glu	1.3E-06	4.57
Sp180_2_chr_00096	Phosphoribosylaminoimgene_idazole-succinocarboxamgene_ide synthase purC	Glu	5.12E-07	4.75
Sp180_2_chr_01172	Hypothetical protein	Glu	3.11E-09	5.19
Sp180_2_chr_01266	Hypothetical protein	Glu	2.3E-06	13.4
Sp180_2_chr_00513	Hypothetical protein	Gal	3.03E-07	4.22
Sp180_2_chr_01194	Glutamine transport system permease protein GlnP	Gal	2.2E-05	3.42
Sp180_2_chr_00602	Major cell-binding factor peb1A	Gal	2.5E-05	3.42
Sp180_2_chr_00511	HTH-type transcriptional regulator GlnR	Gal	7.65E-07	3.15
Sp180_2_chr_00813	Hypothetical protein	Gal	7.65E-07	3.1
Sp180_2_chr_00512	Glutamine synthetase glnA	Gal	2.1E-06	3.08
Sp180_2_chr_01195	Arginine transport ATP-binding protein ArtM	Gal	1.9E-05	3.08
Sp180_2_chr_00603	Glutamine transport ATP-binding protein GlnQ	Gal	0.00069	2.98
Sp180_2_chr_00707	Hypothetical protein	Gal	0.00304	2.91
Sp180_2_chr_01077	Redox-sensing transcriptional repressor Rex	Gal	1.3E-05	2.83
Sp180_2_chr_00161	Hypothetical protein	Gal	0.00079	2.83
Sp180_2_chr_00708	putative copper-transporting ATPase PacS	Gal	0.00375	2.71
Sp180_2_chr_01821	groL 60 kDa chaperonin	Gal	1.8E-05	2.69
Sp180_2_chr_01076	Putative glutamine amgene_idotransferase	Gal	1.5E-05	2.66
Sp180_2_chr_00162	Hypothetical protein	Gal	0.00069	2.66
Sp180_2_chr_01404	Hypothetical protein	Gal	0.0009	2.56
Sp180_2_chr_00152	putative cell wall hydrolase LytN	Gal	0.004	2.54
Sp180_2_chr_00601	putative glutamine ABC transporter permease protein GlnM	Gal	8.9E-05	2.52
Sp180_2_chr_00706	Transcriptional repressor CopY	Gal	0.007	2.48
Sp180_2_chr_01075	Hypothetical protein	Gal	3.5E-05	2.46
Sp180_2_chr_01822	groS 10 kDa chaperonin	Gal	3.9E-05	2.45
Sp180_2_chr_01437	Hypothetical protein	Gal	1.4E-05	2.43
Sp180_2_chr_01435	Multgene_idrug resistance ABC transporter ATP-binding and permease protein lmrA_1	Gal	1.8E-05	2.37
Sp180_2_chr_01436	Multgene_idrug resistance ABC transporter ATP-binding and permease protein lmrA_2	Gal	2.7E-05	2.36
Sp180_2_chr_00160	Hypothetical protein	Gal	0.00443	2.32
Sp180_2_chr_01939	Lichenan permease IIC component licC_5	Gal	0.0012	2.28
Sp180_2_chr_01941	PTS system oligo-beta-mannosgene_ide-specific EIIA component gmuA	Gal	0.00192	2.27
Sp180_2_chr_01196	Glucose-6-phosphate 1-dehydrogenase zwf	Gal	5.8E-05	2.24
Sp180_2_chr_00600	putative glutamine ABC transporter permease protein GlnP	Gal	0.0009	2.24
Sp180_2_chr_01940	PTS system cellobiose-specific EIIB component celA_3	Gal	0.00101	2.23
Sp180_2_chr_01980	Hypothetical protein	Gal	0.00025	2.2
Sp180_2_chr_01434	Cystathionine gamma-synthase/O-acetylhomoserine (thiol)-lyase metI	Gal	2.1E-06	2.16
Sp180_2_chr_01938	6-phospho-beta-glucosgene_idase GmuD	Gal	0.00181	2.14
Sp180_2_chr_01433	Cystathionine beta-lyase PatB	Gal	1.2E-06	2.02
Sp180_2_chr_02141	Secreted 45 kDa protein	Gal	5.8E-05	2.01
Sp180_2_chr_00187	Hypothetical protein	Gal	0.01323	2.01
Sp180_2_chr_01929	tRNA pseudourgene_idine synthase C truC	Gal	5.48E-08	2.02
Sp180_2_chr_00980	Large-conductance mechanosensitive channel mscL	Gal	0.0002	2.03
Sp180_2_chr_00509	Phosphoglycerate kinase pgk	Gal	0.01028	2.03
Sp180_2_chr_01007	putative sgene_iderophore transport system ATP-binding protein YusV	Gal	3.7E-05	2.05
Sp180_2_chr_01111	Glycerate kinase glxK	Gal	0.00011	2.05
Sp180_2_chr_01928	Penicillin-binding protein 1F pbpF_1	Gal	5.48E-08	2.08
Sp180_2_chr_01112	Hypothetical protein	Gal	0.00061	2.08

Sp180_2_chr_00924	Putative ribosomal N-acetyltransferase YdaF	Gal	7.65E-07	2.08
Sp180_2_chr_00373	PTS system mannose-specific EIgene_id component manZ_3	Gal	0.00069	2.1
Sp180_2_chr_01595	Putative ABC transporter substrate-binding protein YesO	Gal	0.01301	2.11
Sp180_2_chr_01372	Capsule biosynthesis protein CapA	Gal	0.00011	2.15
Sp180_2_chr_01095	Riboflavin biosynthesis protein RibF	Gal	0.00044	2.15
Sp180_2_chr_00598	Fructose-bisphosphate aldolase fba	Gal	0.00321	2.15
Sp180_2_chr_02116	IgA FC receptor bag	Gal	3.9E-06	2.16
Sp180_2_chr_01110	Phosphoserine phosphatase serB	Gal	4.6E-05	2.19
Sp180_2_chr_01961	Ubiquinone/menaquinone biosynthesis C-methyltransferase UbiE	Gal	0.00167	2.19
Sp180_2_chr_02117	Hypothetical protein	Gal	2.3E-06	2.2
Sp180_2_chr_01341	Putative ribosomal N-acetyltransferase YdaF	Gal	8.9E-06	2.21
Sp180_2_chr_01124	Dihydrolipoamide dehydrogenase	Gal	0.00052	2.21
Sp180_2_chr_01008	Hypothetical protein	Gal	0.00022	2.24
Sp180_2_chr_00372	N-acetylgalactosamine permease IIC component 1 agaC	Gal	0.00969	2.26
Sp180_2_chr_01593	Inner membrane ABC transporter permease protein YcjP	Gal	0.04518	2.27
Sp180_2_chr_01519	Hypothetical protein	Gal	3.6E-06	2.33
Sp180_2_chr_01371	Sugar phosphatase YbiV	Gal	8.6E-05	2.37
Sp180_2_chr_00571	Hypothetical protein	Gal	0.00096	2.37
Sp180_2_chr_00217	Hypothetical protein	Gal	0.00707	2.37
Sp180_2_chr_01518	Hypothetical protein	Gal	2.8E-05	2.37
Sp180_2_chr_02136	Hypothetical protein	Gal	0.00192	2.4
Sp180_2_chr_00490	PTS system lactose-specific EIICB component lacE_1	Gal	0.00254	2.42
Sp180_2_chr_02082	Alcohol dehydrogenase 2 adhB	Gal	3.4E-06	2.45
Sp180_2_chr_01387	FAD:protein FMN transferase apbE	Gal	0.00055	2.45
Sp180_2_chr_00489	Hypothetical protein	Gal	0.00161	2.48
Sp180_2_chr_01517	Hypothetical protein	Gal	0.00144	2.49
Sp180_2_chr_01370	Hypothetical protein	Gal	2.2E-05	2.51
Sp180_2_chr_01389	NADH-dependent flavin reductase subunit 1 nfr1	Gal	0.00096	2.53
Sp180_2_chr_01749	Cadmium%2C cobalt and zinc/H(+)-K(+) antiporter czcD	Gal	0.02412	2.54
Sp180_2_chr_00926	ComE operon protein 3 comEC	Gal	7.47E-07	2.56
Sp180_2_chr_01591	scyllo-inositol 2-dehydrogenase (NAD(+)) iolX	Gal	0.00254	2.59
Sp180_2_chr_01123	Lipoate-protein ligase LplJ	Gal	0.00013	2.6
Sp180_2_chr_00981	Hypothetical protein	Gal	5.5E-05	2.62
Sp180_2_chr_01592	Sialgene_idase B nanB	Gal	0.0018	2.64
Sp180_2_chr_00925	ComE operon protein 1	Gal	2.05E-07	2.7
Sp180_2_chr_01105	NADP-dependent glyceraldehyde-3-phosphate dehydrogenase	Gal	0.00037	2.73
Sp180_2_chr_01962	Hypothetical protein	Gal	0.0009	2.76
Sp180_2_chr_01342	NH(3)-dependent NAD(+) synthetase nadE	Gal	1.5E-05	2.78
Sp180_2_chr_01596	Toxin-antitoxin biofilm protein TabA	Gal	0.00399	2.81
Sp180_2_chr_01343	Nicotinate phosphoribosyltransferase pncB2	Gal	5.5E-06	2.84
Sp180_2_chr_01388	NADH-dependent flavin reductase subunit 2 nfr2	Gal	0.00101	2.89
Sp180_2_chr_02121	Transcriptional regulator CtsR	Gal	1.16E-08	2.96
Sp180_2_chr_02118	Sensor histgene_idine kinase WalK	Gal	5.48E-08	3.09
Sp180_2_chr_02120	ATP-dependent Clp protease ATP-binding subunit ClpC	Gal	1.37E-08	3.21
Sp180_2_chr_01910	Hypothetical protein	Gal	2.3E-06	3.24
Sp180_2_chr_02119	Phosphate regulon transcriptional regulatory protein PhoB	Gal	1.16E-08	3.3
Sp180_2_chr_01909	Hypothetical protein	Gal	2.1E-06	3.49

Sp180_2_chr_01908	putative ABC transporter ATP-binding protein YxlF	Gal	1.5E-06	3.53
Sp180_2_chr_00979	Ferrochelatase hemH	Gal	4.45E-07	4.25
Sp180_2_chr_01942	Aldehyde-alcohol dehydrogenase adhE	Gal	2.1E-06	4.64
Sp180_2_chr_01971	Alcohol dehydrogenase adh_2	Gal	0.00714	4.84
Sp180_2_chr_01172	Hypothetical protein	Gal	1.5E-05	6.85
Sp180_2_chr_01266	Hypothetical protein	Gal	1.6E-06	11.3
Sp180_2_chr_01076	Putative glutamine amgene_idotransferase	Serum	4.97E-09	43.4
Sp180_2_chr_01077	Redox-sensing transcriptional repressor Rex	Serum	4.24E-08	29.8
Sp180_2_chr_01075	Hypothetical protein	Serum	2.00E-09	20.8
Sp180_2_chr_01712	N-(5'-phosphoribosyl)anthranilate isomerase	Serum	0.00044	5.21
Sp180_2_chr_00096	Phosphoribosylaminoimgene_idazole-succinocarboxamgene_ide synthase purC	Serum	4.27E-05	5.07
Sp180_2_chr_00097	Phosphoribosylformylglycinamgene_idine synthase purL	Serum	0.00017	4.48
Sp180_2_chr_01714	Anthranilate phosphoribosyltransferase trpD	Serum	0.00014	4.34
Sp180_2_chr_01739	Xanthine phosphoribosyltransferase xpt	Serum	7.68E-05	3.97
Sp180_2_chr_01740	Uric acgene_id permease PucK	Serum	7.95E-05	3.95
Sp180_2_chr_01716	Anthranilate synthase component 1 trpE	Serum	0.00011	3.89
Sp180_2_chr_01711	Tryptophan synthase beta chain trpB	Serum	1.76E-05	3.67
Sp180_2_chr_00045	Hypothetical protein	Serum	0.00186	3.44
Sp180_2_chr_01715	Aminodeoxychorismate/anthranilate synthase component 2 pabA	Serum	0.00064	3.31
Sp180_2_chr_00040	Hypothetical protein	Serum	0.00084	3.29
Sp180_2_chr_01713	Indole-3-glycerol phosphate synthase trpC	Serum	0.00037	3.18
Sp180_2_chr_01435	Multgene_idrug resistance ABC transporter ATP-binding and permease protein lmrA_1	Serum	0.00027	3.16
Sp180_2_chr_00044	Single-stranded DNA-binding protein ssb_1	Serum	0.00038	3.15
Sp180_2_chr_00042	Hypothetical protein	Serum	0.00089	3.13
Sp180_2_chr_00098	Amgene_idophosphoribosyltransferase purF	Serum	0.00046	3.12
Sp180_2_chr_01437	Hypothetical protein	Serum	0.00081	3.04
Sp180_2_chr_01436	Multgene_idrug resistance ABC transporter ATP-binding and permease protein lmrA_2	Serum	0.00038	3.04
Sp180_2_chr_00338	Hypothetical protein	Serum	0.00039	2.89
Sp180_2_chr_00041	DNA replication protein DnaC	Serum	8.27E-05	2.87
Sp180_2_chr_00159	Argininosuccinate synthase argG	Serum	0.00376	2.86
Sp180_2_chr_01718	Hypothetical protein	Serum	0.0031	2.79
Sp180_2_chr_00047	Hypothetical protein	Serum	0.00437	2.77
Sp180_2_chr_00103	Phosphoribosylamine--glycine ligase	Serum	2.57E-05	2.73
Sp180_2_chr_00054	Hypothetical protein	Serum	3.20E-05	2.69
Sp180_2_chr_00049	Tyrosine recombinase XerD	Serum	0.00031	2.68
Sp180_2_chr_00064	Chromosome partition protein Smc	Serum	7.68E-05	2.64
Sp180_2_chr_00046	Hypothetical protein	Serum	0.01073	2.63
Sp180_2_chr_00065	Hypothetical protein	Serum	0.00012	2.61
Sp180_2_chr_00106	N5-carboxyaminoimgene_idazole ribonucleotgene_ide synthase purK	Serum	0.00041	2.55
Sp180_2_chr_00048	Hypothetical protein	Serum	0.00024	2.54
Sp180_2_chr_00043	Hypothetical protein	Serum	0.00266	2.53
Sp180_2_chr_00055	Hypothetical protein	Serum	7.68E-05	2.53
Sp180_2_chr_01710	Tryptophan synthase alpha chain trpA	Serum	0.00294	2.52
Sp180_2_chr_00813	Hypothetical protein	Serum	7.68E-05	2.49
Sp180_2_chr_00337	Guanine/hypoxanthine permease PbuO	Serum	0.0002	2.47
Sp180_2_chr_00053	Hypothetical protein	Serum	0.0001	2.45
Sp180_2_chr_00052	Hypothetical protein	Serum	9.14E-05	2.44
Sp180_2_chr_00050	Hypothetical protein	Serum	4.06E-05	2.43
Sp180_2_chr_00062	Hypothetical protein	Serum	7.68E-05	2.42
Sp180_2_chr_00035	Hypothetical protein	Serum	0.0001	2.38
Sp180_2_chr_00056	Hypothetical protein	Serum	9.14E-05	2.36
Sp180_2_chr_00516	Hypothetical protein	Serum	0.00035	2.36

Sp180_2_chr_00051	Hypothetical protein	Serum	0.00058	2.34
Sp180_2_chr_01072	Hypothetical protein	Serum	0.00081	2.34
Sp180_2_chr_00066	Hypothetical protein	Serum	0.00035	2.33
Sp180_2_chr_01789	Bifunctional alpha-galactosgene_idase/sucrose kinase AgaSK	Serum	0.02057	2.32
Sp180_2_chr_00032	Hypothetical protein	Serum	0.00027	2.31
Sp180_2_chr_00515	Hypothetical protein	Serum	0.00035	2.27
Sp180_2_chr_00072	Autolysin lytA_1	Serum	0.00039	2.27
Sp180_2_chr_00063	Hypothetical protein	Serum	9.11E-05	2.27
Sp180_2_chr_00603	Glutamine transport ATP-binding protein GlnQ	Serum	6.15E-06	2.25
Sp180_2_chr_00039	DNA replication protein DnaD	Serum	0.00033	2.25
Sp180_2_chr_00105	N5-carboxyaminoimgene_idazole ribonucleotgene_ide mutase purE	Serum	0.00111	2.24
Sp180_2_chr_00099	Phosphoribosylformylglycinamgene_idine cyclo-ligase purM	Serum	0.00373	2.24
Sp180_2_chr_00162	Hypothetical protein	Serum	0.01243	2.24
Sp180_2_chr_01521	Hypothetical protein	Serum	0.01013	2.24
Sp180_2_chr_00069	Hypothetical protein	Serum	0.00148	2.23
Sp180_2_chr_00033	Hypothetical protein	Serum	0.00628	2.23
Sp180_2_chr_00060	Hypothetical protein	Serum	0.00017	2.22
Sp180_2_chr_00161	Hypothetical protein	Serum	0.01378	2.22
Sp180_2_chr_00059	Hypothetical protein	Serum	0.0004	2.22
Sp180_2_chr_00160	Hypothetical protein	Serum	0.01041	2.18
Sp180_2_chr_00038	Hypothetical protein	Serum	0.00018	2.16
Sp180_2_chr_00031	Hypothetical protein	Serum	6.75E-05	2.16
Sp180_2_chr_00071	Hypothetical protein	Serum	0.00071	2.16
Sp180_2_chr_00034	Hypothetical protein	Serum	3.75E-05	2.15
Sp180_2_chr_00513	Hypothetical protein	Serum	0.00465	2.15
Sp180_2_chr_00036	Hypothetical protein	Serum	7.68E-05	2.13
Sp180_2_chr_00600	putative glutamine ABC transporter permease protein GlnP	Serum	6.15E-06	2.12
Sp180_2_chr_00602	Major cell-binding factor peb1A	Serum	3.48E-05	2.12
Sp180_2_chr_00070	Hypothetical protein	Serum	0.00041	2.12
Sp180_2_chr_00058	Hypothetical protein	Serum	0.0005	2.11
Sp180_2_chr_01317	Putative ABC transporter arginine-binding protein 2 artI	Serum	0.04054	2.11
Sp180_2_chr_00068	Hypothetical protein	Serum	0.0014	2.11
Sp180_2_chr_00100	Phosphoribosylglycinamgene_ide formyltransferase purN	Serum	0.01334	2.1
Sp180_2_chr_00519	putative type I restriction enzymeP M protein	Serum	6.15E-06	2.09
Sp180_2_chr_00158	Arginine-binding extracellular protein ArtP	Serum	0.00848	2.08
Sp180_2_chr_00057	Hypothetical protein	Serum	0.00037	2.08
Sp180_2_chr_00061	Hypothetical protein	Serum	0.00071	2.08
Sp180_2_chr_00005	Peptgene_idyl-tRNA hydrolase pth	Serum	0.00588	2.06
Sp180_2_chr_01404	Hypothetical protein	Serum	3.75E-05	2.05
Sp180_2_chr_01438	Oligopeptgene_ide-binding protein SarA	Serum	0.00484	2.02
Sp180_2_chr_00728	Inosine-5'-monophosphate dehydrogenase guaB_1	Serum	0.00029	2.02
Sp180_2_chr_00006	Transcription-repair-coupling factor mfd	Serum	0.01182	2.01
Sp180_2_chr_00297	Lichenan-specific phosphotransferase enzyme IIA component licA	Serum	0.00064	2
Sp180_2_chr_00295	Glucitol operon repressor srlR_1	Serum	0.0005	2.02
Sp180_2_chr_00142	Hypothetical protein	Serum	1.58E-05	2.03
Sp180_2_chr_00228	Riboflavin biosynthesis protein RibBA	Serum	0.00359	2.03
Sp180_2_chr_00615	Hypothetical protein	Serum	0.00053	2.03
Sp180_2_chr_00450	Malonyl CoA-acyl carrier protein transacylase fabD	Serum	0.00027	2.04
Sp180_2_chr_00635	Hypothetical protein	Serum	0.03563	2.04
Sp180_2_chr_00975	Hypothetical protein	Serum	7.68E-05	2.05

Sp180_2_chr_00451	product=3-oxoacyl-[acyl-carrier-protein] reductase FabG	Serum	0.00041	2.08
Sp180_2_chr_01934	putative nicotinate-nucleotgene_ide pyrophosphorylase [carboxylating] nadC	Serum	3.48E-05	2.08
Sp180_2_chr_00453	Biotin carboxyl carrier protein of acetyl-CoA carboxylase accB	Serum	0.00016	2.09
Sp180_2_chr_00452	3-oxoacyl-[acyl-carrier-protein] synthase 2 fabF	Serum	0.00027	2.09
Sp180_2_chr_01136	Hypothetical protein	Serum	0.00022	2.09
Sp180_2_chr_00459	Hypothetical protein	Serum	0.00075	2.1
Sp180_2_chr_00927	ABC transporter ATP-binding protein NatA	Serum	0.03044	2.1
Sp180_2_chr_00374	Hypothetical protein	Serum	0.00108	2.11
Sp180_2_chr_00454	3-hydroxyacyl-[acyl-carrier-protein] dehydratase FabZ	Serum	0.00018	2.13
Sp180_2_chr_00449	Nitronate monooxygenase	Serum	7.68E-05	2.13
Sp180_2_chr_01552	Neutral endopeptgene_idase pepO	Serum	2.75E-06	2.13
Sp180_2_chr_01932	Hypothetical protein	Serum	1.41E-05	2.16
Sp180_2_chr_00320	Pullulanase pulA	Serum	0.00323	2.17
Sp180_2_chr_00229	Riboflavin synthase ribE	Serum	0.00674	2.18
Sp180_2_chr_01904	Catabolite control protein A ccpA_2	Serum	0.00515	2.19
Sp180_2_chr_00455	Biotin carboxylase accC	Serum	0.00022	2.19
Sp180_2_chr_01749	Cadmium%2C cobalt and zinc/H(+)-K(+) antiporter czcD	Serum	0.01227	2.21
Sp180_2_chr_00804	Pyrimgene_idine-nucleosgene_ide phosphorylase pdp	Serum	5.78E-05	2.22
Sp180_2_chr_00333	PTS system sorbose-specific EIIC component sorA	Serum	0.00422	2.24
Sp180_2_chr_02117	Hypothetical protein	Serum	0.00985	2.25
Sp180_2_chr_00979	Ferrochelatase hemH	Serum	9.11E-06	2.25
Sp180_2_chr_00456	Acetyl-coenzyme A carboxylase carboxyl transferase subunit beta accD	Serum	0.00011	2.26
Sp180_2_chr_01933	Hypothetical protein	Serum	8.27E-05	2.26
Sp180_2_chr_00332	PTS system mannose-specific EIgene_id component manZ_2	Serum	0.00515	2.26
Sp180_2_chr_01172	Hypothetical protein	Serum	7.49E-05	2.26
Sp180_2_chr_00227	6%2C7-dimethyl-8-ribityllumazine synthase ribH	Serum	0.00384	2.29
Sp180_2_chr_00457	Acetyl-coenzyme A carboxylase carboxyl transferase subunit alpha accA	Serum	0.0001	2.32
Sp180_2_chr_01931	Macrolgene_ide export ATP-binding/permease protein MacB	Serum	9.51E-05	2.33
Sp180_2_chr_00616	Hypothetical protein	Serum	0.00024	2.34
Sp180_2_chr_02022	Hypothetical protein	Serum	0.04956	2.44
Sp180_2_chr_01748	HTH-type transcriptional regulator AdhR	Serum	0.00107	2.45
Sp180_2_chr_00445	Trans-2-decenoyl-[acyl-carrier-protein] isomerase fabM	Serum	3.75E-05	2.65
Sp180_2_chr_00973	Hypothetical protein	Serum	1.33E-05	2.76
Sp180_2_chr_01597	Hypothetical protein	Serum	0.01541	3.44
Sp180_2_chr_01127	Acetoin:2%2C6-dichlorophenolindophenol oxgene_idoreductase subunit alpha acoA	Serum	7.22E-07	3.6
Sp180_2_chr_02116	IgA FC receptor bag	Serum	0.00188	3.64
Sp180_2_chr_02020	Phosphate-specific transport system accessory protein PhoU	Serum	0.0017	4.38
Sp180_2_chr_01266	Hypothetical protein	Serum	2.01E-06	4.42
Sp180_2_chr_02019	Phosphate import ATP-binding protein PstB 3	Serum	0.00148	4.77
Sp180_2_chr_02018	Phosphate transport system permease protein PstA 2	Serum	0.00114	4.84
Sp180_2_chr_02017	Phosphate transport system permease protein PstC 1	Serum	0.00123	4.94
Sp180_2_chr_02016	Phosphate-binding protein PstS 2	Serum	0.00048	5.03

Sp180_2_chr_01751	Nicotinamgene_ide ribosgene_ide transporter PnuC	Serum	6.15E-06	5.49
Sp180_2_chr_01126	2-oxoisovalerate dehydrogenase subunit beta bfmBAB	Serum	4.97E-09	6.07
Sp180_2_chr_01123	Lipoate-protein ligase LplJ	Serum	1.02E-08	6.11
Sp180_2_chr_01125	Dihydrolipoyllysine-resgene_idue acetyltransferase component of pyruvate dehydrogenase complex pdhC	Serum	4.97E-09	6.19
Sp180_2_chr_01124	Dihydrolipoamide dehydrogenase	Serum	6.42E-09	6.61

Appendix M. Pneumococcal differential gene expression in the lungs 6 h post-infection, 947 vs 947M. Genes with fold change (FC) greater than 2 and $p < 0.05$ are shown. FC values highlighted in blue = upregulated in 947, while values highlighted in red = upregulated in 947M.

Locus tag in 947	Product	padj	FC
Sp947_chr_00844	Sialidase B	3.08E-10	313.9807
Sp947_chr_02077	hypothetical protein	4.46E-10	306.9412
Sp947_chr_00842	Sodium/glucose cotransporter	2.22E-09	243.4822
Sp947_chr_00841	N-acetylneuraminate lyase	4.53E-09	227.7963
Sp947_chr_00845	scyllo-inositol 2-dehydrogenase (NAD(+))	4.36E-09	221.051
Sp947_chr_00848	hypothetical protein	1.19E-08	202.7867
Sp947_chr_00853	V-type sodium ATPase catalytic subunit A	1.29E-06	100.5411
Sp947_chr_00846	Beta-glucoside kinase	3.42E-06	98.18951
Sp947_chr_00855	V-type sodium ATPase subunit D	8.34E-06	85.94879
Sp947_chr_00851	V-type sodium ATPase subunit C	2.50E-05	72.46612
Sp947_chr_00843	hypothetical protein	2.17E-05	65.97758
Sp947_chr_00839	HTH-type transcriptional regulator RpiR	3.09E-05	61.28171
Sp947_chr_00854	V-type sodium ATPase subunit B	1.32E-06	50.86992
Sp947_chr_00120	hypothetical protein	3.00E-04	45.77325
Sp947_chr_02078	hypothetical protein	1.52E-04	45.42925
Sp947_chr_00852	V-type sodium ATPase subunit G	5.34E-04	44.97311
Sp947_chr_01964	3-keto-L-gulonate-6-phosphate decarboxylase UlaD	1.36E-03	44.2113
Sp947_chr_00850	V-type proton ATPase subunit E	9.39E-04	39.74672
Sp947_chr_00840	Putative N-acetylmannosamine-6-phosphate 2-epimerase	4.32E-04	37.87573
Sp947_chr_01963	L-ribulose-5-phosphate 3-epimerase UlaE	2.11E-03	37.77052
Sp947_chr_01962	L-ribulose-5-phosphate 4-epimerase AraD	2.75E-03	35.23993
Sp947_chr_00849	V-type sodium ATPase subunit K	2.25E-03	34.7923
Sp947_chr_01960	putative L-ascorbate-6-phosphate lactonase UlaG	1.16E-03	34.0495
Sp947_chr_00847	hypothetical protein	3.85E-03	30.78829
Sp947_chr_00118	hypothetical protein	2.13E-03	30.10216
Sp947_chr_00631	hypothetical protein	1.22E-04	28.36211
Sp947_chr_01965	Ascorbate-specific PTS system EIIA component	8.94E-03	28.12967
Sp947_chr_00632	ABC transporter ATP-binding protein YxdL	7.13E-03	26.82578
Sp947_chr_00117	hypothetical protein	9.36E-03	21.85911
Sp947_chr_00116	hypothetical protein	1.27E-02	20.39713
Sp947_chr_02096	hypothetical protein	2.92E-07	18.61494
Sp947_chr_01966	Ascorbate-specific PTS system EIIB component	5.76E-02	18.33251
Sp947_chr_01967	Ascorbate-specific PTS system EIIC component	1.17E-02	14.29112
Sp947_chr_00630	hypothetical protein	4.67E-02	14.26137
Sp947_chr_01105	Transcription antiterminator LicT	5.76E-02	12.54562
Sp947_chr_00122	hypothetical protein	5.11E-02	12.44502
Sp947_chr_00111	Lactococcin-G-processing and transport ATP-binding protein LagD	8.11E-02	12.07699
Sp947_chr_01629	PTS system trehalose-specific EIIBC component	3.15E-18	11.47534
Sp947_chr_00637	hypothetical protein	8.81E-02	11.10599
Sp947_chr_00119	hypothetical protein	2.96E-02	10.07432
Sp947_chr_01187	hypothetical protein	5.24E-02	8.833295
Sp947_chr_01975	Ubiquinone biosynthesis O-methyltransferase	5.86E-02	8.275917
Sp947_chr_00702	Maltose 6'-phosphate phosphatase	2.91E-01	8.131911
Sp947_chr_00121	hypothetical protein	8.44E-02	8.011629

Sp947_chr_01982	ComG operon protein 1	1.19E-04	7.374729
Sp947_chr_00133	hypothetical protein	6.34E-04	7.228914
Sp947_chr_02066	hypothetical protein	2.74E-01	7.180618
Sp947_chr_01949	hypothetical protein	2.49E-01	7.107773
Sp947_chr_02151	ComF operon protein 1	2.86E-01	6.998242
Sp947_chr_01923	tRNA-Pro(tgg)	3.04E-01	6.979745
Sp947_chr_01980	hypothetical protein	3.75E-02	6.946905
Sp947_chr_02094	Ornithine carbamoyltransferase%2C catabolic	1.29E-13	6.850913
Sp947_chr_00240	Glucitol operon repressor	2.50E-01	6.725672
Sp947_chr_00922	ComE operon protein 1	2.64E-01	6.597975
Sp947_chr_01978	hypothetical protein	1.39E-01	6.480978
Sp947_chr_01277	hypothetical protein	1.43E-01	6.459624
Sp947_chr_00112	hypothetical protein	2.91E-01	6.188522
Sp947_chr_02128	putative glycerol uptake facilitator protein	4.20E-14	6.053371
Sp947_chr_01120	hypothetical protein	3.51E-01	6.024365
Sp947_chr_01977	hypothetical protein	6.78E-02	5.999717
Sp947_chr_00794	tRNA-Gln(ttg)	3.91E-01	5.87385
Sp947_chr_01979	hypothetical protein	2.88E-02	5.870884
Sp947_chr_02129	Alpha-glycerophosphate oxidase	1.19E-37	5.867422
Sp947_chr_02097	Putative dipeptidase	1.26E-04	5.831657
Sp947_chr_00134	hypothetical protein	1.28E-02	5.621892
Sp947_chr_00659	Aminopyrimidine aminohydrolase	3.95E-01	5.584997
Sp947_chr_02130	Glycerol kinase	1.19E-27	5.564175
Sp947_chr_00147	UDP-glucose 6-dehydrogenase	6.94E-02	5.536174
Sp947_chr_02065	hypothetical protein	2.63E-01	5.252184
Sp947_chr_01700	Inner membrane ABC transporter permease protein YcjP	2.73E-01	5.193315
Sp947_chr_02072	1-deoxy-D-xylulose-5-phosphate synthase	2.52E-02	5.114776
Sp947_chr_01044	3-isopropylmalate dehydratase small subunit	4.14E-01	4.950902
Sp947_chr_02093	Arginine deiminase	6.29E-05	4.916879
Sp947_chr_00981	Queuosine precursor transporter QueT	2.91E-01	4.902071
Sp947_chr_00135	tRNA threonylcarbamoyladenosine biosynthesis protein TsaB	2.15E-01	4.652439
Sp947_chr_02029	Phosphate-binding protein PstS 2	1.20E-06	4.568416
Sp947_chr_01119	hypothetical protein	3.89E-01	4.33514
Sp947_chr_00105	hypothetical protein	2.35E-06	4.320641
Sp947_chr_01601	hypothetical protein	1.99E-01	4.317593
Sp947_chr_01585	hypothetical protein	9.40E-06	4.244689
Sp947_chr_02095	Carbamate kinase 1	2.88E-02	4.210313
Sp947_chr_01582	Beta-glucoside kinase	8.39E-11	4.021705
Sp947_chr_02074	Ascorbate-specific PTS system EIIC component	4.93E-02	3.969839
Sp947_chr_00983	asd	1.88E-02	3.920181
Sp947_chr_02073	Transketolase	1.04E-01	3.916258
Sp947_chr_00390	Glycine	3.47E-01	3.883027
Sp947_chr_01611	hypothetical protein	4.51E-01	3.86601
Sp947_chr_00146	2'-N-acetylparomamine deacetylase	1.44E-01	3.836192
Sp947_chr_00145	hypothetical protein	2.43E-02	3.78253
Sp947_chr_00149	hypothetical protein	1.96E-43	3.78179
Sp947_chr_01772	Iron-uptake system permease protein FeuB	1.10E-02	3.780349
Sp947_chr_00109	Argininosuccinate synthase	1.38E-01	3.732843
Sp947_chr_01631	HTH-type transcriptional regulator DegA	2.19E-02	3.731615
Sp947_chr_01262	Putative endo-beta-N-acetylglucosaminidase	8.15E-02	3.596429
Sp947_chr_01107	PTS system lactose-specific EIICB component	1.35E-02	3.562908
Sp947_chr_01035	hypothetical protein	9.08E-02	3.496732

Sp947_chr_01250	putative ABC transporter ATP-binding protein YheS	6.78E-02	3.438094
Sp947_chr_00108	Arginine-binding extracellular protein ArtP	1.51E-01	3.41617
Sp947_chr_01108	6-phospho-beta-galactosidase	7.85E-02	3.360241
Sp947_chr_00649	ABC transporter ATP-binding protein NatA	1.01E-01	3.333401
Sp947_chr_01835	Single-stranded DNA-binding protein	7.89E-05	3.281171
Sp947_chr_00055	hypothetical protein	2.19E-04	3.207721
Sp947_chr_00144	hypothetical protein	2.73E-01	3.138686
Sp947_chr_00641	Fluoroquinolones export ATP-binding protein	5.76E-02	3.109696
Sp947_chr_01747	hypothetical protein	4.93E-01	3.109528
Sp947_chr_01587	L-arabinose transport system permease protein AraQ	5.18E-09	3.081995
Sp947_chr_01976	hypothetical protein	1.08E-01	3.078674
Sp947_chr_01155	Glucose-1-phosphate adenylyltransferase	1.41E-05	3.071928
Sp947_chr_01228	Tyrosine-protein phosphatase	3.76E-02	3.048501
Sp947_chr_01154	Glycogen biosynthesis protein GlgD	3.87E-05	2.954565
Sp947_chr_01100	hypothetical protein	4.09E-01	2.889683
Sp947_chr_01993	hypothetical protein	2.76E-03	2.87091
Sp947_chr_01263	Autolysin	2.73E-01	2.870719
Sp947_chr_01613	hypothetical protein	3.54E-01	2.855586
Sp947_chr_01588	Lactose transport system permease protein LacF	8.93E-08	2.852978
Sp947_chr_00608	putative response regulatory protein	1.10E-09	2.84383
Sp947_chr_01600	Sialidase A	1.33E-17	2.819847
Sp947_chr_00173	6%2C7-dimethyl-8-ribityllumazine synthase	4.42E-01	2.814878
Sp947_chr_00069	Putative tagatose-6-phosphate ketose/aldose isomerase	5.19E-08	2.76399
Sp947_chr_01584	hypothetical protein	1.66E-03	2.762851
Sp947_chr_00521	hypothetical protein	3.78E-01	2.762754
Sp947_chr_00250	hypothetical protein	4.70E-01	2.727314
Sp947_chr_00721	hypothetical protein	3.97E-01	2.68465
Sp947_chr_00987	2-hydroxymuconate tautomerase	4.81E-01	2.666089
Sp947_chr_01388	hypothetical protein	1.16E-01	2.622464
Sp947_chr_00923	ComE operon protein 3	2.15E-01	2.594794
Sp947_chr_01013	Serine recombinase PinR	1.76E-01	2.580421
Sp947_chr_01586	Toxin-antitoxin biofilm protein TabA	1.04E-02	2.560526
Sp947_chr_00023	competence protein ComW, recombinase RecX	3.57E-01	2.551904
Sp947_chr_01453	hypothetical protein	2.91E-01	2.548217
Sp947_chr_00480	hypothetical protein	2.60E-01	2.514127
Sp947_chr_00067	PTS system mannose-specific EIID component	4.61E-05	2.500185
Sp947_chr_02076	Mannitol-specific cryptic phosphotransferase enzyme IIA component	4.56E-01	2.444106
Sp947_chr_01589	Putative ABC transporter substrate-binding protein YesO	4.02E-17	2.425022
Sp947_chr_00052	Amidophosphoribosyltransferase	2.35E-06	2.408122
Sp947_chr_00457	hypothetical protein	3.54E-01	2.390357
Sp947_chr_01583	N-acetylneuraminate lyase	4.63E-06	2.376665
Sp947_chr_00925	hypothetical protein	4.93E-02	2.375513
Sp947_chr_01278	50S ribosomal protein L7/L12	2.41E-07	2.35971
Sp947_chr_00053	Phosphoribosylformylglycinamidine cyclo-ligase	1.21E-05	2.353489
Sp947_chr_02127	hypothetical protein	4.95E-02	2.308295
Sp947_chr_02131	hypothetical protein	3.40E-01	2.301176
Sp947_chr_01756	Acyl-coenzyme A thioesterase PaaI	3.75E-01	2.288928
Sp947_chr_01404	hypothetical protein	2.91E-01	2.276784

Sp947_chr_01775	putative ABC transporter solute-binding protein YclQ	1.34E-01	2.268465
Sp947_chr_00005	Peptidyl-tRNA hydrolase	3.69E-01	2.265023
Sp947_chr_01153	Glycogen synthase	5.10E-03	2.260835
Sp947_chr_01101	Galactose-6-phosphate isomerase subunit LacA	2.16E-01	2.243408
Sp947_chr_00476	Protein GrpE	9.93E-04	2.233808
Sp947_chr_00638	hypothetical protein	3.54E-01	2.218743
Sp947_chr_02032	Phosphate import ATP-binding protein PstB 3	2.74E-02	2.215497
Sp947_chr_01224	hypothetical protein	3.49E-01	2.207203
Sp947_chr_01810	tRNA-Ser(tga)	4.13E-01	2.19757
Sp947_chr_00762	Purine nucleoside phosphorylase 1	1.20E-01	2.193752
Sp947_chr_01803	HTH-type transcriptional regulator CdhR	3.03E-01	2.193316
Sp947_chr_02007	tRNA-Gly(tcc)	4.74E-01	2.1921
Sp947_chr_00827	Type-1 restriction enzyme EcoKI specificity protein	2.00E-01	2.190873
Sp947_chr_01630	Sucrose-6-phosphate hydrolase	3.05E-02	2.18504
Sp947_chr_00106	hypothetical protein	3.27E-03	2.177719
Sp947_chr_00066	PTS system sorbose-specific EIIC component	3.08E-03	2.174249
Sp947_chr_02030	Phosphate transport system permease protein PstC 1	8.44E-02	2.167527
Sp947_chr_00150	Nisin biosynthesis protein NisB	7.57E-23	2.163768
Sp947_chr_01099	hypothetical protein	3.93E-01	2.157605
Sp947_chr_01479	DegV domain-containing protein	7.47E-03	2.15692
Sp947_chr_02062	hypothetical protein	2.49E-01	2.144907
Sp947_chr_00607	Peptide methionine sulfoxide reductase MsrA/MsrB	1.57E-06	2.132922
Sp947_chr_00017	tRNA-Ala(tgc)	4.70E-01	2.123204
Sp947_chr_01824	tRNA-Ala(tgc)	4.70E-01	2.123204
Sp947_chr_01934	tRNA-Ala(tgc)	4.70E-01	2.123204
Sp947_chr_02011	tRNA-Ala(tgc)	4.70E-01	2.123204
Sp947_chr_00140	hypothetical protein	4.86E-01	2.122109
Sp947_chr_01612	Molybdenum import ATP-binding protein ModC	3.11E-01	2.120579
Sp947_chr_01773	Ferric enterobactin transport system permease protein FepD	2.48E-01	2.118436
Sp947_chr_00477	Chaperone protein DnaK	3.11E-11	2.118333
Sp947_chr_00645	hypothetical protein	1.33E-01	2.110241
Sp947_chr_00056	Bifunctional purine biosynthesis protein PurH	2.62E-06	2.095397
Sp947_chr_00496	Bacteriocin lactacin-F subunit LafA	4.09E-01	2.074411
Sp947_chr_01478	4-hydroxy-tetrahydrodipicolinate reductase	1.97E-02	2.068728
Sp947_chr_02033	Phosphate-specific transport system accessory protein PhoU	3.11E-02	2.04991
Sp947_chr_00174	Riboflavin biosynthesis protein RibBA	2.98E-01	2.047245
Sp947_chr_01231	hypothetical protein	2.17E-01	2.042865
Sp947_chr_00152	hypothetical protein	1.87E-20	2.035498
Sp947_chr_02063	hypothetical protein	4.93E-01	2.032609
Sp947_chr_00054	Phosphoribosylglycinamide formyltransferase	2.39E-02	2.031196
Sp947_chr_01614	hypothetical protein	3.71E-01	2.028597
Sp947_chr_02031	Phosphate transport system permease protein PstA 2	7.01E-02	2.026564
Sp947_chr_00475	Heat-inducible transcription repressor HrcA	7.89E-05	2.006056
Sp947_chr_02088	Beta-glucoside kinase	5.00E-01	2.004401
Sp947_chr_01317	HTH-type transcriptional regulatory protein GabR	3.80E-01	2.004158
Sp947_chr_02092	hypothetical protein	4.45E-01	2.004096
Sp947_chr_00279	Alcohol dehydrogenase 1	4.32E-03	2.100505

Sp947_chr_01847	putative transcriptional regulatory protein	2.22E-05	2.113858
Sp947_chr_01234	UTP--glucose-1-phosphate uridylyltransferase	6.67E-04	2.154403
Sp947_chr_01238	Ribitol-5-phosphate cytidylyltransferase	1.32E-04	2.183908
Sp947_chr_00859	Arginine regulator	4.52E-03	2.209799
Sp947_chr_01055	Glucose-6-phosphate 1-dehydrogenase	2.31E-14	2.212385
Sp947_chr_01293	Regulatory protein MsrR	2.28E-03	2.222293
Sp947_chr_01640	Ribosomal RNA small subunit methyltransferase B	9.93E-04	2.225681
Sp947_chr_00191	Folylpolyglutamate synthase	3.11E-02	2.250767
Sp947_chr_01653	hypothetical protein	1.43E-02	2.295077
Sp947_chr_01300	3-dehydroquinate synthase	2.71E-02	2.309334
Sp947_chr_00490	Lactococcin-G-processing and transport ATP-binding protein LagD	2.35E-06	2.364015
Sp947_chr_01419	Arginine-binding extracellular protein ArtP	4.40E-07	2.398254
Sp947_chr_01447	Multidrug resistance ABC transporter ATP-binding/permease protein BmrA	1.06E-02	2.404999
Sp947_chr_00613	2-succinyl-6-hydroxy-2%2C4-cyclohexadiene-1-carboxylate synthase	4.54E-02	2.488993
Sp947_chr_02091	hypothetical protein	9.36E-03	2.491938
Sp947_chr_01850	hypothetical protein	4.99E-05	2.506163
Sp947_chr_01236	hypothetical protein	4.88E-06	2.557541
Sp947_chr_01851	hypothetical protein	2.43E-03	2.891242
Sp947_chr_01237	Ribulose-5-phosphate reductase	1.55E-09	2.935155
Sp947_chr_01235	hypothetical protein	4.67E-09	3.067205
Sp947_chr_01848	Pneumolysin	7.93E-20	3.074683
Sp947_chr_01445	Multidrug resistance ABC transporter ATP-binding and permease protein	9.93E-04	3.429428
Sp947_chr_01421	L-cystine transport system permease protein YecS	4.60E-05	3.567119
Sp947_chr_01952	Lichenan permease IIC component	3.40E-03	3.631755
Sp947_chr_01849	hypothetical protein	8.04E-09	3.899592
Sp947_chr_01951	6-phospho-beta-glucosidase GmuD	6.09E-04	4.38906
Sp947_chr_00675	Pyruvate oxidase	2.48E-78	5.288241
Sp947_chr_00722	Biotin transporter BioY2	9.36E-03	7.135698
Sp947_chr_01592	scyllo-inositol 2-dehydrogenase (NAD(+))	7.65E-10	16.61538
Sp947_chr_01596	Inner membrane ABC transporter permease protein YcjO	1.70E-07	17.3257
Sp947_chr_01598	Evolved beta-galactosidase subunit beta	7.36E-05	17.8072
Sp947_chr_01595	Inner membrane ABC transporter permease protein YcjP	1.12E-06	19.42745
Sp947_chr_01599	hypothetical protein	2.80E-03	23.35696
Sp947_chr_01597	Putative ABC transporter substrate-binding protein YesO	1.24E-13	40.51841

Appendix N. Pneumococcal differential gene expression in the lungs 6 h post-infection, 947 vs 4559. Genes with fold change (FC) greater than 2 and $p < 0.05$ are shown. FC values highlighted in blue = upregulated in 947, while values highlighted in red = upregulated in 4559.

Locus tag in 947	Product	padj	FC
Sp947_chr_01964	3-keto-L-gulonate-6-phosphate decarboxylase UlaD	9.92E-03	24.34795
Sp947_chr_00305	Unsaturated chondroitin disaccharide hydrolase	7.83E-03	23.54004
Sp947_chr_01629	PTS system trehalose-specific EIIBC component	2.80E-19	18.65254
Sp947_chr_01663	hypothetical protein	4.24E-02	17.40567
Sp947_chr_00108	Arginine-binding extracellular protein ArtP	9.63E-03	15.89418
Sp947_chr_00309	hypothetical protein	4.66E-02	15.73089
Sp947_chr_01967	Ascorbate-specific PTS system EIIC component	1.09E-02	15.09351
Sp947_chr_00109	Argininosuccinate synthase	1.64E-02	13.49916
Sp947_chr_01318	Glutamine-binding periplasmic protein	2.64E-07	7.648698
Sp947_chr_01667	Accessory Sec system protein Asp3	4.58E-02	7.043576
Sp947_chr_01630	Sucrose-6-phosphate hydrolase	1.00E-06	6.702188
Sp947_chr_02097	Putative dipeptidase	5.39E-05	6.495677
Sp947_chr_01672	General stress protein A	3.63E-19	5.924728
Sp947_chr_01670	Accessory Sec system protein translocase subunit SecY2	3.19E-05	5.757463
Sp947_chr_01631	HTH-type transcriptional regulator DegA	3.19E-03	5.461813
Sp947_chr_00308	PTS system mannose-specific EIID component	3.92E-02	4.864117
Sp947_chr_00854	V-type sodium ATPase subunit B	2.52E-06	4.860106
Sp947_chr_01671	Beta-1%2C6-galactofuranosyltransferase WbbI	2.36E-05	4.837304
Sp947_chr_02096	hypothetical protein	2.73E-05	4.789669
Sp947_chr_01560	putative thiol peroxidase	6.59E-14	4.443783
Sp947_chr_01666	Protein translocase subunit SecA	2.98E-07	4.414981
Sp947_chr_01665	Glycosyltransferase Gtf1	2.51E-05	4.413495
Sp947_chr_01920	putative ABC transporter ATP-binding protein YxlF	1.07E-07	4.401048
Sp947_chr_00855	V-type sodium ATPase subunit D	4.26E-03	4.394869
Sp947_chr_01081	L-methionine gamma-lyase	3.24E-04	4.297872
Sp947_chr_01447	Multidrug resistance ABC transporter ATP-binding/permease protein BmrA	4.48E-03	4.165307
Sp947_chr_01444	Cystathionine gamma-synthase/O-acetylhomoserine (thiol)-lyase	6.76E-04	4.10799
Sp947_chr_01772	Iron-uptake system permease protein FeuB	6.06E-03	4.051281
Sp947_chr_01673	General stress protein A	1.82E-06	4.024977
Sp947_chr_01669	hypothetical protein	2.01E-04	4.019284
Sp947_chr_01443	Cystathionine beta-lyase PatB	6.28E-04	4.001289
Sp947_chr_01664	Glycosyltransferase-stabilizing protein Gtf2	6.80E-05	3.991404
Sp947_chr_00104	putative cell wall hydrolase LytN	6.33E-10	3.97022
Sp947_chr_01448	Oligopeptide-binding protein SarA	8.69E-35	3.885765
Sp947_chr_02094	Ornithine carbamoyltransferase%2C catabolic	2.27E-09	3.843469
Sp947_chr_02093	Arginine deiminase	1.20E-03	3.624133
Sp947_chr_01668	Accessory Sec system protein Asp2	9.01E-04	3.57589
Sp947_chr_01993	hypothetical protein	2.75E-04	3.5502
Sp947_chr_00262	Alkanal monooxygenase alpha chain	4.20E-02	3.513196
Sp947_chr_00631	hypothetical protein	6.86E-03	3.468201
Sp947_chr_01628	Putative fructokinase	3.76E-02	3.396119
Sp947_chr_01674	putative glycosyltransferase EpsJ	3.86E-03	3.263426
Sp947_chr_02070	hypothetical protein	3.40E-02	3.249364
Sp947_chr_00169	hypothetical protein	1.81E-12	3.175252
Sp947_chr_00105	hypothetical protein	9.82E-05	3.113409
Sp947_chr_00544	5%2C10-methylenetetrahydrofolate reductase	6.48E-07	3.063051
Sp947_chr_02127	hypothetical protein	5.20E-03	3.051198

Sp947_chr_01919	hypothetical protein	6.43E-04	3.008033
Sp947_chr_00148	hypothetical protein	3.11E-03	2.944036
Sp947_chr_00846	Beta-glucoside kinase	2.93E-02	2.853877
Sp947_chr_01724	Tryptophan synthase beta chain	8.91E-04	2.848494
Sp947_chr_01917	Transcriptional regulatory protein DesR	1.30E-04	2.799649
Sp947_chr_01157	NADP-dependent glyceraldehyde-3-phosphate dehydrogenase	5.07E-05	2.764121
Sp947_chr_00161	Methionine import ATP-binding protein MetN	6.86E-03	2.745542
Sp947_chr_01732	T-box	4.38E-02	2.72911
Sp947_chr_01840	hypothetical protein	2.90E-03	2.691428
Sp947_chr_00425	Acetolactate synthase large subunit	1.12E-15	2.650045
Sp947_chr_00848	hypothetical protein	5.95E-04	2.637928
Sp947_chr_00845	scyllo-inositol 2-dehydrogenase (NAD(+))	4.49E-07	2.594575
Sp947_chr_01918	Sensor histidine kinase DesK	1.20E-05	2.551678
Sp947_chr_00844	Sialidase B	1.14E-08	2.530319
Sp947_chr_00692	Leucine-%2C isoleucine-%2C valine-%2C threonine-%2C and alanine-binding protein	2.08E-05	2.499057
Sp947_chr_02160	Secreted 45 kDa protein	1.55E-13	2.495737
Sp947_chr_00476	Protein GrpE	2.01E-04	2.420533
Sp947_chr_00787	Branched-chain-amino-acid aminotransferase	1.35E-07	2.395717
Sp947_chr_01424	6-phosphogluconolactonase	5.77E-04	2.345615
Sp947_chr_01660	Serine/threonine transporter SstT	2.89E-04	2.303845
Sp947_chr_00232	2%2C3-bisphosphoglycerate-dependent phosphoglycerate mutase	3.88E-02	2.243558
Sp947_chr_00842	Sodium/glucose cotransporter	2.08E-05	2.238557
Sp947_chr_01276	NADP-specific glutamate dehydrogenase	9.86E-19	2.229232
Sp947_chr_01391	Pyridoxal 5'-phosphate synthase subunit PdxS	1.61E-04	2.172842
Sp947_chr_00696	High-affinity branched-chain amino acid transport ATP-binding protein LivF	4.48E-03	2.171266
Sp947_chr_01661	hypothetical protein	2.04E-02	2.153858
Sp947_chr_00853	V-type sodium ATPase catalytic subunit A	9.55E-03	2.130379
Sp947_chr_00543	5-methyltetrahydropteroyltriglutamate--homocysteine methyltransferase	2.38E-05	2.118701
Sp947_chr_00695	Lipopolysaccharide export system ATP-binding protein LptB	2.08E-02	2.098421
Sp947_chr_00153	hypothetical protein	2.00E-19	2.013755
Sp947_chr_01394	NADH-dependent flavin reductase subunit 2	3.48E-02	2.043274
Sp947_chr_00205	30S ribosomal protein S19	2.68E-08	2.057637
Sp947_chr_00489	Lactococcin A secretion protein LcnD	5.57E-07	2.137788
Sp947_chr_00057	Phosphoribosylamine--glycine ligase	2.04E-02	2.148252
Sp947_chr_00155	hypothetical protein	1.27E-26	2.163473
Sp947_chr_00151	Nisin biosynthesis protein NisC	3.70E-31	2.171804
Sp947_chr_00498	hypothetical protein	3.74E-02	2.222467
Sp947_chr_02091	hypothetical protein	2.88E-02	2.230061
Sp947_chr_01955	Aldehyde-alcohol dehydrogenase	3.36E-10	2.239625
Sp947_chr_00490	Lactococcin-G-processing and transport ATP-binding protein LagD	1.15E-05	2.2462
Sp947_chr_02054	Maltose transport system permease protein MalG	2.55E-03	2.250996
Sp947_chr_00152	hypothetical protein	3.16E-35	2.253763
Sp947_chr_02053	Maltose transport system permease protein MalF	6.34E-05	2.292191
Sp947_chr_00157	L-cystine-binding protein TcyA	2.04E-02	2.305243
Sp947_chr_00491	hypothetical protein	2.93E-08	2.319449
Sp947_chr_00150	Nisin biosynthesis protein NisB	2.65E-31	2.324591
Sp947_chr_00499	hypothetical protein	2.99E-04	2.378979
Sp947_chr_00154	hypothetical protein	4.99E-25	2.443422
Sp947_chr_00281	Guanine/hypoxanthine permease PbuO	5.57E-07	2.494449
Sp947_chr_00041	hypothetical protein	3.18E-02	2.52396

Sp947_chr_01178	NAD kinase	5.94E-03	2.564431
Sp947_chr_00050	Phosphoribosylaminoimidazole-succinocarboxamide synthase	1.84E-02	2.58736
Sp947_chr_00263	Pullulanase	6.02E-06	2.823468
Sp947_chr_00440	Formate acetyltransferase	2.27E-52	2.85616
Sp947_chr_00279	Alcohol dehydrogenase 1	5.38E-07	3.088478
Sp947_chr_01753	Uric acid permease PucK	2.63E-06	3.150544
Sp947_chr_00156	hypothetical protein	1.25E-03	3.349079
Sp947_chr_01798	Sucrose phosphorylase	3.67E-02	3.943655
Sp947_chr_00282	hypothetical protein	5.77E-04	5.106822
Sp947_chr_01802	Bifunctional alpha-galactosidase/sucrose kinase AgaSK	2.44E-03	5.116292
Sp947_chr_00676	hypothetical protein	1.18E-02	6.452692
Sp947_chr_01801	Multiple sugar-binding protein	4.56E-03	6.788077
Sp947_chr_00675	Pyruvate oxidase	7.84E-110	6.915359
Sp947_chr_01592	scyllo-inositol 2-dehydrogenase (NAD(+))	8.87E-15	29.54277
Sp947_chr_01596	Inner membrane ABC transporter permease protein YcjO	2.70E-13	42.27417
Sp947_chr_01598	Evolved beta-galactosidase subunit beta	2.11E-08	45.04628
Sp947_chr_01595	Inner membrane ABC transporter permease protein YcjP	9.79E-12	49.58462
Sp947_chr_01599	hypothetical protein	3.26E-06	80.56657
Sp947_chr_01597	Putative ABC transporter substrate-binding protein YesO	1.55E-21	99.69291

Appendix O. Pneumococcal differential gene expression in the lungs 6 h post-infection, 947 vs 4559M. Genes with fold change (FC) greater than 2 and $p < 0.05$ are shown. FC values highlighted in blue = upregulated in 947, while values highlighted in red = upregulated in 4559M.

Locus tag in 947	Product	padj	FC
Sp947_chr_01081	L-methionine gamma-lyase	2.01E-06	6.049978
Sp947_chr_01629	PTS system trehalose-specific EIIBC component	4.32E-17	5.71303
Sp947_chr_01673	General stress protein A	2.68E-09	4.856349
Sp947_chr_01318	Glutamine-binding periplasmic protein	3.42E-07	4.661576
Sp947_chr_01448	Oligopeptide-binding protein SarA	1.19E-45	4.251728
Sp947_chr_01671	Beta-1%2C6-galactofuranosyltransferase WbbI	5.13E-06	4.200336
Sp947_chr_02096	hypothetical protein	1.64E-05	4.131014
Sp947_chr_02097	Putative dipeptidase	2.74E-04	3.935156
Sp947_chr_00544	5%2C10-methylenetetrahydrofolate reductase	4.34E-11	3.926284
Sp947_chr_01630	Sucrose-6-phosphate hydrolase	1.32E-05	3.842564
Sp947_chr_00105	hypothetical protein	9.16E-07	3.720141
Sp947_chr_01674	putative glycosyltransferase EpsJ	2.97E-04	3.645955
Sp947_chr_02093	Arginine deiminase	6.31E-04	3.638204
Sp947_chr_02094	Ornithine carbamoyltransferase%2C catabolic	2.11E-10	3.595965
Sp947_chr_01669	hypothetical protein	9.12E-05	3.520343
Sp947_chr_00145	hypothetical protein	1.10E-02	3.437721
Sp947_chr_01672	General stress protein A	3.78E-14	3.337295
Sp947_chr_01444	Cystathionine gamma-synthase/O-acetylhomoserine (thiol)-lyase	6.68E-04	3.323343
Sp947_chr_01628	Putative fructokinase	1.81E-02	3.312402
Sp947_chr_01993	hypothetical protein	1.09E-04	3.292474
Sp947_chr_00104	putative cell wall hydrolase LytN	9.04E-10	3.274894
Sp947_chr_01668	Accessory Sec system protein Asp2	3.58E-04	3.271471
Sp947_chr_02070	hypothetical protein	1.33E-02	3.268113
Sp947_chr_01631	HTH-type transcriptional regulator DegA	1.62E-02	3.241793
Sp947_chr_01666	Protein translocase subunit SecA	1.86E-06	3.194154
Sp947_chr_01560	putative thiol peroxidase	1.87E-11	3.156039
Sp947_chr_00148	hypothetical protein	3.69E-04	3.143065
Sp947_chr_00843	hypothetical protein	6.34E-04	3.140506
Sp947_chr_01446	Multidrug resistance ABC transporter ATP-binding and permease protein	2.44E-02	3.095084
Sp947_chr_00631	hypothetical protein	5.70E-03	3.078157
Sp947_chr_01670	Accessory Sec system protein translocase subunit SecY2	6.16E-04	3.060934
Sp947_chr_01447	Multidrug resistance ABC transporter ATP-binding/permease protein BmrA	6.68E-03	3.030447
Sp947_chr_01665	Glycosyltransferase Gtf1	2.91E-04	2.877465
Sp947_chr_00846	Beta-glucoside kinase	1.36E-02	2.854048
Sp947_chr_01664	Glycosyltransferase-stabilizing protein Gtf2	4.96E-04	2.799165
Sp947_chr_01660	Serine/threonine transporter SstT	1.28E-06	2.757889
Sp947_chr_00855	V-type sodium ATPase subunit D	4.10E-02	2.573402
Sp947_chr_01772	Iron-uptake system permease protein FeuB	3.65E-02	2.566198
Sp947_chr_01443	Cystathionine beta-lyase PatB	1.32E-02	2.466567
Sp947_chr_00695	Lipopolysaccharide export system ATP-binding protein LptB	1.70E-03	2.4024
Sp947_chr_00854	V-type sodium ATPase subunit B	2.76E-03	2.359804
Sp947_chr_01157	NADP-dependent glyceraldehyde-3-phosphate dehydrogenase	1.59E-04	2.339795
Sp947_chr_00169	hypothetical protein	4.71E-09	2.339571
Sp947_chr_00692	Leucine-%2C isoleucine-%2C valine-%2C threonine-%2C and alanine-binding protein	2.14E-05	2.312731

Sp947_chr_00543	5-methyltetrahydropteroyltriglutamate--homocysteine methyltransferase	2.80E-07	2.29823
Sp947_chr_01661	hypothetical protein	5.48E-03	2.245706
Sp947_chr_00701	PTS system glucose-specific EIICBA component	2.24E-04	2.216955
Sp947_chr_01985	N-acetylglucosamine-6-phosphate deacetylase	1.28E-06	2.199836
Sp947_chr_00845	scyllo-inositol 2-dehydrogenase (NAD(+))	6.36E-06	2.193442
Sp947_chr_00967	putative amino acid permease YhdG	6.47E-03	2.175611
Sp947_chr_00853	V-type sodium ATPase catalytic subunit A	2.93E-03	2.171867
Sp947_chr_00747	hypothetical protein	1.16E-02	2.164988
Sp947_chr_01984	Alcohol dehydrogenase	6.59E-05	2.143827
Sp947_chr_02160	Secreted 45 kDa protein	5.54E-11	2.11217
Sp947_chr_00696	High-affinity branched-chain amino acid transport ATP-binding protein LivF	2.42E-03	2.088927
Sp947_chr_00844	Sialidase B	1.59E-06	2.076986
Sp947_chr_01840	hypothetical protein	1.72E-02	2.063451
Sp947_chr_00842	Sodium/glucose cotransporter	4.98E-05	2.058073
Sp947_chr_00787	Branched-chain-amino-acid aminotransferase	2.56E-06	2.038246
Sp947_chr_02071	Dihydroxy-acid dehydratase	1.13E-06	2.036651
Sp947_chr_00841	N-acetylneuraminate lyase	2.76E-03	2.028736
Sp947_chr_00219	50S ribosomal protein L30	4.02E-06	2.006281
Sp947_chr_01505	putative MFS-type transporter YhjX	1.81E-02	2.023671
Sp947_chr_00337	Putative O-antigen transporter	1.76E-08	2.108266
Sp947_chr_00285	GTP cyclohydrolase 1	7.38E-03	2.146718
Sp947_chr_01309	Spermidine/putrescine-binding periplasmic protein	9.70E-03	2.183815
Sp947_chr_00051	Phosphoribosylformylglycinamidine synthase	2.50E-18	2.248477
Sp947_chr_00499	hypothetical protein	3.77E-04	2.270129
Sp947_chr_00489	Lactococcin A secretion protein LcnD	4.44E-09	2.301998
Sp947_chr_00057	Phosphoribosylamine--glycine ligase	3.82E-03	2.336422
Sp947_chr_01178	NAD kinase	7.88E-03	2.39753
Sp947_chr_00440	Formate acetyltransferase	4.09E-39	2.453134
Sp947_chr_00491	hypothetical protein	2.44E-11	2.578315
Sp947_chr_01048	GMP reductase	1.47E-04	2.657956
Sp947_chr_00060	hypothetical protein	2.11E-02	2.684809
Sp947_chr_00490	Lactococcin-G-processing and transport ATP-binding protein LagD	8.32E-10	2.783617
Sp947_chr_00281	Guanine/hypoxanthine permease PbuO	1.01E-11	3.141839
Sp947_chr_00050	Phosphoribosylaminoimidazole-succinocarboxamide synthase	8.38E-04	3.197571
Sp947_chr_01752	Xanthine phosphoribosyltransferase	5.58E-03	3.533145
Sp947_chr_01753	Uric acid permease PucK	1.84E-11	4.438869
Sp947_chr_00282	hypothetical protein	5.34E-05	5.973551
Sp947_chr_00675	Pyruvate oxidase	2.07E-119	7.278273
Sp947_chr_00676	hypothetical protein	3.25E-03	7.516116
Sp947_chr_01592	scyllo-inositol 2-dehydrogenase (NAD(+))	1.85E-18	43.48026
Sp947_chr_01598	Evolved beta-galactosidase subunit beta	4.44E-09	49.62974
Sp947_chr_01596	Inner membrane ABC transporter permease protein YcjO	1.62E-14	50.00969
Sp947_chr_01599	hypothetical protein	1.54E-05	59.75261
Sp947_chr_01595	Inner membrane ABC transporter permease protein YcjP	4.01E-13	60.7687
Sp947_chr_01597	Putative ABC transporter substrate-binding protein YesO	7.96E-23	115.2393

Appendix P. Pneumococcal differential gene expression in the lungs 6 h post-infection, 947M vs 4559. Genes with fold change (FC) greater than 2 and $p < 0.05$ are shown. FC values highlighted in blue = upregulated in 947M, while values highlighted in red = upregulated in 4559.

Locus tag in 947	Product	padj	FC
Sp947_chr_00305	Unsaturated chondroitin disaccharide hydrolase	5.14E-05	68.93754
Sp947_chr_00306	PTS system sorbose-specific EIIB component	3.51E-04	49.45218
Sp947_chr_00300	KHG/KDPG aldolase	3.91E-03	24.0683
Sp947_chr_01663	hypothetical protein	4.89E-02	14.9774
Sp947_chr_00307	N-acetylgalactosamine permease IIC component 1	1.38E-02	13.15252
Sp947_chr_01954	PTS system oligo-beta-mannoside-specific EIIA component	1.43E-02	12.11948
Sp947_chr_01722	hypothetical protein	4.94E-02	11.94383
Sp947_chr_00301	2-dehydro-3-deoxygluconokinase	6.47E-04	11.29777
Sp947_chr_01447	Multidrug resistance ABC transporter ATP-binding/permease protein BmrA	7.75E-08	10.01756
Sp947_chr_00308	PTS system mannose-specific EIID component	2.03E-03	7.771254
Sp947_chr_00262	Alkanal monooxygenase alpha chain	1.33E-04	6.912513
Sp947_chr_00193	Cardiolipin synthase	4.62E-03	6.683222
Sp947_chr_01672	General stress protein A	1.61E-20	6.353083
Sp947_chr_01448	Oligopeptide-binding protein SarA	2.32E-67	6.342907
Sp947_chr_01318	Glutamine-binding periplasmic protein	8.47E-06	6.056553
Sp947_chr_01670	Accessory Sec system protein translocase subunit SecY2	3.95E-05	5.615085
Sp947_chr_01951	6-phospho-beta-glucosidase GmuD	2.41E-04	5.149937
Sp947_chr_01671	Beta-1%2C6-galactofuranosyltransferase WbbI	2.30E-05	4.811812
Sp947_chr_01674	putative glycosyltransferase EpsJ	2.18E-05	4.795206
Sp947_chr_01669	hypothetical protein	1.60E-05	4.73273
Sp947_chr_01444	Cystathionine gamma-synthase/O-acetylhomoserine (thiol)-lyase	1.22E-04	4.673266
Sp947_chr_01665	Glycosyltransferase Gtf1	1.18E-05	4.600689
Sp947_chr_01849	hypothetical protein	1.09E-09	4.492743
Sp947_chr_01666	Protein translocase subunit SecA	2.78E-07	4.406684
Sp947_chr_01952	Lichenan permease IIC component	9.92E-04	4.298464
Sp947_chr_01668	Accessory Sec system protein Asp2	1.11E-04	4.155341
Sp947_chr_01673	General stress protein A	1.46E-06	4.054469
Sp947_chr_01445	Multidrug resistance ABC transporter ATP-binding and permease protein	2.20E-04	4.038759
Sp947_chr_00104	putative cell wall hydrolase LytN	6.98E-10	3.983611
Sp947_chr_01664	Glycosyltransferase-stabilizing protein Gtf2	8.77E-05	3.910847
Sp947_chr_01157	NADP-dependent glyceraldehyde-3-phosphate dehydrogenase	1.24E-08	3.804836
Sp947_chr_01920	putative ABC transporter ATP-binding protein YxlF	3.68E-06	3.759168
Sp947_chr_01995	putative FMN/FAD exporter YeeO	4.45E-02	3.737599
Sp947_chr_01446	Multidrug resistance ABC transporter ATP-binding and permease protein	2.66E-03	3.726174
Sp947_chr_01443	Cystathionine beta-lyase PatB	2.07E-03	3.550934
Sp947_chr_00544	5%2C10-methylenetetrahydrofolate reductase	7.79E-09	3.549207
Sp947_chr_00161	Methionine import ATP-binding protein MetN	2.08E-04	3.538504
Sp947_chr_01837	Phenylalanine--tRNA ligase beta subunit	3.15E-02	3.43443
Sp947_chr_01848	Pneumolysin	9.47E-22	3.364311
Sp947_chr_01420	Glutamine transport ATP-binding protein GlnQ	7.35E-08	3.349461
Sp947_chr_00162	Methionine import system permease protein MetP	3.23E-03	3.322192
Sp947_chr_01081	L-methionine gamma-lyase	8.60E-03	3.120338
Sp947_chr_01260	Putative phosphatase	3.26E-02	3.115464
Sp947_chr_01630	Sucrose-6-phosphate hydrolase	1.34E-02	3.067307

Sp947_chr_02070	hypothetical protein	4.65E-02	2.98896
Sp947_chr_00181	putative murein peptide carboxypeptidase	4.94E-02	2.972231
Sp947_chr_01419	Arginine-binding extracellular protein ArtP	1.35E-09	2.930964
Sp947_chr_00482	ABC-type transporter ATP-binding protein EcsA	2.93E-02	2.922061
Sp947_chr_01055	Glucose-6-phosphate 1-dehydrogenase	9.29E-23	2.874562
Sp947_chr_01918	Sensor histidine kinase DesK	6.21E-07	2.828767
Sp947_chr_01851	hypothetical protein	2.91E-03	2.786765
Sp947_chr_01339	Glucosamine-6-phosphate deaminase	9.28E-07	2.746131
Sp947_chr_01850	hypothetical protein	1.10E-05	2.743522
Sp947_chr_01732	T-box	3.58E-02	2.720698
Sp947_chr_00543	5-methyltetrahydropteroyltriglutamate--homocysteine methyltransferase	2.51E-09	2.709082
Sp947_chr_01847	putative transcriptional regulatory protein	6.58E-08	2.646376
Sp947_chr_01238	Ribitol-5-phosphate cytidylyltransferase	4.11E-06	2.589054
Sp947_chr_01056	Arginine transport ATP-binding protein ArtM	2.77E-13	2.557431
Sp947_chr_01421	L-cystine transport system permease protein YecS	2.65E-03	2.512296
Sp947_chr_01282	putative ABC transporter ATP-binding protein	2.62E-03	2.508221
Sp947_chr_01642	Primosomal protein N'	3.98E-04	2.500435
Sp947_chr_00696	High-affinity branched-chain amino acid transport ATP-binding protein LivF	3.30E-04	2.495921
Sp947_chr_01919	hypothetical protein	7.59E-03	2.477463
Sp947_chr_01917	Transcriptional regulatory protein DesR	1.19E-03	2.460707
Sp947_chr_01724	Tryptophan synthase beta chain	6.73E-03	2.43327
Sp947_chr_00434	hypothetical protein	1.20E-02	2.423222
Sp947_chr_00191	Folylpolyglutamate synthase	1.37E-02	2.406573
Sp947_chr_00787	Branched-chain-amino-acid aminotransferase	1.28E-07	2.396524
Sp947_chr_01660	Serine/threonine transporter SstT	1.56E-04	2.365193
Sp947_chr_00817	PTS system fructose-specific EIIABC component	3.52E-05	2.357843
Sp947_chr_02040	N-acetyldiaminopimelate deacetylase	2.44E-03	2.31786
Sp947_chr_00425	Acetolactate synthase large subunit	9.17E-11	2.279343
Sp947_chr_00169	hypothetical protein	4.14E-06	2.275144
Sp947_chr_00944	putative S-adenosyl-L-methionine-dependent methyltransferase TehB	6.05E-03	2.260243
Sp947_chr_01560	putative thiol peroxidase	4.54E-04	2.24987
Sp947_chr_01215	putative peptidoglycan glycosyltransferase FtsW	4.18E-05	2.245616
Sp947_chr_02018	putative ABC transporter ATP-binding protein	2.54E-04	2.232901
Sp947_chr_00985	4-hydroxy-tetrahydrodipicolinate synthase	9.09E-04	2.211691
Sp947_chr_01283	putative ABC transporter ATP-binding protein	9.29E-03	2.209084
Sp947_chr_02056	HTH-type transcriptional regulator MalR	2.43E-02	2.208454
Sp947_chr_00859	Arginine regulator	4.43E-03	2.173132
Sp947_chr_01470	hypothetical protein	1.28E-07	2.172156
Sp947_chr_00967	putative amino acid permease YhdG	8.74E-03	2.141793
Sp947_chr_00695	Lipopolysaccharide export system ATP-binding protein LptB	1.97E-02	2.066565
Sp947_chr_01653	hypothetical protein	2.93E-02	2.065838
Sp947_chr_01057	Glutamine transport system permease protein GlnP	2.03E-12	2.062275
Sp947_chr_01661	hypothetical protein	2.78E-02	2.054099
Sp947_chr_01640	Ribosomal RNA small subunit methyltransferase B	2.91E-03	2.053249
Sp947_chr_01281	5-methylthioadenosine/S-adenosylhomocysteine deaminase	7.78E-03	2.046941
Sp947_chr_00789	hypothetical protein	6.20E-04	2.033781
Sp947_chr_01235	hypothetical protein	1.92E-04	2.031984
Sp947_chr_00258	Putative zinc metalloprotease	6.05E-03	2.019156
Sp947_chr_02160	Secreted 45 kDa protein	1.02E-07	2.017272
Sp947_chr_00790	hypothetical protein	8.94E-06	2.016723
Sp947_chr_01391	Pyridoxal 5'-phosphate synthase subunit PdxS	9.79E-04	2.001587

Sp947_chr_00210	30S ribosomal protein S17	4.67E-07	2.011481
Sp947_chr_01154	Glycogen biosynthesis protein GlgD	1.55E-02	2.038321
Sp947_chr_01279	50S ribosomal protein L10	1.09E-07	2.043546
Sp947_chr_01477	CCA-adding enzyme	4.41E-02	2.051156
Sp947_chr_01432	ATP synthase subunit c	6.93E-03	2.052648
Sp947_chr_00225	30S ribosomal protein S13	1.54E-08	2.076816
Sp947_chr_00498	hypothetical protein	4.94E-02	2.116476
Sp947_chr_00928	50S ribosomal protein L35	2.34E-03	2.124092
Sp947_chr_00608	putative response regulatory protein	3.31E-05	2.136323
Sp947_chr_00228	50S ribosomal protein L17	3.58E-08	2.137006
Sp947_chr_01478	4-hydroxy-tetrahydrodipicolinate reductase	6.93E-03	2.173119
Sp947_chr_00501	hypothetical protein	5.79E-03	2.174678
Sp947_chr_01479	DegV domain-containing protein	3.33E-03	2.221312
Sp947_chr_01591	Putative N-acetylmannosamine-6-phosphate 2-epimerase	7.35E-08	2.23104
Sp947_chr_00059	N5-carboxyaminoimidazole ribonucleotide synthase	6.69E-04	2.236367
Sp947_chr_01589	Putative ABC transporter substrate-binding protein YesO	9.43E-15	2.28675
Sp947_chr_01584	hypothetical protein	1.07E-02	2.333389
Sp947_chr_01590	PTS system glucose-specific EIICBA component	5.93E-17	2.346142
Sp947_chr_00057	Phosphoribosylamine--glycine ligase	6.10E-03	2.431764
Sp947_chr_01596	Inner membrane ABC transporter permease protein YcjO	4.53E-05	2.439969
Sp947_chr_01597	Putative ABC transporter substrate-binding protein YesO	1.57E-11	2.460435
Sp947_chr_00577	Branched-chain amino acid transport system 2 carrier protein	2.12E-06	2.461054
Sp947_chr_00499	hypothetical protein	2.11E-04	2.4774
Sp947_chr_01600	Sialidase A	1.40E-13	2.501157
Sp947_chr_01598	Evolved beta-galactosidase subunit beta	1.08E-03	2.529667
Sp947_chr_00925	hypothetical protein	1.77E-02	2.540488
Sp947_chr_01595	Inner membrane ABC transporter permease protein YcjP	4.13E-05	2.552297
Sp947_chr_00282	hypothetical protein	3.15E-02	2.616579
Sp947_chr_01586	Toxin-antitoxin biofilm protein TabA	2.91E-03	2.76266
Sp947_chr_01101	Galactose-6-phosphate isomerase subunit LacA	4.83E-02	2.778676
Sp947_chr_00493	hypothetical protein	1.56E-04	2.785461
Sp947_chr_02029	Phosphate-binding protein PstS 2	2.15E-03	2.865929
Sp947_chr_01278	50S ribosomal protein L7/L12	3.87E-12	2.996972
Sp947_chr_00488	hypothetical protein	4.04E-02	3.028346
Sp947_chr_01585	hypothetical protein	1.43E-03	3.034917
Sp947_chr_01588	Lactose transport system permease protein LacF	8.20E-09	3.043549
Sp947_chr_01587	L-arabinose transport system permease protein AraQ	4.60E-09	3.098046
Sp947_chr_02129	Alpha-glycerophosphate oxidase	2.28E-14	3.098558
Sp947_chr_01753	Uric acid permease PucK	6.97E-06	3.127739
Sp947_chr_01583	N-acetylneuraminate lyase	8.65E-11	3.160283
Sp947_chr_02130	Glycerol kinase	6.99E-12	3.188476
Sp947_chr_02128	putative glycerol uptake facilitator protein	5.65E-06	3.28419
Sp947_chr_00056	Bifunctional purine biosynthesis protein PurH	4.99E-17	3.314739
Sp947_chr_01233	DNA processing protein DprA	1.59E-02	3.332503
Sp947_chr_00051	Phosphoribosylformylglycinamidine synthase	6.17E-29	3.43114
Sp947_chr_01599	hypothetical protein	6.34E-04	3.44936
Sp947_chr_00156	hypothetical protein	1.20E-03	3.475747
Sp947_chr_00153	hypothetical protein	1.72E-53	3.578283
Sp947_chr_00155	hypothetical protein	3.41E-64	3.592961

Sp947_chr_00053	Phosphoribosylformylglycinamidine cyclo-ligase	3.79E-13	3.631123
Sp947_chr_01107	PTS system lactose-specific EIICB component	7.51E-03	3.644307
Sp947_chr_00154	hypothetical protein	7.99E-47	3.765825
Sp947_chr_01835	Single-stranded DNA-binding protein	4.27E-06	3.783469
Sp947_chr_00050	Phosphoribosylaminoimidazole-succinocarboxamide synthase	1.15E-03	3.934432
Sp947_chr_00151	Nisin biosynthesis protein NisC	1.55E-88	4.039514
Sp947_chr_00054	Phosphoribosylglycinamide formyltransferase	1.05E-08	4.05498
Sp947_chr_01976	hypothetical protein	1.43E-02	4.070542
Sp947_chr_00491	hypothetical protein	1.08E-16	4.148617
Sp947_chr_00157	L-cystine-binding protein TcyA	1.27E-04	4.197553
Sp947_chr_00052	Amidophosphoribosyltransferase	2.70E-18	4.311536
Sp947_chr_01752	Xanthine phosphoribosyltransferase	8.75E-03	4.371717
Sp947_chr_01035	hypothetical protein	1.51E-02	4.523322
Sp947_chr_00152	hypothetical protein	1.47E-102	4.587529
Sp947_chr_00496	Bacteriocin lactacin-F subunit LafA	3.41E-03	4.761852
Sp947_chr_01582	Beta-glucoside kinase	5.11E-14	4.796863
Sp947_chr_01979	hypothetical protein	4.17E-02	4.975354
Sp947_chr_00150	Nisin biosynthesis protein NisB	2.28E-105	5.029877
Sp947_chr_00149	hypothetical protein	9.98E-80	5.84338
Sp947_chr_00055	hypothetical protein	2.54E-10	5.908767
Sp947_chr_00923	ComE operon protein 3	6.38E-04	5.932836
Sp947_chr_01974	Ubiquinone/menaquinone biosynthesis C-methyltransferase UbiE	6.02E-03	6.304239
Sp947_chr_01982	ComG operon protein 1	1.51E-04	7.042161
Sp947_chr_00133	hypothetical protein	5.43E-04	7.078549
Sp947_chr_00631	hypothetical protein	3.43E-02	8.177758
Sp947_chr_01601	hypothetical protein	1.07E-02	8.512209
Sp947_chr_00134	hypothetical protein	4.34E-04	8.597105
Sp947_chr_01187	hypothetical protein	3.55E-02	8.767671
Sp947_chr_00119	hypothetical protein	2.86E-02	9.128069
Sp947_chr_01977	hypothetical protein	3.77E-03	10.4118
Sp947_chr_00854	V-type sodium ATPase subunit B	1.03E-02	10.46683
Sp947_chr_01975	Ubiquinone biosynthesis O-methyltransferase	1.60E-02	10.52488
Sp947_chr_01949	hypothetical protein	4.65E-02	12.94222
Sp947_chr_00632	ABC transporter ATP-binding protein YxdL	2.09E-02	17.25928
Sp947_chr_00111	Lactococcin-G-processing and transport ATP-binding protein LagD	1.55E-02	18.33763
Sp947_chr_00855	V-type sodium ATPase subunit D	7.50E-03	19.55662
Sp947_chr_00850	V-type proton ATPase subunit E	9.84E-03	19.86727
Sp947_chr_00840	Putative N-acetylmannosamine-6-phosphate 2-epimerase	2.06E-03	24.75437
Sp947_chr_00120	hypothetical protein	2.86E-03	25.71408
Sp947_chr_00116	hypothetical protein	2.91E-03	26.96818
Sp947_chr_00851	V-type sodium ATPase subunit C	1.83E-03	28.20511
Sp947_chr_00843	hypothetical protein	6.39E-04	31.47893
Sp947_chr_00117	hypothetical protein	1.32E-03	31.85973
Sp947_chr_00846	Beta-glucoside kinase	6.62E-04	34.40566
Sp947_chr_00118	hypothetical protein	3.54E-04	40.73953
Sp947_chr_02078	hypothetical protein	1.92E-04	40.77519
Sp947_chr_00839	HTH-type transcriptional regulator RpiR	1.25E-04	44.12853
Sp947_chr_00853	V-type sodium ATPase catalytic subunit A	7.65E-05	47.19399
Sp947_chr_00848	hypothetical protein	6.15E-06	76.87348
Sp947_chr_00845	scyllo-inositol 2-dehydrogenase (NAD(+))	2.21E-06	85.19736
Sp947_chr_00842	Sodium/glucose cotransporter	4.67E-07	108.7675
Sp947_chr_00841	N-acetylneuraminate lyase	4.39E-07	115.1438
Sp947_chr_00844	Sialidase B	1.77E-07	124.0874

Sp947_chr_02077	hypothetical protein	8.20E-09	199.0553

Appendix Q. Pneumococcal differential gene expression in the lungs 6 h post-infection, 947M vs 4559M. Genes with fold change (FC) greater than 2 and $p < 0.05$ are shown. FC values highlighted in blue = upregulated in 947M, while values highlighted in red = upregulated in 4559M.

Locus tag in 947	Product	padj	FC
Sp947_chr_00301	2-dehydro-3-deoxygluconokinase	1.17E-04	9.670733
Sp947_chr_01712	Lichenan permease IIC component	3.56E-02	8.609312
Sp947_chr_01445	Multidrug resistance ABC transporter ATP-binding and permease protein	4.16E-08	8.483181
Sp947_chr_00306	PTS system sorbose-specific EIIB component	8.86E-03	7.513945
Sp947_chr_01447	Multidrug resistance ABC transporter ATP-binding/permease protein BmrA	7.53E-09	7.288221
Sp947_chr_01448	Oligopeptide-binding protein SarA	3.21E-85	6.940285
Sp947_chr_00302	hypothetical protein	1.64E-02	6.743771
Sp947_chr_01446	Multidrug resistance ABC transporter ATP-binding and permease protein	2.12E-05	6.075821
Sp947_chr_00307	N-acetylgalactosamine permease IIC component 1	2.53E-02	5.42795
Sp947_chr_01674	putative glycosyltransferase EpsJ	5.67E-07	5.357286
Sp947_chr_00308	PTS system mannose-specific EIID component	2.24E-03	4.992152
Sp947_chr_00305	Unsaturated chondroitin disaccharide hydrolase	9.64E-03	4.929947
Sp947_chr_01673	General stress protein A	3.78E-09	4.891933
Sp947_chr_00664	Putative HMP/thiamine import ATP-binding protein YkoD	4.57E-02	4.859076
Sp947_chr_00544	5%2C10-methylenetetrahydrofolate reductase	1.52E-13	4.549448
Sp947_chr_01081	L-methionine gamma-lyase	2.58E-04	4.3924
Sp947_chr_01802	Bifunctional alpha-galactosidase/sucrose kinase AgaSK	9.20E-03	4.294223
Sp947_chr_01671	Beta-1%2C6-galactofuranosyltransferase WbbI	7.43E-06	4.178201
Sp947_chr_01669	hypothetical protein	6.03E-06	4.145224
Sp947_chr_01668	Accessory Sec system protein Asp2	4.18E-05	3.801593
Sp947_chr_01444	Cystathionine gamma-synthase/O-acetylhomoserine (thiol)-lyase	1.32E-04	3.780648
Sp947_chr_01749	Exodeoxyribonuclease	1.34E-03	3.759186
Sp947_chr_01318	Glutamine-binding periplasmic protein	4.34E-05	3.691227
Sp947_chr_00722	Biotin transporter BioY2	3.56E-02	3.673481
Sp947_chr_01672	General stress protein A	1.09E-15	3.578579
Sp947_chr_01850	hypothetical protein	1.54E-08	3.371368
Sp947_chr_00104	putative cell wall hydrolase LytN	1.48E-09	3.28594
Sp947_chr_01711	Arylsulfatase	3.74E-02	3.285935
Sp947_chr_01951	6-phospho-beta-glucosidase GmuD	2.12E-03	3.238088
Sp947_chr_01952	Lichenan permease IIC component	3.22E-03	3.220857
Sp947_chr_01157	NADP-dependent glyceraldehyde-3-phosphate dehydrogenase	3.10E-08	3.220747
Sp947_chr_01666	Protein translocase subunit SecA	2.62E-06	3.188151
Sp947_chr_01849	hypothetical protein	3.61E-07	3.031185
Sp947_chr_02070	hypothetical protein	2.76E-02	3.006206
Sp947_chr_01665	Glycosyltransferase Gtf1	1.78E-04	2.99951
Sp947_chr_01670	Accessory Sec system protein translocase subunit SecY2	1.04E-03	2.985239
Sp947_chr_00543	5-methyltetrahydropteroyltriglutamate--homocysteine methyltransferase	3.12E-12	2.938637
Sp947_chr_01731	hypothetical protein	1.04E-02	2.933719
Sp947_chr_01851	hypothetical protein	8.59E-04	2.875592
Sp947_chr_01339	Glucosamine-6-phosphate deaminase	2.98E-08	2.866661
Sp947_chr_01660	Serine/threonine transporter SstT	7.70E-07	2.831328
Sp947_chr_01664	Glycosyltransferase-stabilizing protein Gtf2	8.36E-04	2.742671

Sp947_chr_01848	Pneumolysin	5.90E-18	2.731212
Sp947_chr_00967	putative amino acid permease YhdG	2.01E-04	2.694598
Sp947_chr_01281	5-methylthioadenosine/S-adenosylhomocysteine deaminase	1.08E-04	2.610116
Sp947_chr_01238	Ribitol-5-phosphate cytidylyltransferase	5.25E-07	2.603372
Sp947_chr_02040	N-acetyldiaminopimelate deacetylase	3.36E-04	2.491103
Sp947_chr_01847	putative transcriptional regulatory protein	4.75E-08	2.46311
Sp947_chr_01055	Glucose-6-phosphate 1-dehydrogenase	8.83E-19	2.41423
Sp947_chr_00279	Alcohol dehydrogenase 1	1.79E-04	2.402247
Sp947_chr_00696	High-affinity branched-chain amino acid transport ATP-binding protein LivF	1.78E-04	2.40127
Sp947_chr_00161	Methionine import ATP-binding protein MetN	5.07E-03	2.36814
Sp947_chr_00695	Lipopolysaccharide export system ATP-binding protein LptB	2.38E-03	2.365929
Sp947_chr_00162	Methionine import system permease protein MetP	2.47E-02	2.354175
Sp947_chr_01237	Ribulose-5-phosphate reductase	2.21E-07	2.347699
Sp947_chr_00694	High-affinity branched-chain amino acid transport system permease protein LivH	6.27E-04	2.285144
Sp947_chr_02071	Dihydroxy-acid dehydratase	9.70E-09	2.2807
Sp947_chr_01640	Ribosomal RNA small subunit methyltransferase B	2.39E-04	2.277034
Sp947_chr_00985	4-hydroxy-tetrahydrodipicolinate synthase	3.06E-04	2.222209
Sp947_chr_01421	L-cystine transport system permease protein YecS	6.47E-03	2.19205
Sp947_chr_01443	Cystathionine beta-lyase PatB	4.50E-02	2.188948
Sp947_chr_01056	Arginine transport ATP-binding protein ArtM	1.14E-10	2.147633
Sp947_chr_01661	hypothetical protein	1.13E-02	2.141693
Sp947_chr_01287	Adapter protein MecA	6.92E-03	2.108023
Sp947_chr_01420	Glutamine transport ATP-binding protein GlnQ	3.04E-04	2.064193
Sp947_chr_00191	Folylpolyglutamate synthase	3.39E-02	2.058539
Sp947_chr_01057	Glutamine transport system permease protein GlnP	1.08E-13	2.054665
Sp947_chr_00789	hypothetical protein	2.13E-04	2.044356
Sp947_chr_00787	Branched-chain-amino-acid aminotransferase	3.56E-06	2.038933
Sp947_chr_00403	Malonyl CoA-acyl carrier protein transacylase	1.35E-02	2.029537
Sp947_chr_01985	N-acetylglucosamine-6-phosphate deacetylase	4.34E-05	2.007822
Sp947_chr_01955	Aldehyde-alcohol dehydrogenase	2.78E-07	2.00535
Sp947_chr_00283	Dihydropteroate synthase	1.34E-02	2.008932
Sp947_chr_01500	Trehalose import ATP-binding protein SugC	3.16E-06	2.026012
Sp947_chr_00609	Sensor histidine kinase YehU	1.74E-06	2.070439
Sp947_chr_00083	Histidine protein kinase SaeS	5.36E-03	2.073337
Sp947_chr_01155	Glucose-1-phosphate adenylyltransferase	8.09E-03	2.093897
Sp947_chr_01279	50S ribosomal protein L10	1.05E-08	2.096326
Sp947_chr_01154	Glycogen biosynthesis protein GlgD	8.29E-03	2.098713
Sp947_chr_01590	PTS system glucose-specific EIICBA component	5.60E-14	2.138227
Sp947_chr_00500	hypothetical protein	1.66E-06	2.139178
Sp947_chr_00502	hypothetical protein	7.03E-05	2.147247
Sp947_chr_01589	Putative ABC transporter substrate-binding protein YesO	3.23E-13	2.149307
Sp947_chr_00066	PTS system sorbose-specific EIIC component	1.90E-03	2.153142
Sp947_chr_00065	PTS system sorbose-specific EIIB component	2.53E-02	2.169443
Sp947_chr_00069	Putative tagatose-6-phosphate ketose/aldose isomerase	4.34E-05	2.18834
Sp947_chr_00925	hypothetical protein	4.99E-02	2.232677
Sp947_chr_00067	PTS system mannose-specific EIID component	2.72E-04	2.245442
Sp947_chr_01591	Putative N-acetylmannosamine-6-phosphate 2-epimerase	1.55E-08	2.259193
Sp947_chr_00284	Folylpolyglutamate synthase	1.47E-04	2.262639

Sp947_chr_00582	50S ribosomal protein L1	1.92E-11	2.266385
Sp947_chr_01478	4-hydroxy-tetrahydrodipicolinate reductase	1.95E-03	2.316861
Sp947_chr_00228	50S ribosomal protein L17	7.30E-11	2.339842
Sp947_chr_00608	putative response regulatory protein	7.07E-07	2.352334
Sp947_chr_00499	hypothetical protein	3.48E-04	2.364047
Sp947_chr_00930	Lactoylglutathione lyase	3.61E-02	2.382768
Sp947_chr_02030	Phosphate transport system permease protein PstC 1	1.96E-02	2.434936
Sp947_chr_01479	DegV domain-containing protein	4.56E-04	2.439687
Sp947_chr_01600	Sialidase A	1.52E-13	2.448881
Sp947_chr_00281	Guanine/hypoxanthine permease PbuO	1.26E-07	2.458395
Sp947_chr_00059	N5-carboxyaminoimidazole ribonucleotide synthase	6.17E-05	2.458645
Sp947_chr_01584	hypothetical protein	3.37E-03	2.507546
Sp947_chr_01599	hypothetical protein	1.54E-02	2.558236
Sp947_chr_01592	scyllo-inositol 2-dehydrogenase (NAD(+))	4.91E-07	2.616868
Sp947_chr_00285	GTP cyclohydrolase 1	1.08E-03	2.622738
Sp947_chr_00577	Branched-chain amino acid transport system 2 carrier protein	1.03E-07	2.63016
Sp947_chr_00057	Phosphoribosylamine--glycine ligase	1.46E-03	2.644768
Sp947_chr_00493	hypothetical protein	2.13E-04	2.678999
Sp947_chr_02032	Phosphate import ATP-binding protein PstB 3	1.01E-03	2.722278
Sp947_chr_01598	Evolved beta-galactosidase subunit beta	1.56E-04	2.78706
Sp947_chr_00154	hypothetical protein	2.65E-28	2.805147
Sp947_chr_01597	Putative ABC transporter substrate-binding protein YesO	1.60E-16	2.844123
Sp947_chr_01586	Toxin-antitoxin biofilm protein TabA	1.39E-03	2.849225
Sp947_chr_02031	Phosphate transport system permease protein PstA 2	5.46E-04	2.861119
Sp947_chr_01596	Inner membrane ABC transporter permease protein YcjO	2.53E-07	2.886446
Sp947_chr_00153	hypothetical protein	1.82E-37	2.892108
Sp947_chr_00155	hypothetical protein	1.12E-45	2.931856
Sp947_chr_00151	Nisin biosynthesis protein NisC	7.90E-55	2.999037
Sp947_chr_00282	hypothetical protein	6.70E-03	3.060665
Sp947_chr_02033	Phosphate-specific transport system accessory protein PhoU	2.38E-05	3.077587
Sp947_chr_01595	Inner membrane ABC transporter permease protein YcjP	1.02E-07	3.127981
Sp947_chr_01588	Lactose transport system permease protein LacF	6.39E-10	3.167722
Sp947_chr_01583	N-acetylneuraminate lyase	1.77E-11	3.181516
Sp947_chr_00488	hypothetical protein	2.55E-02	3.198131
Sp947_chr_01278	50S ribosomal protein L7/L12	2.57E-14	3.199195
Sp947_chr_02062	hypothetical protein	1.23E-02	3.218262
Sp947_chr_00157	L-cystine-binding protein TcyA	1.97E-03	3.281804
Sp947_chr_02128	putative glycerol uptake facilitator protein	1.40E-06	3.376722
Sp947_chr_00152	hypothetical protein	1.56E-66	3.408858
Sp947_chr_01587	L-arabinose transport system permease protein AraQ	2.04E-11	3.436735
Sp947_chr_01108	6-phospho-beta-galactosidase	3.63E-02	3.572337
Sp947_chr_00150	Nisin biosynthesis protein NisB	3.01E-67	3.640087
Sp947_chr_00053	Phosphoribosylformylglycinamidine cyclo-ligase	7.11E-14	3.646901
Sp947_chr_01835	Single-stranded DNA-binding protein	4.27E-06	3.681599
Sp947_chr_02130	Glycerol kinase	5.10E-16	3.692078
Sp947_chr_01585	hypothetical protein	2.56E-05	3.869586
Sp947_chr_00056	Bifunctional purine biosynthesis protein PurH	3.59E-23	3.888367
Sp947_chr_00496	Bacteriocin lactacin-F subunit LafA	1.15E-02	3.987266

Sp947_chr_00054	Phosphoribosylglycinamide formyltransferase	8.51E-09	3.987798
Sp947_chr_00983	asd	9.32E-03	3.997549
Sp947_chr_02129	Alpha-glycerophosphate oxidase	3.55E-23	4.018257
Sp947_chr_01035	hypothetical protein	2.41E-02	4.140521
Sp947_chr_00051	Phosphoribosylformylglycinamidine synthase	2.28E-42	4.235246
Sp947_chr_00052	Amidophosphoribosyltransferase	1.19E-18	4.268644
Sp947_chr_02029	Phosphate-binding protein PstS 2	1.30E-06	4.397577
Sp947_chr_01753	Uric acid permease PucK	2.01E-10	4.406739
Sp947_chr_01976	hypothetical protein	6.51E-03	4.475349
Sp947_chr_02096	hypothetical protein	2.68E-02	4.506143
Sp947_chr_00491	hypothetical protein	3.28E-20	4.611629
Sp947_chr_01582	Beta-glucoside kinase	2.18E-14	4.75467
Sp947_chr_00050	Phosphoribosylaminoimidazole-succinocarboxamide synthase	7.03E-05	4.86234
Sp947_chr_00149	hypothetical protein	9.11E-65	4.877677
Sp947_chr_00923	ComE operon protein 3	1.39E-03	5.294791
Sp947_chr_01752	Xanthine phosphoribosyltransferase	8.53E-04	5.746786
Sp947_chr_00055	hypothetical protein	9.95E-11	5.925865
Sp947_chr_01974	Ubiquinone/menaquinone biosynthesis C-methyltransferase UbiE	5.04E-03	6.407721
Sp947_chr_01601	hypothetical protein	2.99E-02	6.738993
Sp947_chr_00133	hypothetical protein	3.54E-04	7.246645
Sp947_chr_01979	hypothetical protein	5.49E-03	7.304412
Sp947_chr_01980	hypothetical protein	1.67E-02	7.537585
Sp947_chr_01982	ComG operon protein 1	1.75E-05	8.446919
Sp947_chr_00134	hypothetical protein	4.13E-04	8.447782
Sp947_chr_00631	hypothetical protein	2.15E-02	9.213989
Sp947_chr_01977	hypothetical protein	5.49E-03	9.600591
Sp947_chr_00119	hypothetical protein	2.24E-02	9.657972
Sp947_chr_01975	Ubiquinone biosynthesis O-methyltransferase	1.24E-02	11.19827
Sp947_chr_00849	V-type sodium ATPase subunit K	4.67E-02	12.68675
Sp947_chr_00847	hypothetical protein	4.77E-02	12.75212
Sp947_chr_00632	ABC transporter ATP-binding protein YxdL	3.91E-02	13.87838
Sp947_chr_00115	hypothetical protein	4.98E-02	15.08898
Sp947_chr_00122	hypothetical protein	7.13E-03	19.74573
Sp947_chr_00852	V-type sodium ATPase subunit G	9.01E-03	20.06019
Sp947_chr_00843	hypothetical protein	3.51E-03	21.00858
Sp947_chr_00854	V-type sodium ATPase subunit B	2.61E-04	21.55684
Sp947_chr_00111	Lactococcin-G-processing and transport ATP-binding protein LagD	7.18E-03	22.70188
Sp947_chr_00850	V-type proton ATPase subunit E	1.94E-03	29.81791
Sp947_chr_00116	hypothetical protein	1.53E-03	30.65687
Sp947_chr_00840	Putative N-acetylmannosamine-6-phosphate 2-epimerase	6.27E-04	31.88306
Sp947_chr_00855	V-type sodium ATPase subunit D	7.10E-04	33.3989
Sp947_chr_00851	V-type sodium ATPase subunit C	7.66E-04	33.41091
Sp947_chr_00839	HTH-type transcriptional regulator RpiR	4.17E-04	33.69369
Sp947_chr_00846	Beta-glucoside kinase	6.02E-04	34.40359
Sp947_chr_02078	hypothetical protein	2.89E-04	37.03186
Sp947_chr_00117	hypothetical protein	6.19E-04	37.13564
Sp947_chr_00120	hypothetical protein	3.83E-04	39.34665
Sp947_chr_00853	V-type sodium ATPase catalytic subunit A	8.31E-05	46.29248
Sp947_chr_00118	hypothetical protein	1.01E-04	52.43328
Sp947_chr_00845	scyllo-inositol 2-dehydrogenase (NAD(+))	6.99E-07	100.7781
Sp947_chr_00848	hypothetical protein	5.25E-07	111.61
Sp947_chr_00841	N-acetylneuraminate lyase	4.68E-07	112.2849
Sp947_chr_00842	Sodium/glucose cotransporter	2.63E-07	118.3059

Sp947_chr_00844	Sialidase B	4.59E-08	151.1713
Sp947_chr_02077	hypothetical protein	6.25E-09	206.1168

Appendix R. Pneumococcal differential gene expression in the lungs 6 h post-infection, 4559 vs 4559M. Genes with fold change (FC) greater than 2 and $p < 0.05$ are shown. FC values highlighted in blue = upregulated in 4559, while values highlighted in red = upregulated in 4559M.

Locus tag in 947	Product	padj	FC
Sp947_chr_00279	Alcohol dehydrogenase 1	2.23E-08	3.532144
Sp947_chr_01955	Aldehyde-alcohol dehydrogenase	1.15E-20	3.234431
Sp947_chr_00088	putative multiple-sugar transport system permease YteP	3.50E-02	2.176402
Sp947_chr_02054	Maltose transport system permease protein MalG	9.80E-03	2.120116
Sp947_chr_01917	Transcriptional regulatory protein DesR	1.14E-02	2.254388
Sp947_chr_02033	Phosphate-specific transport system accessory protein PhoU	5.24E-03	2.313659
Sp947_chr_01629	PTS system trehalose-specific EIIBC component	1.03E-02	3.264913
Sp947_chr_01920	putative ABC transporter ATP-binding protein YxlF	1.75E-04	3.369874

Appendix S. Murine differential gene expression in the lungs 6 h post-infection, 947 vs 947M. Genes with fold change (FC) greater than 1.5 and $p < 0.05$ are shown. FC values highlighted in blue = upregulated in 947, while values highlighted in red = upregulated in 947M.

Gene Stable ID	Gene Name	padj	FC
ENSMUSG00000065254	*Gm23973*	1.17E-08	6.0256
ENSMUSG00000088675	*Rprl1*	2.45E-08	5.382293
ENSMUSG00000106222	*Rprl1*	2.45E-08	5.382293
ENSMUSG00000096269	*Rpl31-ps21*	6.02E-06	5.232448
ENSMUSG00000094668	*Gm24871*	1.75E-06	4.724852
ENSMUSG00000064682	*Gm25813*	1.04E-09	4.405394
ENSMUSG00000065870	*Rnu3a*	4.31E-15	4.246867
ENSMUSG00000106147	*Rnu3a*	4.31E-15	4.246867
ENSMUSG00000095676	*Gm25099*	2.12E-22	4.006482
ENSMUSG00000104896	*Rnu3b4*	2.62E-19	3.731483
ENSMUSG00000105115	*Rnu3b2*	1.58E-19	3.730893
ENSMUSG00000098925	*Rnu3b2*	1.58E-19	3.730893
ENSMUSG00000098641	*Rnu3b4*	3.16E-19	3.726678
ENSMUSG00000098943	*Rnu3b1*	5.09E-19	3.713982
ENSMUSG00000105025	*Rnu3b1*	5.09E-19	3.713982
ENSMUSG00000099291	*Rnu3b3*	1.37E-18	3.710655
ENSMUSG00000104856	*Rnu3b3*	1.37E-18	3.710655
ENSMUSG00000065232	*Gm22973*	7.53E-12	3.699468
ENSMUSG00000095738	*Gm25313*	7.10E-11	3.614973
ENSMUSG00000064994	*Gm22422*	2.64E-07	3.494379
ENSMUSG00000065176	*Rnu12*	2.59E-22	3.424881
ENSMUSG00000077254	*Gm26079*	7.16E-09	3.417376
ENSMUSG00000095892	*Rnu5g*	1.98E-10	3.377252
ENSMUSG00000093956	*Gm24497*	1.37E-09	3.358284
ENSMUSG00000094050	*Gm23472*	7.29E-10	3.353025
ENSMUSG00000080465	*Gm22486*	2.03E-10	3.35003
ENSMUSG00000064856	*Gm23444*	1.29E-09	3.346978
ENSMUSG00000064899	*Snord118*	1.39E-05	3.336753
ENSMUSG00000093843	*Gm25939*	5.28E-08	3.334159
ENSMUSG00000094655	*Gm25360*	1.09E-16	3.3217
ENSMUSG00000065820	*Gm26316*	1.36E-09	3.301702
ENSMUSG00000065767	*Gm23849*	3.38E-09	3.230541
ENSMUSG00000064702	*Gm24950*	4.61E-09	3.217205
ENSMUSG00000065251	*Gm23971*	4.61E-09	3.217205
ENSMUSG00000065944	*Rnu2-10*	3.79E-09	3.210903
ENSMUSG00000080538	*Gm25541*	1.66E-11	3.172594
ENSMUSG00000027261	*Hao1*	7.14E-05	3.03458
ENSMUSG00000094377	*Gm24407*	3.83E-10	3.022053
ENSMUSG00000032494	*Tdgf1*	4.29E-04	3.003122
ENSMUSG00000065911	*Gm24447*	3.13E-11	2.969689
ENSMUSG00000065824	*Gm26315*	3.28E-11	2.966459
ENSMUSG00000089255	*Snora78*	5.52E-04	2.891999
ENSMUSG00000096243	*Gm24265*	9.59E-08	2.856449
ENSMUSG00000064945	*Rny3*	3.87E-08	2.845147
ENSMUSG00000085348	*Myhas*	3.19E-07	2.838211
ENSMUSG00000064694	*Gm24146*	1.10E-06	2.83174
ENSMUSG00000065087	*Snord22*	2.41E-26	2.800736
ENSMUSG00000115207	*Gm49132*	4.18E-02	2.775687
ENSMUSG00000084744	*Gm25291*	1.83E-05	2.768169
ENSMUSG00000091993	*B930036N10Rik*	2.04E-05	2.722677
ENSMUSG00000084708	*Gm22988*	4.52E-11	2.714612
ENSMUSG00000114163	*Gm32296*	2.07E-03	2.66448

ENSMUSG00000010362	*Rdm1*	7.28E-09	2.661396
ENSMUSG00000064453	*Snord21*	2.98E-04	2.630897
ENSMUSG00000055170	*Ifng*	3.23E-05	2.609289
ENSMUSG00000044092	*C130050O18Rik*	5.69E-17	2.609004
ENSMUSG00000000386	*Mx1*	3.70E-72	2.588273
ENSMUSG00000065118	*Gm23297*	5.39E-04	2.56856
ENSMUSG00000064966	*Snord15b*	5.58E-08	2.566291
ENSMUSG00000065701	*Rny1*	2.33E-06	2.562933
ENSMUSG00000087819	*Gm25117*	1.86E-10	2.551007
ENSMUSG00000111734	*Gm29825*	1.81E-02	2.544426
ENSMUSG00000010342	*Tex14*	8.31E-10	2.529067
ENSMUSG00000064901	*Snora21*	1.95E-03	2.517886
ENSMUSG00000087775	*Rprl2*	4.05E-05	2.454835
ENSMUSG00000065822	*Snord15a*	1.38E-04	2.451242
ENSMUSG00000097770	*Gm26776*	9.57E-03	2.44156
ENSMUSG00000020641	*Rsad2*	7.09E-26	2.429777
ENSMUSG00000043681	*Fam25c*	1.39E-04	2.404388
ENSMUSG00000003545	*Fosb*	5.64E-13	2.404057
ENSMUSG00000025431	*Crisp1*	9.80E-05	2.397804
ENSMUSG00000101133	*Gm29050*	8.16E-03	2.391731
ENSMUSG00000088252	*Snord13*	6.50E-05	2.386827
ENSMUSG00000077323	*Rnu11*	6.57E-07	2.38433
ENSMUSG00000097131	*D230017M19Rik*	1.76E-08	2.381225
ENSMUSG00000092837	*Rpph1*	7.69E-06	2.372261
ENSMUSG00000071470	*Ccnb1ip1*	7.38E-06	2.360943
ENSMUSG00000092819	*Gm23639*	7.41E-03	2.352266
ENSMUSG00000048806	*Ifnb1*	7.71E-03	2.351491
ENSMUSG00000117269	*AC151275.1*	2.17E-05	2.349181
ENSMUSG00000087477	*Gm13822*	8.85E-05	2.342073
ENSMUSG00000065649	*Snora74a*	1.06E-06	2.339372
ENSMUSG00000105797	*Gm5149*	1.85E-04	2.330504
ENSMUSG00000035692	*Isg15*	4.03E-49	2.315568
ENSMUSG00000069310	*Hist1h3c*	2.16E-03	2.278831
ENSMUSG00000090101	*Snhg9*	2.99E-03	2.269589
ENSMUSG00000020216	*Jsrp1*	4.96E-03	2.263278
ENSMUSG00000069265	*Hist1h3a*	8.88E-03	2.259961
ENSMUSG00000104863	*Gm49347*	5.93E-05	2.258448
ENSMUSG00000099517	*Hist1h3g*	1.60E-02	2.249359
ENSMUSG00000057596	*Trim30d*	3.93E-09	2.247087
ENSMUSG00000064604	*Snora44*	2.55E-04	2.227773
ENSMUSG00000015437	*Gzmb*	1.49E-07	2.22751
ENSMUSG00000046229	*Scand1*	7.61E-03	2.223718
ENSMUSG00000077167	*Gm24119*	2.38E-03	2.220322
ENSMUSG00000065126	*Snord104*	3.21E-09	2.21526
ENSMUSG00000096887	*Gm20594*	7.60E-12	2.198159
ENSMUSG00000080542	*Gm22710*	8.69E-04	2.195982
ENSMUSG00000064999	*Gm26035*	2.79E-06	2.192941
ENSMUSG00000069273	*Hist1h3e*	3.58E-06	2.184059
ENSMUSG00000080365	*Gm25776*	1.43E-04	2.181141
ENSMUSG00000031289	*Il13ra2*	4.89E-06	2.177819
ENSMUSG00000016327	*Atp1b4*	1.73E-02	2.166814
ENSMUSG00000064380	*Gm26448*	1.91E-09	2.16627
ENSMUSG00000111821	*Gm48545*	9.69E-05	2.152735
ENSMUSG00000097060	*Gm26759*	9.57E-10	2.145737
ENSMUSG00000034855	*Cxcl10*	6.33E-14	2.12518
ENSMUSG00000067455	*Hist1h4j*	7.47E-04	2.121665
ENSMUSG00000045932	*Ifit2*	1.49E-41	2.119366

ENSMUSG00000096349	*Gm22513*	1.67E-02	2.109175
ENSMUSG00000064655	*Gm25788*	7.16E-03	2.098184
ENSMUSG00000094344	*Gm11942*	7.06E-20	2.094663
ENSMUSG00000023341	*Mx2*	4.66E-63	2.093454
ENSMUSG00000060093	*Hist1h4a*	7.15E-07	2.093403
ENSMUSG00000030670	*Cyp2r1*	5.70E-03	2.090606
ENSMUSG00000044748	*Defb1*	3.78E-02	2.074292
ENSMUSG00000107722	*2900060B14Rik*	1.19E-03	2.067021
ENSMUSG00000031757	*Mt4*	1.78E-04	2.063615
ENSMUSG00000088025	*Rprl3*	1.20E-03	2.055532
ENSMUSG00000095590	*Gm24305*	4.50E-02	2.053062
ENSMUSG00000081163	*Defa-ps12*	2.72E-02	2.051928
ENSMUSG00000038357	*Camp*	9.67E-07	2.049958
ENSMUSG00000097457	*2310031A07Rik*	4.24E-02	2.038639
ENSMUSG00000064387	*Snora73a*	2.52E-11	2.036576
ENSMUSG00000031343	*Gabra3*	1.84E-06	2.035071
ENSMUSG00000115420	*AL732506.1*	1.46E-06	2.031062
ENSMUSG00000088088	*Rmrp*	1.46E-06	2.031062
ENSMUSG00000086336	*Gm12979*	4.46E-02	2.029161
ENSMUSG00000042761	*Mrap2*	8.11E-03	2.023479
ENSMUSG00000066443	*Gm10163*	1.60E-02	2.02177
ENSMUSG00000110421	*Gm9689*	8.49E-03	2.017106
ENSMUSG00000058385	*Hist1h2bg*	2.16E-05	2.015475
ENSMUSG00000069274	*Hist1h4f*	6.77E-04	2.001288
ENSMUSG00000083596	*Rpl21-ps15*	2.72E-02	1.997761
ENSMUSG00000020638	*Cmpk2*	1.22E-42	1.997189
ENSMUSG00000046748	*Tmem45a2*	1.42E-06	1.980568
ENSMUSG00000114279	*Hist1h2bm*	3.13E-02	1.978823
ENSMUSG00000088948	*Gm23262*	5.31E-05	1.970935
ENSMUSG00000029019	*Nppb*	2.19E-04	1.958092
ENSMUSG00000102189	*Gm37194*	8.10E-06	1.955291
ENSMUSG00000059230	*Defb4*	2.95E-05	1.953494
ENSMUSG00000106366	*Mir3069*	3.60E-02	1.950774
ENSMUSG00000065259	*Snora30*	2.68E-02	1.943307
ENSMUSG00000017300	*Tnnc2*	1.69E-15	1.943187
ENSMUSG00000033213	*AA467197*	1.20E-05	1.94194
ENSMUSG00000065353	*Snora73b*	3.61E-05	1.941924
ENSMUSG00000062461	*Gm5453*	2.89E-10	1.940423
ENSMUSG00000100551	*Gm19503*	1.62E-07	1.936219
ENSMUSG00000060639	*Hist1h4i*	6.90E-04	1.935604
ENSMUSG00000087968	*Gm25395*	8.91E-07	1.934721
ENSMUSG00000106649	*Gm49349*	3.20E-06	1.929867
ENSMUSG00000068397	*Gm10240*	2.63E-02	1.927078
ENSMUSG00000100210	*Hist1h3f*	8.72E-04	1.921571
ENSMUSG00000004814	*Ccl24*	4.06E-02	1.915198
ENSMUSG00000063001	*Gm9701*	1.53E-02	1.914728
ENSMUSG00000047501	*Cldn4*	5.80E-05	1.913371
ENSMUSG00000091028	*Gm10722*	2.29E-02	1.902823
ENSMUSG00000065686	*Snora5c*	2.53E-02	1.902247
ENSMUSG00000114456	*Hist1h2bh*	4.42E-03	1.899751
ENSMUSG00000030107	*Usp18*	4.19E-35	1.891192
ENSMUSG00000108332	*D530033B14Rik*	5.32E-17	1.887082
ENSMUSG00000065226	*Gm25791*	4.61E-06	1.885368
ENSMUSG00000027233	*Patl2*	4.30E-02	1.87672
ENSMUSG00000052837	*Junb*	3.04E-33	1.873304
ENSMUSG00000045027	*Prss22*	2.77E-08	1.873299
ENSMUSG00000095217	*Hist1h2bn*	6.37E-03	1.869101

ENSMUSG00000065145	*Vaultrc5*	1.08E-03	1.86865
ENSMUSG00000046049	*Rp1l1*	1.93E-03	1.864557
ENSMUSG00000085532	*B430319H21Rik*	7.16E-05	1.864074
ENSMUSG00000069266	*Hist1h4b*	1.11E-02	1.861964
ENSMUSG00000074001	*Klhl40*	9.93E-04	1.861333
ENSMUSG00000085806	*Gm12023*	1.61E-04	1.860825
ENSMUSG00000026535	*Ifi202b*	5.49E-24	1.860159
ENSMUSG00000041827	*Oasl1*	1.59E-25	1.858532
ENSMUSG00000038295	*Atg9b*	2.43E-03	1.857709
ENSMUSG00000094392	*Gm3788*	6.33E-05	1.85749
ENSMUSG00000058773	*Hist1h1b*	1.03E-03	1.854963
ENSMUSG00000075031	*Hist1h2bb*	1.13E-02	1.853781
ENSMUSG00000089542	*Gm25835*	2.47E-06	1.852865
ENSMUSG00000106392	*Gm5870*	4.66E-02	1.852755
ENSMUSG00000083832	*Gm13771*	1.90E-05	1.846272
ENSMUSG00000074433	*Lce3e*	1.17E-02	1.844793
ENSMUSG00000090293	*Gm17034*	3.68E-02	1.844258
ENSMUSG00000088008	*Gm25492*	1.09E-02	1.841263
ENSMUSG00000082069	*Gm16242*	2.24E-03	1.83945
ENSMUSG00000107480	*Gm44165*	8.52E-05	1.836863
ENSMUSG00000064288	*Hist1h4k*	1.54E-03	1.836703
ENSMUSG00000091383	*Hist1h2al*	1.56E-06	1.834135
ENSMUSG00000070644	*Etnk2*	2.72E-02	1.83037
ENSMUSG00000034459	*Ifit1*	9.35E-29	1.829028
ENSMUSG00000108414	*Snhg1*	1.47E-18	1.82864
ENSMUSG00000101191	*Gm28809*	1.83E-02	1.825134
ENSMUSG00000095580	*Rnu1b1*	1.57E-03	1.824702
ENSMUSG00000093834	*Rnu1b2*	1.57E-03	1.824702
ENSMUSG00000087090	*Nctc1*	3.87E-14	1.821732
ENSMUSG00000031231	*Cox7b*	1.15E-18	1.818275
ENSMUSG00000064451	*Snora23*	4.39E-02	1.815006
ENSMUSG00000026418	*Tnni1*	8.22E-03	1.811313
ENSMUSG00000022586	*Ly6i*	6.13E-15	1.806331
ENSMUSG00000102135	*Gm37108*	2.29E-04	1.803613
ENSMUSG00000057465	*Saa2*	2.25E-09	1.803135
ENSMUSG00000018930	*Ccl4*	5.57E-23	1.800731
ENSMUSG00000104956	*4930429D17Rik*	1.82E-02	1.800304
ENSMUSG00000049173	*Myoz3*	2.97E-04	1.793444
ENSMUSG00000105361	*AY036118*	4.61E-03	1.788552
ENSMUSG00000104862	*Gm6520*	5.48E-03	1.787612
ENSMUSG00000088529	*Gm26083*	3.15E-03	1.7854
ENSMUSG00000085241	*Snhg3*	8.45E-07	1.784438
ENSMUSG00000068885	*Lce3f*	3.45E-03	1.781149
ENSMUSG00000085609	*1700016P03Rik*	1.93E-02	1.781038
ENSMUSG00000052305	*Hbb-bs*	1.24E-04	1.779109
ENSMUSG00000069306	*Hist1h4m*	8.36E-03	1.776996
ENSMUSG00000074403	*Hist2h3b*	4.10E-02	1.775714
ENSMUSG00000038508	*Gdf15*	1.58E-02	1.774828
ENSMUSG00000111713	*Gm20234*	3.65E-02	1.77292
ENSMUSG00000105826	*Gm42141*	1.78E-02	1.772001
ENSMUSG00000068855	*Hist2h2ac*	3.41E-03	1.763701
ENSMUSG00000064923	*Gm22042*	2.24E-03	1.762643
ENSMUSG00000033196	*Myh2*	1.57E-05	1.760939
ENSMUSG00000095701	*Gm24830*	2.16E-03	1.760782
ENSMUSG00000096838	*Gm26232*	2.16E-03	1.760782
ENSMUSG00000065773	*Rnu1b6*	2.16E-03	1.760782
ENSMUSG00000092702	*Gm24514*	2.48E-03	1.758247

ENSMUSG00000031097	*Tnni2*	2.03E-10	1.757473
ENSMUSG00000021768	*Dusp13*	1.61E-02	1.754751
ENSMUSG00000068697	*Myoz1*	2.09E-06	1.754697
ENSMUSG00000058427	*Cxcl2*	4.52E-11	1.754009
ENSMUSG00000096010	*Hist4h4*	8.63E-04	1.751589
ENSMUSG00000100969	*1700030N03Rik*	1.26E-04	1.75055
ENSMUSG00000065037	*Rn7sk*	2.99E-04	1.749012
ENSMUSG00000061482	*Hist1h4d*	9.27E-08	1.745652
ENSMUSG00000081159	*Gm6023*	3.99E-02	1.745032
ENSMUSG00000077714	*Snord17*	9.77E-04	1.74339
ENSMUSG00000077563	*Snora68*	1.10E-03	1.741607
ENSMUSG00000059434	*Gckr*	1.39E-05	1.737341
ENSMUSG00000036731	*Cysrt1*	2.64E-02	1.736202
ENSMUSG00000009070	*Rsph14*	1.51E-06	1.732995
ENSMUSG00000038037	*Socs1*	3.91E-10	1.729735
ENSMUSG00000115783	*Bc1*	1.91E-02	1.72912
ENSMUSG00000095260	*Gm25890*	3.42E-03	1.728617
ENSMUSG00000094812	*Gm22614*	3.42E-03	1.728617
ENSMUSG00000079434	*Neu2*	2.66E-03	1.727284
ENSMUSG00000066510	*Ankdd1a*	6.66E-07	1.722526
ENSMUSG00000052565	*Hist1h1d*	6.03E-05	1.722286
ENSMUSG00000026573	*Xcl1*	2.28E-02	1.721571
ENSMUSG00000096084	*Gm21850*	5.20E-05	1.721306
ENSMUSG00000076066	*Mir223*	1.46E-04	1.719947
ENSMUSG00000060183	*Cxcl11*	1.19E-05	1.718861
ENSMUSG00000056300	*Zfp981*	3.47E-08	1.717174
ENSMUSG00000112041	*9530020I12Rik*	4.54E-02	1.716234
ENSMUSG00000081642	*Gm13532*	2.45E-02	1.71339
ENSMUSG00000080950	*Gm7278*	4.27E-03	1.71199
ENSMUSG00000102630	*Gm37289*	3.32E-02	1.708678
ENSMUSG00000073902	*Gm1966*	8.32E-11	1.70586
ENSMUSG00000049734	*Trex1*	1.10E-13	1.705391
ENSMUSG00000060981	*Hist1h4h*	1.23E-04	1.704353
ENSMUSG00000032174	*Icam5*	9.90E-03	1.703716
ENSMUSG00000088789	*Scarna13*	2.42E-04	1.703392
ENSMUSG00000103308	*Gm37800*	1.54E-05	1.702856
ENSMUSG00000062727	*Hist1h2bk*	1.47E-02	1.700599
ENSMUSG00000088185	*Scarna2*	3.84E-05	1.700093
ENSMUSG00000113198	*Gm6988*	1.11E-04	1.700093
ENSMUSG00000059108	*Ifitm6*	1.55E-16	1.69831
ENSMUSG00000065862	*Gm24029*	5.06E-03	1.697729
ENSMUSG00000092805	*Gm26461*	8.64E-03	1.69729
ENSMUSG00000070271	*Gm13268*	2.67E-02	1.696212
ENSMUSG00000109052	*Gm45012*	1.88E-02	1.694509
ENSMUSG00000028037	*Ifi44*	9.21E-19	1.693727
ENSMUSG00000097413	*A830052D11Rik*	3.38E-02	1.693497
ENSMUSG00000026358	*Rgs1*	1.60E-07	1.69318
ENSMUSG00000054325	*Lce3a*	4.97E-03	1.691831
ENSMUSG00000053560	*Ier2*	3.16E-19	1.69155
ENSMUSG00000073940	*Hbb-bt*	7.55E-04	1.691523
ENSMUSG00000051319	*1500011K16Rik*	1.19E-02	1.691061
ENSMUSG00000064179	*Tnnt1*	3.07E-03	1.690918
ENSMUSG00000074115	*Saa1*	9.38E-13	1.688411
ENSMUSG00000069305	*Hist1h4n*	9.18E-03	1.688272
ENSMUSG00000028341	*Nr4a3*	5.23E-35	1.683154
ENSMUSG00000071637	*Cebpd*	3.66E-31	1.680871
ENSMUSG00000065637	*Gm26397*	1.11E-04	1.68061

ENSMUSG00000057160	*Gm16372*	1.59E-04	1.680286
ENSMUSG00000105790	*Gm24105*	9.29E-04	1.678237
ENSMUSG00000092674	*Gm24105*	8.40E-04	1.675874
ENSMUSG00000060678	*Hist1h4c*	3.44E-05	1.674695
ENSMUSG00000042918	*Mamstr*	4.07E-16	1.672552
ENSMUSG00000109875	*Gm45456*	1.06E-02	1.6722
ENSMUSG00000030399	*Ckm*	1.29E-07	1.666114
ENSMUSG00000030672	*Mylpf*	3.88E-04	1.662639
ENSMUSG00000005716	*Pvalb*	2.77E-02	1.662341
ENSMUSG00000042031	*Lce3b*	7.71E-03	1.661896
ENSMUSG00000109905	*Gm7380*	1.71E-03	1.660339
ENSMUSG00000025172	*Ankrd2*	2.03E-04	1.659684
ENSMUSG00000026826	*Nr4a2*	3.05E-06	1.659502
ENSMUSG00000094338	*Hist1h2bl*	8.49E-03	1.656315
ENSMUSG00000029379	*Cxcl3*	2.23E-17	1.656114
ENSMUSG00000035852	*Misp*	4.46E-09	1.656018
ENSMUSG00000086777	*Far2os2*	4.90E-02	1.655464
ENSMUSG00000053469	*Tg*	1.99E-19	1.649527
ENSMUSG00000104740	*Mir6516*	2.80E-02	1.648462
ENSMUSG00000071858	*Gm94*	2.34E-02	1.647909
ENSMUSG00000031972	*Acta1*	6.98E-10	1.647593
ENSMUSG00000029635	*Cdk8*	1.63E-05	1.64378
ENSMUSG00000081684	*Rps2-ps13*	1.03E-05	1.64243
ENSMUSG00000067767	*Clec4b2*	1.61E-03	1.642307
ENSMUSG00000045475	*Lce3c*	9.18E-03	1.642182
ENSMUSG00000017204	*Gsdma*	1.46E-02	1.640548
ENSMUSG00000029378	*Areg*	3.84E-05	1.638461
ENSMUSG00000085249	*Gm12847*	1.43E-02	1.636783
ENSMUSG00000097122	*Gm26624*	4.43E-08	1.636704
ENSMUSG00000027913	*Crct1*	1.49E-03	1.63647
ENSMUSG00000050463	*Krt78*	8.75E-06	1.635311
ENSMUSG00000115518	*Gm10791*	1.41E-03	1.634944
ENSMUSG00000086213	*A330040F15Rik*	1.95E-07	1.633556
ENSMUSG00000004885	*Crabp2*	2.87E-02	1.63166
ENSMUSG00000066491	*Cox6c2*	3.99E-07	1.630614
ENSMUSG00000062826	*Ces2f*	8.39E-04	1.627736
ENSMUSG00000046031	*Calhm6*	1.04E-03	1.627261
ENSMUSG00000064382	*Gm26447*	7.12E-04	1.626644
ENSMUSG00000035653	*Lrfn5*	3.15E-02	1.624893
ENSMUSG00000063739	*Gm4963*	8.67E-05	1.623848
ENSMUSG00000074896	*Ifit3*	8.41E-19	1.622777
ENSMUSG00000062028	*Irgc1*	7.95E-04	1.621717
ENSMUSG00000063820	*Arl9*	3.59E-02	1.621614
ENSMUSG00000045377	*Tmem88*	4.72E-06	1.619556
ENSMUSG00000114185	*Gm47662*	3.98E-02	1.619275
ENSMUSG00000041872	*Il17f*	1.86E-04	1.619247
ENSMUSG00000002500	*Rpl3l*	2.59E-03	1.616885
ENSMUSG00000075042	*4930431P03Rik*	1.10E-02	1.615685
ENSMUSG00000044165	*Bcl2l15*	2.68E-05	1.615489
ENSMUSG00000017697	*Ada*	9.34E-11	1.615438
ENSMUSG00000091957	*Rps2-ps10*	3.10E-05	1.615002
ENSMUSG00000025498	*Irf7*	2.69E-23	1.614017
ENSMUSG00000114277	*Gm48583*	7.46E-04	1.611868
ENSMUSG00000104818	*Gm43661*	3.64E-03	1.609404
ENSMUSG00000063651	*Cnfn*	5.49E-04	1.609357
ENSMUSG00000081700	*Atp5k-ps2*	3.69E-03	1.607129
ENSMUSG00000096205	*Gm22068*	9.60E-03	1.604372

ENSMUSG00000098181	*Rps12-ps24*	4.51E-03	1.603992
ENSMUSG00000056054	*S100a8*	3.40E-07	1.600618
ENSMUSG00000028896	*Rcc1*	4.47E-11	1.599941
ENSMUSG00000031780	*Ccl17*	5.39E-06	1.598957
ENSMUSG00000109729	*Gm45418*	3.30E-05	1.597842
ENSMUSG00000029862	*Clcn1*	1.22E-04	1.595774
ENSMUSG00000097134	*1110002J07Rik*	8.36E-04	1.595135
ENSMUSG00000094826	*Gm23804*	1.22E-03	1.594121
ENSMUSG00000074149	*Gm10634*	2.88E-07	1.59407
ENSMUSG00000029371	*Cxcl5*	5.61E-15	1.593155
ENSMUSG00000111752	*Gm38575*	1.27E-10	1.593054
ENSMUSG00000057580	*Gm10012*	1.95E-02	1.592497
ENSMUSG00000114790	*4921509O07Rik*	4.54E-04	1.592138
ENSMUSG00000027368	*Dusp2*	4.18E-09	1.591586
ENSMUSG00000113178	*Mylf-ps*	1.12E-06	1.591195
ENSMUSG00000048572	*Tmem252*	4.44E-31	1.589873
ENSMUSG00000095969	*Rnu1a1*	1.30E-02	1.589137
ENSMUSG00000022602	*Arc*	3.85E-02	1.589088
ENSMUSG00000105145	*Gm47299*	1.40E-02	1.587799
ENSMUSG00000105788	*Gm47295*	1.40E-02	1.587791
ENSMUSG00000020061	*Mybpc1*	1.21E-11	1.587253
ENSMUSG00000000157	*Itgb2l*	7.93E-11	1.586842
ENSMUSG00000028680	*Plk3*	1.73E-13	1.586408
ENSMUSG00000053553	*3110082I17Rik*	4.41E-10	1.586388
ENSMUSG00000070167	*Snora57*	1.06E-03	1.585311
ENSMUSG00000024430	*Cabyr*	2.76E-02	1.584461
ENSMUSG00000087066	*Gm15518*	1.60E-08	1.584091
ENSMUSG00000026166	*Ccl20*	3.82E-11	1.583687
ENSMUSG00000014773	*Dll1*	1.32E-28	1.583278
ENSMUSG00000090582	*Gm17024*	6.03E-07	1.582913
ENSMUSG00000096659	*Gm25679*	1.19E-03	1.5829
ENSMUSG00000093815	*Gm26444*	1.19E-03	1.5829
ENSMUSG00000082838	*Gm14519*	5.79E-05	1.581682
ENSMUSG00000062488	*Ifit3b*	7.88E-13	1.57948
ENSMUSG00000070866	*Zfp804a*	2.93E-03	1.577636
ENSMUSG00000053522	*Lgals7*	4.18E-02	1.57711
ENSMUSG00000038670	*Mybpc2*	9.70E-09	1.576178
ENSMUSG00000115355	*4930445E18Rik*	1.31E-03	1.574801
ENSMUSG00000085434	*Gm11725*	3.76E-02	1.574487
ENSMUSG00000037977	*6430571L13Rik*	1.13E-02	1.573903
ENSMUSG00000089281	*Scarna6*	8.23E-03	1.573558
ENSMUSG00000032327	*Stra6*	5.98E-03	1.572608
ENSMUSG00000064816	*Gm22357*	1.73E-02	1.572211
ENSMUSG00000008384	*Sertad1*	1.12E-13	1.571184
ENSMUSG00000054582	*Pabpc1l*	2.99E-05	1.569168
ENSMUSG00000026628	*Atf3*	3.62E-22	1.569059
ENSMUSG00000057003	*Myh4*	1.65E-08	1.568031
ENSMUSG00000113722	*Snhg10*	1.06E-03	1.566332
ENSMUSG00000001014	*Icam4*	6.99E-03	1.565655
ENSMUSG00000041954	*Tnfrsf18*	6.61E-03	1.563024
ENSMUSG00000051439	*Cd14*	3.56E-27	1.562597
ENSMUSG00000040328	*Olfr56*	4.75E-15	1.562502
ENSMUSG00000096214	*Gm22634*	1.28E-03	1.562461
ENSMUSG00000096206	*Gm22317*	1.28E-03	1.562461
ENSMUSG00000033730	*Egr3*	2.40E-10	1.56174
ENSMUSG00000116961	*AC117662.4*	2.23E-03	1.560197
ENSMUSG00000090698	*Apold1*	1.43E-10	1.560015

ENSMUSG00000109700	*Gm21123*	2.06E-03	1.559279
ENSMUSG00000059741	*Myl3*	2.72E-06	1.558851
ENSMUSG00000057280	*Musk*	2.22E-06	1.556841
ENSMUSG00000053508	*Gtsf2*	6.80E-07	1.553985
ENSMUSG00000030156	*Cd69*	5.45E-07	1.553384
ENSMUSG00000089617	*Scarna10*	1.55E-02	1.551375
ENSMUSG00000099587	*Gm28967*	1.55E-02	1.551375
ENSMUSG00000030669	*Calca*	7.44E-05	1.551054
ENSMUSG00000078616	*Trim30c*	4.08E-08	1.550782
ENSMUSG00000060438	*Rps10-ps1*	1.39E-08	1.550238
ENSMUSG00000024205	*Rpl36-ps2*	1.69E-04	1.549767
ENSMUSG00000054169	*Ceacam10*	1.16E-05	1.548901
ENSMUSG00000103313	*Gm38357*	3.20E-19	1.548815
ENSMUSG00000110697	*Gm31718*	2.21E-17	1.548758
ENSMUSG00000025726	*Slc28a1*	3.17E-02	1.545524
ENSMUSG00000009633	*G0s2*	6.94E-06	1.54482
ENSMUSG00000028435	*Aqp3*	1.82E-03	1.543177
ENSMUSG00000030592	*Ryr1*	4.26E-06	1.541763
ENSMUSG00000022126	*Acod1*	2.57E-26	1.541705
ENSMUSG00000023034	*Nr4a1*	1.81E-17	1.541288
ENSMUSG00000000982	*Ccl3*	6.13E-15	1.541237
ENSMUSG00000078763	*Slfn1*	5.73E-17	1.541102
ENSMUSG00000043953	*Ccrl2*	5.73E-17	1.540659
ENSMUSG00000021250	*Fos*	1.14E-13	1.540618
ENSMUSG00000113998	*Gm40909*	1.24E-05	1.539072
ENSMUSG00000055775	*Myh8*	3.34E-07	1.538545
ENSMUSG00000113778	*Gm40847*	4.05E-02	1.537382
ENSMUSG00000003752	*Itpkc*	4.85E-21	1.537115
ENSMUSG00000039236	*Isg20*	3.09E-19	1.536846
ENSMUSG00000095891	*Gm10717*	4.11E-02	1.536618
ENSMUSG00000039001	*Rps21*	9.90E-03	1.536396
ENSMUSG00000082884	*Gm13339*	7.50E-04	1.536237
ENSMUSG00000048003	*Catsper4*	8.39E-03	1.535787
ENSMUSG00000078122	*F630028O10Rik*	4.20E-06	1.533738
ENSMUSG00000026896	*Ifih1*	3.30E-37	1.533564
ENSMUSG00000044162	*Tnip3*	1.14E-13	1.533448
ENSMUSG00000060988	*Galnt13*	9.45E-06	1.532422
ENSMUSG00000114980	*4933432I03Rik*	8.97E-11	1.532082
ENSMUSG00000022026	*Olfm4*	2.93E-15	1.531757
ENSMUSG00000051627	*Hist1h1e*	2.39E-07	1.530874
ENSMUSG00000088835	*Gm23547*	1.43E-04	1.528212
ENSMUSG00000024912	*Fosl1*	1.80E-06	1.524675
ENSMUSG00000062345	*Serpinb2*	8.22E-08	1.524046
ENSMUSG00000038418	*Egr1*	4.00E-21	1.523384
ENSMUSG00000095280	*Gm21738*	2.33E-02	1.52126
ENSMUSG00000026407	*Cacna1s*	4.38E-06	1.519984
ENSMUSG00000074146	*4930579C12Rik*	7.58E-07	1.519858
ENSMUSG00000099250	*Rn7s2*	1.74E-02	1.51752
ENSMUSG00000099021	*Rn7s1*	1.74E-02	1.517472
ENSMUSG00000059326	*Csf2ra*	1.63E-03	1.517321
ENSMUSG00000089999	*Gm6485*	5.58E-09	1.517
ENSMUSG00000043165	*Lor*	8.24E-05	1.516516
ENSMUSG00000105195	*Gm43584*	5.14E-04	1.516166
ENSMUSG00000089929	*Bcl2a1b*	2.06E-12	1.515751
ENSMUSG00000081857	*Gm13624*	3.76E-02	1.515199
ENSMUSG00000030787	*Lyve1*	1.11E-18	1.514832
ENSMUSG00000116848	*AC138306.1*	1.12E-11	1.514698

ENSMUSG00000104348	*Gm37691*	6.21E-04	1.514665
ENSMUSG00000066861	*Oas1g*	1.81E-08	1.514221
ENSMUSG00000020108	*Ddit4*	2.93E-14	1.513448
ENSMUSG00000089762	*Ier5l*	3.07E-03	1.513212
ENSMUSG00000095616	*Gm26244*	3.81E-02	1.513043
ENSMUSG00000098178	*Gm42418*	7.46E-03	1.512104
ENSMUSG00000081695	*Rpsa-ps5*	2.21E-02	1.510847
ENSMUSG00000073402	*Gm8909*	3.59E-08	1.510563
ENSMUSG00000086591	*Dnah2os*	1.17E-02	1.509414
ENSMUSG00000105398	*Gm47305*	1.69E-02	1.508695
ENSMUSG00000106279	*Gm47287*	1.69E-02	1.508691
ENSMUSG00000087700	*Gm15283*	2.52E-02	1.508122
ENSMUSG00000039070	*Cpa4*	3.68E-02	1.507901
ENSMUSG00000075122	*Cd80*	2.72E-16	1.507703
ENSMUSG00000069792	*Wfdc17*	2.78E-06	1.507287
ENSMUSG00000069372	*Ctxn3*	3.67E-03	1.507089
ENSMUSG00000087590	*Epb41l4aos*	1.11E-02	1.506513
ENSMUSG00000026981	*Il1rn*	3.16E-19	1.505344
ENSMUSG00000026452	*Syt2*	1.70E-09	1.505325
ENSMUSG00000000204	*Slfn4*	4.49E-06	1.504687
ENSMUSG00000046961	*Gpr156*	2.21E-03	1.504602
ENSMUSG00000070692	*Rps12-ps10*	4.70E-02	1.504592
ENSMUSG00000087881	*Gm22442*	1.39E-03	1.50459
ENSMUSG00000086290	*Snhg12*	4.30E-06	1.504012
ENSMUSG00000026121	*Sema4c*	6.49E-23	1.503955
ENSMUSG00000087006	*Gm13889*	6.41E-14	1.501606
ENSMUSG00000102496	*Gm36989*	8.23E-03	1.501532
ENSMUSG00000079597	*Gm5483*	3.51E-09	1.500636
ENSMUSG00000041117	*Ccdc8*	4.06E-05	1.500681
ENSMUSG00000058571	*Gpc6*	1.32E-14	1.500895
ENSMUSG00000036411	*9530077C05Rik*	6.19E-05	1.501083
ENSMUSG00000052117	*D630039A03Rik*	2.45E-02	1.502702
ENSMUSG00000104168	*Gm38250*	2.20E-02	1.503235
ENSMUSG00000075410	*Prcd*	1.29E-02	1.506303
ENSMUSG00000100005	*B130024G19Rik*	2.07E-17	1.507802
ENSMUSG00000075592	*Nynrin*	6.90E-13	1.509107
ENSMUSG00000038236	*Hoxa7*	4.80E-02	1.509405
ENSMUSG00000091183	*Gm5141*	4.66E-03	1.509918
ENSMUSG00000110206	*Flt3l*	1.03E-05	1.510135
ENSMUSG00000078870	*Gm14410*	1.70E-12	1.510221
ENSMUSG00000048402	*Gli2*	2.01E-16	1.510632
ENSMUSG00000027318	*Adam33*	7.24E-05	1.510692
ENSMUSG00000070867	*Trabd2b*	1.19E-23	1.510708
ENSMUSG00000002346	*Slc25a42*	3.08E-09	1.51104
ENSMUSG00000038119	*Cdon*	2.13E-13	1.511472
ENSMUSG00000000901	*Mmp11*	5.59E-04	1.511928
ENSMUSG00000030125	*Lrrc23*	5.32E-04	1.514186
ENSMUSG00000021708	*Rasgrf2*	3.43E-12	1.514585
ENSMUSG00000030494	*Rhpn2*	6.96E-09	1.515185
ENSMUSG00000042788	*Fam166b*	4.27E-02	1.515671
ENSMUSG00000024206	*Rfx2*	1.63E-11	1.516097
ENSMUSG00000026494	*Kif26b*	4.56E-12	1.516931
ENSMUSG00000017167	*Cntnap1*	8.30E-04	1.517416
ENSMUSG00000022456	*3-Sep*	6.51E-04	1.518584
ENSMUSG00000086158	*Ccpg1os*	2.54E-02	1.519402
ENSMUSG00000060548	*Tnfrsf19*	1.99E-11	1.519979
ENSMUSG00000031665	*Sall1*	1.66E-02	1.520783

ENSMUSG00000020642	*Rnf144a*	4.31E-15	1.521445
ENSMUSG00000085517	*Gm12963*	2.62E-08	1.522068
ENSMUSG00000026785	*Pkn3*	1.39E-05	1.522559
ENSMUSG00000041429	*Nthl1*	1.53E-02	1.522772
ENSMUSG00000099564	*Gm28729*	3.26E-02	1.52279
ENSMUSG00000050751	*Pgbd5*	3.26E-03	1.523024
ENSMUSG00000024063	*Lbh*	1.62E-22	1.524459
ENSMUSG00000051590	*Map3k19*	2.04E-03	1.524752
ENSMUSG00000026109	*Tmeff2*	7.24E-05	1.524936
ENSMUSG00000023266	*Frs3*	3.39E-02	1.525124
ENSMUSG00000019945	*Cabcoco1*	1.24E-04	1.52674
ENSMUSG00000026259	*Ngef*	2.29E-07	1.529308
ENSMUSG00000034522	*Zfp395*	1.20E-09	1.531411
ENSMUSG00000101801	*1700020G17Rik*	1.60E-08	1.531815
ENSMUSG00000027656	*Wisp2*	1.30E-21	1.531853
ENSMUSG00000022199	*Slc22a17*	3.25E-05	1.532662
ENSMUSG00000045875	*Adra1a*	2.84E-04	1.533756
ENSMUSG00000072601	*Ear1*	4.22E-05	1.534311
ENSMUSG00000037492	*Zmat4*	1.17E-06	1.534582
ENSMUSG00000050541	*Adra1b*	9.82E-06	1.535536
ENSMUSG00000050014	*Apol10b*	1.20E-02	1.536867
ENSMUSG00000059824	*Dbp*	3.21E-07	1.537822
ENSMUSG00000026691	*Fmo3*	6.57E-08	1.538988
ENSMUSG00000085024	*C230035I16Rik*	9.71E-03	1.539108
ENSMUSG00000026347	*Tmem163*	2.07E-16	1.541624
ENSMUSG00000097591	*A330032B11Rik*	4.27E-02	1.541666
ENSMUSG00000075389	*2810410L24Rik*	2.04E-04	1.542084
ENSMUSG00000022543	*4930451G09Rik*	1.75E-02	1.543206
ENSMUSG00000106951	*5930430L01Rik*	7.93E-03	1.544424
ENSMUSG00000022758	*P2rx6*	8.50E-04	1.545377
ENSMUSG00000026888	*Grb14*	2.00E-26	1.54642
ENSMUSG00000026824	*Kcnj3*	9.08E-11	1.547942
ENSMUSG00000045555	*Mettl24*	1.86E-10	1.550112
ENSMUSG00000022053	*Ebf2*	8.28E-10	1.550167
ENSMUSG00000031489	*Adrb3*	2.08E-05	1.550335
ENSMUSG00000074384	*AI429214*	2.69E-02	1.55054
ENSMUSG00000054021	*Sirt5*	4.74E-06	1.551042
ENSMUSG00000055945	*Prr18*	5.17E-03	1.551295
ENSMUSG00000033595	*Lgi3*	1.84E-11	1.55237
ENSMUSG00000103183	*Gm37090*	2.52E-03	1.5557
ENSMUSG00000061601	*Pclo*	1.11E-04	1.555835
ENSMUSG00000112714	*Gm4798*	2.86E-05	1.556475
ENSMUSG00000020182	*Ddc*	2.94E-02	1.556886
ENSMUSG00000030041	*M1ap*	4.17E-06	1.556913
ENSMUSG00000066319	*Rtp3*	1.02E-03	1.559718
ENSMUSG00000013089	*Etv5*	2.23E-20	1.561183
ENSMUSG00000097805	*Gm17473*	3.87E-07	1.561625
ENSMUSG00000017309	*Cd300lg*	4.88E-06	1.561748
ENSMUSG00000085982	*9530051G07Rik*	4.48E-02	1.563023
ENSMUSG00000029053	*Prkcz*	4.17E-13	1.563284
ENSMUSG00000030607	*Acan*	9.06E-03	1.563675
ENSMUSG00000046456	*Tmem150b*	1.36E-03	1.564973
ENSMUSG00000093479	*Gm20629*	2.73E-09	1.565239
ENSMUSG00000037610	*Kcnmb2*	7.66E-08	1.5685
ENSMUSG00000086368	*Gm13830*	7.26E-03	1.569182
ENSMUSG00000043088	*Il17re*	2.31E-04	1.569494
ENSMUSG00000016262	*Sertad4*	6.83E-03	1.56952

ENSMUSG00000020682	*Mmp28*	4.74E-10	1.570816
ENSMUSG00000084939	*Gm830*	1.84E-02	1.572365
ENSMUSG00000039763	*Dnajc28*	3.97E-02	1.575323
ENSMUSG00000020734	*Grin2c*	3.03E-02	1.577359
ENSMUSG00000026676	*Ccdc3*	6.28E-11	1.578234
ENSMUSG00000028871	*Rspo1*	1.42E-02	1.579214
ENSMUSG00000017007	*Rbpjl*	8.03E-08	1.581836
ENSMUSG00000019831	*Wasf1*	2.22E-02	1.583533
ENSMUSG00000042793	*Lgr6*	1.16E-16	1.585253
ENSMUSG00000087424	*5730405O15Rik*	2.20E-02	1.587279
ENSMUSG00000078794	*Dact3*	2.02E-05	1.590225
ENSMUSG00000095079	*Igha*	8.37E-05	1.592326
ENSMUSG00000050022	*Amz1*	5.27E-05	1.593171
ENSMUSG00000036854	*Hspb6*	2.04E-03	1.597689
ENSMUSG00000021719	*Rgs7bp*	2.95E-09	1.59776
ENSMUSG00000025902	*Sox17*	1.02E-13	1.598591
ENSMUSG00000074219	*Gm10644*	2.18E-02	1.598961
ENSMUSG00000037846	*Rtkn2*	5.55E-07	1.598991
ENSMUSG00000102082	*Gm28675*	4.81E-02	1.599203
ENSMUSG00000086141	*9030622O22Rik*	1.25E-10	1.604845
ENSMUSG00000089941	*Gm16168*	1.79E-03	1.606211
ENSMUSG00000112468	*Gm47720*	2.62E-06	1.608526
ENSMUSG00000068323	*Slc4a5*	6.46E-08	1.609607
ENSMUSG00000116097	*Gm36738*	2.28E-02	1.611492
ENSMUSG00000019312	*Grb7*	8.16E-04	1.611956
ENSMUSG00000059659	*Gm10069*	3.68E-05	1.612558
ENSMUSG00000031220	*Awat2*	1.41E-02	1.613621
ENSMUSG00000090206	*Tepp*	4.13E-03	1.616264
ENSMUSG00000087514	*Gm16076*	2.99E-02	1.62071
ENSMUSG00000041351	*Rap1gap*	2.36E-09	1.621611
ENSMUSG00000069378	*Prdm6*	1.85E-18	1.623444
ENSMUSG00000036923	*Stox1*	5.18E-07	1.623817
ENSMUSG00000050288	*Fzd2*	8.28E-04	1.624159
ENSMUSG00000086607	*4930511M06Rik*	6.52E-03	1.624741
ENSMUSG00000034685	*Fam171a2*	6.79E-04	1.62484
ENSMUSG00000062542	*Syt9*	1.57E-02	1.627124
ENSMUSG00000007279	*Scube2*	2.67E-18	1.629611
ENSMUSG00000054057	*A930004D18Rik*	3.30E-02	1.629982
ENSMUSG00000066438	*Plekhd1*	2.77E-07	1.631307
ENSMUSG00000085682	*Gm14267*	1.18E-03	1.635757
ENSMUSG00000074793	*Hspa12b*	6.74E-21	1.635809
ENSMUSG00000030495	*Slc7a10*	3.89E-09	1.637942
ENSMUSG00000033590	*Myo5c*	1.66E-15	1.641777
ENSMUSG00000030562	*Nox4*	8.94E-09	1.642642
ENSMUSG00000083817	*Gm14400*	1.77E-02	1.642954
ENSMUSG00000099553	*Gm29538*	1.68E-03	1.64385
ENSMUSG00000058420	*Syt17*	3.26E-06	1.643854
ENSMUSG00000054459	*Vsnl1*	1.48E-12	1.644077
ENSMUSG00000037973	*Ccdc129*	8.09E-09	1.644828
ENSMUSG00000059146	*Ntrk3*	4.47E-22	1.645531
ENSMUSG00000056155	*Nanos3*	4.06E-03	1.646041
ENSMUSG00000106749	*Gm43281*	3.37E-06	1.64753
ENSMUSG00000072599	*Ear-ps2*	8.09E-03	1.648472
ENSMUSG00000069518	*Gm10271*	4.49E-02	1.649982
ENSMUSG00000074771	*Ankef1*	3.41E-04	1.656591
ENSMUSG00000041479	*Syt15*	1.37E-05	1.659181
ENSMUSG00000049511	*Htr1b*	2.21E-04	1.662514

ENSMUSG00000063430	*Wscd2*	1.63E-07	1.662763
ENSMUSG00000086596	*Susd5*	3.88E-05	1.663486
ENSMUSG00000011263	*Exoc3l2*	2.11E-02	1.671039
ENSMUSG00000034584	*Exph5*	2.07E-17	1.671345
ENSMUSG00000022840	*Adcy5*	1.15E-24	1.673312
ENSMUSG00000028801	*Stpg1*	1.90E-04	1.675936
ENSMUSG00000027827	*Kcnab1*	1.06E-12	1.685414
ENSMUSG00000020614	*Fam20a*	7.24E-19	1.686889
ENSMUSG00000021499	*Catsper3*	7.33E-03	1.687729
ENSMUSG00000085171	*D830026I12Rik*	4.25E-02	1.689753
ENSMUSG00000035435	*Abca17*	2.81E-10	1.692557
ENSMUSG00000030043	*Tacr1*	7.60E-05	1.693777
ENSMUSG00000041020	*Map7d2*	2.75E-02	1.695372
ENSMUSG00000110380	*Gm45332*	6.76E-03	1.695675
ENSMUSG00000105376	*Gm36535*	1.64E-02	1.696479
ENSMUSG00000101605	*Ace3*	1.74E-05	1.696685
ENSMUSG00000037709	*Fam13a*	2.63E-08	1.704891
ENSMUSG00000109165	*Gm45148*	5.67E-03	1.705895
ENSMUSG00000020169	*Best3*	1.46E-07	1.71572
ENSMUSG00000048728	*Zfp454*	4.49E-02	1.717216
ENSMUSG00000028755	*Cda*	1.99E-02	1.717754
ENSMUSG00000085282	*Gm15663*	1.21E-02	1.718236
ENSMUSG00000048096	*Lmod1*	9.53E-07	1.718553
ENSMUSG00000103738	*Gm37652*	1.24E-03	1.722127
ENSMUSG00000108580	*Gm39094*	1.47E-22	1.733461
ENSMUSG00000027380	*Acoxl*	2.48E-08	1.733573
ENSMUSG00000063535	*Zfp773*	3.78E-03	1.735884
ENSMUSG00000027186	*Elf5*	3.75E-05	1.74138
ENSMUSG00000029193	*Cckar*	1.05E-05	1.742803
ENSMUSG00000108767	*Gm29763*	2.99E-02	1.742917
ENSMUSG00000032357	*Tinag*	2.33E-06	1.748176
ENSMUSG00000092515	*C87198*	4.36E-02	1.750226
ENSMUSG00000070661	*Rnf186*	4.40E-02	1.752275
ENSMUSG00000030380	*Mzf1*	1.63E-02	1.763149
ENSMUSG00000042428	*Mgat3*	6.40E-12	1.763723
ENSMUSG00000044708	*Kcnj10*	2.22E-02	1.767881
ENSMUSG00000041423	*Paqr6*	2.72E-02	1.768799
ENSMUSG00000089712	*Gm15889*	6.62E-03	1.770295
ENSMUSG00000063730	*Hsd3b2*	2.08E-02	1.773821
ENSMUSG00000101693	*Gm19461*	2.09E-02	1.777561
ENSMUSG00000064294	*Aox3*	3.77E-15	1.778141
ENSMUSG00000086313	*Gm15940*	2.10E-02	1.780429
ENSMUSG00000044694	*2010007H06Rik*	1.51E-06	1.781054
ENSMUSG00000108481	*Gm33248*	4.21E-13	1.784046
ENSMUSG00000061397	*Krt79*	6.09E-04	1.786124
ENSMUSG00000094786	*Gm14403*	1.13E-16	1.786856
ENSMUSG00000079436	*Kcnj13*	4.22E-02	1.78992
ENSMUSG00000038233	*Fam198a*	1.05E-06	1.790914
ENSMUSG00000042256	*Ptchd4*	7.00E-05	1.791307
ENSMUSG00000052026	*Slc6a7*	4.86E-05	1.792733
ENSMUSG00000097124	*A530020G20Rik*	7.37E-06	1.792876
ENSMUSG00000048988	*Elfn1*	1.27E-13	1.803612
ENSMUSG00000057719	*Sh3rf2*	2.42E-19	1.804366
ENSMUSG00000111761	*9230112J17Rik*	3.13E-04	1.810487
ENSMUSG00000027886	*1700013F07Rik*	2.43E-02	1.810795
ENSMUSG00000082292	*Gm12250*	3.69E-06	1.81246
ENSMUSG00000049107	*Ntf3*	7.06E-20	1.821726

ENSMUSG00000068373	*D430041D05Rik*	5.87E-17	1.830741
ENSMUSG00000020566	*Atp6v1c2*	1.23E-25	1.832003
ENSMUSG00000114028	*9630002D21Rik*	3.96E-03	1.832354
ENSMUSG00000102590	*Mannr*	1.75E-04	1.836166
ENSMUSG00000006567	*Atp7b*	2.18E-17	1.836476
ENSMUSG00000076613	*Ighg2b*	2.30E-02	1.837406
ENSMUSG00000102437	*Gm38048*	2.54E-08	1.843504
ENSMUSG00000025577	*Cbx2*	1.42E-04	1.846281
ENSMUSG00000037279	*Ovol2*	2.30E-03	1.852727
ENSMUSG00000030093	*Wnt7a*	1.05E-06	1.855136
ENSMUSG00000097453	*Gm26894*	1.59E-03	1.856702
ENSMUSG00000087518	*Gm13561*	3.22E-03	1.859076
ENSMUSG00000044633	*B530045E10Rik*	8.05E-19	1.860022
ENSMUSG00000009394	*Syn2*	1.55E-17	1.865441
ENSMUSG00000085069	*Gm13111*	1.65E-04	1.866473
ENSMUSG00000079173	*Zan*	4.11E-04	1.868008
ENSMUSG00000030098	*Grip2*	4.24E-11	1.871182
ENSMUSG00000074575	*Kcng1*	4.71E-02	1.871584
ENSMUSG00000116766	*AC171205.1*	3.48E-02	1.87324
ENSMUSG00000027513	*Pck1*	3.53E-10	1.874273
ENSMUSG00000056824	*Zfp663*	6.72E-03	1.880195
ENSMUSG00000086843	*E030013I19Rik*	3.55E-05	1.886677
ENSMUSG00000108218	*Olfr1372-ps1*	6.73E-09	1.893798
ENSMUSG00000087413	*Gm11266*	3.96E-14	1.899133
ENSMUSG00000093550	*Higd1c*	3.35E-02	1.906324
ENSMUSG00000020335	*Zfp354b*	1.86E-02	1.906344
ENSMUSG00000027460	*Angpt4*	7.61E-09	1.918001
ENSMUSG00000036295	*Lrrn3*	4.53E-05	1.925128
ENSMUSG00000090166	*Ear10*	1.40E-06	1.929094
ENSMUSG00000099338	*2810030D12Rik*	6.44E-05	1.935947
ENSMUSG00000032502	*Stac*	6.19E-06	1.936727
ENSMUSG00000079039	*Gm11037*	2.50E-02	1.940577
ENSMUSG00000105786	*Gm18957*	1.48E-02	1.942241
ENSMUSG00000117322	*AC154766.4*	2.55E-02	1.953694
ENSMUSG00000022504	*Ciita*	2.96E-28	1.959704
ENSMUSG00000028919	*Arhgef19*	2.26E-03	1.968027
ENSMUSG00000110891	*Gm40639*	3.60E-02	1.972536
ENSMUSG00000104376	*Gm37516*	1.20E-02	1.974628
ENSMUSG00000029601	*Iqcd*	8.65E-03	1.990538
ENSMUSG00000026870	*Cutal*	1.79E-04	1.994395
ENSMUSG00000110631	*Gm42047*	5.59E-03	2.007803
ENSMUSG00000085882	*2610507I01Rik*	5.32E-05	2.01961
ENSMUSG00000109770	*Gm30085*	3.97E-02	2.026925
ENSMUSG00000086390	*1810019D21Rik*	1.01E-09	2.035809
ENSMUSG00000080797	*Gm15760*	2.06E-02	2.049068
ENSMUSG00000033849	*B3galt2*	1.86E-03	2.059198
ENSMUSG00000031725	*Ces1f*	6.83E-03	2.092553
ENSMUSG00000087500	*Gm12426*	5.91E-03	2.107058
ENSMUSG00000092004	*Gm17482*	9.93E-07	2.112466
ENSMUSG00000019909	*Fam162b*	5.07E-04	2.116376
ENSMUSG00000115307	*Gm49313*	1.84E-04	2.139641
ENSMUSG00000060275	*Nrg2*	7.68E-08	2.145009
ENSMUSG00000025789	*St8sia2*	1.28E-15	2.169809
ENSMUSG00000108390	*Gm39038*	1.64E-03	2.192189
ENSMUSG00000026147	*Col9a1*	1.56E-02	2.194131
ENSMUSG00000053961	*Ang5*	2.31E-03	2.198318
ENSMUSG00000086155	*9430041J12Rik*	2.78E-02	2.203234

ENSMUSG00000027796	*Smad9*	3.65E-14	2.220367
ENSMUSG00000103160	*C130012C08Rik*	2.01E-03	2.234457
ENSMUSG00000020081	*Tacr2*	1.82E-02	2.253652
ENSMUSG00000069830	*Nlrp1a*	2.69E-07	2.281738
ENSMUSG00000108617	*Gm31749*	6.04E-03	2.285686
ENSMUSG00000009900	*Wnt3a*	5.16E-09	2.298134
ENSMUSG00000027831	*Veph1*	9.72E-25	2.301924
ENSMUSG00000061171	*Slc38a11*	3.50E-05	2.353128
ENSMUSG00000001494	*Sost*	4.34E-04	2.412139
ENSMUSG00000026304	*Rab17*	1.09E-03	2.608575
ENSMUSG00000031551	*Ido1*	1.39E-05	3.239545
ENSMUSG00000092591	*Gm20429*	2.09E-04	3.383042
ENSMUSG00000071679	*Rtl4*	6.39E-21	4.582634
ENSMUSG00000085154	*C130046K22Rik*	1.28E-13	27.59869

Appendix T. Murine differential gene expression in the lungs 6 h post-infection, 947 vs 4559. Genes with fold change (FC) greater than 1.5 and $p < 0.05$ are shown. FC values highlighted in blue = upregulated in 947, while values highlighted in red = upregulated in 4559.

Gene Stable ID	Gene Name	padj	FC
ENSMUSG00000096349	*Gm22513*	3.77E-18	10.97464
ENSMUSG00000094668	*Gm24871*	1.29E-07	6.745915
ENSMUSG00000064899	*Snord118*	1.08E-09	6.570577
ENSMUSG00000097554	*Gm26825*	7.25E-04	5.791676
ENSMUSG00000109641	*Gm45556*	1.47E-03	5.598475
ENSMUSG00000105361	*AY036118*	3.15E-13	5.461151
ENSMUSG00000080538	*Gm25541*	4.06E-18	5.174635
ENSMUSG00000093843	*Gm25939*	7.29E-13	4.925819
ENSMUSG00000095676	*Gm25099*	9.26E-27	4.906139
ENSMUSG00000065870	*Rnu3a*	1.74E-16	4.884372
ENSMUSG00000106147	*Rnu3a*	1.74E-16	4.884372
ENSMUSG00000095738	*Gm25313*	8.71E-14	4.857934
ENSMUSG00000095892	*Rnu5g*	4.27E-14	4.78872
ENSMUSG00000104896	*Rnu3b4*	9.34E-24	4.622038
ENSMUSG00000098641	*Rnu3b4*	1.21E-23	4.615922
ENSMUSG00000099291	*Rnu3b3*	6.68E-23	4.590292
ENSMUSG00000104856	*Rnu3b3*	6.68E-23	4.590292
ENSMUSG00000105115	*Rnu3b2*	7.99E-24	4.578094
ENSMUSG00000098925	*Rnu3b2*	7.99E-24	4.578094
ENSMUSG00000098943	*Rnu3b1*	3.21E-23	4.559078
ENSMUSG00000105025	*Rnu3b1*	3.21E-23	4.559078
ENSMUSG00000085393	*Gm11280*	1.04E-03	4.538932
ENSMUSG00000064945	*Rny3*	1.19E-15	4.476071
ENSMUSG00000042385	*Gzmk*	5.37E-03	4.35977
ENSMUSG00000094050	*Gm23472*	1.36E-13	4.320851
ENSMUSG00000093956	*Gm24497*	4.43E-13	4.291089
ENSMUSG00000064856	*Gm23444*	2.34E-13	4.288303
ENSMUSG00000088675	*Rprl1*	2.41E-06	4.192998
ENSMUSG00000106222	*Rprl1*	2.41E-06	4.192998
ENSMUSG00000065176	*Rnu12*	1.99E-27	4.109879
ENSMUSG00000065701	*Rny1*	7.64E-13	4.069417
ENSMUSG00000065254	*Gm23973*	3.03E-06	4.059083
ENSMUSG00000032494	*Tdgf1*	1.92E-05	4.053171
ENSMUSG00000065820	*Gm26316*	9.85E-13	4.048075
ENSMUSG00000064682	*Gm25813*	9.90E-09	4.046294
ENSMUSG00000064702	*Gm24950*	3.05E-12	3.981116
ENSMUSG00000065251	*Gm23971*	3.05E-12	3.981116
ENSMUSG00000065944	*Rnu2-10*	2.22E-12	3.976161
ENSMUSG00000065767	*Gm23849*	3.07E-12	3.962822
ENSMUSG00000077323	*Rnu11*	6.04E-13	3.962105
ENSMUSG00000094377	*Gm24407*	2.62E-14	3.808851
ENSMUSG00000065232	*Gm22973*	6.93E-12	3.795942
ENSMUSG00000067455	*Hist1h4j*	3.60E-08	3.778868
ENSMUSG00000060093	*Hist1h4a*	2.31E-16	3.753049
ENSMUSG00000096243	*Gm24265*	2.84E-11	3.648484
ENSMUSG00000065845	*Gm25189*	2.58E-03	3.636942
ENSMUSG00000064943	*Gm23240*	2.39E-03	3.62003
ENSMUSG00000069300	*Hist1h2bj*	2.08E-05	3.616983
ENSMUSG00000095616	*Gm26244*	1.81E-09	3.585974
ENSMUSG00000088252	*Snord13*	3.16E-08	3.500728
ENSMUSG00000064941	*Gm23238*	2.49E-12	3.477513
ENSMUSG00000095969	*Rnu1a1*	4.33E-10	3.447212

ENSMUSG00000096659	*Gm25679*	2.63E-16	3.411828
ENSMUSG00000093815	*Gm26444*	2.63E-16	3.411828
ENSMUSG00000063021	*Hist1h2ak*	2.45E-03	3.406041
ENSMUSG00000095260	*Gm25890*	9.28E-10	3.34811
ENSMUSG00000094812	*Gm22614*	9.28E-10	3.34811
ENSMUSG00000064923	*Gm22042*	8.01E-10	3.347755
ENSMUSG00000095580	*Rnu1b1*	2.34E-09	3.347511
ENSMUSG00000093834	*Rnu1b2*	2.34E-09	3.347511
ENSMUSG00000094306	*Gm24924*	7.72E-09	3.330976
ENSMUSG00000095701	*Gm24830*	1.01E-09	3.296712
ENSMUSG00000096838	*Gm26232*	1.01E-09	3.296712
ENSMUSG00000065773	*Rnu1b6*	1.01E-09	3.296712
ENSMUSG00000094826	*Gm23804*	3.33E-15	3.281135
ENSMUSG00000097131	*D230017M19Rik*	7.32E-15	3.266318
ENSMUSG00000069266	*Hist1h4b*	3.25E-06	3.259907
ENSMUSG00000060981	*Hist1h4h*	4.37E-17	3.254606
ENSMUSG00000101355	*Hist1h3h*	1.42E-03	3.179868
ENSMUSG00000099517	*Hist1h3g*	1.06E-03	3.159837
ENSMUSG00000010362	*Rdm1*	1.06E-11	3.14031
ENSMUSG00000081684	*Rps2-ps13*	4.23E-24	3.13385
ENSMUSG00000069305	*Hist1h4n*	4.43E-08	3.133044
ENSMUSG00000065905	*Gm26110*	1.16E-04	3.130131
ENSMUSG00000069306	*Hist1h4m*	5.27E-07	3.127821
ENSMUSG00000095217	*Hist1h2bn*	2.95E-06	3.119423
ENSMUSG00000064288	*Hist1h4k*	1.87E-08	3.117272
ENSMUSG00000080465	*Gm22486*	2.90E-09	3.11249
ENSMUSG00000047061	*Gm9817*	3.14E-02	3.110749
ENSMUSG00000087963	*Gm25394*	2.00E-03	3.095042
ENSMUSG00000115420	*AL732506.1*	2.92E-15	3.080505
ENSMUSG00000088088	*Rmrp*	2.92E-15	3.080505
ENSMUSG00000096205	*Gm22068*	3.77E-09	3.06075
ENSMUSG00000094655	*Gm25360*	1.37E-14	3.058749
ENSMUSG00000060678	*Hist1h4c*	2.01E-18	3.058247
ENSMUSG00000065824	*Gm26315*	1.04E-11	3.053521
ENSMUSG00000092837	*Rpph1*	4.58E-09	3.031887
ENSMUSG00000088025	*Rprl3*	2.03E-07	3.027158
ENSMUSG00000099583	*Hist1h3d*	3.33E-04	3.01984
ENSMUSG00000071470	*Ccnb1ip1*	4.41E-09	3.011385
ENSMUSG00000065911	*Gm24447*	2.34E-11	2.998729
ENSMUSG00000064694	*Gm24146*	5.78E-07	2.99441
ENSMUSG00000092805	*Gm26461*	4.04E-09	2.980919
ENSMUSG00000069274	*Hist1h4f*	2.64E-07	2.963294
ENSMUSG00000096214	*Gm22634*	3.07E-14	2.955618
ENSMUSG00000096206	*Gm22317*	3.07E-14	2.955618
ENSMUSG00000087775	*Rprl2*	5.59E-07	2.949971
ENSMUSG00000061482	*Hist1h4d*	5.96E-25	2.947909
ENSMUSG00000092819	*Gm23639*	1.31E-03	2.911866
ENSMUSG00000023467	*Tulp2*	8.88E-03	2.887985
ENSMUSG00000010342	*Tex14*	2.11E-12	2.887178
ENSMUSG00000092702	*Gm24514*	3.30E-08	2.857933
ENSMUSG00000105790	*Gm24105*	1.12E-10	2.857786
ENSMUSG00000087943	*Gm24245*	4.70E-13	2.854799
ENSMUSG00000100210	*Hist1h3f*	1.45E-07	2.846879
ENSMUSG00000090625	*Gm20721*	5.27E-04	2.822061
ENSMUSG00000092674	*Gm24105*	1.19E-10	2.820054
ENSMUSG00000046242	*Nme9*	4.34E-05	2.796067
ENSMUSG00000064604	*Snora44*	7.00E-06	2.781139

ENSMUSG00000114279	*Hist1h2bm*	1.67E-03	2.777077
ENSMUSG00000058385	*Hist1h2bg*	2.78E-09	2.77039
ENSMUSG00000064901	*Snora21*	9.99E-04	2.75448
ENSMUSG00000101972	*Hist1h3i*	1.08E-03	2.745319
ENSMUSG00000070167	*Snora57*	2.32E-12	2.741946
ENSMUSG00000069265	*Hist1h3a*	1.82E-03	2.720348
ENSMUSG00000064451	*Snora23*	9.44E-04	2.713527
ENSMUSG00000091383	*Hist1h2al*	5.55E-14	2.672474
ENSMUSG00000114456	*Hist1h2bh*	2.26E-05	2.669249
ENSMUSG00000068855	*Hist2h2ac*	1.06E-06	2.662418
ENSMUSG00000088008	*Gm25492*	6.86E-05	2.660852
ENSMUSG00000105145	*Gm47299*	1.14E-08	2.652374
ENSMUSG00000105788	*Gm47295*	1.14E-08	2.652269
ENSMUSG00000105399	*Mir1843b*	7.66E-03	2.649552
ENSMUSG00000065686	*Snora5c*	9.51E-04	2.647534
ENSMUSG00000062727	*Hist1h2bk*	1.21E-05	2.647047
ENSMUSG00000090208	*Gm15851*	4.93E-02	2.646
ENSMUSG00000096992	*Gm26788*	1.53E-02	2.640965
ENSMUSG00000092386	*Gm20536*	1.21E-02	2.615154
ENSMUSG00000057596	*Trim30d*	2.24E-12	2.613284
ENSMUSG00000064999	*Gm26035*	7.18E-09	2.608373
ENSMUSG00000069267	*Hist1h3b*	1.04E-03	2.564833
ENSMUSG00000093355	*Snora26*	1.95E-02	2.562115
ENSMUSG00000069273	*Hist1h3e*	5.25E-08	2.556766
ENSMUSG00000064994	*Gm22422*	9.17E-05	2.54989
ENSMUSG00000060988	*Galnt13*	1.31E-22	2.547254
ENSMUSG00000081342	*Gm11434*	1.83E-02	2.528216
ENSMUSG00000065649	*Snora74a*	1.80E-07	2.526072
ENSMUSG00000064655	*Gm25788*	1.04E-03	2.525134
ENSMUSG00000097799	*Gm26899*	2.35E-02	2.488561
ENSMUSG00000065145	*Vaultrc5*	2.35E-06	2.476147
ENSMUSG00000085465	*Gm15347*	1.42E-02	2.4729
ENSMUSG00000075031	*Hist1h2bb*	2.05E-04	2.467707
ENSMUSG00000087819	*Gm25117*	1.17E-09	2.467012
ENSMUSG00000074403	*Hist2h3b*	1.52E-03	2.454729
ENSMUSG00000077254	*Gm26079*	1.78E-05	2.438855
ENSMUSG00000115783	*Bc1*	1.63E-04	2.432863
ENSMUSG00000098178	*Gm42418*	3.40E-10	2.426788
ENSMUSG00000065087	*Snord22*	4.68E-20	2.423107
ENSMUSG00000094338	*Hist1h2bl*	5.96E-06	2.421661
ENSMUSG00000096010	*Hist4h4*	1.32E-07	2.421203
ENSMUSG00000076614	*Ighg1*	3.86E-02	2.417765
ENSMUSG00000089536	*Scarna3a*	8.57E-03	2.411926
ENSMUSG00000069268	*Hist1h2bf*	6.11E-03	2.41015
ENSMUSG00000076258	*Gm23935*	6.42E-13	2.406898
ENSMUSG00000097346	*Gm26619*	2.89E-02	2.388088
ENSMUSG00000080365	*Gm25776*	3.68E-05	2.383555
ENSMUSG00000076281	*Gm24270*	1.12E-10	2.373892
ENSMUSG00000097815	*Gm26809*	2.33E-02	2.371395
ENSMUSG00000114969	*Hba-ps3*	9.14E-04	2.369228
ENSMUSG00000065778	*Gm22154*	1.68E-02	2.34964
ENSMUSG00000105448	*Gm25820*	1.08E-02	2.348821
ENSMUSG00000105288	*Gm25820*	1.08E-02	2.348821
ENSMUSG00000064966	*Snord15b*	1.44E-06	2.333139
ENSMUSG00000069308	*Hist1h2bp*	3.62E-03	2.322081
ENSMUSG00000035299	*Mid1*	4.01E-07	2.316383
ENSMUSG00000085790	*Gm12729*	2.53E-02	2.316346

ENSMUSG00000088529	*Gm26083*	2.80E-05	2.314116
ENSMUSG00000113512	*Gm9063*	3.83E-02	2.306271
ENSMUSG00000069310	*Hist1h3c*	2.34E-03	2.302294
ENSMUSG00000115432	*D130009I18Rik*	2.70E-03	2.300679
ENSMUSG00000004814	*Ccl24*	9.80E-03	2.290894
ENSMUSG00000091957	*Rps2-ps10*	1.37E-12	2.275718
ENSMUSG00000077611	*Gm23946*	4.84E-02	2.264088
ENSMUSG00000088609	*Gm24187*	3.72E-12	2.233571
ENSMUSG00000099250	*Rn7s2*	5.82E-07	2.228017
ENSMUSG00000099021	*Rn7s1*	5.82E-07	2.227961
ENSMUSG00000095590	*Gm24305*	2.92E-02	2.221176
ENSMUSG00000060639	*Hist1h4i*	5.98E-05	2.218385
ENSMUSG00000082755	*Gm8692*	3.31E-04	2.214971
ENSMUSG00000112246	*Gm40761*	4.75E-02	2.182331
ENSMUSG00000105398	*Gm47305*	8.24E-07	2.175963
ENSMUSG00000106279	*Gm47287*	8.24E-07	2.175954
ENSMUSG00000063954	*Hist2h2aa2*	3.09E-07	2.164586
ENSMUSG00000052305	*Hbb-bs*	1.32E-07	2.16149
ENSMUSG00000104863	*Gm49347*	2.14E-04	2.145847
ENSMUSG00000064380	*Gm26448*	4.40E-09	2.145839
ENSMUSG00000088246	*Gm25911*	7.67E-12	2.145126
ENSMUSG00000089255	*Snora78*	1.36E-02	2.137569
ENSMUSG00000085297	*Gm11651*	5.25E-03	2.127159
ENSMUSG00000058773	*Hist1h1b*	8.95E-05	2.120617
ENSMUSG00000064220	*Hist2h2aa1*	3.10E-04	2.117751
ENSMUSG00000104740	*Mir6516*	9.92E-04	2.113466
ENSMUSG00000046229	*Scand1*	1.44E-02	2.111608
ENSMUSG00000064387	*Snora73a*	7.47E-12	2.088608
ENSMUSG00000085261	*Gm13814*	1.41E-02	2.077594
ENSMUSG00000080542	*Gm22710*	2.43E-03	2.074884
ENSMUSG00000091993	*B930036N10Rik*	2.07E-03	2.07144
ENSMUSG00000112831	*AC167229.1*	2.82E-02	2.068995
ENSMUSG00000091405	*Hist2h4*	9.28E-10	2.052495
ENSMUSG00000046031	*Calhm6*	1.74E-06	2.048611
ENSMUSG00000084708	*Gm22988*	5.06E-06	2.038794
ENSMUSG00000031289	*Il13ra2*	4.46E-05	2.025167
ENSMUSG00000088185	*Scarna2*	2.45E-08	2.024717
ENSMUSG00000029635	*Cdk8*	3.25E-10	2.022129
ENSMUSG00000088789	*Scarna13*	1.73E-06	2.017749
ENSMUSG00000026573	*Xcl1*	3.45E-03	2.016054
ENSMUSG00000100992	*Gm23925*	3.22E-02	2.01348
ENSMUSG00000102189	*Gm37194*	5.60E-06	2.000652
ENSMUSG00000077167	*Gm24119*	9.88E-03	1.997643
ENSMUSG00000065637	*Gm26397*	4.01E-07	1.997637
ENSMUSG00000084744	*Gm25291*	4.03E-03	1.99723
ENSMUSG00000106649	*Gm49349*	1.43E-06	1.993359
ENSMUSG00000064405	*Gm23925*	3.66E-02	1.98704
ENSMUSG00000082516	*Gm13342*	1.02E-02	1.981125
ENSMUSG00000027233	*Patl2*	3.08E-02	1.979645
ENSMUSG00000092746	*Rn7s6*	1.82E-05	1.965498
ENSMUSG00000073940	*Hbb-bt*	8.75E-06	1.965051
ENSMUSG00000103336	*Gm37993*	4.98E-02	1.954663
ENSMUSG00000100831	*Gm17847*	1.84E-02	1.954622
ENSMUSG00000081058	*Hist2h3c2*	2.98E-03	1.954493
ENSMUSG00000065118	*Gm23297*	1.62E-02	1.944291
ENSMUSG00000030670	*Cyp2r1*	1.52E-02	1.939325
ENSMUSG00000107722	*2900060B14Rik*	3.88E-03	1.935981

ENSMUSG00000001983	*Taco1*	6.95E-08	1.933656
ENSMUSG00000065226	*Gm25791*	3.01E-06	1.926078
ENSMUSG00000062461	*Gm5453*	8.46E-10	1.924129
ENSMUSG00000104690	*Gm47304*	3.05E-05	1.920177
ENSMUSG00000065037	*Rn7sk*	2.04E-05	1.917124
ENSMUSG00000069917	*Hba-a2*	3.52E-13	1.915594
ENSMUSG00000055170	*Ifng*	5.97E-03	1.914606
ENSMUSG00000064841	*Gm26205*	1.80E-02	1.910409
ENSMUSG00000090101	*Snhg9*	2.49E-02	1.888943
ENSMUSG00000065353	*Snora73b*	9.17E-05	1.888933
ENSMUSG00000113136	*Gm19951*	1.01E-03	1.888218
ENSMUSG00000113465	*Gm40271*	5.45E-03	1.872958
ENSMUSG00000066629	*Rpl36-ps3*	5.45E-03	1.872958
ENSMUSG00000024205	*Rpl36-ps2*	1.48E-07	1.856283
ENSMUSG00000089617	*Scarna10*	3.70E-04	1.856044
ENSMUSG00000099587	*Gm28967*	3.70E-04	1.856044
ENSMUSG00000022658	*Tagln3*	3.59E-03	1.852149
ENSMUSG00000117074	*AC121299.1*	4.22E-02	1.849145
ENSMUSG00000087968	*Gm25395*	7.59E-06	1.841096
ENSMUSG00000052565	*Hist1h1d*	8.37E-06	1.839687
ENSMUSG00000091955	*Gm9844*	3.52E-18	1.837563
ENSMUSG00000086196	*Gm13571*	3.25E-04	1.836858
ENSMUSG00000064853	*Gm23442*	2.97E-04	1.832979
ENSMUSG00000077714	*Snord17*	3.52E-04	1.822824
ENSMUSG00000069919	*Hba-a1*	8.16E-13	1.822782
ENSMUSG00000020641	*Rsad2*	3.37E-12	1.822486
ENSMUSG00000049539	*Hist1h1a*	7.38E-03	1.821165
ENSMUSG00000069307	*Hist1h2bq*	4.15E-05	1.818275
ENSMUSG00000035528	*Npffr2*	7.77E-03	1.814241
ENSMUSG00000027220	*Syt13*	1.11E-02	1.812055
ENSMUSG00000067321	*Gm7931*	3.36E-02	1.81009
ENSMUSG00000085348	*Myhas*	3.50E-03	1.803894
ENSMUSG00000065822	*Snord15a*	1.55E-02	1.803286
ENSMUSG00000063234	*Gpr84*	1.21E-08	1.800134
ENSMUSG00000085241	*Snhg3*	6.58E-07	1.798898
ENSMUSG00000085573	*Gm15418*	4.34E-02	1.79681
ENSMUSG00000065304	*Gm23245*	2.53E-02	1.794865
ENSMUSG00000003545	*Fosb*	2.44E-06	1.793447
ENSMUSG00000089762	*Ier5l*	3.00E-05	1.79236
ENSMUSG00000057465	*Saa2*	5.73E-09	1.789508
ENSMUSG00000053553	*3110082I17Rik*	9.75E-15	1.769663
ENSMUSG00000109875	*Gm45456*	4.92E-03	1.768914
ENSMUSG00000069303	*Hist1h2br*	8.01E-05	1.766683
ENSMUSG00000100969	*1700030N03Rik*	1.27E-04	1.764586
ENSMUSG00000053626	*Tll1*	3.72E-29	1.754673
ENSMUSG00000037190	*Cyb561d2*	9.84E-03	1.753648
ENSMUSG00000046470	*Sox18*	1.23E-13	1.751676
ENSMUSG00000044092	*C130050O18Rik*	1.22E-06	1.748316
ENSMUSG00000062778	*Chia1*	4.57E-20	1.747009
ENSMUSG00000035852	*Misp*	1.80E-10	1.74205
ENSMUSG00000025946	*Pth2r*	3.71E-02	1.730767
ENSMUSG00000113722	*Snhg10*	6.72E-05	1.728473
ENSMUSG00000020638	*Cmpk2*	9.44E-27	1.721661
ENSMUSG00000089281	*Scarna6*	1.62E-03	1.712381
ENSMUSG00000077563	*Snora68*	2.00E-03	1.708197
ENSMUSG00000114234	*Gm3131*	3.41E-02	1.706159
ENSMUSG00000045932	*Ifit2*	2.48E-21	1.705861

ENSMUSG00000028461	*Ccdc107*	1.38E-06	1.705554
ENSMUSG00000102349	*Gm37376*	1.71E-02	1.701801
ENSMUSG00000024810	*Il33*	4.65E-23	1.70107
ENSMUSG00000070473	*Cldn3*	2.42E-10	1.696455
ENSMUSG00000048709	*Gm8666*	3.20E-02	1.694683
ENSMUSG00000028678	*Kif2c*	3.69E-02	1.693279
ENSMUSG00000095098	*Ccdc85b*	4.36E-03	1.690404
ENSMUSG00000074576	*Mocs3*	1.14E-02	1.689861
ENSMUSG00000088948	*Gm23262*	2.79E-03	1.686819
ENSMUSG00000075268	*Gm10819*	1.05E-04	1.686108
ENSMUSG00000078141	*Gm2399*	4.75E-03	1.685731
ENSMUSG00000022595	*Lypd2*	4.45E-03	1.685708
ENSMUSG00000063171	*Rps4l*	2.87E-03	1.683014
ENSMUSG00000110528	*Gm1943*	4.81E-02	1.681924
ENSMUSG00000015880	*Ncapg*	1.05E-02	1.677303
ENSMUSG00000056758	*Hmga2*	3.94E-02	1.676199
ENSMUSG00000084783	*Gm15419*	2.22E-02	1.674643
ENSMUSG00000116694	*AC154667.2*	1.48E-03	1.671371
ENSMUSG00000083737	*Prdx6-ps2*	1.28E-02	1.666943
ENSMUSG00000085431	*4930440I19Rik*	1.34E-03	1.66478
ENSMUSG00000097971	*Gm26917*	1.21E-04	1.66206
ENSMUSG00000094344	*Gm11942*	4.89E-10	1.661048
ENSMUSG00000092267	*Gm20417*	6.05E-04	1.651296
ENSMUSG00000042737	*Dpm3*	1.76E-02	1.647963
ENSMUSG00000087247	*Alkal1*	1.04E-10	1.64795
ENSMUSG00000064382	*Gm26447*	5.42E-04	1.647264
ENSMUSG00000083337	*Gm11539*	4.30E-05	1.643919
ENSMUSG00000025226	*Fbxl15*	3.44E-02	1.64349
ENSMUSG00000082241	*Gng5-ps*	3.89E-02	1.641179
ENSMUSG00000105827	*Hist2h2bb*	2.20E-03	1.637237
ENSMUSG00000057160	*Gm16372*	4.55E-04	1.635812
ENSMUSG00000106767	*Gm42727*	1.77E-02	1.635709
ENSMUSG00000020493	*Prr11*	1.30E-02	1.633632
ENSMUSG00000092116	*Gm10320*	3.42E-03	1.631539
ENSMUSG00000117037	*CT010433.2*	2.53E-02	1.628923
ENSMUSG00000024401	*Tnf*	3.17E-19	1.627752
ENSMUSG00000057863	*Rpl36*	9.70E-06	1.626087
ENSMUSG00000047370	*Gm7367*	9.82E-04	1.625595
ENSMUSG00000020895	*Tmem107*	4.41E-02	1.624311
ENSMUSG00000114304	*Gm48099*	1.30E-06	1.623936
ENSMUSG00000028896	*Rcc1*	1.44E-11	1.622009
ENSMUSG00000107349	*Gm6655*	8.45E-03	1.614486
ENSMUSG00000080006	*Rps19-ps7*	3.14E-03	1.611362
ENSMUSG00000060438	*Rps10-ps1*	9.88E-10	1.610232
ENSMUSG00000080811	*Gm14513*	7.39E-05	1.609441
ENSMUSG00000104862	*Gm6520*	2.83E-02	1.607007
ENSMUSG00000028540	*Dph2*	7.43E-05	1.606169
ENSMUSG00000022769	*Sdf2l1*	7.63E-04	1.604934
ENSMUSG00000090942	*F830016B08Rik*	7.69E-06	1.603028
ENSMUSG00000007892	*Rplp1*	2.35E-11	1.602848
ENSMUSG00000022097	*Sftpc*	3.79E-08	1.601389
ENSMUSG00000040936	*Ulk4*	1.79E-13	1.600562
ENSMUSG00000097060	*Gm26759*	2.92E-04	1.600487
ENSMUSG00000091845	*Rpl36-ps12*	6.25E-04	1.600167
ENSMUSG00000030329	*Pianp*	8.93E-03	1.596449
ENSMUSG00000035202	*Lars2*	9.76E-08	1.596336
ENSMUSG00000104325	*Gm37321*	1.08E-02	1.595466

ENSMUSG00000082662	*Gm15516*	4.17E-02	1.594564
ENSMUSG00000063586	*Gm5513*	6.64E-03	1.592966
ENSMUSG00000097679	*Rps19-ps5*	1.49E-02	1.590111
ENSMUSG00000108414	*Snhg1*	2.93E-11	1.588096
ENSMUSG00000085401	*Slc39a1-ps*	5.90E-10	1.587829
ENSMUSG00000060183	*Cxcl11*	2.63E-04	1.587297
ENSMUSG00000027447	*Cst3*	8.64E-19	1.585854
ENSMUSG00000069515	*Lyz1*	3.15E-15	1.584793
ENSMUSG00000071419	*Rps15-ps2*	2.45E-08	1.583911
ENSMUSG00000102135	*Gm37108*	5.48E-03	1.582546
ENSMUSG00000065126	*Snord104*	8.14E-04	1.581336
ENSMUSG00000052837	*Junb*	4.96E-18	1.580061
ENSMUSG00000117187	*CT033749.1*	1.02E-02	1.579981
ENSMUSG00000000386	*Mx1*	2.32E-17	1.579725
ENSMUSG00000036114	*Rpp25l*	1.62E-03	1.578918
ENSMUSG00000079505	*Gm11131*	3.63E-03	1.576721
ENSMUSG00000114321	*Gm8971*	3.66E-04	1.576165
ENSMUSG00000046240	*Hepacam*	5.51E-04	1.575183
ENSMUSG00000083669	*Gm10169*	5.08E-03	1.573737
ENSMUSG00000094955	*Gm3699*	5.08E-03	1.573303
ENSMUSG00000029410	*Ppef2*	5.25E-03	1.572807
ENSMUSG00000068606	*Gm4841*	3.38E-02	1.572259
ENSMUSG00000106352	*5033403H07Rik*	4.74E-06	1.571858
ENSMUSG00000098534	*Gm27167*	3.43E-06	1.571239
ENSMUSG00000111897	*Gm19810*	1.29E-04	1.568539
ENSMUSG00000117269	*AC151275.1*	3.31E-02	1.567532
ENSMUSG00000112290	*Gm33782*	4.90E-03	1.563678
ENSMUSG00000015437	*Gzmb*	5.18E-03	1.561612
ENSMUSG00000024165	*Jpt2*	9.07E-16	1.560746
ENSMUSG00000047443	*Erfe*	1.12E-03	1.559959
ENSMUSG00000089542	*Gm25835*	9.96E-04	1.558194
ENSMUSG00000080747	*Gm14016*	4.05E-03	1.557656
ENSMUSG00000064063	*BC048507*	1.80E-02	1.554995
ENSMUSG00000117046	*AC122746.1*	2.71E-02	1.552568
ENSMUSG00000021070	*Bdkrb2*	5.92E-05	1.552425
ENSMUSG00000060419	*Rps16-ps2*	4.73E-10	1.551902
ENSMUSG00000086324	*Gm15564*	3.09E-05	1.551082
ENSMUSG00000086420	*Gm8865*	4.69E-03	1.548083
ENSMUSG00000041378	*Cldn5*	1.39E-15	1.546994
ENSMUSG00000027496	*Aurka*	4.17E-02	1.546663
ENSMUSG00000095478	*Gm9824*	9.03E-03	1.546072
ENSMUSG00000079330	*Lemd1*	1.45E-03	1.544978
ENSMUSG00000076036	*Gm22133*	4.18E-13	1.544169
ENSMUSG00000082062	*Ftl2-ps*	7.57E-11	1.542066
ENSMUSG00000032425	*Zfp949*	7.47E-12	1.541584
ENSMUSG00000070284	*Gmppb*	4.20E-05	1.539971
ENSMUSG00000081382	*Rpl18-ps1*	1.43E-03	1.538547
ENSMUSG00000099060	*Mir7025*	4.48E-02	1.53617
ENSMUSG00000082609	*Gm15464*	3.50E-02	1.535836
ENSMUSG00000030744	*Rps3*	6.04E-11	1.535727
ENSMUSG00000037169	*Mycn*	3.45E-04	1.535438
ENSMUSG00000094111	*Nutf2-ps2*	4.80E-02	1.534662
ENSMUSG00000087006	*Gm13889*	3.61E-15	1.533387
ENSMUSG00000113212	*Gm47435*	1.57E-02	1.532655
ENSMUSG00000007872	*Id3*	6.85E-12	1.530174
ENSMUSG00000015092	*Edf1*	3.80E-08	1.530159
ENSMUSG00000072235	*Tuba1a*	2.93E-13	1.528993

ENSMUSG00000073144	*4930599N23Rik*	1.03E-03	1.528627
ENSMUSG00000087060	*Eldr*	9.87E-03	1.527571
ENSMUSG00000028179	*Cth*	1.62E-04	1.52673
ENSMUSG00000058900	*Rsl1*	9.35E-05	1.526622
ENSMUSG00000053508	*Gtsf2*	3.10E-06	1.522863
ENSMUSG00000050796	*B3galt6*	1.56E-02	1.522466
ENSMUSG00000050370	*Ch25h*	2.02E-21	1.521802
ENSMUSG00000059835	*Rpl13-ps3*	7.89E-04	1.521415
ENSMUSG00000112003	*Gm4864*	3.60E-02	1.520838
ENSMUSG00000043099	*Hic1*	1.04E-03	1.518516
ENSMUSG00000033368	*Trim69*	4.03E-03	1.516764
ENSMUSG00000046731	*Kctd11*	1.05E-14	1.516698
ENSMUSG00000070392	*Gm20634*	2.49E-03	1.515844
ENSMUSG00000093674	*Rpl41*	1.91E-12	1.515683
ENSMUSG00000096942	*Rps19-ps6*	1.09E-06	1.515244
ENSMUSG00000104560	*Gm8115*	7.31E-03	1.514801
ENSMUSG00000070462	*Tlnrd1*	1.52E-09	1.513754
ENSMUSG00000036992	*Nxt1*	1.64E-03	1.513731
ENSMUSG00000061848	*Gm5805*	1.54E-10	1.512703
ENSMUSG00000099544	*Gm18699*	2.13E-03	1.511865
ENSMUSG00000059434	*Gckr*	1.64E-03	1.511175
ENSMUSG00000042842	*Serpinb6b*	2.39E-16	1.510922
ENSMUSG00000068240	*Gm11808*	9.62E-10	1.510582
ENSMUSG00000109658	*Gm45660*	3.74E-05	1.510374
ENSMUSG00000044197	*Gpr146*	8.83E-19	1.510371
ENSMUSG00000105472	*Gm43024*	2.61E-02	1.509917
ENSMUSG00000075020	*Mir670hg*	8.54E-03	1.509891
ENSMUSG00000008140	*Emc10*	3.81E-09	1.509274
ENSMUSG00000029371	*Cxcl5*	1.04E-11	1.507055
ENSMUSG00000024925	*Rnaseh2c*	3.97E-02	1.506518
ENSMUSG00000110275	*Gm5905*	2.92E-15	1.506379
ENSMUSG00000115143	*Fkbp1a-ps1*	3.40E-04	1.504907
ENSMUSG00000074115	*Saa1*	4.30E-08	1.504478
ENSMUSG00000091639	*Gm3756*	5.43E-10	1.504454
ENSMUSG00000101449	*Gm17791*	1.23E-02	1.504151
ENSMUSG00000098181	*Rps12-ps24*	1.77E-02	1.503082
ENSMUSG00000116358	*Gm49450*	2.31E-13	1.502451
ENSMUSG00000059461	*Gm7331*	1.06E-06	1.502048
ENSMUSG00000091269	*Gm6682*	9.38E-11	1.501853
ENSMUSG00000022408	Fam83f	1.13E-02	1.500479
ENSMUSG00000027843	Ptpn22	4.55E-11	1.500715
ENSMUSG00000026414	Tnnt2	2.59E-14	1.500887
ENSMUSG00000046961	Gpr156	7.92E-04	1.503034
ENSMUSG00000030468	Siglecg	1.69E-05	1.503144
ENSMUSG00000059900	Tmem40	3.18E-02	1.503359
ENSMUSG00000015568	Lpl	1.57E-32	1.503627
ENSMUSG00000048794	Cfap100	1.97E-05	1.504035
ENSMUSG00000043789	Vwce	1.10E-02	1.504138
ENSMUSG00000021751	Acox2	2.40E-04	1.504181
ENSMUSG00000050600	Zfp831	4.21E-09	1.504376
ENSMUSG00000020892	Aloxe3	1.83E-02	1.504792
ENSMUSG00000078234	Klhdc7a	7.85E-04	1.505376
ENSMUSG00000114937	Gm30054	1.87E-05	1.505389
ENSMUSG00000046186	Cd109	2.33E-05	1.505728
ENSMUSG00000038167	Plekhg6	2.51E-03	1.506016
ENSMUSG00000028017	Egf	4.01E-07	1.506454
ENSMUSG00000019577	Pdk4	8.43E-28	1.506585

ENSMUSG00000025271	Pfkfb1	7.66E-13	1.507316
ENSMUSG00000029123	Stk32b	1.69E-02	1.507913
ENSMUSG00000024049	Myom1	1.17E-21	1.508449
ENSMUSG00000007122	Casq1	6.70E-07	1.509955
ENSMUSG00000003476	Crhr2	1.35E-04	1.511069
ENSMUSG00000056366	Fabp3-ps1	2.81E-06	1.512819
ENSMUSG00000108955	Gm44775	3.93E-02	1.513353
ENSMUSG00000111907	Gm48202	6.46E-03	1.514782
ENSMUSG00000002007	Srpk3	3.83E-03	1.514899
ENSMUSG00000006345	Ggt1	1.00E-04	1.514981
ENSMUSG00000073968	Trim68	1.66E-08	1.515157
ENSMUSG00000112230	Ifngas1	3.52E-02	1.515642
ENSMUSG00000090124	Ugt1a7c	1.52E-11	1.516108
ENSMUSG00000089943	Ugt1a5	7.03E-06	1.516142
ENSMUSG00000090165	Ugt1a10	6.59E-12	1.516306
ENSMUSG00000097579	Gm26799	2.23E-03	1.517356
ENSMUSG00000112023	Lilr4b	1.77E-04	1.517729
ENSMUSG00000005951	Shpk	1.11E-04	1.51779
ENSMUSG00000035296	Sgcg	1.16E-09	1.517805
ENSMUSG00000032925	Itgbl1	1.02E-17	1.518245
ENSMUSG00000043873	Chil5	7.73E-03	1.518859
ENSMUSG00000109371	Gm44626	2.32E-02	1.519236
ENSMUSG00000090175	Ugt1a9	7.00E-12	1.519384
ENSMUSG00000060275	Nrg2	6.87E-03	1.52007
ENSMUSG00000089675	Ugt1a8	6.80E-12	1.520697
ENSMUSG00000041608	Entpd3	1.12E-10	1.520924
ENSMUSG00000069808	Fam57a	1.25E-06	1.521054
ENSMUSG00000100510	AV026068	5.30E-03	1.521178
ENSMUSG00000086607	4930511M06Rik	2.52E-02	1.521734
ENSMUSG00000040247	Tbc1d10c	6.96E-07	1.522149
ENSMUSG00000041642	Kif21b	3.24E-10	1.522398
ENSMUSG00000090799	Klhl33	8.11E-05	1.522621
ENSMUSG00000070498	Tmem132b	3.43E-08	1.523157
ENSMUSG00000018796	Acsl1	8.24E-30	1.523655
ENSMUSG00000078937	Cpt1b	5.04E-08	1.523826
ENSMUSG00000034570	Inpp5j	8.55E-03	1.523892
ENSMUSG00000044551	9930012K11Rik	7.95E-04	1.524065
ENSMUSG00000032053	Pou2af1	6.57E-06	1.524753
ENSMUSG00000089804	Gm16136	3.66E-02	1.525379
ENSMUSG00000031958	Ldhd	1.14E-03	1.526
ENSMUSG00000073988	Ttpa	2.43E-06	1.52693
ENSMUSG00000043639	Rbm20	4.76E-16	1.527208
ENSMUSG00000046971	Pla2g4f	1.67E-05	1.527252
ENSMUSG00000058207	Serpina3k	5.08E-04	1.5276
ENSMUSG00000062257	Opcml	5.34E-11	1.527897
ENSMUSG00000066108	Muc5b	2.76E-21	1.528023
ENSMUSG00000020256	Aldh1l2	1.82E-04	1.530481
ENSMUSG00000031303	Map3k15	1.02E-08	1.532052
ENSMUSG00000006014	Prg4	3.62E-08	1.532224
ENSMUSG00000007107	Atp1a4	2.62E-06	1.53242
ENSMUSG00000038777	Sema6c	8.09E-05	1.533598
ENSMUSG00000030470	Csrp3	6.81E-10	1.534077
ENSMUSG00000024039	Cbs	3.49E-02	1.534538
ENSMUSG00000000686	Abhd15	8.63E-05	1.535291
ENSMUSG00000051910	Sox6	9.77E-26	1.536789
ENSMUSG00000002997	Prkar2b	2.00E-17	1.537187
ENSMUSG00000024803	Ankrd1	1.13E-12	1.537284

ENSMUSG00000110397	Gm45540	4.65E-06	1.537736
ENSMUSG00000029228	Lnx1	1.73E-19	1.537867
ENSMUSG00000031382	Asb11	2.82E-04	1.538155
ENSMUSG00000020303	Stc2	3.41E-05	1.538946
ENSMUSG00000026824	Kcnj3	2.07E-10	1.539467
ENSMUSG00000054545	Ugt1a6a	9.67E-10	1.539483
ENSMUSG00000097193	Gm26664	1.10E-02	1.539627
ENSMUSG00000032066	Bco2	3.66E-02	1.539965
ENSMUSG00000090145	Ugt1a6b	6.45E-12	1.540465
ENSMUSG00000030098	Grip2	2.01E-05	1.541304
ENSMUSG00000030650	Tmc5	3.57E-04	1.543931
ENSMUSG00000113165	Gm47863	4.70E-02	1.547216
ENSMUSG00000096981	Gm16845	7.49E-05	1.547297
ENSMUSG00000058498	Rnf207	5.23E-03	1.547335
ENSMUSG00000104094	Gm37314	4.58E-03	1.547567
ENSMUSG00000087172	Gm12153	2.27E-09	1.547691
ENSMUSG00000000197	Nalcn	4.06E-06	1.549339
ENSMUSG00000097885	5031434O11Rik	4.83E-03	1.549511
ENSMUSG00000085779	Atcayos	8.31E-10	1.550724
ENSMUSG00000038583	Pln	3.75E-10	1.550962
ENSMUSG00000047940	Stpg2	3.85E-03	1.55183
ENSMUSG00000032495	Lrrc2	1.65E-06	1.553009
ENSMUSG00000046818	Ddit4l	1.98E-02	1.554266
ENSMUSG00000031808	Slc27a1	6.93E-12	1.555141
ENSMUSG00000027796	Smad9	1.44E-04	1.555153
ENSMUSG00000064368	mt-Nd6	4.83E-18	1.555459
ENSMUSG00000074497	A430078G23Rik	5.03E-17	1.557086
ENSMUSG00000087579	Hectd2os	3.22E-07	1.557447
ENSMUSG00000097917	Gm26839	3.13E-02	1.55764
ENSMUSG00000113184	AC125351.1	6.09E-05	1.558477
ENSMUSG00000043531	Sorcs1	2.00E-07	1.560471
ENSMUSG00000112947	Gm47493	2.90E-03	1.560632
ENSMUSG00000042474	Fcmr	3.47E-04	1.561669
ENSMUSG00000039521	Foxp3	3.68E-03	1.562481
ENSMUSG00000030219	Erp27	2.46E-02	1.563639
ENSMUSG00000029158	Yipf7	1.40E-02	1.563821
ENSMUSG00000079015	Serpina1c	2.41E-03	1.56468
ENSMUSG00000038132	Rbm24	4.06E-11	1.564762
ENSMUSG00000028116	Myoz2	2.18E-12	1.566472
ENSMUSG00000114138	Gm36423	1.97E-02	1.566955
ENSMUSG00000044938	Klhl31	1.10E-08	1.567813
ENSMUSG00000012705	Retn	1.11E-02	1.567825
ENSMUSG00000030278	Cidec	1.15E-06	1.56902
ENSMUSG00000075307	Klhl41	1.95E-09	1.569759
ENSMUSG00000043165	Lor	7.00E-06	1.56992
ENSMUSG00000060962	Dmkn	6.45E-08	1.570534
ENSMUSG00000038242	Aox4	5.04E-03	1.571204
ENSMUSG00000091712	Sec14l5	1.06E-03	1.572691
ENSMUSG00000013523	Bcas1	3.93E-02	1.572801
ENSMUSG00000092201	A530058N18Rik	1.98E-06	1.572952
ENSMUSG00000083120	Gm15854	3.07E-03	1.573014
ENSMUSG00000034009	Rxfp1	2.53E-03	1.573695
ENSMUSG00000029499	Pxmp2	6.54E-04	1.574213
ENSMUSG00000097062	Gm17586	4.09E-02	1.574318
ENSMUSG00000078486	Perm1	7.00E-10	1.575601
ENSMUSG00000053024	Cntn2	3.82E-02	1.576448
ENSMUSG00000044694	2010007H06Rik	3.28E-04	1.576597

ENSMUSG00000101640	Gm28376	4.52E-02	1.576948
ENSMUSG00000093938	Evi2b	2.47E-13	1.577235
ENSMUSG00000029838	Ptn	3.62E-03	1.578484
ENSMUSG00000074433	Lce3e	4.14E-02	1.579193
ENSMUSG00000113178	Mylf-ps	5.90E-07	1.579344
ENSMUSG00000043629	1700019D03Rik	8.68E-03	1.58036
ENSMUSG00000099966	2810402E24Rik	1.76E-03	1.580758
ENSMUSG00000026989	Dapl1	4.53E-02	1.581376
ENSMUSG00000030598	Fbxo17	3.90E-05	1.582412
ENSMUSG00000054598	9130230L23Rik	5.99E-08	1.582807
ENSMUSG00000033508	Asprv1	6.88E-04	1.583878
ENSMUSG00000038295	Atg9b	1.40E-02	1.58412
ENSMUSG00000096351	Samd11	9.99E-04	1.584324
ENSMUSG00000039084	Chad	9.78E-06	1.586243
ENSMUSG00000076617	Ighm	5.17E-12	1.586353
ENSMUSG00000086968	4933431E20Rik	3.14E-02	1.586354
ENSMUSG00000040086	Tnni3k	4.57E-09	1.587296
ENSMUSG00000035606	Ky	2.23E-04	1.588323
ENSMUSG00000038170	Pde4dip	3.86E-39	1.588667
ENSMUSG00000029055	Plch2	6.80E-08	1.588932
ENSMUSG00000061013	Mkx	2.08E-04	1.589186
ENSMUSG00000041782	Lad1	1.14E-06	1.589714
ENSMUSG00000027456	Sdcbp2	1.49E-07	1.5906
ENSMUSG00000020836	Coro6	8.35E-11	1.591197
ENSMUSG00000060180	Myh13	3.21E-04	1.591427
ENSMUSG00000053093	Myh7	2.88E-07	1.593422
ENSMUSG00000109510	Gm42417	7.99E-14	1.595001
ENSMUSG00000057092	Fxyd3	3.96E-03	1.596509
ENSMUSG00000117297	CT571247.2	9.90E-03	1.597064
ENSMUSG00000090173	Fbxw10	2.39E-04	1.598188
ENSMUSG00000054889	Dsp	3.20E-46	1.598377
ENSMUSG00000041616	Nppa	1.28E-03	1.59881
ENSMUSG00000056271	Lman1l	4.16E-02	1.599281
ENSMUSG00000057280	Musk	5.50E-08	1.600621
ENSMUSG00000031377	Bmx	1.66E-10	1.601368
ENSMUSG00000064340	mt-Tl1	1.92E-09	1.601856
ENSMUSG00000027559	Car3	1.93E-38	1.60232
ENSMUSG00000061462	Obscn	1.92E-25	1.602458
ENSMUSG00000102305	Gm38192	2.46E-02	1.603866
ENSMUSG00000038173	Enpp6	2.21E-02	1.604535
ENSMUSG00000028150	Rorc	9.93E-07	1.604951
ENSMUSG00000029167	Ppargc1a	2.14E-18	1.605113
ENSMUSG00000092397	C130080G10Rik	7.30E-06	1.605123
ENSMUSG00000103984	Gm37447	3.69E-02	1.605238
ENSMUSG00000040055	Gjb6	2.24E-03	1.605389
ENSMUSG00000024347	Psd2	2.70E-02	1.606216
ENSMUSG00000068885	Lce3f	8.58E-03	1.607541
ENSMUSG00000037989	Wnk2	1.81E-14	1.608343
ENSMUSG00000085184	4933439K11Rik	3.15E-03	1.608853
ENSMUSG00000031097	Tnni2	2.26E-08	1.6098
ENSMUSG00000017400	Stac2	4.29E-02	1.612166
ENSMUSG00000024673	Ms4a1	8.11E-06	1.612963
ENSMUSG00000033544	Angptl1	1.17E-02	1.613351
ENSMUSG00000097652	Mhrt	2.82E-07	1.613894
ENSMUSG00000085971	Gm15411	3.02E-05	1.613896
ENSMUSG00000075289	Carns1	1.74E-06	1.615629
ENSMUSG00000026163	Sphkap	7.15E-09	1.617694

ENSMUSG00000040694	Apobec2	6.16E-08	1.620042
ENSMUSG00000043008	Klhl6	3.96E-14	1.62231
ENSMUSG00000018893	Mb	2.71E-08	1.623243
ENSMUSG00000027861	Casq2	1.05E-11	1.623312
ENSMUSG00000020067	Mypn	1.05E-14	1.623658
ENSMUSG00000028115	Bnipl	1.13E-02	1.623683
ENSMUSG00000054659	Pm20d2	1.90E-02	1.623767
ENSMUSG00000055415	Atp10b	9.65E-03	1.624498
ENSMUSG00000039891	Txlnb	6.59E-16	1.625928
ENSMUSG00000020169	Best3	3.97E-06	1.62632
ENSMUSG00000085194	Platr32	1.32E-02	1.628265
ENSMUSG00000063297	Luzp2	9.47E-06	1.63024
ENSMUSG00000025815	Dhtkd1	2.73E-06	1.630385
ENSMUSG00000021123	Rdh12	1.62E-12	1.631252
ENSMUSG00000046056	Sbsn	8.20E-05	1.631281
ENSMUSG00000076275	Mir675	3.45E-04	1.631535
ENSMUSG00000036560	Lgi4	6.45E-08	1.632499
ENSMUSG00000111818	Gm17749	8.46E-06	1.632708
ENSMUSG00000052496	Pkdrej	1.85E-02	1.635592
ENSMUSG00000085417	Gm13919	1.14E-02	1.637562
ENSMUSG00000031700	Gpt2	2.20E-10	1.638222
ENSMUSG00000086564	Cd101	2.04E-15	1.638923
ENSMUSG00000067149	Jchain	6.64E-03	1.639225
ENSMUSG00000049123	Catsperg2	3.63E-02	1.639878
ENSMUSG00000057719	Sh3rf2	1.37E-13	1.640066
ENSMUSG00000027887	Sypl2	7.30E-06	1.641809
ENSMUSG00000066510	Ankdd1a	8.15E-07	1.642186
ENSMUSG00000102191	Gm36569	1.33E-02	1.642411
ENSMUSG00000022523	Fgf12	9.16E-19	1.642983
ENSMUSG00000058470	Gm8369	1.21E-10	1.644013
ENSMUSG00000096646	CR974586.6	4.85E-02	1.647968
ENSMUSG00000079853	Klra1	4.74E-04	1.648672
ENSMUSG00000029862	Clcn1	3.16E-06	1.649099
ENSMUSG00000007279	Scube2	3.52E-19	1.651431
ENSMUSG00000032564	Cpne4	1.36E-05	1.651458
ENSMUSG00000043487	Acot6	1.05E-02	1.65192
ENSMUSG00000014453	Blk	1.77E-09	1.652393
ENSMUSG00000059857	Ntng1	2.28E-05	1.653485
ENSMUSG00000057246	BC051142	2.48E-04	1.653565
ENSMUSG00000033569	Adgrb3	4.62E-07	1.653669
ENSMUSG00000041538	H2-Ob	1.37E-05	1.653876
ENSMUSG00000029361	Nos1	1.56E-11	1.653885
ENSMUSG00000106547	B230303O12Rik	1.21E-08	1.654582
ENSMUSG00000072720	Myo18b	4.14E-27	1.655567
ENSMUSG00000086962	Gm12248	3.67E-04	1.656171
ENSMUSG00000020374	Rasgef1c	1.48E-09	1.656757
ENSMUSG00000033182	Kbtbd12	1.02E-07	1.656789
ENSMUSG00000105646	Gm30211	1.89E-10	1.657828
ENSMUSG00000054582	Pabpc1l	1.93E-07	1.660152
ENSMUSG00000047228	A2ml1	2.62E-03	1.660287
ENSMUSG00000098381	Mir7225	3.46E-03	1.660541
ENSMUSG00000085532	B430319H21Rik	1.21E-03	1.661812
ENSMUSG00000079764	AC087559.1	4.29E-02	1.662417
ENSMUSG00000108436	Gm44851	1.77E-02	1.663035
ENSMUSG00000078817	Nlrp12	1.01E-15	1.663158
ENSMUSG00000110195	Pde2a	7.09E-18	1.665411
ENSMUSG00000075555	Gm10863	1.92E-04	1.665852

ENSMUSG00000037572	Wdhd1	5.63E-09	1.666104
ENSMUSG00000021506	Pitx1	2.48E-02	1.668955
ENSMUSG00000026564	Dusp27	2.96E-09	1.67013
ENSMUSG00000037188	Grhl3	5.01E-04	1.670721
ENSMUSG00000028834	Trim63	5.36E-07	1.67122
ENSMUSG00000038077	Kcna6	3.83E-05	1.672132
ENSMUSG00000063651	Cnfn	3.01E-05	1.673857
ENSMUSG00000031245	Hmgn5	1.75E-06	1.674099
ENSMUSG00000028544	Slc5a9	4.27E-03	1.67494
ENSMUSG00000058966	Fam57b	2.45E-04	1.676352
ENSMUSG00000022416	Cacna1i	7.73E-05	1.678167
ENSMUSG00000036731	Cysrt1	1.69E-02	1.678982
ENSMUSG00000046352	Gjb2	7.16E-07	1.679256
ENSMUSG00000028459	Cd72	3.05E-05	1.679816
ENSMUSG00000045534	Kcna5	2.06E-03	1.681084
ENSMUSG00000000244	Tspan32	1.65E-11	1.681161
ENSMUSG00000108985	A930030B08Rik	2.28E-02	1.682419
ENSMUSG00000032942	Ucp3	6.10E-07	1.684317
ENSMUSG00000087336	Gm15860	2.35E-02	1.684872
ENSMUSG00000002831	Plin4	1.20E-31	1.686763
ENSMUSG00000020848	Doc2b	1.14E-10	1.686804
ENSMUSG00000052726	Kcnt2	2.57E-21	1.687119
ENSMUSG00000024105	Themis3	1.57E-02	1.68772
ENSMUSG00000112707	D830005E20Rik	1.41E-09	1.688501
ENSMUSG00000030317	Timp4	1.18E-08	1.688584
ENSMUSG00000095438	Mir133a-1hg	2.49E-05	1.688705
ENSMUSG00000034308	Sdr42e1	1.55E-04	1.688804
ENSMUSG00000070385	Ampd1	9.23E-08	1.689044
ENSMUSG00000086405	9330198N18Rik	9.76E-07	1.689856
ENSMUSG00000029660	Tex26	5.91E-07	1.690097
ENSMUSG00000032262	Elovl4	6.32E-05	1.690396
ENSMUSG00000031461	Myom2	2.01E-27	1.69079
ENSMUSG00000040740	Slc25a34	2.14E-05	1.690811
ENSMUSG00000000049	Apoh	2.58E-02	1.69197
ENSMUSG00000023019	Gpd1	5.00E-16	1.693018
ENSMUSG00000030510	Cers3	7.37E-07	1.693354
ENSMUSG00000076937	Iglc2	2.70E-03	1.693807
ENSMUSG00000038763	Alpk3	6.16E-26	1.693831
ENSMUSG00000067889	Sptbn2	2.00E-07	1.694539
ENSMUSG00000106245	Gm43824	1.15E-02	1.694809
ENSMUSG00000042567	Nek10	1.91E-12	1.695091
ENSMUSG00000048764	Tmprss11f	8.49E-03	1.696489
ENSMUSG00000022878	Adipoq	5.10E-07	1.69666
ENSMUSG00000026527	Rgs7	1.36E-33	1.696693
ENSMUSG00000090206	Tepp	1.43E-03	1.696892
ENSMUSG00000002500	Rpl3l	1.67E-04	1.698266
ENSMUSG00000054057	A930004D18Rik	1.98E-02	1.699027
ENSMUSG00000079644	Gm1110	1.53E-02	1.699165
ENSMUSG00000059201	Lep	5.30E-03	1.70052
ENSMUSG00000061816	Myl1	3.42E-12	1.701209
ENSMUSG00000043366	Olfr78	4.74E-03	1.701217
ENSMUSG00000039092	Sptlc3	1.10E-03	1.702114
ENSMUSG00000053964	Lgals4	6.56E-05	1.702508
ENSMUSG00000025892	Gria4	3.55E-03	1.703464
ENSMUSG00000019906	Lin7a	1.80E-05	1.704483
ENSMUSG00000041020	Map7d2	2.72E-02	1.705429
ENSMUSG00000100147	1700047M11Rik	4.18E-08	1.706711

ENSMUSG00000028773	Fabp3	1.13E-08	1.706932
ENSMUSG00000031385	Plxnb3	2.72E-03	1.709339
ENSMUSG00000110411	Gm45457	9.03E-03	1.710479
ENSMUSG00000034282	Evpl	1.07E-08	1.710621
ENSMUSG00000087628	Gm13028	1.40E-03	1.71063
ENSMUSG00000036960	Clca2	2.27E-02	1.712431
ENSMUSG00000052013	Btla	1.86E-06	1.713815
ENSMUSG00000025754	Agbl1	1.29E-20	1.714057
ENSMUSG00000034634	Ly6d	7.90E-04	1.715269
ENSMUSG00000061126	Cyp4f39	3.92E-03	1.718439
ENSMUSG00000035580	Kcnh8	9.67E-06	1.718443
ENSMUSG00000021340	Gpld1	5.88E-10	1.718732
ENSMUSG00000040350	Trim7	7.94E-08	1.718782
ENSMUSG00000116987	AC150035.3	1.76E-02	1.719502
ENSMUSG00000038204	Asb10	2.36E-02	1.719976
ENSMUSG00000020334	Slc22a4	1.93E-07	1.720261
ENSMUSG00000064346	mt-Tw	2.44E-04	1.721955
ENSMUSG00000007033	Hspa1l	2.73E-02	1.722982
ENSMUSG00000038239	Hrc	6.28E-14	1.724801
ENSMUSG00000073492	Gm10521	2.63E-03	1.725675
ENSMUSG00000020279	Il9r	3.97E-02	1.726651
ENSMUSG00000040899	Ccr6	4.51E-09	1.728272
ENSMUSG00000073985	Gm10602	5.77E-04	1.7291
ENSMUSG00000069733	Ube2u	5.69E-03	1.72999
ENSMUSG00000036123	Slc9a3	8.61E-03	1.729994
ENSMUSG00000019787	Trdn	2.22E-33	1.730141
ENSMUSG00000099364	5730419F03Rik	1.15E-02	1.732264
ENSMUSG00000093577	Gm20632	4.01E-02	1.733244
ENSMUSG00000027077	Smtnl1	4.61E-06	1.734518
ENSMUSG00000057003	Myh4	3.19E-14	1.734608
ENSMUSG00000000031	H19	5.10E-18	1.735173
ENSMUSG00000003271	Sult2b1	1.84E-03	1.735974
ENSMUSG00000038354	Ankrd35	3.79E-03	1.736278
ENSMUSG00000015879	Fam184b	6.83E-03	1.737161
ENSMUSG00000079243	Xirp1	1.34E-16	1.737887
ENSMUSG00000079588	Tmem182	9.64E-13	1.738319
ENSMUSG00000031376	Atp2b3	9.23E-04	1.73926
ENSMUSG00000042010	Acacb	9.27E-37	1.739339
ENSMUSG00000022871	Fetub	5.57E-05	1.739701
ENSMUSG00000010066	Cacna2d2	4.85E-04	1.74003
ENSMUSG00000027831	Veph1	7.22E-11	1.743301
ENSMUSG00000005268	Prlr	1.86E-05	1.743362
ENSMUSG00000038665	Dgki	7.51E-11	1.743848
ENSMUSG00000040536	Necab1	6.32E-03	1.744057
ENSMUSG00000062713	Sim2	3.32E-09	1.745706
ENSMUSG00000037139	Myom3	3.04E-14	1.746519
ENSMUSG00000014030	Pax5	3.89E-07	1.746801
ENSMUSG00000031626	Sorbs2	8.87E-27	1.746865
ENSMUSG00000048142	Nat8l	3.69E-04	1.747147
ENSMUSG00000067341	H2-Eb2	8.84E-03	1.748009
ENSMUSG00000025172	Ankrd2	1.45E-06	1.749393
ENSMUSG00000096974	Gm26881	1.04E-02	1.749441
ENSMUSG00000020000	Moxd1	4.65E-03	1.750501
ENSMUSG00000070423	Olfr558	4.01E-02	1.750691
ENSMUSG00000099449	Gm28401	4.06E-02	1.754089
ENSMUSG00000067653	Ankrd23	1.06E-15	1.754635
ENSMUSG00000019102	Aldh3a1	7.57E-08	1.754898

ENSMUSG00000027868	Tbx15	4.21E-14	1.755594
ENSMUSG00000051747	Ttn	1.12E-46	1.757967
ENSMUSG00000032033	Barx2	1.39E-07	1.759194
ENSMUSG00000022622	Acr	1.21E-08	1.760657
ENSMUSG00000057054	Inca1	1.12E-04	1.76172
ENSMUSG00000115610	Gm31251	3.90E-14	1.761914
ENSMUSG00000061259	Tmprss11d	1.42E-02	1.761956
ENSMUSG00000069830	Nlrp1a	1.11E-03	1.76325
ENSMUSG00000110010	Gm45629	1.53E-03	1.764151
ENSMUSG00000038663	Fsd2	1.08E-14	1.765708
ENSMUSG00000100627	A830008E24Rik	1.45E-02	1.766465
ENSMUSG00000001095	Slc13a2	5.92E-04	1.767172
ENSMUSG00000024827	Gldc	3.59E-02	1.767944
ENSMUSG00000027913	Crct1	4.51E-05	1.768545
ENSMUSG00000013483	Card14	4.06E-05	1.769133
ENSMUSG00000030592	Ryr1	3.35E-10	1.769178
ENSMUSG00000102759	Gm10463	4.04E-02	1.770039
ENSMUSG00000074254	Cyp2a4	3.39E-02	1.770248
ENSMUSG00000058975	Kcnc1	6.09E-05	1.770841
ENSMUSG00000054325	Lce3a	5.92E-04	1.771249
ENSMUSG00000022040	Ephx2	1.34E-07	1.77423
ENSMUSG00000069670	Nkain2	1.14E-30	1.775621
ENSMUSG00000099994	1700024B18Rik	3.27E-02	1.775772
ENSMUSG00000039873	Neurl2	3.62E-03	1.776821
ENSMUSG00000086765	Gm11827	4.14E-05	1.779138
ENSMUSG00000093765	Gm20658	4.32E-02	1.779401
ENSMUSG00000044708	Kcnj10	2.20E-02	1.780045
ENSMUSG00000010476	Ebf3	2.43E-10	1.782939
ENSMUSG00000043681	Fam25c	5.16E-03	1.783067
ENSMUSG00000026220	Slc16a14	1.02E-02	1.783575
ENSMUSG00000048078	Tenm4	8.65E-33	1.786182
ENSMUSG00000074625	Arhgap40	1.61E-05	1.786986
ENSMUSG00000024334	H2-Oa	2.83E-02	1.78792
ENSMUSG00000005373	Mlxipl	1.48E-14	1.792638
ENSMUSG00000031757	Mt4	1.02E-03	1.792943
ENSMUSG00000104927	Gm43388	8.61E-03	1.794412
ENSMUSG00000031594	Fgl1	3.86E-02	1.796159
ENSMUSG00000017300	Tnnc2	5.41E-14	1.797829
ENSMUSG00000087307	Gm12925	4.11E-02	1.79825
ENSMUSG00000100199	Gm20324	5.05E-04	1.800659
ENSMUSG00000109754	Gm39214	4.56E-02	1.800915
ENSMUSG00000040490	Lrfn2	2.65E-03	1.803413
ENSMUSG00000110631	Gm42047	2.58E-02	1.804324
ENSMUSG00000111809	Gm49334	5.99E-03	1.805073
ENSMUSG00000048070	Pirt	4.90E-02	1.805324
ENSMUSG00000111299	4930540M03Rik	3.88E-02	1.805841
ENSMUSG00000026489	Coq8a	5.21E-32	1.80787
ENSMUSG00000085171	D830026I12Rik	1.96E-02	1.808535
ENSMUSG00000000673	Haao	2.83E-04	1.808707
ENSMUSG00000037661	Gpr160	1.16E-06	1.8137
ENSMUSG00000074215	Gm10643	2.95E-02	1.814076
ENSMUSG00000096449	Gm4076	4.29E-02	1.815678
ENSMUSG00000022383	Ppara	2.50E-24	1.817544
ENSMUSG00000109157	Gm44829	3.21E-05	1.818829
ENSMUSG00000020698	Cct6b	6.42E-04	1.823548
ENSMUSG00000049336	Tenm2	1.31E-16	1.8238
ENSMUSG00000074199	Krtdap	2.27E-03	1.824717

ENSMUSG00000005547	Cyp2a5	1.12E-09	1.826543
ENSMUSG00000027261	Hao1	1.24E-02	1.82689
ENSMUSG00000037446	Tulp1	5.73E-03	1.828912
ENSMUSG00000086547	Gm11755	1.77E-02	1.832213
ENSMUSG00000087090	Nctc1	7.99E-18	1.832231
ENSMUSG00000047419	Cmya5	3.32E-33	1.832861
ENSMUSG00000031425	Plp1	8.47E-11	1.833127
ENSMUSG00000067616	Klk11	1.67E-03	1.835648
ENSMUSG00000079025	Gsdmc	4.96E-03	1.835798
ENSMUSG00000085479	9430073C21Rik	4.93E-02	1.836068
ENSMUSG00000027674	Pex5l	3.20E-11	1.836523
ENSMUSG00000001027	Scn4a	8.93E-13	1.838172
ENSMUSG00000038020	Rapgefl1	3.35E-07	1.842817
ENSMUSG00000037509	Arhgef4	1.01E-11	1.84526
ENSMUSG00000056569	Mpz	2.39E-15	1.845464
ENSMUSG00000018862	Otop3	2.40E-03	1.847993
ENSMUSG00000027022	Xirp2	2.79E-35	1.849448
ENSMUSG00000116508	Gm49463	1.89E-02	1.850853
ENSMUSG00000044788	Fads6	2.44E-04	1.85333
ENSMUSG00000031372	Trex2	3.78E-02	1.854308
ENSMUSG00000028573	Fggy	2.26E-05	1.854817
ENSMUSG00000029683	Lmod2	1.32E-16	1.857354
ENSMUSG00000022491	Glycam1	8.74E-05	1.858915
ENSMUSG00000030724	Cd19	1.17E-10	1.860844
ENSMUSG00000087242	C78197	4.25E-02	1.86137
ENSMUSG00000040340	Tex45	7.93E-03	1.861819
ENSMUSG00000021613	Hapln1	2.16E-04	1.864932
ENSMUSG00000112895	Gm47567	7.34E-05	1.86531
ENSMUSG00000085743	8430419K02Rik	6.18E-22	1.866081
ENSMUSG00000101930	Gm5441	1.11E-09	1.866612
ENSMUSG00000042251	Pm20d1	6.12E-05	1.867473
ENSMUSG00000103965	Gm30173	2.07E-04	1.869946
ENSMUSG00000028996	Rbp7	6.66E-03	1.871717
ENSMUSG00000042031	Lce3b	1.73E-04	1.872678
ENSMUSG00000042895	Abra	1.62E-09	1.874549
ENSMUSG00000026697	Myoc	1.02E-02	1.875415
ENSMUSG00000026100	Mstn	8.60E-03	1.877754
ENSMUSG00000091119	Ccdc152	2.42E-05	1.879304
ENSMUSG00000062515	Fabp4	8.53E-23	1.879539
ENSMUSG00000062372	Otof	6.43E-03	1.881054
ENSMUSG00000021622	Ckmt2	1.81E-18	1.882596
ENSMUSG00000096960	A230028O05Rik	2.40E-09	1.883268
ENSMUSG00000104453	Gm37829	6.61E-05	1.884749
ENSMUSG00000039496	Cdnf	4.66E-03	1.887309
ENSMUSG00000034645	Zyg11a	2.17E-02	1.88839
ENSMUSG00000074862	BC025920	2.90E-03	1.888707
ENSMUSG00000030577	Cd22	5.61E-10	1.888805
ENSMUSG00000046480	Scn4b	2.33E-10	1.889073
ENSMUSG00000061723	Tnnt3	3.36E-12	1.895792
ENSMUSG00000073602	Serpinb3b	8.46E-04	1.896022
ENSMUSG00000042250	Pglyrp4	1.68E-02	1.896106
ENSMUSG00000037977	6430571L13Rik	1.82E-05	1.897294
ENSMUSG00000071858	Gm94	1.11E-03	1.898142
ENSMUSG00000043461	Sptssb	3.69E-04	1.8982
ENSMUSG00000027470	Mylk2	8.39E-14	1.898313
ENSMUSG00000084929	Foxo6os	1.25E-02	1.898699
ENSMUSG00000059832	Kprp	6.59E-08	1.901066

ENSMUSG00000020061	Mybpc1	4.60E-23	1.903022
ENSMUSG00000000223	Drp2	6.47E-08	1.90562
ENSMUSG00000042514	Klhl14	9.78E-05	1.906063
ENSMUSG00000097286	Gm26684	2.80E-02	1.914855
ENSMUSG00000038602	Slc35f1	6.46E-23	1.915687
ENSMUSG00000029602	Rasal1	7.61E-04	1.918457
ENSMUSG00000025431	Crisp1	6.65E-04	1.918683
ENSMUSG00000047586	Nccrp1	3.55E-02	1.920616
ENSMUSG00000086980	Gm13791	1.98E-02	1.922479
ENSMUSG00000049134	Nrap	2.40E-35	1.926123
ENSMUSG00000044737	Klk14	1.25E-07	1.926874
ENSMUSG00000071540	3425401B19Rik	1.95E-20	1.927593
ENSMUSG00000039763	Dnajc28	1.34E-03	1.92807
ENSMUSG00000041423	Paqr6	9.00E-03	1.931307
ENSMUSG00000045475	Lce3c	5.69E-05	1.931506
ENSMUSG00000032311	Nrg4	1.59E-17	1.932314
ENSMUSG00000039269	2300002M23Rik	5.11E-03	1.934349
ENSMUSG00000050840	Cdh20	3.44E-04	1.936624
ENSMUSG00000032278	Paqr5	8.26E-10	1.937115
ENSMUSG00000039376	Synpo2l	3.96E-21	1.938741
ENSMUSG00000007653	Gabrb2	6.55E-03	1.938974
ENSMUSG00000056328	Myh1	2.30E-34	1.944869
ENSMUSG00000032503	Arpp21	1.12E-06	1.948018
ENSMUSG00000090118	Gm16163	7.49E-08	1.950295
ENSMUSG00000005355	Casp14	2.78E-02	1.950333
ENSMUSG00000019851	Perp	2.82E-14	1.951709
ENSMUSG00000026950	Neb	2.63E-19	1.958489
ENSMUSG00000041476	Smpx	7.49E-08	1.958962
ENSMUSG00000055333	Fat2	8.85E-09	1.964371
ENSMUSG00000032281	Acsbg1	6.04E-11	1.96499
ENSMUSG00000026450	Chit1	3.30E-03	1.966851
ENSMUSG00000110580	D830024N08Rik	3.00E-09	1.967915
ENSMUSG00000039070	Cpa4	2.42E-05	1.968184
ENSMUSG00000021223	Papln	5.90E-05	1.970017
ENSMUSG00000050808	Muc15	3.15E-02	1.970166
ENSMUSG00000096169	Olfr1564	4.84E-02	1.970537
ENSMUSG00000067242	Lgi1	1.81E-04	1.972543
ENSMUSG00000001497	Pax9	7.05E-07	1.973159
ENSMUSG00000041737	Tmem45b	1.68E-09	1.973324
ENSMUSG00000055561	Spink5	1.65E-11	1.975498
ENSMUSG00000037129	Tmprss13	2.20E-05	1.978708
ENSMUSG00000112471	Gm5779	6.88E-03	1.980462
ENSMUSG00000027833	Shox2	1.87E-02	1.981285
ENSMUSG00000043286	Pnpla1	1.95E-03	1.981508
ENSMUSG00000105986	Gm43065	5.52E-04	1.983525
ENSMUSG00000030935	Acsm3	9.82E-03	1.984411
ENSMUSG00000059742	Kcnh7	1.36E-03	1.986178
ENSMUSG00000050650	Mrgpra1	3.24E-02	1.986835
ENSMUSG00000034730	Adgrb1	1.54E-02	1.986876
ENSMUSG00000050663	Trhde	2.20E-03	1.987786
ENSMUSG00000034774	Dsg1c	2.60E-02	1.98819
ENSMUSG00000030178	Klra13-ps	3.18E-03	1.989497
ENSMUSG00000030730	Atp2a1	2.28E-32	1.98969
ENSMUSG00000027376	Prom2	3.25E-06	1.991537
ENSMUSG00000025105	Bnc1	5.33E-04	1.99208
ENSMUSG00000039956	Mrap	5.20E-09	1.993265
ENSMUSG00000104213	Ighd	3.20E-10	1.994516

ENSMUSG00000024331	Dsc2	6.73E-10	1.997784
ENSMUSG00000103243	Lce1d	3.79E-03	1.999738
ENSMUSG00000050463	Krt78	3.05E-12	2.000453
ENSMUSG00000021359	Tfap2a	1.09E-03	2.000592
ENSMUSG00000025329	Padi1	1.62E-02	2.00394
ENSMUSG00000031204	Asb12	4.92E-02	2.004544
ENSMUSG00000039518	Cdsn	8.05E-07	2.005848
ENSMUSG00000031844	Hsd17b2	1.89E-04	2.007414
ENSMUSG00000099906	Gm28653	1.27E-02	2.010149
ENSMUSG00000075296	Aldh3b2	1.77E-03	2.010847
ENSMUSG00000031936	Hephl1	1.35E-02	2.013642
ENSMUSG00000102590	Mannr	1.14E-05	2.01519
ENSMUSG00000026834	Acvr1c	4.87E-08	2.015446
ENSMUSG00000030834	Abcc6	6.84E-03	2.015784
ENSMUSG00000025425	St8sia5	2.17E-02	2.018317
ENSMUSG00000036854	Hspb6	1.10E-06	2.019132
ENSMUSG00000019853	Hebp2	4.55E-03	2.019308
ENSMUSG00000050359	Sprr1a	4.50E-07	2.019357
ENSMUSG00000110390	Gm45869	4.89E-02	2.02195
ENSMUSG00000090356	Teddm3	1.30E-03	2.026459
ENSMUSG00000050296	Abca12	8.96E-08	2.026805
ENSMUSG00000047746	Fbxo40	8.92E-18	2.029312
ENSMUSG00000032726	Bmp8a	5.87E-03	2.030065
ENSMUSG00000029154	Cwh43	1.88E-02	2.030933
ENSMUSG00000055489	Ano5	8.68E-17	2.033201
ENSMUSG00000017204	Gsdma	3.20E-05	2.033369
ENSMUSG00000044086	Lmod3	3.08E-06	2.045815
ENSMUSG00000110843	Gm35552	4.00E-02	2.047718
ENSMUSG00000033579	Fa2h	3.55E-03	2.048412
ENSMUSG00000028989	Angptl7	3.95E-11	2.049447
ENSMUSG00000114493	Gm47071	9.81E-10	2.052629
ENSMUSG00000074489	Bglap3	1.66E-03	2.058281
ENSMUSG00000060621	Nkpd1	1.03E-02	2.065488
ENSMUSG00000062826	Ces2f	1.92E-08	2.067273
ENSMUSG00000030546	Plin1	8.52E-14	2.067798
ENSMUSG00000109311	AI314278	4.74E-04	2.069279
ENSMUSG00000023473	Celsr3	1.86E-12	2.073428
ENSMUSG00000096001	2610528A11Rik	3.36E-02	2.073506
ENSMUSG00000089941	Gm16168	2.39E-07	2.073697
ENSMUSG00000074647	Fam83c	2.18E-02	2.076138
ENSMUSG00000067081	Asb18	2.76E-08	2.077407
ENSMUSG00000044594	Serpinb3a	5.80E-06	2.079432
ENSMUSG00000044499	Hs3st5	3.23E-11	2.080027
ENSMUSG00000030713	Klk7	1.62E-02	2.081978
ENSMUSG00000043472	Lce3d	2.62E-02	2.084031
ENSMUSG00000045019	Acer1	2.71E-02	2.084468
ENSMUSG00000047976	Kcna1	2.86E-12	2.088442
ENSMUSG00000032013	Trim29	1.72E-10	2.088868
ENSMUSG00000026327	Serpinb11	1.47E-04	2.090204
ENSMUSG00000026592	Tex35	4.71E-09	2.091662
ENSMUSG00000047216	Cdh19	9.22E-24	2.093022
ENSMUSG00000050830	Vwc2	6.27E-05	2.093227
ENSMUSG00000078907	Fam186b	4.10E-02	2.094674
ENSMUSG00000016179	Camk1g	3.72E-02	2.098511
ENSMUSG00000026407	Cacna1s	4.35E-21	2.098587
ENSMUSG00000059994	Fcrl1	2.55E-10	2.10039
ENSMUSG00000027961	Lrrc39	1.44E-08	2.10099

ENSMUSG00000010064	Slc38a3	3.35E-10	2.106878
ENSMUSG00000031448	Adprhl1	1.43E-16	2.1087
ENSMUSG00000045776	Lrtm1	1.67E-11	2.109699
ENSMUSG00000053522	Lgals7	5.24E-05	2.111441
ENSMUSG00000069873	4930438A08Rik	3.96E-05	2.11536
ENSMUSG00000022053	Ebf2	2.57E-28	2.116937
ENSMUSG00000049598	Vsig8	5.27E-03	2.118056
ENSMUSG00000056966	Gjc3	1.05E-02	2.118632
ENSMUSG00000094814	Gm21973	5.63E-03	2.122571
ENSMUSG00000026621	Mar1	2.60E-02	2.123251
ENSMUSG00000021255	Esrrb	5.97E-07	2.124457
ENSMUSG00000109293	Dcst2	1.99E-02	2.125564
ENSMUSG00000026147	Col9a1	2.36E-02	2.125738
ENSMUSG00000067001	Serpinb7	1.24E-02	2.128035
ENSMUSG00000024076	Vit	7.49E-08	2.128736
ENSMUSG00000048399	Tprg	5.27E-05	2.129159
ENSMUSG00000048721	Fndc9	4.81E-02	2.129168
ENSMUSG00000028865	Cd164l2	6.80E-05	2.131367
ENSMUSG00000029195	Klb	1.90E-02	2.135638
ENSMUSG00000032401	Lctl	4.28E-02	2.141541
ENSMUSG00000051965	Nanos2	2.43E-02	2.142158
ENSMUSG00000028736	Pax7	1.19E-02	2.142682
ENSMUSG00000044041	Krt13	2.13E-07	2.145789
ENSMUSG00000035686	Thrsp	1.00E-21	2.14587
ENSMUSG00000059956	Serpinb12	6.27E-06	2.148141
ENSMUSG00000030484	Lypd5	1.18E-07	2.149653
ENSMUSG00000057454	Lypd3	8.72E-05	2.150403
ENSMUSG00000025479	Cyp2e1	2.34E-37	2.150779
ENSMUSG00000097768	2310043M15Rik	2.17E-03	2.151001
ENSMUSG00000020007	Il20ra	8.82E-04	2.163851
ENSMUSG00000027359	Slc27a2	3.11E-04	2.163887
ENSMUSG00000045539	Sprr3	1.12E-09	2.16411
ENSMUSG00000032807	Alox12b	2.37E-06	2.164244
ENSMUSG00000032454	Rbp2	2.18E-02	2.166851
ENSMUSG00000050108	Bpifc	6.18E-03	2.167485
ENSMUSG00000043460	Elfn2	2.40E-02	2.16877
ENSMUSG00000041984	Rptn	1.76E-11	2.170781
ENSMUSG00000043468	Adam30	5.96E-03	2.173031
ENSMUSG00000073601	Serpinb3c	2.50E-03	2.175747
ENSMUSG00000024471	Myot	2.51E-26	2.176575
ENSMUSG00000065445	Mir143	2.74E-02	2.17762
ENSMUSG00000005716	Pvalb	2.86E-05	2.18435
ENSMUSG00000022510	Trp63	1.40E-18	2.189235
ENSMUSG00000026984	Il1f6	3.02E-03	2.189606
ENSMUSG00000062044	Lmtk3	3.45E-02	2.190846
ENSMUSG00000052581	Lrrtm4	1.15E-11	2.192309
ENSMUSG00000045569	Mc2r	3.78E-02	2.192408
ENSMUSG00000017309	Cd300lg	6.73E-18	2.195374
ENSMUSG00000024526	Cidea	2.31E-06	2.199377
ENSMUSG00000081689	Gm9166	4.77E-02	2.201972
ENSMUSG00000102574	Gm33206	1.64E-02	2.204692
ENSMUSG00000025064	Col17a1	1.23E-11	2.208855
ENSMUSG00000074445	Sprr2a3	3.39E-03	2.210458
ENSMUSG00000116659	AC158985.1	1.19E-02	2.215346
ENSMUSG00000027401	Tgm3	2.06E-08	2.229316
ENSMUSG00000026985	Il1f8	3.43E-03	2.233766
ENSMUSG00000028186	Uox	1.47E-02	2.235586

ENSMUSG00000041991	Hrnr	2.86E-07	2.235634
ENSMUSG00000024972	Lgals12	4.44E-07	2.236885
ENSMUSG00000054146	Krt15	4.97E-10	2.240443
ENSMUSG00000021509	Slc25a48	9.46E-04	2.243699
ENSMUSG00000044322	Dsc1	1.20E-04	2.247548
ENSMUSG00000059668	Krt4	3.30E-08	2.252859
ENSMUSG00000102698	Gm37777	4.88E-02	2.254948
ENSMUSG00000031725	Ces1f	2.39E-03	2.264564
ENSMUSG00000028396	2310002L09Rik	6.45E-05	2.264786
ENSMUSG00000105128	Gm42870	1.67E-03	2.265372
ENSMUSG00000117222	AC060761.1	1.12E-09	2.268436
ENSMUSG00000039238	Zfp750	1.91E-05	2.270028
ENSMUSG00000028148	Them5	4.51E-09	2.271649
ENSMUSG00000027966	Col11a1	1.37E-12	2.271918
ENSMUSG00000117029	CT030155.1	3.50E-04	2.274179
ENSMUSG00000085615	A330035P11Rik	3.82E-03	2.27617
ENSMUSG00000097364	Gm26719	1.09E-03	2.281662
ENSMUSG00000046764	A530053G22Rik	3.40E-04	2.285877
ENSMUSG00000069441	Dsg1a	1.19E-12	2.293298
ENSMUSG00000106871	Gm3289	3.38E-02	2.300456
ENSMUSG00000026413	Pkp1	1.59E-11	2.301027
ENSMUSG00000043430	Psapl1	6.34E-09	2.302115
ENSMUSG00000026983	Il1f5	7.17E-04	2.303818
ENSMUSG00000044359	P2ry4	3.22E-04	2.308913
ENSMUSG00000023041	Krt6b	2.05E-02	2.310622
ENSMUSG00000094335	Igkv1-117	4.70E-02	2.317249
ENSMUSG00000040154	Wfdc5	1.56E-04	2.317891
ENSMUSG00000044505	Lingo4	4.11E-02	2.324002
ENSMUSG00000086155	9430041J12Rik	1.78E-02	2.328883
ENSMUSG00000051596	Otop1	5.62E-03	2.333939
ENSMUSG00000040283	Btnl9	4.98E-05	2.341489
ENSMUSG00000071019	Sdr16c6	6.69E-04	2.347186
ENSMUSG00000061928	Dsg1b	2.79E-10	2.356478
ENSMUSG00000044453	Ffar1	6.83E-03	2.359339
ENSMUSG00000074771	Ankef1	3.32E-11	2.367063
ENSMUSG00000102713	Gm29994	4.96E-02	2.37116
ENSMUSG00000033268	Duox1	1.02E-07	2.373757
ENSMUSG00000087382	Ctcflos	3.00E-06	2.374574
ENSMUSG00000022860	Chodl	2.17E-03	2.383702
ENSMUSG00000097335	Gm26563	3.11E-04	2.388002
ENSMUSG00000074113	Gm10629	2.59E-02	2.396626
ENSMUSG00000061527	Krt5	1.53E-10	2.400635
ENSMUSG00000102788	Gm38255	2.20E-02	2.411338
ENSMUSG00000063130	Calml3	1.42E-10	2.41536
ENSMUSG00000027761	Aadac	1.39E-02	2.416545
ENSMUSG00000021565	Slc6a19	1.11E-07	2.422981
ENSMUSG00000017607	Tns4	1.21E-08	2.42721
ENSMUSG00000086584	Gm12002	9.27E-09	2.431887
ENSMUSG00000056078	Lipm	3.36E-06	2.434023
ENSMUSG00000048455	Sprr1b	7.22E-04	2.435726
ENSMUSG00000074623	Gm826	2.01E-05	2.447222
ENSMUSG00000117322	AC154766.4	1.42E-03	2.450311
ENSMUSG00000074652	Myh7b	3.23E-04	2.464603
ENSMUSG00000097074	4833428L15Rik	3.94E-03	2.46861
ENSMUSG00000044748	Defb1	6.87E-04	2.475512
ENSMUSG00000109656	Gm45548	1.18E-02	2.476315
ENSMUSG00000028236	Sdr16c5	2.53E-03	2.481761

ENSMUSG00000030972	Acsm5	4.43E-02	2.484046
ENSMUSG00000082141	Gm11212	1.17E-02	2.488085
ENSMUSG00000114898	Gm49390	2.70E-02	2.494279
ENSMUSG00000043795	Prr33	9.14E-05	2.508198
ENSMUSG00000095079	Igha	3.83E-18	2.559163
ENSMUSG00000070719	Pla2g4d	2.65E-03	2.562518
ENSMUSG00000057913	Gm10032	3.14E-02	2.585521
ENSMUSG00000023176	Cpn2	4.45E-03	2.587907
ENSMUSG00000068893	Sprr2a2	1.16E-09	2.589158
ENSMUSG00000042662	Dusp15	9.84E-03	2.602635
ENSMUSG00000067006	Serpinb5	9.95E-09	2.602844
ENSMUSG00000086032	Gm15929	3.41E-02	2.608879
ENSMUSG00000092222	Gm20506	6.46E-03	2.617156
ENSMUSG00000055301	Adh7	5.78E-18	2.63083
ENSMUSG00000102762	4930403P22Rik	1.44E-03	2.635338
ENSMUSG00000028427	Aqp7	2.36E-05	2.650459
ENSMUSG00000078664	Sprr2a1	9.93E-05	2.651024
ENSMUSG00000019936	Epyc	2.77E-02	2.652037
ENSMUSG00000046095	Krt32	1.20E-03	2.667941
ENSMUSG00000114091	Gm40655	5.12E-07	2.678247
ENSMUSG00000099798	Gm29168	1.20E-02	2.686459
ENSMUSG00000027048	Abcb11	3.96E-02	2.686539
ENSMUSG00000032373	Car12	1.07E-30	2.712374
ENSMUSG00000035861	Tmprss11b	5.06E-03	2.728767
ENSMUSG00000097850	4631405K08Rik	6.26E-04	2.731215
ENSMUSG00000030046	Bmp10	2.22E-02	2.748688
ENSMUSG00000079451	Tmprss11g	2.47E-07	2.766776
ENSMUSG00000033765	Calm4	2.29E-07	2.770286
ENSMUSG00000074156	Ces1h	1.20E-08	2.790568
ENSMUSG00000078964	Ces1b	7.10E-05	2.800191
ENSMUSG00000029019	Nppb	4.80E-12	2.809285
ENSMUSG00000074183	Gsta1	1.83E-03	2.825282
ENSMUSG00000045545	Krt14	8.07E-21	2.845235
ENSMUSG00000033849	B3galt2	1.28E-06	2.854439
ENSMUSG00000037942	Crp	4.26E-04	2.872187
ENSMUSG00000032852	Rspo4	3.66E-02	2.874898
ENSMUSG00000028011	Tdo2	5.25E-03	2.883112
ENSMUSG00000053675	Tgm5	1.57E-02	2.88705
ENSMUSG00000114922	Ppifos	6.49E-06	2.892979
ENSMUSG00000092586	Ly6g6c	8.58E-10	2.894076
ENSMUSG00000075217	4833423E24Rik	5.12E-09	2.895953
ENSMUSG00000016327	Atp1b4	2.46E-06	2.972894
ENSMUSG00000028356	Ambp	1.17E-04	3.000966
ENSMUSG00000031710	Ucp1	1.67E-14	3.002674
ENSMUSG00000116482	Gm34152	1.61E-02	3.020639
ENSMUSG00000033196	Myh2	1.40E-20	3.128999
ENSMUSG00000013936	Myl2	1.78E-08	3.151791
ENSMUSG00000111709	Gm3776	1.40E-03	3.198663
ENSMUSG00000059898	Dsc3	1.21E-15	3.210725
ENSMUSG00000111556	Gm19299	4.63E-06	3.219853
ENSMUSG00000058354	Krt6a	5.91E-07	3.268707
ENSMUSG00000004872	Pax3	4.21E-04	3.300239
ENSMUSG00000106056	4930500L23Rik	1.18E-03	3.320195
ENSMUSG00000115207	Gm49132	2.01E-04	3.358344
ENSMUSG00000028001	Fga	2.45E-06	3.395634
ENSMUSG00000056632	Dsg3	1.17E-26	3.443911
ENSMUSG00000027513	Pck1	2.05E-42	3.544075

ENSMUSG00000017950	Hnf4a	3.71E-04	3.786185
ENSMUSG00000025003	Cyp2c39	1.57E-03	4.069422
ENSMUSG00000102098	2310016D03Rik	8.49E-06	4.610042
ENSMUSG00000056656	Apol8	1.42E-18	4.685594
ENSMUSG00000033860	Fgg	2.32E-12	4.837005
ENSMUSG00000022875	Kng1	3.51E-06	4.98915
ENSMUSG00000025194	Abcc2	1.51E-05	5.208255
ENSMUSG00000054422	Fabp1	9.90E-07	5.384976
ENSMUSG00000021364	Elovl2	1.66E-05	5.766093
ENSMUSG00000001670	Tat	8.99E-06	8.225412
ENSMUSG00000030131	Mug2	4.90E-08	8.940782
ENSMUSG00000030359	Pzp	5.53E-19	10.7158
ENSMUSG00000028307	Aldob	4.66E-11	13.80692
ENSMUSG00000020609	Apob	3.96E-21	14.75844
ENSMUSG00000085154	C130046K22Rik	5.61E-09	14.96049
ENSMUSG00000022868	Ahsg	1.17E-21	15.70773
ENSMUSG00000035540	Gc	1.39E-15	17.68534
ENSMUSG00000019932	Kera	9.46E-13	17.79842
ENSMUSG00000003053	Cyp2c29	3.02E-11	21.15165
ENSMUSG00000059481	Plg	1.20E-08	22.09324
ENSMUSG00000056035	Cyp3a11	1.28E-13	54.83161
ENSMUSG00000032083	Apoa1	5.63E-16	55.84116
ENSMUSG00000061808	Ttr	6.66E-07	82.413
ENSMUSG00000059908	Mug1	1.60E-17	99.55708
ENSMUSG00000029630	Cyp3a25	1.25E-06	123.9654
ENSMUSG00000029368	Alb	2.26E-43	153.3651
ENSMUSG00000025991	Cps1	2.28E-07	180.3232
ENSMUSG00000033831	Fgb	4.13E-09	409.5904

Appendix U. Murine differential gene expression in the lungs 6 h post-infection, 947 vs 4559M. Genes with fold change (FC) greater than 1.5 and $p < 0.05$ are shown. FC values highlighted in blue = upregulated in 947, while values highlighted in red = upregulated in 4559M.

Gene Stable ID	Gene Name	padj	FC
ENSMUSG00000096349	*Gm22513*	4.55E-03	2.606374
ENSMUSG00000045932	*Ifit2*	6.67E-41	2.120213
ENSMUSG00000003545	*Fosb*	1.28E-08	2.101081
ENSMUSG00000094392	*Gm3788*	2.89E-05	2.057367
ENSMUSG00000057596	*Trim30d*	5.07E-06	1.986075
ENSMUSG00000000386	*Mx1*	2.11E-34	1.933773
ENSMUSG00000020641	*Rsad2*	1.35E-13	1.923719
ENSMUSG00000059434	*Gckr*	5.94E-06	1.899378
ENSMUSG00000097312	*Gm26870*	9.81E-06	1.880663
ENSMUSG00000060183	*Cxcl11*	4.50E-06	1.864222
ENSMUSG00000035852	*Misp*	1.64E-10	1.805939
ENSMUSG00000015437	*Gzmb*	7.02E-04	1.803683
ENSMUSG00000108289	*Gm44174*	1.88E-06	1.793558
ENSMUSG00000048003	*Catsper4*	2.11E-03	1.765394
ENSMUSG00000052353	*Cemip*	5.51E-17	1.762085
ENSMUSG00000084823	*Gm17216*	1.45E-02	1.726759
ENSMUSG00000020638	*Cmpk2*	4.84E-24	1.693086
ENSMUSG00000103824	*Gm38177*	1.68E-02	1.688716
ENSMUSG00000031757	*Mt4*	3.02E-02	1.675168
ENSMUSG00000037962	*Rflna*	2.29E-02	1.671596
ENSMUSG00000114553	*Gm7644*	1.01E-02	1.623832
ENSMUSG00000026826	*Nr4a2*	1.18E-04	1.600445
ENSMUSG00000059832	*Kprp*	2.90E-03	1.592978
ENSMUSG00000014543	*Klra17*	2.61E-06	1.58641
ENSMUSG00000063651	*Cnfn*	4.88E-03	1.573752
ENSMUSG00000116660	*CT030736.1*	1.20E-05	1.572765
ENSMUSG00000028031	*Dkk2*	3.03E-04	1.572515
ENSMUSG00000059230	*Defb4*	2.16E-02	1.569063
ENSMUSG00000086196	*Gm13571*	2.78E-02	1.568524
ENSMUSG00000067767	*Clec4b2*	1.74E-02	1.568218
ENSMUSG00000073902	*Gm1966*	8.80E-07	1.554048
ENSMUSG00000111229	*Gm39323*	1.70E-02	1.52393
ENSMUSG00000034855	*Cxcl10*	3.16E-04	1.523329
ENSMUSG00000070866	*Zfp804a*	2.31E-02	1.521761
ENSMUSG00000097134	*1110002J07Rik*	1.21E-02	1.519142
ENSMUSG00000032502	*Stac*	4.38E-02	1.517901
ENSMUSG00000043664	*Tmem221*	3.80E-02	1.516904
ENSMUSG00000086213	*A330040F15Rik*	1.39E-04	1.503579
ENSMUSG00000096349	*Gm22513*	4.55E-03	2.606374
ENSMUSG00000045932	*Ifit2*	6.67E-41	2.120213
ENSMUSG00000003545	*Fosb*	1.28E-08	2.101081
ENSMUSG00000094392	*Gm3788*	2.89E-05	2.057367
ENSMUSG00000057596	*Trim30d*	5.07E-06	1.986075
ENSMUSG00000000386	*Mx1*	2.11E-34	1.933773
ENSMUSG00000020641	*Rsad2*	1.35E-13	1.923719
ENSMUSG00000059434	*Gckr*	5.94E-06	1.899378
ENSMUSG00000097312	*Gm26870*	9.81E-06	1.880663
ENSMUSG00000060183	*Cxcl11*	4.50E-06	1.864222
ENSMUSG00000035852	*Misp*	1.64E-10	1.805939
ENSMUSG00000015437	*Gzmb*	7.02E-04	1.803683
ENSMUSG00000108289	*Gm44174*	1.88E-06	1.793558
ENSMUSG00000048003	*Catsper4*	2.11E-03	1.765394

ENSMUSG00000052353	*Cemip*	5.51E-17	1.762085
ENSMUSG00000084823	*Gm17216*	1.45E-02	1.726759
ENSMUSG00000020638	*Cmpk2*	4.84E-24	1.693086
ENSMUSG00000103824	*Gm38177*	1.68E-02	1.688716
ENSMUSG00000031757	*Mt4*	3.02E-02	1.675168
ENSMUSG00000037962	*Rflna*	2.29E-02	1.671596
ENSMUSG00000114553	*Gm7644*	1.01E-02	1.623832
ENSMUSG00000026826	*Nr4a2*	1.18E-04	1.600445
ENSMUSG00000059832	*Kprp*	2.90E-03	1.592978
ENSMUSG00000014543	*Klra17*	2.61E-06	1.58641
ENSMUSG00000063651	*Cnfn*	4.88E-03	1.573752
ENSMUSG00000116660	*CT030736.1*	1.20E-05	1.572765
ENSMUSG00000028031	*Dkk2*	3.03E-04	1.572515
ENSMUSG00000059230	*Defb4*	2.16E-02	1.569063
ENSMUSG00000086196	*Gm13571*	2.78E-02	1.568524
ENSMUSG00000067767	*Clec4b2*	1.74E-02	1.568218
ENSMUSG00000073902	*Gm1966*	8.80E-07	1.554048
ENSMUSG00000111229	*Gm39323*	1.70E-02	1.52393
ENSMUSG00000034855	*Cxcl10*	3.16E-04	1.523329
ENSMUSG00000070866	*Zfp804a*	2.31E-02	1.521761
ENSMUSG00000097134	*1110002J07Rik*	1.21E-02	1.519142
ENSMUSG00000032502	*Stac*	4.38E-02	1.517901
ENSMUSG00000043664	*Tmem221*	3.80E-02	1.516904
ENSMUSG00000086213	*A330040F15Rik*	1.39E-04	1.503579
ENSMUSG00000101930	*Gm5441*	8.04E-04	1.501768
ENSMUSG00000116031	*D030024E09Rik*	1.14E-03	1.505026
ENSMUSG00000109157	*Gm44829*	2.31E-02	1.513042
ENSMUSG00000047976	*Kcna1*	1.32E-03	1.515831
ENSMUSG00000098708	*Gm27252*	9.38E-03	1.516922
ENSMUSG00000066510	*Ankdd1a*	2.65E-04	1.517129
ENSMUSG00000096084	*Gm21850*	3.46E-03	1.51884
ENSMUSG00000021259	*Cyp46a1*	4.91E-02	1.520911
ENSMUSG00000056569	*Mpz*	1.47E-06	1.521436
ENSMUSG00000092267	*Gm20417*	4.50E-03	1.523107
ENSMUSG00000030350	*Prmt8*	2.14E-06	1.527589
ENSMUSG00000108929	*Cc2d2b*	2.94E-02	1.536074
ENSMUSG00000000197	*Nalcn*	3.23E-05	1.543563
ENSMUSG00000089844	*A530032D15Rik*	2.07E-05	1.544398
ENSMUSG00000054582	*Pabpc1l*	5.95E-05	1.549878
ENSMUSG00000090877	*Hspa1b*	1.31E-04	1.554299
ENSMUSG00000094125	*Gm13698*	1.01E-02	1.558384
ENSMUSG00000094336	*Gm13693*	1.01E-02	1.558384
ENSMUSG00000096484	*Gm13696*	1.01E-02	1.558384
ENSMUSG00000096337	*Gm13694*	1.01E-02	1.558384
ENSMUSG00000095824	*Gm13697*	1.01E-02	1.558384
ENSMUSG00000079247	*Gm13691*	1.01E-02	1.558384
ENSMUSG00000020698	*Cct6b*	4.95E-02	1.558508
ENSMUSG00000097071	*4930544I03Rik*	2.71E-03	1.558902
ENSMUSG00000111818	*Gm17749*	3.50E-04	1.559008
ENSMUSG00000096729	*Gm13695*	9.65E-03	1.560095
ENSMUSG00000000157	*Itgb2l*	1.35E-10	1.563713
ENSMUSG00000102590	*Mannr*	3.05E-02	1.566127
ENSMUSG00000100457	*D830032E09Rik*	4.66E-02	1.566802
ENSMUSG00000069830	*Nlrp1a*	3.96E-02	1.567104
ENSMUSG00000027513	*Pck1*	9.84E-05	1.579451
ENSMUSG00000109002	*Gm38405*	3.97E-02	1.583287
ENSMUSG00000087113	*Gm11714*	7.53E-03	1.586987

ENSMUSG00000019577	*Pdk4*	7.99E-35	1.589981
ENSMUSG00000109032	*Gm7972*	1.78E-03	1.592848
ENSMUSG00000017309	*Cd300lg*	1.27E-05	1.593726
ENSMUSG00000042895	*Abra*	1.07E-04	1.59373
ENSMUSG00000093482	*Gm20619*	4.17E-04	1.595111
ENSMUSG00000025038	*Efhc2*	1.41E-03	1.595115
ENSMUSG00000028989	*Angptl7*	2.82E-04	1.597595
ENSMUSG00000028573	*Fggy*	6.11E-03	1.598726
ENSMUSG00000096351	*Samd11*	2.77E-03	1.599425
ENSMUSG00000001482	*Def8*	1.63E-08	1.601844
ENSMUSG00000103620	*Gm37359*	6.80E-03	1.602521
ENSMUSG00000034755	*Pcdh11x*	2.76E-04	1.607959
ENSMUSG00000112707	*D830005E20Rik*	3.55E-07	1.612262
ENSMUSG00000025716	*Myo3a*	1.00E-02	1.616705
ENSMUSG00000039376	*Synpo2l*	3.29E-10	1.617835
ENSMUSG00000043487	*Acot6*	4.05E-02	1.619862
ENSMUSG00000040740	*Slc25a34*	5.61E-04	1.620673
ENSMUSG00000083898	*Gm7340*	2.52E-05	1.62131
ENSMUSG00000047216	*Cdh19*	3.15E-09	1.621717
ENSMUSG00000087436	*Gm16156*	3.54E-02	1.622122
ENSMUSG00000046748	*Tmem45a2*	5.95E-04	1.63198
ENSMUSG00000042451	*Mybph*	3.29E-11	1.633192
ENSMUSG00000112895	*Gm47567*	9.03E-03	1.63877
ENSMUSG00000031626	*Sorbs2*	2.96E-20	1.6396
ENSMUSG00000030607	*Acan*	1.15E-02	1.640047
ENSMUSG00000004668	*Abca13*	4.50E-22	1.64663
ENSMUSG00000025892	*Gria4*	2.09E-02	1.648351
ENSMUSG00000079243	*Xirp1*	1.13E-12	1.649967
ENSMUSG00000025172	*Ankrd2*	1.14E-04	1.655491
ENSMUSG00000032496	*Ltf*	1.64E-24	1.662871
ENSMUSG00000087353	*Gm13727*	9.58E-05	1.669227
ENSMUSG00000084783	*Gm15419*	2.41E-02	1.67799
ENSMUSG00000043789	*Vwce*	2.45E-03	1.682827
ENSMUSG00000092397	*C130080G10Rik*	3.31E-06	1.687017
ENSMUSG00000052581	*Lrrtm4*	1.05E-04	1.698365
ENSMUSG00000041476	*Smpx*	1.39E-04	1.709086
ENSMUSG00000103288	*Gm37273*	2.47E-03	1.713415
ENSMUSG00000091971	*Hspa1a*	2.89E-05	1.735291
ENSMUSG00000027014	*Cwc22*	4.55E-06	1.737258
ENSMUSG00000038357	*Camp*	1.72E-04	1.743837
ENSMUSG00000086354	*Gm13938*	1.32E-12	1.744173
ENSMUSG00000048388	*Fam171b*	3.75E-15	1.772987
ENSMUSG00000091119	*Ccdc152*	7.27E-04	1.775671
ENSMUSG00000092201	*A530058N18Rik*	3.96E-09	1.775799
ENSMUSG00000027966	*Col11a1*	1.22E-05	1.791424
ENSMUSG00000087362	*Gm13710*	7.49E-07	1.797954
ENSMUSG00000028865	*Cd164l2*	7.33E-03	1.840898
ENSMUSG00000026592	*Tex35*	4.20E-06	1.902222
ENSMUSG00000050830	*Vwc2*	2.01E-03	1.925254
ENSMUSG00000020848	*Doc2b*	7.33E-16	1.935334
ENSMUSG00000021071	*Trim9*	7.02E-07	1.951751
ENSMUSG00000031710	*Ucp1*	7.62E-05	1.957941
ENSMUSG00000042567	*Nek10*	5.83E-20	1.985917
ENSMUSG00000105361	*AY036118*	2.16E-04	2.072411
ENSMUSG00000032484	*Ngp*	7.92E-53	2.07311
ENSMUSG00000096960	*A230028O05Rik*	1.84E-11	2.079473
ENSMUSG00000029019	*Nppb*	1.68E-06	2.216413

ENSMUSG00000020609	*Apob*	5.06E-03	2.792234
ENSMUSG00000056656	*Apol8*	3.96E-09	3.055558
ENSMUSG00000013936	*Myl2*	4.89E-18	5.494857
ENSMUSG00000029368	*Alb*	2.47E-14	19.45594

Appendix V. Murine differential gene expression in the lungs 6 h post-infection, 947M vs 4559. Genes with fold change (FC) greater than 1.5 and $p < 0.05$ are shown. FC values highlighted in blue = upregulated in 947M, while values highlighted in red = upregulated in 4559.

Gene Stable ID	Gene Name	padj	FC
ENSMUSG00000096349	*Gm22513*	4.24E-09	5.203286
ENSMUSG00000086468	*Etaa1os*	3.06E-03	4.383019
ENSMUSG00000071679	*Rtl4*	2.82E-18	4.145063
ENSMUSG00000097554	*Gm26825*	3.15E-02	3.419807
ENSMUSG00000031551	*Ido1*	1.65E-05	3.222093
ENSMUSG00000085465	*Gm15347*	7.57E-04	3.20346
ENSMUSG00000089874	*9230117E06Rik*	4.64E-02	3.119926
ENSMUSG00000112246	*Gm40761*	1.67E-03	3.067346
ENSMUSG00000046242	*Nme9*	5.99E-06	3.059333
ENSMUSG00000105361	*AY036118*	7.94E-06	3.053392
ENSMUSG00000001494	*Sost*	8.97E-05	2.742959
ENSMUSG00000030114	*Klrg1*	6.18E-03	2.73067
ENSMUSG00000092591	*Gm20429*	2.74E-03	2.725606
ENSMUSG00000102608	*Gm37267*	3.18E-02	2.662128
ENSMUSG00000064941	*Gm23238*	4.50E-07	2.561069
ENSMUSG00000091694	*Apol11b*	3.42E-02	2.557668
ENSMUSG00000076612	*Ighg2c*	1.66E-02	2.526225
ENSMUSG00000117074	*AC121299.1*	9.05E-04	2.484582
ENSMUSG00000063594	*Gng8*	1.64E-02	2.483359
ENSMUSG00000102795	*Gm6236*	3.35E-02	2.457189
ENSMUSG00000095616	*Gm26244*	1.72E-04	2.370041
ENSMUSG00000025578	*Cbx8*	3.26E-04	2.32664
ENSMUSG00000086843	*E030013I19Rik*	1.04E-07	2.322747
ENSMUSG00000094306	*Gm24924*	2.98E-04	2.262227
ENSMUSG00000115432	*D130009I18Rik*	4.24E-03	2.229274
ENSMUSG00000070530	*Wfdc16*	2.71E-02	2.177114
ENSMUSG00000095969	*Rnu1a1*	3.65E-04	2.169236
ENSMUSG00000101603	*Gm28730*	4.48E-02	2.160864
ENSMUSG00000115307	*Gm49313*	2.36E-04	2.155958
ENSMUSG00000096659	*Gm25679*	1.87E-06	2.155429
ENSMUSG00000093815	*Gm26444*	1.87E-06	2.155429
ENSMUSG00000090667	*Gm765*	4.68E-02	2.133759
ENSMUSG00000082292	*Gm12250*	2.39E-09	2.123222
ENSMUSG00000080797	*Gm15760*	1.81E-02	2.120402
ENSMUSG00000108481	*Gm33248*	1.01E-19	2.098355
ENSMUSG00000070720	*Tmem200b*	5.47E-05	2.088404
ENSMUSG00000069300	*Hist1h2bj*	3.40E-02	2.08459
ENSMUSG00000065778	*Gm22154*	4.98E-02	2.079887
ENSMUSG00000094826	*Gm23804*	9.42E-06	2.058273
ENSMUSG00000091956	*C2cd4b*	2.21E-02	2.046617
ENSMUSG00000052026	*Slc6a7*	1.35E-06	2.03982
ENSMUSG00000114969	*Hba-ps3*	8.89E-03	2.039639
ENSMUSG00000109491	*Gm15396*	4.44E-03	2.0348
ENSMUSG00000046470	*Sox18*	7.42E-22	2.034619
ENSMUSG00000087943	*Gm24245*	4.06E-06	2.030591
ENSMUSG00000112831	*AC167229.1*	4.48E-02	1.969926
ENSMUSG00000044952	*Kctd21*	6.08E-12	1.954796
ENSMUSG00000116809	*AC122538.1*	1.49E-02	1.952285
ENSMUSG00000072599	*Ear-ps2*	4.25E-04	1.942615
ENSMUSG00000095260	*Gm25890*	2.93E-03	1.936872
ENSMUSG00000094812	*Gm22614*	2.93E-03	1.936872
ENSMUSG00000048988	*Elfn1*	3.07E-16	1.934531

ENSMUSG00000104965	*Gm43437*	2.42E-02	1.930614
ENSMUSG00000071661	*Zbtb3*	1.99E-02	1.929765
ENSMUSG00000035299	*Mid1*	1.10E-04	1.921743
ENSMUSG00000079330	*Lemd1*	3.53E-07	1.913457
ENSMUSG00000060981	*Hist1h4h*	2.00E-05	1.909585
ENSMUSG00000068696	*Gpr88*	1.30E-02	1.908856
ENSMUSG00000081684	*Rps2-ps13*	6.39E-08	1.908057
ENSMUSG00000064063	*BC048507*	1.73E-04	1.907851
ENSMUSG00000096205	*Gm22068*	2.30E-03	1.907755
ENSMUSG00000082192	*Gm14719*	7.60E-03	1.90406
ENSMUSG00000092118	*Fancf*	3.09E-02	1.903835
ENSMUSG00000050578	*Mmp13*	1.52E-03	1.899788
ENSMUSG00000064923	*Gm22042*	3.99E-03	1.899281
ENSMUSG00000055945	*Prr18*	4.95E-05	1.895915
ENSMUSG00000096214	*Gm22634*	3.91E-05	1.891642
ENSMUSG00000096206	*Gm22317*	3.91E-05	1.891642
ENSMUSG00000063681	*Crb1*	3.96E-02	1.887394
ENSMUSG00000116097	*Gm36738*	2.84E-03	1.876667
ENSMUSG00000095701	*Gm24830*	4.71E-03	1.8723
ENSMUSG00000096838	*Gm26232*	4.71E-03	1.8723
ENSMUSG00000065773	*Rnu1b6*	4.71E-03	1.8723
ENSMUSG00000107794	*Gm44095*	1.32E-03	1.871248
ENSMUSG00000083737	*Prdx6-ps2*	1.41E-03	1.870411
ENSMUSG00000035435	*Abca17*	1.48E-13	1.866967
ENSMUSG00000038233	*Fam198a*	3.68E-07	1.865708
ENSMUSG00000069305	*Hist1h4n*	9.20E-03	1.855769
ENSMUSG00000041479	*Syt15*	1.78E-07	1.853036
ENSMUSG00000112969	*Gm48496*	9.76E-03	1.84879
ENSMUSG00000032357	*Tinag*	3.44E-07	1.84595
ENSMUSG00000085154	*C130046K22Rik*	1.34E-02	1.844771
ENSMUSG00000114028	*9630002D21Rik*	4.31E-03	1.844134
ENSMUSG00000036264	*Fstl4*	3.58E-03	1.839891
ENSMUSG00000108580	*Gm39094*	5.20E-27	1.83939
ENSMUSG00000095580	*Rnu1b1*	9.28E-03	1.834552
ENSMUSG00000093834	*Rnu1b2*	9.28E-03	1.834552
ENSMUSG00000060678	*Hist1h4c*	1.39E-05	1.826151
ENSMUSG00000045410	*Akr1e1*	8.33E-04	1.825984
ENSMUSG00000085297	*Gm11651*	3.62E-02	1.823187
ENSMUSG00000110634	*Gm45895*	4.27E-02	1.812488
ENSMUSG00000035528	*Npffr2*	8.19E-03	1.809944
ENSMUSG00000088246	*Gm25911*	1.52E-07	1.809528
ENSMUSG00000086368	*Gm13830*	4.51E-04	1.80628
ENSMUSG00000042988	*Notum*	1.04E-02	1.800697
ENSMUSG00000087247	*Alkal1*	1.02E-14	1.799935
ENSMUSG00000037279	*Ovol2*	4.81E-03	1.799681
ENSMUSG00000060093	*Hist1h4a*	1.67E-03	1.792799
ENSMUSG00000088609	*Gm24187*	7.72E-07	1.790795
ENSMUSG00000085982	*9530051G07Rik*	8.90E-03	1.790428
ENSMUSG00000029193	*Cckar*	6.00E-06	1.790204
ENSMUSG00000086822	*5330413P13Rik*	2.14E-02	1.781756
ENSMUSG00000067455	*Hist1h4j*	4.84E-02	1.781086
ENSMUSG00000009900	*Wnt3a*	7.74E-05	1.780263
ENSMUSG00000092240	*Gm4246*	6.92E-04	1.769107
ENSMUSG00000084998	*Gm16279*	3.51E-03	1.767919
ENSMUSG00000053961	*Ang5*	3.61E-02	1.764068
ENSMUSG00000027070	*Lrp2*	5.22E-34	1.760968
ENSMUSG00000069306	*Hist1h4m*	3.39E-02	1.760173

ENSMUSG00000085882	*2610507I01Rik*	1.69E-03	1.759883
ENSMUSG00000092805	*Gm26461*	4.98E-03	1.756282
ENSMUSG00000024925	*Rnaseh2c*	2.34E-03	1.756123
ENSMUSG00000031831	*Dnaaf1*	3.63E-02	1.748301
ENSMUSG00000052117	*D630039A03Rik*	1.92E-03	1.746534
ENSMUSG00000031220	*Awat2*	4.93E-03	1.738885
ENSMUSG00000101605	*Ace3*	9.36E-06	1.738835
ENSMUSG00000106229	*Gm19409*	3.20E-02	1.738286
ENSMUSG00000030043	*Tacr1*	5.14E-05	1.733899
ENSMUSG00000101674	*4930444A19Rik*	4.33E-02	1.733428
ENSMUSG00000103160	*C130012C08Rik*	4.54E-02	1.730458
ENSMUSG00000047085	*Lrrc4b*	2.55E-04	1.729971
ENSMUSG00000086596	*Susd5*	1.35E-05	1.729874
ENSMUSG00000070167	*Snora57*	5.72E-04	1.729595
ENSMUSG00000050188	*Lsm10*	1.05E-03	1.72668
ENSMUSG00000037649	*H2-DMa*	1.45E-08	1.723012
ENSMUSG00000086390	*1810019D21Rik*	4.92E-06	1.722576
ENSMUSG00000020734	*Grin2c*	9.25E-03	1.722135
ENSMUSG00000106373	*Gm6522*	1.37E-03	1.721283
ENSMUSG00000100041	*Gm5702*	2.41E-02	1.71842
ENSMUSG00000040936	*Ulk4*	1.20E-17	1.714171
ENSMUSG00000046240	*Hepacam*	2.58E-05	1.711621
ENSMUSG00000030041	*M1ap*	2.40E-08	1.711292
ENSMUSG00000035504	*Reep6*	3.13E-04	1.70748
ENSMUSG00000036295	*Lrrn3*	1.27E-03	1.70554
ENSMUSG00000105790	*Gm24105*	3.99E-03	1.70285
ENSMUSG00000053318	*Slamf8*	2.80E-02	1.700939
ENSMUSG00000082571	*Gm8737*	7.77E-03	1.698276
ENSMUSG00000034324	*Tmem132c*	9.33E-22	1.697915
ENSMUSG00000064288	*Hist1h4k*	2.67E-02	1.697211
ENSMUSG00000117037	*CT010433.2*	1.34E-02	1.69681
ENSMUSG00000037628	*Cdkn3*	2.99E-02	1.696525
ENSMUSG00000037962	*Rflna*	3.78E-03	1.692265
ENSMUSG00000061482	*Hist1h4d*	3.50E-06	1.688716
ENSMUSG00000050288	*Fzd2*	3.65E-04	1.688423
ENSMUSG00000076258	*Gm23935*	4.28E-05	1.682922
ENSMUSG00000092674	*Gm24105*	4.53E-03	1.682736
ENSMUSG00000034532	*Fbxo16*	1.50E-02	1.679353
ENSMUSG00000032502	*Stac*	5.86E-04	1.678126
ENSMUSG00000072601	*Ear1*	1.06E-06	1.671809
ENSMUSG00000105145	*Gm47299*	5.17E-03	1.670472
ENSMUSG00000105788	*Gm47295*	5.18E-03	1.670415
ENSMUSG00000035910	*Dcdc2a*	2.61E-02	1.666406
ENSMUSG00000097399	*Gm26555*	2.67E-02	1.664266
ENSMUSG00000060988	*Galnt13*	6.00E-07	1.662241
ENSMUSG00000077323	*Rnu11*	3.05E-02	1.661727
ENSMUSG00000039672	*Kcne2*	2.18E-02	1.658794
ENSMUSG00000070873	*Lilra5*	5.27E-04	1.658722
ENSMUSG00000030093	*Wnt7a*	1.03E-04	1.65745
ENSMUSG00000022504	*Ciita*	2.11E-16	1.65614
ENSMUSG00000042985	*Upk3b*	4.24E-09	1.655501
ENSMUSG00000033053	*1700028P14Rik*	1.36E-02	1.654074
ENSMUSG00000058057	*Mettl7a3*	3.23E-02	1.653564
ENSMUSG00000049511	*Htr1b*	3.81E-04	1.649535
ENSMUSG00000076281	*Gm24270*	3.95E-04	1.648636
ENSMUSG00000079505	*Gm11131*	1.20E-03	1.646768
ENSMUSG00000048696	*Mex3d*	4.84E-05	1.646018

ENSMUSG00000027186	*Elf5*	3.61E-04	1.63763
ENSMUSG00000106416	*Gm5857*	3.80E-02	1.636649
ENSMUSG00000110380	*Gm45332*	1.47E-02	1.634963
ENSMUSG00000097453	*Gm26894*	1.65E-02	1.633469
ENSMUSG00000020493	*Prr11*	1.30E-02	1.633102
ENSMUSG00000061171	*Slc38a11*	2.46E-02	1.631519
ENSMUSG00000114566	*Gm48500*	2.22E-02	1.631147
ENSMUSG00000080538	*Gm25541*	4.24E-02	1.631042
ENSMUSG00000041431	*Ccnb1*	3.24E-02	1.628007
ENSMUSG00000025789	*St8sia2*	7.94E-07	1.627729
ENSMUSG00000090166	*Ear10*	5.45E-04	1.627571
ENSMUSG00000063779	*Chil4*	4.43E-04	1.627486
ENSMUSG00000062545	*Tlr12*	1.63E-02	1.627004
ENSMUSG00000092702	*Gm24514*	2.88E-02	1.625445
ENSMUSG00000030800	*Prss8*	1.50E-08	1.624743
ENSMUSG00000060969	*Irx1*	1.52E-09	1.623286
ENSMUSG00000027656	*Wisp2*	1.04E-26	1.618407
ENSMUSG00000042210	*Abhd14a*	9.45E-03	1.615522
ENSMUSG00000022097	*Sftpc*	1.49E-08	1.614898
ENSMUSG00000037190	*Cyb561d2*	3.40E-02	1.614444
ENSMUSG00000056665	*Them6*	2.04E-02	1.61301
ENSMUSG00000085069	*Gm13111*	5.74E-03	1.611789
ENSMUSG00000038094	*Atp13a4*	5.04E-06	1.611226
ENSMUSG00000112468	*Gm47720*	4.04E-06	1.61105
ENSMUSG00000106352	*5033403H07Rik*	1.21E-06	1.61053
ENSMUSG00000023147	*Wrb*	8.63E-06	1.609411
ENSMUSG00000043719	*Col6a6*	5.13E-12	1.607024
ENSMUSG00000097805	*Gm17473*	1.31E-07	1.60527
ENSMUSG00000099338	*2810030D12Rik*	6.11E-03	1.605182
ENSMUSG00000098178	*Gm42418*	1.65E-03	1.604909
ENSMUSG00000024810	*Il33*	1.71E-18	1.603739
ENSMUSG00000026870	*Cutal*	1.49E-02	1.601874
ENSMUSG00000036114	*Rpp25l*	1.15E-03	1.599792
ENSMUSG00000074480	*Mex3a*	4.38E-02	1.598909
ENSMUSG00000013089	*Etv5*	2.42E-22	1.598533
ENSMUSG00000042766	*Trim46*	1.71E-03	1.598267
ENSMUSG00000075020	*Mir670hg*	2.15E-03	1.596736
ENSMUSG00000087424	*5730405O15Rik*	2.37E-02	1.595889
ENSMUSG00000040841	*Six5*	3.01E-05	1.595572
ENSMUSG00000027380	*Acoxl*	3.11E-06	1.593887
ENSMUSG00000108218	*Olfr1372-ps1*	4.02E-05	1.592729
ENSMUSG00000041380	*Htr2c*	1.13E-06	1.592272
ENSMUSG00000019909	*Fam162b*	4.28E-02	1.591414
ENSMUSG00000090704	*Trp53-ps*	2.03E-07	1.591127
ENSMUSG00000022844	*Pdia5*	8.24E-13	1.590662
ENSMUSG00000033595	*Lgi3*	2.28E-12	1.588201
ENSMUSG00000065701	*Rny1*	4.19E-02	1.587797
ENSMUSG00000037610	*Kcnmb2*	5.28E-08	1.587617
ENSMUSG00000043895	*S1pr2*	1.57E-16	1.586409
ENSMUSG00000102175	*Gm6119*	1.44E-02	1.583275
ENSMUSG00000037846	*Rtkn2*	8.92E-07	1.58299
ENSMUSG00000030329	*Pianp*	1.03E-02	1.58274
ENSMUSG00000027932	*Slc27a3*	3.43E-03	1.582304
ENSMUSG00000030732	*Chrdl2*	4.82E-02	1.581585
ENSMUSG00000094786	*Gm14403*	1.30E-10	1.579975
ENSMUSG00000107290	*Gm43282*	3.94E-02	1.578205
ENSMUSG00000022615	*Tymp*	2.61E-03	1.57791

ENSMUSG00000075389	*2810410L24Rik*	1.42E-04	1.575503
ENSMUSG00000091780	*Sco2*	3.28E-03	1.574907
ENSMUSG00000064945	*Rny3*	3.69E-02	1.573231
ENSMUSG00000009114	*2610028H24Rik*	8.71E-05	1.569539
ENSMUSG00000074283	*Zfp109*	6.83E-04	1.567793
ENSMUSG00000019295	*Tmem129*	8.45E-07	1.564808
ENSMUSG00000026941	*Mamdc4*	2.12E-05	1.563251
ENSMUSG00000086549	*Gm13648*	7.89E-03	1.559935
ENSMUSG00000055134	*9130017K11Rik*	1.15E-02	1.55658
ENSMUSG00000033952	*Aspm*	2.58E-05	1.55636
ENSMUSG00000003779	*Kif20a*	3.46E-02	1.556308
ENSMUSG00000025035	*Arl3*	2.31E-07	1.556136
ENSMUSG00000044030	*Irf2bp1*	2.69E-06	1.55373
ENSMUSG00000093327	*Mir5107*	5.85E-09	1.552336
ENSMUSG00000107349	*Gm6655*	1.81E-02	1.551154
ENSMUSG00000106633	*Gm43431*	4.58E-02	1.551081
ENSMUSG00000078794	*Dact3*	8.48E-05	1.549569
ENSMUSG00000027954	*Efna1*	1.86E-10	1.54683
ENSMUSG00000021700	*Rab3c*	3.56E-05	1.5459
ENSMUSG00000025902	*Sox17*	9.62E-12	1.5454
ENSMUSG00000078772	*Gm12353*	3.08E-08	1.545118
ENSMUSG00000070473	*Cldn3*	4.38E-07	1.5441
ENSMUSG00000069515	*Lyz1*	8.64E-14	1.543848
ENSMUSG00000030796	*Tead2*	4.76E-10	1.543617
ENSMUSG00000040809	*Chil3*	4.58E-05	1.543465
ENSMUSG00000037101	*Ttc29*	7.26E-06	1.542686
ENSMUSG00000040289	*Hey1*	6.55E-13	1.542366
ENSMUSG00000022595	*Lypd2*	2.36E-02	1.542217
ENSMUSG00000051817	*Sox12*	2.88E-02	1.54192
ENSMUSG00000029053	*Prkcz*	4.18E-12	1.538465
ENSMUSG00000113212	*Gm47435*	1.47E-02	1.538088
ENSMUSG00000049625	*Tifab*	1.51E-07	1.537426
ENSMUSG00000032224	*Fam81a*	6.07E-03	1.535556
ENSMUSG00000112343	*Sfta3-ps*	1.96E-21	1.534461
ENSMUSG00000027849	*Syt6*	2.09E-04	1.533147
ENSMUSG00000024206	*Rfx2*	7.51E-12	1.530804
ENSMUSG00000006567	*Atp7b*	5.51E-09	1.529838
ENSMUSG00000073424	*Cyp4f15*	1.31E-02	1.529096
ENSMUSG00000044081	*Zfp85os*	2.57E-02	1.528554
ENSMUSG00000058396	*Gpr182*	1.82E-07	1.527896
ENSMUSG00000086141	*9030622O22Rik*	1.39E-08	1.526052
ENSMUSG00000029651	*Mtus2*	1.31E-14	1.524294
ENSMUSG00000040009	*Gnaz*	1.48E-02	1.522347
ENSMUSG00000089694	*Nat8f7*	3.13E-02	1.518666
ENSMUSG00000034685	*Fam171a2*	4.78E-03	1.518575
ENSMUSG00000041261	*Car8*	9.86E-22	1.517297
ENSMUSG00000057123	*Gja5*	2.89E-12	1.517113
ENSMUSG00000115420	*AL732506.1*	8.45E-03	1.516697
ENSMUSG00000088088	*Rmrp*	8.45E-03	1.516697
ENSMUSG00000081093	*Gm12565*	3.28E-02	1.515801
ENSMUSG00000117046	*AC122746.1*	3.96E-02	1.515479
ENSMUSG00000104114	*Gm37297*	5.73E-04	1.515439
ENSMUSG00000021496	*Pcbd2*	8.78E-13	1.515151
ENSMUSG00000028540	*Dph2*	7.17E-04	1.514882
ENSMUSG00000043668	*Tox3*	3.57E-13	1.513681
ENSMUSG00000111409	*Gm49380*	3.92E-07	1.511921
ENSMUSG00000027424	*Mgme1*	1.40E-02	1.511053

ENSMUSG00000103738	*Gm37652*	2.01E-02	1.50916
ENSMUSG00000044217	*Aqp5*	2.95E-15	1.509144
ENSMUSG00000027490	*E2f1*	4.24E-02	1.508243
ENSMUSG00000001444	*Tbx21*	2.37E-04	1.504887
ENSMUSG00000066319	*Rtp3*	3.35E-03	1.504256
ENSMUSG00000025512	*Chid1*	8.49E-12	1.504081
ENSMUSG00000009394	*Syn2*	4.75E-08	1.503605
ENSMUSG00000115143	*Fkbp1a-ps1*	3.78E-04	1.502351
ENSMUSG00000033282	*Rpgrip1l*	6.03E-09	1.502144
ENSMUSG00000036192	*Rorb*	1.76E-04	1.50102
ENSMUSG00000099553	*Gm29538*	1.36E-02	1.500991
ENSMUSG00000072596	*Ear2*	2.39E-06	1.500831
ENSMUSG00000090737	*Gm6788*	2.53E-03	1.500806
ENSMUSG00000085043	*Gm13184*	3.64E-02	1.500172
ENSMUSG00000030428	*Ttyh1*	1.19E-02	1.502203
ENSMUSG00000050357	*Carmil2*	4.60E-05	1.502416
ENSMUSG00000032089	*Il10ra*	4.81E-21	1.502903
ENSMUSG00000030107	*Usp18*	1.51E-14	1.502976
ENSMUSG00000001014	*Icam4*	1.79E-02	1.502992
ENSMUSG00000030785	*Cox6a2*	2.61E-07	1.503108
ENSMUSG00000079434	*Neu2*	3.87E-02	1.503483
ENSMUSG00000105677	*Gm43328*	4.53E-05	1.503833
ENSMUSG00000101751	*Gm2427*	5.37E-05	1.503916
ENSMUSG00000113668	*Gm47451*	1.42E-03	1.50528
ENSMUSG00000052374	*Actn2*	3.36E-22	1.50534
ENSMUSG00000057897	*Camk2b*	6.39E-04	1.505487
ENSMUSG00000105337	*1700094M23Rik*	2.95E-06	1.505662
ENSMUSG00000042678	*Myo15*	2.07E-03	1.506355
ENSMUSG00000033107	*Rnf125*	1.82E-24	1.50685
ENSMUSG00000036390	*Gadd45a*	1.65E-09	1.507699
ENSMUSG00000058470	*Gm8369*	1.45E-07	1.507965
ENSMUSG00000032369	*Plscr1*	5.18E-17	1.508682
ENSMUSG00000105355	*Gm40117*	4.51E-02	1.508939
ENSMUSG00000040899	*Ccr6*	1.50E-05	1.509044
ENSMUSG00000011305	*Plin5*	1.11E-03	1.509246
ENSMUSG00000102343	*Gm37381*	4.52E-02	1.509423
ENSMUSG00000078937	*Cpt1b*	1.25E-07	1.509518
ENSMUSG00000021250	*Fos*	1.72E-12	1.509638
ENSMUSG00000006763	*Saal1*	3.57E-13	1.509651
ENSMUSG00000074452	*Pate2*	1.01E-06	1.509912
ENSMUSG00000109700	*Gm21123*	5.59E-03	1.510051
ENSMUSG00000030433	*Sbk2*	7.43E-06	1.510461
ENSMUSG00000053040	*Aph1c*	2.31E-08	1.510621
ENSMUSG00000101344	*Gm29183*	7.91E-11	1.510713
ENSMUSG00000035208	*Slfn8*	1.32E-11	1.510878
ENSMUSG00000024778	*Fas*	1.01E-25	1.5111
ENSMUSG00000028862	*Map3k6*	1.35E-20	1.511475
ENSMUSG00000034833	*Tespa1*	1.65E-09	1.512576
ENSMUSG00000115344	*Gm49364*	3.50E-09	1.512709
ENSMUSG00000057092	*Fxyd3*	1.24E-02	1.513268
ENSMUSG00000034959	*Rubcnl*	4.29E-14	1.514234
ENSMUSG00000034842	*Art3*	1.48E-18	1.514796
ENSMUSG00000003134	*Tbc1d8*	2.32E-15	1.51505
ENSMUSG00000048004	*Tmem196*	1.46E-02	1.516581
ENSMUSG00000012123	*Crybg2*	6.60E-05	1.516896
ENSMUSG00000112808	*Gm4739*	1.85E-05	1.516929
ENSMUSG00000025271	*Pfkfb1*	3.17E-13	1.51768

ENSMUSG00000091412	*Gm2895*	1.63E-06	1.518936
ENSMUSG00000026535	*Ifi202b*	5.15E-11	1.518943
ENSMUSG00000044244	*Il20rb*	2.54E-19	1.519567
ENSMUSG00000056755	*Grm7*	9.05E-05	1.519614
ENSMUSG00000085908	*Gm14209*	7.71E-04	1.519669
ENSMUSG00000029377	*Ereg*	1.71E-06	1.520092
ENSMUSG00000024590	*Lmnb1*	2.04E-16	1.521965
ENSMUSG00000071342	*Lsmem1*	5.96E-06	1.522759
ENSMUSG00000069808	*Fam57a*	1.08E-06	1.522864
ENSMUSG00000109371	*Gm44626*	2.28E-02	1.523263
ENSMUSG00000051650	*B3gnt2*	2.04E-28	1.524523
ENSMUSG00000033065	*Pfkm*	5.41E-13	1.52463
ENSMUSG00000087589	*D430040D24Rik*	2.69E-06	1.524663
ENSMUSG00000092201	*A530058N18Rik*	1.19E-05	1.524752
ENSMUSG00000030077	*Chl1*	1.64E-18	1.526046
ENSMUSG00000038665	*Dgki*	1.02E-06	1.526881
ENSMUSG00000032661	*Oas3*	2.11E-10	1.526922
ENSMUSG00000104010	*Gm37366*	8.49E-03	1.527991
ENSMUSG00000032338	*Hcn4*	1.08E-07	1.528197
ENSMUSG00000021125	*Arg2*	6.25E-15	1.528694
ENSMUSG00000109279	*Gm45220*	7.04E-07	1.52872
ENSMUSG00000025804	*Ccr1*	1.42E-12	1.528934
ENSMUSG00000058498	*Rnf207*	6.72E-03	1.530495
ENSMUSG00000074625	*Arhgap40*	2.06E-03	1.530634
ENSMUSG00000108929	*Cc2d2b*	1.62E-02	1.532023
ENSMUSG00000014198	*Zfp385c*	4.22E-02	1.532252
ENSMUSG00000035818	*Plekhs1*	3.36E-03	1.532308
ENSMUSG00000035580	*Kcnh8*	6.34E-04	1.532597
ENSMUSG00000051748	*Wfdc21*	7.29E-08	1.53281
ENSMUSG00000038663	*Fsd2*	8.48E-09	1.533131
ENSMUSG00000022523	*Fgf12*	2.76E-14	1.533583
ENSMUSG00000037904	*Ankrd9*	6.45E-03	1.535904
ENSMUSG00000104406	*Gm38014*	4.26E-03	1.536295
ENSMUSG00000109764	*Klkb1*	2.91E-02	1.53632
ENSMUSG00000026628	*Atf3*	2.70E-20	1.537981
ENSMUSG00000029915	*Clec5a*	1.81E-14	1.538051
ENSMUSG00000042254	*Cilp*	4.11E-06	1.538166
ENSMUSG00000078963	*Hsbp1l1*	4.27E-02	1.538173
ENSMUSG00000004360	*9330159F19Rik*	2.37E-04	1.53843
ENSMUSG00000073489	*Ifi204*	9.86E-22	1.540317
ENSMUSG00000024481	*Lvrn*	2.04E-11	1.541111
ENSMUSG00000057246	*BC051142*	1.99E-03	1.541414
ENSMUSG00000086564	*Cd101*	4.69E-12	1.541652
ENSMUSG00000064340	*mt-Tl1*	4.10E-08	1.54264
ENSMUSG00000032125	*Robo4*	1.62E-20	1.542785
ENSMUSG00000044405	*Adig*	4.27E-02	1.543087
ENSMUSG00000052212	*Cd177*	4.55E-16	1.543341
ENSMUSG00000032355	*Mlip*	2.15E-13	1.543416
ENSMUSG00000042828	*Trim72*	5.22E-08	1.543717
ENSMUSG00000056300	*Zfp981*	1.45E-05	1.543885
ENSMUSG00000004864	*Mapk13*	6.25E-10	1.546096
ENSMUSG00000063129	*Aldoart2*	1.66E-05	1.54623
ENSMUSG00000042010	*Acacb*	3.59E-23	1.54649
ENSMUSG00000070354	*Evi2*	8.63E-14	1.546718
ENSMUSG00000034990	*Otoa*	4.05E-03	1.547561
ENSMUSG00000049093	*Il23r*	5.93E-07	1.54799
ENSMUSG00000071691	*Gm960*	7.83E-05	1.548087

ENSMUSG00000022026	*Olfm4*	7.52E-16	1.548559
ENSMUSG00000026452	*Syt2*	1.23E-10	1.548817
ENSMUSG00000061578	*Ksr2*	1.01E-03	1.54969
ENSMUSG00000032816	*Igdcc4*	5.80E-05	1.549734
ENSMUSG00000104728	*Gm42462*	1.51E-06	1.55063
ENSMUSG00000098702	*1500015A07Rik*	1.10E-03	1.552174
ENSMUSG00000064147	*Rab44*	7.19E-18	1.55308
ENSMUSG00000092397	*C130080G10Rik*	3.48E-05	1.554863
ENSMUSG00000003849	*Nqo1*	1.35E-03	1.555535
ENSMUSG00000057054	*Inca1*	3.20E-03	1.557038
ENSMUSG00000009292	*Trpm2*	8.56E-13	1.558139
ENSMUSG00000001943	*Vsig2*	1.50E-12	1.560479
ENSMUSG00000025701	*Alox5*	2.14E-20	1.561191
ENSMUSG00000105053	*Gm43064*	2.35E-10	1.564013
ENSMUSG00000068794	*Col28a1*	4.53E-05	1.564183
ENSMUSG00000021950	*Anxa8*	2.41E-06	1.565581
ENSMUSG00000113918	*Gm6566*	7.52E-03	1.565835
ENSMUSG00000055027	*Smyd1*	9.41E-12	1.566011
ENSMUSG00000047746	*Fbxo40*	6.40E-08	1.566184
ENSMUSG00000016349	*Eef1a2*	2.02E-12	1.566216
ENSMUSG00000034308	*Sdr42e1*	1.45E-03	1.566555
ENSMUSG00000029204	*Rhoh*	1.15E-21	1.56695
ENSMUSG00000021061	*Sptb*	7.50E-20	1.567256
ENSMUSG00000020698	*Cct6b*	1.31E-02	1.567908
ENSMUSG00000045102	*Poln*	7.37E-20	1.567926
ENSMUSG00000020077	*Srgn*	3.93E-19	1.568811
ENSMUSG00000090582	*Gm17024*	1.32E-06	1.570766
ENSMUSG00000017830	*Dhx58*	5.45E-13	1.571673
ENSMUSG00000044716	*Dok7*	1.96E-05	1.57206
ENSMUSG00000070604	*Vsig10l*	5.39E-07	1.572936
ENSMUSG00000053338	*Tarm1*	1.01E-19	1.573966
ENSMUSG00000005800	*Mmp8*	2.88E-22	1.574036
ENSMUSG00000113778	*Gm40847*	2.80E-02	1.574565
ENSMUSG00000037572	*Wdhd1*	2.94E-07	1.574592
ENSMUSG00000032561	*Acpp*	2.04E-16	1.575351
ENSMUSG00000053914	*Kdm4d*	6.99E-07	1.57607
ENSMUSG00000002769	*Gnmt*	4.11E-02	1.576947
ENSMUSG00000021579	*Lrrc14b*	1.53E-02	1.577637
ENSMUSG00000031452	*1700029H14Rik*	4.92E-11	1.578495
ENSMUSG00000112707	*D830005E20Rik*	1.67E-07	1.578937
ENSMUSG00000024517	*Grp*	1.13E-02	1.579229
ENSMUSG00000030577	*Cd22*	1.23E-05	1.580173
ENSMUSG00000051351	*Zfp46*	5.74E-27	1.580489
ENSMUSG00000000204	*Slfn4*	1.72E-07	1.580569
ENSMUSG00000062007	*Hsh2d*	6.70E-05	1.580819
ENSMUSG00000070000	*Fcho1*	1.23E-04	1.580984
ENSMUSG00000105572	*Gm43300*	8.23E-05	1.581967
ENSMUSG00000027360	*Hdc*	5.77E-25	1.582111
ENSMUSG00000024803	*Ankrd1*	1.68E-14	1.582117
ENSMUSG00000031872	*Bean1*	2.56E-09	1.582908
ENSMUSG00000108313	*Gm45052*	3.46E-02	1.583486
ENSMUSG00000024210	*Ip6k3*	2.10E-09	1.583691
ENSMUSG00000037849	*Ifi206*	8.40E-04	1.584723
ENSMUSG00000050663	*Trhde*	4.90E-02	1.585677
ENSMUSG00000039891	*Txlnb*	2.06E-14	1.58583
ENSMUSG00000024593	*Megf10*	6.07E-05	1.585923
ENSMUSG00000059901	*Adamts14*	1.44E-19	1.586361

ENSMUSG00000053024	*Cntn2*	3.57E-02	1.587941
ENSMUSG00000071561	*BC100530*	2.30E-07	1.588282
ENSMUSG00000114138	*Gm36423*	1.66E-02	1.589727
ENSMUSG00000043789	*Vwce*	3.78E-03	1.5899
ENSMUSG00000042851	*Zc3h6*	1.02E-14	1.590111
ENSMUSG00000116604	*AC087898.2*	3.16E-02	1.590457
ENSMUSG00000010476	*Ebf3*	5.07E-07	1.590556
ENSMUSG00000004609	*Cd33*	3.48E-28	1.592001
ENSMUSG00000098875	*Gm27211*	1.13E-06	1.592609
ENSMUSG00000029205	*Chrna9*	2.74E-02	1.592947
ENSMUSG00000050840	*Cdh20*	1.45E-02	1.593388
ENSMUSG00000006457	*Actn3*	7.83E-07	1.59497
ENSMUSG00000104348	*Gm37691*	1.06E-04	1.595263
ENSMUSG00000024076	*Vit*	1.11E-03	1.595268
ENSMUSG00000024972	*Lgals12*	4.52E-03	1.595515
ENSMUSG00000040055	*Gjb6*	2.71E-03	1.595537
ENSMUSG00000049336	*Tenm2*	1.62E-10	1.596005
ENSMUSG00000104213	*Ighd*	3.47E-05	1.596239
ENSMUSG00000022383	*Ppara*	2.03E-15	1.597777
ENSMUSG00000054169	*Ceacam10*	2.78E-06	1.598518
ENSMUSG00000109232	*Gm44577*	1.35E-02	1.598735
ENSMUSG00000035692	*Isg15*	6.47E-15	1.601526
ENSMUSG00000032523	*Hhatl*	3.08E-03	1.601819
ENSMUSG00000040747	*Cd53*	9.31E-18	1.602191
ENSMUSG00000053469	*Tg*	4.33E-17	1.602498
ENSMUSG00000059974	*Ntm*	1.81E-26	1.602733
ENSMUSG00000018425	*Dhx40*	3.14E-21	1.604037
ENSMUSG00000075122	*Cd80*	1.39E-21	1.605419
ENSMUSG00000002831	*Plin4*	3.11E-26	1.606197
ENSMUSG00000095079	*Igha*	1.40E-05	1.607185
ENSMUSG00000078902	*Gm14443*	1.56E-02	1.607245
ENSMUSG00000115855	*Gm34643*	1.33E-02	1.60811
ENSMUSG00000073492	*Gm10521*	1.01E-02	1.608342
ENSMUSG00000058818	*Pirb*	1.25E-16	1.608386
ENSMUSG00000071562	*Stfa1*	1.20E-02	1.608568
ENSMUSG00000058755	*Osm*	9.87E-06	1.608663
ENSMUSG00000025479	*Cyp2e1*	1.75E-15	1.608811
ENSMUSG00000116975	*AC097366.1*	4.70E-02	1.609642
ENSMUSG00000061126	*Cyp4f39*	1.24E-02	1.611491
ENSMUSG00000086756	*Gm14051*	4.26E-03	1.612421
ENSMUSG00000054383	*Pnma1*	1.58E-02	1.612439
ENSMUSG00000084788	*Gm11342*	1.75E-08	1.6151
ENSMUSG00000102776	*Gm38162*	1.33E-04	1.615539
ENSMUSG00000104453	*Gm37829*	3.14E-03	1.616164
ENSMUSG00000049709	*Nlrp10*	1.69E-03	1.616218
ENSMUSG00000047798	*Cd300lf*	2.12E-26	1.616545
ENSMUSG00000093938	*Evi2b*	9.87E-15	1.61906
ENSMUSG00000031303	*Map3k15*	8.44E-11	1.619429
ENSMUSG00000110195	*Pde2a*	3.98E-16	1.622023
ENSMUSG00000109819	*B930018H19Rik*	2.50E-04	1.622025
ENSMUSG00000028860	*Sytl1*	2.85E-04	1.623336
ENSMUSG00000034570	*Inpp5j*	2.35E-03	1.623616
ENSMUSG00000026220	*Slc16a14*	3.53E-02	1.625516
ENSMUSG00000116290	*Gm49518*	1.89E-02	1.626577
ENSMUSG00000096957	*E230013L22Rik*	7.49E-09	1.626815
ENSMUSG00000003153	*Slc2a3*	1.50E-16	1.627617
ENSMUSG00000074419	*Gm15448*	4.65E-11	1.62794

ENSMUSG00000067577	*A430093F15Rik*	6.34E-09	1.628234
ENSMUSG00000079597	*Gm5483*	5.40E-13	1.628886
ENSMUSG00000018507	*Trpv2*	5.02E-19	1.629285
ENSMUSG00000032023	*Jhy*	7.50E-07	1.630081
ENSMUSG00000042567	*Nek10*	7.69E-11	1.630143
ENSMUSG00000022876	*Samsn1*	1.31E-21	1.6304
ENSMUSG00000113998	*Gm40909*	5.76E-07	1.630854
ENSMUSG00000022454	*Nell2*	1.66E-02	1.631056
ENSMUSG00000107480	*Gm44165*	2.95E-03	1.631572
ENSMUSG00000115355	*4930445E18Rik*	5.26E-04	1.631708
ENSMUSG00000040287	*Stac3*	6.79E-06	1.632241
ENSMUSG00000116747	*AC144408.2*	2.16E-02	1.633409
ENSMUSG00000056071	*S100a9*	5.19E-11	1.634188
ENSMUSG00000066800	*Rnasel*	7.15E-19	1.63539
ENSMUSG00000000386	*Mx1*	3.52E-19	1.638433
ENSMUSG00000030669	*Calca*	6.86E-06	1.640644
ENSMUSG00000099364	*5730419F03Rik*	2.51E-02	1.642235
ENSMUSG00000041754	*Trem3*	2.37E-12	1.64293
ENSMUSG00000048416	*Mlf1*	3.35E-12	1.64339
ENSMUSG00000056054	*S100a8*	5.09E-08	1.644216
ENSMUSG00000011148	*Adssl1*	5.36E-13	1.645005
ENSMUSG00000052726	*Kcnt2*	2.51E-19	1.645058
ENSMUSG00000029228	*Lnx1*	2.29E-25	1.645255
ENSMUSG00000116031	*D030024E09Rik*	2.72E-05	1.645676
ENSMUSG00000099092	*Mir7062*	3.90E-02	1.646838
ENSMUSG00000109096	*Gm44888*	1.16E-02	1.647995
ENSMUSG00000038132	*Rbm24*	2.05E-13	1.648088
ENSMUSG00000000673	*Haao*	2.61E-03	1.648454
ENSMUSG00000026073	*Il1r2*	8.70E-09	1.64854
ENSMUSG00000037731	*Themis2*	6.62E-24	1.649889
ENSMUSG00000091438	*Gm17088*	1.47E-02	1.650306
ENSMUSG00000064346	*mt-Tw*	8.31E-04	1.65172
ENSMUSG00000034855	*Cxcl10*	1.23E-06	1.652425
ENSMUSG00000031312	*Itgb1bp2*	3.28E-08	1.652551
ENSMUSG00000059657	*Stfa2l1*	1.02E-14	1.652763
ENSMUSG00000024379	*Tslp*	1.96E-07	1.652917
ENSMUSG00000032648	*Pygm*	1.27E-25	1.653929
ENSMUSG00000064360	*mt-Nd3*	6.22E-34	1.653955
ENSMUSG00000005686	*Ampd3*	5.07E-44	1.654326
ENSMUSG00000036067	*Slc2a6*	2.22E-21	1.655183
ENSMUSG00000110125	*Gm33148*	4.23E-02	1.655315
ENSMUSG00000021071	*Trim9*	4.06E-04	1.655679
ENSMUSG00000012819	*Cdh23*	5.33E-08	1.655851
ENSMUSG00000029602	*Rasal1*	1.09E-02	1.6569
ENSMUSG00000038204	*Asb10*	3.79E-02	1.657364
ENSMUSG00000034755	*Pcdh11x*	2.75E-05	1.65877
ENSMUSG00000038067	*Csf3*	2.30E-17	1.659219
ENSMUSG00000029059	*Fam213b*	2.03E-02	1.659422
ENSMUSG00000032033	*Barx2*	2.86E-06	1.659698
ENSMUSG00000034686	*Prr7*	4.58E-13	1.660366
ENSMUSG00000101939	*Gm28438*	1.42E-34	1.661494
ENSMUSG00000100510	*AV026068*	6.71E-04	1.66215
ENSMUSG00000046610	*Oacyl*	7.18E-05	1.662776
ENSMUSG00000028834	*Trim63*	7.79E-07	1.663212
ENSMUSG00000003863	*Ppfia3*	3.09E-02	1.664438
ENSMUSG00000031626	*Sorbs2*	1.22E-22	1.665918
ENSMUSG00000047501	*Cldn4*	2.88E-03	1.66654

ENSMUSG00000087579	*Hectd2os*	4.33E-09	1.666956
ENSMUSG00000022821	*Hgd*	9.49E-04	1.667405
ENSMUSG00000020067	*Mypn*	2.91E-16	1.668111
ENSMUSG00000074071	*Fam169b*	1.03E-40	1.669004
ENSMUSG00000093806	*Asmt*	3.89E-02	1.669364
ENSMUSG00000031258	*Xkrx*	2.29E-02	1.669615
ENSMUSG00000040435	*Ppp1r15a*	1.10E-25	1.669806
ENSMUSG00000097643	*A130051J06Rik*	3.09E-02	1.669883
ENSMUSG00000079644	*Gm1110*	2.01E-02	1.67036
ENSMUSG00000042717	*Ppp1r3a*	8.51E-16	1.670789
ENSMUSG00000075042	*4930431P03Rik*	6.43E-03	1.670913
ENSMUSG00000054717	*Hmgb2*	8.73E-07	1.670984
ENSMUSG00000082179	*Gm11407*	1.60E-02	1.671338
ENSMUSG00000056133	*Unc93a2*	1.34E-02	1.672597
ENSMUSG00000101640	*Gm28376*	2.21E-02	1.673873
ENSMUSG00000030156	*Cd69*	2.53E-09	1.674983
ENSMUSG00000113185	*Gm47127*	3.62E-10	1.675362
ENSMUSG00000038239	*Hrc*	1.25E-12	1.67644
ENSMUSG00000078486	*Perm1*	3.53E-12	1.677159
ENSMUSG00000059741	*Myl3*	2.68E-08	1.677439
ENSMUSG00000027843	*Ptpn22*	1.42E-17	1.677529
ENSMUSG00000098670	*Gm27818*	6.52E-03	1.678782
ENSMUSG00000003476	*Crhr2*	1.34E-06	1.679035
ENSMUSG00000091712	*Sec14l5*	1.80E-04	1.679152
ENSMUSG00000103308	*Gm37800*	3.21E-05	1.680186
ENSMUSG00000026358	*Rgs1*	3.15E-07	1.680205
ENSMUSG00000109864	*Eid3*	9.84E-08	1.682789
ENSMUSG00000073771	*Btbd19*	4.74E-06	1.683039
ENSMUSG00000090439	*Gm17455*	2.54E-02	1.683429
ENSMUSG00000035653	*Lrfn5*	2.04E-02	1.684683
ENSMUSG00000086335	*Gm12107*	4.07E-02	1.684829
ENSMUSG00000111809	*Gm49334*	1.68E-02	1.687123
ENSMUSG00000006724	*Cyp27b1*	2.49E-02	1.688563
ENSMUSG00000097028	*Ptgs2os*	4.00E-03	1.688812
ENSMUSG00000027966	*Col11a1*	6.48E-06	1.689108
ENSMUSG00000042251	*Pm20d1*	9.34E-04	1.689267
ENSMUSG00000104554	*Gm4610*	2.85E-03	1.689388
ENSMUSG00000028544	*Slc5a9*	3.63E-03	1.690419
ENSMUSG00000027861	*Casq2*	1.46E-13	1.690798
ENSMUSG00000087684	*1200007C13Rik*	9.26E-19	1.692709
ENSMUSG00000046223	*Plaur*	3.12E-25	1.69343
ENSMUSG00000086727	*4931428L18Rik*	4.68E-02	1.694028
ENSMUSG00000018470	*Kcnab3*	4.44E-02	1.695106
ENSMUSG00000020722	*Cacng1*	3.42E-03	1.695444
ENSMUSG00000050966	*Lin28a*	3.70E-02	1.696226
ENSMUSG00000031245	*Hmgn5*	1.10E-06	1.696266
ENSMUSG00000084760	*Gm15472*	4.94E-02	1.699259
ENSMUSG00000029379	*Cxcl3*	3.14E-19	1.699755
ENSMUSG00000106741	*4930513D17Rik*	2.78E-04	1.700156
ENSMUSG00000033676	*Gabrb3*	9.53E-03	1.700516
ENSMUSG00000111827	*Gm8131*	2.03E-02	1.701357
ENSMUSG00000026989	*Dapl1*	1.87E-02	1.702816
ENSMUSG00000021298	*Gpr132*	1.17E-13	1.705667
ENSMUSG00000005373	*Mlxipl*	2.58E-12	1.705754
ENSMUSG00000022651	*Retnlg*	1.15E-21	1.705788
ENSMUSG00000036557	*Stpg4*	7.22E-03	1.706336
ENSMUSG00000060600	*Eno3*	1.40E-17	1.70718

ENSMUSG00000092134	*Gm17089*	2.08E-03	1.708295
ENSMUSG00000115610	*Gm31251*	8.64E-13	1.708416
ENSMUSG00000027824	*Vmn2r1*	3.39E-02	1.71058
ENSMUSG00000057580	*Gm10012*	5.95E-03	1.711245
ENSMUSG00000090785	*Gm17116*	3.94E-02	1.712965
ENSMUSG00000109005	*Gm45221*	9.18E-13	1.713519
ENSMUSG00000097652	*Mhrt*	5.45E-09	1.713729
ENSMUSG00000039376	*Synpo2l*	2.08E-14	1.714714
ENSMUSG00000030935	*Acsm3*	4.85E-02	1.714851
ENSMUSG00000085792	*Gm15414*	4.12E-02	1.715017
ENSMUSG00000032845	*Alpk2*	8.22E-25	1.71506
ENSMUSG00000024215	*Spdef*	3.57E-05	1.715667
ENSMUSG00000040490	*Lrfn2*	6.64E-03	1.717782
ENSMUSG00000067049	*Unc93a*	3.95E-04	1.719453
ENSMUSG00000020836	*Coro6*	4.06E-14	1.719576
ENSMUSG00000025236	*Adpgk*	9.28E-08	1.720655
ENSMUSG00000069670	*Nkain2*	2.61E-27	1.720935
ENSMUSG00000054204	*Alkal2*	9.31E-03	1.721026
ENSMUSG00000050439	*Enthd1*	1.61E-03	1.722314
ENSMUSG00000058966	*Fam57b*	1.21E-04	1.722847
ENSMUSG00000039521	*Foxp3*	3.73E-04	1.722974
ENSMUSG00000042451	*Mybph*	4.32E-14	1.725736
ENSMUSG00000025746	*Il6*	5.63E-08	1.726006
ENSMUSG00000087382	*Ctcflos*	3.89E-03	1.729287
ENSMUSG00000024521	*Pmaip1*	5.17E-21	1.731247
ENSMUSG00000113321	*Gm8075*	1.52E-03	1.732541
ENSMUSG00000028125	*Abca4*	1.40E-15	1.733301
ENSMUSG00000109510	*Gm42417*	2.03E-18	1.733587
ENSMUSG00000056643	*Chst13*	3.89E-02	1.737568
ENSMUSG00000109002	*Gm38405*	3.68E-03	1.738016
ENSMUSG00000066366	*Serpina1a*	4.81E-04	1.739086
ENSMUSG00000030144	*Clec4d*	1.24E-21	1.739304
ENSMUSG00000074899	*Sptbn5*	8.93E-15	1.741636
ENSMUSG00000019933	*Mrln*	6.47E-04	1.74233
ENSMUSG00000117297	*CT571247.2*	2.12E-03	1.742747
ENSMUSG00000029838	*Ptn*	3.58E-04	1.745315
ENSMUSG00000110626	*Gm45805*	3.93E-03	1.746875
ENSMUSG00000114638	*Gm31834*	1.32E-02	1.748994
ENSMUSG00000004902	*Slc25a18*	9.40E-11	1.748994
ENSMUSG00000021886	*Gpr65*	1.38E-16	1.751875
ENSMUSG00000111334	*AC162938.1*	2.19E-03	1.751922
ENSMUSG00000090141	*Gm614*	1.79E-07	1.752594
ENSMUSG00000028116	*Myoz2*	1.41E-18	1.753998
ENSMUSG00000024912	*Fosl1*	4.81E-11	1.757523
ENSMUSG00000047281	*Sfn*	1.96E-12	1.758427
ENSMUSG00000048489	*Depp1*	5.70E-10	1.75859
ENSMUSG00000052769	*Gm9889*	3.49E-03	1.758749
ENSMUSG00000038242	*Aox4*	3.63E-04	1.759686
ENSMUSG00000047940	*Stpg2*	1.76E-04	1.761496
ENSMUSG00000067242	*Lgi1*	2.15E-03	1.76182
ENSMUSG00000079015	*Serpina1c*	9.81E-05	1.762405
ENSMUSG00000028573	*Fggy*	9.93E-05	1.763622
ENSMUSG00000106547	*B230303O12Rik*	1.91E-10	1.763742
ENSMUSG00000110010	*Gm45629*	1.72E-03	1.764186
ENSMUSG00000106478	*Gm36551*	2.69E-03	1.766268
ENSMUSG00000034919	*Ttc22*	1.21E-03	1.767889
ENSMUSG00000028773	*Fabp3*	1.25E-09	1.769041

ENSMUSG00000026564	*Dusp27*	4.71E-11	1.770954
ENSMUSG00000079429	*Mroh2a*	4.95E-02	1.771987
ENSMUSG00000030510	*Cers3*	8.43E-08	1.773692
ENSMUSG00000094334	*Fabp5l2*	1.94E-02	1.773759
ENSMUSG00000030235	*Slco1c1*	6.91E-16	1.775853
ENSMUSG00000037989	*Wnk2*	2.70E-20	1.777419
ENSMUSG00000027674	*Pex5l*	4.64E-10	1.777644
ENSMUSG00000004668	*Abca13*	5.69E-29	1.778516
ENSMUSG00000062713	*Sim2*	1.19E-09	1.779309
ENSMUSG00000116961	*AC117662.4*	3.90E-05	1.7808
ENSMUSG00000026669	*Mcm10*	2.70E-08	1.780809
ENSMUSG00000049598	*Vsig8*	3.66E-02	1.781692
ENSMUSG00000051747	*Ttn*	1.20E-50	1.787185
ENSMUSG00000085417	*Gm13919*	2.58E-03	1.789173
ENSMUSG00000033544	*Angptl1*	2.01E-03	1.789715
ENSMUSG00000020000	*Moxd1*	3.38E-03	1.789741
ENSMUSG00000001249	*Hpn*	8.32E-15	1.79272
ENSMUSG00000034648	*Lrrn1*	4.21E-04	1.792909
ENSMUSG00000090173	*Fbxw10*	4.07E-06	1.793362
ENSMUSG00000110580	*D830024N08Rik*	3.86E-07	1.79383
ENSMUSG00000027559	*Car3*	1.14E-58	1.794165
ENSMUSG00000049173	*Myoz3*	3.68E-04	1.794511
ENSMUSG00000097579	*Gm26799*	1.22E-05	1.798591
ENSMUSG00000108322	*5430431A17Rik*	9.26E-04	1.79877
ENSMUSG00000041954	*Tnfrsf18*	1.91E-04	1.798838
ENSMUSG00000086236	*5830418P13Rik*	3.97E-02	1.799096
ENSMUSG00000107667	*C530044C16Rik*	2.55E-03	1.799886
ENSMUSG00000032484	*Ngp*	7.22E-33	1.802514
ENSMUSG00000097543	*Gm805*	3.14E-03	1.804272
ENSMUSG00000042045	*Sln*	1.59E-14	1.805054
ENSMUSG00000031382	*Asb11*	5.07E-07	1.807798
ENSMUSG00000039653	*Baat*	1.72E-02	1.807968
ENSMUSG00000109921	*Gm33326*	4.27E-02	1.808594
ENSMUSG00000046818	*Ddit4l*	1.37E-03	1.809116
ENSMUSG00000044083	*Efcab8*	1.54E-22	1.80916
ENSMUSG00000101639	*Gm8597*	2.68E-02	1.810383
ENSMUSG00000000223	*Drp2*	8.23E-07	1.810905
ENSMUSG00000085584	*Rtl9*	4.99E-02	1.814506
ENSMUSG00000006345	*Ggt1*	2.21E-08	1.817124
ENSMUSG00000086448	*9330162012Rik*	3.73E-02	1.817998
ENSMUSG00000067889	*Sptbn2*	4.24E-09	1.818248
ENSMUSG00000038763	*Alpk3*	1.96E-32	1.81872
ENSMUSG00000085194	*Platr32*	2.24E-03	1.819714
ENSMUSG00000030470	*Csrp3*	2.08E-18	1.819847
ENSMUSG00000043008	*Klhl6*	2.15E-21	1.820648
ENSMUSG00000019987	*Arg1*	2.20E-03	1.822152
ENSMUSG00000039264	*Gimap3*	3.51E-14	1.824217
ENSMUSG00000060470	*Adgrg3*	1.14E-17	1.824816
ENSMUSG00000025488	*Cox8b*	1.08E-07	1.825697
ENSMUSG00000097071	*4930544I03Rik*	5.59E-06	1.830008
ENSMUSG00000028680	*Plk3*	8.61E-23	1.830772
ENSMUSG00000020007	*Il20ra*	1.06E-02	1.831433
ENSMUSG00000074340	*Ovgp1*	2.09E-12	1.832669
ENSMUSG00000112148	*Lilrb4a*	1.06E-12	1.832695
ENSMUSG00000034145	*Tmem63c*	7.44E-03	1.833488
ENSMUSG00000031837	*Necab2*	4.40E-02	1.833535
ENSMUSG00000040694	*Apobec2*	1.11E-11	1.834504

ENSMUSG00000021255	*Esrrb*	6.95E-05	1.835067
ENSMUSG00000092008	*Cyp2c69*	1.42E-02	1.83538
ENSMUSG00000103485	*Gm38001*	2.57E-02	1.836426
ENSMUSG00000029660	*Tex26*	9.36E-09	1.837627
ENSMUSG00000086405	*9330198N18Rik*	1.69E-08	1.837669
ENSMUSG00000037509	*Arhgef4*	1.46E-11	1.84023
ENSMUSG00000041737	*Tmem45b*	8.44E-08	1.840717
ENSMUSG00000027359	*Slc27a2*	5.04E-03	1.841241
ENSMUSG00000047419	*Cmya5*	5.22E-34	1.843129
ENSMUSG00000033182	*Kbtbd12*	1.30E-10	1.843376
ENSMUSG00000044938	*Klhl31*	4.21E-15	1.843504
ENSMUSG00000109675	*Nxpe1-ps*	2.49E-02	1.843549
ENSMUSG00000000049	*Apoh*	9.36E-03	1.843946
ENSMUSG00000105107	*Gm43412*	3.93E-05	1.845797
ENSMUSG00000023341	*Mx2*	2.68E-43	1.846495
ENSMUSG00000053641	*Dennd4a*	7.82E-42	1.846884
ENSMUSG00000029158	*Yipf7*	5.09E-04	1.849072
ENSMUSG00000032278	*Paqr5*	1.41E-08	1.850269
ENSMUSG00000031098	*Syt8*	9.62E-03	1.851676
ENSMUSG00000090118	*Gm16163*	8.91E-07	1.853032
ENSMUSG00000024526	*Cidea*	2.58E-04	1.853747
ENSMUSG00000115919	*Gm31583*	2.47E-02	1.853826
ENSMUSG00000114372	*2310067P03Rik*	2.35E-03	1.854639
ENSMUSG00000081700	*Atp5k-ps2*	8.27E-05	1.855005
ENSMUSG00000066491	*Cox6c2*	5.55E-11	1.856124
ENSMUSG00000031461	*Myom2*	1.24E-37	1.857642
ENSMUSG00000104956	*4930429D17Rik*	1.29E-02	1.859359
ENSMUSG00000041616	*Nppa*	8.40E-06	1.859817
ENSMUSG00000030834	*Abcc6*	1.85E-02	1.86125
ENSMUSG00000044367	*Slc16a13*	1.02E-23	1.863682
ENSMUSG00000026100	*Mstn*	1.03E-02	1.863901
ENSMUSG00000058975	*Kcnc1*	1.48E-05	1.864086
ENSMUSG00000044086	*Lmod3*	5.83E-05	1.864089
ENSMUSG00000032262	*Elovl4*	1.84E-06	1.865299
ENSMUSG00000022824	*Muc13*	2.46E-06	1.871007
ENSMUSG00000105986	*Gm43065*	1.82E-03	1.871109
ENSMUSG00000091119	*Ccdc152*	3.30E-05	1.87189
ENSMUSG00000109198	*D7Bwg0826e*	6.88E-03	1.872806
ENSMUSG00000087187	*Gm13431*	2.85E-04	1.873198
ENSMUSG00000106245	*Gm43824*	2.54E-03	1.874635
ENSMUSG00000110411	*Gm45457*	2.24E-03	1.87632
ENSMUSG00000025069	*Gsto2*	7.14E-04	1.878743
ENSMUSG00000090066	*1110002E22Rik*	4.80E-18	1.881563
ENSMUSG00000110498	*A630001O12Rik*	2.05E-05	1.881948
ENSMUSG00000032174	*Icam5*	1.60E-03	1.884311
ENSMUSG00000040350	*Trim7*	3.16E-10	1.886702
ENSMUSG00000063001	*Gm9701*	2.00E-02	1.886992
ENSMUSG00000028017	*Egf*	2.98E-15	1.887283
ENSMUSG00000070498	*Tmem132b*	7.38E-17	1.887425
ENSMUSG00000028427	*Aqp7*	6.69E-03	1.888129
ENSMUSG00000038508	*Gdf15*	6.53E-03	1.888853
ENSMUSG00000027513	*Pck1*	9.43E-13	1.890906
ENSMUSG00000059900	*Tmem40*	4.20E-04	1.893524
ENSMUSG00000115518	*Gm10791*	1.65E-05	1.895648
ENSMUSG00000090293	*Gm17034*	2.96E-02	1.897849
ENSMUSG00000025004	*Cyp2c40*	1.94E-02	1.898265
ENSMUSG00000112895	*Gm47567*	5.03E-05	1.899642

ENSMUSG00000031958	*Ldhd*	4.49E-07	1.899952
ENSMUSG00000022582	*Ly6g*	4.01E-07	1.902278
ENSMUSG00000062077	*Trim54*	1.10E-15	1.902342
ENSMUSG00000024617	*Camk2a*	4.89E-09	1.903979
ENSMUSG00000007122	*Casq1*	2.89E-15	1.904008
ENSMUSG00000069733	*Ube2u*	1.19E-03	1.904037
ENSMUSG00000024430	*Cabyr*	1.01E-03	1.904429
ENSMUSG00000056569	*Mpz*	1.14E-16	1.905577
ENSMUSG00000032942	*Ucp3*	9.12E-10	1.909391
ENSMUSG00000044165	*Bcl2l15*	4.24E-09	1.911503
ENSMUSG00000079588	*Tmem182*	5.78E-17	1.91235
ENSMUSG00000007877	*Tcap*	1.05E-20	1.912751
ENSMUSG00000025473	*Adam8*	9.12E-15	1.913184
ENSMUSG00000031376	*Atp2b3*	1.10E-04	1.915267
ENSMUSG00000099760	*Gm28800*	1.04E-02	1.918089
ENSMUSG00000085249	*Gm12847*	6.44E-04	1.921004
ENSMUSG00000105826	*Gm42141*	5.75E-03	1.921732
ENSMUSG00000112082	*Gm35035*	1.26E-03	1.922335
ENSMUSG00000033213	*AA467197*	2.17E-05	1.926523
ENSMUSG00000046764	*A530053G22Rik*	5.14E-03	1.927384
ENSMUSG00000074623	*Gm826*	1.94E-03	1.931273
ENSMUSG00000030399	*Ckm*	2.68E-12	1.931828
ENSMUSG00000101930	*Gm5441*	1.33E-10	1.932682
ENSMUSG00000027456	*Sdcbp2*	5.13E-14	1.933121
ENSMUSG00000086765	*Gm11827*	2.95E-06	1.933308
ENSMUSG00000027505	*Fam209*	8.82E-04	1.935233
ENSMUSG00000054905	*Stfa3*	8.40E-04	1.935879
ENSMUSG00000062515	*Fabp4*	8.09E-25	1.936282
ENSMUSG00000024223	*Armc12*	3.96E-02	1.94095
ENSMUSG00000026068	*Il18rap*	6.22E-34	1.941935
ENSMUSG00000026489	*Coq8a*	2.76E-39	1.94642
ENSMUSG00000105542	*Gm34248*	2.05E-02	1.947483
ENSMUSG00000022468	*Endou*	3.09E-13	1.95126
ENSMUSG00000062372	*Otof*	4.14E-03	1.953074
ENSMUSG00000060962	*Dmkn*	4.46E-16	1.954338
ENSMUSG00000075307	*Klhl41*	3.80E-19	1.954528
ENSMUSG00000013936	*Myl2*	8.34E-04	1.957148
ENSMUSG00000074218	*Cox7a1*	4.66E-09	1.957494
ENSMUSG00000103965	*Gm30173*	8.23E-05	1.957865
ENSMUSG00000015879	*Fam184b*	9.58E-04	1.958074
ENSMUSG00000030236	*Slco1b2*	6.11E-03	1.958235
ENSMUSG00000116641	*AC165271.1*	3.93E-02	1.960352
ENSMUSG00000029683	*Lmod2*	2.29E-19	1.962142
ENSMUSG00000058427	*Cxcl2*	7.52E-16	1.965001
ENSMUSG00000097468	*Mdrl*	1.18E-02	1.9652
ENSMUSG00000085739	*Gm15862*	4.50E-02	1.966473
ENSMUSG00000099906	*Gm28653*	1.68E-02	1.966573
ENSMUSG00000097622	*A330033J07Rik*	9.21E-03	1.967677
ENSMUSG00000025929	*Il17a*	6.98E-03	1.968258
ENSMUSG00000101969	*Gm20125*	7.68E-08	1.970172
ENSMUSG00000109881	*Gm45507*	3.61E-02	1.972472
ENSMUSG00000025892	*Gria4*	1.74E-04	1.973108
ENSMUSG00000028786	*Tmem54*	2.69E-02	1.973491
ENSMUSG00000037188	*Grhl3*	3.13E-06	1.976128
ENSMUSG00000028736	*Pax7*	2.68E-02	1.978015
ENSMUSG00000117029	*CT030155.1*	3.35E-03	1.980083
ENSMUSG00000072720	*Myo18b*	5.67E-49	1.980402

ENSMUSG00000001027	*Scn4a*	1.63E-15	1.982106
ENSMUSG00000020848	*Doc2b*	7.17E-17	1.983107
ENSMUSG00000071540	*3425401B19Rik*	1.11E-21	1.983567
ENSMUSG00000059108	*Ifitm6*	1.39E-27	1.986147
ENSMUSG00000026166	*Ccl20*	1.87E-24	1.988087
ENSMUSG00000032021	*Crtam*	1.62E-20	1.988346
ENSMUSG00000048939	*Atp13a5*	8.98E-03	1.988773
ENSMUSG00000027961	*Lrrc39*	1.97E-07	1.989628
ENSMUSG00000050211	*Pla2g4e*	2.57E-15	1.990622
ENSMUSG00000050612	*Txndc2*	9.64E-03	1.991405
ENSMUSG00000097476	*Gm26583*	2.67E-02	1.992121
ENSMUSG00000018893	*Mb*	2.96E-16	1.995476
ENSMUSG00000001497	*Pax9*	5.45E-07	1.99584
ENSMUSG00000022871	*Fetub*	5.14E-07	1.996529
ENSMUSG00000040536	*Necab1*	6.95E-04	1.9986
ENSMUSG00000109831	*Gm36431*	7.50E-03	1.99936
ENSMUSG00000102762	*4930403P22Rik*	2.46E-02	2.001551
ENSMUSG00000041782	*Lad1*	3.08E-13	2.002946
ENSMUSG00000043873	*Chil5*	7.40E-06	2.00396
ENSMUSG00000085806	*Gm12023*	2.03E-05	2.005786
ENSMUSG00000035686	*Thrsp*	3.08E-18	2.008526
ENSMUSG00000067653	*Ankrd23*	7.18E-23	2.012683
ENSMUSG00000021622	*Ckmt2*	2.18E-22	2.016924
ENSMUSG00000046480	*Scn4b*	3.61E-12	2.018601
ENSMUSG00000114656	*2810403G07Rik*	2.60E-02	2.018932
ENSMUSG00000022525	*Hrasls*	1.48E-02	2.019224
ENSMUSG00000070644	*Etnk2*	8.41E-03	2.020491
ENSMUSG00000042306	*S100a14*	4.36E-12	2.021351
ENSMUSG00000098132	*Rassf10*	1.04E-02	2.021448
ENSMUSG00000062593	*Gm49339*	1.64E-14	2.024042
ENSMUSG00000111299	*4930540M03Rik*	1.34E-02	2.024137
ENSMUSG00000021340	*Gpld1*	6.91E-16	2.028941
ENSMUSG00000046352	*Gjb2*	1.21E-11	2.030651
ENSMUSG00000103620	*Gm37359*	4.58E-06	2.031625
ENSMUSG00000085743	*8430419K02Rik*	1.91E-27	2.032356
ENSMUSG00000089854	*Gm16133*	2.61E-06	2.035203
ENSMUSG00000006204	*5430419D17Rik*	3.20E-02	2.035247
ENSMUSG00000021509	*Slc25a48*	4.04E-03	2.035611
ENSMUSG00000061462	*Obscn*	5.68E-58	2.038968
ENSMUSG00000059994	*Fcrl1*	1.30E-09	2.039878
ENSMUSG00000076275	*Mir675*	1.77E-07	2.041447
ENSMUSG00000069372	*Ctxn3*	3.18E-08	2.043908
ENSMUSG00000037129	*Tmprss13*	8.77E-06	2.050404
ENSMUSG00000021223	*Papln*	2.43E-05	2.052027
ENSMUSG00000085779	*Atcayos*	9.38E-24	2.05238
ENSMUSG00000031231	*Cox7b*	6.58E-27	2.052756
ENSMUSG00000049100	*Pcdh10*	8.51E-03	2.052949
ENSMUSG00000085996	*A830012C17Rik*	1.30E-03	2.057668
ENSMUSG00000034282	*Evpl*	8.05E-15	2.062518
ENSMUSG00000027887	*Sypl2*	3.80E-11	2.066455
ENSMUSG00000032503	*Arpp21*	1.46E-07	2.066522
ENSMUSG00000047976	*Kcna1*	7.38E-12	2.070587
ENSMUSG00000032066	*Bco2*	2.78E-04	2.073257
ENSMUSG00000044359	*P2ry4*	1.91E-03	2.076374
ENSMUSG00000093577	*Gm20632*	6.14E-03	2.077013
ENSMUSG00000013483	*Card14*	1.31E-07	2.078412
ENSMUSG00000000157	*Itgb2l*	9.04E-27	2.079323

ENSMUSG00000043029	*Trpv3*	1.44E-02	2.081377
ENSMUSG00000039238	*Zfp750*	1.47E-04	2.082281
ENSMUSG00000110752	*D730003K21Rik*	4.64E-02	2.082774
ENSMUSG00000028778	*Hcrtr1*	3.59E-02	2.085093
ENSMUSG00000058207	*Serpina3k*	1.26E-09	2.085453
ENSMUSG00000067081	*Asb18*	2.65E-08	2.090381
ENSMUSG00000086628	*Gm16157*	1.73E-02	2.090745
ENSMUSG00000024105	*Themis3*	5.35E-04	2.093314
ENSMUSG00000061259	*Tmprss11d*	1.09E-03	2.098869
ENSMUSG00000090698	*Apold1*	9.53E-29	2.09911
ENSMUSG00000019102	*Aldh3a1*	7.05E-13	2.102843
ENSMUSG00000083832	*Gm13771*	1.13E-07	2.104884
ENSMUSG00000102630	*Gm37289*	1.55E-03	2.105392
ENSMUSG00000110278	*Gm5608*	5.85E-19	2.108069
ENSMUSG00000034768	*Asb16*	1.07E-02	2.111324
ENSMUSG00000039956	*Mrap*	4.45E-10	2.112034
ENSMUSG00000103923	*Gm37896*	8.60E-03	2.11783
ENSMUSG00000097335	*Gm26563*	2.10E-03	2.118682
ENSMUSG00000078907	*Fam186b*	3.97E-02	2.120724
ENSMUSG00000059742	*Kcnh7*	5.20E-04	2.121118
ENSMUSG00000069581	*Tspear*	4.61E-03	2.12407
ENSMUSG00000111582	*Gm47347*	3.71E-02	2.125209
ENSMUSG00000110101	*Gm6249*	2.05E-02	2.12537
ENSMUSG00000114838	*Gm48703*	2.07E-02	2.125697
ENSMUSG00000110622	*Iqcn*	5.56E-03	2.126382
ENSMUSG00000032013	*Trim29*	7.42E-11	2.126553
ENSMUSG00000019787	*Trdn*	6.78E-61	2.127457
ENSMUSG00000103502	*9330121J05Rik*	4.80E-02	2.127771
ENSMUSG00000059201	*Lep*	5.78E-05	2.128026
ENSMUSG00000072573	*Gm10369*	3.96E-02	2.129896
ENSMUSG00000035923	*Myf6*	2.65E-02	2.130758
ENSMUSG00000028989	*Angptl7*	5.47E-12	2.131128
ENSMUSG00000055775	*Myh8*	4.26E-21	2.138598
ENSMUSG00000108436	*Gm44851*	3.51E-04	2.138805
ENSMUSG00000100551	*Gm19503*	1.04E-09	2.138828
ENSMUSG00000038670	*Mybpc2*	7.68E-24	2.148925
ENSMUSG00000079243	*Xirp1*	5.72E-30	2.150145
ENSMUSG00000104340	*Gm10522*	2.43E-02	2.151948
ENSMUSG00000031448	*Adprhl1*	2.72E-17	2.153714
ENSMUSG00000021359	*Tfap2a*	3.33E-04	2.154076
ENSMUSG00000021702	*Thbs4*	2.51E-18	2.160411
ENSMUSG00000082884	*Gm13339*	7.91E-11	2.160938
ENSMUSG00000072845	*Tmprss11a*	1.18E-02	2.165947
ENSMUSG00000025370	*Cdh9*	1.48E-02	2.168399
ENSMUSG00000028356	*Ambp*	6.80E-03	2.16969
ENSMUSG00000019851	*Perp*	7.61E-19	2.171313
ENSMUSG00000108985	*A930030B08Rik*	5.86E-04	2.171742
ENSMUSG00000089948	*Far2os1*	3.02E-02	2.174011
ENSMUSG00000024973	*Hrasls5*	6.29E-03	2.174329
ENSMUSG00000038751	*Ptk6*	2.90E-04	2.175162
ENSMUSG00000055489	*Ano5*	2.65E-19	2.176035
ENSMUSG00000036960	*Clca2*	8.46E-04	2.179341
ENSMUSG00000064371	*mt-Tt*	3.00E-02	2.180972
ENSMUSG00000111514	*E230014E18Rik*	6.75E-12	2.182891
ENSMUSG00000086777	*Far2os2*	7.84E-04	2.185863
ENSMUSG00000020892	*Aloxe3*	1.75E-06	2.187315
ENSMUSG00000032726	*Bmp8a*	2.54E-03	2.1889

ENSMUSG00000117092	*AC166110.1*	2.83E-03	2.190222
ENSMUSG00000023176	*Cpn2*	2.07E-02	2.192113
ENSMUSG00000027196	*Alkbh3os1*	3.46E-02	2.193943
ENSMUSG00000032292	*Nr2e3*	4.12E-03	2.196921
ENSMUSG00000042918	*Mamstr*	1.20E-37	2.197597
ENSMUSG00000046056	*Sbsn*	2.83E-10	2.198103
ENSMUSG00000027902	*Chil6*	1.73E-02	2.200008
ENSMUSG00000091238	*Gm17103*	7.14E-04	2.200115
ENSMUSG00000096351	*Samd11*	9.26E-09	2.20062
ENSMUSG00000109157	*Gm44829*	6.38E-08	2.201996
ENSMUSG00000042250	*Pglyrp4*	3.18E-03	2.203176
ENSMUSG00000102759	*Gm10463*	4.03E-03	2.205769
ENSMUSG00000007653	*Gabrb2*	1.16E-03	2.208491
ENSMUSG00000047216	*Cdh19*	1.60E-26	2.20978
ENSMUSG00000096887	*Gm20594*	7.85E-12	2.211799
ENSMUSG00000045027	*Prss22*	4.56E-13	2.221258
ENSMUSG00000041872	*Il17f*	3.11E-11	2.222913
ENSMUSG00000104314	*Gm37907*	4.45E-02	2.226011
ENSMUSG00000025754	*Agbl1*	1.47E-44	2.226428
ENSMUSG00000019853	*Hebp2*	1.26E-03	2.230586
ENSMUSG00000111818	*Gm17749*	3.92E-13	2.231279
ENSMUSG00000047686	*Rtl3*	3.27E-02	2.237085
ENSMUSG00000017607	*Tns4*	2.61E-07	2.237262
ENSMUSG00000028435	*Aqp3*	1.87E-10	2.240723
ENSMUSG00000034683	*Ppp1r1c*	4.89E-04	2.242066
ENSMUSG00000031936	*Hephl1*	4.37E-03	2.253413
ENSMUSG00000087477	*Gm13822*	2.34E-04	2.260881
ENSMUSG00000046961	*Gpr156*	1.14E-11	2.261469
ENSMUSG00000068890	*Lce1a2*	5.61E-03	2.26277
ENSMUSG00000112023	*Lilr4b*	2.80E-15	2.264239
ENSMUSG00000038020	*Rapgefl1*	7.31E-12	2.268906
ENSMUSG00000042662	*Dusp15*	2.80E-02	2.282184
ENSMUSG00000036123	*Slc9a3*	7.66E-05	2.282388
ENSMUSG00000070385	*Ampd1*	2.67E-16	2.283597
ENSMUSG00000111765	*Gm10635*	3.06E-03	2.287427
ENSMUSG00000042895	*Abra*	4.53E-15	2.29493
ENSMUSG00000040340	*Tex45*	2.95E-04	2.297836
ENSMUSG00000027022	*Xirp2*	1.00E-64	2.303434
ENSMUSG00000032281	*Acsbg1*	1.63E-15	2.307473
ENSMUSG00000106746	*2900064F13Rik*	3.81E-02	2.307491
ENSMUSG00000085564	*Gm12198*	3.19E-02	2.309238
ENSMUSG00000000031	*H19*	9.37E-41	2.316057
ENSMUSG00000017697	*Ada*	2.19E-32	2.316335
ENSMUSG00000108964	*Gm18600*	2.02E-02	2.316741
ENSMUSG00000040258	*Nxph4*	1.61E-02	2.322015
ENSMUSG00000034634	*Ly6d*	7.55E-08	2.32215
ENSMUSG00000085434	*Gm11725*	1.18E-05	2.32389
ENSMUSG00000041827	*Oasl1*	1.27E-48	2.333376
ENSMUSG00000046049	*Rp1l1*	8.88E-06	2.335651
ENSMUSG00000029361	*Nos1*	2.34E-29	2.336301
ENSMUSG00000022860	*Chodl*	3.02E-03	2.338522
ENSMUSG00000025329	*Padi1*	3.46E-03	2.339451
ENSMUSG00000004885	*Crabp2*	2.14E-05	2.342472
ENSMUSG00000097076	*Platr7*	7.34E-03	2.342649
ENSMUSG00000073602	*Serpinb3b*	7.91E-06	2.343508
ENSMUSG00000049134	*Nrap*	7.61E-59	2.345431
ENSMUSG00000048764	*Tmprss11f*	1.67E-05	2.348341

ENSMUSG00000056966	*Gjc3*	3.67E-03	2.35148
ENSMUSG00000068697	*Myoz1*	3.99E-14	2.351495
ENSMUSG00000009070	*Rsph14*	5.67E-15	2.352471
ENSMUSG00000022622	*Acr*	2.57E-18	2.353769
ENSMUSG00000114457	*Gm36346*	1.55E-02	2.357304
ENSMUSG00000037469	*Acp7*	6.67E-04	2.357911
ENSMUSG00000096084	*Gm21850*	1.15E-11	2.358208
ENSMUSG00000031972	*Acta1*	3.59E-28	2.359297
ENSMUSG00000026983	*Il1f5*	5.52E-04	2.359573
ENSMUSG00000059832	*Kprp*	5.63E-13	2.360512
ENSMUSG00000043286	*Pnpla1*	1.03E-04	2.366505
ENSMUSG00000033508	*Asprv1*	8.12E-12	2.36952
ENSMUSG00000085511	*Gm11738*	1.72E-03	2.370938
ENSMUSG00000044737	*Klk14*	4.19E-12	2.372258
ENSMUSG00000111556	*Gm19299*	6.49E-04	2.375603
ENSMUSG00000024771	*Lipk*	3.83E-03	2.37619
ENSMUSG00000027376	*Prom2*	7.96E-09	2.376333
ENSMUSG00000021123	*Rdh12*	6.55E-37	2.378531
ENSMUSG00000043165	*Lor*	6.90E-19	2.380809
ENSMUSG00000097069	*Gm16998*	3.57E-02	2.384026
ENSMUSG00000060180	*Myh13*	2.82E-11	2.384598
ENSMUSG00000026621	*Mar1*	1.07E-02	2.385001
ENSMUSG00000024331	*Dsc2*	7.84E-15	2.385649
ENSMUSG00000095438	*Mir133a-1hg*	5.55E-12	2.386779
ENSMUSG00000069873	*4930438A08Rik*	2.56E-06	2.387168
ENSMUSG00000041476	*Smpx*	1.20E-12	2.388318
ENSMUSG00000097281	*Gm26685*	4.14E-02	2.39049
ENSMUSG00000022510	*Trp63*	1.37E-22	2.394718
ENSMUSG00000034730	*Adgrb1*	2.15E-03	2.399098
ENSMUSG00000108448	*Gm21269*	1.77E-02	2.402324
ENSMUSG00000081619	*Gm13351*	4.66E-02	2.402361
ENSMUSG00000097850	*4631405K08Rik*	3.02E-03	2.406628
ENSMUSG00000109372	*Gm19410*	2.96E-02	2.407345
ENSMUSG00000092222	*Gm20506*	1.38E-02	2.407749
ENSMUSG00000064179	*Tnnt1*	6.04E-08	2.41389
ENSMUSG00000050808	*Muc15*	4.42E-03	2.423088
ENSMUSG00000030672	*Mylpf*	4.00E-11	2.425658
ENSMUSG00000037942	*Crp*	3.22E-03	2.427037
ENSMUSG00000075296	*Aldh3b2*	7.70E-05	2.42977
ENSMUSG00000044499	*Hs3st5*	1.87E-15	2.429999
ENSMUSG00000038357	*Camp*	4.41E-10	2.437799
ENSMUSG00000081163	*Defa-ps12*	4.11E-03	2.439291
ENSMUSG00000097413	*A830052D11Rik*	6.08E-05	2.440113
ENSMUSG00000040283	*Btnl9*	2.24E-05	2.447538
ENSMUSG00000074695	*Il22*	2.53E-04	2.451827
ENSMUSG00000026592	*Tex35*	3.15E-12	2.456187
ENSMUSG00000109311	*AI314278*	2.12E-05	2.458668
ENSMUSG00000042092	*Lce1c*	1.91E-03	2.46598
ENSMUSG00000061816	*Myl1*	1.65E-32	2.468997
ENSMUSG00000027868	*Tbx15*	3.60E-32	2.473286
ENSMUSG00000067001	*Serpinb7*	2.67E-03	2.476115
ENSMUSG00000043461	*Sptssb*	4.59E-07	2.477048
ENSMUSG00000067616	*Klk11*	2.13E-06	2.484335
ENSMUSG00000032807	*Alox12b*	2.99E-08	2.487194
ENSMUSG00000050830	*Vwc2*	9.16E-07	2.489155
ENSMUSG00000057280	*Musk*	7.35E-26	2.491914
ENSMUSG00000052581	*Lrrtm4*	1.35E-14	2.496839

ENSMUSG00000026984	*Il1f6*	6.08E-04	2.49812
ENSMUSG00000075394	*Hoxc4*	3.49E-02	2.499153
ENSMUSG00000042761	*Mrap2*	3.01E-04	2.502625
ENSMUSG00000027077	*Smtnl1*	6.53E-14	2.503067
ENSMUSG00000023153	*Tmem52*	1.52E-03	2.503879
ENSMUSG00000028865	*Cd164l2*	1.88E-06	2.505749
ENSMUSG00000100147	*1700047M11Rik*	1.89E-21	2.506465
ENSMUSG00000045019	*Acer1*	5.56E-03	2.51065
ENSMUSG00000050359	*Sprr1a*	6.00E-11	2.511127
ENSMUSG00000113178	*Mylf-ps*	7.37E-25	2.513042
ENSMUSG00000028186	*Uox*	5.38E-03	2.521096
ENSMUSG00000021506	*Pitx1*	4.13E-05	2.524928
ENSMUSG00000100410	*2310020H05Rik*	5.52E-04	2.525092
ENSMUSG00000099798	*Gm29168*	1.95E-02	2.530757
ENSMUSG00000023473	*Celsr3*	5.94E-19	2.534816
ENSMUSG00000042124	*Lce1f*	2.44E-03	2.541445
ENSMUSG00000027470	*Mylk2*	2.72E-26	2.549178
ENSMUSG00000044322	*Dsc1*	5.79E-06	2.554197
ENSMUSG00000037139	*Myom3*	1.14E-36	2.554969
ENSMUSG00000026327	*Serpinb11*	1.65E-06	2.557138
ENSMUSG00000096960	*A230028O05Rik*	1.73E-18	2.567768
ENSMUSG00000057609	*Lce1a1*	1.62E-04	2.572862
ENSMUSG00000025064	*Col17a1*	5.34E-16	2.577045
ENSMUSG00000024365	*Cyp21a1*	1.60E-02	2.581649
ENSMUSG00000025317	*Car5a*	3.01E-02	2.589695
ENSMUSG00000026418	*Tnni1*	3.68E-06	2.58989
ENSMUSG00000061928	*Dsg1b*	2.34E-12	2.593438
ENSMUSG00000114493	*Gm47071*	2.06E-15	2.5951
ENSMUSG00000081689	*Gm9166*	1.74E-02	2.598563
ENSMUSG00000028148	*Them5*	1.44E-11	2.59946
ENSMUSG00000048455	*Sprr1b*	3.10E-04	2.603137
ENSMUSG00000054582	*Pabpc1l*	3.75E-22	2.605057
ENSMUSG00000047586	*Nccrp1*	1.96E-03	2.608167
ENSMUSG00000103382	*Gm37755*	1.50E-03	2.610909
ENSMUSG00000021768	*Dusp13*	4.51E-06	2.617201
ENSMUSG00000021565	*Slc6a19*	1.45E-08	2.620258
ENSMUSG00000069441	*Dsg1a*	1.77E-16	2.627138
ENSMUSG00000029862	*Clcn1*	1.98E-18	2.631589
ENSMUSG00000066897	*Olfr872*	7.98E-03	2.634158
ENSMUSG00000038354	*Ankrd35*	3.43E-07	2.634991
ENSMUSG00000016942	*Tmprss6*	2.91E-02	2.635952
ENSMUSG00000074199	*Krtdap*	1.84E-07	2.63948
ENSMUSG00000026450	*Chit1*	2.83E-05	2.645391
ENSMUSG00000034774	*Dsg1c*	1.69E-03	2.648044
ENSMUSG00000055561	*Spink5*	2.81E-21	2.649507
ENSMUSG00000049593	*Lce1h*	1.12E-02	2.651785
ENSMUSG00000087410	*2310065F04Rik*	1.84E-02	2.652839
ENSMUSG00000031710	*Ucp1*	8.66E-12	2.653905
ENSMUSG00000074001	*Klhl40*	2.22E-08	2.659211
ENSMUSG00000031343	*Gabra3*	8.60E-12	2.660099
ENSMUSG00000040154	*Wfdc5*	1.24E-05	2.663952
ENSMUSG00000112041	*9530020I12Rik*	3.40E-05	2.669075
ENSMUSG00000116482	*Gm34152*	3.36E-02	2.674711
ENSMUSG00000059956	*Serpinb12*	2.21E-09	2.67661
ENSMUSG00000060621	*Nkpd1*	5.88E-04	2.680095
ENSMUSG00000063651	*Cnfn*	1.68E-15	2.693832
ENSMUSG00000086980	*Gm13791*	4.89E-04	2.702456

ENSMUSG00000040127	*Sdr9c7*	7.30E-03	2.70979
ENSMUSG00000059230	*Defb4*	4.63E-11	2.713218
ENSMUSG00000053675	*Tgm5*	2.41E-02	2.71792
ENSMUSG00000112471	*Gm5779*	8.23E-05	2.719729
ENSMUSG00000057003	*Myh4*	8.95E-42	2.71992
ENSMUSG00000097768	*2310043M15Rik*	6.60E-05	2.725258
ENSMUSG00000100781	*Gm29481*	3.64E-04	2.726074
ENSMUSG00000026950	*Neb*	4.90E-43	2.726723
ENSMUSG00000030592	*Ryr1*	3.70E-30	2.727653
ENSMUSG00000034362	*Csta1*	4.08E-04	2.728502
ENSMUSG00000111821	*Gm48545*	1.08E-07	2.729446
ENSMUSG00000050296	*Abca12*	2.65E-14	2.739696
ENSMUSG00000002500	*Rpl3l*	1.16E-12	2.745902
ENSMUSG00000084228	*Gm8080*	1.10E-02	2.75149
ENSMUSG00000041991	*Hrnr*	4.02E-11	2.752579
ENSMUSG00000091376	*Aadacl2*	1.73E-03	2.759068
ENSMUSG00000028011	*Tdo2*	8.06E-03	2.760958
ENSMUSG00000084929	*Foxo6os*	9.14E-05	2.765202
ENSMUSG00000090356	*Teddm3*	5.80E-06	2.767835
ENSMUSG00000074489	*Bglap3*	9.79E-06	2.770307
ENSMUSG00000061762	*Tac1*	9.92E-03	2.773699
ENSMUSG00000031844	*Hsd17b2*	7.25E-08	2.776301
ENSMUSG00000027401	*Tgm3*	2.87E-13	2.777067
ENSMUSG00000041984	*Rptn*	1.46E-19	2.778259
ENSMUSG00000048806	*Ifnb1*	9.77E-04	2.781116
ENSMUSG00000058260	*Serpina9*	4.93E-03	2.790483
ENSMUSG00000045539	*Sprr3*	1.26E-16	2.802851
ENSMUSG00000030484	*Lypd5*	2.30E-12	2.803817
ENSMUSG00000028396	*2310002L09Rik*	8.35E-07	2.810987
ENSMUSG00000061723	*Tnnt3*	7.78E-31	2.811141
ENSMUSG00000108371	*Gm38832*	4.21E-03	2.817575
ENSMUSG00000074113	*Gm10629*	9.39E-03	2.826311
ENSMUSG00000066510	*Ankdd1a*	1.97E-24	2.828707
ENSMUSG00000031097	*Tnni2*	5.06E-35	2.82918
ENSMUSG00000039518	*Cdsn*	2.66E-13	2.831018
ENSMUSG00000043468	*Adam30*	2.93E-04	2.837999
ENSMUSG00000106056	*4930500L23Rik*	4.77E-03	2.840989
ENSMUSG00000045776	*Lrtm1*	1.50E-19	2.850709
ENSMUSG00000043460	*Elfn2*	2.64E-03	2.850978
ENSMUSG00000057454	*Lypd3*	1.13E-07	2.855151
ENSMUSG00000018862	*Otop3*	4.00E-07	2.861507
ENSMUSG00000068885	*Lce3f*	3.57E-09	2.863271
ENSMUSG00000032401	*Lctl*	5.17E-03	2.865397
ENSMUSG00000032373	*Car12*	2.44E-33	2.866191
ENSMUSG00000046748	*Tmem45a2*	3.29E-15	2.875771
ENSMUSG00000116659	*AC158985.1*	1.03E-03	2.879651
ENSMUSG00000111555	*Gm47326*	4.82E-02	2.882505
ENSMUSG00000079025	*Gsdmc*	9.10E-07	2.885077
ENSMUSG00000056328	*Myh1*	2.08E-87	2.886996
ENSMUSG00000027913	*Crct1*	2.20E-14	2.894169
ENSMUSG00000020216	*Jsrp1*	1.18E-04	2.896039
ENSMUSG00000071019	*Sdr16c6*	3.06E-05	2.897926
ENSMUSG00000025172	*Ankrd2*	3.28E-18	2.90344
ENSMUSG00000074433	*Lce3e*	9.33E-07	2.913285
ENSMUSG00000036731	*Cysrt1*	8.18E-07	2.915053
ENSMUSG00000010064	*Slc38a3*	5.21E-18	2.918093
ENSMUSG00000030730	*Atp2a1*	5.75E-78	2.932671

ENSMUSG00000085479	*9430073C21Rik*	5.71E-04	2.934549
ENSMUSG00000059668	*Krt4*	4.18E-14	2.937284
ENSMUSG00000114163	*Gm32296*	5.99E-04	2.941019
ENSMUSG00000038295	*Atg9b*	6.02E-09	2.942834
ENSMUSG00000099449	*Gm28401*	1.09E-04	2.950106
ENSMUSG00000026413	*Pkp1*	5.96E-19	2.956086
ENSMUSG00000028386	*Slc46a2*	8.03E-03	2.960449
ENSMUSG00000039070	*Cpa4*	3.59E-11	2.967827
ENSMUSG00000037977	*6430571L13Rik*	1.15E-12	2.986157
ENSMUSG00000110426	*Gm45757*	2.83E-02	2.990865
ENSMUSG00000032454	*Rbp2*	9.49E-04	2.991761
ENSMUSG00000073601	*Serpinb3c*	2.89E-05	2.992627
ENSMUSG00000029154	*Cwh43*	3.21E-04	2.995754
ENSMUSG00000054325	*Lce3a*	3.84E-11	2.996653
ENSMUSG00000105160	*A530030E21Rik*	7.94E-03	3.00639
ENSMUSG00000074183	*Gsta1*	1.18E-03	3.011134
ENSMUSG00000068889	*Lce1e*	3.36E-03	3.016024
ENSMUSG00000020061	*Mybpc1*	4.58E-66	3.020577
ENSMUSG00000027048	*Abcb11*	2.16E-02	3.040284
ENSMUSG00000039269	*2300002M23Rik*	1.76E-06	3.045743
ENSMUSG00000117222	*AC060761.1*	8.51E-16	3.048258
ENSMUSG00000025129	*Ppp1r27*	6.54E-04	3.050154
ENSMUSG00000020908	*Myh3*	2.90E-04	3.053928
ENSMUSG00000097364	*Gm26719*	2.09E-05	3.072513
ENSMUSG00000054422	*Fabp1*	5.44E-04	3.078014
ENSMUSG00000044041	*Krt13*	2.04E-15	3.079995
ENSMUSG00000063821	*Dupd1*	1.16E-02	3.080693
ENSMUSG00000043430	*Psapl1*	2.65E-14	3.082218
ENSMUSG00000044594	*Serpinb3a*	5.68E-13	3.087602
ENSMUSG00000085532	*B430319H21Rik*	1.32E-14	3.09774
ENSMUSG00000042031	*Lce3b*	1.13E-11	3.112196
ENSMUSG00000005355	*Casp14*	2.13E-04	3.113601
ENSMUSG00000087038	*2900079G21Rik*	4.50E-03	3.1195
ENSMUSG00000114922	*Ppifos*	2.43E-06	3.120941
ENSMUSG00000031372	*Trex2*	1.04E-04	3.124283
ENSMUSG00000086584	*Gm12002*	6.34E-13	3.127654
ENSMUSG00000071858	*Gm94*	2.60E-09	3.127964
ENSMUSG00000092586	*Ly6g6c*	8.86E-11	3.133452
ENSMUSG00000101133	*Gm29050*	2.40E-04	3.136949
ENSMUSG00000048399	*Tprg*	1.51E-09	3.169198
ENSMUSG00000045475	*Lce3c*	3.14E-12	3.171884
ENSMUSG00000110735	*Gm47173*	8.51E-03	3.184631
ENSMUSG00000054146	*Krt15*	8.74E-19	3.18484
ENSMUSG00000103243	*Lce1d*	2.93E-06	3.187473
ENSMUSG00000026407	*Cacna1s*	1.08E-45	3.18982
ENSMUSG00000024471	*Myot*	5.42E-54	3.196349
ENSMUSG00000030713	*Klk7*	1.82E-04	3.197459
ENSMUSG00000097214	*Gm19791*	2.77E-02	3.223603
ENSMUSG00000068893	*Sprr2a2*	2.58E-13	3.229494
ENSMUSG00000050108	*Bpifc*	5.73E-05	3.240719
ENSMUSG00000028236	*Sdr16c5*	1.03E-04	3.243863
ENSMUSG00000078664	*Sprr2a1*	4.79E-06	3.253984
ENSMUSG00000033268	*Duox1*	2.09E-12	3.257037
ENSMUSG00000063130	*Calml3*	1.60E-17	3.258145
ENSMUSG00000050463	*Krt78*	7.67E-32	3.271363
ENSMUSG00000096269	*Rpl31-ps21*	2.93E-03	3.274694
ENSMUSG00000074652	*Myh7b*	5.39E-06	3.28996

ENSMUSG00000061527	*Krt5*	7.51E-19	3.292118
ENSMUSG00000030155	*Clec2e*	8.29E-03	3.314901
ENSMUSG00000047884	*Klk9*	1.29E-04	3.323011
ENSMUSG00000114091	*Gm40655*	1.54E-09	3.328511
ENSMUSG00000053522	*Lgals7*	1.35E-10	3.329974
ENSMUSG00000017204	*Gsdma*	4.28E-12	3.335837
ENSMUSG00000087090	*Nctc1*	2.38E-59	3.337836
ENSMUSG00000096001	*2610528A11Rik*	4.77E-04	3.356603
ENSMUSG00000062826	*Ces2f*	1.27E-20	3.364975
ENSMUSG00000031344	*Gabrq*	9.36E-03	3.374101
ENSMUSG00000085257	*Gm13264*	2.59E-02	3.380709
ENSMUSG00000082141	*Gm11212*	1.11E-03	3.415103
ENSMUSG00000067006	*Serpinb5*	3.69E-13	3.437795
ENSMUSG00000074156	*Ces1h*	2.13E-11	3.444764
ENSMUSG00000046676	*Lce1l*	1.08E-02	3.449777
ENSMUSG00000021364	*Elovl2*	1.25E-03	3.464127
ENSMUSG00000074445	*Sprr2a3*	8.74E-06	3.468969
ENSMUSG00000078964	*Ces1b*	2.78E-06	3.472679
ENSMUSG00000045545	*Krt14*	4.41E-27	3.472881
ENSMUSG00000059898	*Dsc3*	2.86E-17	3.473919
ENSMUSG00000033765	*Calm4*	5.17E-10	3.476147
ENSMUSG00000105961	*Gm40123*	8.89E-03	3.493003
ENSMUSG00000048721	*Fndc9*	1.16E-03	3.493393
ENSMUSG00000017300	*Tnnc2*	2.61E-56	3.493517
ENSMUSG00000101840	*Gm28294*	1.22E-02	3.494083
ENSMUSG00000046095	*Krt32*	6.38E-05	3.511431
ENSMUSG00000043795	*Prr33*	3.14E-07	3.513074
ENSMUSG00000074647	*Fam83c*	1.30E-04	3.523902
ENSMUSG00000091172	*Gm17120*	7.31E-03	3.529014
ENSMUSG00000110207	*Gm33586*	2.10E-02	3.530274
ENSMUSG00000051965	*Nanos2*	3.22E-04	3.536107
ENSMUSG00000051431	*Gpr87*	7.37E-05	3.549606
ENSMUSG00000025229	*Pitx3*	6.86E-03	3.553927
ENSMUSG00000005716	*Pvalb*	2.81E-11	3.631134
ENSMUSG00000031757	*Mt4*	1.87E-13	3.699945
ENSMUSG00000058354	*Krt6a*	8.73E-08	3.701633
ENSMUSG00000026985	*Il1f8*	4.85E-06	3.747629
ENSMUSG00000055301	*Adh7*	9.72E-31	3.762133
ENSMUSG00000097770	*Gm26776*	2.69E-05	3.767514
ENSMUSG00000115270	*5430430K15Rik*	1.03E-02	3.813184
ENSMUSG00000075217	*4833423E24Rik*	7.79E-13	3.828324
ENSMUSG00000043472	*Lce3d*	9.57E-05	3.852596
ENSMUSG00000030244	*Gys2*	3.13E-03	3.866888
ENSMUSG00000056078	*Lipm*	5.55E-12	3.878651
ENSMUSG00000047428	*Dlk2*	6.06E-04	3.942878
ENSMUSG00000013766	*Ly6g6e*	6.75E-03	3.95354
ENSMUSG00000017950	*Hnf4a*	2.61E-04	4.02923
ENSMUSG00000025194	*Abcc2*	1.91E-04	4.03213
ENSMUSG00000030046	*Bmp10*	5.70E-04	4.173749
ENSMUSG00000056632	*Dsg3*	2.00E-33	4.176681
ENSMUSG00000030237	*Slco1a4*	4.96E-03	4.192899
ENSMUSG00000028001	*Fga*	1.73E-08	4.260873
ENSMUSG00000109685	*Gm45912*	2.62E-03	4.273195
ENSMUSG00000111709	*Gm3776*	1.46E-04	4.284462
ENSMUSG00000043681	*Fam25c*	7.65E-12	4.287186
ENSMUSG00000079451	*Tmprss11g*	6.62E-12	4.355436
ENSMUSG00000097189	*Gm26594*	1.21E-02	4.459896

ENSMUSG00000025431	*Crisp1*	1.13E-13	4.600625
ENSMUSG00000023041	*Krt6b*	7.88E-05	4.619968
ENSMUSG00000011632	*Pinlyp*	1.13E-03	4.658043
ENSMUSG00000022875	*Kng1*	9.90E-06	4.667574
ENSMUSG00000035031	*C8a*	2.65E-03	4.905581
ENSMUSG00000044748	*Defb1*	2.48E-08	5.134939
ENSMUSG00000102098	*2310016D03Rik*	3.16E-06	5.282878
ENSMUSG00000035861	*Tmprss11b*	1.93E-05	5.434747
ENSMUSG00000027761	*Aadac*	2.12E-05	5.483728
ENSMUSG00000029019	*Nppb*	2.05E-26	5.500836
ENSMUSG00000033196	*Myh2*	1.31E-45	5.509976
ENSMUSG00000027261	*Hao1*	4.23E-11	5.543845
ENSMUSG00000070719	*Pla2g4d*	3.51E-07	5.701431
ENSMUSG00000025003	*Cyp2c39*	1.58E-04	6.085577
ENSMUSG00000004872	*Pax3*	1.87E-06	6.162959
ENSMUSG00000016327	*Atp1b4*	4.64E-12	6.441707
ENSMUSG00000027249	*F2*	5.25E-04	6.44469
ENSMUSG00000033860	*Fgg*	1.30E-15	6.79552
ENSMUSG00000056656	*Apol8*	2.35E-27	6.857002
ENSMUSG00000073375	*Lrrc30*	2.39E-04	7.131156
ENSMUSG00000024512	*Dynap*	2.79E-05	7.653523
ENSMUSG00000001670	*Tat*	1.65E-05	8.104061
ENSMUSG00000029671	*Wnt16*	5.12E-05	8.122169
ENSMUSG00000019932	*Kera*	9.32E-11	9.197208
ENSMUSG00000115207	*Gm49132*	6.77E-08	9.321712
ENSMUSG00000030131	*Mug2*	3.68E-08	10.01166
ENSMUSG00000020609	*Apob*	1.70E-16	10.07445
ENSMUSG00000003053	*Cyp2c29*	1.58E-09	11.55749
ENSMUSG00000022868	*Ahsg*	1.79E-19	12.68437
ENSMUSG00000035540	*Gc*	2.58E-14	14.12206
ENSMUSG00000030359	*Pzp*	3.60E-20	14.37129
ENSMUSG00000059481	*Plg*	3.52E-08	19.5621
ENSMUSG00000057400	*Ces1c*	8.80E-07	19.90682
ENSMUSG00000028307	*Aldob*	1.46E-10	20.84021
ENSMUSG00000005681	*Apoa2*	3.99E-05	38.11525
ENSMUSG00000059908	*Mug1*	1.99E-19	49.75901
ENSMUSG00000029630	*Cyp3a25*	3.05E-06	60.85914
ENSMUSG00000056035	*Cyp3a11*	2.89E-12	61.11608
ENSMUSG00000025991	*Cps1*	1.52E-07	68.002
ENSMUSG00000061808	*Ttr*	9.12E-07	72.79417
ENSMUSG00000033831	*Fgb*	2.27E-10	80.34186
ENSMUSG00000032083	*Apoa1*	1.86E-13	85.92226
ENSMUSG00000029368	*Alb*	8.71E-39	89.99856

Appendix W. Murine differential gene expression in the lungs 6 h post-infection, 947M vs 4559M. Genes with fold change (FC) greater than 1.5 and $p < 0.05$ are shown. FC values highlighted in blue = upregulated in 947M, while values highlighted in red = upregulated in 4559M.

Gene Stable ID	Gene Name	padj	FC
ENSMUSG00000085261	*Gm13814*	1.01E-05	5.162232
ENSMUSG00000031551	*Ido1*	1.63E-07	4.116956
ENSMUSG00000071679	*Rtl4*	1.67E-17	4.081086
ENSMUSG00000063594	*Gng8*	7.78E-04	3.837051
ENSMUSG00000009900	*Wnt3a*	3.97E-16	3.498319
ENSMUSG00000092591	*Gm20429*	6.56E-04	3.202419
ENSMUSG00000115574	*Gm49245*	6.79E-04	3.163799
ENSMUSG00000115307	*Gm49313*	7.11E-07	2.940982
ENSMUSG00000032502	*Stac*	7.16E-13	2.939761
ENSMUSG00000085982	*9530051G07Rik*	4.37E-06	2.908872
ENSMUSG00000085235	*Gm12576*	1.23E-05	2.830949
ENSMUSG00000030114	*Klrg1*	5.25E-03	2.807412
ENSMUSG00000068428	*Gmnc*	8.48E-03	2.716893
ENSMUSG00000001494	*Sost*	1.53E-04	2.681953
ENSMUSG00000020081	*Tacr2*	7.50E-03	2.609488
ENSMUSG00000105402	*Gm3716*	8.05E-03	2.563662
ENSMUSG00000108617	*Gm31749*	3.03E-03	2.550466
ENSMUSG00000060275	*Nrg2*	1.89E-11	2.543613
ENSMUSG00000114028	*9630002D21Rik*	2.18E-05	2.514966
ENSMUSG00000048485	*Zbtb8b*	1.10E-02	2.476257
ENSMUSG00000076613	*Ighg2b*	8.81E-04	2.473764
ENSMUSG00000053961	*Ang5*	8.04E-04	2.455475
ENSMUSG00000092389	*Gm20483*	1.60E-02	2.454367
ENSMUSG00000090166	*Ear10*	5.22E-10	2.447762
ENSMUSG00000114566	*Gm48500*	3.34E-05	2.443691
ENSMUSG00000087500	*Gm12426*	1.87E-03	2.430623
ENSMUSG00000086843	*E030013I19Rik*	9.29E-08	2.368294
ENSMUSG00000061171	*Slc38a11*	6.50E-05	2.368149
ENSMUSG00000087355	*Gm13187*	2.64E-02	2.35886
ENSMUSG00000076612	*Ighg2c*	2.96E-02	2.329747
ENSMUSG00000079436	*Kcnj13*	3.92E-03	2.327287
ENSMUSG00000052026	*Slc6a7*	2.97E-08	2.315711
ENSMUSG00000070530	*Wfdc16*	1.76E-02	2.314729
ENSMUSG00000109056	*A630009H07Rik*	2.27E-02	2.292291
ENSMUSG00000056824	*Zfp663*	6.59E-04	2.279782
ENSMUSG00000072599	*Ear-ps2*	2.14E-05	2.246685
ENSMUSG00000009394	*Syn2*	3.23E-27	2.246363
ENSMUSG00000051969	*Tlr11*	1.09E-02	2.239618
ENSMUSG00000086313	*Gm15940*	1.71E-03	2.238922
ENSMUSG00000036295	*Lrrn3*	1.33E-06	2.227998
ENSMUSG00000085882	*2610507I01Rik*	1.42E-05	2.211385
ENSMUSG00000116097	*Gm36738*	2.22E-04	2.2066
ENSMUSG00000030041	*M1ap*	6.18E-16	2.204481
ENSMUSG00000011263	*Exoc3l2*	4.87E-04	2.194716
ENSMUSG00000086822	*5330413P13Rik*	1.81E-03	2.193201
ENSMUSG00000102082	*Gm28675*	9.97E-04	2.179205
ENSMUSG00000099338	*2810030D12Rik*	7.38E-06	2.170948
ENSMUSG00000030495	*Slc7a10*	8.33E-20	2.14737
ENSMUSG00000087042	*Gm11611*	2.21E-02	2.145158
ENSMUSG00000099553	*Gm29538*	2.37E-06	2.13579
ENSMUSG00000066319	*Rtp3*	5.27E-08	2.127259
ENSMUSG00000041479	*Syt15*	4.13E-10	2.125265

ENSMUSG00000110427	*4933406B17Rik*	1.98E-02	2.10939
ENSMUSG00000025789	*St8sia2*	8.02E-14	2.104873
ENSMUSG00000028755	*Cda*	1.82E-03	2.099281
ENSMUSG00000026304	*Rab17*	1.54E-02	2.091565
ENSMUSG00000029193	*Cckar*	1.80E-08	2.087954
ENSMUSG00000019909	*Fam162b*	9.91E-04	2.085813
ENSMUSG00000039179	*Tekt5*	3.66E-03	2.083175
ENSMUSG00000044633	*B530045E10Rik*	2.46E-24	2.082099
ENSMUSG00000108084	*Gm7932*	3.36E-02	2.079352
ENSMUSG00000060615	*Ang4*	3.19E-02	2.073621
ENSMUSG00000000901	*Mmp11*	1.21E-09	2.071062
ENSMUSG00000051920	*Rspo2*	3.77E-02	2.060566
ENSMUSG00000024968	*Rcor2*	7.64E-03	2.054541
ENSMUSG00000048988	*Elfn1*	2.26E-18	2.049999
ENSMUSG00000028919	*Arhgef19*	1.84E-03	2.045006
ENSMUSG00000085282	*Gm15663*	1.26E-03	2.042585
ENSMUSG00000101605	*Ace3*	1.64E-08	2.033861
ENSMUSG00000063730	*Hsd3b2*	4.33E-03	2.031267
ENSMUSG00000037962	*Rflna*	9.51E-05	2.029917
ENSMUSG00000048455	*Sprr1b*	4.70E-02	2.029009
ENSMUSG00000054622	*D730045B01Rik*	3.09E-03	2.018059
ENSMUSG00000092353	*Gm20539*	1.07E-02	2.004409
ENSMUSG00000029601	*Iqcd*	9.80E-03	2.001456
ENSMUSG00000026109	*Tmeff2*	3.23E-11	1.998603
ENSMUSG00000009114	*2610028H24Rik*	2.03E-09	1.997699
ENSMUSG00000029477	*Morn3*	2.44E-03	1.99663
ENSMUSG00000074505	*Fat3*	3.95E-40	1.986612
ENSMUSG00000108481	*Gm33248*	9.66E-17	1.983101
ENSMUSG00000026494	*Kif26b*	6.07E-29	1.976902
ENSMUSG00000103857	*Gm37249*	2.44E-02	1.97662
ENSMUSG00000055945	*Prr18*	2.04E-05	1.976009
ENSMUSG00000087142	*Gm12454*	1.40E-03	1.974069
ENSMUSG00000022491	*Glycam1*	9.58E-05	1.972925
ENSMUSG00000070720	*Tmem200b*	2.56E-04	1.963692
ENSMUSG00000116660	*CT030736.1*	1.35E-13	1.960853
ENSMUSG00000020218	*Wif1*	3.37E-14	1.957565
ENSMUSG00000047085	*Lrrc4b*	1.22E-05	1.939777
ENSMUSG00000027656	*Wisp2*	6.19E-47	1.938229
ENSMUSG00000027380	*Acoxl*	1.13E-11	1.935006
ENSMUSG00000017007	*Rbpjl*	2.17E-14	1.933213
ENSMUSG00000033533	*Acsm1*	1.08E-07	1.933132
ENSMUSG00000079039	*Gm11037*	3.17E-02	1.927416
ENSMUSG00000092004	*Gm17482*	3.73E-05	1.925619
ENSMUSG00000052353	*Cemip*	1.08E-23	1.921299
ENSMUSG00000067714	*Lpar5*	4.75E-02	1.916894
ENSMUSG00000086368	*Gm13830*	1.34E-04	1.915922
ENSMUSG00000107230	*Gm19265*	2.82E-03	1.914934
ENSMUSG00000022504	*Ciita*	3.98E-26	1.914004
ENSMUSG00000050288	*Fzd2*	1.07E-05	1.912167
ENSMUSG00000086585	*Gm16126*	3.81E-02	1.91092
ENSMUSG00000040841	*Six5*	6.58E-09	1.910496
ENSMUSG00000084998	*Gm16279*	9.76E-04	1.908554
ENSMUSG00000072596	*Ear2*	7.41E-14	1.907457
ENSMUSG00000063681	*Crb1*	3.66E-02	1.90717
ENSMUSG00000026870	*Cutal*	7.86E-04	1.907001
ENSMUSG00000105547	*Iglc3*	3.49E-02	1.904731
ENSMUSG00000103824	*Gm38177*	4.20E-04	1.893794

ENSMUSG00000034324	*Tmem132c*	6.54E-30	1.893682
ENSMUSG00000108390	*Gm39038*	1.42E-02	1.893336
ENSMUSG00000097591	*A330032B11Rik*	2.92E-03	1.889618
ENSMUSG00000108195	*Gm44415*	1.81E-02	1.887889
ENSMUSG00000038233	*Fam198a*	3.94E-07	1.883042
ENSMUSG00000103839	*Gm37607*	3.89E-02	1.879446
ENSMUSG00000030043	*Tacr1*	4.32E-06	1.878906
ENSMUSG00000074480	*Mex3a*	5.57E-03	1.877201
ENSMUSG00000063260	*Syt10*	2.50E-02	1.87586
ENSMUSG00000072601	*Ear1*	3.55E-09	1.87466
ENSMUSG00000025577	*Cbx2*	1.79E-04	1.874541
ENSMUSG00000043110	*Lrrn4*	8.40E-06	1.874015
ENSMUSG00000045087	*S1pr5*	2.29E-03	1.872791
ENSMUSG00000085069	*Gm13111*	2.88E-04	1.871815
ENSMUSG00000014543	*Klra17*	1.24E-12	1.871249
ENSMUSG00000092515	*C87198*	2.73E-02	1.870875
ENSMUSG00000114161	*Gm48662*	1.37E-02	1.868726
ENSMUSG00000108289	*Gm44174*	3.34E-08	1.868318
ENSMUSG00000034467	*Dynlrb2*	1.07E-04	1.864633
ENSMUSG00000030125	*Lrrc23*	3.21E-07	1.862472
ENSMUSG00000037492	*Zmat4*	1.44E-11	1.858985
ENSMUSG00000089713	*Gm16564*	3.70E-02	1.858329
ENSMUSG00000110380	*Gm45332*	2.12E-03	1.856669
ENSMUSG00000026616	*Cr2*	1.36E-07	1.856455
ENSMUSG00000027831	*Veph1*	6.53E-14	1.85639
ENSMUSG00000108580	*Gm39094*	9.91E-27	1.847514
ENSMUSG00000085419	*Gm11734*	9.18E-03	1.8441
ENSMUSG00000024440	*Pcdh12*	1.29E-20	1.843863
ENSMUSG00000044952	*Kctd21*	5.91E-10	1.842085
ENSMUSG00000116609	*AC122141.1*	1.30E-02	1.840951
ENSMUSG00000086154	*Gm16196*	1.33E-02	1.840383
ENSMUSG00000046242	*Nme9*	1.23E-02	1.838804
ENSMUSG00000063320	*1190007I07Rik*	1.48E-02	1.836405
ENSMUSG00000086390	*1810019D21Rik*	4.43E-07	1.836126
ENSMUSG00000087518	*Gm13561*	5.48E-03	1.835776
ENSMUSG00000100041	*Gm5702*	1.11E-02	1.835727
ENSMUSG00000102175	*Gm6119*	1.10E-03	1.833252
ENSMUSG00000087514	*Gm16076*	7.80E-03	1.831068
ENSMUSG00000079355	*Ackr4*	1.42E-05	1.830347
ENSMUSG00000021234	*Fam161b*	1.93E-04	1.828797
ENSMUSG00000097339	*Gm26671*	6.23E-05	1.828632
ENSMUSG00000046182	*Gsg1l*	2.43E-05	1.826043
ENSMUSG00000047787	*Flrt1*	4.73E-02	1.825861
ENSMUSG00000021708	*Rasgrf2*	7.04E-24	1.822346
ENSMUSG00000029651	*Mtus2*	3.04E-27	1.820688
ENSMUSG00000079173	*Zan*	1.05E-03	1.82063
ENSMUSG00000042256	*Ptchd4*	8.22E-05	1.819936
ENSMUSG00000063430	*Wscd2*	1.07E-09	1.81492
ENSMUSG00000104168	*Gm38250*	8.48E-04	1.810521
ENSMUSG00000103738	*Gm37652*	6.73E-04	1.809033
ENSMUSG00000056155	*Nanos3*	8.78E-04	1.806709
ENSMUSG00000044338	*Aplnr*	1.37E-34	1.806317
ENSMUSG00000038402	*Foxf2*	1.43E-09	1.806283
ENSMUSG00000110660	*Gm5362*	1.46E-02	1.804937
ENSMUSG00000020642	*Rnf144a*	4.67E-29	1.804772
ENSMUSG00000086283	*2810433D01Rik*	4.15E-02	1.804678
ENSMUSG00000033249	*Hsf4*	2.62E-04	1.798369

ENSMUSG00000105376	*Gm36535*	8.45E-03	1.797718
ENSMUSG00000030098	*Grip2*	2.83E-09	1.795977
ENSMUSG00000027796	*Smad9*	7.70E-08	1.788007
ENSMUSG00000052563	*D930048N14Rik*	1.75E-06	1.786953
ENSMUSG00000045555	*Mettl24*	4.87E-17	1.786089
ENSMUSG00000039037	*St6galnac5*	9.72E-33	1.782983
ENSMUSG00000084866	*A930006K02Rik*	7.02E-03	1.779173
ENSMUSG00000050022	*Amz1*	1.30E-06	1.779075
ENSMUSG00000115333	*Gm34590*	6.00E-03	1.77317
ENSMUSG00000091415	*Ak9*	7.15E-10	1.77086
ENSMUSG00000036923	*Stox1*	1.49E-08	1.769288
ENSMUSG00000025902	*Sox17*	1.61E-18	1.76508
ENSMUSG00000026301	*Iqca*	1.77E-05	1.764688
ENSMUSG00000079330	*Lemd1*	1.10E-05	1.764372
ENSMUSG00000057123	*Gja5*	5.68E-21	1.76359
ENSMUSG00000112468	*Gm47720*	6.31E-08	1.762303
ENSMUSG00000027932	*Slc27a3*	3.01E-04	1.757901
ENSMUSG00000027318	*Adam33*	5.00E-08	1.756879
ENSMUSG00000034584	*Exph5*	9.73E-20	1.754362
ENSMUSG00000042359	*Osbpl6*	1.37E-20	1.752867
ENSMUSG00000086141	*9030622O22Rik*	6.75E-14	1.748517
ENSMUSG00000087413	*Gm11266*	1.49E-10	1.7464
ENSMUSG00000043088	*Il17re*	8.79E-06	1.745302
ENSMUSG00000073877	*Gm13306*	1.50E-02	1.741028
ENSMUSG00000058420	*Syt17*	5.21E-07	1.739965
ENSMUSG00000054966	*Lmntd1*	3.10E-21	1.739876
ENSMUSG00000044156	*Hepacam2*	8.78E-03	1.7394
ENSMUSG00000112343	*Sfta3-ps*	6.02E-35	1.73883
ENSMUSG00000025578	*Cbx8*	2.05E-02	1.738267
ENSMUSG00000049420	*Tmem200a*	4.62E-16	1.737708
ENSMUSG00000094786	*Gm14403*	2.31E-14	1.73598
ENSMUSG00000052516	*Robo2*	3.01E-29	1.732225
ENSMUSG00000052117	*D630039A03Rik*	2.49E-03	1.730316
ENSMUSG00000095247	*Ccl27a*	1.67E-02	1.729601
ENSMUSG00000035829	*Ppp1r26*	4.19E-05	1.727533
ENSMUSG00000031489	*Adrb3*	1.72E-07	1.727349
ENSMUSG00000022844	*Pdia5*	7.32E-17	1.727186
ENSMUSG00000030732	*Chrdl2*	1.63E-02	1.727151
ENSMUSG00000034685	*Fam171a2*	2.13E-04	1.726734
ENSMUSG00000063535	*Zfp773*	5.88E-03	1.725168
ENSMUSG00000030302	*Atp2b2*	1.69E-08	1.723946
ENSMUSG00000024063	*Lbh*	4.98E-36	1.722771
ENSMUSG00000068246	*Apol9b*	3.02E-02	1.721537
ENSMUSG00000027849	*Syt6*	2.77E-06	1.721018
ENSMUSG00000023011	*Faim2*	1.27E-05	1.718468
ENSMUSG00000037709	*Fam13a*	1.35E-08	1.718152
ENSMUSG00000037973	*Ccdc129*	1.14E-09	1.717358
ENSMUSG00000030093	*Wnt7a*	3.68E-05	1.717134
ENSMUSG00000054459	*Vsnl1*	3.49E-14	1.71657
ENSMUSG00000106749	*Gm43281*	1.17E-06	1.71649
ENSMUSG00000038453	*Srcin1*	3.73E-09	1.71294
ENSMUSG00000020169	*Best3*	4.21E-07	1.7127
ENSMUSG00000070802	*Pnmal2*	2.73E-03	1.712669
ENSMUSG00000108767	*Gm29763*	4.23E-02	1.712211
ENSMUSG00000106617	*Gm36266*	4.87E-02	1.708878
ENSMUSG00000037846	*Rtkn2*	5.59E-09	1.707006
ENSMUSG00000046916	*Myct1*	1.96E-11	1.7066

ENSMUSG00000020734	*Grin2c*	1.11E-02	1.70189
ENSMUSG00000020135	*Apc2*	5.57E-05	1.700572
ENSMUSG00000029510	*Gpc2*	3.36E-02	1.699228
ENSMUSG00000011658	*Fuz*	2.30E-07	1.696259
ENSMUSG00000028871	*Rspo1*	5.07E-03	1.694801
ENSMUSG00000059323	*Tonsl*	8.20E-04	1.693202
ENSMUSG00000051727	*Kctd14*	3.92E-02	1.692769
ENSMUSG00000021496	*Pcbd2*	5.81E-19	1.692202
ENSMUSG00000024206	*Rfx2*	4.60E-17	1.691263
ENSMUSG00000034771	*Tle2*	8.58E-09	1.690916
ENSMUSG00000105637	*Gm42480*	4.36E-02	1.690621
ENSMUSG00000110206	*Flt3l*	3.41E-08	1.689626
ENSMUSG00000020566	*Atp6v1c2*	6.88E-19	1.689203
ENSMUSG00000026347	*Tmem163*	2.61E-23	1.688979
ENSMUSG00000038422	*Hdhd3*	1.93E-02	1.688234
ENSMUSG00000110893	*Gm47392*	3.19E-02	1.684205
ENSMUSG00000020546	*Stxbp4*	8.52E-19	1.682897
ENSMUSG00000031147	*Magix*	1.99E-02	1.682316
ENSMUSG00000097399	*Gm26555*	2.40E-02	1.681825
ENSMUSG00000057719	*Sh3rf2*	5.96E-15	1.681035
ENSMUSG00000078794	*Dact3*	3.49E-06	1.680713
ENSMUSG00000026676	*Ccdc3*	9.32E-13	1.678664
ENSMUSG00000113585	*Gm19605*	3.31E-04	1.676504
ENSMUSG00000112714	*Gm4798*	2.16E-06	1.675832
ENSMUSG00000082192	*Gm14719*	3.57E-02	1.675599
ENSMUSG00000104244	*2900018N21Rik*	2.55E-02	1.67496
ENSMUSG00000098022	*Zfp82*	2.20E-02	1.672994
ENSMUSG00000040543	*Pitpnm3*	2.42E-15	1.670307
ENSMUSG00000040009	*Gnaz*	2.72E-03	1.670102
ENSMUSG00000074282	*Zfp94*	1.02E-04	1.669767
ENSMUSG00000041431	*Ccnb1*	2.46E-02	1.668727
ENSMUSG00000037101	*Ttc29*	1.48E-07	1.668254
ENSMUSG00000044694	*2010007H06Rik*	4.57E-05	1.664324
ENSMUSG00000074283	*Zfp109*	1.27E-04	1.664311
ENSMUSG00000042750	*Bex2*	2.12E-02	1.660556
ENSMUSG00000037610	*Kcnmb2*	3.48E-09	1.660213
ENSMUSG00000029206	*Nsun7*	8.95E-03	1.65966
ENSMUSG00000048096	*Lmod1*	4.51E-06	1.658969
ENSMUSG00000087424	*5730405O15Rik*	1.41E-02	1.658718
ENSMUSG00000043664	*Tmem221*	1.85E-03	1.657821
ENSMUSG00000036962	*Cfap221*	1.50E-04	1.657207
ENSMUSG00000104658	*Gm30275*	9.01E-04	1.656842
ENSMUSG00000059588	*Calcrl*	5.46E-25	1.656551
ENSMUSG00000032606	*Nicn1*	4.61E-05	1.655171
ENSMUSG00000042988	*Notum*	3.14E-02	1.651852
ENSMUSG00000090135	*Gm15809*	7.06E-05	1.651829
ENSMUSG00000026785	*Pkn3*	3.37E-07	1.651277
ENSMUSG00000036864	*Proser3*	1.85E-04	1.650066
ENSMUSG00000021573	*Tppp*	1.72E-15	1.64999
ENSMUSG00000047146	*Tet1*	9.98E-15	1.649532
ENSMUSG00000022763	*Aifm3*	4.57E-02	1.648956
ENSMUSG00000029074	*Ttll10*	4.54E-08	1.648169
ENSMUSG00000106951	*5930430L01Rik*	2.79E-03	1.648167
ENSMUSG00000066129	*Kndc1*	1.48E-05	1.648069
ENSMUSG00000036218	*Pdzrn4*	1.20E-13	1.64797
ENSMUSG00000049349	*Gm5105*	4.33E-02	1.647966
ENSMUSG00000034522	*Zfp395*	2.88E-12	1.647198

ENSMUSG00000004996	*Mri1*	6.19E-05	1.646009
ENSMUSG00000030209	*Grin2b*	1.06E-03	1.644894
ENSMUSG00000083640	*Gm8876*	2.25E-02	1.644745
ENSMUSG00000022199	*Slc22a17*	2.43E-06	1.644577
ENSMUSG00000097115	*1810019N24Rik*	4.68E-02	1.644237
ENSMUSG00000053730	*Tmem39b*	5.53E-05	1.642946
ENSMUSG00000022615	*Tymp*	9.68E-04	1.641539
ENSMUSG00000038605	*Samd10*	3.89E-05	1.640188
ENSMUSG00000028801	*Stpg1*	5.81E-04	1.639582
ENSMUSG00000024579	*Pcyox1l*	2.73E-06	1.639339
ENSMUSG00000109394	*A230057D06Rik*	1.24E-15	1.639166
ENSMUSG00000038576	*Susd4*	5.59E-13	1.639016
ENSMUSG00000097453	*Gm26894*	1.64E-02	1.637894
ENSMUSG00000027186	*Elf5*	3.99E-04	1.637037
ENSMUSG00000067629	*Syngap1*	1.04E-10	1.636623
ENSMUSG00000042474	*Fcmr*	1.58E-04	1.636419
ENSMUSG00000049625	*Tifab*	3.19E-09	1.636014
ENSMUSG00000102437	*Gm38048*	9.87E-06	1.635702
ENSMUSG00000032357	*Tinag*	5.76E-05	1.635216
ENSMUSG00000033952	*Aspm*	3.64E-06	1.635025
ENSMUSG00000106993	*Gm43417*	1.87E-02	1.634425
ENSMUSG00000085682	*Gm14267*	1.56E-03	1.633309
ENSMUSG00000050705	*2310061I04Rik*	1.46E-05	1.632802
ENSMUSG00000035504	*Reep6*	1.13E-03	1.631873
ENSMUSG00000029521	*Chek2*	1.57E-03	1.62588
ENSMUSG00000085237	*Gm15406*	4.19E-08	1.6257
ENSMUSG00000031220	*Awat2*	1.51E-02	1.624394
ENSMUSG00000054555	*Adam12*	2.00E-23	1.623831
ENSMUSG00000112694	*Gm33037*	1.78E-02	1.620917
ENSMUSG00000042826	*Fgf11*	1.79E-03	1.618808
ENSMUSG00000040282	*BC052040*	2.59E-16	1.618536
ENSMUSG00000032064	*Dixdc1*	5.04E-09	1.617751
ENSMUSG00000111229	*Gm39323*	1.15E-03	1.617613
ENSMUSG00000052921	*Arhgef15*	1.73E-18	1.61749
ENSMUSG00000031870	*Pgr*	3.58E-10	1.617384
ENSMUSG00000051811	*Cox6b2*	1.16E-02	1.617084
ENSMUSG00000035435	*Abca17*	2.04E-08	1.615687
ENSMUSG00000022179	*4931414P19Rik*	3.70E-05	1.615439
ENSMUSG00000028031	*Dkk2*	2.04E-05	1.613944
ENSMUSG00000049811	*Fam161a*	3.97E-06	1.611627
ENSMUSG00000097805	*Gm17473*	1.63E-07	1.610565
ENSMUSG00000027560	*Dok5*	1.58E-03	1.609425
ENSMUSG00000045875	*Adra1a*	3.66E-05	1.608373
ENSMUSG00000074793	*Hspa12b*	3.94E-19	1.607954
ENSMUSG00000068551	*Zfp467*	5.27E-10	1.605012
ENSMUSG00000022442	*Ttll1*	1.44E-05	1.604733
ENSMUSG00000058396	*Gpr182*	6.53E-09	1.603606
ENSMUSG00000001496	*Nkx2-1*	1.73E-11	1.599734
ENSMUSG00000116116	*Gm671*	1.39E-07	1.599663
ENSMUSG00000030796	*Tead2*	3.21E-11	1.599608
ENSMUSG00000057060	*Slc35f3*	1.38E-03	1.599499
ENSMUSG00000046806	*Cyren*	2.91E-05	1.5994
ENSMUSG00000003779	*Kif20a*	2.39E-02	1.599212
ENSMUSG00000066235	*Pomgnt2*	2.51E-04	1.597016
ENSMUSG00000055333	*Fat2*	2.60E-04	1.596568
ENSMUSG00000030873	*Scnn1b*	2.04E-20	1.594799
ENSMUSG00000097915	*A330009N23Rik*	3.03E-03	1.594615

ENSMUSG00000020614	*Fam20a*	1.16E-14	1.594492
ENSMUSG00000062542	*Syt9*	2.52E-02	1.59351
ENSMUSG00000068263	*Efcc1*	1.34E-09	1.593299
ENSMUSG00000097124	*A530020G20Rik*	5.09E-04	1.593002
ENSMUSG00000078607	*1810010H24Rik*	7.09E-07	1.592582
ENSMUSG00000043668	*Tox3*	5.03E-16	1.591389
ENSMUSG00000022676	*Snai2*	1.80E-03	1.591354
ENSMUSG00000042210	*Abhd14a*	1.25E-02	1.591316
ENSMUSG00000024403	*Atp6v1g2*	5.74E-03	1.591076
ENSMUSG00000026860	*Sh3glb2*	5.11E-12	1.590949
ENSMUSG00000027217	*Tspan18*	4.38E-21	1.590887
ENSMUSG00000082292	*Gm12250*	3.96E-04	1.59078
ENSMUSG00000105135	*Gm43667*	1.64E-02	1.589917
ENSMUSG00000031665	*Sall1*	9.47E-03	1.589292
ENSMUSG00000108207	*1810059H22Rik*	2.37E-02	1.589229
ENSMUSG00000087013	*2610027K06Rik*	5.70E-14	1.589185
ENSMUSG00000044548	*Dact1*	2.47E-07	1.587675
ENSMUSG00000110279	*Gm45552*	1.29E-02	1.585905
ENSMUSG00000115301	*Gm6330*	2.91E-02	1.585784
ENSMUSG00000055150	*Zfp78*	2.68E-03	1.584768
ENSMUSG00000057751	*Megf6*	1.53E-14	1.584688
ENSMUSG00000054517	*Trim65*	3.34E-06	1.584269
ENSMUSG00000002771	*Grin2d*	3.01E-05	1.583762
ENSMUSG00000107736	*Gm44148*	4.72E-09	1.583468
ENSMUSG00000030680	*Pagr1a*	7.90E-04	1.5832
ENSMUSG00000037025	*Foxa2*	1.28E-03	1.582839
ENSMUSG00000103766	*Gm38392*	2.13E-04	1.580705
ENSMUSG00000033233	*Trim45*	1.95E-02	1.578751
ENSMUSG00000046240	*Hepacam*	4.39E-04	1.578062
ENSMUSG00000098465	*Mir1668*	3.82E-05	1.577691
ENSMUSG00000089769	*Gm16574*	3.22E-02	1.577572
ENSMUSG00000029790	*Cep41*	1.21E-04	1.576274
ENSMUSG00000046470	*Sox18*	1.24E-09	1.57479
ENSMUSG00000036598	*Ccdc113*	2.12E-02	1.574563
ENSMUSG00000084939	*Gm830*	2.06E-02	1.573865
ENSMUSG00000069378	*Prdm6*	2.91E-16	1.572953
ENSMUSG00000042766	*Trim46*	2.68E-03	1.572774
ENSMUSG00000034848	*Ttc21b*	1.51E-11	1.572038
ENSMUSG00000064284	*Cdpf1*	2.94E-03	1.571986
ENSMUSG00000115095	*Gm49311*	8.92E-03	1.571257
ENSMUSG00000020182	*Ddc*	2.97E-02	1.571232
ENSMUSG00000032492	*Pth1r*	1.36E-04	1.570378
ENSMUSG00000027574	*Nkain4*	3.42E-06	1.570249
ENSMUSG00000021684	*Pde8b*	6.66E-17	1.570207
ENSMUSG00000039552	*Rsph4a*	1.53E-02	1.570094
ENSMUSG00000102305	*Gm38192*	4.40E-02	1.56988
ENSMUSG00000041117	*Ccdc8*	7.59E-06	1.569825
ENSMUSG00000033590	*Myo5c*	7.37E-13	1.569346
ENSMUSG00000043932	*Klri2*	2.44E-03	1.5688
ENSMUSG00000108218	*Olfr1372-ps1*	8.01E-05	1.567865
ENSMUSG00000055134	*9130017K11Rik*	1.04E-02	1.567643
ENSMUSG00000038725	*Pkhd1l1*	2.18E-08	1.56719
ENSMUSG00000037279	*Ovol2*	3.58E-02	1.566143
ENSMUSG00000050947	*Amigo1*	1.16E-07	1.566084
ENSMUSG00000022416	*Cacna1i*	1.45E-03	1.565741
ENSMUSG00000038379	*Ttk*	3.20E-02	1.564059
ENSMUSG00000018395	*Kif3a*	5.66E-10	1.563864

ENSMUSG00000078772	*Gm12353*	1.41E-08	1.563774
ENSMUSG00000115157	*Gm49397*	8.53E-23	1.563261
ENSMUSG00000079164	*Tlr5*	3.12E-06	1.563178
ENSMUSG00000068323	*Slc4a5*	5.95E-07	1.56313
ENSMUSG00000054967	*Zfp647*	3.16E-03	1.563113
ENSMUSG00000086533	*Mypopos*	8.00E-09	1.560072
ENSMUSG00000064294	*Aox3*	2.44E-09	1.560014
ENSMUSG00000025933	*Tmem14a*	2.01E-02	1.559242
ENSMUSG00000061397	*Krt79*	1.26E-02	1.559113
ENSMUSG00000062861	*Zfp28*	1.43E-05	1.558974
ENSMUSG00000114553	*Gm7644*	7.76E-03	1.558629
ENSMUSG00000039577	*Nphp4*	5.79E-05	1.558615
ENSMUSG00000085936	*2610307P16Rik*	1.35E-26	1.558192
ENSMUSG00000041429	*Nthl1*	1.26E-02	1.55773
ENSMUSG00000030351	*Tspan11*	1.91E-24	1.555549
ENSMUSG00000017167	*Cntnap1*	5.58E-04	1.555233
ENSMUSG00000030800	*Prss8*	4.00E-07	1.554977
ENSMUSG00000026824	*Kcnj3*	1.18E-10	1.55393
ENSMUSG00000022759	*Lrrc74b*	1.13E-02	1.553927
ENSMUSG00000102691	*Gm37780*	9.59E-03	1.553868
ENSMUSG00000027424	*Mgme1*	8.77E-03	1.553739
ENSMUSG00000038797	*Zscan2*	3.13E-04	1.553465
ENSMUSG00000112121	*C230072F16Rik*	1.48E-06	1.553102
ENSMUSG00000039304	*Tnfsf10*	1.86E-18	1.552207
ENSMUSG00000054074	*Skida1*	4.97E-02	1.551638
ENSMUSG00000074646	*6430550D23Rik*	3.75E-02	1.550595
ENSMUSG00000051550	*Zfp579*	4.82E-05	1.549596
ENSMUSG00000029053	*Prkcz*	2.72E-12	1.549462
ENSMUSG00000045410	*Akr1e1*	1.81E-02	1.547976
ENSMUSG00000108365	*Gm44951*	3.56E-03	1.547705
ENSMUSG00000083817	*Gm14400*	4.50E-02	1.547364
ENSMUSG00000024299	*Adamts10*	6.54E-19	1.546832
ENSMUSG00000029603	*Dtx1*	4.99E-03	1.546727
ENSMUSG00000075592	*Nynrin*	8.46E-14	1.546558
ENSMUSG00000031517	*Gpm6a*	1.10E-11	1.546528
ENSMUSG00000099564	*Gm28729*	2.89E-02	1.546472
ENSMUSG00000022701	*Ccdc191*	1.34E-10	1.546372
ENSMUSG00000039058	*Ak5*	3.48E-05	1.546267
ENSMUSG00000048498	*Cd300e*	4.94E-02	1.545969
ENSMUSG00000106633	*Gm43431*	4.81E-02	1.544944
ENSMUSG00000066438	*Plekhd1*	9.20E-06	1.544901
ENSMUSG00000060548	*Tnfrsf19*	5.99E-12	1.544576
ENSMUSG00000020682	*Mmp28*	3.42E-09	1.544554
ENSMUSG00000042073	*Abhd14b*	8.46E-08	1.543843
ENSMUSG00000074384	*AI429214*	3.33E-02	1.543505
ENSMUSG00000082264	*Gm12799*	1.72E-04	1.543452
ENSMUSG00000048897	*Zfp710*	6.90E-19	1.542688
ENSMUSG00000109165	*Gm45148*	3.20E-02	1.542583
ENSMUSG00000022543	*4930451G09Rik*	2.13E-02	1.542361
ENSMUSG00000032609	*Klhdc8b*	1.78E-05	1.541974
ENSMUSG00000062785	*Kcnc3*	7.41E-09	1.541955
ENSMUSG00000034532	*Fbxo16*	4.66E-02	1.5419
ENSMUSG00000020513	*Tubd1*	2.22E-06	1.541575
ENSMUSG00000035547	*Capn5*	1.06E-11	1.541062
ENSMUSG00000020268	*Lyrm7*	1.22E-03	1.541004
ENSMUSG00000106758	*Gm42731*	3.30E-02	1.540776
ENSMUSG00000107436	*Gm44416*	2.31E-02	1.540763

ENSMUSG00000041460	*Cacna2d4*	2.80E-02	1.540666
ENSMUSG00000037813	*D630003M21Rik*	1.59E-03	1.540376
ENSMUSG00000037892	*Pcdh18*	2.52E-14	1.540206
ENSMUSG00000078552	*Dcdc2b*	3.72E-02	1.539768
ENSMUSG00000113543	*Gm36264*	2.91E-02	1.539705
ENSMUSG00000029335	*Bmp3*	1.77E-12	1.539659
ENSMUSG00000107068	*Gm42742*	4.89E-06	1.538758
ENSMUSG00000095987	*Gm13104*	1.34E-02	1.538362
ENSMUSG00000046456	*Tmem150b*	2.91E-03	1.538263
ENSMUSG00000106247	*Gm43720*	4.73E-02	1.538062
ENSMUSG00000070873	*Lilra5*	3.76E-03	1.53778
ENSMUSG00000022818	*Cyp2ab1*	2.94E-02	1.537532
ENSMUSG00000058656	*Samd12*	1.10E-19	1.536867
ENSMUSG00000059851	*Kmt5c*	1.85E-08	1.536592
ENSMUSG00000104114	*Gm37297*	4.16E-04	1.536347
ENSMUSG00000018740	*Slc25a35*	2.79E-05	1.536163
ENSMUSG00000103845	*Gm19026*	3.48E-03	1.536156
ENSMUSG00000112627	*4933412E12Rik*	2.50E-08	1.535554
ENSMUSG00000035863	*Palm*	2.73E-10	1.535105
ENSMUSG00000033763	*Mtss1l*	3.13E-14	1.535088
ENSMUSG00000024787	*Snx15*	1.16E-06	1.534706
ENSMUSG00000028088	*Fmo5*	1.52E-06	1.534518
ENSMUSG00000106892	*Gm42791*	4.56E-09	1.534363
ENSMUSG00000051359	*Ncald*	1.38E-26	1.534218
ENSMUSG00000049532	*Sall2*	6.86E-05	1.534187
ENSMUSG00000112164	*Gm19990*	4.48E-02	1.533334
ENSMUSG00000026888	*Grb14*	1.31E-24	1.5329
ENSMUSG00000026586	*Prrx1*	1.15E-18	1.532838
ENSMUSG00000023147	*Wrb*	8.70E-05	1.531827
ENSMUSG00000022941	*Ripply3*	1.87E-10	1.531256
ENSMUSG00000021055	*Esr2*	9.86E-08	1.531097
ENSMUSG00000050069	*Grem2*	2.17E-14	1.53098
ENSMUSG00000042784	*Muc1*	1.74E-15	1.530839
ENSMUSG00000030361	*Klrb1a*	1.98E-02	1.530589
ENSMUSG00000036278	*Macrod1*	1.31E-10	1.530463
ENSMUSG00000027500	*Stmn2*	5.55E-12	1.529312
ENSMUSG00000079671	*2610203C22Rik*	1.17E-16	1.529211
ENSMUSG00000070737	*Tmem35b*	1.01E-03	1.528272
ENSMUSG00000026443	*Lrrn2*	3.23E-03	1.52766
ENSMUSG00000036882	*Arhgap33*	2.72E-04	1.527118
ENSMUSG00000076431	*Sox4*	1.22E-10	1.526384
ENSMUSG00000049107	*Ntf3*	3.97E-10	1.526123
ENSMUSG00000097354	*2310001H17Rik*	1.98E-27	1.525662
ENSMUSG00000102326	*Gm37788*	2.52E-02	1.525393
ENSMUSG00000115970	*8430426J06Rik*	1.78E-06	1.52498
ENSMUSG00000000627	*Sema4f*	1.29E-05	1.524743
ENSMUSG00000051855	*Mest*	2.70E-08	1.524224
ENSMUSG00000019312	*Grb7*	4.43E-03	1.524165
ENSMUSG00000041361	*Myzap*	3.12E-18	1.523261
ENSMUSG00000036983	*Tfb1m*	1.77E-06	1.521731
ENSMUSG00000024673	*Ms4a1*	3.20E-04	1.521639
ENSMUSG00000019945	*Cabcoco1*	2.38E-04	1.52083
ENSMUSG00000026748	*Plxdc2*	3.63E-19	1.520549
ENSMUSG00000107499	*Ccdc142*	4.86E-02	1.520041
ENSMUSG00000029456	*Acad10*	4.39E-07	1.520036
ENSMUSG00000023949	*Tcte1*	3.76E-02	1.5199
ENSMUSG00000036555	*Iqce*	2.95E-11	1.518721

ENSMUSG00000060862	*Zbtb40*	1.39E-13	1.517839
ENSMUSG00000027490	*E2f1*	3.92E-02	1.517055
ENSMUSG00000032680	*6820408C15Rik*	1.89E-02	1.516845
ENSMUSG00000022103	*Gfra2*	1.63E-10	1.516841
ENSMUSG00000000402	*Egfl6*	8.17E-08	1.516514
ENSMUSG00000026390	*Marco*	1.23E-08	1.516135
ENSMUSG00000107794	*Gm44095*	3.87E-02	1.515819
ENSMUSG00000111761	*9230112J17Rik*	1.69E-02	1.51564
ENSMUSG00000056228	*Cars2*	3.79E-12	1.514966
ENSMUSG00000079003	*Samd1*	1.24E-04	1.514814
ENSMUSG00000038302	*Afg1l*	7.32E-25	1.514245
ENSMUSG00000022309	*Angpt1*	1.03E-07	1.514084
ENSMUSG00000045114	*Prrt2*	9.94E-04	1.51398
ENSMUSG00000037922	*Bank1*	1.10E-03	1.512972
ENSMUSG00000034800	*Zfp661*	9.55E-03	1.512619
ENSMUSG00000036411	*9530077C05Rik*	8.03E-05	1.512568
ENSMUSG00000035459	*Stab2*	1.02E-04	1.512457
ENSMUSG00000062960	*Kdr*	3.63E-21	1.511554
ENSMUSG00000050936	*Gm42743*	1.63E-07	1.511039
ENSMUSG00000021719	*Rgs7bp*	4.17E-07	1.510943
ENSMUSG00000031802	*Phxr4*	1.18E-04	1.510821
ENSMUSG00000085207	*Gm11767*	2.22E-03	1.50959
ENSMUSG00000057396	*Zfp759*	1.29E-03	1.509269
ENSMUSG00000031736	*Crnde*	1.62E-06	1.509225
ENSMUSG00000027977	*Ndst3*	7.76E-05	1.508506
ENSMUSG00000025395	*Prim1*	4.62E-03	1.507443
ENSMUSG00000030551	*Nr2f2*	3.20E-10	1.507264
ENSMUSG00000028003	*Lrat*	1.08E-05	1.507135
ENSMUSG00000100707	*Gm28523*	2.77E-03	1.50701
ENSMUSG00000050222	*Il17d*	1.67E-02	1.506503
ENSMUSG00000056185	*Snx32*	3.36E-07	1.506257
ENSMUSG00000098318	*Lockd*	1.28E-03	1.50611
ENSMUSG00000031775	*Pllp*	1.05E-06	1.506048
ENSMUSG00000002346	*Slc25a42*	8.80E-09	1.506014
ENSMUSG00000007207	*Stx1a*	7.57E-06	1.5059
ENSMUSG00000030084	*Plxna1*	1.91E-16	1.505539
ENSMUSG00000059146	*Ntrk3*	4.22E-15	1.504398
ENSMUSG00000073424	*Cyp4f15*	1.80E-02	1.503825
ENSMUSG00000039062	*Anpep*	4.19E-13	1.503782
ENSMUSG00000001288	*Rarg*	2.33E-13	1.503681
ENSMUSG00000051817	*Sox12*	4.13E-02	1.502765
ENSMUSG00000076609	*Igkc*	4.41E-05	1.502726
ENSMUSG00000013033	*Adgrl1*	1.28E-14	1.502317
ENSMUSG00000033948	*Zswim5*	6.73E-05	1.501944
ENSMUSG00000079620	*Muc4*	1.41E-14	1.501612
ENSMUSG00000024018	*Ccdc167*	3.57E-09	1.501095
ENSMUSG00000045441	*Gprin3*	3.83E-11	1.500851
ENSMUSG00000036959	*Bcorl1*	3.46E-14	1.500655
ENSMUSG00000044701	*Il27*	1.05E-02	1.500073
ENSMUSG00000028773	*Fabp3*	3.89E-05	1.501682
ENSMUSG00000070031	*Sp140*	3.17E-21	1.501904
ENSMUSG00000105053	*Gm43064*	1.55E-08	1.501933
ENSMUSG00000029552	*Tes*	1.46E-22	1.502499
ENSMUSG00000047976	*Kcna1*	4.87E-04	1.502872
ENSMUSG00000045349	*Sh2d5*	1.76E-02	1.502987
ENSMUSG00000058755	*Osm*	1.79E-04	1.503113
ENSMUSG00000104348	*Gm37691*	1.01E-03	1.503512

ENSMUSG00000113041	*Gm48302*	4.83E-03	1.503595
ENSMUSG00000100969	*1700030N03Rik*	9.26E-03	1.503827
ENSMUSG00000030595	*Nfkbib*	5.68E-12	1.503921
ENSMUSG00000090141	*Gm614*	3.44E-04	1.504654
ENSMUSG00000035208	*Slfn8*	3.12E-11	1.504893
ENSMUSG00000004951	*Hspb1*	3.20E-15	1.505858
ENSMUSG00000059498	*Fcgr3*	5.02E-25	1.506788
ENSMUSG00000043953	*Ccrl2*	2.05E-15	1.507145
ENSMUSG00000041754	*Trem3*	1.95E-08	1.507303
ENSMUSG00000112707	*D830005E20Rik*	3.83E-06	1.507644
ENSMUSG00000084208	*Gm12792*	3.21E-02	1.508358
ENSMUSG00000053560	*Ier2*	6.51E-12	1.508916
ENSMUSG00000021886	*Gpr65*	5.04E-09	1.509174
ENSMUSG00000105337	*1700094M23Rik*	2.68E-06	1.510638
ENSMUSG00000075042	*4930431P03Rik*	3.69E-02	1.511896
ENSMUSG00000101969	*Gm20125*	2.94E-03	1.51201
ENSMUSG00000039005	*Tlr4*	9.61E-33	1.512543
ENSMUSG00000102476	*Gm37245*	3.69E-08	1.512732
ENSMUSG00000036557	*Stpg4*	4.97E-02	1.513017
ENSMUSG00000108368	*Gm45053*	8.49E-05	1.513592
ENSMUSG00000034640	*Tiparp*	3.82E-23	1.514228
ENSMUSG00000004609	*Cd33*	1.53E-22	1.514366
ENSMUSG00000097558	*Gm26902*	2.40E-02	1.514485
ENSMUSG00000030069	*Prok2*	3.12E-09	1.51466
ENSMUSG00000079012	*Serpina3m*	9.97E-15	1.515028
ENSMUSG00000037833	*Sh2d4b*	1.28E-10	1.515452
ENSMUSG00000036181	*Hist1h1c*	8.16E-07	1.515838
ENSMUSG00000032942	*Ucp3*	2.72E-04	1.515872
ENSMUSG00000078915	*Hsp25-ps1*	1.89E-14	1.515918
ENSMUSG00000045763	*Basp1*	8.22E-23	1.516202
ENSMUSG00000023964	*Calcr*	2.13E-09	1.51776
ENSMUSG00000074449	*Gm15319*	1.18E-02	1.518175
ENSMUSG00000027748	*Trpc4*	4.48E-02	1.518209
ENSMUSG00000084093	*Gm16418*	4.51E-02	1.518297
ENSMUSG00000025716	*Myo3a*	1.15E-02	1.518517
ENSMUSG00000019787	*Trdn*	5.00E-18	1.51858
ENSMUSG00000089281	*Scarna6*	1.66E-02	1.519358
ENSMUSG00000090248	*Gm14027*	1.67E-02	1.519727
ENSMUSG00000086320	*Gm12840*	2.45E-10	1.519868
ENSMUSG00000028573	*Fggy*	5.40E-03	1.520122
ENSMUSG00000033730	*Egr3*	6.03E-09	1.520144
ENSMUSG00000089716	*Gm6264*	6.83E-06	1.520708
ENSMUSG00000051650	*B3gnt2*	7.54E-28	1.520857
ENSMUSG00000104108	*Gm37876*	2.97E-03	1.520932
ENSMUSG00000051439	*Cd14*	2.28E-24	1.521574
ENSMUSG00000020732	*Rab37*	4.19E-04	1.521864
ENSMUSG00000037904	*Ankrd9*	7.83E-03	1.522534
ENSMUSG00000105195	*Gm43584*	5.16E-04	1.522603
ENSMUSG00000027360	*Hdc*	4.67E-21	1.522604
ENSMUSG00000001014	*Icam4*	1.36E-02	1.522651
ENSMUSG00000022126	*Acod1*	4.82E-25	1.523696
ENSMUSG00000031448	*Adprhl1*	1.56E-05	1.524028
ENSMUSG00000056328	*Myh1*	4.72E-14	1.524211
ENSMUSG00000087593	*Gm16174*	6.08E-03	1.524313
ENSMUSG00000020275	*Rel*	1.32E-22	1.524463
ENSMUSG00000016559	*H3f3b*	1.21E-21	1.524786
ENSMUSG00000116614	*AC151299.1*	5.83E-04	1.526535

ENSMUSG00000099250	*Rn7s2*	1.32E-02	1.526701
ENSMUSG00000099021	*Rn7s1*	1.32E-02	1.526715
ENSMUSG00000023067	*Cdkn1a*	1.39E-25	1.527143
ENSMUSG00000095294	*Gm21119*	1.32E-02	1.527698
ENSMUSG00000026073	*Il1r2*	1.36E-06	1.527927
ENSMUSG00000031231	*Cox7b*	1.64E-09	1.528049
ENSMUSG00000025161	*Slc16a3*	3.55E-18	1.528109
ENSMUSG00000097543	*Gm805*	4.90E-02	1.528998
ENSMUSG00000059974	*Ntm*	4.19E-21	1.529013
ENSMUSG00000103288	*Gm37273*	8.69E-03	1.529304
ENSMUSG00000052769	*Gm9889*	3.93E-02	1.529381
ENSMUSG00000024590	*Lmnb1*	8.45E-17	1.529562
ENSMUSG00000114277	*Gm48583*	4.03E-03	1.529671
ENSMUSG00000106497	*Gm43195*	3.51E-02	1.529948
ENSMUSG00000085147	*Gm12609*	2.37E-02	1.529985
ENSMUSG00000068697	*Myoz1*	6.25E-04	1.530719
ENSMUSG00000029660	*Tex26*	1.65E-04	1.530841
ENSMUSG00000046480	*Scn4b*	9.28E-05	1.530902
ENSMUSG00000115946	*Mirt2*	7.87E-13	1.531478
ENSMUSG00000021622	*Ckmt2*	1.46E-08	1.531721
ENSMUSG00000039753	*Fbxl5*	8.84E-17	1.532351
ENSMUSG00000108486	*Gm44836*	8.76E-04	1.533293
ENSMUSG00000082057	*Gm15789*	2.89E-02	1.533491
ENSMUSG00000028862	*Map3k6*	6.29E-22	1.534354
ENSMUSG00000061462	*Obscn*	6.82E-21	1.535088
ENSMUSG00000029204	*Rhoh*	1.11E-19	1.535236
ENSMUSG00000072620	*Slfn2*	1.20E-17	1.535662
ENSMUSG00000098670	*Gm27818*	3.10E-02	1.536024
ENSMUSG00000107029	*Gm43123*	2.37E-04	1.536945
ENSMUSG00000087066	*Gm15518*	2.95E-07	1.537162
ENSMUSG00000031682	*1700011L22Rik*	6.64E-04	1.537235
ENSMUSG00000078763	*Slfn1*	2.40E-16	1.537518
ENSMUSG00000074149	*Gm10634*	4.40E-06	1.540107
ENSMUSG00000030669	*Calca*	1.35E-04	1.540221
ENSMUSG00000030088	*Aldh1l1*	8.07E-17	1.541343
ENSMUSG00000030107	*Usp18*	3.01E-16	1.541655
ENSMUSG00000071342	*Lsmem1*	3.17E-06	1.541988
ENSMUSG00000027861	*Casq2*	2.44E-09	1.542362
ENSMUSG00000074419	*Gm15448*	1.08E-08	1.542588
ENSMUSG00000062077	*Trim54*	3.72E-07	1.543231
ENSMUSG00000031289	*Il13ra2*	2.50E-02	1.544205
ENSMUSG00000094344	*Gm11942*	5.03E-07	1.545029
ENSMUSG00000055602	*Tcp10b*	1.12E-04	1.545251
ENSMUSG00000022902	*Stfa2*	2.23E-06	1.546076
ENSMUSG00000097579	*Gm26799*	2.14E-03	1.546157
ENSMUSG00000028116	*Myoz2*	3.48E-11	1.546592
ENSMUSG00000029915	*Clec5a*	1.27E-14	1.546688
ENSMUSG00000087135	*Gm16096*	3.13E-02	1.547248
ENSMUSG00000026669	*Mcm10*	6.49E-05	1.547768
ENSMUSG00000026358	*Rgs1*	2.94E-05	1.548109
ENSMUSG00000114790	*4921509O07Rik*	1.41E-03	1.54851
ENSMUSG00000115855	*Gm34643*	2.49E-02	1.548911
ENSMUSG00000097062	*Gm17586*	4.91E-02	1.549771
ENSMUSG00000037139	*Myom3*	5.04E-08	1.550368
ENSMUSG00000028012	*Rrh*	5.89E-04	1.551343
ENSMUSG00000052270	*Fpr2*	8.89E-17	1.551885
ENSMUSG00000025017	*Pik3ap1*	2.80E-32	1.552126

ENSMUSG00000042680	*Garem1*	2.43E-28	1.553264
ENSMUSG00000083500	*Gm15470*	2.33E-02	1.553699
ENSMUSG00000089617	*Scarna10*	1.33E-02	1.554248
ENSMUSG00000099587	*Gm28967*	1.33E-02	1.554248
ENSMUSG00000061723	*Tnnt3*	3.59E-06	1.554618
ENSMUSG00000101930	*Gm5441*	4.71E-05	1.554924
ENSMUSG00000047281	*Sfn*	1.18E-07	1.554958
ENSMUSG00000003134	*Tbc1d8*	2.31E-17	1.555831
ENSMUSG00000095098	*Ccdc85b*	1.46E-02	1.556789
ENSMUSG00000105572	*Gm43300*	1.75E-04	1.557092
ENSMUSG00000007877	*Tcap*	8.03E-10	1.557367
ENSMUSG00000028896	*Rcc1*	6.05E-10	1.558192
ENSMUSG00000104093	*A330015K06Rik*	2.94E-04	1.558524
ENSMUSG00000049515	*Espnl*	1.85E-06	1.558599
ENSMUSG00000105145	*Gm47299*	1.61E-02	1.559865
ENSMUSG00000105788	*Gm47295*	1.61E-02	1.560047
ENSMUSG00000030470	*Csrp3*	2.57E-10	1.560127
ENSMUSG00000086350	*B230369F24Rik*	3.44E-02	1.561156
ENSMUSG00000092134	*Gm17089*	1.34E-02	1.562976
ENSMUSG00000087684	*1200007C13Rik*	1.65E-13	1.563081
ENSMUSG00000031626	*Sorbs2*	1.55E-17	1.563623
ENSMUSG00000109279	*Gm45220*	1.65E-07	1.564122
ENSMUSG00000031780	*Ccl17*	2.29E-05	1.565128
ENSMUSG00000110251	*Gm2996*	4.56E-09	1.565506
ENSMUSG00000021591	*Glrx*	1.01E-19	1.565524
ENSMUSG00000079597	*Gm5483*	5.00E-11	1.565997
ENSMUSG00000097282	*5031415H12Rik*	2.32E-03	1.566965
ENSMUSG00000086554	*9530034E10Rik*	1.85E-02	1.567387
ENSMUSG00000109005	*Gm45221*	4.72E-09	1.567699
ENSMUSG00000050439	*Enthd1*	1.23E-02	1.568498
ENSMUSG00000020644	*Id2*	5.12E-18	1.570106
ENSMUSG00000086584	*Gm12002*	1.57E-02	1.570339
ENSMUSG00000079190	*AC133103.1*	6.72E-04	1.570523
ENSMUSG00000107352	*Gm43660*	2.34E-04	1.570886
ENSMUSG00000056569	*Mpz*	2.72E-08	1.570995
ENSMUSG00000069873	*4930438A08Rik*	3.36E-02	1.571682
ENSMUSG00000085249	*Gm12847*	2.96E-02	1.571826
ENSMUSG00000052212	*Cd177*	3.33E-17	1.571901
ENSMUSG00000031382	*Asb11*	2.67E-04	1.571915
ENSMUSG00000087597	*Gm15345*	5.12E-03	1.573455
ENSMUSG00000101751	*Gm2427*	5.74E-06	1.573571
ENSMUSG00000024774	*Ankrd22*	7.98E-10	1.573578
ENSMUSG00000078122	*F630028O10Rik*	7.10E-07	1.57378
ENSMUSG00000104801	*Gm43834*	1.91E-08	1.574775
ENSMUSG00000095260	*Gm25890*	2.05E-02	1.575215
ENSMUSG00000094812	*Gm22614*	2.05E-02	1.575215
ENSMUSG00000044997	*E130304I02Rik*	4.00E-02	1.575721
ENSMUSG00000098702	*1500015A07Rik*	6.89E-04	1.576298
ENSMUSG00000019933	*Mrln*	7.38E-03	1.577435
ENSMUSG00000055972	*2810407A14Rik*	3.65E-09	1.577756
ENSMUSG00000104406	*Gm38014*	2.17E-03	1.5782
ENSMUSG00000046223	*Plaur*	3.97E-19	1.578531
ENSMUSG00000031452	*1700029H14Rik*	7.05E-11	1.578888
ENSMUSG00000044639	*Gm11507*	3.21E-02	1.580159
ENSMUSG00000047604	*Frat2*	6.81E-03	1.580191
ENSMUSG00000086765	*Gm11827*	2.45E-03	1.580289
ENSMUSG00000090582	*Gm17024*	1.06E-06	1.58119

ENSMUSG00000029377	*Ereg*	1.30E-07	1.581718
ENSMUSG00000005686	*Ampd3*	3.84E-36	1.582624
ENSMUSG00000055639	*Dach1*	2.45E-49	1.582772
ENSMUSG00000048572	*Tmem252*	2.15E-30	1.583456
ENSMUSG00000106741	*4930513D17Rik*	2.31E-03	1.583518
ENSMUSG00000104449	*Gm37255*	6.66E-04	1.583657
ENSMUSG00000034226	*Rhov*	1.51E-03	1.583825
ENSMUSG00000034990	*Otoa*	2.27E-03	1.584135
ENSMUSG00000038059	*Smim3*	2.50E-27	1.584279
ENSMUSG00000064288	*Hist1h4k*	2.55E-02	1.584323
ENSMUSG00000067049	*Unc93a*	3.55E-03	1.584342
ENSMUSG00000114662	*Gm31683*	3.36E-03	1.584857
ENSMUSG00000071561	*BC100530*	2.75E-07	1.585823
ENSMUSG00000056025	*Clca3a1*	1.39E-09	1.586042
ENSMUSG00000064923	*Gm22042*	1.82E-02	1.586766
ENSMUSG00000087362	*Gm13710*	3.87E-05	1.588172
ENSMUSG00000115764	*Gm18811*	4.77E-02	1.588766
ENSMUSG00000102135	*Gm37108*	6.83E-03	1.589787
ENSMUSG00000018930	*Ccl4*	3.25E-14	1.592018
ENSMUSG00000092920	*Mirt2*	2.33E-03	1.593218
ENSMUSG00000003484	*Cyp4f18*	1.28E-11	1.594494
ENSMUSG00000068855	*Hist2h2ac*	2.26E-02	1.595197
ENSMUSG00000077192	*Snora17*	1.22E-02	1.595366
ENSMUSG00000112148	*Lilrb4a*	6.29E-08	1.595991
ENSMUSG00000053914	*Kdm4d*	3.47E-07	1.598458
ENSMUSG00000078905	*Gm14393*	2.09E-02	1.598898
ENSMUSG00000055301	*Adh7*	3.36E-04	1.599546
ENSMUSG00000025804	*Ccr1*	2.69E-15	1.600075
ENSMUSG00000025236	*Adpgk*	4.54E-06	1.600129
ENSMUSG00000028747	*Htr6*	3.61E-02	1.600441
ENSMUSG00000026452	*Syt2*	4.75E-12	1.600466
ENSMUSG00000095438	*Mir133a-1hg*	8.40E-04	1.60088
ENSMUSG00000107092	*Gm7993*	3.05E-09	1.601292
ENSMUSG00000099061	*Gm28050*	3.42E-06	1.601401
ENSMUSG00000100182	*1810006J02Rik*	2.34E-03	1.601528
ENSMUSG00000080845	*Gm9115*	9.28E-06	1.602056
ENSMUSG00000021702	*Thbs4*	5.37E-07	1.602758
ENSMUSG00000094733	*Gm5416*	2.35E-02	1.603974
ENSMUSG00000044719	*E230025N22Rik*	7.14E-03	1.604274
ENSMUSG00000031538	*Plat*	1.12E-27	1.6045
ENSMUSG00000071562	*Stfa1*	1.25E-02	1.604593
ENSMUSG00000116760	*AC164314.1*	1.55E-18	1.605019
ENSMUSG00000062028	*Irgc1*	1.27E-03	1.605428
ENSMUSG00000020108	*Ddit4*	3.87E-18	1.605556
ENSMUSG00000097168	*C230088H06Rik*	1.53E-07	1.607501
ENSMUSG00000059657	*Stfa2l1*	4.70E-13	1.608177
ENSMUSG00000054383	*Pnma1*	1.59E-02	1.609741
ENSMUSG00000030235	*Slco1c1*	8.01E-11	1.610186
ENSMUSG00000079800	*AC125149.3*	5.67E-04	1.610687
ENSMUSG00000047330	*Kcne4*	1.72E-12	1.611245
ENSMUSG00000011179	*Odc1*	6.77E-19	1.611702
ENSMUSG00000088185	*Scarna2*	2.29E-04	1.611916
ENSMUSG00000029635	*Cdk8*	2.85E-05	1.613325
ENSMUSG00000040747	*Cd53*	2.71E-18	1.613354
ENSMUSG00000104740	*Mir6516*	3.89E-02	1.613694
ENSMUSG00000086275	*1700121C08Rik*	1.98E-03	1.614578
ENSMUSG00000046178	*Nxph1*	3.18E-02	1.614789

ENSMUSG00000046101	*Mcmdc2*	2.24E-02	1.615786
ENSMUSG00000114980	*4933432I03Rik*	3.86E-13	1.617126
ENSMUSG00000112105	*Rps7-ps2*	2.09E-03	1.617464
ENSMUSG00000024215	*Spdef*	3.27E-04	1.617571
ENSMUSG00000087436	*Gm16156*	1.33E-02	1.618843
ENSMUSG00000095701	*Gm24830*	1.23E-02	1.619865
ENSMUSG00000096838	*Gm26232*	1.23E-02	1.619865
ENSMUSG00000065773	*Rnu1b6*	1.23E-02	1.619865
ENSMUSG00000029378	*Areg*	8.57E-05	1.620274
ENSMUSG00000030144	*Clec4d*	1.13E-16	1.621129
ENSMUSG00000089999	*Gm6485*	1.16E-11	1.621898
ENSMUSG00000097060	*Gm26759*	2.64E-04	1.622397
ENSMUSG00000043613	*Mmp3*	2.40E-04	1.624738
ENSMUSG00000106607	*Gm43178*	2.36E-02	1.625189
ENSMUSG00000064941	*Gm23238*	2.37E-03	1.625244
ENSMUSG00000045102	*Poln*	6.51E-23	1.627181
ENSMUSG00000074146	*4930579C12Rik*	9.25E-09	1.627321
ENSMUSG00000061878	*Sphk1*	2.13E-23	1.628004
ENSMUSG00000067555	*Gm10212*	4.20E-03	1.628146
ENSMUSG00000086993	*Rsf1os2*	1.93E-02	1.629504
ENSMUSG00000116747	*AC144408.2*	2.19E-02	1.630024
ENSMUSG00000069273	*Hist1h3e*	8.64E-03	1.630123
ENSMUSG00000085743	*8430419K02Rik*	5.99E-13	1.63082
ENSMUSG00000053338	*Tarm1*	1.27E-22	1.63113
ENSMUSG00000024471	*Myot*	2.74E-09	1.631316
ENSMUSG00000046610	*Oacyl*	1.57E-04	1.631988
ENSMUSG00000114125	*1700037F03Rik*	1.56E-02	1.632073
ENSMUSG00000027832	*Ptx3*	2.36E-34	1.633264
ENSMUSG00000092397	*C130080G10Rik*	3.11E-06	1.634192
ENSMUSG00000099803	*Gm28863*	4.44E-02	1.634596
ENSMUSG00000100779	*Gm29292*	5.73E-14	1.635041
ENSMUSG00000032523	*Hhatl*	1.82E-03	1.63623
ENSMUSG00000028125	*Abca4*	1.97E-12	1.637562
ENSMUSG00000038037	*Socs1*	4.73E-08	1.638886
ENSMUSG00000031872	*Bean1*	1.38E-10	1.639807
ENSMUSG00000049734	*Trex1*	2.49E-11	1.640014
ENSMUSG00000095580	*Rnu1b1*	1.33E-02	1.641977
ENSMUSG00000093834	*Rnu1b2*	1.33E-02	1.641977
ENSMUSG00000009633	*G0s2*	2.23E-07	1.642205
ENSMUSG00000002847	*Pla1a*	3.33E-22	1.642753
ENSMUSG00000043008	*Klhl6*	7.14E-15	1.642823
ENSMUSG00000062461	*Gm5453*	8.90E-06	1.643537
ENSMUSG00000045455	*Gm9797*	4.46E-02	1.644519
ENSMUSG00000082884	*Gm13339*	5.60E-05	1.644853
ENSMUSG00000052477	*C130026I21Rik*	6.00E-27	1.645118
ENSMUSG00000040490	*Lrfn2*	1.41E-02	1.645149
ENSMUSG00000113701	*B230303A05Rik*	4.29E-04	1.645667
ENSMUSG00000104560	*Gm8115*	6.75E-04	1.645915
ENSMUSG00000028396	*2310002L09Rik*	4.23E-02	1.649697
ENSMUSG00000024521	*Pmaip1*	2.02E-17	1.652637
ENSMUSG00000066361	*Serpina3c*	4.62E-21	1.652992
ENSMUSG00000091971	*Hspa1a*	3.82E-05	1.65332
ENSMUSG00000027014	*Cwc22*	6.70E-06	1.653834
ENSMUSG00000085779	*Atcayos*	1.32E-11	1.655658
ENSMUSG00000079462	*Gm15737*	4.27E-02	1.655772
ENSMUSG00000069305	*Hist1h4n*	1.34E-02	1.65667
ENSMUSG00000108414	*Snhg1*	6.02E-13	1.656675

ENSMUSG00000023341	*Mx2*	6.24E-29	1.656679
ENSMUSG00000096957	*E230013L22Rik*	2.31E-09	1.657441
ENSMUSG00000082838	*Gm14519*	1.01E-05	1.657928
ENSMUSG00000095500	*AC132444.5*	1.55E-02	1.658094
ENSMUSG00000035692	*Isg15*	5.98E-17	1.659027
ENSMUSG00000031972	*Acta1*	2.51E-10	1.660693
ENSMUSG00000115518	*Gm10791*	1.14E-03	1.661218
ENSMUSG00000028989	*Angptl7*	1.47E-05	1.661267
ENSMUSG00000030592	*Ryr1*	3.10E-08	1.662936
ENSMUSG00000087968	*Gm25395*	3.29E-04	1.663115
ENSMUSG00000074218	*Cox7a1*	2.46E-05	1.664493
ENSMUSG00000097927	*Gm6999*	1.40E-06	1.664539
ENSMUSG00000024481	*Lvrn*	1.55E-15	1.664843
ENSMUSG00000051748	*Wfdc21*	6.59E-11	1.665772
ENSMUSG00000056133	*Unc93a2*	1.42E-02	1.666035
ENSMUSG00000022821	*Hgd*	9.91E-04	1.666819
ENSMUSG00000077391	*Gm24336*	9.21E-03	1.667557
ENSMUSG00000112895	*Gm47567*	1.94E-03	1.668933
ENSMUSG00000097414	*B130046B21Rik*	5.30E-06	1.670513
ENSMUSG00000057003	*Myh4*	1.07E-10	1.67121
ENSMUSG00000096010	*Hist4h4*	2.64E-03	1.673569
ENSMUSG00000113960	*4933412O06Rik*	5.41E-03	1.673653
ENSMUSG00000041616	*Nppa*	2.60E-04	1.674788
ENSMUSG00000108436	*Gm44851*	2.65E-02	1.675059
ENSMUSG00000052496	*Pkdrej*	8.35E-03	1.675102
ENSMUSG00000032845	*Alpk2*	2.46E-22	1.67545
ENSMUSG00000006345	*Ggt1*	2.80E-06	1.675688
ENSMUSG00000030672	*Mylpf*	2.51E-04	1.677392
ENSMUSG00000075122	*Cd80*	1.39E-25	1.678083
ENSMUSG00000100301	*6030407O03Rik*	1.46E-17	1.678651
ENSMUSG00000091952	*Gm17709*	3.50E-11	1.679019
ENSMUSG00000022876	*Samsn1*	2.79E-24	1.680546
ENSMUSG00000113178	*Mylf-ps*	3.93E-08	1.680637
ENSMUSG00000095620	*2010005H15Rik*	3.96E-03	1.680691
ENSMUSG00000054258	*Gm5082*	3.59E-02	1.681204
ENSMUSG00000070498	*Tmem132b*	3.01E-11	1.68225
ENSMUSG00000056856	*Jakmip3*	3.89E-03	1.683214
ENSMUSG00000111324	*Gm31410*	6.04E-03	1.68436
ENSMUSG00000054204	*Alkal2*	1.32E-02	1.6846
ENSMUSG00000078902	*Gm14443*	6.61E-03	1.684691
ENSMUSG00000076135	*Gm24276*	3.81E-02	1.685494
ENSMUSG00000000204	*Slfn4*	1.36E-09	1.686
ENSMUSG00000005800	*Mmp8*	3.48E-29	1.686464
ENSMUSG00000001249	*Hpn*	7.62E-12	1.687075
ENSMUSG00000041827	*Oasl1*	9.65E-18	1.687086
ENSMUSG00000074452	*Pate2*	1.83E-10	1.688618
ENSMUSG00000045551	*Fpr1*	1.35E-39	1.689129
ENSMUSG00000053641	*Dennd4a*	2.32E-30	1.689402
ENSMUSG00000104818	*Gm43661*	1.29E-03	1.689966
ENSMUSG00000109232	*Gm44577*	4.63E-03	1.690024
ENSMUSG00000048489	*Depp1*	1.22E-08	1.690058
ENSMUSG00000093378	*Gm20663*	1.10E-02	1.691727
ENSMUSG00000049134	*Nrap*	6.44E-22	1.692374
ENSMUSG00000051832	*E230016K23Rik*	8.52E-07	1.694895
ENSMUSG00000052837	*Junb*	1.10E-23	1.695927
ENSMUSG00000069274	*Hist1h4f*	1.44E-02	1.701594
ENSMUSG00000086836	*Gm13748*	1.50E-03	1.701696

ENSMUSG00000028680	*Plk3*	1.48E-17	1.701976
ENSMUSG00000032174	*Icam5*	1.01E-02	1.705483
ENSMUSG00000087113	*Gm11714*	3.79E-04	1.706526
ENSMUSG00000111514	*E230014E18Rik*	7.88E-06	1.708494
ENSMUSG00000064382	*Gm26447*	1.31E-04	1.709249
ENSMUSG00000107667	*C530044C16Rik*	6.95E-03	1.709767
ENSMUSG00000057580	*Gm10012*	5.96E-03	1.711919
ENSMUSG00000062593	*Gm49339*	8.13E-09	1.712107
ENSMUSG00000047216	*Cdh19*	5.39E-12	1.712183
ENSMUSG00000092626	*9130230N09Rik*	3.71E-02	1.712613
ENSMUSG00000109032	*Gm7972*	5.34E-05	1.712639
ENSMUSG00000087159	*Gm15246*	5.79E-06	1.712843
ENSMUSG00000071637	*Cebpd*	2.78E-33	1.713579
ENSMUSG00000027737	*Slc7a11*	7.04E-24	1.713985
ENSMUSG00000109729	*Gm45418*	1.79E-06	1.714339
ENSMUSG00000026068	*Il18rap*	1.63E-22	1.714997
ENSMUSG00000097263	*Gm26804*	1.62E-02	1.715908
ENSMUSG00000109052	*Gm45012*	1.67E-02	1.716023
ENSMUSG00000029862	*Clcn1*	8.39E-06	1.716184
ENSMUSG00000022582	*Ly6g*	3.58E-05	1.718298
ENSMUSG00000042918	*Mamstr*	7.60E-18	1.719004
ENSMUSG00000027505	*Fam209*	8.93E-03	1.720522
ENSMUSG00000092201	*A530058N18Rik*	6.08E-09	1.721383
ENSMUSG00000102349	*Gm37376*	7.33E-03	1.722299
ENSMUSG00000102051	*I830127L07Rik*	2.66E-06	1.722921
ENSMUSG00000094306	*Gm24924*	3.54E-03	1.723532
ENSMUSG00000027470	*Mylk2*	8.88E-09	1.72462
ENSMUSG00000088008	*Gm25492*	2.74E-02	1.727829
ENSMUSG00000029384	*2010109A12Rik*	9.32E-06	1.729412
ENSMUSG00000104010	*Gm37366*	3.43E-04	1.729563
ENSMUSG00000031710	*Ucp1*	4.71E-04	1.730521
ENSMUSG00000064841	*Gm26205*	3.76E-02	1.732023
ENSMUSG00000087059	*Gm12339*	3.57E-10	1.73504
ENSMUSG00000059741	*Myl3*	2.57E-09	1.735257
ENSMUSG00000030399	*Ckm*	6.58E-09	1.737508
ENSMUSG00000072720	*Myo18b*	2.53E-31	1.738448
ENSMUSG00000100733	*4932411K12Rik*	8.48E-06	1.74245
ENSMUSG00000013483	*Card14*	1.29E-04	1.743775
ENSMUSG00000026407	*Cacna1s*	4.58E-10	1.743939
ENSMUSG00000085241	*Snhg3*	2.11E-06	1.74396
ENSMUSG00000097122	*Gm26624*	2.89E-10	1.744094
ENSMUSG00000032661	*Oas3*	1.63E-17	1.74446
ENSMUSG00000060639	*Hist1h4i*	6.34E-03	1.746403
ENSMUSG00000092539	*Gm20468*	3.84E-02	1.747708
ENSMUSG00000100147	*1700047M11Rik*	3.91E-08	1.748016
ENSMUSG00000070524	*Fcrlb*	1.24E-02	1.748075
ENSMUSG00000095616	*Gm26244*	3.02E-03	1.749841
ENSMUSG00000069306	*Hist1h4m*	1.13E-02	1.750899
ENSMUSG00000101191	*Gm28809*	3.20E-02	1.7511
ENSMUSG00000097358	*Gm26773*	2.59E-03	1.753117
ENSMUSG00000061816	*Myl1*	1.60E-12	1.754682
ENSMUSG00000054169	*Ceacam10*	9.98E-09	1.754693
ENSMUSG00000105826	*Gm42141*	2.16E-02	1.754897
ENSMUSG00000105790	*Gm24105*	3.07E-04	1.75526
ENSMUSG00000092674	*Gm24105*	2.58E-04	1.75676
ENSMUSG00000056071	*S100a9*	2.01E-14	1.760172
ENSMUSG00000069792	*Wfdc17*	2.66E-11	1.760299

ENSMUSG00000022651	*Retnlg*	1.87E-24	1.766124
ENSMUSG00000023473	*Celsr3*	3.06E-07	1.767531
ENSMUSG00000101344	*Gm29183*	4.83E-20	1.767788
ENSMUSG00000050931	*Sgms2*	5.11E-55	1.768559
ENSMUSG00000091119	*Ccdc152*	2.18E-04	1.768666
ENSMUSG00000097413	*A830052D11Rik*	2.01E-02	1.771034
ENSMUSG00000091383	*Hist1h2al*	9.26E-06	1.771647
ENSMUSG00000064853	*Gm23442*	3.06E-04	1.773453
ENSMUSG00000099092	*Mir7062*	1.37E-02	1.773986
ENSMUSG00000052767	*Gm12703*	5.22E-04	1.775187
ENSMUSG00000111752	*Gm38575*	1.61E-15	1.776614
ENSMUSG00000043789	*Vwce*	1.79E-04	1.778777
ENSMUSG00000109831	*Gm36431*	3.33E-02	1.779631
ENSMUSG00000039653	*Baat*	2.08E-02	1.779818
ENSMUSG00000050553	*Gk2*	1.02E-02	1.780074
ENSMUSG00000022824	*Muc13*	2.08E-05	1.781872
ENSMUSG00000027855	*Sycp1*	2.52E-02	1.785086
ENSMUSG00000102343	*Gm37381*	2.22E-03	1.785986
ENSMUSG00000058427	*Cxcl2*	6.05E-12	1.786152
ENSMUSG00000031097	*Tnni2*	6.59E-11	1.786684
ENSMUSG00000072875	*Gpr27*	2.99E-05	1.787666
ENSMUSG00000026100	*Mstn*	1.84E-02	1.787836
ENSMUSG00000090698	*Apold1*	1.30E-17	1.788991
ENSMUSG00000027824	*Vmn2r1*	1.85E-02	1.78902
ENSMUSG00000116508	*Gm49463*	2.15E-02	1.789422
ENSMUSG00000088529	*Gm26083*	3.34E-03	1.790452
ENSMUSG00000081857	*Gm13624*	1.87E-03	1.79269
ENSMUSG00000077323	*Rnu11*	2.17E-03	1.793382
ENSMUSG00000022602	*Arc*	6.32E-03	1.79405
ENSMUSG00000044367	*Slc16a13*	8.06E-21	1.795745
ENSMUSG00000109096	*Gm44888*	2.17E-03	1.796222
ENSMUSG00000085792	*Gm15414*	2.28E-02	1.796476
ENSMUSG00000115432	*D130009I18Rik*	1.25E-02	1.7966
ENSMUSG00000074001	*Klhl40*	2.39E-03	1.804207
ENSMUSG00000024827	*Gldc*	2.59E-02	1.808096
ENSMUSG00000110626	*Gm45805*	1.93E-03	1.809283
ENSMUSG00000102759	*Gm10463*	4.37E-02	1.811725
ENSMUSG00000108929	*Cc2d2b*	3.12E-04	1.814541
ENSMUSG00000048388	*Fam171b*	3.36E-17	1.816202
ENSMUSG00000089844	*A530032D15Rik*	3.03E-10	1.816284
ENSMUSG00000043795	*Prr33*	4.01E-02	1.817973
ENSMUSG00000027456	*Sdcbp2*	1.73E-11	1.818137
ENSMUSG00000095969	*Rnu1a1*	7.72E-04	1.823663
ENSMUSG00000041872	*Il17f*	1.92E-06	1.828096
ENSMUSG00000001482	*Def8*	2.17E-14	1.828763
ENSMUSG00000006724	*Cyp27b1*	7.32E-03	1.82998
ENSMUSG00000101279	*Gm18342*	1.51E-05	1.831412
ENSMUSG00000109157	*Gm44829*	8.56E-05	1.83179
ENSMUSG00000056300	*Zfp981*	3.27E-10	1.83268
ENSMUSG00000077714	*Snord17*	2.21E-04	1.835137
ENSMUSG00000034683	*Ppp1r1c*	1.37E-02	1.836685
ENSMUSG00000087700	*Gm15283*	3.63E-04	1.838693
ENSMUSG00000096214	*Gm22634*	4.41E-06	1.840548
ENSMUSG00000096206	*Gm22317*	4.41E-06	1.840548
ENSMUSG00000110411	*Gm45457*	3.21E-03	1.842368
ENSMUSG00000115420	*AL732506.1*	3.41E-05	1.84363
ENSMUSG00000088088	*Rmrp*	3.41E-05	1.84363

ENSMUSG00000070167	*Snora57*	6.49E-06	1.843722
ENSMUSG00000044083	*Efcab8*	8.89E-24	1.847127
ENSMUSG00000096205	*Gm22068*	4.44E-04	1.848083
ENSMUSG00000034755	*Pcdh11x*	1.69E-07	1.849981
ENSMUSG00000064655	*Gm25788*	3.42E-02	1.850018
ENSMUSG00000112082	*Gm35035*	2.70E-03	1.850562
ENSMUSG00000096659	*Gm25679*	6.20E-06	1.851418
ENSMUSG00000093815	*Gm26444*	6.20E-06	1.851418
ENSMUSG00000044092	*C130050O18Rik*	4.16E-07	1.85322
ENSMUSG00000060093	*Hist1h4a*	6.83E-05	1.854758
ENSMUSG00000112023	*Lilr4b*	3.87E-09	1.856512
ENSMUSG00000030730	*Atp2a1*	2.57E-25	1.856765
ENSMUSG00000113185	*Gm47127*	2.52E-14	1.857191
ENSMUSG00000087203	*Gm13986*	9.23E-38	1.857802
ENSMUSG00000017300	*Tnnc2*	2.32E-13	1.860495
ENSMUSG00000005716	*Pvalb*	5.17E-03	1.862103
ENSMUSG00000064179	*Tnnt1*	3.30E-04	1.865691
ENSMUSG00000103907	*Gm37498*	2.41E-19	1.868144
ENSMUSG00000094826	*Gm23804*	6.28E-06	1.870232
ENSMUSG00000107480	*Gm44165*	6.63E-05	1.871722
ENSMUSG00000050304	*Slc25a2*	1.14E-02	1.87573
ENSMUSG00000065862	*Gm24029*	6.61E-04	1.875777
ENSMUSG00000064453	*Snord21*	3.67E-02	1.876243
ENSMUSG00000096972	*Gm26883*	3.02E-04	1.878023
ENSMUSG00000002500	*Rpl3l*	4.07E-05	1.878812
ENSMUSG00000065145	*Vaultrc5*	9.73E-04	1.881338
ENSMUSG00000097052	*Snora43*	4.79E-02	1.882312
ENSMUSG00000025473	*Adam8*	3.65E-14	1.883209
ENSMUSG00000025929	*Il17a*	1.27E-02	1.884795
ENSMUSG00000069733	*Ube2u*	1.49E-03	1.885786
ENSMUSG00000060988	*Galnt13*	6.96E-12	1.886176
ENSMUSG00000064387	*Snora73a*	4.95E-09	1.88777
ENSMUSG00000110125	*Gm33148*	6.45E-03	1.888934
ENSMUSG00000082069	*Gm16242*	1.52E-03	1.890196
ENSMUSG00000042451	*Mybph*	7.08E-19	1.89042
ENSMUSG00000074071	*Fam169b*	1.22E-62	1.892733
ENSMUSG00000062393	*Dgkk*	3.95E-02	1.894875
ENSMUSG00000104554	*Gm4610*	1.51E-04	1.897808
ENSMUSG00000032021	*Crtam*	1.06E-17	1.89973
ENSMUSG00000092805	*Gm26461*	7.94E-04	1.903632
ENSMUSG00000060470	*Adgrg3*	5.50E-20	1.903686
ENSMUSG00000097081	*Gm10425*	2.22E-02	1.906599
ENSMUSG00000032066	*Bco2*	1.74E-03	1.906705
ENSMUSG00000092267	*Gm20417*	5.68E-07	1.908725
ENSMUSG00000025892	*Gria4*	4.06E-04	1.909271
ENSMUSG00000042567	*Nek10*	1.49E-18	1.909826
ENSMUSG00000115426	*Gm19510*	3.61E-02	1.911947
ENSMUSG00000116641	*AC165271.1*	4.77E-02	1.912683
ENSMUSG00000108332	*D530033B14Rik*	3.38E-17	1.912716
ENSMUSG00000038067	*Csf3*	5.24E-28	1.912958
ENSMUSG00000043681	*Fam25c*	9.06E-03	1.913562
ENSMUSG00000064999	*Gm26035*	1.27E-04	1.915529
ENSMUSG00000084929	*Foxo6os*	2.44E-02	1.916095
ENSMUSG00000113321	*Gm8075*	1.08E-04	1.9166
ENSMUSG00000080542	*Gm22710*	9.10E-03	1.916605
ENSMUSG00000097622	*A330033J07Rik*	1.30E-02	1.916889
ENSMUSG00000111971	*Gm48678*	1.01E-02	1.918064

ENSMUSG00000065353	*Snora73b*	4.31E-05	1.92082
ENSMUSG00000079451	*Tmprss11g*	1.05E-02	1.922677
ENSMUSG00000057280	*Musk*	4.21E-13	1.924024
ENSMUSG00000026166	*Ccl20*	6.82E-22	1.924662
ENSMUSG00000043873	*Chil5*	3.16E-05	1.926813
ENSMUSG00000099470	*Gm29340*	6.43E-03	1.928433
ENSMUSG00000038508	*Gdf15*	4.48E-03	1.930522
ENSMUSG00000085434	*Gm11725*	1.19E-03	1.931465
ENSMUSG00000049173	*Myoz3*	4.24E-05	1.93273
ENSMUSG00000097417	*Gm26669*	3.24E-02	1.932952
ENSMUSG00000052581	*Lrrtm4*	1.64E-07	1.934282
ENSMUSG00000116975	*AC097366.1*	2.80E-03	1.934645
ENSMUSG00000107722	*2900060B14Rik*	4.30E-03	1.93608
ENSMUSG00000044165	*Bcl2l15*	2.49E-09	1.936183
ENSMUSG00000104728	*Gm42462*	3.00E-14	1.936263
ENSMUSG00000022622	*Acr*	4.06E-11	1.941514
ENSMUSG00000065226	*Gm25791*	1.83E-06	1.942482
ENSMUSG00000109002	*Gm38405*	2.93E-04	1.943877
ENSMUSG00000055523	*Gucy2g*	2.09E-02	1.944978
ENSMUSG00000024912	*Fosl1*	4.08E-15	1.946069
ENSMUSG00000049100	*Pcdh10*	1.63E-02	1.947579
ENSMUSG00000100334	*C230024C17Rik*	1.73E-02	1.947699
ENSMUSG00000102416	*4933424G06Rik*	2.21E-02	1.951006
ENSMUSG00000042895	*Abra*	1.14E-09	1.951135
ENSMUSG00000102630	*Gm37289*	5.47E-03	1.953604
ENSMUSG00000037705	*Tecta*	1.30E-02	1.953664
ENSMUSG00000085750	*Gm14009*	2.26E-02	1.959056
ENSMUSG00000106392	*Gm5870*	2.74E-02	1.959897
ENSMUSG00000116961	*AC117662.4*	7.69E-07	1.970064
ENSMUSG00000029379	*Cxcl3*	5.85E-31	1.970535
ENSMUSG00000056054	*S100a8*	2.08E-14	1.971878
ENSMUSG00000009070	*Rsph14*	1.08E-09	1.971919
ENSMUSG00000106649	*Gm49349*	1.69E-06	1.97517
ENSMUSG00000115355	*4930445E18Rik*	3.15E-07	1.98206
ENSMUSG00000084783	*Gm15419*	3.73E-04	1.984549
ENSMUSG00000048806	*Ifnb1*	4.47E-02	1.985866
ENSMUSG00000112683	*Gm18904*	5.10E-03	1.988548
ENSMUSG00000103626	*Gm37358*	4.92E-04	1.992354
ENSMUSG00000087090	*Nctc1*	3.78E-18	1.993635
ENSMUSG00000110498	*A630001O12Rik*	2.63E-06	1.993703
ENSMUSG00000097643	*A130051J06Rik*	1.72E-03	1.997776
ENSMUSG00000024430	*Cabyr*	3.39E-04	1.999224
ENSMUSG00000065701	*Rny1*	7.04E-04	2.000426
ENSMUSG00000104956	*4930429D17Rik*	4.22E-03	2.000856
ENSMUSG00000046049	*Rp1l1*	5.00E-04	2.002651
ENSMUSG00000089647	*Gm2245*	4.25E-03	2.00392
ENSMUSG00000034145	*Tmem63c*	1.54E-03	2.004762
ENSMUSG00000097300	*Gm26835*	2.99E-02	2.005741
ENSMUSG00000058740	*Kcnt1*	1.78E-11	2.006095
ENSMUSG00000032496	*Ltf*	1.13E-45	2.006145
ENSMUSG00000065126	*Snord104*	6.05E-07	2.006554
ENSMUSG00000097071	*4930544I03Rik*	1.01E-07	2.006732
ENSMUSG00000077167	*Gm24119*	1.08E-02	2.009462
ENSMUSG00000110622	*Iqcn*	1.16E-02	2.011367
ENSMUSG00000071470	*Ccnb1ip1*	2.89E-04	2.016759
ENSMUSG00000037977	*6430571L13Rik*	2.38E-05	2.018356
ENSMUSG00000053469	*Tg*	9.23E-38	2.022512

ENSMUSG00000080950	*Gm7278*	9.59E-05	2.024914
ENSMUSG00000092837	*Rpph1*	2.95E-04	2.025336
ENSMUSG00000040340	*Tex45*	2.80E-03	2.026678
ENSMUSG00000086754	*Gm16098*	3.57E-02	2.033401
ENSMUSG00000088025	*Rprl3*	1.21E-03	2.034205
ENSMUSG00000116031	*D030024E09Rik*	3.10E-10	2.034724
ENSMUSG00000079243	*Xirp1*	1.63E-25	2.041369
ENSMUSG00000054905	*Stfa3*	2.46E-04	2.044116
ENSMUSG00000032292	*Nr2e3*	1.06E-02	2.046336
ENSMUSG00000089854	*Gm16133*	2.44E-06	2.047282
ENSMUSG00000116606	*AC163633.2*	3.18E-02	2.047702
ENSMUSG00000103382	*Gm37755*	2.66E-02	2.049867
ENSMUSG00000077563	*Snora68*	1.19E-05	2.052854
ENSMUSG00000106224	*Gm43823*	1.06E-02	2.054673
ENSMUSG00000103308	*Gm37800*	1.61E-09	2.055329
ENSMUSG00000115151	*Gm19276*	5.37E-03	2.055894
ENSMUSG00000086649	*Gm15286*	3.26E-02	2.064189
ENSMUSG00000020216	*Jsrp1*	1.65E-02	2.064977
ENSMUSG00000097036	*1110036E04Rik*	2.16E-02	2.065813
ENSMUSG00000089536	*Scarna3a*	2.33E-02	2.0728
ENSMUSG00000113447	*Gm48538*	3.67E-05	2.078097
ENSMUSG00000087477	*Gm13822*	1.26E-03	2.082278
ENSMUSG00000041476	*Smpx*	3.41E-09	2.083676
ENSMUSG00000065824	*Gm26315*	1.20E-05	2.084426
ENSMUSG00000103485	*Gm38001*	4.48E-03	2.088313
ENSMUSG00000109311	*AI314278*	8.28E-04	2.092515
ENSMUSG00000065911	*Gm24447*	1.06E-05	2.092602
ENSMUSG00000108985	*A930030B08Rik*	1.21E-03	2.092679
ENSMUSG00000094088	*Ighv1-64*	4.84E-02	2.093497
ENSMUSG00000093577	*Gm20632*	5.25E-03	2.099577
ENSMUSG00000097468	*Mdrl*	4.60E-03	2.100337
ENSMUSG00000103923	*Gm37896*	9.28E-03	2.102126
ENSMUSG00000112471	*Gm5779*	5.98E-03	2.104841
ENSMUSG00000093908	*Gm5784*	1.59E-06	2.105369
ENSMUSG00000047501	*Cldn4*	3.24E-06	2.10583
ENSMUSG00000108677	*Gm44759*	1.85E-02	2.11069
ENSMUSG00000087775	*Rprl2*	7.23E-04	2.112469
ENSMUSG00000033213	*AA467197*	7.56E-07	2.116442
ENSMUSG00000117092	*AC166110.1*	4.57E-03	2.122036
ENSMUSG00000110278	*Gm5608*	4.80E-19	2.124723
ENSMUSG00000033196	*Myh2*	2.12E-09	2.129399
ENSMUSG00000021123	*Rdh12*	1.23E-27	2.13007
ENSMUSG00000111818	*Gm17749*	1.56E-11	2.130559
ENSMUSG00000022026	*Olfm4*	1.74E-47	2.133503
ENSMUSG00000097131	*D230017M19Rik*	8.10E-07	2.14415
ENSMUSG00000113998	*Gm40909*	1.98E-16	2.150507
ENSMUSG00000090101	*Snhg9*	6.89E-03	2.150509
ENSMUSG00000074398	*Gm15441*	1.46E-03	2.151127
ENSMUSG00000035653	*Lrfn5*	2.00E-04	2.153773
ENSMUSG00000086220	*Gm16599*	1.86E-03	2.158383
ENSMUSG00000116237	*Gm30339*	3.53E-03	2.162938
ENSMUSG00000028865	*Cd164l2*	1.12E-04	2.164257
ENSMUSG00000114457	*Gm36346*	3.31E-02	2.164377
ENSMUSG00000064604	*Snora44*	5.26E-04	2.16931
ENSMUSG00000084708	*Gm22988*	4.87E-07	2.171425
ENSMUSG00000089542	*Gm25835*	1.60E-09	2.171658
ENSMUSG00000024907	*Gal*	4.18E-02	2.171949

ENSMUSG00000103620	*Gm37359*	3.97E-07	2.173343
ENSMUSG00000093355	*Snora26*	4.17E-02	2.191494
ENSMUSG00000043468	*Adam30*	1.06E-02	2.195772
ENSMUSG00000101845	*Gm28198*	4.01E-02	2.207421
ENSMUSG00000064380	*Gm26448*	9.55E-10	2.208699
ENSMUSG00000025431	*Crisp1*	6.59E-04	2.208969
ENSMUSG00000111867	*Gm31013*	2.68E-02	2.214693
ENSMUSG00000087819	*Gm25117*	1.67E-07	2.214707
ENSMUSG00000091366	*Gm17040*	4.44E-02	2.216824
ENSMUSG00000064694	*Gm24146*	4.82E-04	2.217621
ENSMUSG00000009551	*6330409D20Rik*	4.87E-02	2.221007
ENSMUSG00000096351	*Samd11*	6.92E-09	2.221597
ENSMUSG00000080365	*Gm25776*	1.17E-04	2.222028
ENSMUSG00000065259	*Snora30*	5.73E-03	2.223572
ENSMUSG00000107841	*Gm44185*	1.38E-02	2.224563
ENSMUSG00000046961	*Gpr156*	4.17E-11	2.227765
ENSMUSG00000026592	*Tex35*	1.15E-09	2.233732
ENSMUSG00000103502	*9330121J05Rik*	3.03E-02	2.239685
ENSMUSG00000086354	*Gm13938*	8.15E-26	2.24405
ENSMUSG00000114697	*Gm30806*	2.67E-02	2.246899
ENSMUSG00000004668	*Abca13*	2.61E-57	2.24728
ENSMUSG00000085573	*Gm15418*	3.19E-04	2.250028
ENSMUSG00000092819	*Gm23639*	1.25E-02	2.258412
ENSMUSG00000104863	*Gm49347*	6.55E-05	2.266581
ENSMUSG00000096887	*Gm20594*	2.13E-12	2.268158
ENSMUSG00000113868	*Gm34719*	1.46E-03	2.270756
ENSMUSG00000096243	*Gm24265*	3.92E-05	2.270994
ENSMUSG00000085599	*Gm13449*	3.60E-04	2.273353
ENSMUSG00000020848	*Doc2b*	4.53E-24	2.275294
ENSMUSG00000088948	*Gm23262*	4.47E-07	2.276029
ENSMUSG00000092702	*Gm24514*	2.89E-06	2.276899
ENSMUSG00000109921	*Gm33326*	2.14E-03	2.281901
ENSMUSG00000111765	*Gm10635*	3.03E-03	2.28596
ENSMUSG00000053615	*Gm9913*	3.32E-02	2.288715
ENSMUSG00000050830	*Vwc2*	1.21E-05	2.28941
ENSMUSG00000045027	*Prss22*	4.65E-14	2.295806
ENSMUSG00000059108	*Ifitm6*	3.62E-40	2.296863
ENSMUSG00000111639	*1700019L13Rik*	1.07E-02	2.297301
ENSMUSG00000006764	*Tph2*	1.53E-02	2.300399
ENSMUSG00000099760	*Gm28800*	5.16E-04	2.300754
ENSMUSG00000108171	*Gm43915*	1.82E-02	2.304507
ENSMUSG00000051965	*Nanos2*	3.15E-02	2.309161
ENSMUSG00000065649	*Snora74a*	1.83E-06	2.319528
ENSMUSG00000111821	*Gm48545*	1.45E-05	2.341304
ENSMUSG00000074652	*Myh7b*	2.41E-03	2.354961
ENSMUSG00000023153	*Tmem52*	3.20E-03	2.37334
ENSMUSG00000113778	*Gm40847*	2.82E-06	2.385725
ENSMUSG00000102189	*Gm37194*	2.59E-09	2.389093
ENSMUSG00000091238	*Gm17103*	1.31E-04	2.395524
ENSMUSG00000110237	*Gm18258*	2.84E-02	2.417341
ENSMUSG00000088252	*Snord13*	5.28E-05	2.418714
ENSMUSG00000098975	*Gm27177*	1.24E-02	2.419022
ENSMUSG00000097346	*Gm26619*	8.29E-03	2.422694
ENSMUSG00000054582	*Pabpc1l*	8.18E-19	2.43202
ENSMUSG00000094377	*Gm24407*	5.41E-07	2.44395
ENSMUSG00000090625	*Gm20721*	5.29E-04	2.452874
ENSMUSG00000010342	*Tex14*	2.41E-09	2.454352

ENSMUSG00000033860	*Fgg*	1.06E-03	2.454493
ENSMUSG00000043460	*Elfn2*	1.29E-02	2.455388
ENSMUSG00000110114	*Gm45471*	1.99E-02	2.456678
ENSMUSG00000064945	*Rny3*	2.32E-06	2.465394
ENSMUSG00000085297	*Gm11651*	3.64E-05	2.473195
ENSMUSG00000089655	*Gm16004*	2.40E-03	2.475649
ENSMUSG00000108720	*Gm44672*	7.98E-03	2.479163
ENSMUSG00000000157	*Itgb2l*	5.28E-41	2.481365
ENSMUSG00000086980	*Gm13791*	1.78E-03	2.484391
ENSMUSG00000024729	*1700017D01Rik*	1.57E-02	2.495512
ENSMUSG00000069310	*Hist1h3c*	5.35E-04	2.501758
ENSMUSG00000065087	*Snord22*	1.02E-20	2.504791
ENSMUSG00000077254	*Gm26079*	5.09E-05	2.508432
ENSMUSG00000023467	*Tulp2*	3.92E-03	2.545698
ENSMUSG00000084744	*Gm25291*	1.27E-04	2.547348
ENSMUSG00000080538	*Gm25541*	1.65E-07	2.547886
ENSMUSG00000086628	*Gm16157*	1.31E-03	2.549909
ENSMUSG00000116657	*AC127341.3*	6.32E-03	2.552284
ENSMUSG00000085532	*B430319H21Rik*	2.25E-10	2.571664
ENSMUSG00000095590	*Gm24305*	5.01E-03	2.571674
ENSMUSG00000040258	*Nxph4*	5.24E-03	2.575445
ENSMUSG00000097069	*Gm16998*	1.82E-02	2.578575
ENSMUSG00000010362	*Rdm1*	1.63E-08	2.583826
ENSMUSG00000107179	*Gm43069*	7.95E-03	2.585741
ENSMUSG00000064966	*Snord15b*	2.43E-08	2.605397
ENSMUSG00000066510	*Ankdd1a*	1.64E-20	2.613295
ENSMUSG00000031343	*Gabra3*	2.60E-11	2.613416
ENSMUSG00000096084	*Gm21850*	1.82E-14	2.614388
ENSMUSG00000090208	*Gm15851*	1.89E-02	2.614614
ENSMUSG00000074113	*Gm10629*	1.77E-02	2.621575
ENSMUSG00000064901	*Snora21*	1.20E-03	2.626929
ENSMUSG00000090293	*Gm17034*	1.90E-04	2.681395
ENSMUSG00000037942	*Crp*	7.71E-04	2.683734
ENSMUSG00000111582	*Gm47347*	3.20E-03	2.685612
ENSMUSG00000085511	*Gm11738*	1.89E-04	2.70767
ENSMUSG00000064371	*mt-Tt*	2.94E-03	2.714465
ENSMUSG00000114649	*3110006O06Rik*	8.08E-03	2.716208
ENSMUSG00000065822	*Snord15a*	1.62E-05	2.722509
ENSMUSG00000085806	*Gm12023*	8.06E-11	2.725972
ENSMUSG00000021071	*Trim9*	6.06E-15	2.732965
ENSMUSG00000025172	*Ankrd2*	4.58E-16	2.747592
ENSMUSG00000064899	*Snord118*	3.85E-04	2.765016
ENSMUSG00000110790	*Gm47079*	8.78E-03	2.791718
ENSMUSG00000016327	*Atp1b4*	7.76E-04	2.794331
ENSMUSG00000096960	*A230028O05Rik*	2.22E-22	2.835285
ENSMUSG00000089255	*Snora78*	7.85E-04	2.851741
ENSMUSG00000032484	*Ngp*	3.65E-107	2.860267
ENSMUSG00000064943	*Gm23240*	8.10E-03	2.878259
ENSMUSG00000114922	*Ppifos*	1.68E-05	2.879757
ENSMUSG00000022249	*Ttc23l*	3.38E-03	2.910968
ENSMUSG00000030359	*Pzp*	1.62E-03	2.922478
ENSMUSG00000065118	*Gm23297*	4.76E-05	2.968259
ENSMUSG00000111734	*Gm29825*	3.88E-03	2.997991
ENSMUSG00000115532	*Gm41206*	2.62E-03	3.003723
ENSMUSG00000106056	*4930500L23Rik*	2.55E-03	3.004773
ENSMUSG00000093843	*Gm25939*	6.49E-07	3.015148
ENSMUSG00000065176	*Rnu12*	9.49E-18	3.015627

ENSMUSG00000094050	*Gm23472*	2.00E-08	3.0215
ENSMUSG00000064856	*Gm23444*	2.61E-08	3.025159
ENSMUSG00000093956	*Gm24497*	3.05E-08	3.03474
ENSMUSG00000059908	*Mug1*	4.53E-02	3.062787
ENSMUSG00000064994	*Gm22422*	7.84E-06	3.063734
ENSMUSG00000109464	*Gm34350*	1.03E-02	3.073399
ENSMUSG00000042761	*Mrap2*	4.40E-06	3.081864
ENSMUSG00000089948	*Far2os1*	4.72E-04	3.104791
ENSMUSG00000065944	*Rnu2-10*	7.80E-09	3.107609
ENSMUSG00000064702	*Gm24950*	9.28E-09	3.114592
ENSMUSG00000065251	*Gm23971*	9.28E-09	3.114592
ENSMUSG00000065767	*Gm23849*	7.91E-09	3.116902
ENSMUSG00000087038	*2900079G21Rik*	4.45E-03	3.117026
ENSMUSG00000091993	*B930036N10Rik*	9.73E-07	3.120615
ENSMUSG00000022868	*Ahsg*	3.12E-04	3.161068
ENSMUSG00000095892	*Rnu5g*	3.38E-09	3.162782
ENSMUSG00000065820	*Gm26316*	3.08E-09	3.189586
ENSMUSG00000046748	*Tmem45a2*	1.25E-18	3.232248
ENSMUSG00000097554	*Gm26825*	1.50E-03	3.233552
ENSMUSG00000095738	*Gm25313*	4.08E-09	3.26894
ENSMUSG00000110735	*Gm47173*	6.45E-03	3.273965
ENSMUSG00000099291	*Rnu3b3*	2.67E-15	3.306299
ENSMUSG00000104856	*Rnu3b3*	2.67E-15	3.306299
ENSMUSG00000105115	*Rnu3b2*	5.42E-16	3.31235
ENSMUSG00000098925	*Rnu3b2*	5.42E-16	3.31235
ENSMUSG00000104896	*Rnu3b4*	7.98E-16	3.316405
ENSMUSG00000098641	*Rnu3b4*	8.89E-16	3.316683
ENSMUSG00000027233	*Patl2*	9.28E-06	3.317931
ENSMUSG00000098943	*Rnu3b1*	9.63E-16	3.32264
ENSMUSG00000105025	*Rnu3b1*	9.63E-16	3.32264
ENSMUSG00000085348	*Myhas*	2.21E-09	3.342376
ENSMUSG00000065254	*Gm23973*	3.63E-04	3.375179
ENSMUSG00000088675	*Rprl1*	9.25E-05	3.390244
ENSMUSG00000106222	*Rprl1*	9.25E-05	3.390244
ENSMUSG00000086777	*Far2os2*	8.53E-09	3.410703
ENSMUSG00000013936	*Myl2*	1.38E-11	3.412107
ENSMUSG00000065870	*Rnu3a*	8.20E-11	3.438606
ENSMUSG00000106147	*Rnu3a*	8.20E-11	3.438606
ENSMUSG00000094655	*Gm25360*	9.25E-18	3.476566
ENSMUSG00000099449	*Gm28401*	3.66E-06	3.512495
ENSMUSG00000080465	*Gm22486*	3.79E-11	3.525781
ENSMUSG00000097770	*Gm26776*	7.15E-05	3.556066
ENSMUSG00000095676	*Gm25099*	1.48E-18	3.569557
ENSMUSG00000038357	*Camp*	2.10E-20	3.574791
ENSMUSG00000110588	*Gm45774*	2.37E-05	3.651499
ENSMUSG00000105361	*AY036118*	4.75E-13	3.706614
ENSMUSG00000114163	*Gm32296*	1.06E-05	3.753819
ENSMUSG00000097815	*Gm26809*	4.14E-06	3.770845
ENSMUSG00000101133	*Gm29050*	4.66E-06	3.935451
ENSMUSG00000094668	*Gm24871*	3.50E-05	3.990369
ENSMUSG00000065232	*Gm22973*	1.47E-13	4.080121
ENSMUSG00000096269	*Rpl31-ps21*	1.07E-04	4.321736
ENSMUSG00000029019	*Nppb*	3.13E-19	4.33994
ENSMUSG00000097364	*Gm26719*	2.54E-09	4.440093
ENSMUSG00000056656	*Apol8*	1.21E-16	4.471575
ENSMUSG00000064682	*Gm25813*	4.91E-11	4.908819
ENSMUSG00000115207	*Gm49132*	2.67E-04	5.036502

ENSMUSG00000028307	*Aldob*	2.14E-03	5.215422
ENSMUSG00000027261	*Hao1*	2.14E-10	5.270442
ENSMUSG00000056035	*Cyp3a11*	1.02E-03	8.674899
ENSMUSG00000025991	*Cps1*	9.04E-03	9.941545
ENSMUSG00000032083	*Apoa1*	5.02E-04	10.21736
ENSMUSG00000029368	*Alb*	1.23E-11	11.41724
ENSMUSG00000033831	*Fgb*	1.09E-04	16.81357

Appendix X. Murine differential gene expression in the lungs 6 h post-infection, 4559 vs 4559M. Genes with fold change (FC) greater than 1.5 and $p < 0.05$ are shown. FC values highlighted in blue = upregulated in 4559, while values highlighted in red = upregulated in 4559M.

Gene Stable ID	Gene Name	padj	FC
ENSMUSG00000029630	*Cyp3a25*	1.75E-05	49.7977
ENSMUSG00000059908	*Mug1*	3.28E-16	16.2463
ENSMUSG00000061808	*Ttr*	2.84E-06	14.48
ENSMUSG00000032083	*Apoa1*	1.40E-09	8.40944
ENSMUSG00000029368	*Alb*	7.42E-10	7.88269
ENSMUSG00000056035	*Cyp3a11*	2.46E-09	7.04516
ENSMUSG00000003053	*Cyp2c29*	1.29E-06	6.94961
ENSMUSG00000025991	*Cps1*	1.02E-02	6.84018
ENSMUSG00000059481	*Plg*	5.17E-05	6.64669
ENSMUSG00000035540	*Gc*	4.99E-09	6.39712
ENSMUSG00000019932	*Kera*	1.93E-07	5.71283
ENSMUSG00000058354	*Krt6a*	2.39E-09	5.47428
ENSMUSG00000020609	*Apob*	7.58E-09	5.28553
ENSMUSG00000048455	*Sprr1b*	8.94E-08	5.28178
ENSMUSG00000030131	*Mug2*	7.90E-05	4.9728
ENSMUSG00000030359	*Pzp*	5.04E-10	4.9175
ENSMUSG00000074647	*Fam83c*	3.54E-05	4.88673
ENSMUSG00000033831	*Fgb*	8.00E-03	4.77839
ENSMUSG00000023041	*Krt6b*	6.28E-04	4.23661
ENSMUSG00000046095	*Krt32*	6.56E-05	4.06888
ENSMUSG00000022875	*Kng1*	1.83E-04	4.04028
ENSMUSG00000022868	*Ahsg*	6.92E-08	4.01269
ENSMUSG00000028307	*Aldob*	4.31E-05	3.99588
ENSMUSG00000068888	*Lce1i*	1.87E-03	3.93124
ENSMUSG00000035861	*Tmprss11b*	9.18E-04	3.92883
ENSMUSG00000025194	*Abcc2*	8.61E-04	3.90941
ENSMUSG00000027761	*Aadac*	1.07E-03	3.88939
ENSMUSG00000092586	*Ly6g6c*	2.26E-12	3.86378
ENSMUSG00000074445	*Sprr2a3*	1.99E-05	3.71115
ENSMUSG00000059898	*Dsc3*	2.90E-17	3.70907
ENSMUSG00000054422	*Fabp1*	3.27E-04	3.66856
ENSMUSG00000053675	*Tgm5*	1.06E-02	3.59152
ENSMUSG00000032373	*Car12*	2.24E-43	3.56925
ENSMUSG00000021364	*Elovl2*	3.03E-03	3.52501
ENSMUSG00000026450	*Chit1*	1.24E-06	3.51671
ENSMUSG00000033268	*Duox1*	7.07E-12	3.43887
ENSMUSG00000056632	*Dsg3*	8.74E-24	3.40573
ENSMUSG00000067006	*Serpinb5*	8.21E-12	3.40296
ENSMUSG00000017950	*Hnf4a*	3.10E-03	3.39187
ENSMUSG00000040127	*Sdr9c7*	3.52E-03	3.33689
ENSMUSG00000045545	*Krt14*	1.09E-22	3.26379
ENSMUSG00000061527	*Krt5*	1.31E-17	3.25295
ENSMUSG00000097850	*4631405K08Rik*	3.80E-04	3.17772
ENSMUSG00000026985	*Il1f8*	1.88E-04	3.17313
ENSMUSG00000078664	*Sprr2a1*	4.06E-05	3.14672
ENSMUSG00000054146	*Krt15*	8.77E-17	3.1094
ENSMUSG00000028236	*Sdr16c5*	5.99E-04	3.09328
ENSMUSG00000026413	*Pkp1*	2.42E-19	3.08859
ENSMUSG00000102098	*2310016D03Rik*	2.45E-03	3.03012
ENSMUSG00000059832	*Kprp*	2.49E-18	3.02836
ENSMUSG00000068893	*Sprr2a2*	5.63E-11	3.01925
ENSMUSG00000031757	*Mt4*	2.82E-09	3.00348

ENSMUSG00000038295	*Atg9b*	3.71E-08	3.00088
ENSMUSG00000097768	*2310043M15Rik*	6.14E-05	2.99467
ENSMUSG00000048399	*Tprg*	8.10E-08	2.97043
ENSMUSG00000071858	*Gm94*	8.27E-08	2.95766
ENSMUSG00000042031	*Lce3b*	8.70E-10	2.94911
ENSMUSG00000085261	*Gm13814*	1.65E-02	2.93578
ENSMUSG00000075217	*4833423E24Rik*	3.24E-08	2.93359
ENSMUSG00000041984	*Rptn*	2.63E-20	2.90552
ENSMUSG00000033765	*Calm4*	4.66E-07	2.90141
ENSMUSG00000005355	*Casp14*	1.53E-03	2.89567
ENSMUSG00000026327	*Serpinb11*	7.21E-07	2.86034
ENSMUSG00000044748	*Defb1*	4.03E-04	2.84373
ENSMUSG00000079025	*Gsdmc*	6.93E-06	2.8424
ENSMUSG00000053522	*Lgals7*	1.41E-07	2.82395
ENSMUSG00000043472	*Lce3d*	5.15E-03	2.80644
ENSMUSG00000045539	*Sprr3*	1.03E-15	2.79819
ENSMUSG00000018862	*Otop3*	4.58E-06	2.79571
ENSMUSG00000114091	*Gm40655*	1.03E-06	2.79416
ENSMUSG00000071019	*Sdr16c6*	2.08E-04	2.79341
ENSMUSG00000099906	*Gm28653*	9.77E-04	2.78803
ENSMUSG00000004872	*Pax3*	6.22E-03	2.78741
ENSMUSG00000045019	*Acer1*	5.37E-03	2.78363
ENSMUSG00000057609	*Lce1a1*	1.99E-04	2.77319
ENSMUSG00000056078	*Lipm*	6.48E-07	2.76931
ENSMUSG00000033860	*Fgg*	1.23E-05	2.7686
ENSMUSG00000047428	*Dlk2*	1.85E-02	2.76136
ENSMUSG00000025064	*Col17a1*	6.87E-17	2.75765
ENSMUSG00000034774	*Dsg1c*	3.15E-03	2.75484
ENSMUSG00000017607	*Tns4*	1.32E-09	2.74798
ENSMUSG00000030484	*Lypd5*	7.90E-11	2.74454
ENSMUSG00000074156	*Ces1h*	1.86E-07	2.73844
ENSMUSG00000026983	*Il1f5*	2.08E-04	2.73336
ENSMUSG00000059668	*Krt4*	1.06E-11	2.72465
ENSMUSG00000050359	*Sprr1a*	2.66E-11	2.71649
ENSMUSG00000105160	*A530030E21Rik*	3.10E-02	2.71344
ENSMUSG00000050808	*Muc15*	3.46E-03	2.71087
ENSMUSG00000050463	*Krt78*	1.01E-21	2.70916
ENSMUSG00000029154	*Cwh43*	3.03E-03	2.6846
ENSMUSG00000044041	*Krt13*	1.85E-11	2.68386
ENSMUSG00000103243	*Lce1d*	2.22E-04	2.66703
ENSMUSG00000078964	*Ces1b*	5.60E-04	2.66571
ENSMUSG00000070719	*Pla2g4d*	4.58E-03	2.66266
ENSMUSG00000027224	*Duoxa1*	1.53E-02	2.65474
ENSMUSG00000062826	*Ces2f*	5.60E-13	2.64193
ENSMUSG00000074199	*Krtdap*	6.33E-07	2.64017
ENSMUSG00000050108	*Bpifc*	2.11E-03	2.63956
ENSMUSG00000055561	*Spink5*	2.42E-19	2.63531
ENSMUSG00000063651	*Cnfn*	1.48E-13	2.63424
ENSMUSG00000042124	*Lce1f*	4.49E-03	2.6302
ENSMUSG00000044594	*Serpinb3a*	3.67E-09	2.62271
ENSMUSG00000028001	*Fga*	6.07E-04	2.61124
ENSMUSG00000074489	*Bglap3*	1.19E-04	2.60397
ENSMUSG00000017204	*Gsdma*	1.43E-07	2.603
ENSMUSG00000033196	*Myh2*	4.95E-14	2.58757
ENSMUSG00000030834	*Abcc6*	1.07E-03	2.57913
ENSMUSG00000081163	*Defa-ps12*	6.10E-03	2.57856
ENSMUSG00000034634	*Ly6d*	1.25E-08	2.56812

ENSMUSG00000061928	*Dsg1b*	3.62E-11	2.56262
ENSMUSG00000106871	*Gm3289*	3.48E-02	2.55403
ENSMUSG00000022491	*Glycam1*	5.93E-08	2.552
ENSMUSG00000057454	*Lypd3*	9.96E-06	2.54396
ENSMUSG00000084228	*Gm8080*	3.66E-02	2.53954
ENSMUSG00000061259	*Tmprss11d*	1.47E-04	2.53596
ENSMUSG00000027376	*Prom2*	7.87E-09	2.53276
ENSMUSG00000022860	*Chodl*	3.30E-03	2.53009
ENSMUSG00000036960	*Clca2*	3.16E-04	2.52337
ENSMUSG00000045475	*Lce3c*	9.57E-08	2.52299
ENSMUSG00000063130	*Calml3*	1.43E-10	2.51428
ENSMUSG00000040154	*Wfdc5*	1.42E-04	2.51022
ENSMUSG00000117222	*AC060761.1*	1.75E-10	2.50439
ENSMUSG00000059956	*Serpinb12*	1.32E-07	2.48356
ENSMUSG00000021506	*Pitx1*	2.41E-04	2.46822
ENSMUSG00000043029	*Trpv3*	6.01E-03	2.45237
ENSMUSG00000034362	*Csta1*	4.02E-03	2.44214
ENSMUSG00000099146	*0610031O16Rik*	1.31E-02	2.42834
ENSMUSG00000044499	*Hs3st5*	4.61E-14	2.42328
ENSMUSG00000116659	*AC158985.1*	1.31E-02	2.41132
ENSMUSG00000027401	*Tgm3*	1.67E-09	2.41084
ENSMUSG00000037188	*Grhl3*	1.79E-08	2.41062
ENSMUSG00000093385	*A330044P14Rik*	4.33E-02	2.40792
ENSMUSG00000030713	*Klk7*	9.32E-03	2.40587
ENSMUSG00000043430	*Psapl1*	1.18E-08	2.40429
ENSMUSG00000044628	*Rnf208*	3.62E-02	2.40152
ENSMUSG00000039238	*Zfp750*	2.57E-05	2.39905
ENSMUSG00000037129	*Tmprss13*	4.41E-07	2.39884
ENSMUSG00000032013	*Trim29*	1.24E-12	2.39013
ENSMUSG00000109656	*Gm45548*	3.25E-02	2.38688
ENSMUSG00000051431	*Gpr87*	1.20E-02	2.38474
ENSMUSG00000044322	*Dsc1*	7.89E-05	2.38231
ENSMUSG00000069441	*Dsg1a*	1.65E-12	2.37371
ENSMUSG00000032807	*Alox12b*	8.10E-07	2.37178
ENSMUSG00000039269	*2300002M23Rik*	6.30E-04	2.36131
ENSMUSG00000055301	*Adh7*	2.74E-13	2.352
ENSMUSG00000022510	*Trp63*	3.19E-20	2.34287
ENSMUSG00000092222	*Gm20506*	3.27E-02	2.34271
ENSMUSG00000038020	*Rapgefl1*	1.54E-11	2.33861
ENSMUSG00000028148	*Them5*	1.43E-08	2.32907
ENSMUSG00000032454	*Rbp2*	2.18E-02	2.32839
ENSMUSG00000054325	*Lce3a*	1.60E-06	2.31499
ENSMUSG00000016327	*Atp1b4*	9.25E-04	2.30528
ENSMUSG00000047884	*Klk9*	1.51E-02	2.29768
ENSMUSG00000041991	*Hrnr*	2.88E-07	2.29503
ENSMUSG00000010064	*Slc38a3*	9.74E-11	2.28605
ENSMUSG00000027913	*Crct1*	1.33E-08	2.2855
ENSMUSG00000050296	*Abca12*	2.98E-09	2.27557
ENSMUSG00000039518	*Cdsn*	3.75E-08	2.27368
ENSMUSG00000079451	*Tmprss11g*	1.35E-04	2.2653
ENSMUSG00000073602	*Serpinb3b*	7.22E-05	2.25697
ENSMUSG00000027513	*Pck1*	7.41E-18	2.24387
ENSMUSG00000043681	*Fam25c*	2.27E-04	2.24042
ENSMUSG00000047586	*Nccrp1*	1.89E-02	2.24009
ENSMUSG00000026984	*Il1f6*	6.03E-03	2.23995
ENSMUSG00000039070	*Cpa4*	3.31E-06	2.23183
ENSMUSG00000023176	*Cpn2*	3.39E-02	2.23093

ENSMUSG00000060621	*Nkpd1*	1.11E-02	2.2285
ENSMUSG00000048764	*Tmprss11f*	1.97E-04	2.22505
ENSMUSG00000076613	*Ighg2b*	8.46E-03	2.22301
ENSMUSG00000025329	*Padi1*	1.34E-02	2.22281
ENSMUSG00000044359	*P2ry4*	2.00E-03	2.21873
ENSMUSG00000079644	*Gm1110*	8.55E-04	2.19573
ENSMUSG00000059230	*Defb4*	1.15E-06	2.17928
ENSMUSG00000112267	*Gm47903*	3.79E-02	2.17842
ENSMUSG00000021359	*Tfap2a*	8.96E-04	2.17337
ENSMUSG00000031844	*Hsd17b2*	1.45E-04	2.16161
ENSMUSG00000067714	*Lpar5*	2.70E-02	2.15751
ENSMUSG00000068885	*Lce3f*	5.02E-05	2.15408
ENSMUSG00000031372	*Trex2*	1.77E-02	2.15218
ENSMUSG00000073601	*Serpinb3c*	7.40E-03	2.14657
ENSMUSG00000024331	*Dsc2*	6.87E-11	2.14446
ENSMUSG00000090356	*Teddm3*	1.75E-03	2.13866
ENSMUSG00000032281	*Acsbg1*	5.63E-12	2.13831
ENSMUSG00000021509	*Slc25a48*	5.40E-03	2.13414
ENSMUSG00000086448	*9330162012Rik*	1.57E-02	2.12691
ENSMUSG00000047787	*Flrt1*	1.70E-02	2.12205
ENSMUSG00000068890	*Lce1a2*	2.23E-02	2.12041
ENSMUSG00000046818	*Ddit4l*	1.82E-04	2.11443
ENSMUSG00000045776	*Lrtm1*	3.90E-10	2.10474
ENSMUSG00000038242	*Aox4*	1.01E-05	2.10471
ENSMUSG00000027923	*Lce1b*	2.48E-02	2.10373
ENSMUSG00000055333	*Fat2*	2.95E-09	2.09985
ENSMUSG00000091376	*Aadacl2*	4.12E-02	2.09943
ENSMUSG00000086585	*Gm16126*	2.80E-02	2.08292
ENSMUSG00000074625	*Arhgap40*	4.55E-07	2.08272
ENSMUSG00000025431	*Crisp1*	3.94E-04	2.0827
ENSMUSG00000003271	*Sult2b1*	1.40E-04	2.07941
ENSMUSG00000074771	*Ankef1*	1.86E-07	2.06756
ENSMUSG00000030577	*Cd22*	9.58E-12	2.0664
ENSMUSG00000042092	*Lce1c*	2.56E-02	2.06455
ENSMUSG00000075296	*Aldh3b2*	3.22E-03	2.06241
ENSMUSG00000048078	*Tenm4*	4.36E-46	2.05431
ENSMUSG00000043165	*Lor*	1.66E-12	2.053
ENSMUSG00000046056	*Sbsn*	6.79E-08	2.04981
ENSMUSG00000049336	*Tenm2*	1.73E-20	2.03138
ENSMUSG00000020061	*Mybpc1*	1.29E-26	2.0298
ENSMUSG00000038354	*Ankrd35*	5.87E-04	2.02604
ENSMUSG00000021255	*Esrrb*	2.34E-05	2.00726
ENSMUSG00000106245	*Gm43824*	2.26E-03	2.00651
ENSMUSG00000026616	*Cr2*	8.19E-09	2.0019
ENSMUSG00000087500	*Gm12426*	3.86E-02	1.99964
ENSMUSG00000074433	*Lce3e*	3.42E-03	1.99487
ENSMUSG00000086584	*Gm12002*	3.67E-05	1.99171
ENSMUSG00000104927	*Gm43388*	4.85E-03	1.99016
ENSMUSG00000033849	*B3galt2*	3.89E-03	1.98493
ENSMUSG00000035606	*Ky*	1.89E-07	1.98363
ENSMUSG00000100781	*Gm29481*	2.81E-02	1.98361
ENSMUSG00000049598	*Vsig8*	2.47E-02	1.98235
ENSMUSG00000028544	*Slc5a9*	3.70E-04	1.97676
ENSMUSG00000036731	*Cysrt1*	3.63E-03	1.97512
ENSMUSG00000038115	*Ano2*	1.53E-17	1.96639
ENSMUSG00000027833	*Shox2*	3.91E-02	1.96557
ENSMUSG00000009900	*Wnt3a*	1.55E-04	1.96506

ENSMUSG00000022416	*Cacna1i*	1.15E-06	1.96482
ENSMUSG00000032278	*Paqr5*	5.13E-09	1.96334
ENSMUSG00000043461	*Sptssb*	5.50E-04	1.96325
ENSMUSG00000026109	*Tmeff2*	5.04E-10	1.96288
ENSMUSG00000024471	*Myot*	1.16E-18	1.95937
ENSMUSG00000115919	*Gm31583*	2.72E-02	1.95861
ENSMUSG00000037469	*Acp7*	1.65E-02	1.95823
ENSMUSG00000056966	*Gjc3*	4.48E-02	1.95084
ENSMUSG00000005716	*Pvalb*	1.10E-03	1.95002
ENSMUSG00000055489	*Ano5*	1.63E-13	1.94962
ENSMUSG00000043286	*Pnpla1*	6.54E-03	1.94448
ENSMUSG00000015879	*Fam184b*	2.97E-03	1.94
ENSMUSG00000001497	*Pax9*	7.64E-06	1.93926
ENSMUSG00000021565	*Slc6a19*	2.86E-04	1.93609
ENSMUSG00000114493	*Gm47071*	1.55E-07	1.93539
ENSMUSG00000043795	*Prr33*	1.22E-02	1.93241
ENSMUSG00000024972	*Lgals12*	1.56E-04	1.92981
ENSMUSG00000037157	*Il22ra1*	2.63E-02	1.92792
ENSMUSG00000085184	*4933439K11Rik*	1.66E-04	1.92699
ENSMUSG00000031936	*Hephl1*	4.23E-02	1.92403
ENSMUSG00000024673	*Ms4a1*	1.09E-08	1.92013
ENSMUSG00000111556	*Gm19299*	2.18E-02	1.91814
ENSMUSG00000030178	*Klra13-ps*	1.23E-02	1.91485
ENSMUSG00000000673	*Haao*	2.01E-04	1.91426
ENSMUSG00000019102	*Aldh3a1*	2.82E-09	1.90858
ENSMUSG00000104213	*Ighd*	1.37E-08	1.90673
ENSMUSG00000034282	*Evpl*	4.31E-11	1.90263
ENSMUSG00000021223	*Papln*	5.43E-04	1.89985
ENSMUSG00000041782	*Lad1*	1.90E-10	1.89447
ENSMUSG00000067889	*Sptbn2*	3.18E-09	1.89422
ENSMUSG00000056328	*Myh1*	5.41E-31	1.89409
ENSMUSG00000048142	*Nat8l*	2.19E-04	1.88665
ENSMUSG00000116290	*Gm49518*	4.80E-03	1.88407
ENSMUSG00000027359	*Slc27a2*	8.34E-03	1.88103
ENSMUSG00000061126	*Cyp4f39*	1.85E-03	1.87931
ENSMUSG00000019853	*Hebp2*	2.38E-02	1.8788
ENSMUSG00000024347	*Psd2*	6.76E-03	1.8787
ENSMUSG00000049123	*Catsperg2*	1.49E-02	1.87815
ENSMUSG00000017300	*Tnnc2*	5.40E-15	1.87774
ENSMUSG00000026950	*Neb*	1.41E-16	1.87734
ENSMUSG00000032033	*Barx2*	3.20E-08	1.87675
ENSMUSG00000046182	*Gsg1l*	2.78E-05	1.8741
ENSMUSG00000044737	*Klk14*	2.20E-06	1.87252
ENSMUSG00000046971	*Pla2g4f*	1.78E-09	1.87121
ENSMUSG00000044086	*Lmod3*	1.84E-04	1.86547
ENSMUSG00000084162	*Gm11251*	4.13E-02	1.86137
ENSMUSG00000033508	*Asprv1*	4.71E-06	1.85815
ENSMUSG00000034579	*Pla2g3*	9.27E-03	1.85233
ENSMUSG00000106617	*Gm36266*	3.40E-02	1.85212
ENSMUSG00000037509	*Arhgef4*	9.74E-11	1.8494
ENSMUSG00000028435	*Aqp3*	6.38E-06	1.84168
ENSMUSG00000060180	*Myh13*	1.20E-05	1.8367
ENSMUSG00000030935	*Acsm3*	4.56E-02	1.83384
ENSMUSG00000028031	*Dkk2*	1.01E-07	1.83252
ENSMUSG00000039092	*Sptlc3*	6.41E-04	1.83181
ENSMUSG00000026407	*Cacna1s*	2.79E-13	1.82909
ENSMUSG00000000031	*H19*	2.56E-20	1.82543

ENSMUSG00000073492	*Gm10521*	2.31E-03	1.81983
ENSMUSG00000087382	*Ctcflos*	3.63E-03	1.81593
ENSMUSG00000014030	*Pax5*	1.30E-07	1.81402
ENSMUSG00000030724	*Cd19*	4.30E-09	1.8132
ENSMUSG00000029361	*Nos1*	2.87E-14	1.81035
ENSMUSG00000069808	*Fam57a*	1.84E-11	1.80929
ENSMUSG00000061723	*Tnnt3*	3.90E-10	1.80825
ENSMUSG00000054966	*Lmntd1*	3.80E-23	1.80655
ENSMUSG00000003863	*Ppfia3*	2.28E-02	1.80404
ENSMUSG00000060275	*Nrg2*	1.27E-04	1.80254
ENSMUSG00000085235	*Gm12576*	4.86E-02	1.79966
ENSMUSG00000039809	*Gabbr2*	3.16E-02	1.79942
ENSMUSG00000102305	*Gm38192*	1.07E-02	1.79922
ENSMUSG00000030510	*Cers3*	3.38E-07	1.79054
ENSMUSG00000037922	*Bank1*	5.44E-06	1.7892
ENSMUSG00000027077	*Smtnl1*	6.91E-06	1.78907
ENSMUSG00000049349	*Gm5105*	2.80E-02	1.78388
ENSMUSG00000072591	*5930412G12Rik*	3.66E-02	1.78195
ENSMUSG00000042306	*S100a14*	9.20E-08	1.77984
ENSMUSG00000042474	*Fcmr*	2.09E-05	1.77414
ENSMUSG00000067616	*Klk11*	7.10E-03	1.77343
ENSMUSG00000040283	*Btnl9*	1.58E-02	1.77128
ENSMUSG00000001095	*Slc13a2*	1.63E-03	1.76877
ENSMUSG00000095079	*Igha*	6.91E-07	1.76823
ENSMUSG00000071540	*3425401B19Rik*	2.42E-14	1.76757
ENSMUSG00000042514	*Klhl14*	1.86E-03	1.76512
ENSMUSG00000032502	*Stac*	1.48E-03	1.75181
ENSMUSG00000004885	*Crabp2*	1.22E-02	1.74533
ENSMUSG00000022871	*Fetub*	2.02E-04	1.74369
ENSMUSG00000025754	*Agbl1*	7.55E-21	1.74292
ENSMUSG00000057802	*Gm10030*	2.61E-02	1.74044
ENSMUSG00000032564	*Cpne4*	7.97E-06	1.73707
ENSMUSG00000013523	*Bcas1*	2.19E-02	1.73402
ENSMUSG00000030546	*Plin1*	1.25E-07	1.73097
ENSMUSG00000085417	*Gm13919*	1.02E-02	1.72944
ENSMUSG00000079853	*Klra1*	3.86E-04	1.72252
ENSMUSG00000105646	*Gm30211*	5.74E-11	1.72189
ENSMUSG00000033182	*Kbtbd12*	8.41E-08	1.72084
ENSMUSG00000038751	*Ptk6*	2.49E-02	1.71998
ENSMUSG00000026989	*Dapl1*	3.16E-02	1.71791
ENSMUSG00000112041	*9530020I12Rik*	4.23E-02	1.71514
ENSMUSG00000019851	*Perp*	5.28E-09	1.71321
ENSMUSG00000026418	*Tnni1*	1.91E-02	1.71016
ENSMUSG00000062515	*Fabp4*	9.13E-16	1.70935
ENSMUSG00000026834	*Acvr1c*	1.49E-04	1.70449
ENSMUSG00000028396	*2310002L09Rik*	2.22E-02	1.70394
ENSMUSG00000060962	*Dmkn*	1.01E-09	1.69805
ENSMUSG00000074862	*BC025920*	2.99E-02	1.69659
ENSMUSG00000091712	*Sec14l5*	4.66E-04	1.69507
ENSMUSG00000025479	*Cyp2e1*	3.83E-17	1.69172
ENSMUSG00000029055	*Plch2*	9.19E-09	1.68869
ENSMUSG00000087514	*Gm16076*	4.55E-02	1.68559
ENSMUSG00000038167	*Plekhg6*	3.73E-04	1.6825
ENSMUSG00000076617	*Ighm*	3.37E-14	1.68243
ENSMUSG00000076275	*Mir675*	4.98E-04	1.68125
ENSMUSG00000021768	*Dusp13*	2.66E-02	1.68064
ENSMUSG00000027868	*Tbx15*	5.26E-11	1.67891

ENSMUSG00000014543	*Klra17*	3.90E-08	1.67493
ENSMUSG00000086564	*Cd101*	3.09E-15	1.6748
ENSMUSG00000087090	*Nctc1*	3.84E-12	1.67425
ENSMUSG00000022053	*Ebf2*	5.76E-13	1.67262
ENSMUSG00000097312	*Gm26870*	4.70E-04	1.67024
ENSMUSG00000044788	*Fads6*	6.63E-03	1.66957
ENSMUSG00000067081	*Asb18*	4.14E-04	1.66683
ENSMUSG00000067242	*Lgi1*	1.29E-02	1.66527
ENSMUSG00000025330	*Padi4*	2.91E-05	1.65776
ENSMUSG00000079015	*Serpina1c*	1.52E-03	1.65711
ENSMUSG00000040536	*Necab1*	2.89E-02	1.65665
ENSMUSG00000029603	*Dtx1*	2.06E-03	1.65369
ENSMUSG00000032311	*Nrg4*	1.05E-09	1.65365
ENSMUSG00000038457	*Tmem255b*	1.95E-03	1.65304
ENSMUSG00000098488	*Pla2g4b*	8.22E-03	1.65198
ENSMUSG00000066366	*Serpina1a*	4.02E-03	1.64939
ENSMUSG00000029120	*Ppp2r2c*	3.19E-03	1.64868
ENSMUSG00000027022	*Xirp2*	1.28E-22	1.64858
ENSMUSG00000037139	*Myom3*	8.53E-11	1.64798
ENSMUSG00000033544	*Angptl1*	1.83E-02	1.64513
ENSMUSG00000024136	*Dnase1l2*	3.42E-03	1.64394
ENSMUSG00000030592	*Ryr1*	1.75E-07	1.64026
ENSMUSG00000103824	*Gm38177*	1.79E-02	1.6397
ENSMUSG00000006411	*Nectin4*	3.58E-05	1.63718
ENSMUSG00000096974	*Gm26881*	4.82E-02	1.63547
ENSMUSG00000005547	*Cyp2a5*	4.57E-06	1.63304
ENSMUSG00000113543	*Gm36264*	2.07E-02	1.63225
ENSMUSG00000026494	*Kif26b*	2.39E-14	1.63132
ENSMUSG00000070802	*Pnmal2*	1.50E-02	1.62883
ENSMUSG00000057003	*Myh4*	1.66E-10	1.62751
ENSMUSG00000028017	*Egf*	1.08E-08	1.62681
ENSMUSG00000082674	*Gm11914*	2.98E-02	1.62365
ENSMUSG00000059994	*Fcrl1*	1.55E-04	1.62354
ENSMUSG00000020169	*Best3*	2.24E-05	1.62346
ENSMUSG00000046352	*Gjb2*	1.75E-05	1.62257
ENSMUSG00000058498	*Rnf207*	4.30E-03	1.6175
ENSMUSG00000033533	*Acsm1*	5.95E-04	1.61748
ENSMUSG00000017697	*Ada*	1.08E-10	1.61747
ENSMUSG00000005373	*Mlxipl*	2.73E-09	1.61612
ENSMUSG00000056755	*Grm7*	2.64E-05	1.6147
ENSMUSG00000082179	*Gm11407*	4.66E-02	1.61227
ENSMUSG00000001027	*Scn4a*	1.74E-07	1.60993
ENSMUSG00000050600	*Zfp831*	3.33E-11	1.60941
ENSMUSG00000056155	*Nanos3*	2.00E-02	1.60734
ENSMUSG00000025105	*Bnc1*	3.90E-02	1.60648
ENSMUSG00000075555	*Gm10863*	1.79E-03	1.6055
ENSMUSG00000054889	*Dsp*	3.74E-45	1.60391
ENSMUSG00000074604	*Mgst2*	1.19E-07	1.60185
ENSMUSG00000036218	*Pdzrn4*	1.90E-11	1.60165
ENSMUSG00000058975	*Kcnc1*	3.09E-03	1.60068
ENSMUSG00000000244	*Tspan32*	1.03E-08	1.5999
ENSMUSG00000031937	*Vstm5*	6.27E-03	1.5993
ENSMUSG00000034648	*Lrrn1*	1.12E-02	1.59815
ENSMUSG00000030495	*Slc7a10*	2.96E-07	1.59742
ENSMUSG00000017639	*Rab11fip4*	7.16E-06	1.59393
ENSMUSG00000029602	*Rasal1*	3.67E-02	1.59345
ENSMUSG00000026676	*Ccdc3*	1.21E-09	1.59159

ENSMUSG00000034308	*Sdr42e1*	2.38E-03	1.5912
ENSMUSG00000059900	*Tmem40*	2.36E-02	1.59117
ENSMUSG00000089941	*Gm16168*	3.31E-03	1.59041
ENSMUSG00000020892	*Aloxe3*	1.31E-02	1.58477
ENSMUSG00000115095	*Gm49311*	1.45E-02	1.58455
ENSMUSG00000031097	*Tnni2*	2.64E-07	1.58348
ENSMUSG00000031245	*Hmgn5*	9.24E-05	1.58329
ENSMUSG00000067653	*Ankrd23*	7.42E-10	1.58165
ENSMUSG00000039264	*Gimap3*	5.32E-08	1.58068
ENSMUSG00000030730	*Atp2a1*	4.52E-14	1.57945
ENSMUSG00000083834	*Gm12577*	3.00E-02	1.57726
ENSMUSG00000076609	*Igkc*	1.26E-05	1.5742
ENSMUSG00000021579	*Lrrc14b*	3.06E-02	1.57311
ENSMUSG00000030598	*Fbxo17*	1.83E-04	1.57292
ENSMUSG00000008999	*Bmp7*	9.10E-03	1.5718
ENSMUSG00000036214	*Znrd1as*	3.27E-02	1.57078
ENSMUSG00000030468	*Siglecg*	7.97E-06	1.56997
ENSMUSG00000085971	*Gm15411*	3.59E-04	1.56795
ENSMUSG00000024617	*Camk2a*	1.83E-04	1.56649
ENSMUSG00000021340	*Gpld1*	1.71E-06	1.56545
ENSMUSG00000031933	*Izumo1r*	4.04E-02	1.56461
ENSMUSG00000090799	*Klhl33*	9.45E-05	1.56433
ENSMUSG00000036854	*Hspb6*	5.71E-03	1.56314
ENSMUSG00000047419	*Cmya5*	1.22E-17	1.56238
ENSMUSG00000114014	*Gm48350*	2.45E-03	1.56063
ENSMUSG00000063522	*2010109I03Rik*	1.10E-02	1.56032
ENSMUSG00000037661	*Gpr160*	1.12E-03	1.56002
ENSMUSG00000055775	*Myh8*	2.99E-07	1.55915
ENSMUSG00000097899	*Gm16894*	8.00E-03	1.55851
ENSMUSG00000039521	*Foxp3*	9.57E-03	1.55602
ENSMUSG00000070385	*Ampd1*	4.23E-05	1.55169
ENSMUSG00000050106	*Tmc8*	7.90E-05	1.5508
ENSMUSG00000035686	*Thrsp*	2.97E-07	1.54774
ENSMUSG00000041460	*Cacna2d4*	4.52E-02	1.5477
ENSMUSG00000026824	*Kcnj3*	9.29E-10	1.54542
ENSMUSG00000020758	*Itgb4*	4.89E-09	1.54438
ENSMUSG00000032503	*Arpp21*	4.76E-03	1.54437
ENSMUSG00000043110	*Lrrn4*	7.92E-03	1.5421
ENSMUSG00000014453	*Blk*	1.27E-06	1.54192
ENSMUSG00000027419	*Pcsk2*	5.87E-03	1.54191
ENSMUSG00000034656	*Cacna1a*	7.55E-12	1.54042
ENSMUSG00000015702	*Anxa9*	7.23E-03	1.5397
ENSMUSG00000062713	*Sim2*	2.58E-05	1.53934
ENSMUSG00000068697	*Myoz1*	5.79E-04	1.5362
ENSMUSG00000038602	*Slc35f1*	8.70E-10	1.53615
ENSMUSG00000079110	*Capn3*	9.20E-06	1.5356
ENSMUSG00000036856	*Wnt4*	2.59E-06	1.53379
ENSMUSG00000000223	*Drp2*	1.32E-03	1.53365
ENSMUSG00000031710	*Ucp1*	7.53E-03	1.53359
ENSMUSG00000056656	*Apol8*	4.49E-02	1.53347
ENSMUSG00000029862	*Clcn1*	2.78E-04	1.5334
ENSMUSG00000024526	*Cidea*	2.67E-02	1.53274
ENSMUSG00000042251	*Pm20d1*	1.64E-02	1.5326
ENSMUSG00000079055	*Slc8a3*	2.56E-06	1.53124
ENSMUSG00000031377	*Bmx*	4.19E-08	1.5308
ENSMUSG00000034570	*Inpp5j*	1.71E-02	1.52977
ENSMUSG00000048368	*Omd*	4.45E-02	1.52965

ENSMUSG00000057719	*Sh3rf2*	1.60E-09	1.52797
ENSMUSG00000035189	*Ano4*	1.29E-06	1.52212
ENSMUSG00000043932	*Klri2*	1.09E-02	1.51956
ENSMUSG00000024112	*Cacna1h*	1.02E-02	1.51951
ENSMUSG00000072812	*Ahnak2*	2.64E-06	1.51917
ENSMUSG00000024669	*Cd5*	8.63E-04	1.51847
ENSMUSG00000037989	*Wnk2*	1.82E-10	1.51835
ENSMUSG00000074497	*A430078G23Rik*	3.97E-14	1.51676
ENSMUSG00000054708	*Ankrd24*	3.01E-04	1.51618
ENSMUSG00000032243	*Itga11*	6.65E-04	1.51519
ENSMUSG00000087150	*BC064078*	4.96E-03	1.51421
ENSMUSG00000044461	*Shisa2*	4.62E-02	1.50751
ENSMUSG00000114937	*Gm30054*	6.11E-05	1.50651
ENSMUSG00000038605	*Samd10*	2.26E-03	1.50622
ENSMUSG00000040350	*Trim7*	2.15E-04	1.50563
ENSMUSG00000100551	*Gm19503*	3.16E-03	1.5047
ENSMUSG00000015314	*Slamf6*	1.76E-09	1.50457
ENSMUSG00000032262	*Elovl4*	5.29E-03	1.50436
ENSMUSG00000090166	*Ear10*	2.48E-02	1.50393
ENSMUSG00000058207	*Serpina3k*	2.37E-03	1.50282
ENSMUSG00000040694	*Apobec2*	2.65E-05	1.50189
ENSMUSG00000113447	*Gm48538*	4.54E-02	1.50191
ENSMUSG00000026646	*Suv39h2*	4.57E-02	1.5074
ENSMUSG00000030744	*Rps3*	1.27E-09	1.50807
ENSMUSG00000085025	*Gm13715*	3.50E-02	1.50829
ENSMUSG00000059835	*Rpl13-ps3*	2.53E-03	1.51027
ENSMUSG00000032496	*Ltf*	3.04E-16	1.51096
ENSMUSG00000084104	*Gm13578*	2.62E-05	1.51286
ENSMUSG00000091845	*Rpl36-ps12*	7.00E-03	1.51322
ENSMUSG00000100969	*1700030N03Rik*	1.54E-02	1.51588
ENSMUSG00000082062	*Ftl2-ps*	3.39E-09	1.51711
ENSMUSG00000076036	*Gm22133*	2.46E-11	1.51828
ENSMUSG00000083337	*Gm11539*	1.80E-03	1.52589
ENSMUSG00000040809	*Chil3*	1.62E-04	1.52703
ENSMUSG00000024774	*Ankrd22*	3.56E-08	1.53049
ENSMUSG00000052565	*Hist1h1d*	7.00E-03	1.53071
ENSMUSG00000024026	*Glo1*	8.15E-12	1.53202
ENSMUSG00000057863	*Rpl36*	4.20E-04	1.53263
ENSMUSG00000080811	*Gm14513*	1.25E-03	1.5339
ENSMUSG00000109658	*Gm45660*	4.65E-05	1.53887
ENSMUSG00000097366	*Gm8177*	1.12E-02	1.54012
ENSMUSG00000094955	*Gm3699*	1.48E-02	1.5463
ENSMUSG00000094125	*Gm13698*	6.40E-03	1.55008
ENSMUSG00000094336	*Gm13693*	6.40E-03	1.55008
ENSMUSG00000096484	*Gm13696*	6.40E-03	1.55008
ENSMUSG00000096337	*Gm13694*	6.40E-03	1.55008
ENSMUSG00000095824	*Gm13697*	6.40E-03	1.55008
ENSMUSG00000079247	*Gm13691*	6.40E-03	1.55008
ENSMUSG00000096729	*Gm13695*	5.93E-03	1.55266
ENSMUSG00000112908	*Gm7392*	3.88E-04	1.5528
ENSMUSG00000022097	*Sftpc*	6.96E-07	1.55295
ENSMUSG00000046031	*Calhm6*	1.49E-02	1.5541
ENSMUSG00000082978	*Rpsa-ps11*	2.04E-02	1.55812
ENSMUSG00000085264	*Gm15581*	3.86E-02	1.56146
ENSMUSG00000028179	*Cth*	1.60E-04	1.56198
ENSMUSG00000080950	*Gm7278*	2.72E-02	1.56602
ENSMUSG00000097679	*Rps19-ps5*	3.50E-02	1.56618

ENSMUSG00000114304	*Gm48099*	2.47E-05	1.56873
ENSMUSG00000065968	*Ifitm7*	3.54E-02	1.57151
ENSMUSG00000077391	*Gm24336*	3.92E-02	1.57527
ENSMUSG00000073940	*Hbb-bt*	7.22E-03	1.57539
ENSMUSG00000028896	*Rcc1*	7.42E-10	1.57968
ENSMUSG00000085401	*Slc39a1-ps*	5.82E-09	1.58067
ENSMUSG00000049932	*H2afx*	6.34E-03	1.58133
ENSMUSG00000087968	*Gm25395*	2.95E-03	1.58263
ENSMUSG00000032484	*Ngp*	5.93E-21	1.58682
ENSMUSG00000083898	*Gm7340*	3.68E-05	1.58939
ENSMUSG00000097971	*Gm26917*	8.77E-04	1.59222
ENSMUSG00000050796	*B3galt6*	1.23E-02	1.59236
ENSMUSG00000048388	*Fam171b*	2.37E-10	1.59429
ENSMUSG00000024205	*Rpl36-ps2*	4.35E-04	1.59832
ENSMUSG00000007892	*Rplp1*	5.42E-11	1.61046
ENSMUSG00000052305	*Hbb-bs*	3.42E-03	1.61115
ENSMUSG00000065037	*Rn7sk*	4.20E-03	1.61406
ENSMUSG00000079505	*Gm11131*	4.60E-03	1.61438
ENSMUSG00000087700	*Gm15283*	1.12E-02	1.61608
ENSMUSG00000096972	*Gm26883*	1.24E-02	1.62189
ENSMUSG00000063779	*Chil4*	1.09E-03	1.62825
ENSMUSG00000062461	*Gm5453*	4.23E-05	1.62974
ENSMUSG00000083836	*Ldha-ps2*	2.54E-03	1.63004
ENSMUSG00000084708	*Gm22988*	4.90E-03	1.63084
ENSMUSG00000106373	*Gm6522*	8.32E-03	1.64441
ENSMUSG00000075391	*Gm13443*	5.63E-08	1.6457
ENSMUSG00000077192	*Snora17*	1.41E-02	1.64917
ENSMUSG00000021071	*Trim9*	2.44E-04	1.65066
ENSMUSG00000089281	*Scarna6*	7.09E-03	1.6534
ENSMUSG00000025716	*Myo3a*	4.50E-03	1.65551
ENSMUSG00000030329	*Pianp*	7.04E-03	1.66575
ENSMUSG00000097168	*C230088H06Rik*	6.39E-08	1.67154
ENSMUSG00000063586	*Gm5513*	4.76E-03	1.67361
ENSMUSG00000070473	*Cldn3*	4.42E-09	1.67916
ENSMUSG00000083737	*Prdx6-ps2*	2.04E-02	1.6846
ENSMUSG00000088789	*Scarna13*	1.82E-03	1.68485
ENSMUSG00000035299	*Mid1*	3.52E-03	1.71244
ENSMUSG00000070524	*Fcrlb*	2.80E-02	1.72336
ENSMUSG00000064382	*Gm26447*	2.21E-04	1.73092
ENSMUSG00000032425	*Zfp949*	1.91E-18	1.74133
ENSMUSG00000013936	*Myl2*	4.07E-03	1.74341
ENSMUSG00000104560	*Gm8115*	3.84E-04	1.74573
ENSMUSG00000089762	*Ier5l*	2.27E-04	1.74658
ENSMUSG00000087353	*Gm13727*	7.20E-06	1.75524
ENSMUSG00000085241	*Snhg3*	4.49E-06	1.75809
ENSMUSG00000113960	*4933412O06Rik*	4.05E-03	1.76721
ENSMUSG00000075268	*Gm10819*	4.64E-05	1.77825
ENSMUSG00000106497	*Gm43195*	7.66E-03	1.77886
ENSMUSG00000044117	*2900011O08Rik*	6.16E-03	1.78002
ENSMUSG00000086420	*Gm8865*	2.40E-04	1.78093
ENSMUSG00000027014	*Cwc22*	5.52E-07	1.781
ENSMUSG00000077254	*Gm26079*	1.93E-02	1.79018
ENSMUSG00000062464	*Cyp4f37*	2.53E-04	1.80716
ENSMUSG00000082755	*Gm8692*	2.33E-02	1.80988
ENSMUSG00000080542	*Gm22710*	3.28E-02	1.81091
ENSMUSG00000107722	*2900060B14Rik*	2.04E-02	1.81334
ENSMUSG00000103103	*4833445I07Rik*	5.75E-03	1.81998

ENSMUSG00000089542	*Gm25835*	8.85E-06	1.82629
ENSMUSG00000085599	*Gm13449*	1.80E-02	1.82911
ENSMUSG00000084744	*Gm25291*	2.45E-02	1.83791
ENSMUSG00000029372	*Ppbp*	1.41E-06	1.83838
ENSMUSG00000095098	*Ccdc85b*	1.56E-03	1.84033
ENSMUSG00000088609	*Gm24187*	4.85E-07	1.84671
ENSMUSG00000001482	*Def8*	5.29E-14	1.84897
ENSMUSG00000089617	*Scarna10*	6.74E-04	1.85948
ENSMUSG00000099587	*Gm28967*	6.74E-04	1.85948
ENSMUSG00000088246	*Gm25911*	1.03E-07	1.86065
ENSMUSG00000001983	*Taco1*	8.81E-07	1.86641
ENSMUSG00000065353	*Snora73b*	2.44E-04	1.8684
ENSMUSG00000086354	*Gm13938*	1.03E-15	1.8767
ENSMUSG00000091405	*Hist2h4*	4.81E-07	1.88798
ENSMUSG00000091957	*Rps2-ps10*	4.59E-07	1.89014
ENSMUSG00000069273	*Hist1h3e*	1.12E-03	1.9083
ENSMUSG00000104690	*Gm47304*	5.92E-05	1.91679
ENSMUSG00000077714	*Snord17*	1.66E-04	1.91875
ENSMUSG00000088185	*Scarna2*	7.71E-07	1.9197
ENSMUSG00000049097	*Ankrd34a*	1.63E-02	1.91985
ENSMUSG00000036264	*Fstl4*	2.89E-03	1.92434
ENSMUSG00000114456	*Hist1h2bh*	1.82E-02	1.92447
ENSMUSG00000098178	*Gm42418*	1.34E-05	1.92525
ENSMUSG00000058385	*Hist1h2bg*	1.06E-03	1.92534
ENSMUSG00000064387	*Snora73a*	5.40E-09	1.936
ENSMUSG00000094338	*Hist1h2bl*	3.08E-03	1.94362
ENSMUSG00000088948	*Gm23262*	1.49E-04	1.94793
ENSMUSG00000064220	*Hist2h2aa1*	3.69E-03	1.95446
ENSMUSG00000028461	*Ccdc107*	1.54E-09	1.96853
ENSMUSG00000065226	*Gm25791*	3.14E-06	1.98442
ENSMUSG00000029635	*Cdk8*	2.29E-09	1.98467
ENSMUSG00000092746	*Rn7s6*	2.46E-05	1.98632
ENSMUSG00000065259	*Snora30*	3.24E-02	1.99136
ENSMUSG00000060639	*Hist1h4i*	1.64E-03	2.00154
ENSMUSG00000065822	*Snord15a*	5.99E-03	2.00285
ENSMUSG00000063954	*Hist2h2aa2*	1.91E-05	2.0103
ENSMUSG00000077563	*Snora68*	6.54E-05	2.01347
ENSMUSG00000074398	*Gm15441*	7.12E-03	2.02986
ENSMUSG00000069308	*Hist1h2bp*	3.32E-02	2.03521
ENSMUSG00000106649	*Gm49349*	2.06E-06	2.04015
ENSMUSG00000116237	*Gm30339*	1.38E-02	2.04542
ENSMUSG00000089655	*Gm16004*	2.91E-02	2.05643
ENSMUSG00000076281	*Gm24270*	2.24E-07	2.06413
ENSMUSG00000104740	*Mir6516*	3.24E-03	2.06889
ENSMUSG00000097263	*Gm26804*	2.12E-03	2.10305
ENSMUSG00000089255	*Snora78*	2.81E-02	2.10781
ENSMUSG00000065911	*Gm24447*	2.25E-05	2.11307
ENSMUSG00000062727	*Hist1h2bk*	3.23E-03	2.11378
ENSMUSG00000093378	*Gm20663*	7.20E-04	2.11505
ENSMUSG00000085348	*Myhas*	2.48E-04	2.12433
ENSMUSG00000064841	*Gm26205*	8.37E-03	2.1269
ENSMUSG00000081684	*Rps2-ps13*	5.49E-10	2.13212
ENSMUSG00000101972	*Hist1h3i*	3.84E-02	2.13658
ENSMUSG00000064231	*Gm5321*	1.89E-02	2.13892
ENSMUSG00000087819	*Gm25117*	2.03E-06	2.14179
ENSMUSG00000065824	*Gm26315*	1.47E-05	2.1456
ENSMUSG00000106279	*Gm47287*	2.67E-06	2.1466

ENSMUSG00000105398	*Gm47305*	2.67E-06	2.14661
ENSMUSG00000097300	*Gm26835*	3.09E-02	2.15296
ENSMUSG00000104863	*Gm49347*	5.00E-04	2.15358
ENSMUSG00000065087	*Snord22*	1.78E-14	2.16707
ENSMUSG00000100210	*Hist1h3f*	5.03E-04	2.17714
ENSMUSG00000069265	*Hist1h3a*	3.80E-02	2.18419
ENSMUSG00000064380	*Gm26448*	7.15E-09	2.18787
ENSMUSG00000064853	*Gm23442*	3.71E-06	2.1894
ENSMUSG00000065304	*Gm23245*	2.59E-03	2.20662
ENSMUSG00000110588	*Gm45774*	1.44E-02	2.22306
ENSMUSG00000064655	*Gm25788*	1.17E-02	2.22647
ENSMUSG00000064994	*Gm22422*	2.44E-03	2.23564
ENSMUSG00000099250	*Rn7s2*	9.79E-07	2.24149
ENSMUSG00000099021	*Rn7s1*	9.79E-07	2.24153
ENSMUSG00000105460	*Gm42671*	4.96E-02	2.24303
ENSMUSG00000065118	*Gm23297*	4.50E-03	2.24685
ENSMUSG00000065254	*Gm23973*	2.55E-02	2.27365
ENSMUSG00000064999	*Gm26035*	2.23E-06	2.27841
ENSMUSG00000065686	*Snora5c*	1.32E-02	2.28658
ENSMUSG00000117074	*AC121299.1*	6.16E-03	2.29666
ENSMUSG00000086220	*Gm16599*	1.82E-03	2.30969
ENSMUSG00000096010	*Hist4h4*	2.23E-06	2.31336
ENSMUSG00000076258	*Gm23935*	1.76E-11	2.31549
ENSMUSG00000103626	*Gm37358*	6.88E-05	2.31983
ENSMUSG00000088529	*Gm26083*	7.90E-05	2.32066
ENSMUSG00000112246	*Gm40761*	4.60E-02	2.33454
ENSMUSG00000064694	*Gm24146*	5.87E-04	2.34501
ENSMUSG00000114969	*Hba-ps3*	2.31E-03	2.35684
ENSMUSG00000086649	*Gm15286*	2.21E-02	2.36528
ENSMUSG00000064966	*Snord15b*	1.96E-06	2.36869
ENSMUSG00000091993	*B930036N10Rik*	3.93E-04	2.3742
ENSMUSG00000053615	*Gm9913*	4.61E-02	2.38787
ENSMUSG00000108866	*Gm35082*	4.48E-02	2.40681
ENSMUSG00000068855	*Hist2h2ac*	5.77E-05	2.40805
ENSMUSG00000099517	*Hist1h3g*	3.11E-02	2.42777
ENSMUSG00000080365	*Gm25776*	6.97E-05	2.42824
ENSMUSG00000102189	*Gm37194*	5.60E-09	2.44452
ENSMUSG00000061482	*Hist1h4d*	2.67E-16	2.45181
ENSMUSG00000043340	*6530409C15Rik*	1.55E-02	2.46462
ENSMUSG00000099583	*Hist1h3d*	9.81E-03	2.47409
ENSMUSG00000105448	*Gm25820*	1.07E-02	2.49056
ENSMUSG00000105288	*Gm25820*	1.07E-02	2.49056
ENSMUSG00000065145	*Vaultrc5*	5.90E-06	2.49296
ENSMUSG00000088008	*Gm25492*	6.25E-04	2.49693
ENSMUSG00000064451	*Snora23*	6.01E-03	2.49877
ENSMUSG00000095217	*Hist1h2bn*	8.20E-04	2.50304
ENSMUSG00000065649	*Snora74a*	9.27E-07	2.50464
ENSMUSG00000092267	*Gm20417*	2.33E-11	2.5151
ENSMUSG00000069274	*Hist1h4f*	6.17E-05	2.51954
ENSMUSG00000093650	*Gm20631*	3.45E-02	2.52141
ENSMUSG00000069310	*Hist1h3c*	1.27E-03	2.52752
ENSMUSG00000087775	*Rprl2*	4.48E-05	2.53855
ENSMUSG00000071470	*Ccnb1ip1*	1.51E-06	2.57238
ENSMUSG00000091383	*Hist1h2al*	3.90E-12	2.58142
ENSMUSG00000092837	*Rpph1*	1.54E-06	2.5885
ENSMUSG00000092386	*Gm20536*	2.30E-02	2.58947
ENSMUSG00000019865	*Nmbr*	2.79E-02	2.5947

ENSMUSG00000102349	*Gm37376*	5.22E-06	2.59474
ENSMUSG00000060678	*Hist1h4c*	1.34E-12	2.602
ENSMUSG00000097417	*Gm26669*	3.90E-03	2.60481
ENSMUSG00000105145	*Gm47299*	4.92E-08	2.60571
ENSMUSG00000105788	*Gm47295*	4.92E-08	2.60593
ENSMUSG00000089536	*Scarna3a*	6.53E-03	2.6208
ENSMUSG00000101355	*Hist1h3h*	1.95E-02	2.63462
ENSMUSG00000088675	*Rprl1*	4.46E-03	2.64112
ENSMUSG00000106222	*Rprl1*	4.46E-03	2.64112
ENSMUSG00000069266	*Hist1h4b*	5.61E-04	2.64927
ENSMUSG00000069267	*Hist1h3b*	1.36E-03	2.66856
ENSMUSG00000060981	*Hist1h4h*	3.18E-11	2.67747
ENSMUSG00000064288	*Hist1h4k*	6.70E-06	2.68893
ENSMUSG00000064604	*Snora44*	4.05E-05	2.70815
ENSMUSG00000093355	*Snora26*	1.76E-02	2.76757
ENSMUSG00000095590	*Gm24305*	5.74E-03	2.78226
ENSMUSG00000092819	*Gm23639*	4.60E-03	2.79569
ENSMUSG00000115420	*AL732506.1*	1.91E-12	2.79623
ENSMUSG00000088088	*Rmrp*	1.91E-12	2.79623
ENSMUSG00000086953	*Aknaos*	4.22E-02	2.79896
ENSMUSG00000010342	*Tex14*	2.50E-11	2.80189
ENSMUSG00000067455	*Hist1h4j*	1.31E-04	2.80961
ENSMUSG00000084783	*Gm15419*	5.16E-07	2.81003
ENSMUSG00000111971	*Gm48678*	1.46E-04	2.81027
ENSMUSG00000064901	*Snora21*	1.28E-03	2.87377
ENSMUSG00000087943	*Gm24245*	1.66E-12	2.89193
ENSMUSG00000087963	*Gm25394*	8.18E-03	2.89624
ENSMUSG00000096243	*Gm24265*	1.61E-07	2.90069
ENSMUSG00000065905	*Gm26110*	9.26E-04	2.91055
ENSMUSG00000105399	*Mir1843b*	5.37E-03	2.9215
ENSMUSG00000097131	*D230017M19Rik*	5.32E-12	2.94112
ENSMUSG00000092674	*Gm24105*	7.90E-11	2.95616
ENSMUSG00000077323	*Rnu11*	1.61E-07	2.98011
ENSMUSG00000096992	*Gm26788*	9.33E-03	2.98078
ENSMUSG00000117227	*AC105304.3*	2.95E-02	2.9812
ENSMUSG00000065778	*Gm22154*	2.44E-03	2.9846
ENSMUSG00000105790	*Gm24105*	8.13E-11	2.98894
ENSMUSG00000088025	*Rprl3*	6.04E-07	2.99575
ENSMUSG00000095580	*Rnu1b1*	3.38E-07	3.01229
ENSMUSG00000093834	*Rnu1b2*	3.38E-07	3.01229
ENSMUSG00000064923	*Gm22042*	1.44E-07	3.01372
ENSMUSG00000095701	*Gm24830*	9.14E-08	3.03287
ENSMUSG00000096838	*Gm26232*	9.14E-08	3.03287
ENSMUSG00000065773	*Rnu1b6*	9.14E-08	3.03287
ENSMUSG00000010362	*Rdm1*	9.37E-11	3.04878
ENSMUSG00000095260	*Gm25890*	1.10E-07	3.05099
ENSMUSG00000094812	*Gm22614*	1.10E-07	3.05099
ENSMUSG00000069300	*Hist1h2bj*	7.93E-04	3.06257
ENSMUSG00000069305	*Hist1h4n*	3.36E-07	3.0744
ENSMUSG00000094377	*Gm24407*	6.03E-10	3.08024
ENSMUSG00000069306	*Hist1h4m*	2.82E-06	3.08188
ENSMUSG00000060988	*Galnt13*	9.80E-33	3.13528
ENSMUSG00000065701	*Rny1*	1.52E-08	3.17627
ENSMUSG00000070167	*Snora57*	1.98E-15	3.18889
ENSMUSG00000094655	*Gm25360*	5.67E-15	3.20136
ENSMUSG00000108563	*Gm44686*	1.39E-02	3.23591
ENSMUSG00000080465	*Gm22486*	2.04E-09	3.27578

ENSMUSG00000091165	*Gm17036*	1.50E-02	3.27618
ENSMUSG00000060093	*Hist1h4a*	1.46E-12	3.32521
ENSMUSG00000092805	*Gm26461*	1.31E-10	3.34331
ENSMUSG00000096214	*Gm22634*	5.90E-18	3.48166
ENSMUSG00000096206	*Gm22317*	5.90E-18	3.48166
ENSMUSG00000027233	*Patl2*	1.67E-05	3.4999
ENSMUSG00000065845	*Gm25189*	7.04E-03	3.50714
ENSMUSG00000096205	*Gm22068*	8.03E-11	3.52569
ENSMUSG00000088252	*Snord13*	8.10E-08	3.5475
ENSMUSG00000065176	*Rnu12*	1.76E-21	3.61877
ENSMUSG00000097799	*Gm26899*	1.05E-03	3.63697
ENSMUSG00000092702	*Gm24514*	7.15E-12	3.70097
ENSMUSG00000064943	*Gm23240*	3.63E-03	3.72556
ENSMUSG00000085573	*Gm15418*	1.61E-07	3.75952
ENSMUSG00000110790	*Gm47079*	2.36E-03	3.78383
ENSMUSG00000065767	*Gm23849*	2.98E-11	3.82342
ENSMUSG00000065944	*Rnu2-10*	1.90E-11	3.84825
ENSMUSG00000094826	*Gm23804*	1.21E-18	3.84945
ENSMUSG00000064702	*Gm24950*	2.50E-11	3.85414
ENSMUSG00000065251	*Gm23971*	2.50E-11	3.85414
ENSMUSG00000064856	*Gm23444*	3.12E-11	3.87597
ENSMUSG00000093956	*Gm24497*	6.05E-11	3.87768
ENSMUSG00000064945	*Rny3*	1.84E-12	3.87863
ENSMUSG00000094050	*Gm23472*	2.54E-11	3.89363
ENSMUSG00000094306	*Gm24924*	1.54E-10	3.89902
ENSMUSG00000108171	*Gm43915*	7.23E-04	3.89946
ENSMUSG00000065820	*Gm26316*	9.58E-12	3.91062
ENSMUSG00000097346	*Gm26619*	2.86E-04	3.94457
ENSMUSG00000065870	*Rnu3a*	1.51E-11	3.95478
ENSMUSG00000106147	*Rnu3a*	1.51E-11	3.95478
ENSMUSG00000095969	*Rnu1a1*	1.19E-11	3.95595
ENSMUSG00000096659	*Gm25679*	1.03E-19	3.9906
ENSMUSG00000093815	*Gm26444*	1.03E-19	3.9906
ENSMUSG00000115432	*D130009I18Rik*	1.17E-07	4.00512
ENSMUSG00000105115	*Rnu3b2*	3.78E-19	4.06451
ENSMUSG00000098925	*Rnu3b2*	3.78E-19	4.06451
ENSMUSG00000098943	*Rnu3b1*	6.81E-19	4.07869
ENSMUSG00000105025	*Rnu3b1*	6.81E-19	4.07869
ENSMUSG00000099291	*Rnu3b3*	1.50E-18	4.09008
ENSMUSG00000104856	*Rnu3b3*	1.50E-18	4.09008
ENSMUSG00000104896	*Rnu3b4*	3.78E-19	4.1079
ENSMUSG00000098641	*Rnu3b4*	4.19E-19	4.1081
ENSMUSG00000095616	*Gm26244*	5.63E-11	4.1472
ENSMUSG00000080538	*Gm25541*	1.15E-12	4.15571
ENSMUSG00000064941	*Gm23238*	2.71E-15	4.16236
ENSMUSG00000065232	*Gm22973*	6.24E-13	4.18652
ENSMUSG00000085393	*Gm11280*	4.14E-03	4.19886
ENSMUSG00000096349	*Gm22513*	1.18E-06	4.21069
ENSMUSG00000090625	*Gm20721*	7.53E-07	4.26306
ENSMUSG00000095676	*Gm25099*	1.09E-21	4.3711
ENSMUSG00000095738	*Gm25313*	2.50E-11	4.39293
ENSMUSG00000093843	*Gm25939*	6.33E-11	4.45452
ENSMUSG00000095892	*Rnu5g*	3.84E-12	4.48461
ENSMUSG00000064682	*Gm25813*	1.88E-09	4.50868
ENSMUSG00000085297	*Gm11651*	8.54E-10	4.5091
ENSMUSG00000085465	*Gm15347*	3.44E-06	4.85263
ENSMUSG00000090208	*Gm15851*	5.99E-04	4.92229

ENSMUSG00000023467	*Tulp2*	2.27E-05	5.12205
ENSMUSG00000064899	*Snord118*	2.09E-07	5.44474
ENSMUSG00000094668	*Gm24871*	6.67E-06	5.69726
ENSMUSG00000097815	*Gm26809*	9.27E-08	5.9877
ENSMUSG00000047061	*Gm9817*	3.07E-05	7.37847
ENSMUSG00000097554	*Gm26825*	2.08E-06	11.0581
ENSMUSG00000105361	*AY036118*	1.29E-26	11.3177

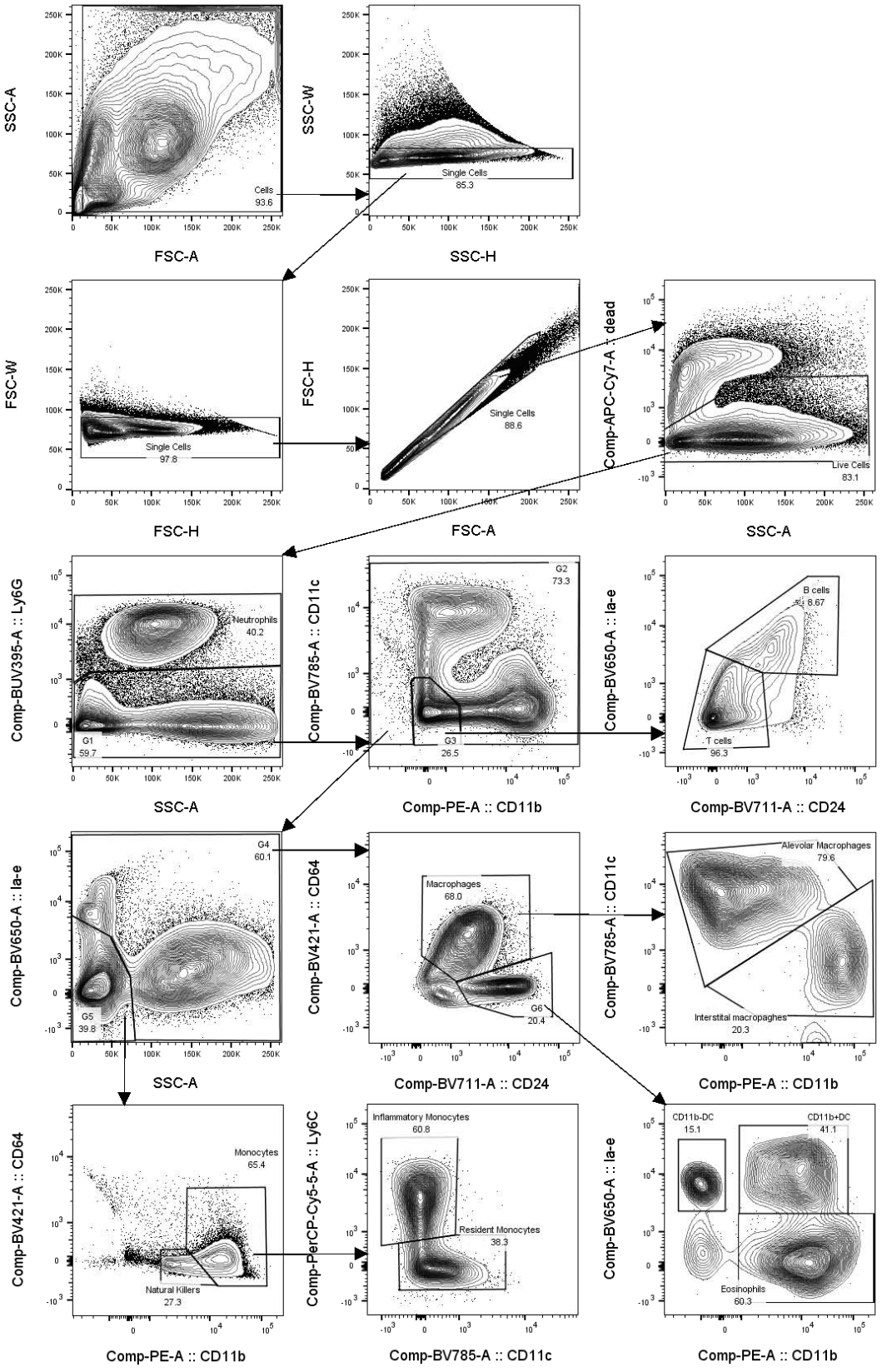

Appendix Y. Gating strategy 1. Contour plots of windows and gating strategy used for the identification of major immune cell populations in pneumococcal infected mouse lungs. Cells were first gated for size and singularity, followed by exclusion of dead cells. Gates containing multiple cell populations other than single cell gates are numbered G1-G6. Gates containing single cell populations are labelled with the cell types that include: T cells, B cells, natural killer cells, neutrophils, eosinophils, inflammatory monocytes, resident monocytes, alveolar macrophages, interstitial macrophages, CD11b^{-} dendritic cells (CD11b^{-} DC), and CD11b^{+} dendritic cells (CD11b^{+} DC).

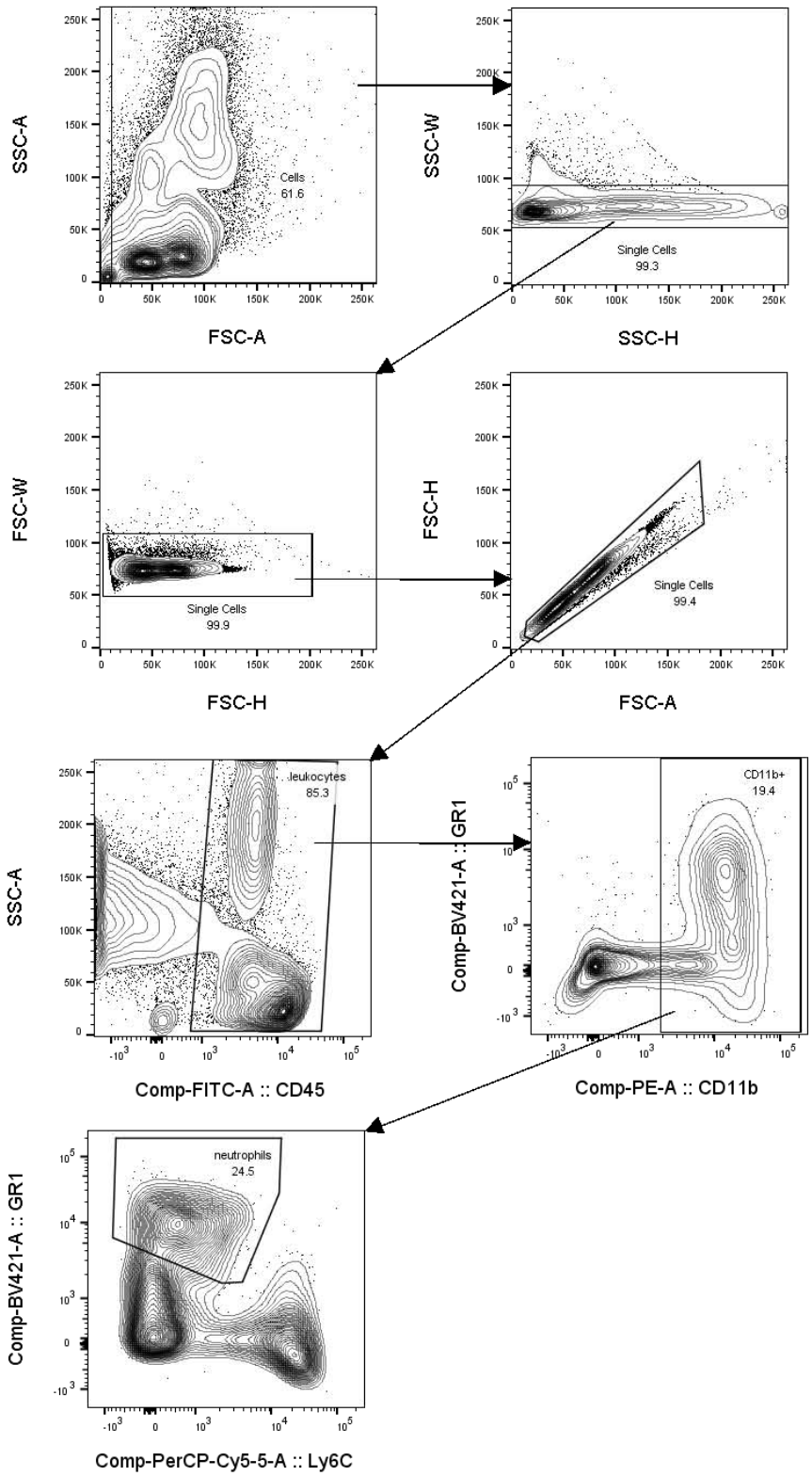

Appendix Z. Gating strategy 2. Contour plots of windows and gating strategy used to validate anti-Ly6G mediated neutrophil depletion. Cells were first gated for size and singularity, followed by gating for leukocytes. CD11b^{+} cells were then gated for, and subsequently neutrophils were detected as GR1$^{int/hi}$ and Ly6C^{int}.

Statement of Authorship

Title of Paper	Capacity To Utilize Raffinose Dictates Pneumococcal Disease Phenotype
Publication Status	☑ Published ☐ Accepted for Publication ☐ Submitted for Publication ☐ Unpublished and Unsubmitted work written in manuscript style
Publication Details	V. Minhas *et al.*, "Capacity To Utilize Raffinose Dictates Pneumococcal Disease Phenotype," *mBio*, vol. 10, no. 1, pp. e02596-18, Feb. 2019, doi: 10.1128/mBio.02596-18

Principal Author

Name of Principal Author (Candidate)	Vikrant Minhas
Contribution to the Paper	Designed and performed experiments, performed analysis on all data and aided in writing the manuscript
Overall percentage (%)	80
Certification:	This paper reports on original research I conducted during the period of my Higher Degree by Research candidature and is not subject to any obligations or contractual agreements with a third party that would constrain its inclusion in this thesis. I am the primary author of this paper.
Signature	Date: 24/03/2020

Co-Author Contributions

By signing the Statement of Authorship, each author certifies that:

i. the candidate's stated contribution to the publication is accurate (as detailed above);

ii. permission is granted for the candidate in include the publication in the thesis; and

iii. the sum of all co-author contributions is equal to 100% less the candidate's stated contribution.

Name of Co-Author	Richard M. Harvey
Contribution to the Paper	Supervised development of work and aided in experiments, data analysis and manuscript writing
Signature	Date: 25/3/2020

Name of Co-Author	Lauren J. McAllister
Contribution to the Paper	Aided in experiments and manuscript editing
Signature	Date: 24/03/2020

Please cut and paste additional co-author panels here as required.

Name of Co-Author	Torsten Seemann		
Contribution to the Paper	Constructed genome sequences and data management		
Signature		Date	18/05/2020

Name of Co-Author	Anna E. Syme		
Contribution to the Paper	Constructed genome sequences and data management		
Signature		Date	24/03/2020

Name of Co-Author	Sarah L. Baines		
Contribution to the Paper	Constructed genome sequences and data management		
Signature		Date	24/03/2020

Name of Co-Author	James Paton		
Contribution to the Paper	Conceived and designed the study, supervised development of work, aided in data interpretation and manuscript writing, and was corresponding author		
Signature		Date	24/03/2020

Name of Co-Author	Claudia Trappetti		
Contribution to the Paper	Conceived and designed the study, supervised development of work, aided in experiments, data interpretation and manuscript writing		
Signature		Date	30/4/2020

RESEARCH ARTICLE
Host-Microbe Biology

Capacity To Utilize Raffinose Dictates Pneumococcal Disease Phenotype

Vikrant Minhas,[a] Richard M. Harvey,[a] Lauren J. McAllister,[a] Torsten Seemann,[b,c] Anna E. Syme,[b] Sarah L. Baines,[c] James C. Paton,[a] Claudia Trappetti[a]

[a]Research Centre for Infectious Diseases, Department of Molecular and Biomedical Science, University of Adelaide, Adelaide, Australia
[b]Melbourne Bioinformatics, The University of Melbourne, Melbourne, Australia
[c]Department of Microbiology and Immunology, The University of Melbourne, Melbourne, Australia

ABSTRACT *Streptococcus pneumoniae* is commonly carried asymptomatically in the human nasopharynx, but it also causes serious and invasive diseases such as pneumonia, bacteremia, and meningitis, as well as less serious but highly prevalent infections such as otitis media. We have previously shown that closely related pneumococci (of the same capsular serotype and multilocus sequence type [ST]) can display distinct pathogenic profiles in mice that correlate with clinical isolation site (e.g., blood versus ear), suggesting stable niche adaptation within a clonal lineage. This has provided an opportunity to identify determinants of disease tropism. Genomic analysis identified 17 and 27 single nucleotide polymorphisms (SNPs) or insertions/deletions in protein coding sequences between blood and ear isolates of serotype 14 ST15 and serotype 3 ST180, respectively. SNPs in raffinose uptake and utilization genes (*rafR* or *rafK*) were detected in both serotypes/lineages. Ear isolates were consistently defective in growth in media containing raffinose as the sole carbon source, as well as in expression of raffinose pathway genes *aga*, *rafG*, and *rafK*, relative to their serotype/ST-matched blood isolates. Similar differences were also seen between serotype 23F ST81 blood and ear isolates. Analysis of *rafR* allelic exchange mutants of the serotype 14 ST15 blood and ear isolates demonstrated that the SNP in *rafR* was entirely responsible for their distinct *in vitro* phenotypes and was also the determinant of differential tropism for the lungs versus ear and brain in a mouse intranasal challenge model. These data suggest that the ability of pneumococci to utilize raffinose determines the nature of disease.

IMPORTANCE *S. pneumoniae* is a component of the commensal nasopharyngeal microflora of humans, but from this reservoir, it can progress to localized or invasive disease with a frequency that translates into massive global morbidity and mortality. However, the factors that govern the switch from commensal to pathogen, as well as those that determine disease tropism, are poorly understood. Here we show that capacity to utilize raffinose can determine the nature of the disease caused by a given pneumococcal strain. Moreover, our findings provide an interesting example of convergent evolution, whereby pneumococci belonging to two unrelated serotypes/lineages exhibit SNPs in separate genes affecting raffinose uptake and utilization that correlate with distinct pathogenic profiles *in vivo*. This further underscores the critical role of differential carbohydrate metabolism in the pathogenesis of localized versus invasive pneumococcal disease.

KEYWORDS *Streptococcus pneumoniae*, carbohydrate metabolism, otitis media, pneumonia, single nucleotide polymorphisms, virulence

Citation Minhas V, Harvey RM, McAllister LJ, Seemann T, Syme AE, Baines SL, Paton JC, Trappetti C. 2019. Capacity to utilize raffinose dictates pneumococcal disease phenotype. mBio 10:e02596-18. https://doi.org/10.1128/mBio.02596-18.

Editor Larry S. McDaniel, University of Mississippi Medical Center

Address correspondence to James C. Paton, james.paton@adelaide.edu.au, or Claudia Trappetti, claudia.trappetti@adelaide.edu.au.

This article is a direct contribution from a Fellow of the American Academy of Microbiology. Solicited external reviewers: Jeffrey Weiser, NYU Lagone Health; Andrew Camilli, Tufts University School of Medicine.

Received 22 November 2018
Accepted 29 November 2018
Published 15 January 2019

Streptococcus pneumoniae (the pneumococcus) is one of the world's foremost bacterial pathogens, killing 1 to 2 million people each year. In spite of this, it is considered part of the "normal" nasopharyngeal microflora, asymptomatically colonizing up to 65% of individuals; these carriers are the principal reservoirs for transmission of *S. pneumoniae* in the community (1, 2). In a small proportion of carriers, which nevertheless translates into globally significant numbers, *S. pneumoniae* invades from its nasopharyngeal reservoir to cause disease: e.g., by aspiration into the lungs to cause pneumonia, by direct or indirect invasion of the blood (bacteremia) or central nervous system (meningitis), or by ascension of the eustachian tube to access the middle ear and cause otitis media (OM) (1, 2). However, the molecular mechanisms whereby pneumococci transition from a commensal lifestyle to cause either localized or invasive disease are poorly understood.

The pneumococcus is a genetically plastic and diverse species, comprising at least 98 capsular serotypes, superimposed on more than 12,000 clonal lineages (sequence types [STs]) recognizable by multilocus sequence typing (3). It has a core genome of roughly 1,500 genes, with the remaining 30% of the genome present as accessory regions (ARs), present in some but not all clonal lineages. Individual *S. pneumoniae* strains can differ markedly in their virulence phenotypes, including their capacity to colonize the nasopharynx, spread from person to person, or progress to either localized or invasive infections. Capsule switching experiments have shown that both serotype and genetic background (i.e., ST) influence virulence (4, 5), but strain complexity has complicated attempts to examine whether there is any association between a given clonal lineage or serotype and propensity to cause localized rather than invasive infections.

Previous studies in our laboratory have shown that *S. pneumoniae* clinical isolates belonging to the same serotype and ST may display distinct virulence phenotypes in mice, in accordance with their original site of isolation in humans (blood versus ear). After intranasal (i.n.) challenge, serotype 3 blood isolates belonging to ST180, ST232, and ST233 did not stably colonize the nasopharynx, but spread to the blood in the majority of mice; none spread to the ear. In contrast, ear isolates colonized the nasopharynx at higher levels than the respective ST-matched blood isolates and also spread to the ear compartment; none caused bacteremia (6). In a separate study, serotype 14 (ST15) blood and ear isolates all exhibited a similar capacity to colonize the nasopharynx, but significant differences were observed between bacterial loads in other host niches. Blood isolates caused pneumonia in most animals, whereas ear isolates were not detected in the lungs of any of the mice 24 h post-intranasal challenge. Conversely, ST15 ear isolates, but not blood isolates, were able to spread to the brain, and in the ear compartment, the bacterial load and proportion of infected mice were significantly greater for mice challenged with ear rather than blood isolates (7). Thus, strains within a clonal lineage appear to be exhibiting stable niche adaptation.

Although members of the same serotype and ST type have very closely related genetic backbones, they are not necessarily identical and may have acquired distinct ARs or other genetic changes, such as single nucleotide polymorphisms (SNPs) or insertions or deletions (indels). In the present study, we have compared the genomes of representative serotype 14 ST15 and serotype 3 ST180 blood and ear isolates to determine whether such differences can account for their distinct virulence phenotypes. We show that SNPs in loci responsible for uptake and utilization of the trisaccharide raffinose are the ultimate determinant of disease progression.

RESULTS

Genetic differences between serotype/ST-matched blood and ear isolates. In the first instance, draft genomes of serotype 14 ST15 strains 4559 (blood isolate) and 947 (ear isolate) were assembled from PacBio and MiSeq data and then compared (see Materials and Methods). The only differences in ARs were the presence of a 35-kb prophage and a 3.2-kb plasmid in 4559 and not 947, but these ARs were not present in other serotype 14 ST15 blood isolates in our collection (results not shown). Seven-

TABLE 1 Genes containing indels or SNPs that led to amino acid changes, identified from the whole-genome variant calling analysis between 4559 and 947[a]

Locus tag in 947	Gene	Product	Change in aa sequence in 4559 relative to 947
0862	*pfkA*	ATP-dependent 6-phosphofructokinase	S212G
1153	*glgA*	Glycogen synthase	E174G
1345	*pncB*	Nicotinate phosphoribosyltransferase	N434D
1631	*scrR*	HTH-type transcriptional regulator	ΔL27-G28
1803	***rafR***	**HTH-type transcriptional regulator**	**D249G**
1255	*pyrP*	Uracil permease	V65A
1737	*piuA*	Fe^{3+} import ATP-binding protein	G141V
2020		ABC transporter ATP-binding protein	Y508N
0330	*cpsE*	CPS glycosyltransferase	L43P
1139	*iga*	Immunoglobulin A1 protease	Premature stop 1905 (4559) due to indel
1594	*nanB*	Sialidase B	Premature stop 362 (947) due to indel
1741	*pfbA*	Plasmin and fibronectin-binding protein A	T318M
0945	*coiA*	Competence protein	E78K
1141	*addA*	ATP-dependent helicase/nuclease subunit A	I980M
1060		Acetyl transferase	C101G
1194		Cytosolic protein containing multiple CBS domains	Premature stop 104 (947) due to SNP
1731		Hypothetical protein (no Pfam match)	H32P

[a]Results for the raffinose pathway gene *rafR* are in boldface.

teen SNPs and indels present within protein coding sequences of 4559 and 947 resulting in a change in the predicted amino acid sequence are listed in Table 1. The genes affected included those predicted to be involved in metabolism and energy production, transcriptional regulation, transporters, and putative virulence factors. Among the latter category, an SNP resulting in a L43P substitution was identified in *cpsE*, which encodes the glycosyl transferase that initiates assembly of the capsular polysaccharide (CPS) repeat unit. However, we have previously shown that there is no difference in total CPS production between 4559 and 947 (7). The SNP in the putative plasmin and fibronectin-binding protein gene *pfbA* is also a conservative T318M substitution. The protein encoded by *iga* is truncated in 4559 compared to 947, but only by four amino acids. On the other hand, the *nanB* sequence in 947 has a premature stop codon that truncates the protein by 330 amino acids (47% of the 4559 protein), presumably inactivating the gene product. Mutagenesis studies have previously shown that NanB contributes to colonization of both the upper and lower respiratory tract of mice, albeit to a lesser extent than the major neuraminidase NanA (8). Nevertheless, 4559 and 947 colonize the nasopharynx equally well (7). Interestingly, SNPs were identified in two metabolic genes, coding for ATP-dependent 6-phosphofructokinase (*pfkA*) and a glycogen synthase (*glgA*), as well as in two helix-turn-helix (HTH)-type transcriptional regulators, *scrR* and *rafR*, involved in metabolism of sucrose and raffinose, respectively. Given the importance of carbohydrate metabolism to *S. pneumoniae* (9), we employed a phenotypic microarray to compare the capacity of 4559 and 947 to metabolize over 100 different carbohydrates (see Materials and Methods). The only difference observed between the ear and blood isolates was a reduced capacity of the former (947) to grow in medium containing raffinose as the sole carbon source (data not shown).

Genetic differences between ear/blood isolate pairs that are common to two unrelated serotypes/ST lineages would be strong candidates for determinants of tissue tropism. Genomic comparisons were therefore also made between two serotype 3 ST180 ear and blood isolates (strains 180/2 and 180/15, respectively), which like the serotype 14 ST15 isolates, have previously been shown to exhibit distinct tissue tropism in mice in accordance with clinical isolation site (6). There were no differences in ARs between the two strains, while SNPs and indels impacting the deduced amino acid sequence for 27 genes were identified (Table 2). Interestingly, there were no affected genes in common with those in Table 1. However, an I227T SNP was detected in the serotype 3 *rafK* gene, encoding the ATP-binding protein component of the raffinose

TABLE 2 Genes containing indels or SNPs that led to amino acid changes, identified from the whole-genome variant calling analysis between 180/2 and 180/15[a]

Locus tag in 180/2	Gene	Product[b]	Change in aa sequence of 180/15 relative to 180/2
100	*purN*	Phosphoribosyl-glycinamide	G81A
254	*rpsJ*	30S ribosomal protein S10	Y58D
285		Hypothetical protein	A81S
314	*cdsA*	Phosphatidate cytidylyltransferase	M14I
335	*adhP*	Alcohol dehydrogenase 1	M210V
403	*fabK*	Enoyl-[acyl-carrier-protein] reductase	I1029T
449		Nitronate monooxygenase	I55M
512	*glnA*	Glutamine synthetase	F22L
645	*nhaK*	Sodium, potassium, lithium and rubidium/H^+ antiporter	G190D
741		VanZ family protein	C149W
996		Hypothetical protein	H38R
1121	*clcA*	H^+/Cl^- exchange transporter	M131I
1138	*ptsH*	Phosphocarrier protein HPr	I14V
1172		Formate/nitrate transporter	A211E
1194	*glnP*	Glutamine transport system permease protein	S662A
1234		SpF43_sRNA	Y31C
1306	*alaS*	Alanine-tRNA ligase	E18A
1387	*apbE*	FAD:protein FMN transferase	M52I
1404		LPXTG cell wall anchor domain-containing protein	ΔK112-Q119; G125K, E126T, P127E, E130V, K131N, I133D; ΔQ135-P178
1491	***rafK***	**Raffinose import ATP-binding protein**	**I227T**
1616	*dnaB*	DNA helicase	C375R
1760	*fepD_2*	Ferric enterobactin transport system permease protein	S248G
1863	*rpoC*	DNA-directed RNA polymerase subunit beta	D76E
1878	*acyP*	Acylphosphatase	V4I
1887	*rsgA*	Small ribosomal subunit biogenesis	G40S
2045	*aspS*	Aspartate tRNA ligase	E51V
2100	*dltD*	D-Alanyl-lipoteichoic acid biosynthesis protein	D151E

[a]Results for the raffinose pathway gene *rafK* are in boldface.
[b]FAD, flavin adenine dinucleotide; FMN, flavin mononucleotide.

ABC transporter. RafK is known to be essential for activation of other *raf* operon genes, and the SNP identified in ST180 isolates is located in the conserved regulatory domain motif 1 (10). Thus, potential defects in raffinose uptake/metabolism appear to be a common feature of ear isolates from both serotypes/lineages.

Blood isolates utilize raffinose more efficiently than ear isolates. In view of the SNPs in genes associated with raffinose metabolism between ear and blood isolates in two unrelated serotypes/STs and the fact that the serotype 14 ear and blood isolates differed only in their ability to metabolize raffinose on phenotypic microarray analysis, *in vitro* growth phenotypes were further investigated. Strains 4559 and 947, as well as another pair of serotype 14 ST15 blood and ear isolates (4534 and 51742, respectively), were grown in a chemically defined medium (CDM) with either glucose or raffinose as the sole carbon source (designated CDM+Glc and CDM+Raf, respectively) (Fig. 1). In CDM+Glc, there were no significant differences in growth rates between blood and ear isolates. However, in CDM+Raf, the two blood isolates grew at a higher rate and to a higher final culture density (optical density at 600 nm [OD_{600}]) than either of the serotype 14 ST15 ear isolates. Similarly, there was no significant difference in growth rates of the serotype 3 ST180 ear and blood isolates (180/15 and 180/2, respectively) in CDM+Glc, but the blood isolate grew better than the ear isolate in CDM+Raf (Fig. 1). Thus, defective growth in raffinose appears to be a common defect in ear isolates relative to serotype/ST-matched blood isolates.

The raffinose uptake/utilization operon in *S. pneumoniae* comprises genes encoding transcriptional regulators (*rafR* and *rafS*), an α-galactosidase (*aga*), the ABC transporter substrate-binding protein and two cognate permeases (*rafE*, *rafF*, and *rafG*), a sucrose phosphorylase (*gtfA*), and a protein of unknown function (*rafX*), as well as the ATP binding protein component of the transporter (*rafK*), which is independently located in the genome (11) (Fig. 2). To determine if the difference in ability to utilize raffinose

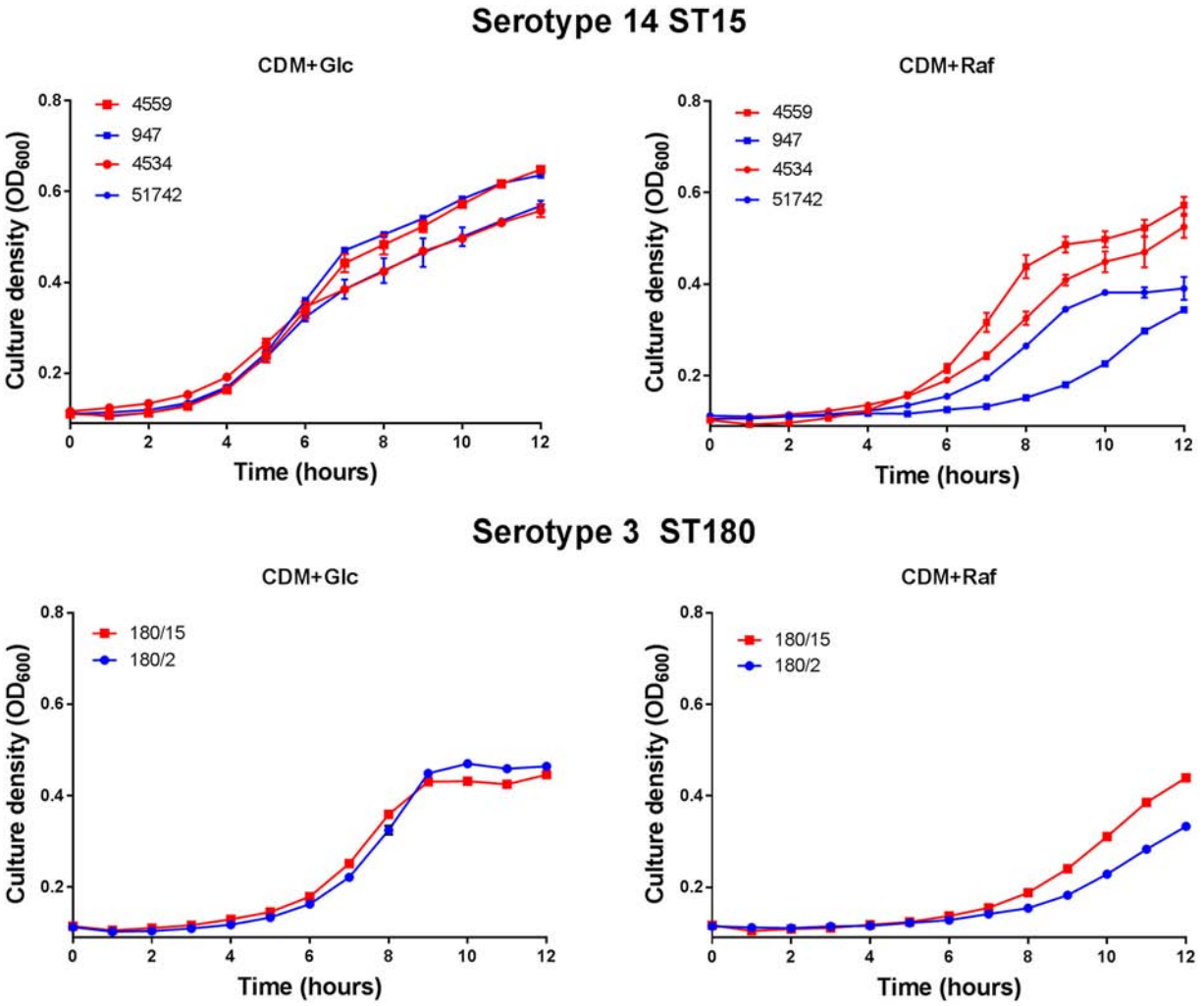

FIG 1 Differential growth of blood and ear isolates in raffinose. *S. pneumoniae* serotype 14 ST15 blood isolates 4559 and 4534 and ear isolates 947 and 51742 were grown in 200 μl CDM supplemented with 0.5% glucose (CDM+Glc) or 0.5% raffinose (CDM+Raf). Similar growth studies were also performed for serotype 3 ST180 strains 180/15 (blood isolate) and 180/2 (ear isolate). OD_{600} was measured every hour for 12 h. Data are mean OD_{600} ± standard deviation (SD) from triplicate assays.

between the blood and ear isolates corresponded with raffinose operon gene expression, *S. pneumoniae* serotype 14 ST15 strains 4559, 947, 4534, and 51742 and serotype 3 ST180 strains 180/2 and 180/15 were grown to the same OD_{600} (0.2) in CDM+Glc and then washed and resuspended in CDM+Raf and incubated for a further 30 min. RNA

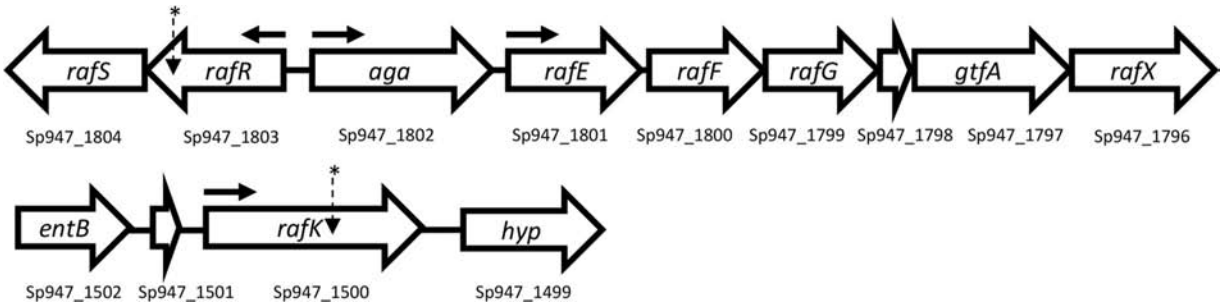

FIG 2 Genetic loci encoding raffinose uptake and utilization in *S. pneumoniae*. The numbers below each gene refer to the locus tags in the serotype 14 ST15 947 genome. The locations of SNPs in serotype 14 ST15 and serotype 3 ST180 isolates are indicated with asterisks; horizontal arrows show the locations of promoters.

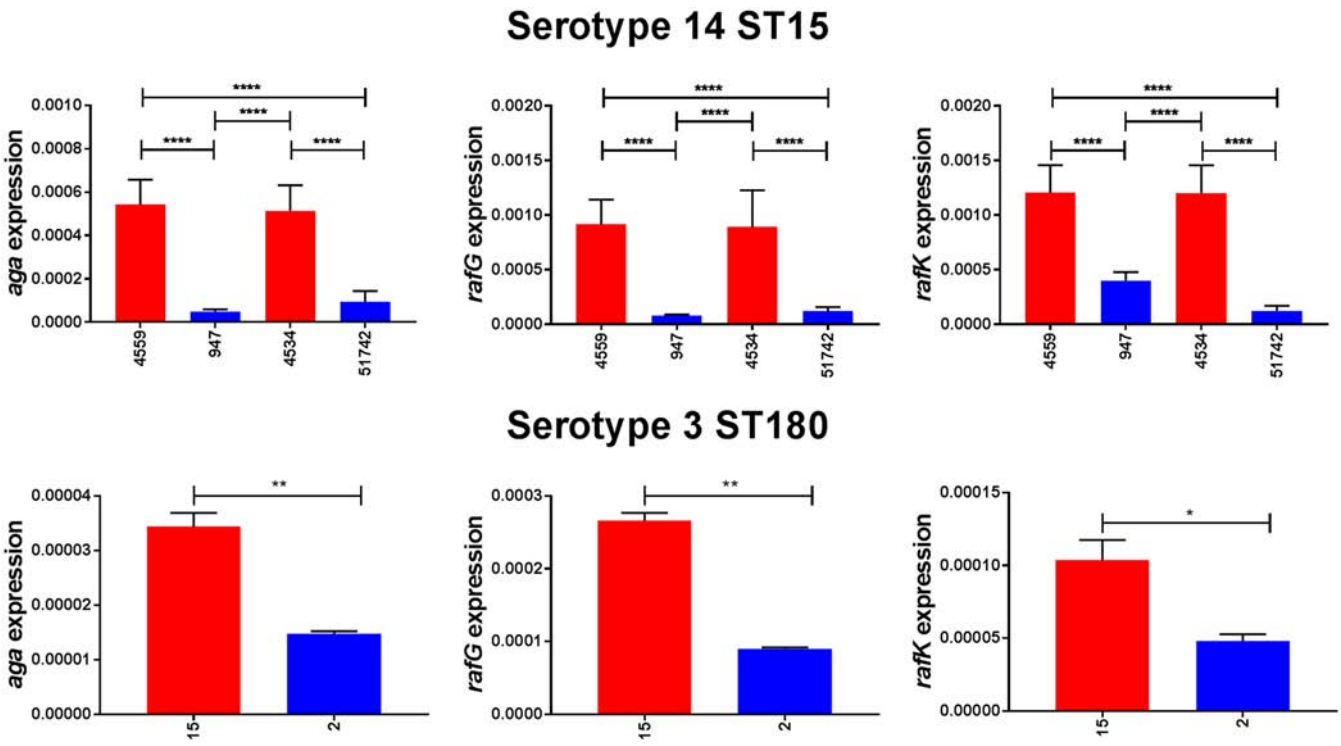

FIG 3 Expression of raffinose pathway genes by serotype 14 and 3 blood and ear isolates. The indicated strains were grown in CDM+Glc to an OD_{600} of 0.2, washed and resuspended in CDM+Raf, and then incubated at 37°C for a further 30 min. RNA was then extracted, and levels of *aga*, *rafG*, and *rafK* mRNA were analyzed by qRT-PCR using 16S rRNA as an internal control (see Materials and Methods). The data presented are the means ± SD from three independent experiments. *, $P < 0.05$, **, $P < 0.01$, and ****, $P < 0.0001$, by unpaired *t* test.

was then extracted, and levels of *aga*, *rafG*, and *rafK* mRNA, representative of each of the three *rafR*-regulated transcriptional units, were then measured relative to 16S rRNA by quantitative real-time reverse transcription-PCR (qRT-PCR). In every case, expression levels for all three genes were significantly greater in the blood isolates than in the respective ear isolates (Fig. 3).

As further confirmation, blood and ear isolates belonging to serotype 23F ST81 were also tested for growth in CDM+Glc and CDM+Raf, as well as for expression of *aga*, *rafG*, and *rafK* (Fig. 4). Again, the blood isolate grew to a higher OD_{600} than the ear isolate in CDM+Raf, but not in CDM+Glc. Moreover, expression of all three *raf* genes was significantly higher in the blood isolate than in the ear isolate.

The SNP in 947 *rafR* is responsible for its raffinose phenotype. In order to test whether the distinct *in vitro* and *in vivo* phenotype of 947 relative to 4559 was attributable to the SNP in *rafR*, allelic-exchange mutagenesis was performed in 4559 and 947, generating a 4559 derivative with its *rafR* allele replaced by that from 947 (designated $4559^{947rafR}$) and a 947 derivative expressing the 4559 *rafR* allele ($947^{4559rafR}$) (see Materials and Methods). Growth assays in CDM+Glc showed no significant differences in growth rates between 4559, 947, $4559^{947rafR}$, and $947^{4559rafR}$. However, in CDM+Raf, growth of $4559^{947rafR}$ was at least as poor as that of 947, while growth of $947^{4559rafR}$ was similar to that of 4559 (Fig. 5A). Expression of *aga*, *rafG*, and *rafK* was then examined in 4559, 947, $4559^{947rafR}$, and $947^{4559rafR}$ by qRT-PCR after 30 min of growth in CDM+Raf. For all three genes, expression levels in $947^{4559rafR}$ were indistinguishable from those in 4559, while expression in $4559^{947rafR}$ was essentially the same as that in 947 (Fig. 5B). Thus, exchange of *rafR* alleles between 4559 and 947 significantly impacts both growth phenotype and *raf* operon gene expression in CDM+Raf.

Virulence phenotypes of 4559 and 947 and their *rafR* exchange mutants. In order to determine whether the marked difference in virulence phenotypes of 4559 and

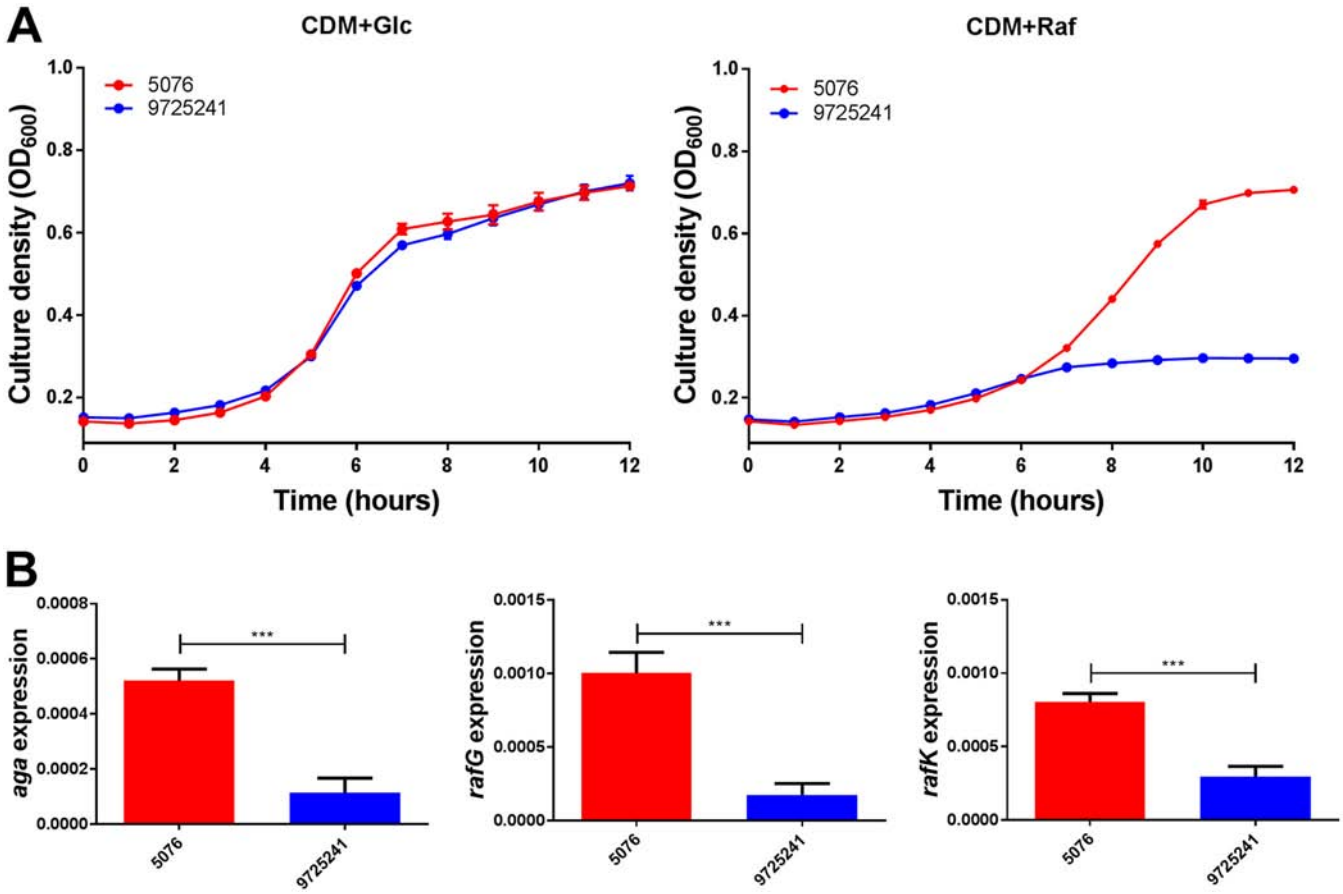

FIG 4 Growth phenotype and raffinose pathway gene expression in serotype 23F ST81 blood and ear isolates. (A) Growth of blood isolate 5076 and ear isolate 9725241 in CDM+Glc or CDM+Raf was monitored by OD_{600} for 12 h. Data are mean OD_{600} ± SD from triplicate assays. (B) The indicated strains were grown in CDM+Glc to an OD_{600} of 0.2, washed and resuspended in CDM+Raf, and then incubated at 37°C for a further 30 min. RNA was then extracted, and levels of *aga*, *rafG*, and *rafK* mRNA were analyzed by qRT-PCR using 16S rRNA as an internal control. The data presented are the means ± SD from three independent experiments. ***, $P < 0.001$ by unpaired *t* test.

947 is also directly attributable to the SNP in *rafR*, 4559, 947, $4559^{947rafR}$, and $947^{4559rafR}$ were tested in a murine intranasal challenge model. Groups of Swiss mice were challenged with 10^8 CFU of each strain, and bacterial loads were quantitated in various tissues 24 h postchallenge (Fig. 6). No significant differences in bacterial numbers in the nasopharynx were seen between any groups (Fig. 6), and no bacteria were detected in the blood of any mice (data not presented). However, 4559 was better able than 947 to persist in the lungs of infected mice, with significantly higher geometric mean (GM) bacterial load ($P < 0.0001$) and a significantly greater proportion of infected animals (14/16 versus 6/16; $P < 0.01$) (Fig. 6). On the other hand, bacterial loads of 947 in the ear were significantly greater than that for mice challenged with 4559 ($P < 0.01$), and the proportion of infected mice was also significantly greater (16/16 versus 7/16; $P < 0.001$) (Fig. 6). A similar trend was also seen in the brain (Fig. 6), in accordance with our previous report (4).

Exchanging the *rafR* alleles has a striking impact on virulence phenotype. In the lungs, both the GM CFU and proportion of infected mice for the group challenged with $4559^{947rafR}$ were significantly lower than those for the 4559 group ($P < 0.0001$ and $P < 0.001$, respectively). Indeed, the virulence phenotype of $4559^{947rafR}$ was indistinguishable from that of 947. Conversely, the GM bacterial load and proportion of infected mice for the $947^{4559rafR}$ group were significantly greater than those for the 947 group ($P < 0.01$ and $P < 0.05$, respectively); there were no significant differences in these parameters between the $947^{4559rafR}$ and 4559 groups. In the ear, both the GM

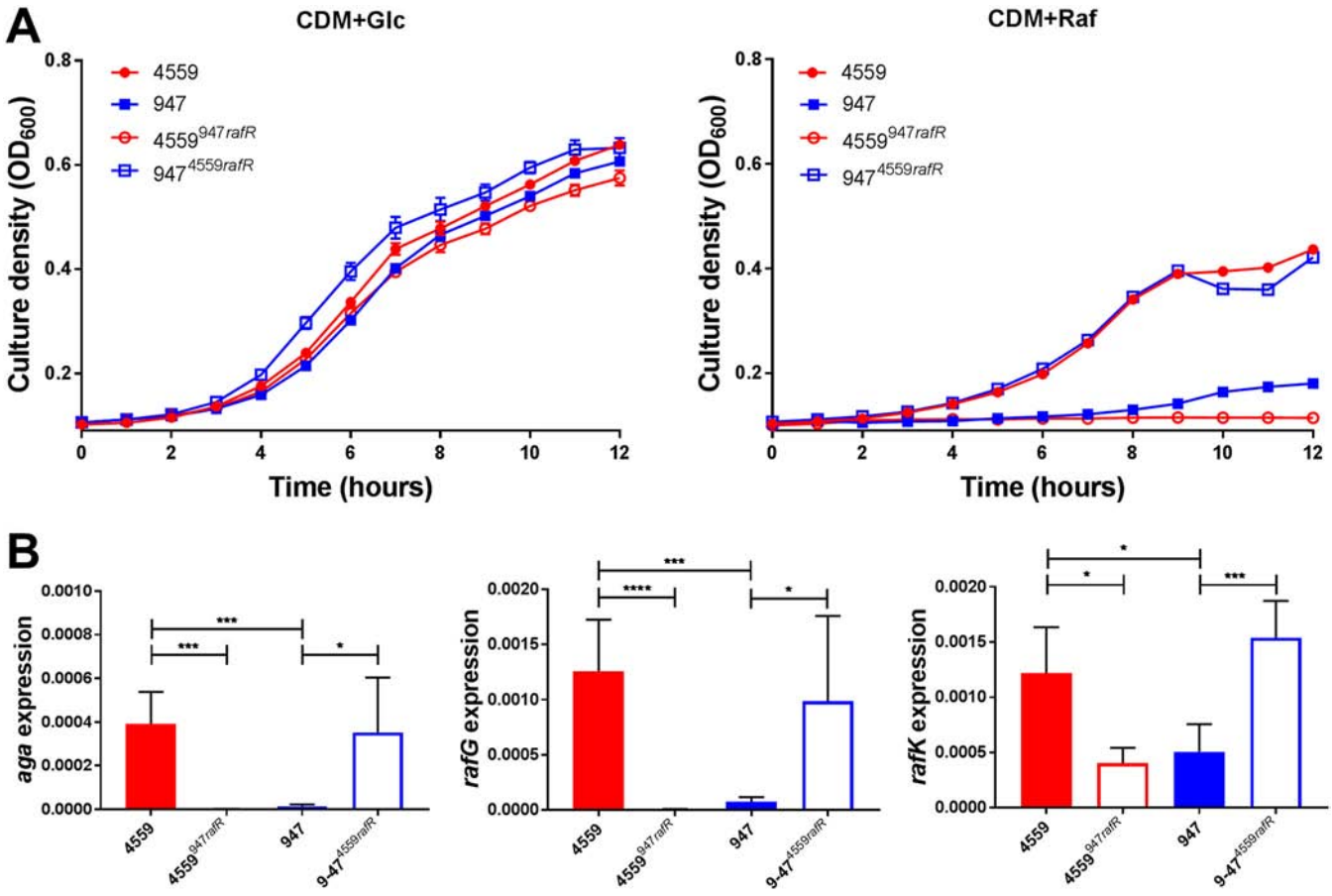

FIG 5 Growth phenotype and raffinose operon gene expression in *rafR* exchange mutants. (A) *S. pneumoniae* strains 4559, 947, $4559^{947rafR}$, and $947^{4559rafR}$ were grown in CDM+Glc or CDM+Raf, and OD_{600} was monitored for 12 h. Data are mean OD_{600} ± SD from triplicate assays. (B) The indicated strains were grown in CDM+Glc to an OD_{600} of 0.2, washed and resuspended in CDM+Raf, and then incubated at 37°C for a further 30 min. RNA was then extracted, and levels of *aga*, *rafG*, and *rafK* mRNA were analyzed by qRT-PCR. Data are the means ± SD from three independent experiments. *, $P < 0.05$, ***, $P < 0.001$, and ****, $P < 0.0001$, by unpaired *t* test.

CFU and proportion of infected mice for the group challenged with $4559^{947rafR}$ were significantly greater than those for the 4559 group ($P < 0.05$ and $P < 0.01$, respectively). Conversely, both the GM CFU and proportion of infected mice for the group challenged with $947^{4559rafR}$ were significantly lower than those for the 947 group ($P < 0.01$ in both cases). Moreover, there was no significant difference in either GM bacterial loads or proportions of infected mice between the $4559^{947rafR}$ and 947 groups or between the $947^{4559rafR}$ and 4559 groups (Fig. 6). A similar pattern is seen in the brain; the GM CFU for the $4559^{947rafR}$ group was significantly greater than those for either the 4559 or $947^{4559rafR}$ groups ($P < 0.01$ in both cases). Moreover, there was no significant difference in either GM bacterial loads or proportions of infected mice between the $4559^{947rafR}$ and 947 groups or between the $947^{4559rafR}$ and 4559 group (Fig. 6). Collectively, these data show that swapping the *rafR* allele between 4559 and 947 leads to a switch in their respective virulence profiles, and thus, the D49G SNP in *rafR* is entirely responsible for the observed difference in tissue tropisms between the serotype 14 ST15 blood and ear isolates.

Mutagenesis of *rafK* in serotype 3 ST180 blood and ear isolates. Attempts to construct *rafK* exchange mutants of serotype 3 ST180 blood and ear isolates (180/15 and 180/2, respectively) analogous to the *rafR* exchange mutants constructed for the serotype 14 strains were not successful. Thus, the impact of the SNP in RafK could not be directly tested. However, we were able to delete the native *rafK* genes from both type 3 strains (designated 180/15 Δ*rafK* and 180/2 Δ*rafK*, respectively). Both mutants

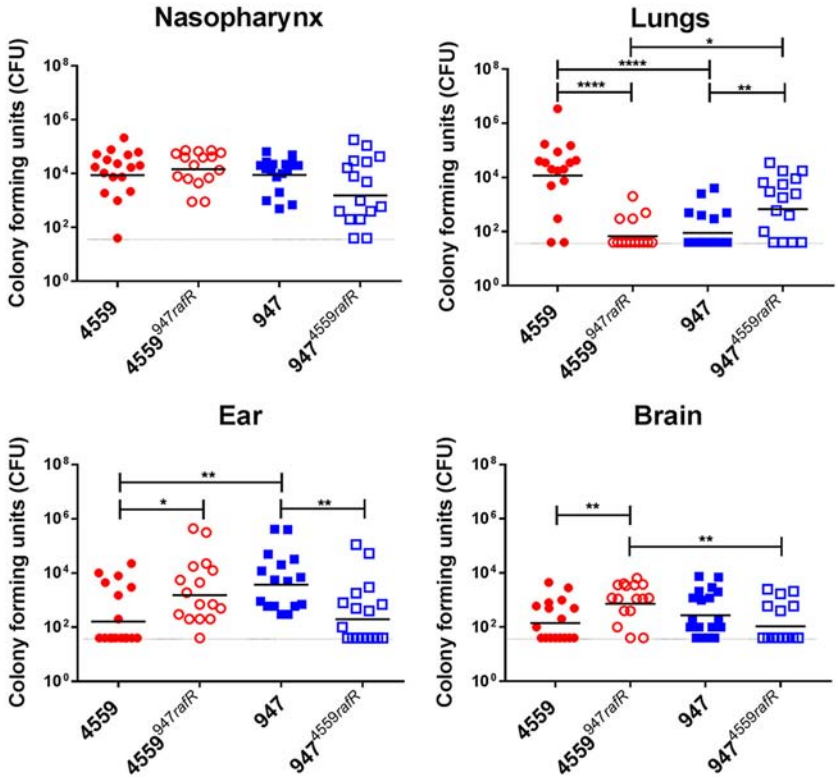

FIG 6 Virulence phenotype of *rafR* exchange mutants. Groups of 16 mice were infected intranasally with 10^8 CFU of the indicated strain. At 24 h, all mice from each group were euthanized and numbers of pneumococci in the indicated tissues/sites were quantitated (see Materials and Methods). Viable counts (total CFU per tissue) are shown for each mouse at each site; horizontal bars indicate the geometric mean (GM) CFU for each group; the broken line indicates the threshold for detection. Differences in GM bacterial loads between groups are indicated by asterisks: *, $P < 0.05$, **, $P < 0.01$, and ****, $P < 0.0001$, by unpaired *t* test.

were incapable of growth in CDM+Raf, and expression of *aga* and *rafG* was virtually undetectable by qRT-PCR; *rafK* expression was also undetectable, as expected (Fig. 7). Thus, the ear isolate 180/2 exhibits a phenotype that is intermediate between that of the blood isolate 180/15 and either of the two Δ*rafK* mutants, consistent with partial functionality of the ear isolate RafK. *S. pneumoniae rafK* deletion mutants have previously been shown to be outcompeted by the wild type in the murine lung and nasopharynx (10, 12). Similarly, in the present study, bacterial loads in the lungs, blood, ear, and brain were also lower for mice challenged with the 180/2 and 180/15 Δ*rafK* mutants relative to those challenged with the respective wild types at 48 h after intranasal challenge (result not presented). This indicates that even the intermediate level of raffinose pathway gene expression exhibited by ear isolate 180/2 contributes to virulence.

DISCUSSION

Pneumococci are strictly fermentative bacteria, relying solely on carbohydrate metabolism for energy and growth (13). However, carbohydrate availability differs between host niches, and so the ability to respond to and utilize distinct carbohydrates is crucial for pneumococcal fitness *in vivo*. The *S. pneumoniae* genome encodes 21 phosphotransferase systems (PTSs) and up to 8 ATP binding cassette (ABC) transporters for the import of carbohydrates (9, 14), accounting for roughly 30% of all transport systems. Previous studies have shown that several of these carbohydrate transporters, present in both the core and accessory genome, impact pneumococcal virulence. For example, a sucrose PTS and ABC transporter system of serotype 4 pneumococci have been shown to play roles in murine colonization and pneumonia, respectively (15),

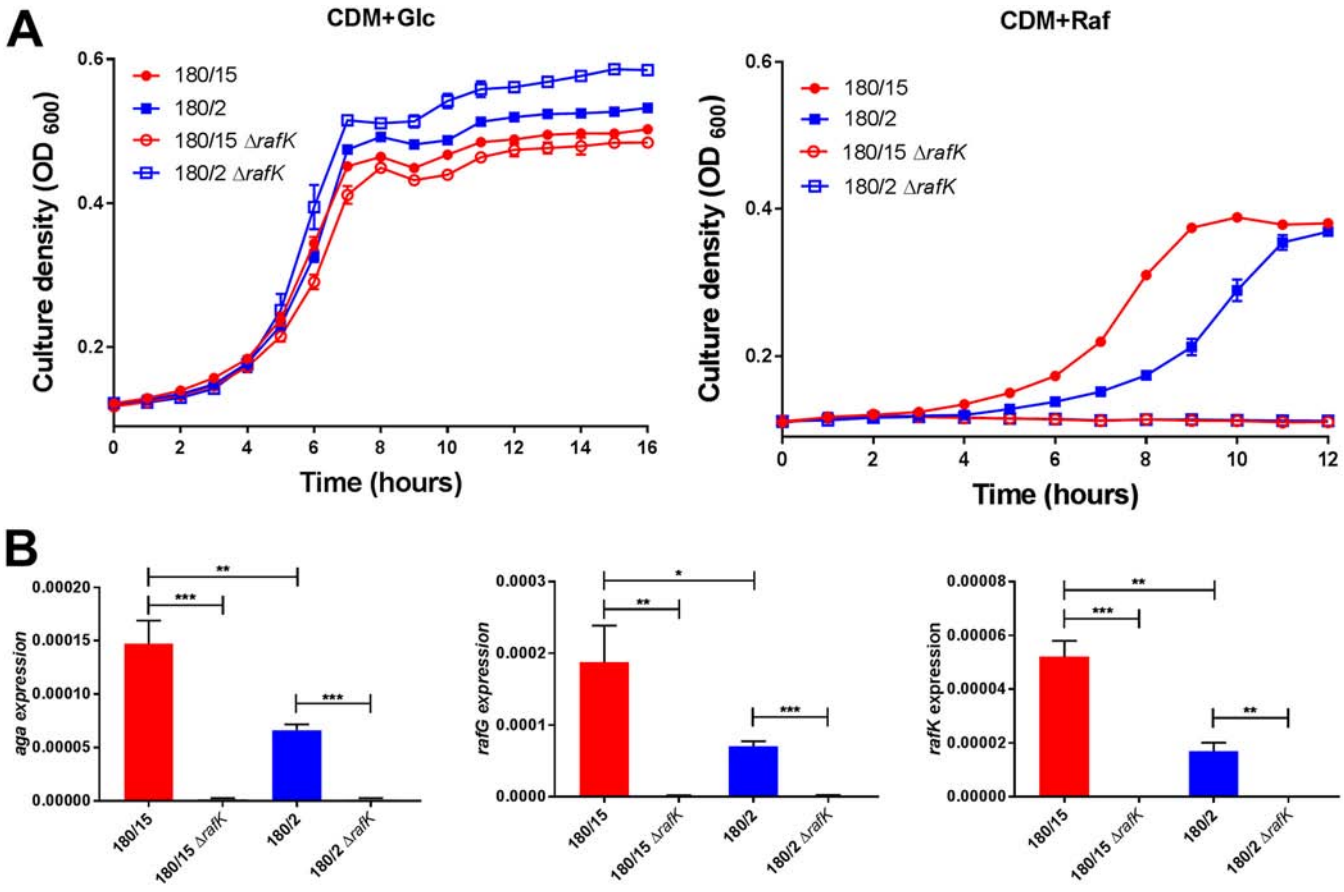

FIG 7 Growth phenotype and raffinose operon gene expression in Δ*rafK* mutants. (A) *S. pneumoniae* serotype 3 strains 180/15, 180/2, 180/15Δ*rafK*, and 180/2Δ*rafK* were grown in CDM+Glc or CDM+Raf, and OD_{600} was monitored for 12 h. Data are mean OD_{600} ± SD from triplicate assays. (B) The indicated strains were grown in CDM+Glc to an OD_{600} of 0.2, washed and resuspended in CDM+Raf, and then incubated at 37°C for a further 30 min. RNA was then extracted, and levels of *aga*, *rafG*, and *rafK* mRNA were analyzed by qRT-PCR. Data are the means ± SD from three independent experiments. *, $P < 0.05$, **, $P < 0.01$, and ***, $P < 0.001$, by unpaired *t* test.

while transporters for carbohydrates such as glucose, galactose, and mannose were shown to impact invasive pneumococcal disease (16–18).

The present study further underscores the critical role played by differential carbohydrate metabolism in pneumococcal pathogenesis. It demonstrates that reduced capacity to utilize raffinose does not simply reduce pneumococcal virulence, but rather changes the nature of disease caused. In multiple serotypes/ST lineages, ear isolates had defective growth in CDM+Raf and reduced expression of raffinose pathway genes relative to their serotype/ST-matched blood isolates. Exchange of *rafR* alleles between ear and blood isolates of serotype 14 ST15 reversed these *in vitro* phenotypes. Moreover, *rafR* exchange caused blood isolates to now cause otitis media and meningitis rather than pneumonia, after intranasal challenge, and conversely cause ear isolates to now target the lungs. This striking switch in *in vitro* and *in vivo* behaviors was attributable to a single, nonconservative SNP (D249G) in RafR, identifying this residue as one of critical functional importance. Significantly, the region of RafR from amino acids 226 to 268 comprises a conserved signature sequence for the AraC/XylS family of transcriptional regulators (11).

Interestingly, in spite of exhibiting similarly distinct *in vitro* and *in vivo* phenotypes, the serotype 3 ST180 blood and ear isolates did not share the SNP in *rafR*, but rather had an SNP in *rafK*, which encodes the ATPase required for raffinose uptake via the ABC transport system encoded by *rafEFG*. RafK-mediated uptake of raffinose has previously been shown to be essential for induction of the *raf* operons in *S. pneumoniae* D39 (10). Attempts to construct *rafK* exchange mutants in this lineage (analogous to the serotype

14 ST15 *rafR* exchange mutants) were not successful. However, *rafK* deletion mutants of both 180/2 and 180/15 were obtained. Whereas the wild-type ear isolate 180/2 exhibited reduced growth in CDM+Raf and expression of *aga*, *rafG*, and *rafK* relative to the wild-type blood isolate 180/15, both *rafK* deletion mutants were unable to grow in CDM+Raf at all, and expression of any of the *raf* operon transcripts was undetectable. Clearly, the RafK allele carried by 180/2 retains partial function. The I227T SNP that distinguishes the RafK alleles of 180/2 and 180/15 is located in the conserved regulatory domain motif 1. This domain is believed to be involved in the interaction between RafK and the enzyme dihydrolipoamide dehydrogenase (DLDH), which has been shown to modulate raffinose uptake and *raf* operon expression in *S. pneumoniae* D39 (10). In the murine model, both *rafK* deletion mutants exhibited reduced bacterial loads in multiple host niches relative to their respective wild-type strains, consistent with previous reports (10, 12).

Our findings provide an interesting example of convergent evolution, whereby pneumococci belonging to two unrelated serotypes/lineages exhibit SNPs in separate genes, each affecting raffinose uptake and utilization, which in turn correlate with distinct pathogenic profiles in both mice and humans (the latter by inference from the clinical isolation site). In *S. pneumoniae* D39, induction of expression of the *raf* operon gene *aga* required the presence of raffinose; reduced but nevertheless significant *aga* expression also occurred in a *rafR* knockout mutant (11). Thus, *raf* operon expression in pneumococci can be impacted either by defects in raffinose import (e.g., due to a defective RafK), such that insufficient exogenous raffinose (if present) is internalized to induce *raf* expression, or by functional defects in the transcriptional activator RafR, such that baseline levels of expression induced by the presence of raffinose are not further upregulated. The *raf* operons are part of the core genome of *S. pneumoniae*, and BLASTX analysis of available genomes shows that there is between 1% and 3% deduced amino acid sequence variation within any of the *raf* genes. Thus, SNPs are widespread, but it is not known which (if any) of these other SNPs impact the capacity to import or utilize raffinose or the virulence phenotype.

Notwithstanding the results presented above, the precise mechanism whereby differential raffinose uptake/utilization determines the virulence phenotype is uncertain. Raffinose is a plant-derived trisaccharide present in many staple foods, particularly beans and soy (19, 20). Although humans are unable to metabolize it, dietary raffinose is known to be absorbed by the intestinal epithelium (21), raising the possibility of at least small amounts being present on mucosal surfaces. As part of the present study, we confirmed that expression of *aga*, *rafG*, and *rafK* was not detectable by qRT-PCR when pneumococci are grown *in vitro* in media lacking raffinose. However, expression of all three genes was detected in RNA extracts of mouse lung tissue 6 h after intranasal challenge with either of the serotype 14 ST15 blood or ear isolates (results not shown). Since raffinose is the only known inducer of the *raf* operon in *S. pneumoniae*, this finding is strongly indicative of the presence of bioavailable raffinose in the murine lung. A potential complicating factor is that RafEFG is reported to be also capable of importing stachyose (14), while RafK has been reported to also energize uptake of sialic acid and maltotetraose via unrelated transporters (12). Thus, the SNPs observed in the present study could have pleiotropic effects. However, no differences in metabolism of these sugars between the serotype 14 ST15 blood and ear isolates were observed using phenotypic microarray analysis, and the serotype 3 ST180 strains were unable to grow in CDM with stachyose or sialic acid as the sole carbon source. Moreover, there was no significant difference in the growth rates of the ST180 blood and ear isolates when grown in CDM with maltotetraose (results not presented). A particularly intriguing finding of the present study was that lower raffinose uptake/utilization by the ear isolates provided an advantage over blood isolates in the ear compartment. Interestingly, exogenous raffinose has recently been shown to promote biofilm formation by *Streptococcus mutans* by promoting aggregation of extracellular DNA into the biofilm matrix. Biofilm formation was unaffected by deletion of the α-galactosidase gene *agaL*, indicating that the effect was unrelated to metabolism of any internalized raffinose (22). Thus, it is conceivable that the reduced

TABLE 3 *S. pneumoniae* strains used in this study

Strain	Description	Source	Reference
4559	Serotype 14 ST15	Blood	7
947	Serotype 14 ST15	Ear	7
4534	Serotype 14 ST15	Blood	7
51742	Serotype 14 ST15	Ear	7
$4559^{947rafR}$	4559 expressing 947 *rafR* gene		This study
$947^{4559rafR}$	947 expressing 4559 *rafR* gene		This study
180/15	Serotype 3 ST180	Blood	6
180/2	Serotype 3 ST180	Ear	6
5076	Serotype 23F ST81	Blood	This study
9725241	Serotype 23F ST81	Ear	This study

capacity of *S. pneumoniae* ear isolates to assimilate (and thereby deplete) raffinose from the middle ear mucosa may similarly promote pneumococcal biofilm formation in that niche, leading to otitis media. Further studies are in progress in our laboratory to elucidate the precise molecular mechanism whereby fine-tuning of levels of expression of raffinose uptake and utilization genes can have such a profound impact on pathogenic profiles of clinical isolates of *S. pneumoniae*.

MATERIALS AND METHODS

Bacterial strains and growth conditions. The *S. pneumoniae* strains used in this study are listed in Table 3. Cells were routinely grown in casein-based, semisynthetic liquid medium (C+Y) (23) or serum broth (SB) as required. Growth assays were performed using a chemically medium (CDM) comprising RPMI 1640 medium (Sigma), supplemented with amino acids, vitamins, choline, and catalase as described previously (24), with either 0.5% glucose or 0.5% raffinose. Bacteria were plated on Columbia agar supplemented with 5% (vol/vol) horse blood (BA) with or without gentamicin (40 μg/ml), kanamycin (500 μg/ml), or streptomycin (150 μg/ml) (as required) and incubated at 37°C in 5% CO_2 overnight. For gene expression analyses, strains were grown in CDM+Glc medium to an OD_{600} of 0.2, before being incubated in CDM+Raf for 30 min.

Genome sequencing. *S. pneumoniae* strains were grown to mid-exponential phase in Todd-Hewitt broth supplemented with 1% yeast extract. Genomic DNA (gDNA) was extracted using the Qiagen genomic DNA buffer set with 100/g Genomic Tips according to the manufacturer's instructions, except mutanolysin (20 U) and sodium deoxycholate (0.1%) were included to aid cell lysis. The gDNA was sequenced at the Ramaciotti Centre for Genomics (University of New South Wales, Sydney, Australia) on an Illumina MiSeq (250-bp paired-end reads), as well as a PacBio RSII instrument using one SMRT cell per strain, a 20-kb insert library, and the P6 polymerase and C4 sequencing chemistry.

Bioinformatic analyses. The Artemis Comparison Tool was used to compare genomes (25). MiSeq reads of 4559 and 947 and 180/15 and 180/2 were mapped to the assembled reference genome of the opposing strain with BOWTIE2 version 2.2.6 (26). Variant calling was then performed using SAMTools version 0.1.18 (27), and variants were mapped to coding sequences of the reference strain using BEDTools version 2.25.0 (28). Single nucleotide polymorphisms (SNPs) and insertions/deletions (indels) were filtered for those with scores of 100 or greater. Artemis was used to visualize SNPs and indels (29). Sanger sequencing was performed to confirm the SNPs in *rafR* and *rafK* (Australian Genome Research Facility, Adelaide).

Phenotypic microarrays. Carbon phenotype microarray analysis was performed on the serotype 14 ST 15 strains, using the PM microplates PM1 and PM2A (Biolog, Inc.), which tested for the catabolism of 190 different carbon sources. Each well of the microarrays contained a different carbon source. Briefly, cells were suspended in the provided buffer (as per the manufacturer's instructions) to an A_{590} of 0.37. One hundred microliters of this suspension was added to the wells, and the A_{590} was measured after 17 h of incubation at 37°C. Catabolism was measured through the reduction of a colorless tetrazolium dye by NADH, produced during catabolic activity. Absorbance values above 0.65 after subtraction of that for the zero carbon source blank were considered positive.

Growth assays. Each tested strain was grown in CDM supplemented with either 0.5% Glc (CDM+Glc), 0.5% Raf (CDM+Raf), or no sugar (CDM) and then incubated at 37°C for 12 h in 96-well flat bottom plates (Costar). The OD_{600} was measured every 15 min using a SPECTRAmax M2 spectrophotometer (Millennium Science). All experiments were conducted in triplicate and repeated at least two times.

qRT-PCR. Differences in levels of gene expression were assayed by one-step relative quantitative real-time RT-PCR (qRT-PCR) in a Roche LC480 real-time cycler essentially as described previously (30). The specific primers used for the various genes are listed in Table 4 and were used at a final concentration of 200 nM per reaction. As an internal control, primers specific for 16S rRNA were employed. Amplification data were analyzed using the comparative critical threshold cycle ($2^{-\Delta\Delta CT}$) method (31).

Mutagenesis. The *rafR* gene swap between serotype 14 ST15 4559 and 947 strains, to produce $4559^{947rafR}$ and $947^{4559rafR}$, was achieved via allelic exchange mutagenesis utilizing the Janus cassette, as described previously (32, 33). This involved a three-step process in which endogenous *rpsL* (which confers

TABLE 4 Oligonucleotide primers used in this study

Primer	Sequence (5′→3′)	Reference
rafR Flank F	GCGAACGTAGGTTACAATCGT	This study
rafR R j tail	GGAAAGGGGCCCAGGTCTCTCTAGCATGTGCTACCTCCTACC	This study
rafR F j tail	CATTATCCATTAAAAATCAAAGGGGAAATCCTACCAAGCTGTCTACC	This study
rafR Flank R	CGAACGTAGTTCAGTGGTAGAA	This study
Janus F	CCGTTTGATTTTTAATGGATAATG	33
Janus R	AGAGACCTGGGCCCCTTTCC	33
aga F	AAGGTCAGAATGGTCCACAG	This study
aga R	GCTGGAAAATCAGCCATAAA	This study
rafG F	CCTATGGCAGCCTACTCCATC	This study
rafG R	GGGTCTGTGGAATCGCATAGG	This study
rafK F	AACGACGTAGCTCCAAAAGA	This study
rafK R	GCTGGTTTACGTTCCAAGAA	This study
16s rRNA F	GGTGAGTAACGCGTAGGTAA	34
16s rRNA R	ACGATCCGAAAACCTTCTTC	34
rafR sanger	AGTAGAAGAGCTGGTGTTTG	This study
rafR sanger	TCTGTGACTAAGCCAGTTTC	This study
rafK Flank F	AGGACTTGGTTCTTGTTGAG	This study
rafK R ery tail	TTGTTCATGTAATCACTCCTTCCTACCATGAGGTGAACTCC	This study
rafK F ery tail	CGGGAGGAAATAATTCTATGAGATCAGTTAATCTAGGGAGAG	This study
rafK Flank R	CTCAAAGGCAACTGGACAAC	This study

streptomycin sensitivity) was first replaced with the streptomycin-resistant *rpsL1* allele by direct transformation of the blood and ear isolates. The Janus cassette (comprising a kanamycin resistance marker and a dominant counterselectable *rpsL*$^+$ marker) was then used to replace the native *rafR* gene by direct transformation with a linear PCR product comprising the Janus cassette flanked by sequences 5′ and 3′ to *rafR* (selecting on kanamycin). In the final step, the Janus cassette in Kan^r/Strep^s transformants is replaced by transformation with the alternative *rafR* allele and flanking sequences, counterselecting on streptomycin (loss of the Janus cassette reinstates the Strep^r phenotype). Gene swap constructs were confirmed by Sanger DNA sequencing (AGRF, Adelaide). The *rafK* gene was also deleted from serotype 3 ST180/2 and ST180/15 by direct transformation with a linear DNA fragment comprising an erythromycin resistance cassette flanked by sequences 5′ and 3′ to *rafK* generated by overlap PCR, essentially as previously described (34). The primers used are listed in Table 4. Mutant constructs were confirmed by PCR.

Animal studies. Animal experiments were approved by the University of Adelaide Animal Ethics Committee. Groups of outbred 6-week-old female Swiss (CD-1) mice were anesthetized by intraperitoneal injection of pentobarbital sodium (Nembutal; Rhone-Merieux) and challenged intranasally (i.n.) with 50 μl of bacterial suspension containing approximately 1×10^8 CFU in SB (7). The challenge dose was confirmed retrospectively by serial dilution and plating on BA. Mice were euthanized by CO_2 asphyxiation at 24 h, and then tissue samples (lungs, nasopharynx, brain, ear, and blood) were harvested and pneumococci enumerated in tissue homogenates as described previously via serial dilution and plating on plates containing BA plus gentamicin (35).

Data availability. Genome sequences have been deposited with ENA under accession no. SAMEA5092021, SAMEA5092022, SAMEA5092023, and SAMEA5092024, for strains 947, 4559, 180/2, and 180/15, respectively.

ACKNOWLEDGMENTS

We acknowledge the contribution of the Antibiotic Resistant Sepsis Pathogens Framework Initiative consortium (https://data.bioplatforms.com/organization/pages/bpa-sepsis/consortium) in the generation of genome sequence data used in this publication. The Initiative is supported by funding from Bioplatforms Australia through the Australian Government National Collaborative Research Infrastructure Strategy (NCRIS). We also thank Kimberley McLean for assistance with animal experiments.

This work was supported by National Health and Medical Research Council (NHMRC) Program Grant 1071659 and NHMRC Senior Principal Research Fellowship 1043070 to J.C.P. as well as Australian Research Council DECRA Fellowship DE140100963 and a University of Adelaide Beacon Fellowship to C.T. The funders had no role in study design, data collection and interpretation, or the decision to submit the work for publication.

REFERENCES

1. Kadioglu A, Weiser JN, Paton JC, Andrew PW. 2008. The role of *Streptococcus pneumoniae* virulence factors in host respiratory colonization and disease. Nat Rev Microbiol 6:288–301. https://doi.org/10.1038/nrmicro1871.

2. Weiser JN, Ferreira DM, Paton JC. 2018. *Streptococcus pneumoniae*: transmission, colonization and invasion. Nat Rev Microbiol 16:355–367. https://doi.org/10.1038/s41579-018-0001-8.

3. Enright MC, Spratt BG. 1998. A multilocus sequence typing scheme for *Streptococcus pneumoniae*: identification of clones associated with serious invasive disease. Microbiology 144:3049–3060. https://doi.org/10.1099/00221287-144-11-3049.
4. McAllister LJ, Ogunniyi AD, Stroeher UH, Leach AJ, Paton JC. 2011. Contribution of serotype and genetic background to virulence of serotype 3 and serogroup 11 pneumococcal isolates. Infect Immun 79:4839–4849. https://doi.org/10.1128/IAI.05663-11.
5. Kelly T, Dillard JP, Yother J. 1994. Effect of genetic switching of capsular type on virulence of *Streptococcus pneumoniae*. Infect Immun 62:1813–1819.
6. Trappetti C, van der Maten E, Amin Z, Potter AJ, Chen AY, van Mourik PM, Lawrence AJ, Paton AW, Paton JC. 2013. Site of isolation determines biofilm formation and virulence phenotypes of *Streptococcus pneumoniae* serotype 3 clinical isolates. Infect Immun 81:505–513. https://doi.org/10.1128/IAI.01033-12.
7. Amin Z, Harvey RM, Wang H, Hughes CE, Paton AW, Paton JC, Trappetti C. 2015. Isolation site influences virulence phenotype of serotype 14 *Streptococcus pneumoniae* strains belonging to multilocus sequence type 15. Infect Immun 83:4781–4790. https://doi.org/10.1128/IAI.01081-15.
8. Manco S, Hernon F, Yesilkaya H, Paton JC, Andrew PW, Kadioglu A. 2006. Pneumococcal neuraminidases A and B both have essential roles during infection of the respiratory tract and sepsis. Infect Immun 74:4014–4020. https://doi.org/10.1128/IAI.01237-05.
9. Buckwalter CM, King SJ. 2012. Pneumococcal carbohydrate transport: food for thought. Trends Microbiol 20:517–522. https://doi.org/10.1016/j.tim.2012.08.008.
10. Tyx RE, Roche-Hakansson H, Hakansson AP. 2011. Role of dihydrolipoamide dehydrogenase in regulation of raffinose transport in *Streptococcus pneumoniae*. J Bacteriol 193:3512–3524. https://doi.org/10.1128/JB.01410-10.
11. Rosenow C, Maniar M, Trias J. 1999. Regulation of the alpha-galactosidase activity in *Streptococcus pneumoniae*: characterization of the raffinose utilization system. Genome Res 9:1189–1197. https://doi.org/10.1101/gr.9.12.1189.
12. Marion C, Aten AE, Woodiga SA, King SJ. 2011. Identification of an ATPase, MsmK, which energizes multiple carbohydrate ABC transporters in *Streptococcus pneumoniae*. Infect Immun 79:4193–4200. https://doi.org/10.1128/IAI.05290-11.
13. Paixão L, Caldas J, Kloosterman TG, Kuipers OP, Vinga S, Neves AR. 2015. Transcriptional and metabolic effects of glucose on *Streptococcus pneumoniae* sugar metabolism. Front Microbiol 6:1041. https://doi.org/10.3389/fmicb.2015.01041.
14. Bidossi A, Mulas L, Decorosi F, Colomba L, Ricci S, Pozzi G, Deutscher J, Viti C, Oggioni MR. 2012. A functional genomics approach to establish the complement of carbohydrate transporters in *Streptococcus pneumoniae*. PLoS One 7:e33320. https://doi.org/10.1371/journal.pone.0033320.
15. Iyer R, Camilli A. 2007. Sucrose metabolism contributes to in vivo fitness of *Streptococcus pneumoniae*. Mol Microbiol 66:1–13. https://doi.org/10.1111/j.1365-2958.2007.05878.x.
16. Hava DL, Camilli A. 2002. Large-scale identification of serotype 4 *Streptococcus pneumoniae* virulence factors. Mol Microbiol 45:1389–1406.
17. Orihuela CJ, Radin JN, Sublett JE, Gao G, Kaushal D, Tuomanen EI. 2004. Microarray analysis of pneumococcal gene expression during invasive disease. Infect Immun 72:5582–5596. https://doi.org/10.1128/IAI.72.10.5582-5596.2004.
18. Ogunniyi AD, Mahdi LK, Trappetti C, Verhoeven N, Mermans D, Van der Hoek MB, Plumptre CD, Paton JC. 2012. Identification of genes that contribute to the pathogenesis of invasive pneumococcal disease by in vivo transcriptomic analysis. Infect Immun 80:3268–3278. https://doi.org/10.1128/IAI.00295-12.
19. Díaz-Batalla L, Widholm JM, Fahey GC, Jr, Castaño-Tostado E, Paredes-López O. 2006. Chemical components with health implications in wild and cultivated Mexican common bean seeds (*Phaseolus vulgaris* L.). J Agric Food Chem 54:2045–2052. https://doi.org/10.1021/jf051706l.
20. Kumar V, Rani A, Goyal L, Dixit AK, Manjaya JG, Dev J, Swamy M. 2010. Sucrose and raffinose family oligosaccharides (RFOs) in soybean seeds as influenced by genotype and growing location. J Agric Food Chem 58:5081–5085. https://doi.org/10.1021/jf903141s.
21. Lobley RW, Burrows PC, Warwick R, Dawson DJ, Holmes R. 1990. Simultaneous assessment of intestinal permeability and lactose tolerance with orally administered raffinose, lactose and L-arabinose. Clin Sci (Lond) 79:175–183. https://doi.org/10.1042/cs0790175.
22. Nagasawa R, Sato T, Senpuku H. 2017. Raffinose induces biofilm formation by *Streptococcus* mutans in low concentrations of sucrose by increasing production of extracellular DNA and fructan. Appl Environ Microbiol 83:e00869-17. https://doi.org/10.1128/AEM.00869-17.
23. Lacks S, Hotchkiss RD. 1960. A study of the genetic material determining an enzyme in Pneumococcus. Biochim Biophys Acta 39:508–518. https://doi.org/10.1016/0006-3002(60)90205-5.
24. Kloosterman TG, Bijlsma JJ, Kok J, Kuipers OP. 2006. To have neighbour's fare: extending the molecular toolbox for Streptococcus pneumoniae. Microbiology 152:351–359. https://doi.org/10.1099/mic.0.28521-0.
25. Carver TJ, Rutherford KM, Berriman M, Rajandream MA, Barrell BG, Parkhill J. 2005. ACT: the Artemis Comparison Tool. Bioinformatics 21:3422–3423. https://doi.org/10.1093/bioinformatics/bti553.
26. Langmead B, Salzberg SL. 2012. Fast gapped-read alignment with Bowtie 2. Nat Methods 9:357–359. https://doi.org/10.1038/nmeth.1923.
27. Li H, Handsaker B, Wysoker A, Fennell T, Ruan J, Homer N, Marth G, Abecasis G, Durbin R, 1000 Genome Project Data Processing Subgroup. 2009. The Sequence Alignment/Map format and SAMtools. Bioinformatics 25:2078–2079. https://doi.org/10.1093/bioinformatics/btp352.
28. Quinlan AR, Hall IM. 2010. BEDTools: a flexible suite of utilities for comparing genomic features. Bioinformatics 26:841–842. https://doi.org/10.1093/bioinformatics/btq033.
29. Rutherford K, Parkhill J, Crook J, Horsnell T, Rice P, Rajandream MA, Barrell B. 2000. Artemis: sequence visualization and annotation. Bioinformatics 16:944–945. https://doi.org/10.1093/bioinformatics/16.10.944.
30. Mahdi LK, Ogunniyi AD, LeMessurier KS, Paton JC. 2008. Pneumococcal virulence gene expression and host cytokine profiles during pathogenesis of invasive disease. Infect Immun 76:646–657. https://doi.org/10.1128/IAI.01161-07.
31. Livak KJ, Schmittgen TD. 2001. Analysis of relative gene expression data using real-time quantitative PCR and the $2^{-\Delta\Delta}CT$ method. Methods 25:402–408. https://doi.org/10.1006/meth.2001.1262.
32. Harvey RM, Hughes CE, Paton AW, Trappetti C, Tweten RK, Paton JC. 2014. The impact of pneumolysin on the macrophage response to *Streptococcus pneumoniae* is strain-dependent. PLoS One 9:e103625. https://doi.org/10.1371/journal.pone.0103625.
33. Sung CK, Li H, Claverys JP, Morrison DA. 2001. An *rpsL* cassette, Janus, for gene replacement through negative selection in *Streptococcus pneumoniae*. Appl Environ Microbiol 67:5190–5196. https://doi.org/10.1128/AEM.67.11.5190-5196.2001.
34. Trappetti C, McAllister LJ, Chen A, Wang H, Paton AW, Oggioni MR, McDevitt CA, Paton JC. 2017. Autoinducer 2 signaling via the phosphotransferase FruA drives galactose utilization by *Streptococcus pneumoniae*, resulting in hypervirulence. mBio 8:e02269-16. https://doi.org/10.1128/mBio.02269-16.
35. Trappetti C, Ogunniyi AD, Oggioni MR, Paton JC. 2011. Extracellular matrix formation enhances the ability of *Streptococcus pneumoniae* to cause invasive disease. PLoS One 6:e19844. https://doi.org/10.1371/journal.pone.0019844.

Statement of Authorship

Title of Paper	*In Vivo* Dual RNA-seq Analysis Reveals the Basis for Differential Tissue Tropism of Clinical Isolates of *Streptococcus Pneumoniae*	
Publication Status	☒ Published	☐ Accepted for Publication
	☐ Submitted for Publication	☐ Unpublished and Unsubmitted work written in manuscript style
Publication Details	V. Minhas *et al.*, "*In Vivo* Dual RNA-seq Analysis Reveals the Basis for Differential Tissue Tropism of Clinical Isolates of *Streptococcus Pneumoniae*," Nature Communications Biology 2020	

Principal Author

Name of Principal Author (Candidate)	Vikrant Minhas		
Contribution to the Paper	Conceived and designed the study, designed and performed experiments, performed analysis on data from all wet lab experiments and aided in writing the manuscript		
Overall percentage (%)	70		
Certification:	This paper reports on original research I conducted during the period of my Higher Degree by Research candidature and is not subject to any obligations or contractual agreements with a third party that would constrain its inclusion in this thesis. I am the primary author of this paper.		
Signature		Date	19/05/2020

Co-Author Contributions

By signing the Statement of Authorship, each author certifies that:

i. the candidate's stated contribution to the publication is accurate (as detailed above);

ii. permission is granted for the candidate in include the publication in the thesis; and

iii. the sum of all co-author contributions is equal to 100% less the candidate's stated contribution.

Name of Co-Author	Rieza Aprianto		
Contribution to the Paper	Performed bioinformatic analyses and aided in writing the manuscript		
Signature		Date	19/05/2020

Name of Co-Author	Lauren J. McAllister		
Contribution to the Paper	Aided in experiments and manuscript editing		
Signature		Date	20/05/2020

Name of Co-Author	Hui Wang		
Contribution to the Paper	Aided in experiments and manuscript editing		
Signature		Date	19/05/2020

Name of Co-Author	Shannon C. David		
Contribution to the Paper	Aided in experiments and manuscript editing		
Signature		Date	21/05/2020

Name of Co-Author	Kimberley T. McLean		
Contribution to the Paper	Aided in experiments and manuscript editing		
Signature		Date	19/05/2020

Name of Co-Author	Iain Comerford		
Contribution to the Paper	Designed, supervised development and aided in analysis of immunological experiments		
Signature		Date	19/05/2020

Name of Co-Author	Shaun R. McColl		
Contribution to the Paper	Designed, supervised development and aided in analysis of immunological experiments		
Signature		Date	25/05/20

Name of Co-Author	James C. Paton		
Contribution to the Paper	Supervised development of work, conceived and designed the study, and aided in writing the manuscript		
Signature		Date	19/05/2020

Name of Co-Author	Jan-Willem Veening		
Contribution to the Paper	Supervised development of work, conceived and designed the study and aided in writing the manuscript		
Signature		Date	19/05/2020

Name of Co-Author	Claudia Trappetti		
Contribution to the Paper	Supervised development of work, conceived and designed the study, aided in experiments and aided in writing the manuscript		
Signature		Date	26/5/20

COMMUNICATIONS BIOLOGY

ARTICLE

https://doi.org/10.1038/s42003-020-1018-x OPEN

In vivo dual RNA-seq reveals that neutrophil recruitment underlies differential tissue tropism of *Streptococcus pneumoniae*

Vikrant Minhas[1,4], Rieza Aprianto[2,4], Lauren J. McAllister[1], Hui Wang[1], Shannon C. David[1], Kimberley T. McLean[1], Iain Comerford[3], Shaun R. McColl[3], James C. Paton[1,5✉], Jan-Willem Veening[2,5] & Claudia Trappetti[1,5]

Streptococcus pneumoniae is a genetically diverse human-adapted pathogen commonly carried asymptomatically in the nasopharynx. We have recently shown that a single nucleotide polymorphism (SNP) in the raffinose pathway regulatory gene *rafR* accounts for a difference in the capacity of clonally-related strains to cause localised versus systemic infection. Using dual RNA-seq, we show that this SNP affects expression of bacterial genes encoding multiple sugar transporters, and fine-tunes carbohydrate metabolism, along with extensive rewiring of host transcriptional responses to infection, particularly expression of genes encoding cytokine and chemokine ligands and receptors. The data predict a crucial role for differential neutrophil recruitment (confirmed by in vivo neutrophil depletion and IL-17 neutralization) indicating that early detection of bacteria by the host in the lung environment is crucial for effective clearance. Thus, dual RNA-seq provides a powerful tool for understanding complex host-pathogen interactions and reveals how a single bacterial SNP can drive differential disease outcomes.

[1] Research Centre for Infectious Diseases, Department of Molecular and Biomedical Science, University of Adelaide, Adelaide 5005, Australia. [2] Department of Fundamental Microbiology, Faculty of Biology and Medicine, University of Lausanne, 1015 Lausanne, Switzerland. [3] Department of Molecular and Biomedical Science, University of Adelaide, Adelaide 5005, Australia. [4] These authors contributed equally: Vikrant Minhas, Rieza Aprianto. [5] These authors jointly supervised this work: James C. Paton, Jan-Willem Veening, Claudia Trappetti. ✉email: james.paton@adelaide.edu.au

Streptococcus pneumoniae is a major human pathogen responsible for massive global morbidity and mortality. Despite this, the pneumococcus makes up the part of the commensal human nasopharyngeal flora, colonizing up to 65% of individuals[1,2]. *S. pneumoniae* can invade from this reservoir to cause disease, for example, by aspiration into the lungs to cause pneumonia, by invasion of the blood (bacteremia) or central nervous system (meningitis), or by ascension of the eustachian tube to cause otitis media (OM)[1,2]. *S. pneumoniae* is an extremely heterogeneous species, comprising at least 98 capsular serotypes and over 12,000 clonal lineages (sequence types; ST) recognizable by multi-locus sequence typing[3,4]. Unsurprisingly, *S. pneumoniae* strains differ markedly in their capacity to progress from carriage to disease and/or the nature of the disease that they cause[1,2].

We have previously reported marked differences in virulence in a murine intranasal (IN) challenge model between *S. pneumoniae* strains belonging to the same serotype and ST, which correlated with clinical isolation site in humans (ear versus blood). In serotype 3 ST180, ST232, and ST233, and in serotype 14 ST15, human ear isolates had greater capacity to cause OM in mice relative to their respective serotype-/ST-matched blood isolates, while blood isolates preferentially caused pneumonia or sepsis in mice, suggesting stable niche adaptation within a clonal lineage[5,6]. Recently we have shown that although the genomes of serotype-/ST-matched blood and ear isolates differ by several single nucleotide polymorphisms (SNPs), the distinct virulence phenotypes correlated with single SNPs in genes encoding uptake and utilization of the sugar raffinose[7]. In serotype 14 ST15, the SNP was in the regulatory gene *rafR*, while in serotype 3 ST180, the SNP was in *rafK*, which encodes the raffinose ABC transporter ATPase[7]. Both SNPs result in non-conservative amino acid changes in functionally critical domains of the respective gene product (D249G for RafR; I227T for RafK). Moreover, in both serotypes/lineages, ear isolates had in vitro growth defects in a chemically-defined medium with raffinose as sole carbon source, correlating with defective transcription of raffinose pathway operons. Remarkably, in serotype 14 ST15, exchanging the *rafR* alleles between blood and ear isolates reversed both the in vitro and in vivo phenotypes[7]. Thus, the D249G SNP in *rafR* appears to be the determinant of differential virulence phenotype between the blood and ear isolates of this lineage, which may reflect differential engagement of innate host defenses and/or differential bacterial nutritional fitness in distinct host niches (Fig. 1).

Dual RNA-seq applies deep sequencing to simultaneously quantify genome-wide transcriptional responses of host and pathogen[8,9]. This approach offers higher efficiency and more restricted technical bias compared to conventional approaches, such as assaying single species or array-based methods. Here, we have used dual RNA-seq analysis to examine host-pathogen transcriptional cross-talk in the blood and ear isolates and *rafR*-swapped derivatives thereof, during the early stages of infection. Our data strongly suggest that the *rafR* SNP interacts with the pneumococcal genetic background in the different clinical isolates, which in turn, induces variegated transcriptional responses in the pathogen; this response, in turn, initiates a diverging host response that determines the outcome of infection.

Results

Comparative host/pathogen transcriptomics. Our previous studies have shown that at 6 h after IN challenge with serotype 14 ST15 *S. pneumoniae*, numbers of blood and ear isolates (strains 4559-Blood and 9–47-Ear, respectively) in murine lungs are similar (10^6–10^7 CFU per lung). However, by 24 h, the ear isolate had been cleared from the lungs, instead spreading to the ear and brain. In contrast, the blood isolate persisted in the lungs at 24 h, but did not spread to the ear or brain[6]. Thus, 6 h post infection is a critical decision point in the pathogenic process, and the similar bacterial loads in the lung at this time enables examination of host/pathogen transcriptional cross-talk without the complication of bacterial dose effects. Accordingly, groups of 12 mice were anaesthetized and challenged IN with 10^8 CFU of 4559-Blood, 9–47-Ear or their respective *rafR*-swapped mutants; at 6 h, mice were euthanized and total RNA was extracted from perfused lungs and purified. RNA from lungs of four mice was pooled for dual RNA-seq analysis in triplicate (see "Methods" section).

Within the sequencing libraries, an overwhelming majority of reads originate from the host genome (average 99.5%; range 99.1–99.7%), which translates into an average depth of 1.3 times (range 0.8–1.8 times). Conversely, 0.52% of the total reads originated from the pathogen genome (0.33–0.93%) (Supplementary Table 1). Of these pneumococcal reads, 64.5% (61.4–67.3%) mapped onto rRNA genes and 35.5% (32.7–38.6%) mapped onto non-rRNA genes. Previous data indicate that non-depleted libraries only contain 5% non-ribosomal RNA reads; thus, this treatment enriched the non-ribosomal RNAs sevenfold. Non-ribosomal read depth was 2.7 times (1.4–4.6 times) for the pathogen genome. Further downstream analysis, including

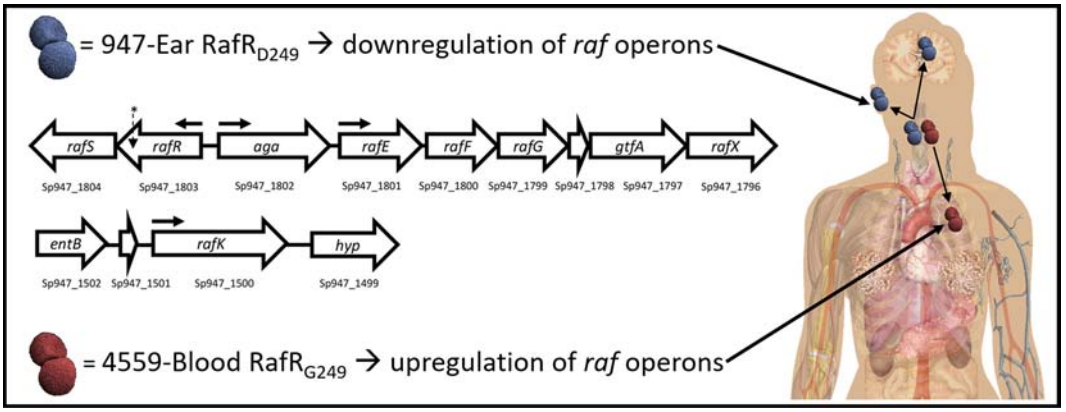

Fig. 1 Impact of *rafR* SNP. A SNP in *rafR* between the serotype 14 sequence type 15 clonal isolates 4559-Blood and 947-Ear leads to a non-conservative G249D amino acid substitution in the raffinose pathway regulator RafR. RafR$_{G249}$ results in upregulation of *raf* operons (horizontal arrows denote transcriptional start sites) in 4559-Blood relative to 947-Ear, favouring persistence in the lung after intranasal challenge. Lower *raf* pathway expression mediated by RafR$_{D249}$ facilitates clearance of 947-Ear from the lung, but promotes spread to and/or persistence in the ear and brain. The location of the SNP in *rafR* is indicated by an asterisk[7].

differential gene expression, excluded ribosomal reads from the pathogen library. Supplementary Data 1–6 list pneumococcal genes that are significantly differentially expressed (fold change (FC) > 2, $p < 0.05$) for each of the six pairwise comparisons between the four strains. Supplementary Data 7–12 list murine genes that are significantly differentially expressed (FC > 1.5, $p < 0.05$) for the same pairwise comparisons. The lower FC cut-off for murine genes was chosen to strike a balance between simplicity of analysis and sensitivity. Heat maps displaying the top 50 murine and top 50 pneumococcal genes (Fig. 2) showcase the breadth of transcriptomic rewiring due to the *rafR* SNP.

RafR fine tunes carbohydrate metabolism during infection. In order to directly compare pathogen transcriptional responses in murine lung, we listed homologous genes between the wild type ear and blood isolates and used these to visualize the transcriptional response in a principal component analysis (PCA) plot (Fig. 3a). Here, the pneumococcal transcriptional response of the ear isolate (strain 9–47-Ear, dark orange) to murine lung infection diverges considerably from the response of the blood isolate (strain 4559-Blood, dark purple). Specifically, 76 homologous genes are upregulated in the ear isolate, while 40 are upregulated in the blood isolate. Upregulated genes in strain 9–47-Ear include genes involved in carbohydrate metabolism, general stress response and nutrient transporters, while upregulated genes in the blood isolate include genes encoding small molecule permeases and nisin biosynthesis orthologous proteins.

Furthermore, replacing *rafR* of 9–47-Ear with the allele from the 4559-Blood (designated strain 9–47M) dissociates its transcriptional response considerably from its parental strain (Fig. 3a; 9–47-Ear, dark orange to 9–47M, light orange). These large scale transcriptomic differences between 9–47-Ear and 9–47M may explain the impact of the *rafR* SNP on in vivo tissue tropism. Specifically, 87 genes are upregulated in the wild type strain (9–47-Ear) while 36 genes are upregulated in the otherwise isogenic *rafR* swap strain (9–47M, Fig. 3b), with differentially expressed genes spread across the pneumococcal genome. Presence of the blood isolate *rafR* allele in 9–47-Ear activates the expression of major genes pertaining to carbohydrate metabolism, including *adhA* (alcohol dehydrogenase) and *spxB* (pyruvate oxidase), as well as genes encoding permeases, including *glnH6P6* (transporting arginine, cysteine) and *ycjOP-yesO* (transporting multiple sugars). Also, a subset of genes with function in carbohydrate metabolism are repressed in the *rafR*-swap strain, such as glycogen synthesis (*glgACD*), sucrose metabolism (*scrB*) and ribulose metabolism (*ulaDEF*). Expression of seven genes encoding ATPase subunits (*ntpABCDEGK*) and genes for iron (*piuB*) and sugar (*scrA, satABC*, and *gadEW*) permeases are also repressed.

On the other hand, replacing the blood isolate *rafR* with the ear allele (strain 4559M) does not noticeably interrupt pneumococcal transcriptional response to murine lung (Fig. 3a; 4559-Blood, dark purple to 4559M, light purple), despite the different in vivo behaviors of 4559-Blood and 4559M. Essentially, the *rafR* swap activates only two genes: *yxlF*, encoding a putative subunit of an ABC transporter and *phoU1* encoding a phosphate transporter; and represses 35 genes, mostly contained in a single genomic island (Fig. 3c, upregulated in 4559-Blood). The genomic island consists of 28 consecutive genes encoding subunits of bacteriophage(s), interspaced by *dnaC*, encoding a DNA replication protein and *lytA*, encoding autolysin. The activation of bacteriophage-associated genes indicates that the original isolate (strain 4559-Blood) endures host-derived stress, unlike the *rafR* swap mutant (strain 4559M). Other genes repressed in 4559M include *adhAE* (alcohol dehydrogenases), *gtfA* (sucrose phosphorylase) and *rafEG* (raffinose transporter). Conversely, 9–47M and 4559-Blood showcase similar in vivo behaviors yet display varied transcriptomes in murine lungs post-infection (Fig. 3a). Hence, transcriptional profiling was unable to predict tissue tropism in this case. Taken together, the single D249G SNP in *rafR* interferes with global gene expression within the already transcriptionally-distinct parental clinical isolates. This effect is more pronounced in 9–47-Ear than 4559-Blood.

Next, we performed quantified enrichment analyses on specific gene functions. Carbohydrate metabolism is enriched in the differentially expressed genes between the strains, particularly when comparing the ear isolate to its cognate *rafR* swap (Fig. 3d; *comparison A*, 9–47-Ear versus 9–47M, $p = 0.03$), comparing the two clinical isolates (*comparison B*, 9–47-Ear versus 4559-Blood, $p = 0.017$) and comparing the swap cognates (*comparison E*, 9–47M versus 4559M, $p = 0.041$). Another function, ABC transporters, is also enriched in the comparison within the ear isolates (Fig. 3e; *comparison A*, 9–47-Ear versus 9–47M, $p = 0.049$), between the original isolates (*comparison B*, 9–47-Ear versus 4559-Blood, $p = 0.014$), between ear isolate and *rafR* 746G in the blood isolate background (*comparison C*, 9–47-Ear versus 4559M, $p = 0.01$) and between the *rafR* cognates (*comparison E*, 9–47M versus 4559M, $p = 1.8 \times 10^{-4}$).

Additionally, since the pneumococcal genome has an exceptionally high number of sugar transporters[10], we quantified enrichment for this function (Fig. 3f). Sugar transporters are enriched in almost all comparisons (except between 4559-Blood and 4559M), highlighting the role of *rafR* in the widespread regulation of pneumococcal sugar importers. Specifically, ear and blood isolates behave differently in regard to sugar transporter expression (9–47-Ear versus 4559-Blood; Fig. 3f, *comparison B*). The ear isolate upregulates *scrA* (encoding a mannose and trehalose transporter) and *ulaA* (ascorbate transporter), while the blood isolate upregulates *ycjOP-yesO* (alternative sugar transporters), *rafE* (raffinose transporter) and *malFG* (maltose transporter). Furthermore, *rafR* swap in the ear isolate background (9–47-Ear versus 9–47M; Fig. 3f, *comparison A*) reduces the expression of *gadEW* (encoding sorbose and mannose transporter), *satABC* (arabinose and lactose transporter), *ulaAC* and *glpF* (glycerol transporter), while the swap activates the expression of *ycjOP-yesO* and *bguD* (encoding complex polysaccharide transporters). In contrast, *rafR* swap in the blood isolate background (4559-Blood versus 4559M; Fig. 3f, *comparison F*) downregulates the expression of *rafEG* and *malD* (maltose transporter). The enrichment analysis reveals that the D249G SNP in *rafR* directly and indirectly affects the expression of genes encoding sugar transporters, other (ABC) transporters and carbohydrate metabolism.

We also identified genes that were commonly up or down-regulated between the strains with a given virulence phenotype (Supplementary Table 2). *adhP* (Sp947_00279) was upregulated in both strains that persisted in lungs (9–47M and 4559-Blood), while eight genes from the genomic region Sp947_0842 to Sp947_0855, as well as Sp947_00631 and Sp947_02096, were upregulated in strains that were cleared from lungs by 24 h (9–47-Ear and 4559M). These genes include neuraminidase *nanB*, and alpha-glycerophosphate oxidase *glpO* (Supplementary Table 2). All other differentially expressed pneumococcal genes are listed in Supplementary Data 1–6.

RafR-specific rewiring of host transcriptional responses. The measured murine transcriptional response represents aggregate gene expression of all (host) cells present during pneumococcal lung infection. These include epithelial cells, endothelial cells of lung vasculature, smooth muscle cells, fibroblasts, activated, and

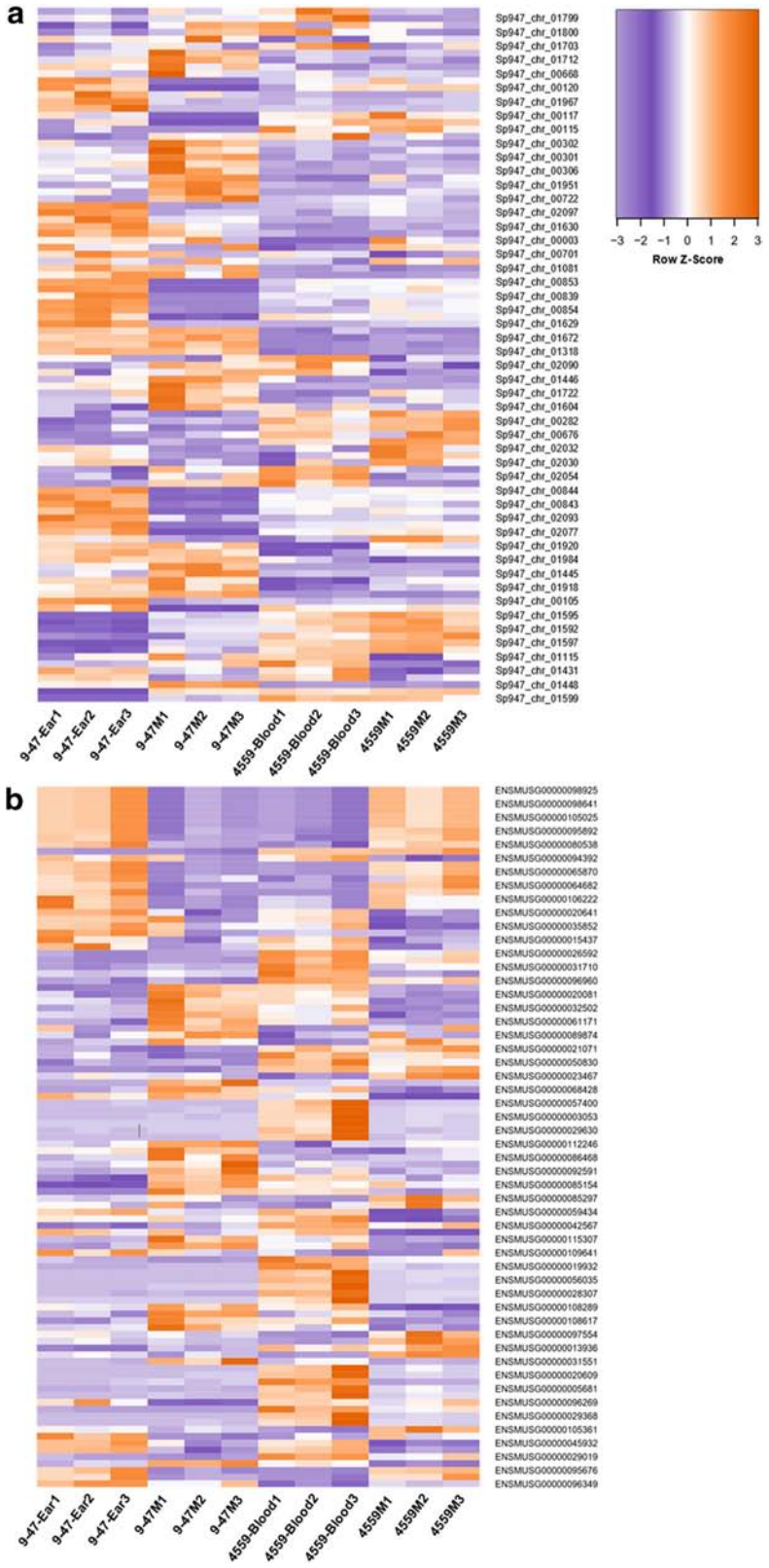

Fig. 2 Heat maps displaying differentially expressed genes from the dual RNA-seq data in murine lungs 6 h after infection with either 9–47-Ear, 4559-Blood, 9–47M, or 4559M. Purple indicates relatively low expression, while orange indicates relatively higher expression values. Top 50 differentially expressed pneumococcal (**a**) and murine (**b**) genes are shown. Fold change values of all statistically significantly expressed genes can be found in Supplementary Data 1–12.

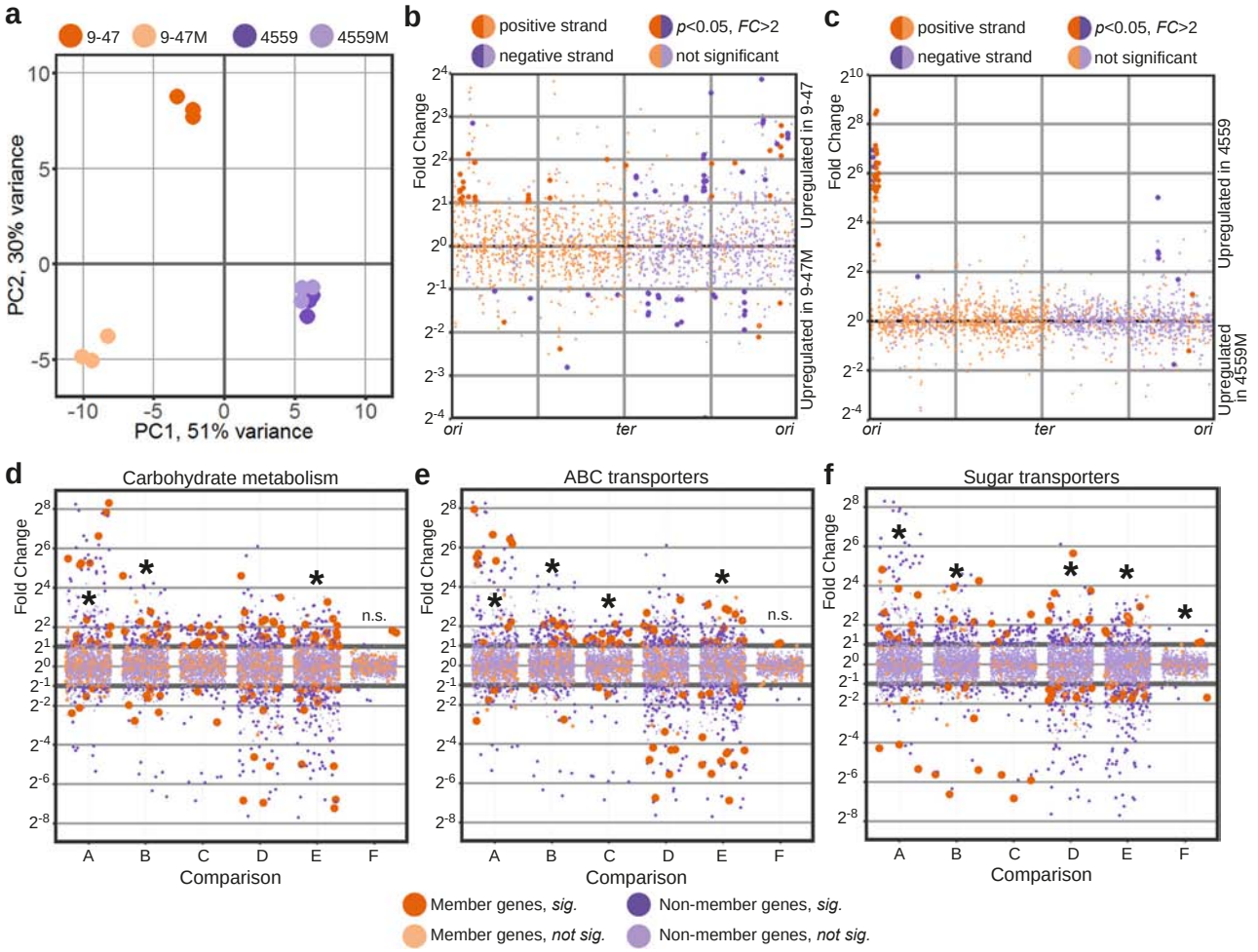

Fig. 3 Pathogen transcriptional responses in murine lung. a PCA plot showing divergence of transcriptional response to lung infection within the ear (9–47-Ear) and blood isolates (4559-Blood). *rafR* swap (9–47M) rewires pneumococcal transcriptional response only in the ear isolate background but not in the blood isolate. **b** Differential expression due to the *rafR* swap in the ear isolate background is spread throughout the pneumococcal genome. **c** Differential expression due to the *rafR* swap in the blood isolate background is limited to a genomic island. **d**–**f** Functional enrichment showed specific function being differentially expressed, including carbohydrate metabolism (**d**), ABC transporters (**e**), and sugar transporters (**f**). A: comparison of 9–47-Ear to 9–47M; B: 9–47-Ear to 4559-Blood; C: 9–47-Ear to 4559M; D: 9–47M to 4559-Blood; E: 9–47M to 4559M and F: 4559-Blood to 4559M. Asterisk (*) denotes statistically significant functional enrichment for the indicated strain–strain comparison.

non-activated immune cells. The host transcriptional response was specific to the infecting pneumococcal strain (Fig. 4a). Specifically, there was a diverging host response to the ear isolate (9–47-Ear, dark orange) and blood isolate (4559-Blood, dark purple). Interestingly, *rafR* swap in blood isolate background (4559M, light purple) mimics the lung response to the wild type ear isolate (9–47-Ear, dark orange); these two strains harbor the D249 *rafR* allele. Surprisingly, the *rafR* swap in the 9–47-Ear background (9–47M, light orange) which harbors the G249 allele, does not drive the host response to mimic those of the wild type 4559-Blood strain (dark purple) that also has the G249 allele, but rather towards a new, third position of genome-wide expression.

Genome-wide plotting of murine transcriptional responses to *S. pneumoniae* strains 9–47-Ear and 4559-Blood shows extensive rewiring of gene expression across the murine chromosomes, consistent with their different tissue tropisms in vivo (Fig. 4b). Specifically, 433 murine genes are activated upon infection by 9–47-Ear (FC > 1.5, $p < 0.05$), while 787 genes are activated by infection with 4559-Blood (FC > 1.5, $p < 0.05$). Of the 9–47-Ear-upregulated murine genes, only 37% were protein-coding, with the majority encoding pseudogenes and small RNAs. Conversely, of the 787 4559-Blood-upregulated murine genes, 80% were protein-coding, while the rest encoded small RNAs. The 4559-Blood-upregulated genes encode proteins involved in multiple pathways such as general metabolism, peroxisome proliferator-activated receptor (PPAR) signaling, steroid hormone biosynthesis and cAMP signaling. Although both strains belong to the same capsular serotype and ST[6], our data strongly suggest wildly diverging isolate-specific host responses during early infection, with the *rafR* SNP varying the host response considerably. Interestingly, the host transcriptional response to 4559M closely resembles that of 9–47-Ear (Fig. 4a), suggesting that the *rafR* SNP plays a crucial role in the distinct response to 9–47-Ear versus 4559-Blood. However, the host transcriptional response to 4559-Blood does not closely resemble the response to 9–47M, despite the similar in vivo tissue tropism these strains display. This suggests, unsurprisingly, that the host transcriptional response to pneumococcal infection does not perfectly correlate with in vivo outcomes.

In addition, *rafR* swap in the ear isolate background (9–47M) expressing the G249 *rafR* allele activates 271 murine genes (FC > 1.5, $p < 0.05$), while it represses 479 genes. The G249 *rafR*-activated genes include those involved in the Wnt signaling pathway (*Fzd2, Lgr6, Rspo1, Sost, Sox17, Wnt3a, Wnt7a*) and

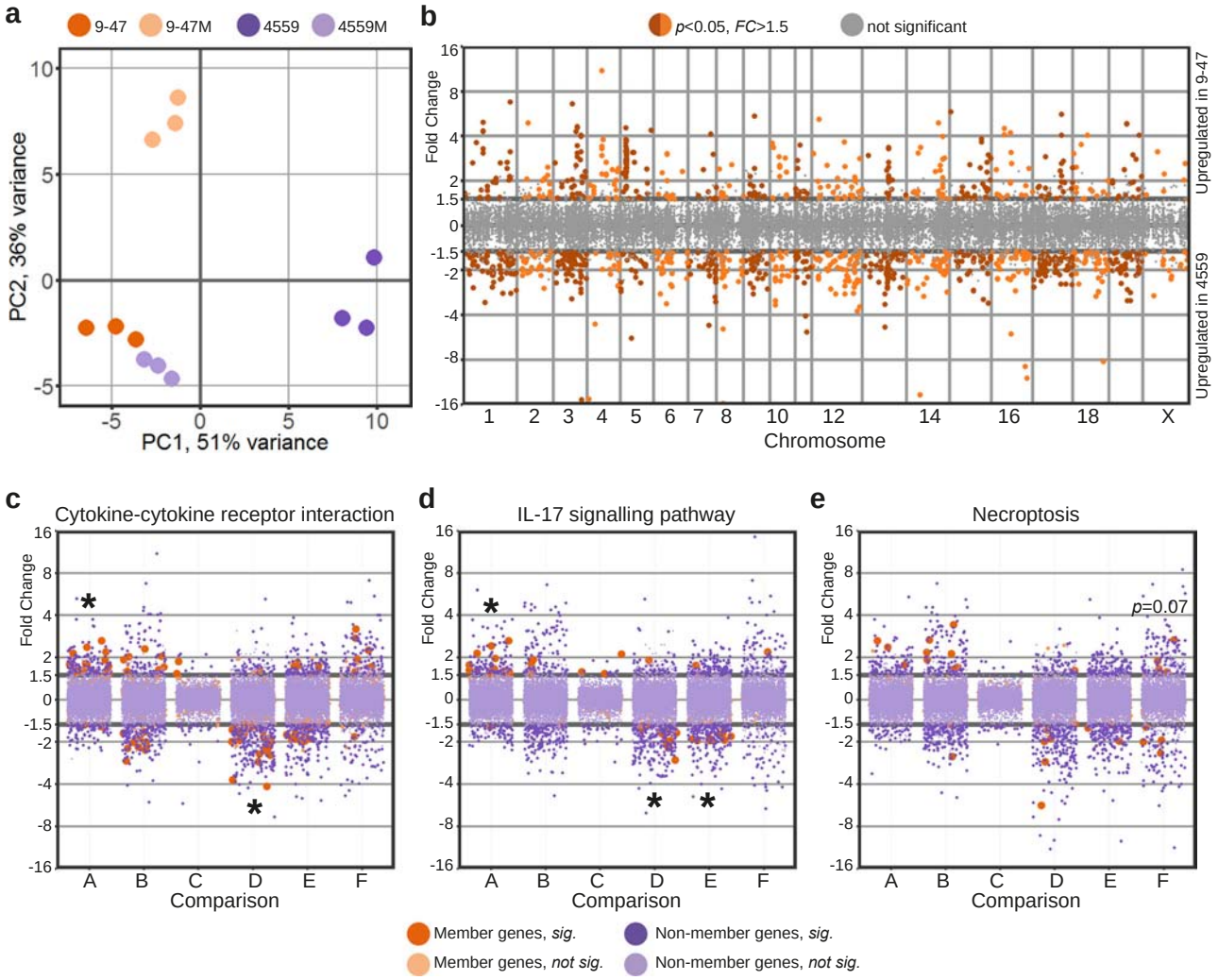

Fig. 4 The SNP in pneumococcal *rafR* drives diverging host response. a PCA plot illustrates murine lung response to the pneumococcal strains. Interestingly, host transcriptional response to *rafR* swap in blood isolate (4559M, light purple) is similar to the murine response to the original ear strain (9–47-Ear, dark orange). **b** Differential gene expression of transcriptional response to pneumococcal ear and blood isolates shows a widespread transcriptional rewiring. Specifically, 433 genes are activated in response to infection by ear isolate (9–47-Ear) while 787 genes are activated ($FC > 1.5$, $p < 0.05$) by blood isolate (4559-Blood). **c**–**e** Specific gene ontology terms are enriched in differentially expressed host genes in response to pneumococcal infection: cytokine–cytokine receptor interaction (**c**), interleukin-17 signaling pathway (**d**), and necroptosis (**e**). A: comparison between 9–47-Ear to 9–47M; B: 9–47-Ear to 4559-Blood; C: 9–47-Ear to 4559M; D: 9–47M to 4559-Blood; E: 9–47M to 4559M and F: 4559-Blood to 4559M. Asterisk (*) denotes statistically significant functional enrichment for the indicated strain–strain comparison.

general calcium signaling pathway (*Adra1a, Adra1b, Adrb3, Cckar, Grin2c, P2rx6, Tacr1, Tacr2*). Conversely, 52% of the G249 *rafR*-repressed genes in lungs infected with 9–47M encode RNA features and 18 chemokines, chemokine ligands, interferons and interleukins. On the other hand, *rafR* swap in the blood isolate background (4559M) expressing the D249 *rafR* allele activates 328 murine genes ($FC > 1.5$, $p < 0.05$), and represses 472 genes. Seventy-three percent of the D249 *rafR*-activated murine genes encode RNA features and 33 encode histone proteins. The activation of these histone proteins suggests a massive reorganization of gene regulation with numerous potential downstream impacts. In contrast, D249 *rafR*-repressed genes include genes encoding calmodulins (*Calm4, Calm13*, and *Camk2a*) and phospholipases A2 (*Pla2g4b, Pla2g4d*, and *Pla2g4f*).

Moreover, there are only 132 differentially expressed host genes in response to wild type 9–47-Ear compared to the response to strain 4559M (both having the D249 *rafR* allele), with 38 genes upregulated in strain 9–47-Ear and 94 in strain 4559M. Intriguingly, the D249 *rafR* allele (strains 9–47-Ear and 4559M) is associated with a upregulation of RNA features, including antisense, intronic, long intergenic non-coding RNAs (lincRNAs) and micro RNAs (miRNAs). The resulting abundance of RNA species in murine cells upon pneumococcal infection has the potential for even more widespread transcriptional rewiring and fine-tuning of gene products later in the infection.

A quantified functional enrichment showed that certain gene functions are enriched in the murine response to pneumococcal strains. In particular, cytokine-cytokine receptor interaction is enriched in differentially expressed host genes because of *rafR* swap in the ear isolate background (Fig. 4c, *comparison A*, 9–47-Ear versus 9–47M, $p = 9.5 \times 10^{-4}$). Concurrently, the function is enriched in differentially expressed genes between mice infected with 9–47M and those infected with 4559-Blood (*comparison D*, $p = 1.8 \times 10^{-4}$). Since both strains harbor the G249 *rafR* allele, the differentially expressed genes encoding cytokines and cytokine receptors are most likely attributable to unrelated genetic differences between the clinical isolates. Interestingly, this function is not enriched in differentially expressed genes

between the *rafR* swap in the blood isolate background (4559M) and the wild type 9–47-Ear (*comparison C*), both of which have the D249 *rafR* allele. Genes encoding chemokine ligands (*Cxcl2, Cxcl3, Cxcl10*, and *Ccl20*), interleukin 17F (*Il17f*), interferon beta (*Ifnb1*) and a receptor of TNF (*Tnfrsf18*) are the common differentially expressed genes in lungs of mice infected with 9–47-Ear, 9–47M, and 4559-Blood, with ascending expression from responses to 9–47M, 9–47-Ear and 4559-Blood. Other genes encoding chemokine ligands (*Ccl3, Ccl4, Ccl17, Ccl24, Cxcl5, Cxcl11*, and *Xcl1*), interleukins (*Il1rn* and *Il13ra2*) and interferon gamma (*Ifng*) are more highly expressed in the ear isolate-infected lung (9–47-Ear) than in lungs infected by the *rafR* swap ear isolate (9–47M). Finally, genes encoding chemokine receptors (*Ccr1* and *Ccr6*), interleukin receptors (*Il1r2, Il10ra, Il17a, Il18rap, Il20ra, Il20rb, Il22*, and *Il23r*), and interleukins (*Il1f5, Il1f6, Il1f8*, and *Il6*) are more highly expressed in lungs infected by 4559-Blood compared to the *rafR* swap in the ear isolate background (9–47M).

Interleukin 17, as part of the cytokine response, activates multitudes of downstream targets in defense against infectious agents[11], and thus plays a central role in host response to pneumococcal infection. Here, we observe the same pattern of diverging activation among murine responses to the pneumococcal strains (Fig. 4d), with IL-17-associated genes being enriched in differentially expressed genes among the host transcriptional response to the *rafR* swap in the ear isolate background (*comparison A*, 9–47-Ear versus 9–47M, $p = 9.5 \times 10^{-4}$). These genes are also enriched amongst the host response to pneumococcal strains with the G249 *rafR* allele (*comparison D*, 9–47M versus 4559-Blood, $p = 7.5{\times}10^{-4}$) and to the *rafR* swap cognates (*comparison E*, 9–47M versus 4559M, $p = 0.022$). However, there was no enrichment of IL-17 associated genes amongst the host response to pneumococcal strains with the D249 *rafR* allele (*comparison C*, 9–47-Ear versus 4559M). Common differentially expressed genes of this function include genes encoding interleukin 17F (*Il17f*) and chemokine ligands (*Cxcl2, Cxcl3* and *Ccl20*), with ascending expression level of response to 9–47M, 9–47-Ear, and 4559-Blood. Specifically, the products of these genes regulate the recruitment of neutrophils and activate immune responses to extracellular pathogens.

In addition to the above, necroptosis, a programmed cell death, exhibits a trend for its enrichment ($p = 0.07$) in differentially expressed murine genes because of the *rafR* swap in the blood isolate background (Fig. 4e, *comparison F*, 4559-Blood versus 4559M). Genes encoding histone cluster 2 (*Hist2h2ac, Hisr2-h2aa1, Hist2h2aa2*, and *H2afx*) are more highly expressed in murine lungs infected with 4559-Blood, while those encoding phospholipases A2 (*Pla2g4b, Pla2g4f*, and *Pla2g4d*) and a subunit of calcium/calmodulin-dependent protein kinase II (*Camk2a*) are more highly expressed in the transcriptional response to the *rafR* swap in the blood isolate background (4559M).

Validation of host/pathogen transcriptomics. To validate the findings from the dual RNA-seq, quantitative real time RT-PCR was performed on the same RNA samples from the lungs 6 h post-infection. 19 pneumococcal and 18 murine genes were chosen for this validation, with the primers used listed in Supplementary Table 3. A total of 76 pneumococcal and 72 murine gene Log_2 FC comparisons were performed, with a high degree of correlation observed for both pneumococcal ($R^2 > 0.73$, Pearson) and murine genes ($R^2 > 0.81$, Pearson) (Fig. 5a). To validate the reproducibility of the dual RNA-seq data, lung RNA samples 6 h post-infection from a different experiment were analysed with qRT-PCR. Here, 6 pneumococcal and 6 murine genes were chosen, and 24 pneumococcal and 24 murine gene log_2 FC comparisons were performed. A high degree of correlation was also observed here, for both pneumococcal ($R^2 > 0.77$, Pearson) and murine genes ($R^2 > 0.73$, Pearson) (Fig. 5b).

Immune cell subsets present in infected lung tissue. The host RNA-seq data represent the pooled transcriptional responses of all cell types present in the lungs at the time of RNA extraction. Thus, some of the transcriptomic differences may be attributable to alterations in the relative abundance of given cell types, for example by differential recruitment of immune cell subsets to the site of infection. Accordingly, flow cytometry was used to quantify immune cell subsets present in lung tissue 6 h after infection with either 9–47-Ear, 4559-Blood, 9–47M or 4559M. The surface marker staining panel used (Supplementary Table 4) and appropriate gating strategy (Supplementary Fig. 1) allowed the identification and enumeration of natural killer (NK) cells, neutrophils, eosinophils, inflammatory monocytes (iMono), resident monocytes (rMono), alveolar macrophages (AMΦ), interstitial macrophages (iMΦ), CD11b-negative dendritic cells (CD11b-DC), CD11b-positive dendritic cells (CD11b + DC), T cells and B cells[12]. Of these, neutrophils, by far the most abundant cell type, were present in significantly higher numbers in murine lungs infected with 9–47-Ear (versus 4559-Blood, $p < 0.01$; versus 9–47M, $p < 0.05$) and 4559M (versus 4559-Blood, $p < 0.05$) (Fig. 6), both of which have the D249 *rafR* allele and were cleared from the lungs 24 h post-infection. NK cells were also found to be significantly higher in lungs infected with 9–47-Ear (versus 4559-Blood, $p < 0.01$; versus 9–47M, $p < 0.05$), while eosinophils were raised in 4559M infected lungs (versus 4559-Blood, $p < 0.05$) (Fig. 6). However, since the numbers of NK cells and eosinophils were much lower than neutrophils, their contribution to total lung mRNA and their impact on tissue tropism may be less pronounced. Moreover, the large difference in neutrophil recruitment to the lungs at 6 h post-infection aligns with the differential IL-17 response highlighted in the dual RNA-seq data. The higher number of neutrophils in murine lungs infected with 9–47-Ear and 4559M is likely to facilitate their clearance from this niche.

Impact of neutrophil depletion and IL-17A neutralization. The greater abundance of neutrophils in lungs infected with strains containing the D249 *rafR* allele that are cleared from the lungs by 24 h suggests that the recruitment and presence of neutrophils is crucial for bacterial clearance from the lung. Thus, differential neutrophil recruitment might be the underlying mechanism for the observed RafR-dependent tropism. To test this, we investigated the importance of neutrophils for persistence of pneumococci in the lungs in the IN challenge model. Injection of anti-mouse Ly6G was used to deplete neutrophils in 32 mice, alongside an isotype control group treated with rat IgG2a. Neutrophil depletion was confirmed in the blood prior to challenge using flow cytometry (Supplementary Fig. 2), with a 76.35% decrease in neutrophils in the anti-mouse ly6G treated mice, relative to the isotype control-treated group ($p < 0.0001$) (Supplementary Fig. 3A). Mice were then challenged with 10^8 CFU of each strain, for both treatment groups. Bacterial loads were quantified in the nasopharynx and lungs 24 h post-challenge. No significant differences in bacterial numbers in the nasopharynx were seen between strains within each treatment group (Fig. 7a). Also, for both treatments, the numbers of bacteria in the lungs infected with 4559-Blood and 9–47M were higher than 9–47-Ear and 4559M (Fig. 7b), which is consistent with our previous findings[7]. However, the anti-Ly6G-treated groups showed significantly higher lung bacterial loads compared to their respective isotype controls: 4559-Blood anti-Ly6G versus 4559-Blood

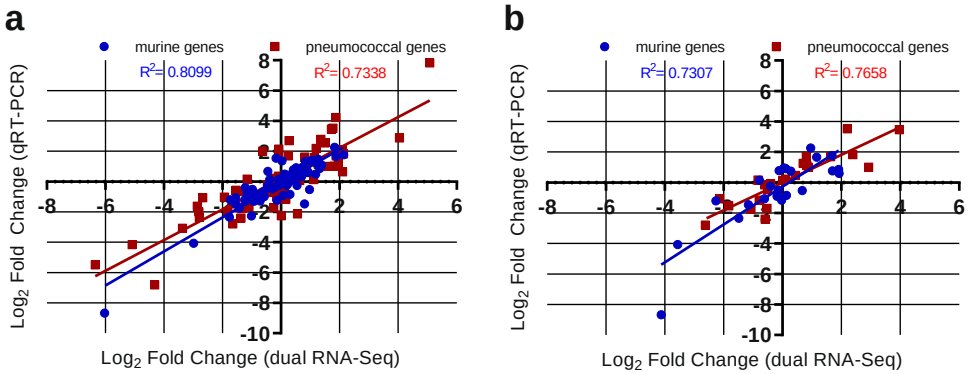

Fig. 5 Validation of transcriptomic data. Gene expression values from the dual RNA-seq were confirmed by qRT-PCR, using **a** the same isolated RNA used for the dual RNA-seq or **b** isolated RNA from a repeated experiment. **a** 18 murine and 19 pneumococcal genes were chosen as experimental validation targets. Log_2 fold changes were plotted from qRT-PCR against dual RNA-seq log fold changes for 9–47-Ear versus 4559-Blood, 9–47-Ear versus 9–47M, 9–47M versus 4559M, and 4559-Blood versus 4559M comparisons. A total of 72 murine and 76 pneumococcal comparisons were plotted, with a high degree of correlation observed for both species ($R^2 > 0.73$, Pearson). **b** 6 murine and 6 pneumococcal genes were chosen as targets to test the reproducibility of the dual RNA-seq data. Log_2 fold changes were plotted from qRT-PCR against dual RNA-seq log fold changes for 9–47-Ear versus 4559-Blood, 9–47-Ear versus 9–47M, 9–47M versus 4559M and 4559-Blood versus 4559M comparisons. A total of 24 murine and 24 pneumococcal comparisons were plotted, with a high degree of correlation observed for both species ($R^2 > 0.73$, Pearson).

control ($p < 0.001$), 947-Blood anti-Ly6G versus 947-Blood control ($p < 0.01$), 4559M anti-Ly6G versus 4559M control ($p < 0.01$), and 947M anti-Ly6G versus 947M control ($p < 0.05$) (Fig. 7b). Importantly, the lung bacterial loads of anti-Ly6G-treated 9–47-Ear and 4559M groups were not significantly different to the isotype control-treated 4559-Blood group (Fig. 7b). Thus, restriction of neutrophil infiltration into the lungs by depleting circulating neutrophils in mice challenged with the strains expressing the D249 *rafR* allele resulted in enhanced lung bacterial loads at 24 h similar to that seen in untreated mice challenged with the strains expressing the G249 *rafR* allele.

Given the known involvement of IL-17 in neutrophil recruitment into the lungs after infection[13–16], we also investigated the in vivo significance of the *rafR*-mediated differential expression of IL-17-associated genes between the various *S. pneumoniae* strains. Groups of mice were injected with anti-mouse IL-17A, or a control murine IgG1 antibody, before and after pneumococcal challenge. IL-17A depletion was confirmed by ELISA on separate 9–47-infected bronchoalveolar lavage (BAL) samples, with a 55.63% reduction in IL-17A levels seen in anti-mouse IL-17A treated mice relative to the isotype control group ($p < 0.0001$) (Supplementary Fig. 3b). The effect of this IL-17A depletion on neutrophil levels was also tested using flow cytometry on infected 9–47 lung tissue, with a 22.23% decrease in neutrophils seen in the anti-mouse IL-17A-treated mice, relative to the isotype control-treated group ($p < 0.05$) (Supplementary Fig. 3C). Bacterial loads were quantified in the nasopharynx and lungs for 24 h of post-challenge. Again, no significant differences between strains in bacterial numbers in the nasopharynx were seen within each treatment group (Fig. 7c). However, similar to the results obtained using anti-Ly6G, groups treated with anti-IL-17A showed significantly higher bacterial numbers in the lungs compared to their respective isotype controls; 4559-Blood anti-IL-17A versus 4559-Blood control ($p < 0.05$); 947-Blood anti-IL-17A versus 947-Blood control ($p < 0.05$); 4559M anti-IL-17A versus 4559M control ($p < 0.05$); and 947M anti-IL-17A versus 947M control ($p < 0.01$) (Fig. 7d). Nevertheless, the impact of anti-IL-17 treatment on lung bacterial loads was not quite as dramatic as that of anti-Ly6G, as the number of bacteria in the lungs of anti-IL-17A-treated 9–47-Ear and 4559M groups remained significantly lower relative to the isotype control treated 4559-Blood group (both $p < 0.05$) (Fig. 7d). Together, these results show that pneumococcal strains carrying the D249 *rafR* allele cause a rapid influx of neutrophils, partly controlled by IL-17 expression in the host, leading to clearance from the lung, while the G249 *rafR* strains manage to remain "stealthy" and hence can persist.

Discussion

In this study, we have used a dual RNA-seq approach, validated by qRT-PCR, to elucidate the complex interspecies interactions between murine lung cells and infecting *S. pneumoniae* blood and ear isolates that are closely related (same capsular serotype and ST type), but exhibit distinct virulence phenotypes in accordance with their original clinical isolation site. These differences are largely, but not completely, driven by a D249G SNP in the raffinose pathway transcriptional regulator gene *rafR*, which extensively impacts the bacterial transcriptome in the lung environment. The SNP affects expression of genes encoding multiple transmembrane transporters, including those for various sugars, and fine-tunes pneumococcal carbohydrate metabolism. This indicates that the differential expression of sugar catabolism pathways provides specific advantages in distinct host niches, implying differential niche-specific availability of one carbohydrate source versus another. Free sugars are in low abundance in the upper respiratory tract, but *S. pneumoniae* expresses a range of surface-associated exoglycosidases enabling it to scavenge constituent sugars (including galactose, *N*-acetylglucosamine, sialic acid, and mannose) from complex host glycans present in respiratory secretions and on the epithelial surface[17–21]. On the other hand, glucose is readily available in the blood and also in inflamed tissues, implying a marked alteration in the availability of this preferred carbohydrate source as invasive disease progresses[22]. All these variations, and the downstream consequences thereof, are ultimately sensed by host cells, including epithelial and immune cells, resulting in the observed divergence of host response to the various strains, particularly with respect to expression of genes encoding cytokine and chemokine ligands and receptors, as well as those associated with programmed cell death.

Examination of the nature of the host response has provided important clues regarding the mechanism whereby the *rafR* SNP impacts virulence phenotype. By way of example, the dual RNA-seq data showed that expression of IL-17-related genes was

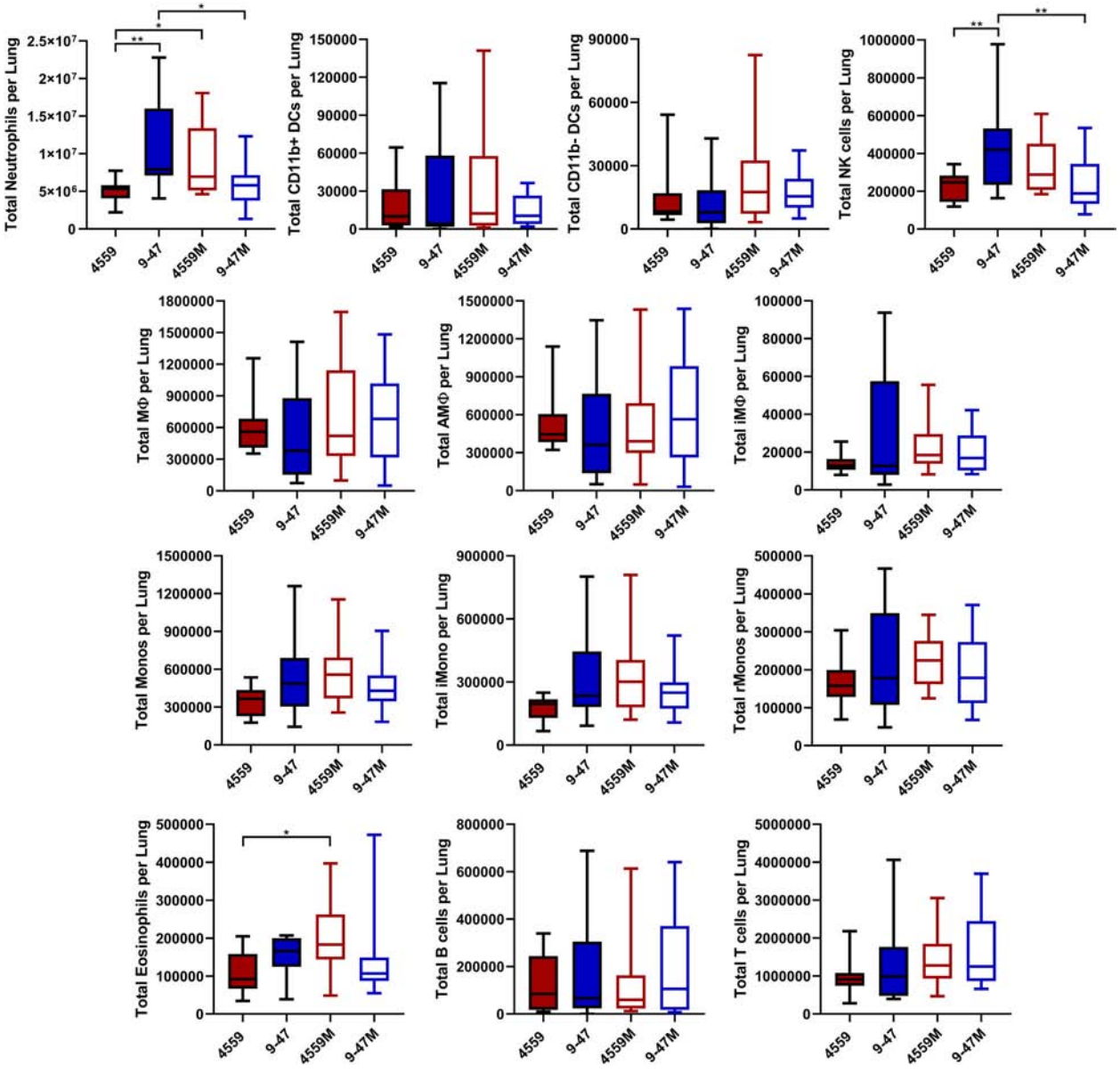

Fig. 6 Quantification of immune cell subsets in murine lungs 6 h post infection. Groups of 8 mice per strain were challenged with either 9-47-Ear, 4559-Blood, 9-47M or 4559M. Single cell lung suspensions were prepared and stained with antibodies against various surface markers (Supplementary Table 4) then analyzed by flow cytometry. Populations enumerated include: NK natural killer cells, iMono neutrophils, eosinophils, inflammatory monocytes, rMono resident monocytes, AMΦ alveolar macrophages, iMΦ interstitial macrophages, CD11b−DC CD11b-negative dendritic cells, CD11b+DC CD11b-positive dendritic cells, T cells and B cells. Graphs shown represent pooled data from two independent experiments. All quantitative data are presented as mean ± S.E.M ($n = 16$ for each group), analyzed by one-way ANOVA (*$p < 0.05$; **$p < 0.01$).

enriched in mice infected with 9–47-Ear and 4559M, the strains that express the D249 *rafR* allele and which are cleared from the lungs after 24 h of post-challenge. It is well known that IL-17 drives neutrophil recruitment into the lungs after infection[13–16]. Additionally, neutrophil extravasation genes were shown to be upregulated in murine lungs for 48 h of post pneumococcal challenge[23]. Indeed, we have shown here that neutrophils were present in the lungs at 6 h of post challenge at higher numbers in mice infected with 9–47-Ear and 4559M compared with the strains expressing the G249 *rafR* allele (Fig. 6), as predicted by the dual RNA-seq data. Moreover, we went on to show that neutrophil depletion by treatment with anti-Ly6G increased bacterial numbers in the lungs of mice, relative to the isotype controls. Strikingly, pneumococcal numbers in the lungs of anti-Ly6G treated mice infected with 9–47-Ear and 4559M were not significantly different to that for isotype control-treated 4559-Blood-infected mice (Fig. 7b). In vivo neutralization of IL-17A also resulted in an increase in bacterial loads in the lungs of mice, relative to the isotype controls, for all challenge strains (Fig. 7d), although not to the same extent as seen with for neutrophil-depleted mice (Fig. 7b). The difference between the impact of IL-17A neutralization versus neutrophil depletion is likely due to the action of alternative neutrophil recruitment pathways[24,25]. Our findings demonstrate that the *rafR* SNP examined in this study has a wide spread effect on both the bacterial and host transcriptomes, with the strains expressing the G249 allele triggering a strong pro-inflammatory IL-17 response in the lungs post-infection. This response leads to an influx of neutrophils to the

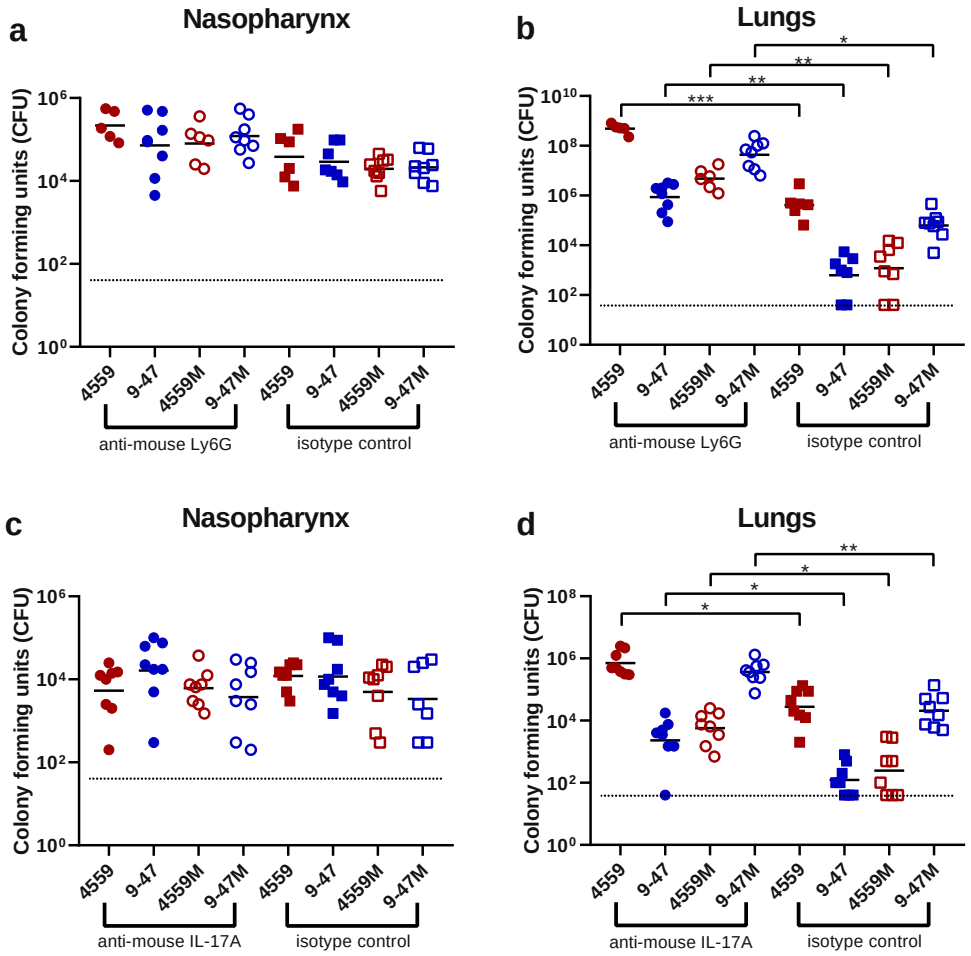

Fig. 7 Impact of neutrophil depletion or IL-17A neutralization on pneumococcal virulence. Groups of eight mice were treated with either 350 µg of rat anti-mouse Ly6G or rat IgG2a isotype control, one and two days prior to pneumococcal challenge (**a**, **b**), or with anti-IL-17A or mouse IgG1 isotype control (**c**, **d**), one day before, 2 h before and 6 h after intranasal challenge (see "Methods" section). Twenty-four hours of post-infection, numbers of pneumococci in the nasopharynx and lungs were quantitated (see "Methods" section). NB: *n* is <8 for some groups because some mice didn't survive the challenge procedure, or until the time of harvest. Viable counts (total CFU per tissue) are shown for each mouse at each site; horizontal bars indicate the geometric mean (GM) CFU for each group; the broken line indicates the threshold for detection. Differences in GM bacterial loads between groups are indicated by asterisks: $*p < 0.05$, $**p < 0.01$, $***p < 0.001$, by unpaired *t*-test.

lungs, resulting in the clearance of bacteria. Conversely, expression of the D249 *rafR* allele results in a more subdued IL-17 host response, allowing for bacterial persistence in the lungs. Thus, our findings clearly indicate that modulation of neutrophil recruitment during the early stage of infection plays a key role in the capacity of a given *S. pneumoniae* strain to persist in the lungs, and the nature of disease ultimately caused by it.

Our previous studies have shown that in spite of early clearance from the lung, strains 9–47 Ear and 4559M, expressing the G249 *rafR* allele, have an enhanced capacity to spread to and/or proliferate in the ear and brain compartments[6,7]. It is not known whether differential carbohydrate metabolism better adapts these strains to available carbohydrate sources in these niches, or whether altered host pro-inflammatory responses contribute to ascension of the Eustachian tube or penetration of the blood-brain barrier. Unfortunately, the total numbers of pneumococci present in these niches are too low for pathogen–host transcriptomic analyses using available technologies.

Intra-species variation in virulence phenotype is a common feature of pathogenic microorganisms, which by nature are genetically diverse. *S. pneumoniae* is an exemplar of such diversity comprising at least 98 capsular serotypes superimposed on over 12,000 MLST types, and with a core genome that accounts for only 70% of genes[2]. Nevertheless, stark differences in pathogenic profile can result from the smallest of genetic differences between strains, as exemplified by the profound impact of a single SNP on both bacterial and host transcriptomes reported in this study.

Methods

Bacterial strains and growth conditions. *S. pneumoniae* strains used in this study are listed in Supplementary Table 4. Cells were routinely grown in serum broth (SB) as required. Bacteria were plated on Columbia agar supplemented with 5% (vol/vol) horse blood (BA) and incubated at 37 °C in 5% CO_2 overnight.

Intranasal challenge of mice and extraction of RNA. Animal experiments were approved by the University of Adelaide Animal Ethics Committee. Groups of 12 outbred 5–6-week-old female Swiss (CD-1) mice (48 in total), were anesthetized by intraperitoneal injection of pentobarbital sodium (Nembutal) and challenged intranasally (IN) with 50 µl of bacterial suspension containing approximately 1×10^8 CFU in SB of 4559-Blood, 9–47-Ear, 4559M or 9–47M. The challenge dose was confirmed retrospectively by serial dilution and plating on BA. Mice were euthanized by CO_2 asphyxiation at 6 h and lungs placed in 1 ml TRIzol (Thermo Fisher). RNA was then extracted using acid-phenol-chloroform-isoamyl alcohol (125:21:1; pH 4.5; Ambion) and purified using the RNeasy minikit (Qiagen). For subsequent dual RNA-seq analyses, there were three replicates per strain, with each replicate derived from the lungs of four mice.

RNA library preparation and sequencing. RNA quality was checked using chip-based capillary electrophoresis. Samples were then simultaneously depleted of

murine and pneumococcal ribosomal RNAs by dual rRNA-depletion as previously described[26]. Stranded cDNA library preparation was performed according to the prescribed protocol (Illumina, US). Sequencing was performed for twelve samples in one lane of an Illumina NextSeq 500, High Output Flowcell in 85 single end mode. Libraries were demultiplexed and analyzed further. Raw libraries are accessible at https://www.ncbi.nlm.nih.gov/geo/ with the accession number GSE123982.

Sequence data analysis. Quality of raw libraries was checked (FastQC v0.11.8, Babraham Bioinformatics, UK)[27]. In order to improve the quality of alignment, we trimmed the reads using the following criteria: (i) removal of adapter sequence, if any, based on TruSeq3-SE library, (ii) removal of low quality leading and trailing nucleotides, (iii) a five-nucleotide sliding window was created for surviving reads, in which the average quality score must be above 20 and (iv) minimum remaining length must be above 50 (Trimmomatic v0.38)[28]. The quality of trimmed reads was confirmed using FastQC[27].

As reference genomes, we created chimeric genomes by concatenating the in-house generated *S. pneumoniae* strain 9–47-Ear or 4559-Blood circular genomes[7] into the genome of *Mus musculus* (ENSEMBL, release 94, downloaded 9 October 2018). The corresponding annotation file was downloaded at the same time. The chimeric mouse/9–47-Ear genome was used as reference to align libraries from lungs infected by strain 9–47-Ear (and its corresponding swap mutant 9–47M) while the mouse/4559-Blood chimeric genome was used to align 4559-Blood and 4559 M libraries. Notably, the genome of *S. pneumoniae* isolate 4559-Blood has a plasmid. Alignment was performed by RNA-STAR (v2.6.0a)[29] with the following options: (i) alignIntronMax 1 and (ii) sjdbOverhang 84. The aligned reads were then summarized (featureCount v1.6.3) according to the chimeric annotation file in stranded, multimapping (-M), fractionized (--fraction) and overlapping (-O) modes[30]. In order to compare gene expression between strains from ear and blood isolate backgrounds, we prepared a common pneumococcal annotation file using Mauve v20150226[31]. Common genes between 9–47-Ear and 4559-Blood were defined as having common coverage at least 90% and identity at least 90%. This single-pass alignment was selected to minimize false discovery rate. However, due to this approach, we had to adjust the summarizing process, taking into account the overlapping nature of bacterial genes and its organization into operon structures.

We then analyzed host and pathogen libraries separately in R (R v3.5.2). Since reads coming from pneumococcal genes encoding bacterial rRNA dominate the pathogen libraries (average 64.5%; range 61.4–67.3%), we excluded these pneumococcal ribosomal RNA reads from downstream analysis, but we did not do the same exclusion to reads from murine ribosomal RNA genes due to effective rRNA depletion. Differential gene analysis was performed by DESeq2 v1.22.1[32] and genome-wide fold change was calculated within host and pathogen libraries for every two possible comparisons: strains 9–47-Ear to 9–47M, strains 9–47-Ear to 4559-Blood, strains 9–47-Ear to 4559M, strains 9–47M to 4559-Blood, strains 9–47M to 4559M and strains 4559-Blood to 4559M. Value of fold change was set to zero if the corresponding adjusted *p*-value (*p*adj) is reported to be NA.

Quantitative real time RT-PCR. Differences in levels of gene expression observed in the dual RNA-seq data were validated by one-step relative quantitative real-time RT-PCR (qRT-PCR) in a Roche LC480 real-time cycler essentially as previously described[33]. The same RNA that was used for the dual RNA-seq was used in the qRT-PCR experimental validation. 19 pneumococcal genes and 18 murine genes were chosen for the experimental validation. The murine intranasal challenge and RNA isolation was repeated to test the reproducibility of the dual RNA-seq data. 6 pneumococcal and 6 murine genes were chosen for the reproducibility validation. The specific primers used for the various genes are listed in Supplementary Table 3 and were used at a final concentration of 200 nM per reaction. As an internal control, primers specific for *gyrA* for pneumococcal genes, and GAPDH for murine genes, were employed. Amplification data were analysed using the comparative critical threshold ($2^{-\Delta\Delta C_T}$) method[34].

Flow cytometry analysis of infected murine lungs. Groups of 8 outbred 6-week-old female Swiss (CD-1) mice (32 in total) were anesthetized and challenged with the bacterial suspension as outlined above in the total RNA extraction method. Mice were euthanized by CO_2 asphyxiation at 6 h, then lungs were finely macerated in 1 mL prewarmed digestion medium (DMEM + 5% FCS, 10 mM HEPES, 2.5 mM $CaCl_2$, 0.2 U mL^{-1} penicillin/gentamicin, 1 mg mL^{-1} collagenase IA, 30 U mL^{-1} DNase) and incubated at 37 °C for 1 h with mixing every 20 min. Single cells were then prepared for acquisition on a BD LSRFortessa X20 flow cytometer as previously described[35]. The single cell suspensions were stained using antibodies against surface markers listed in Supplementary Table 4, allowing the enumeration of a number of immune cell subsets, as previously described[12].

Neutrophil depletion, IL-17A blockade and bacterial loads. Groups of 8 outbred 6-week-old female Swiss (CD-1) mice (64 in total) were intraperitoneally administered with either 350 µg of rat anti-mouse Ly6G or rat IgG2a isotype control antibodies, one and two days prior to pneumococcal challenge, or 200 µg of either monoclonal anti-mouse IL-17A or mouse IgG1 isotype control antibodies one day prior to, 2 h before and 6 h after pneumococcal challenge. Mice were also cheek bled on the day of challenge for confirmation of depletion of Ly6G-positive cells via flow cytometry, as previously described[36]. Mice were then anesthetized and challenged with the bacterial suspension as outlined above in the total RNA extraction method, for each treatment group. Mice were euthanized by CO_2 asphyxiation at 24 h, then nasopharynx and lung tissue samples were harvested and pneumococci enumerated in tissue homogenates as described previously via serial dilution and plating on BA containing gentamicin[37].

Neutrophil and IL-17A levels after IL-17A neutralization. Groups of three outbred 6-week-old female Swiss (CD-1) mice were intraperitoneally administered with 200 µg of either monoclonal anti-mouse IL-17A or mouse IgG1 isotype control antibodies one day prior to and 2 h before intranasal challenge with 9–47, as described above. Six hours of post-infection, lung tissue and bronchoalveolar lavage (BAL) were harvested. To quantify IL-17 levels, a mouse IL-17 DuoSet® ELISA (R&D Systems) was performed on BAL samples in duplicate, according to the manufacturer's instructions. Flow cytometry was performed on lung tissue samples, as described above, to quantify neutrophil levels after anti-mouse IL-17A treatment.

Statistics and reproducibility. For the RNA-seq data, enrichment tests to assess enrichment were performed by the built-in function, *fisher.test()*. Corresponding *p*-values of the enrichment test were adjusted by Bonferroni correction. Resultant figures encompass data derived from three replicates per group, with each replicate derived from lungs of four mice. All other data are presented as mean ± standard error of mean (SEM) or geometric mean, and were analyzed by two-tailed unpaired Student's *t*-test, one way ANOVA or Pearson correlation coefficient, using Prism v8.0d (GraphPad). Statistical significance was defined as $p < 0.05$. Data presented in figures are representative of at least two independent in vivo experiments, or at least 3 independent in vitro experiments.

Reporting summary. Further information on research design is available in the Nature Research Reporting Summary linked to this article.

Data availability

Raw RNA libraries are accessible at https://www.ncbi.nlm.nih.gov/geo/ with the accession number GSE123982. Source data for Figs. 2–7 are provided in Supplementary Data 13.

Received: 19 December 2019; Accepted: 15 May 2020;
Published online: 05 June 2020

References

1. Kadioglu, A., Weiser, J. N., Paton, J. C. & Andrew, P. W. The role of *Streptococcus pneumoniae* virulence factors in host respiratory colonization and disease. *Nat. Rev. Microbiol.* **6**, 288–301 (2008).
2. Weiser, J. N., Ferreira, D. M. & Paton, J. C. *Streptococcus pneumoniae*: transmission, colonization and invasion. *Nat. Rev. Microbiol.* **16**, 355–367 (2018).
3. Enright, M. C. & Spratt, B. G. A multilocus sequence typing scheme for *Streptococcus pneumoniae*: identification of clones associated with serious invasive disease. *Microbiology* **144**, 3049–3060 (1998).
4. van Tonder, A. J. et al. Putative novel *cps* loci in a large global collection of pneumococci. *Microb. Genom.* **5**, e000274 (2019).
5. Trappetti, C. et al. Site of isolation determines biofilm formation and virulence phenotypes of *Streptococcus pneumoniae* serotype 3 clinical isolates. *Infect. Immun.* **81**, 505–513 (2013).
6. Amin, Z. et al. Isolation site influences virulence phenotype of serotype 14 *Streptococcus pneumoniae* strains belonging to multilocus sequence type 15. *Infect. Immun.* **83**, 4781–4790 (2015).
7. Minhas, V. et al. Capacity to utilize raffinose dictates pneumococcal disease phenotype. *mBio* **10**, e02596–18 (2019).
8. Westermann, A. J., Barquist, L. & Vogel, J. Resolving host-pathogen interactions by dual RNA-seq. *PLoS Pathog.* **13**, e1006033 (2017).
9. Wolf, T., Kämmer, P., Brunke, S. & Linde, J. Two's company: studying interspecies relationships with dual RNA-seq. *Curr. Opin. Microbiol.* **42**, 7–12 (2018).
10. Bidossi, A. et al. A functional genomics approach to establish the complement of carbohydrate transporters in *Streptococcus pneumoniae*. *PLoS ONE* **7**, e33320 (2012).
11. Onishi, R. M. & Gaffen, S. L. Interleukin-17 and its target genes: mechanisms of interleukin-17 function in disease. *Immunology* **129**, 311–321 (2010).

12. Yu, Y.-R. A. et al. A protocol for the comprehensive flow cytometric analysis of immune cells in normal and inflamed murine non-lymphoid tissues. *PLoS ONE* **11**, e0150606 (2016).
13. Lindén, A., Laan, M. & Anderson, G. P. Neutrophils, interleukin-17A and lung disease. *Eur. Resp. J.* **25**, 159–172 (2005).
14. McCarthy, M. K., Zhu, L., Procario, M. C. & Weinberg, J. B. IL-17 contributes to neutrophil recruitment but not to control of viral replication during acute mouse adenovirus type 1 respiratory infection. *Virology* **456-457**, 259–267 (2014).
15. Ritchie, N. D., Ritchie, R., Bayes, H. K., Mitchell, T. J. & Evans, T. J. IL-17 can be protective or deleterious in murine pneumococcal pneumonia. *PLoS Pathog.* **14**, e1007099 (2018).
16. Stoppelenburg, A. J. et al. Local IL-17A potentiates early neutrophil recruitment to the respiratory tract during severe RSV infection. *PLoS ONE* **8**, e78461 (2013).
17. King, S. J., Hippe, K. R. & Weiser, J. N. Deglycosylation of human glycoconjugates by the sequential activities of exoglycosidases expressed by *Streptococcus pneumoniae*. *Mol. Microbiol.* **59**, 961–974 (2006).
18. Shelburne, S. A., Davenport, M. T., Keith, D. B. & Musser, J. M. The role of complex carbohydrate catabolism in the pathogenesis of invasive streptococci. *Trends Microbiol.* **16**, 318–325 (2008).
19. Buckwalter, C. M. & King, S. J. Pneumococcal carbohydrate transport: food for thought. *Trends Microbiol.* **20**, 517–522 (2012).
20. Paixão, L. et al. Transcriptional and metabolic effects of glucose on *Streptococcus pneumoniae* sugar metabolism. *Front. Microbiol.* **6**, 1041 (2015).
21. Robb, M. Molecular characterization of *N*-glycan degradation and transport in *Streptococcus pneumoniae* and its contribution to virulence. *PLoS Pathog.* **13**, e1006090 (2017).
22. Philips, B. J., Meguer, J. X., Redman, J. & Baker, E. H. Factors determining the appearance of glucose in upper and lower respiratory tract secretions. *Intensive Care Med.* **29**, 2204–2210 (2003).
23. Ritchie, N. D. & Evans, T. J. Dual RNA-seq in *Streptococcus pneumoniae* infection reveals compartmentalized neutrophil responses in lung and pleural space. *mSystems* **4**, e00216–e00219 (2019).
24. Craig, A., Mai, J., Cai, S. & Jeyaseelan, S. Neutrophil recruitment to the lungs during bacterial pneumonia. *Infect. Immun.* **77**, 568–575 (2009).
25. Peñaloza, H. F. et al. Interleukin-10 plays a key role in the modulation of neutrophils recruitment and lung inflammation during infection by *Streptococcus pneumoniae*. *Immunology* **146**, 100–112 (2015).
26. Aprianto, R., Slager, J., Holsappel, S. & Veening, J.-W. Time-resolved dual RNA-seq reveals extensive rewiring of lung epithelial and pneumococcal transcriptomes during early infection. *Genome Biol.* **17**, 198 (2016).
27. Andrews, S. & Babraham Bioinformatics. FastQC: a quality control tool for high throughput sequence data. Babraham Bioinformatics Manual (2010).
28. Bolger, A. M., Lohse, M. & Usadel, B. Trimmomatic: a flexible trimmer for Illumina sequence data. *Bioinformatics* **30**, 2114–2120 (2014).
29. Dobin, A. et al. STAR: ultrafast universal RNA-seq aligner. *Bioinformatics* **29**, 15–21 (2013).
30. Liao, Y., Smyth, G. K. & Shi, W. featureCounts: an efficient general purpose program for assigning sequence reads to genomic features. *Bioinformatics* **30**, 923–930 (2014).
31. Darling, A. C. E., Mau, B., Blattner, F. R. & Perna, N. T. Mauve: multiple alignment of conserved genomic sequence with rearrangements. *Genome Res.* **14**, 1394–1403 (2004).
32. Love, M. I., Huber, W. & Anders, S. Moderated estimation of fold change and dispersion for RNA-seq data with DESeq2. *Genome Biol.* **15**, 550 (2014).
33. Mahdi, L. K., Ogunniyi, A. D., LeMessurier, K. S. & Paton, J. C. Pneumococcal virulence gene expression and host cytokine profiles during pathogenesis of invasive disease. *Infect. Immun.* **76**, 646–657 (2008).
34. Livak, K. J. & Schmittgen, T. D. Analysis of relative gene expression data using real-time quantitative PCR and the 2(-Delta Delta C(T)) method. *Methods* **25**, 402–408 (2001).
35. David, S. C. et al. Enhanced safety and immunogenicity of a pneumococcal surface antigen A mutant whole-cell inactivated pneumococcal vaccine. *Immunol. Cell Biol.* **97**, 726–739 (2019).
36. Faget, J. et al. Efficient and specific Ly6G+ cell depletion: a change in the current practices toward more relevant functional analyses of neutrophils. *BioRxiv*. https://doi.org/10.1101/498881 (2018).
37. Trappetti, C., Ogunniyi, A. D., Oggioni, M. R. & Paton, J. C. Extracellular matrix formation enhances the ability of *Streptococcus pneumoniae* to cause invasive disease. *PLoS ONE* **6**, e19844 (2011).

Acknowledgements

We thank V Benes (GeneCore, EMBL, Heidelberg) for support in library preparation and sequencing and the Center for Information Technology of the University of Groningen for support and for providing access to the Peregrine high-performance computing cluster. We also thank Timona Tyllis and Todd Norton for assistance in acquiring the flow cytometry samples, and Alexandra Tikhomirova for assistance with the murine experiments. This work was supported by the Swiss National Science Foundation (SNSF) (project grant 31003A_172861) to J.W.V., National Health and Medical Research Council (NHMRC) Program Grant 1071659 and Investigator Grant 1174876 to J.C.P. and a University of Adelaide Beacon Fellowship to C.T. The funders had no role in study design, data collection and interpretation, or the decision to submit the work for publication.

Author contributions

Conceptualization: V.M., J.C.P., J.W.V. and C.T.; Methodology: V.M., R.A., J.W.V. and C.T.; Formal analysis: V.M., R.A., L.J.M., I.C., S.R.M., J.C.P., J.W.V. and C.T.; Investigation: V.M., R.A., H.W., S.C.D., K.T.M., and C.T.; Writing—original draft: V.M., R.A., J.C.P., J.W.V. and C.T.; Writing—review and editing: all authors; Supervision: J.C.P., J.W.V., and C.T.; Funding acquisition: J.C.P., J.W.V., and C.T.

Competing interests

The authors declare no competing interests.

Additional information

Supplementary information is available for this paper at https://doi.org/10.1038/s42003-020-1018-x.

Correspondence and requests for materials should be addressed to J.C.P.

Reprints and permission information is available at http://www.nature.com/reprints

Publisher's note Springer Nature remains neutral with regard to jurisdictional claims in published maps and institutional affiliations.